THE PHYSICAL REVIEW

A journal of experimental and theoretical physics established by E. L. Nichols in 1893

VOLUME 77

Second Series

JANUARY 1–MARCH 15, 1950

Published for the

AMERICAN PHYSICAL SOCIETY

by the

AMERICAN INSTITUTE OF PHYSICS

Incorporated

Astronomy Library
QC
1
.P5812
V. 77

THE PHYSICAL REVIEW

A journal of experimental and theoretical physics established by E. L. Nichols in 1893

Published by the American Institute of Physics for the

AMERICAN PHYSICAL SOCIETY

Officers

President

F. W. LOOMIS
University of Illinois
Urbana, Illinois

Vice-President

I. I. RABI
Columbia University
New York, New York

Secretary

K. K. DARROW
Bell Telephone Laboratories
Office:
Columbia University
New York 27, New York

Treasurer

G. B. PEGRAM
Columbia University
New York 27, New York

Local Secretary for the Pacific Coast

J. KAPLAN
University of California at Los Angeles
Los Angeles, California

Managing Editor

JOHN T. TATE
University of Minnesota
Minneapolis, Minnesota

BOARD OF EDITORS

Editor
JOHN T. TATE

Assistant Editor
J. W. BUCHTA

Associate Editors

H. A. BETHE — S. A. GOUDSMIT — W. E. LAMB, JR.
L. A. RIDENOUR — E. M. PURCELL — R. G. HERB
W. H. ZACHARIASEN — V. F. WEISSKOPF — J. BARDEEN

Manuscripts for publication should be submitted to John T. Tate, University of Minnesota, Minneapolis, Minnesota. The authors' institutions are requested to pay a publication charge of $8 per page which, if honored, entitles them to 100 free reprints. Instructions will be sent with galley proofs.

Proof and all correspondence concerning papers in the process of publication should be addressed to the Publication Manager, American Institute of Physics, 57 East 55 Street, New York 22, New York.

Subscription Price

United States and Canada $25.00
Elsewhere $27.00

Back Numbers [1]

Yearly back number rate when complete year is available:
Prior to 1949: $20.00
Thereafter: $27.00
Single copies: $2.00 each, prior to July, 1929;
$1.00 each, July, 1929–December, 1941;
$2.00 each, January, 1942–December, 1946;
$1.00 each, January, 1947–December, 1948;
$1.25 each, thereafter.
General index, 1893–1920: $4.00.

Subscriptions and orders for back numbers should be addressed to Prince and Lemon Streets, Lancaster, Pennsylvania, or to the American Institute of Physics, 57 East 55 Street, New York 22, New York.

Changes of address in the case of members of the American Physical Society should be addressed to the Treasurer; in the case of other subscribers to the Circulation Manager, American Institute of Physics.

[1] For Series 1 inquire of Physics Department, Cornell University, Ithaca, New York.

The Physical Review is published semi-monthly at Prince and Lemon Streets, Lancaster, Pennsylvania.

Entered as second-class matter March 6, 1947, at the Post Office at Lancaster, Pennsylvania, under the Act of March 3, 1879.

Acceptance for mailing at special rate of postage provided for in paragraph 4, section 538, P. L. & R., authorized January 27, 1933.

950

THE

PHYSICAL REVIEW

Vol. 1 Series 1 Number 1

JANUARY 1, 1950

Published for the

AMERICAN PHYSICAL SOCIETY

by the

UNIVERSITY OF ILLINOIS

Urbana, Illinois

Suggestions for Contributors

Manuscripts

Send manuscripts to John T. Tate, Department of Physics, University of Minnesota, Minneapolis 14, Minnesota.

Each article submitted will in general consist of (a) textual material, i.e., all material which is to be set in type, and (b) drawings or photographs from which zinc etchings or copper halftones will be made. Textual material will consist of an abstract, the body of the paper, tabular material, references, and figure captions. All of this material must be in English, typewritten (except mathematical expressions) double spaced with wide margins (for editorial instructions to the printer) on a durable, white paper, preferably letter size. The original copy, not the carbon, should be submitted.

For general style, spellings, abbreviations, and form, recent issues of this journal should be consulted.

The prime requisite is that the copy shall be clear to the typesetter, who is neither a physicist nor a mathematician.

Abstracts

An abstract must accompany each article. It should be adequate as an index and as a summary. As an index, it should give all subjects, major and minor, concerning which new information is presented. As a summary it should give the conclusions of the article and all numerical results of general interest.

Mathematical Expressions

All but the simplest mathematical expressions should be carefully printed in by hand. Be sure to distinguish between capital and small letters. Indicate clearly superscripts and subscripts by inverted carets and carets, respectively. Avoid complicated superscripts and subscripts. Avoid repetition of a complicated expression by representing it by some convenient symbol. Identify in the margin Greek letters and unusual symbols. Use fractional exponents instead of root signs. Use the solidus (/) for fractions wherever its use will save vertical space.

References

References should appear as footnotes, numbered consecutively, and arranged thus:

[1] A. B. Smith, Phys. Rev. 41, 852 (1932).
[2] H. Lamb, *Hydrodynamics* (Cambridge University Press, Teddington, England), sixth edition, pp. 573, 643.

Tables

All but the simplest tabular material should be organized in tabular form rather than as a part of the running text. Tables may be typewritten on sheets separate from the running text with indications in the margin of the running text where the table is to be inserted. Each table must have a caption which will make the data in the table intelligible without reference to the text. Avoid complicated column headings; if necessary, use symbols which are explained in the table caption.

Figures

Wherever possible figures should be planned for the width of a column of the *Physical Review* (3 inches). A convenient reduction ratio is about 2:1 or 3:1. The original drawings or photographs should therefore be in general about 6 to 9 inches wide and the lettering and symbols should be large enough on the original that when reduced they shall not be less than about $\frac{1}{16}$ in. (≈1.5 mm). If the reduction is 3:1, the original lettering should be not less than $\frac{1}{8}$ in. high.

The process of making zinc etchings or copper halftones is a black and white photographic one. Therefore line drawings must be in *India ink* on white paper or tracing cloth. Coordinate paper is not desirable but if used must be blue lined and the coordinate lines which are to show must be inked over.

Photographs should have maximum black and white contrast.

Plan figures to use space efficiently. Avoid wasting space, particularly at the top or bottom.

Identify on the back or other suitable place each original drawing or photograph with the author's name and the figure number. Figures should be numbered consecutively and their approximate position indicated in the margin of the running text. Figure captions should be typed and included with the manuscript (not as part of the figure).

Avoid round and oval photographs.

Alterations

Take great care that each manuscript is typographically accurate. A limited number of alterations in proof are unavoidable, but the cost of making extensive alterations after the article has been set in type will be charged to the author.

Proof and all correspondence concerning papers in the process of publication should be addressed to the Publication Manager, American Institute of Physics, 57 East 55 Street, New York 22, New York.

Astron. Gb.

THE
PHYSICAL REVIEW

A journal of experimental and theoretical physics established by E. L. Nichols in 1893

SECOND SERIES, VOL. 77, NO. 1 JANUARY 1, 1950

Local Production of Mesons at 11,300 Feet*

O. PICCIONI
Brookhaven National Laboratory, Upton, Long Island, New York
(Received September 6, 1949)

Mesons produced in association with local penetrating showers have been investigated at 11,300 ft. above sea level. The apparatus recorded delayed coincidences arising from the 2.2-μsec. decay process of μ-mesons and distinguished the delayed coincidences which were associated with a local penetrating shower from those which were not. It is found that the fraction of penetrating showers which gives a delayed coincidence is in accordance with the assumption that the local penetrating showers are the typical events in which mesons are produced. The comparison of the delayed coincidences rate using carbon as the material stopping the mesons, with the rate using sulfur shows that the locally produced particles are π-mesons.

Since a recent latitude experiment on local penetrating showers indicates that the average energy of the particles producing such events is above 10 Bev, the result of the present work extends to that energy the conclusion originated from observations in photographic emulsion, that only π-mesons, and not μ's are directly created in the collision of fast particles.

I. INTRODUCTION

LOCAL penetrating showers, or hard showers (HS) have been observed by Wataghin, De Souza Santos and Pompeia, and by Janossy, Ingleby, Rochester, and others. The main characteristic of these events is that one observes a number of penetrating particles crossing simultaneously an absorber, the thickness of which is equal to a large number of radiation units. Also, HS are only rarely accompanied by other particles falling on the area surrounding the apparatus which detects their occurrence. This experimental fact makes the HS easily distinguishable from the large Auger showers, and proves that the many penetrating particles observed in a HS are actually produced locally in the apparatus itself. Even more compelling evidence for local production is given by cloud-chamber pictures.[1]

Not enough information is yet available about the identity of the secondary particles. Rochester, Butler, Mitra, and Rosser[2] operated a cloud chamber triggered by showers containing penetrating particles, and identified a number of low energy particles. Almost all of them were protons. However, five heavily ionizing particles were identified as mesons. The values of their masses could not be determined with good accuracy, but an indication was there that some of those five particles might have been μ-mesons. Though not definite, the indication was particularly interesting after the experiments showing small interaction between μ-mesons and nuclei[3] and the observations in photographic plates regarding the existence of π-mesons and their decay into μ-mesons.[4] Indeed, both those lines of investigations strongly suggested that in the very act of the creation only π-mesons arise, which then decay in μ's. However, one should not forget that the events observed in photographic emulsions, as well as the experiments on the non-capture of μ-mesons, concerned mesons of small energies. On the contrary, an event such as a penetrating shower produces mesons of energy of the order of the Bev.

Further investigation on the identity of the penetrating particles, secondaries of a HS, seemed therefore desirable, both to prove that the produced mesons are

* Reported at the New York meeting of the American Physical Society (Phys. Rev. 75, 1281A (1949)).

[1] W. B. Fretter, Phys. Rev. 73, 41 (1948), see other references there.

[2] Rochester, Butler, Mitra, and Rosser, reported by G. D. Rochester, Symposium of Cosmic Rays, California Institute of Technology (June 21–23, 1948), Rev. Mod. Phys. 21, 20 (1949).

[3] Conversi, Pancini, and Piccioni, Phys. Rev. 71, 318 (1947); T. Sigurgeirson and A. Yamakawa, Phys. Rev. 71, 318 (1947); G. E. Valley, Phys. Rev. 72, 772 (1947); S. Tomonaga and G. Araki, Phys. Rev. 58, 90 (1940); Fermi, Teller, and Weisskopf, Phys. Rev. 71, 314 (1947).

[4] Lattes, Occhialini, and Powell, Nature 160, 486 (1947).

π-mesons, and to see if the HS are the typical events in which mesons are produced.

The present experiment was thus performed, using the delayed coincidence technique to distinguish mesons by their typical decay with a mean life of 2.2 μsec. For this purpose it did not matter whether we were dealing with π- or μ-mesons, because in either case the only delay registered by the apparatus was the delay arising from the μ-decay into an electron. The π–μ-decay involves delays of $\sim 10^{-8}$ sec.,[5] much too short to be detected by an apparatus using normal G-M counters.

However, by changing the absorber in which mesons were stopped, from carbon to sulfur, it was possible to establish their identification.

II. THE APPARATUS AND THE RECORDED EVENTS

The apparatus is shown schematically in Fig. 1. The material surrounding Trays A and B was lead. Adjacent counters of Tray A were separated by $1\frac{1}{2}$ in. of lead. Absorbers of carbon and sulfur were put in the place marked "absorber," at different times. The electronic circuit was designed to register the following types of coincidences[5] AB, prompt coincidences between A and B; ABC, prompt coincidences between A, B, and C; A_2BC, prompt coincidences between A, B, C, in which at least two counters of Tray A were discharged. ABC_{del}, prompt coincidences between A and B with *no more than one counter* discharged in A, followed by a delayed pulse in C; A_2BC_{del}, prompt coincidences between A and B with *two counters or more* being discharged in A, followed by a delayed pulse in C.

All the prompt coincidences were detected within a resolving time of five μsec. The delayed coincidences** were registed if the amount of delay was more than 1.3 μsec. and less than 8.4.

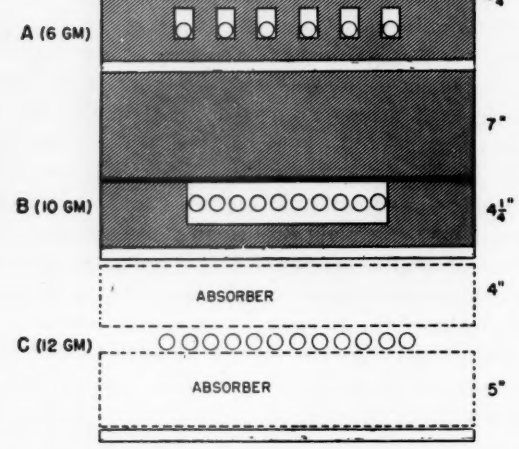

FIG. 1. Sketch of the apparatus. The Geiger-Müller counters (G-M) have an active length of 22 in. Their diameter is approximately 1 in.

If such was the case, for instance, in an event ABC_{del}, the delayed coincidence was registered in one of four registers, according to the actual amount of delay. The limits for the first register were 1.3 and 3.3 μsec., and for the others were 3.04, and 5.04, 4.76 and 6.76, 6.51 and 8.51. In the following, the four delay registers will be sometimes referred to as the "four channels." The same division in four channels was made for the coincidences of types A_2BC_{del}. While this obviously required four other registers, the same electronic circuit supplied the discrimination as to the amount of delay for both ABC_{del} and A_2BC_{del}. The distinction between the two types of delayed coincidences was made after the delay discriminators. This allowed a continuous check of the important part of the apparatus by means of the ABC_{del} events, which obviously occurred at a much higher rate than A_2BC_{del}.

It is rather important to mention that Tray C fed its pulses to a circuit of very short recovery time. Even if all but one of the 12 counters were discharged at the time zero, and the remaining counter was discharged one microsecond later, the corresponding delayed pulse was very much the same as if only one counter were discharged with a delay of one microsecond. The coincidence ABC_{del} or A_2BC_{del} was therefore registered whether or not a prompt coincidence ABC or A_2BC was also registered in the same event. This feature is desirable if one wants to register decay electrons arising from mesons generated in a local penetrating shower, since it permits the registration of a delayed coincidence also in the case that an undelayed particle and a delayed one cross the same tray. Of course the individual counter which has been crossed by the undelayed particle cannot detect the decay electron. However, the average number of counters discharged in Tray C when a local penetrating shower occurs is about one and the correspondent decrease in the efficiency is not serious.

The events like AB, ABC are due to the normal penetrating particles, which for the large majority, are μ-mesons generated in the higher levels of the atmosphere. The π-mesons, having a mean life two hundred times smaller than μ-mesons, cannot constitute any appreciable fraction of such coincidences.

The intensity of fast protons and neutrons, which also could give an ABC coincidence, is not known with good accuracy. However, from several delayed coincidence experiments performed at sea level, and considering that the lead of our apparatus is about equivalent to the amount of air between 11,300 ft. and sea level, one can easily argue that the fraction of ABC coincidences caused by protons or neutrons in our apparatus is no more than a few percent. Finally, electrons and photons cannot give any appreciable contribution to the rate ABC, due to the large thickness of lead which they should cross in order to reach Trays B and C.

[5] J. R. Richardson, Phys. Rev. 74, 1720 (1948).

** Our acquaintance with the delay discriminator built by M. Sands at M.I.T. was very helpful in designing the circuit.

TABLE I.

Absorber (4 in. above C, 5 in below C)	ABC (NP)	ABC_{del} 1.30–3.27 μsec. I	3.04–4.97 μsec. II	4.76–6.74 μsec. III	6.51–8.40 μ-sec. IV	Casuals per each channel*	True delays in all four channels per hour	Time (hr.)	Ratio C/S
Graphite	1,303,500	4556	2337	1339	873	550±15	30.4±0.5	227.95	1.85±0.05
Sulfur	1,225,100	2581	1338	938	650	495±15	16.4±0.4	216.50	
	A_2B(HS)		A_2BC_{del}						
Graphite	21,824	134	77	38	16	3.0	1.17±0.07	216.13	1.11±0.1
Sulfur	22,040	137	58	31	15	2.9	1.06±0.07	216.50	

* For ABC_{del}, this number is equal to the resolving time (1.94×10^{-4} sec.) multiplied by the background counting rate of C (71 sec.$^{-1}$ for graphite and 67.5 sec.$^{-1}$ for sulfur) multiplied by the coincidence rate AB (1.75×10^{4} hr.$^{-1}$) multiplied by the number of hours. While the statistical error in the computed casuals is only one percent, a larger error has been put in the table to take account of time variations of the rate AB, which was not constantly measured. The casuals for HS delays are computed analogously to the ABC casuals substituting to the AB rate the A_2B, which was constantly measured.

In the following we will often refer to the ABC coincidences as the NP (normal particles).

The ABC_{del}, when the casuals are subtracted, are then to be interpreted as given by the decay electrons of μ-mesons, and their frequency-*versus*-delay distribution is expected to follow the exponential law of the typical 2.2-μsec. decay.

The A_2B coincidences as well as the A_2BC, are meant to give the rate of the local penetrating showers. They imply the presence of two penetrating particles, except for the cases in which a single penetrating particle produces secondary electrons which cause the discharge of another counter of the same tray. However, the presence of $1\frac{1}{2}$ in. of lead between adjacent counters of A, makes those cases improbable. The fractions of the A_2B and A_2BC coincidences due to the normal hard component can be computed from the altitude dependence, as we will see later.

Large air showers, also can give an A_2BC or A_2B coincidence. Checking on this point, we found that such showers contribute not more than eight percent of the total rate at 11,300 ft. This is in agreement with the results of Gregory and Tinlot, as well as of Cocconi and Greisen.[6]

The factors by which the rates of the various coincidences increase, between sea level and 11,300 ft. (690 g/cm^{-2}), have been measured with the same apparatus of Fig. 1, having only 9 G-M counters in Tray C instead of 12, spread more apart, in order that the distance between extreme counters was kept equal to that shown in Fig. 1. The electronic circuit registered coincidences of Type A_2BC_n, where the subscript n indicates that the discharge of *n or more* counters of C was required. The result was:

R=ratio: $\frac{\text{rate at 11,300 ft.}}{\text{rate at sea level}}$	ABC	A_2B	A_2BC_1	A_2BC_2	A_2BC_3	A_2BC_4
	1.95	8.6	10.9	17.1	17.6	15.5
		±0.25	±0.5	±1.6	±2.2	±2.3

From those values it appears that NP contribute to the rate of A_2B and A_2BC_1, but A_2BC_2, A_2BC_3, A_2BC_4 are practically all caused by fast nucleons. The value 17 seems to be the exact value of R for the "true" HS detected by our apparatus. Using the absorption coefficient $L=118$ g/cm^{-2} found by Tinlot[7] we would find $R=18$.

From the data $R=18$ for HS, and $R=1.95$ for NP, one can easily evaluate how many of the events which we call HS are "true" HS, and how many are possibly caused by the normal hard component. At 11,300 ft., 92 percent of the A_2BC_1 coincidences and 87 percent of the A_2B are due to HS events, which means that the large majority of the A_2BC coincidences are the result of the collision of a fast nucleon with a nucleus of the lead above Tray A. When the same type of collision happens in the lead *below* Tray A, the probability for more than one counter in A to be discharged must be small. Therefore, not much preference, if any, is made by the apparatus between protons and neutrons, as particles producing a HS coincidence or a HS delayed coincidence. This last type of coincidence has then to be interpreted as follows: a HS is initiated above A, and among the secondary particles is a meson which stops in the absorber either above or below Tray C, giving rise to a delayed electron which crosses C. As we have already said, the double decay π–μ- and μ-electron gives exactly the same result as the μ-decay alone.

III. RESULTS

The delayed coincidence rates are shown in Table I, both for HS and NP. If we refer to the same number of particles crossing the bottom Tray C, we see that, using sulfur as absorber, the apparatus registered 3 A_2BC_{del} coincidences per 1000 ABC coincidences, while per 1000 A_2BC coincidences the number of A_2BC_{del} coincidences registered was 15. This was to be expected, and furnishes an additional proof that the HS delayed coincidences are given by locally produced mesons. Indeed, while the differential spectrum of NP is depleted in the low energy end by the 2.2-μsec. decay during the long flight through the atmosphere, such a decay can

[6] J. Tinlot and B. Gregory, Phys. Rev. **75**, 519 (1949); G. Cocconi and K. Greisen, Phys. Rev. **74**, 62 (1948).

[7] J. Tinlot, Phys. Rev. **74**, 1137 (1948).

have no effect on the spectrum of the locally produced mesons, because of the small distance between the top of the apparatus and Tray C. This fact has also the consequence that while 92 percent of A_2BC represent HS event, 97 percent of A_2BC delayed coincidences are actually associated with a HS.

The rate A_2BC_{del} is 6.5 percent of the ABC_{del}. However, we cannot assume that the apparatus will always register a HS event as such, even if it originated in the lead above A. A real evaluation of the efficiency of the apparatus as a HS detector cannot be made, and therefore the fraction of the locally produced mesons to all mesons cannot be considered as accurately measured. Assuming any reasonable value for the "over-all efficiency," for instance, less than 50 percent, and considering the altitude dependences of the HS ($\sim\exp[-x/118]$),[7] and of the slow mesons ($\sim\exp[-x/240]$),[8] one expects that if our apparatus had been working at a residual pressure of 200 g/cm^{-2}, and if it had 100 percent efficiency, the HS delayed coincidences would have been just as many as the NP delayed coincidences. At a higher altitude, the HS delayed coincidences would be in large prevalence.

We are thus led to conclude that the *local penetrating showers* of the very same type as detected by our apparatus, *constitute the main process where mesons of relevant energy are produced.*

In the preceding discussion, the comparison of A_2BC_{del} with ABC_{del} has been done referring to the data with sulfur as the material stopping mesons, in order not to favor the μ-mesons with respect to π's. This will be clear after the next section of this paper.

IV. DISTINCTION BETWEEN π- AND μ-MESONS

The differential decay curves of Fig. 2, which are based on measurements using either carbon or sulfur as the absorber, show beyond any doubt that the A_2BC_{del} are caused by the 2.2-μsec. decay process typical of μ-mesons.

The separate measurements with carbon and sulfur as absorbers enable us to specify the nature of the mesons directly produced in the nuclear collisions,

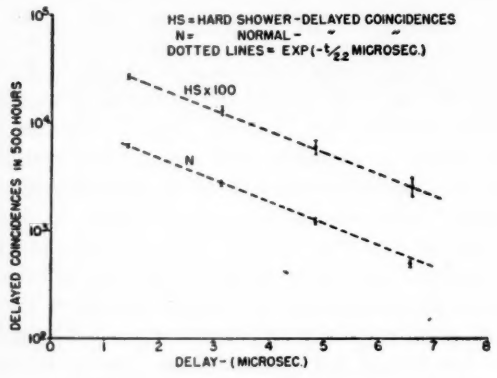
HS = HARD SHOWER - DELAYED COINCIDENCES
N = NORMAL - " "
DOTTED LINES = EXP(-t/2.2 MICROSEC.)
HS x 100
N
DELAYED COINCIDENCES IN 500 HOURS
DELAY - (MICROSEC.)

FIG. 2. Differential decay curves.

namely, whether they are π or μ. We only need to recall the typical behavior of the negative μ-mesons, concerning their capture by nuclei.[3]

In carbon, practically all negative μ-mesons decay, while in sulfur 72 percent of them undergo nuclear capture, according to Ticho.[9] The remaining 28 percent undergo the decay process with a mean life of 0.55 μsec., again after Ticho. Therefore, by setting the minimum registered delay at 1.3 μsec. in our apparatus, we detect the decay of only 2.8 percent of all the negative μ-mesons. With the same minimum delay, we detect the decay of 60 percent of the positive μ-mesons. For the accuracy needed in the conclusions that will follow, we can very well assume that in sulfur all the delayed coincidence are due to positive μ-mesons.

If now mesons are created as μ's with a positive excess of 20 percent (we shall return later to this point), the ratio C/S (delayed coincidence rate in carbon/delayed coincidence rate in sulfur) will be the ratio of the total number of mesons to the number of positive ones, namely, 1.8.

If, on the contrary, mesons are created in our apparatus as π's the ratio C/S is expected to be 1, since in both carbon and sulfur the positive π always decays to μ, which in turn decays into an electron, while the negative π will always be captured at the end of its range, and never decays to μ. On the other hand, for the μ-mesons registered as NP we do expect for the ratio C/S the value 1.8, since the positive excess of μ-mesons arriving at sea level can be accepted for our NP.

It pays to make two remarks. First, the probability that locally produced π-mesons would decay before the end of their range, turns out to be less than five percent, on the basis of the measured mean life of 10^{-8} sec. and the dimensions of the apparatus.

Hence, locally produced π-mesons would practically always decay at rest, and the μ-mesons produced by them would have a range of about one millimeter.

As a second remark, one sees that into the ratio C/S also enters, as a factor, the ratio of the ranges of the decay electrons in carbon and sulfur. However, this factor which is not much different from unity, appears in the case of π-mesons as well as in the case of μ-mesons, without influencing the comparison between the two cases.

The thickness of the counter walls was 0.33 g/cm^2 of glass, and could not introduce an appreciable effect, considering also that the absorber was both above and below Tray C.

We thus expect, for the ratio C/S, the value $1+k$ for π-mesons, and $1.8(1+k)$ for μ-mesons. The correction k represents the difference in the ranges of decay electrons. The experimental values, which can be deduced from Table I, are the following:

$$\text{Hard showers } C/S = 1.1 \pm 0.1,$$
$$\text{Normal particles } C/S = 1.85 \pm 0.05$$

[8] Rossi, Sands, and Sard, Phys. Rev. **72**, 120 (1947).

[9] H. K. Ticho, Phys. Rev. **74**, 1337 (1948).

Such a result strongly indicates that the locally produced mesons are π-mesons. If we would want to interpret the disparity between 1.85 and 1.1 in terms of a large positive excess of locally produced μ-mesons, we would have to assume that practically all locally produced mesons are positive.

This assumption clearly appears to be very far from the truth. We would like to discuss what is the maximum value which we may expect for the locally produced mesons. Such a value will also have a bearing on the quantitative conclusions of the next paper on the nuclear interactions of π-mesons.

There is a fair agreement between various determinations of the positive excess of μ-mesons arriving at sea level. Recently, Conversi[10] reported an experiment where he and Nappo measured the positive excess, at sea level, in the energy band between 310 and 430 Mev. They obtained 1.24 ± 0.05 for the ratio N_+/N_-. Of course, that represents the positive excess of the μ-mesons produced in the atmosphere, and provides no direct information as to the positive excess of the mesons locally produced in our apparatus. But we may recall the experiments of Quercia, Rispoli, and Sciuti, at 17,000 and 25,000 ft.[11] where they detected mesons produced respectively in 530 and 380 g/cm^{-2} of air above the apparatus, therefore in a similar condition to our HS experiment. We have to take into account the already noted fact that the rate of our HS delayed coincidences implies that HS events such as those registered by us constitute the main process for the production of mesons. Thus we consider that the results at 17,000 and 25,000 ft., which show no indication of a large increase of the positive excess respect to the sea level value, stand to prove that we cannot expect for our HS mesons a positive excess much larger than 20 percent.

Another datum, which supplies the same indication, from a different point of view, is the latitude effect of HS recently obtained by Walsh and Piccioni[12] which shows that the average energy of the particles producing HS in an apparatus substantially similar to the present one, is above 10 Bev. Actually the latitude effect for HS, was 1.1 and for the normal hard component was not larger. Now, we consider very reasonable the qualitative assumption that the positive excess decreases when the energy of primary particles increases, and therefore, recalling that our apparatus does not favor protons with respect to neutrons as producers of a HS, we are led to the conclusion that the HS positive excess is not much larger than 20 percent.

On the other hand, let us suppose that not all mesons are produced in our apparatus by high energy nuclear collisions above Tray A of Fig. 1, as implicitly we have assumed so far, and allow for some of them to be produced in secondary low energy collisions between nuclei of lead and nucleons of few hundreds Mev arising from a conspicuous nucleonic cascade process.*** Then we must think that of the secondary nucleons a substantial fraction consists of neutrons, and therefore we cannot expect a large positive excess. Indeed in photographic emulsions positive and negative π-mesons are found in comparable numbers.[13] It seems therefore quite safe to take a value like 1.4 as a maximum value for the ratio of positive to negative mesons produced in our HS events.

The result of the comparison of carbon and sulfur cannot then be interpreted in terms of μ-mesons being created only with a positive charge. The locally produced mesons are of a different type from μ's, and at the end of their range they undergo a process which is practically independent of the atomic number of the material where they are absorbed, at least for $Z\geqslant 6$. They ultimately give rise to μ-mesons, since the obtained decay curve is very characteristic for such particles. Therefore, their identification as π-mesons appears to be quite reliable.

ACKNOWLEDGMENTS

Thanks are due Dr. T. H. Johnson for his continuous encouragement of the work. Mr. C. S. Kemic assembled most of the apparatus and assisted very helpfully in taking data and checking the apparatus throughout the duration of the experiment. Mr. M. Lustgarten and Mrs. B. Lustgarten contributed by building part of the equipment.

The writer and Mr. C. S. Kemic also wish to thank Mr. S. S. Huntington, President of the "Berthoud Pass Lodge, Inc.," for his kind cooperation during their stay at Berthoud Pass, Colorado.

[10] M. Conversi (to be published).

[11] Quercia, Rispoli, and Sciuti, Phys. Rev. **74**, 1728 (1948).

[12] T. G. Walsh and O. Piccioni, Echo Lake Conference on Cosmic Ray (June 22–28, 1949).

*** An experiment (III) reported in our next paper shows that from these low energy processes do not arise more than 20 percent of the HS delayed coincidences.

[13] Lattes, Muirhead, Occhialini, and Powell, Nature **159**, 694 (1947); Lattes, Occhialini, and Powell, Nature **160**, 453 (1947).

On the Secondary Particles of Local Penetrating Showers*

O. PICCIONI
Brookhaven National Laboratory, Upton, Long Island, New York
(Received September 6, 1949)

An analysis of the secondary particles of the local penetrating showers has been done by means of absorption experiments and delayed coincidence measurements. The large majority of those particles, filtered with about 12 in. of lead, appear to be mesons, which have been identified as π-mesons in our preceding paper. The average number of those mesons per shower is about four. The analysis appears to give a lower limit of 1200 g/cm² for the mean free path for nuclear absorption of π-mesons having energies of some hundred Mev. This result is discussed in connection with other experiments on local penetrating showers.

THE results reported in our previous paper[1] show that very likely the mesons produced in a hard shower event (HS) are π-mesons, but they give no indication about the fraction of the secondary particles which is composed of mesons. In what follows we will describe further experiments (I, II, III, IV) which we performed at 11,300 ft., in order to make an analysis of the secondary particles as well as to obtain evidence for nuclear interactions of the π-mesons.

I

The first experiment, I, was made with the same apparatus as described in our previous paper. We measured the absorption in lead and iron of the secondary particles of a HS and of the normal penetrating component (NP). Since only the measurement of the absorption in lead was originally planned, the experiment was made in two different series, as Table I shows. The absorbers were inserted just above Tray C (Fig. 1 of first paper), and a plate of sulfur five inches thick was constantly kept under the same tray. The absorbing powers could then be determined as the ratios:

$$[(ABC)_{\text{no abs}}-(ABC)_{\text{abs}}]:\tfrac{1}{2}[(ABC)_{\text{no abs}}+(ABC)_{\text{abs}}].$$

We will refer to such ratios as $(A_{Fe})_{NP}$, $(A_{Pb})_{NP}$. The analogous ratios for A_2BC coincidences, which represent HS events, will be referred to as $(A_{Fe})_{HS}$ and $(A_{Pb})_{HS}$. The identification of the number of secondary particles absorbed, with the decrease in the rate A_2BC, is certainly incorrect because when two counters of C were discharged, the apparatus, during this experiment I, only registered them as one. However, the *comparison* between lead and iron is not affected appreciably, especially since it turns out that $(A_{Pb})_{HS}$ is about equal to $(A_{Fe})_{HS}$. An error of a few percent, due to the use of a mechanical register not preceded by a scaling circuit, must be supposed to affect both $(A_{Fe})_{NP}$ and $(A_{Pb})_{NP}$ about in the same amount, thus affecting only slightly the ratio $(A_{Fe}/A_{Pb})_{NP}$. The obtained value in $g^{-1}cm^2$, were

$$(A_{Pb})_{NP}=6.57\times10^{-4};\quad (A_{Fe})_{NP}=7.56\times10^{-4};$$
$$(A_{Pb})_{HS}=(2.82\pm0.3)\times10^{-3};$$
$$(A_{Fe})_{HS}=(2.88\pm0.25)\times10^{-3}$$

from which

$$(A_{Fe}/A_{Pb})_{NP}=1.15,\quad (A_{Fe}/A_{Pb})_{HS}=1.02\pm0.15.$$

Our value of 1.15 for $(A_{Fe}/A_{Pb})_{NP}$ compares well with the one obtained by Koenig[2] who measured the absorption of the hard component at sea level. $(A_{Fe}/A_{Pb})_{HS}$ is practically equal to $(A_{Fe}/A_{Pb})_{NP}$. This result, which shows that among the secondary particles emerging downward from the lead block, the proportion of electrons is unimportant, also gives a first indication that π-mesons are not removed by nuclear interactions with an absorption cross section as large as the geometrical cross section of iron nuclei.

For in the case of such a large cross section, we would obtain the values $(A_{Pb})_{HS}=6.25\times10^{-3}$ and $(A_{Fe})_{HS}=9.65\times10^{-3}$, which are much higher than the obtained ones, even allowing for the multiplicity mentioned before. But even more remarkable, the ratio $(A_{Fe})_{HS}/(A_{Pb})_{HS}$ should be 1.55, while it is only 1.02 ± 0.15.

TABLE I. Absorption of HS and NP particles in lead and in iron (Experiment I).

$ABC\times h^{-1}$	$A_2B\times h^{-1}$	$A_2BC\times h^{-1}$	Absorber
5580	108.2±1.2	39.9±0.7	90 g/cm² Pb+¼ in. brass +¼ in. Al
5920	107.9±1.3	51.5±0.9	no Pb+¼ in. brass+¼ in. Al
5405	104±1	40.5±0.6	83 g/cm² Fe
5755	103.7±1	51.5±0.6	None

Absorption powers (g^{-1}/cm^2)

$$(A_{Pb})_{NP}=\frac{340}{5750\times90}=6.57\times10^{-4}$$

$$(A_{Pb})_{HS}=\frac{11.6}{45.7\times90}=(2.82\pm0.3)\times10^{-3}$$

$$(A_{Fe})_{NP}=\frac{350}{5580\times83}=7.56\times10^{-4}$$

$$(A_{Fe})_{HS}=\frac{11}{46\times83}=(2.88\pm0.25)\times10^{-3}$$

* Reported at the Echo Lake Conference of Cosmic Rays (June 22–28, 1949).

[1] O. Piccioni, Phys. Rev. 77, 1 (1950).

[2] H. P. Koenig, Phys. Rev. 69, 590 (1946).

II

In Experiment II, again using the apparatus described in our previous paper, we measured the rates of the delayed coincidences when the absorber above Tray C was, in periodical alternation, 1, 3, and 5 in. of iron. Below Tray C, as we have said, there was always 5 in. of sulfur. The three rates of the delayed coincidences are obviously proportional to the three values of the differential range spectrum corresponding to the three values of the range 1, 3, and 5 in. of iron. Table II shows that such a spectrum is flat in the rather narrow region considered. Unfortunately, practical reasons prevented from extending such a measurement to a wider interval of ranges. Nevertheless, we think that the obtained values are of some significance.

Let $N(E)dE$ be the energy spectrum of the mesons emerging from the lead block, and E_1, E_3, E_5 the energies corresponding to the three ranges of 1, 3, 5 in. of iron.[a] The ratio $N(E_1)/N(E_5)$ would be equal to the ratio of the rates of the delayed coincidences D_1/D_5 if the mesons were affected only by ionization losses. If the mesons were strongly interacting with the nuclei, some of the mesons which emerge from the lead with energy E_5 would be prevented by such nuclear interactions from crossing all the iron. Thus they could not give all the "due" delayed coincidences with the 5-in. iron absorber, with the consequence that $N(E_1)/N(E_5)$ would be smaller than D_1/D_5. Now the experimental value of D_1/D_5 is 0.95 ± 0.1 and if $N(E_1)/N(E_5)$ were to be less than that, we should conclude that the energy spectrum of the locally produced mesons, as they emerge from 15 in. of lead, increases with their energy. Other data on the spectrum of mesons produced by nucleons of average energy of the order of 10 Bev, such as those which suuposedly cause our HS [3] are not yet available.

However, even though it is obvious that the determination of the range spectrum and of the nuclear interaction interfere with each other to some extent, it does not seem likely that, in the narrow interval of ranges which is of interest to us, the shape of the energy spectrum can have a very important role. If we assume that the energy spectrum is flat in the interval E_1 to E_5, then we can say that the probability for a π-meson to undergo a nuclear absorption along its path does not increase by more than 0.1, in absolute value, when the path itself increases by 4 in. of iron. This determines a mean free path of more than 800 g/cm^{-2}, which must be considered as an average over the whole path of the meson, except the last one inch of iron. As to the corresponding interval of energies, we can say that the low limit is 60 Mev and the high limit is the initial energy

[a] The decay electrons may be produced either above or below Tray C, hence the range of the mesons entering the absorber and decaying in the vicinity of Tray C is not well defined. The total thickness of the absorber seems to be the best average of the range. This point has however but little bearing on the whole discussion.

[3] T. G. Walsh and O. Piccioni, Echo Lake Conference on Cosmic Rays (June 22–28, 1949).

TABLE II. Delayed coincidences as function of the thickness of the absorber.

Time (hr.)	ABC_{del}/h^{-1} (total delays in 4 channels less casuals)	A_1BX/h^{-1}	A_1BC_{del}/h^{-1} (total delays in 4 channels, less casuals)	Absorber
210.98	14.5±0.42	104.0	0.86±0.06	1 in. iron+¼ in. brass
188.10	15.5±0.45	105.2	0.98±0.07	3 in. iron+¼ in. brass
227.20	15.3±0.4	104.2	0.90±0.06	5 in. iron+¼ in. brass

E_0 of the meson at its production. To determine the value of E_0 we should know where the mesons are actually produced. Again, the flatness of the obtained range spectrum suggests that the place of production is well above Tray C, at least for most the mesons. It is then reasonable to believe that most mesons giving delayed coincidences are produced above Tray A with an energy E_0 of about 0.5 Bev. Of course, the mesons which do not stop in the absorber are produced with higher energy.

III

Experiment III was made in order to determine the fraction of HS delayed coincidences in which no ionizing secondary emerged from the lead, entering the iron absorber. Such a case would correspond for instance to the production in the iron of a low energy meson by a secondary neutron. The possibility that a large fraction of the delayed coincidences is due to mesons generated with a low initial energy by secondary nucleons in the part of the absorber which is nearest to Tray C, can already be ruled out by the dependence of the delayed coincidence rate with the thickness of the iron, as determined in Experiment II. The 4 in. of iron would indeed absorb considerably the secondary nucleons, while the observed flat curve gives no indication of a strong absorption. However, a fraction like 20 percent for the delayed coincidences due to a meson production in such low energy events, is not in contrast with the experimental errors of Experiment II.

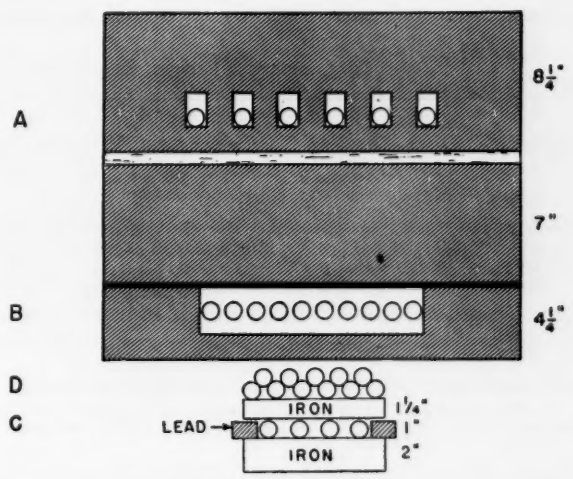

FIG. 1. Arrangement of apparatus.

TABLE III. HS delayed coincidences not accompanied by an ionizing secondary (Experiment III, see also Fig. 1).

Time (hr.)	Total counts A_2BC	A_2BD	A_2BCD	A_2BC_{del} not accompanied by a discharge in D	A_2BC_{del} accompanied by a discharge in D
131.8	2853	6795	2674	11	49

The apparatus was arranged as shown in Fig. 1 of this paper. The coincidences A_2BC, A_2BD, A_2BDC, A_2BC_{del}, and A_2BDC_{del} were registered.

The result of this experiment (Table III) shows that very likely a fraction perhaps more than 10 percent of the delayed coincidence are not accompanied by an incoming ionizing secondary particle. If we are to interpret such a result on the basis of the hypothesis sketched above, we would say that for each registered HS, neutrons of energy of some hundred Mev enter the iron in number of the order of one. This does not appear to be much in contrast with any available experimental datum.

Whether the above explanation is true or not, it appears that the rate of the HS delayed coincidences should be corrected on the basis of Experiment III, if we want to associate a delayed coincidence with an ionizing particle reaching the end of its range in the aborber. This conclusion is of interest for the interpretation of the following experiment.

IV

Experiment IV was performed in order to determine the number of secondary particles when the absorber was, alternatively, 1 and 5 in. of iron. The experiment was made with the same apparatus of Fig. 1 of our first paper, except for Tray C, which was substituted by Tray C_1 of nine counters, 1 in. diameter having $2\frac{1}{2}$ in. center-to-center distance. Tray C_1 was also 1 in. lower than the Tray C of Fig. 1, first paper. The absorber below Tray C_1 was always 5 in. sulfur. The electronic circuit connected with Tray C_1 registered separately the coincidences A_2BC_1, A_2BC_2, A_2BC_3, A_2BC_4, where the subscript in C_n means that *more* than n counters were discharged among the nine of the tray. From the progressive decrease of the rates $A_2BC_1 \cdots A_2BC_4$ (Table IV), it is felt that the neglect of the cases where more than four counters are discharged does not constitute an error more than a very few percent. The same argument, together with the fact that the angle subtended by a counter of C_1, in a plane perpendicular to the axis of the counter itself, with respect to a point at the level of Tray A is only about two degrees, suggests that only seldom must one counter of C_1 be crossed by two secondary particles.[b] Similarly, the practical constancy of the ratio of $(ABC_{del})/(A_2BC_{del})$ measured with three different combinations for Tray C and the absorber above[c] shows that the efficiency of the same tray, as detector of delayed electrons, is not too much affected by the multiplicity of the HS.

The data of Table IV allow us to make a comparison between the number $(HS)_F$ of secondary particles which fail to cross four inches of iron and the number $(HS)_{\pi\text{-ion}}$ of secondary particles which are mesons and reach the end of their range because of ionization losses, therefore producing a decay electron approximately one-half of the times. We know that the number of HS delayed coincidences, $(HS)_{del}$, is proportional to $(HS)_{\pi\text{-ion}}$. The coefficient of proportionality can be written GE, where G represents the coefficient of proportionality which should be used if all the mesons had a positive charge. E is the ratio of the number of positive mesons to the total number of mesons, and is equal to $(1+\epsilon)/(2+\epsilon)$, ϵ being the positive excess. G obviously depends on the geometry and on the thickness of the absorber, as well as on the energy spectrum of the delayed electrons and on the limits of delay within which the delayed coincidences are registered. Rather than compute G, we note that the product GE is about equal to the ratio of $(NP)_{del}/(NP)_F$, where $(NP)_F$, the decrease in the ABC coincidences when four inches of iron are inserted, is to be identified with $(NP)_{\mu\text{-ion}}$, namely, the number of μ-mesons stopped in the four

TABLE IV. Comparison between the absorption power and the decay-electron emitting power.

1 Time (hr.)	2 $ABC\times h^{-1}$**	3 $ABC_{del}\times h^{-1}$ (total of the delays in 3 channels, less casuals)	4 $A_2B\times h^{-1}$	5 $A_2BC_{del}\times h^{-1}$ (total of the delays in 3 channels, less casuals)	6 $A_2BC_1\times h^{-1}$	7 $A_2BC_2\times h^{-1}$	8 $A_2BC_3\times h^{-1}$	9 $A_2BC_4\times h^{-1}$	10* Total of columns 6, 7, 8, 9 (h^{-1})	Absorber above Tray C
165.33	5890	8.45±0.3	108.8	0.56±0.06	44.8	17.8	9.68	5.53	77.8±0.7	1 in. of iron
156.50	5550	8.95±0.3	108.7	0.45±0.06	35.5	14.5	7.73	4.35	62.1±0.6	5 in. of iron
		8.7 ±0.2		0.505±0.04						Averages between 1 and 5 in.
	340								15.7±0.1	Differences between 1 and 5 in.

* A_2BC_n means a HS which discharged *more* than n counters in C. For instance a HS discharging 3 counters, gives one count A_2BC_1, one A_2BC_2, and one A_2BC_3. Column 10 gives thus the total number of counters discharged, with the errors that multiplicities higher than four are taken into account as four.
** Measured with a scaling circuit.

[b] See, for instance, the data on angular divergence, obtained with a cloud chamber by W. Fretter, Phys. Rev. **76**, 511 (1949).
[c] See Table I of the first paper and Tables II and III of the present one.

inches of iron by ionization losses. Indeed, as we have said in Section II of the first paper, within few percent $(NP)_F$ represent nothing else but μ-mesons stopped by ionization in the four inches iron, namely, the analog of $(HS)_{\pi\text{-ion}}$ for NP. Concerning the factor E, however, we should take into account the possibility for the positive excess ϵ_{HS} of the locally produced mesons, to be different from the positive excess ϵ_{NP} of the normal mesons. We note that if ϵ is changed by a factor two, namely, from 0.2 to 0.4, E only changes by a factor 1.07. From the considerations made in Section IV of the first paper, we are led to believe that neglecting such a possible difference between ϵ_{HS} and ϵ_{NP} we make an error not greater than 10 percent. We will take into account this 10 percent indeterminacy in the discussion. The factor G is the same for NP and HS, because the geometry, the circuit, the energy spectrum of the decay electrons, and the mean life for their production are the same in both cases. Our conclusion[1] that the HS mesons are π's, obviously does not imply any practical difference in the value of G to be accepted for HS.

The number $(HS)_{\pi\text{-ion}}$ can then be obtained from the expression:

$$(HS)_{\pi\text{-ion}}=(NP)_F\frac{A_2BC_{del}}{ABC_{del}}$$

and, from Table IV, $(HS)_{\pi\text{-ion}}=19.8\pm1.8$ hr.$^{-1}$.

On the other hand, $(HS)_F$ is supposed to be equal to $(HS)_{\pi\text{-ion}}$, the number of mesons stopped by ionization, plus $(HS)_{\pi\text{-nuc}}$, the number of mesons absorbed by nuclear interaction, plus $(HS)_F$ the number of other particles than mesons, stopped or scattered away by the four inches iron absorber.

Now $(HS)_F$ is only 15.7 ± 1, namely, less than $(HS)_{\pi\text{-ion}}$, which suggests that we should apply some correction either to $(HS)_F$ or to $(HS)_{\pi\text{-ion}}$ which is deduced from A_2BC_{del}. We already mentioned two corrections which might be needed. First, we concluded that from the uncertainty in the value of the positive excess of HS mesons may arise an uncertainty of ~10 percent in the computation of $(HS)_{\pi\text{-ion}}$. Second, and more important, in Experiment III we actually found evidence that a fraction of the A_2BC_{del} were due to non-ionizing particles. We estimated that such a fraction is not likely to be more than 20 percent, because of Experiment III. Introducing those two corrections, we can reduce the value of $(HS)_{\pi\text{-ion}}$ to about 14. But one would say that the difference $(HS)_F-(HS)_{\pi\text{-ion}}$ cannot be as large as 5, without introducing some rather artificial assumption. Taking such a number as an upper limit, we conclude that no more than five out of 77 particles are absorbed by the nuclei in the four inches of iron. That is to say that, the absorption mean free path of the π-mesons in iron is more than 1200 g/cm^{-2}. As to the average energy of the mesons to which such datum is referred, we can give an estimate extrapolating the iron absorption curve. The obtained average, is about 400 Mev.

The result of this experiment also show that $(HS)_X$, the number of particles different from mesons and stopping in the absorber, is unimportant. The proton component is practically extinguished by the lead above Tray C.

V. DISCUSSION

We see that, in progressive order of importance, the comparison of the absorption of lead and iron, the curve of the delayed coincidence rate-*versus*-thickness of absorber, the comparison of the absorption in iron with the rate of delayed coincidences, all point toward the conclusion that Λ_π, the absorption mean free path of π-mesons of energy of the order of few hundred Mev is much larger than the value corresponding to the geometrical size of iron nuclei (~100 g/cm^{-2}).

We should notice that in our apparatus a nuclear non-Coulombian scattering would have the same effect as a nuclear absorption only if the angle of scattering would be as large as 90 degrees. According to Marshak,[4] if one uses the pseudoscalar theory of meson forces, the scattering cross sections, per unit solid angle, in the foreward, transverse and backward directions are, respectively, proportional to the numbers 7; 2.5; 1. Referring to those values the ratio of the scattering in the backward hemisphere to the total scattering would then be as low as $\frac{1}{4}$, therefore we could not learn much about the nuclear scattering of π-mesons from our value of Λ_π. Experiments already reported by Fretter[5] and by Lovati, Mura, Salvini, and Tagliaferri[6] where secondary particles of penetrating showers were observed in a cloud chamber, gave very little evidence, if any, for the scattering of those particles. A number of secondary nuclear events were found in both of those experiments, from which a collision mean free path, in lead, of about 370 g/cm^{-2} according to the Italian group, and of less than 750 g/cm^{-2} according to Fretter could be derived. The last number is a result of a much larger number of events than was obtained by the Italian group, but is not corrected for the probability that a nuclear event would escape observation. We believe that, as the authors pointed out, the question of how many protons are among the particles observed in those experiments, is still an open one.

If the fraction of protons would be reasonably small, our result would appear to be in disagreement at least with the value reported by the Italian group. It is perhaps worth notice that the thickness of lead to be *crossed by the secondary particles* is much larger in our apparatus than it is in both the previously mentioned cloud-chamber experiments. That makes it impossible to assume that the fractional number of protons is the same in our experiment and in the cloud-chamber ones.

[4] R. E. Marshak, Echo Lake Conference on Cosmic Rays (June 22–28, 1949).

[5] W. B. Fretter, Echo Lake Conference on Cosmic Rays (June 22–28, 1949).

[6] Lovati, Mura, Salvini, and Tagliaferri, Nuovo Cimento VI, 207 (1949).

On the other hand, it may be noted that Rochester, Butler, Mitra, and Rosser,[7] working with a cloud chamber covered with 16.8 cm or less, of lead, found among the secondary particles of hard showers, 14 positive lightly ionizing tracks and two negatives, which, as noted by the authors, suggests that such particles were mainly protons. And it is significant that of the slow particles for which the British authors were able to recognize the mass, 23 were protons and 5 mesons.

We thus think that no real discrepancy can be found between our result on the nuclear absorption of π-mesons and any of the experimental evidence now available.

Our lower limit of 1200 g/cm^{-2} for Λ_π seems therefore to be significant.

Finally, we would like to underline that from Experiment III we conclude that the locally produced mesons detected with the delayed coincidence method are mainly generated not in low energy processes by secondary nucleons, but in high energy ones, and most likely in the very first nuclear collision of the arriving nucleon. This supports the standpoint which we have taken in the previous paper.

The average number of particles arriving on Tray C from the lead block for every HS (A_2BC) turns out to be about four, from the average number of counters discharged in Tray C_1 (1.7) and the fraction of the surface covered by the counters (1/2.25).

[7] Rochester, Butler, Mitra, and Rosser, reported by G. D. Rochester, Symposium on Cosmic Rays, California Institute of Technology (June 21–23, 1948), Rev. Mod. Phys. 21, 20 (1949).

ACKNOWLEDGMENTS

The author takes pleasure in thanking Dr. T. H. Johnson for stimulating discussions on the subject.

The important help of Mr. C. S. Kemic is deeply acknowledged.

Thanks are also due Mr. M. Lustgarten and Mrs. B. Lustgarten for their cooperation in building part of the equipment, and Mr. S. S. Hungtinton, President of the "Berthoud Pass Lodge, Inc.," for his courtesy.

PHYSICAL REVIEW VOLUME 77, NUMBER 1 JANUARY 1, 1950

The Effect of Screening on Beta-Ray Spectra and Internal Conversion*

JOHN R. REITZ**
Department of Physics, University of Chicago, Chicago, Illinois
(Received September 1, 1949)

The Dirac equation for an electron in the field of a Thomas-Fermi-Dirac atom is solved numerically on the ENIAC for a large number of cases. The resulting wave functions are used to calculate the effect of screening (by the atomic electrons) on allowed beta-spectra and on the internal conversion coefficients of gamma-rays. It is seen that the negatron spectra are essentially unaffected by screening; positron spectra are affected appreciably in a direction such as to increase the number of low energy positrons. Where a comparison can be made between the present calculations and previous ones in which the screening has been neglected, it is seen that the effect of screening is to increase the conversion coefficients slightly. Most of the present calculations, however, are for the soft gamma-ray region, for which only approximate formulas for the conversion coefficients exist. Thus the results of this paper are used to test the accuracy of these formulas. An attempt is also made to classify a number of experimentally observed gamma-rays.

I. INTRODUCTION

THE purpose of the work described in this paper is to obtain solutions of the relativistic motion of an electron in an atomic potential, this potential being supplied by the statistical model of the atom, and to use the wave functions obtained to calculate internal conversion coefficients and beta-ray spectra. These results, when compared with those calculated using Coulomb wave functions, give the so-called "screening correction" due to atomic electrons.

Whereas the Coulomb correction to the shape of the allowed beta-ray spectrum (obtained by using Coulomb eigenfunctions instead of free particle functions) is quite large, giving a factor of about 100 for elements of high nuclear charge and negatrons of low energy, the screening correction is generally assumed to be small. Approximate calculations of the screening correction by Rose[1] and Longmire and Brown[2] have verified this assumption, although the correction for low energy positrons was found to be appreciable. More accurate calculations of the screening correction seemed desirable since the deviations from the theoretical spectra found experimentally in Cu^{64} and S^{35} (both of the allowed type) have been interpreted[3,4] as a failure of the Fermi

* This paper was written as a Ph.D. thesis in the Department of Physics, University of Chicago, Chicago, Illinois.

** National Research Council Predoctoral Fellow; now at Los Alamos Scientific Laboratory, Los Alamos, New Mexico.

[1] M. E. Rose, Phys. Rev. 49, 727 (1936).
[2] C. Longmire and H. Brown, Phys. Rev. 75, 1102, 264 (1949).
[3] C. S. Cook and L. M. Langer, Phys. Rev. 73, 601 (1948).
[4] Cook, Langer, and Price, Phys. Rev. 74, 548 (1948).

theory. It should be noted, however, that the more recent experiments of Albert and Wu[5,6] with thinner sources and source backings have shown that these discrepancies are in part due to scattering of the higher energy electrons in the source and backing.

An accurate knowledge of the internal conversion coefficient is helpful in establishing the angular momentum state of an isomeric level and for determining the mode of nuclear vibration when the level decays. Accurate calculations of the internal conversion coefficients (using relativistic Coulomb eigenfunctions) have been made by Hulme,[7] Taylor and Mott[8,9] and Fisk[10,11] for the gamma-rays of radium C, and by Griffith and Stanley[12] and Rose and collaborators[13] for various elements with $Z \geqslant 40$. All of these calculations are for gamma-rays with energies greater than 150 kev; thus the results should not be affected much by a consideration of screening. Approximate formulas for the internal conversion coefficient have been derived by Hebb and Uhlenbeck[14] for light elements (non-relativistic calculations), by Dancoff and Morrison[15] for hard gamma-rays, and by Drell[16] for magnetic conversion. The results which are described in the present paper, when compared with the other calculations, give essentially the screening correction to the internal conversion coefficient; actually many of our results are in a range (heavy elements, soft gamma-rays) not covered by previous work.

II. OBTAINING THE WAVE FUNCTIONS

The first step in computing the effect of screening is to obtain the appropriate wave functions. These functions are taken to be solutions of the Dirac equation for a single electron moving in the field of an atomic nucleus and the statistical average field of the atomic electrons. When the Dirac equation for a central field of force is separated in spherical coordinates according to standard methods, the angular and spin parts of the wave function can be replaced by appropriate constants, and we are left with an equation which involves only one independent variable, r. We need now concern ourselves only with the radial part of the wave function, which has a two-component structure:

$$\begin{pmatrix} r^{-1}F(r) \\ r^{-1}G(r) \end{pmatrix}. \tag{1}$$

The Dirac equation then reduces to a set of coupled equations,

$$\begin{aligned} dF/dr \pm r^{-1}(j+\tfrac{1}{2})F + [W-1-V(r)]G = 0, \\ -dG/dr \pm r^{-1}(j+\tfrac{1}{2})G + [W+1-V(r)]F = 0. \end{aligned} \tag{2}$$

Here W is the total energy of the electron, $V(r)$ is potential energy, and j is the total angular momentum quantum number. (In this paper, all distances are given in units of $\hbar/mc$, all energies in units of mc^2, and all momenta in units of mc.) The upper signs in Eq. (2) refer to type a wave functions in which $j=l+\frac{1}{2}$; the lower signs to type b functions ($j=l-\frac{1}{2}$). l is the non-relativistic quantum number which gives the orbital angular momentum.

The set of Eqs. (2) was integrated numerically, for atomic potentials corresponding to sulfur, copper, indium, polonium, and uranium, on the Electronic Numerical Integrator and Calculator (ENIAC), which is located at Aberdeen Proving Ground, Maryland. Angular momentum values up to $j=5/2$, $l=2$, and various energy values, W, were considered. Most of the wave functions calculated belong to continuum electrons (or electrons of positive energy);[17] their energies range from five to about 300 kilovolts. The integration of the equations was started at a point quite close to the origin, where the wave functions were assumed Coulomb-like; and was carried out point-by-point to a distance at which the functions could be converted to their values at infinity by means of an asymptotic expression. The normalization condition was applied at the end of the calculation.[18]

The potential energy, $V(r)$, which was used in the solution of Eq. (2), consists of several parts:

$$V = -V_e - D + K, \tag{3}$$

where $-V_e$ is the electrostatic interaction between the electron in question and the rest of the atom, $-D$ is the "exchange" interaction, and K is a potential correction which may be necessary for the problem under consideration. Since we would like to get V from the sta-

TABLE I. Energy eigenvalues for the 1s and 2s levels. Energy $E=W-1$.

Element	1s level X-ray	1s level T.F.D.	1s level Coulomb	2s level X-ray	2s level T.F.D.	2s level Coulomb
Cu	−0.01762	−0.017619	−0.022650	−0.00219	−0.002207	−0.005679
In	−0.05472	−0.054995	−0.066147	−0.008313	−0.008435	−0.016677
Po	−0.1820	−0.18507	−0.21002	−0.0333	−0.03407	−0.05393
U	−0.2276	−0.23046	−0.25903	−0.04273	−0.04387	−0.06700

[5] R. D. Albert and C. S. Wu, Phys. Rev. **74**, 847 (1948).
[6] C. S. Wu and R. D. Albert, Phys. Rev. **75**, 315 (1949).
[7] H. R. Hulme, Proc. Roy. Soc. **A138**, 643 (1932).
[8] H. M. Taylor and N. F. Mott, Proc. Roy. Soc. **A138**, 665 (1932).
[9] H. M. Taylor and N. F. Mott, Proc. Roy. Soc. **A142**, 215 (1933).
[10] J. B. Fisk, Proc. Roy. Soc. **A143**, 674 (1934).
[11] J. B. Fisk and H. M. Taylor, Proc. Roy. Soc. **A146**, 178 (1934).
[12] B. A. Griffith and J. P. Stanley, Phys. Rev. **75**, 534 (1949).
[13] Rose, Goertzel, Spinrad, Harr, and Strong, Phys. Rev. **76**, 184 (1949). These authors have distributed privately an extensive table of their results.
[14] M. H. Hebb and G. E. Uhlenbeck, Physica **5**, 605 (1938).
[15] S. M. Dancoff and P. Morrison, Phys. Rev. **55**, 128 (1939).
[16] S. D. Drell. Phys. Rev. **75**, 132 (1949).

[17] 1s and 2s bound levels were also computed for copper, indium, polonium, and uranium.
[18] The wave functions and the details of the numerical integration of Eq. (2) will be described in a future publication to be submitted to the Physical Review; tables of the 240 radial wave functions have been published by the University of Chicago Physics Department: J. R. Reitz, *Relativistic Electron Wave Functions for a Thomas-Fermi-Dirac Statistical Atom* (Department of Physics, University of Chicago, 1949).

TABLE II. Screening correction factors ($F_{T.F.D.}/F_{coulomb}$) to allowed beta-spectra (negatrons).

Energy $(W-1)$	($F_{T.F.D.}/F_{coulomb}$) for the elements S $Z=16$	Cu 29	In 49	Po 84	U 92
0.003	0.990				
0.01	0.996	0.988			
0.02	0.998	0.991	0.965		
0.04	0.999*	0.992*	0.971		
0.05	0.999*	0.993	0.973*	0.945	0.933
0.08	0.999	0.994*	0.976	0.951*	0.941*
0.10	0.999*	0.994*	0.978*	0.954	0.944
0.12	0.999*	0.995	0.979*	0.956*	0.947*
0.20	1.000*	0.995	0.983	0.961	0.955*
0.25	1.000*	0.996*	0.984*	0.964*	0.958
0.30	1.000	0.996*	0.985*	0.966*	0.960*
0.40	1.000*	0.996*	0.987	0.968*	0.964*
0.50	1.000*	0.997*	0.988*	0.971	0.967*
0.60	1.000*	0.997	0.989*	0.973*	0.969
0.80	1.000*	0.998*	0.990	0.976*	0.973*

* Values obtained from graphical interpolation.

TABLE III. Screening correction factors ($F_{T.F.D.}/F_{coulomb}$) to allowed positron spectra.

Energy $(W-1)$	($F_{T.F.D.}/F_{coulomb}$) for the elements S $Z=16$	Cu 29	In 49	Po 84	U 92
0.003	8.08				
0.01	1.745	5.44			
0.02	1.325	2.20	7.71		
0.04	1.150*	1.38*	2.64		
0.05	1.130*	1.277	2.09*	7.27	10.44
0.08	1.083	1.154*	1.505	3.41*	4.00*
0.10	1.072*	1.123*	1.37*	2.62	2.93
0.12	1.065*	1.105	1.29*	2.18*	2.41*
0.20	1.051*	1.075	1.173	1.535	1.64*
0.25	1.046*	1.066*	1.146*	1.40*	1.478
0.30	1.042	1.060*	1.128*	1.32*	1.38*
0.40	1.038*	1.053*	1.106	1.245*	1.258*
0.50	1.035*	1.048*	1.094*	1.203	1.233*
0.60	1.033*	1.045	1.084*	1.176*	1.203
0.80	1.030*	1.040*	1.073	1.145*	1.165*
1.30				1.110	

* Values obtained from graphical interpolation.

tistical model of the atom, we write

$$V_c=\begin{cases}\alpha Z r^{-1}\varphi(\mu r)-\alpha^2/2\pi^2-E_0, & \text{for } r\leqslant r_A;\\ 0, & \text{for } r>r_A.\end{cases} \quad (4)$$

$$\mu=4\alpha(2Z/9\pi^2)^{\frac{1}{3}}, \quad \alpha\equiv e^2/\hbar c.$$

Here $\varphi(\mu r)$ is the Thomas-Fermi-Dirac function,[19–21] which is a solution of the equation

$$d^2\varphi(x)/dx^2=x(d+\varphi^{\frac{1}{2}}/x^{\frac{1}{2}})^3; \quad d=(3/32\pi^2)^{\frac{1}{3}}Z^{-\frac{1}{3}}. \quad (5)$$

Equation (5) results from Poisson's equation when we make the substitution (4), assuming that the charge density has been expressed statistically as $\rho(V_c)$. E_0 is the maximum Fermi energy for an electron bound in this statistical distribution; r_A is the radius of the atom. V_c, obtained from Eq. (4), represents a statistical or semiclassical approximation to the Fock-Dirac self-consistent field.

The function $\varphi(\mu r)$ is determined by the boundary conditions that $\varphi(0)=1$, and for the case of a neutral atom that the electric field vanishes at r_A. This procedure for obtaining φ assumes that r_A is known; actually another condition is needed to determine both φ and r_A. If we assume that the momentum, P, of a particle with the maximum Fermi energy, E_0, is zero for distances greater than r_A (this assumption is reasonable, since valence electrons have essentially zero binding energy compared to electrons deep in the atomic cores), then we find that $E_0=0$. Making V_c continuous at $r=r_A$, we get the other condition on φ and r_A from Eq. (4), namely

$$\alpha Z r_A^{-1}\varphi(\mu r_A)=\alpha^2/2\pi^2. \quad (6)$$

Thomas-Fermi-Dirac solutions for various elements have been given by Slater and Krutter[20] and Feynman.[21]

[19] See L. Brillouin, *L'Atome de Thomas-Fermi*, Actualités Scientifiques et Industrielles (Hermann and Cie, Paris, 1934), No. 160.
[20] J. C. Slater and H. M. Krutter, Phys. Rev. **47**, 559 (1935).
[21] Feynman, Metropolis, and Teller, Phys. Rev. **75**, 1561 (1949).

The exchange energy, $-D$, can also be expressed as a statistical approximation which is spherically symmetric.[19] The statistical form is

$$D(r, p_i)=4\alpha P\xi(|p_i|/P),$$

where

$$P(r)=\begin{cases}\alpha/\pi+(\alpha^2/\pi^2+2V_c(r))^{\frac{1}{2}}, & \text{for } r\leqslant r_A,\\ 0, & \text{for } r>r_A,\end{cases} \quad (7)$$

and

$$\xi(w)=\frac{1}{2}+\frac{1-w^2}{4w}\ln\frac{1+w}{|1-w|}.$$

Here $p_i(r)$ is the momentum of the electron in question at point r. Thus Eq. (3) for the potential energy, V, becomes

$$V=-\alpha Z r^{-1}\varphi(\mu r)+\alpha^2/2\pi^2 -4\alpha P(r)\xi(|p_i|/P)+K(r). \quad (8)$$

For bound-level calculations made on the ENIAC, the neutral atom potential was used, i.e., $K(r)=0$. The

TABLE IV. $F_{T.F.D.}(Z, W)$ for copper.

W	$F^-_{T.F.D.}(Z, W)$	$F^+_{T.F.D.}(Z, W)$
1.01	13.45	0.001283
1.02	9.58	0.01273
1.05	6.19	0.0829
1.08	5.06	0.1536
1.12	4.33	0.228
1.2	3.61	0.325
1.3	3.22	0.400
1.4	3.00	0.444
1.5	2.86	0.474
1.6	2.76	0.496
1.7	2.69	0.512
1.8	2.63	0.524
1.9	2.59	0.533
2.0	2.56	0.542
2.12		0.549

bound solutions were obtained essentially by trial and error; first an eigenvalue was guessed, then an ENIAC run was made. This procedure was repeated until a well-behaved solution could be interpolated from the results; at this point the eigenvalue was good to about five significant figures. Table I gives the eigenvalue as determined by ENIAC solution using the potential (8), (potential abbreviated T.F.D.). For comparison the x-ray energies as computed from the K and L_I absorption edges[22] and corresponding Coulomb energies (Dirac eigenvalues for a Coulomb field) are also given. It is seen that the eigenvalues of these functions agree with the x-ray energies within a few percent, whereas the corresponding Coulomb eigenvalues may be off as much as a factor of two.

For the continuum electron calculations, representing electrons ejected by the internal conversion process, it is necessary to correct for the absence of one of the bound electrons (namely the $1s$ electron). The ejected electron leaves the field of the atom in a time which is short compared to an electronic rearrangement time, so that the potential can be considered as made up of the neutral atom potential minus the potential of a $1s$ electron distribution. For this case then, $K(r)$ equals minus the potential created by a $1s$ electron distribution.

Wave functions were also evaluated for electrons which are emitted in the beta-decay of nuclei. Here again the electron traverses the atomic field in a time short compared to an electronic rearrangement time; thus the potential is considered made up of the neutral atom potential of the parent atom plus an attractive term due to the excess positive charge on the nucleus (i.e., $K=-\alpha/r$). For the case of positrons the "neutral atom" part of the potential, due to the parent atom, is of the opposite sign, and $K(r)$ again equals $-\alpha/r$.

Actually the refinements to the potential which have been considered here do not influence the results of this paper. The principal effect comes from the screening of the electric field, and therefore in most cases, we could have taken $V=-V_e$. An exception is, of course, $K(r)=-\alpha/r$ which is necessary in the beta-decay problems to convert to the potential of the *daughter* atom; on the other hand we could have used the V_e corresponding to the daughter and made $K(r)=0$. Another possible exception is the exchange energy, $-D$, for bound electrons; $D(r, p_i)$ is proportional to $r^{-\frac{1}{2}}$ in the vicinity of the nucleus and is thus less than one percent of V_e inside the K-orbit, but for bound electrons it becomes approximately equal to V_e in the outer regions of the atom. Thus, the wave functions and energy eigenvalues would be affected slightly if D were neglected.

[22] See A. H. Compton and S. K. Allison, *X-Rays in Theory and Experiment* (D. Van Nostrand Company, Inc., New York, 1935), pp. 792–794 for a table of x-ray absorption edges.

III. THE SHAPE OF THE ALLOWED BETA-RAY SPECTRUM

According to the Fermi theory of beta-decay[23] the allowed spectrum is given by

$$P(p)dp \propto |M|^2 F(Z, W) p^2 (W_0 - W)^2 dp, \qquad (9)$$

where W is the energy and $p=(W^2-1)^{\frac{1}{2}}$ is the momentum of the emitted particle, W_0 is the maximum energy of particles emitted during the beta-decay, M is the nuclear matrix element, and $F(Z, W)$ is a factor which gives the effect of the atomic field on the spectrum.[24] For wave-functions of spherical symmetry normalized to one particle in a sphere of radius R_s, the function $F(Z, W)$ can be shown to be

$$F(Z, W) = 2\pi R_s p^{-2} \sum_{l=0}^{1} \psi_e^* \psi_e$$

$$(j=\tfrac{1}{2}, \text{ components independent of } \theta, \varphi)$$

$$= (R_s/2p^2r^2)[G^2_{(l=0,\, j=\frac{1}{2})} + F^2_{(l=1,\, j=\frac{1}{2})}]. \qquad (10)$$

Here the wave functions ψ_e are evaluated at the nucleus; $r^{-1}G$ and $r^{-1}F$ are the normalized radial components of ψ_e given in Eq. (1). For the Coulomb field, $F(Z, W)$ reduces to (see Konopinski)[24]

$$F_{\text{coulomb}}(Z, W) = 4(2pR_N)^{2s-2} e^{\pi\alpha ZW/p} \times \frac{|\Gamma(s+i\alpha ZW/p)|^2}{[\Gamma(2s+1)]^2} \cdot \frac{(1+s)}{2}, \qquad (11)$$

where R_N is the radius of the nucleus, and $s=(1-\alpha^2Z^2)^{\frac{1}{2}}$. In this expression the nuclear charge, Z, is to be taken negative for positron emitters. For other atomic fields where the wave functions are known in numerical form, $F(Z, W)$ can be evaluated from Eq. (10).

In Table II are given the screening correction factors to the allowed beta-spectra of sulfur, copper, indium, polonium, and uranium. The correction factors are given as the ratios of $F_{\text{T.F.D.}}(Z, W)/F_{\text{coulomb}}(Z, W,)$ where $F_{\text{T.F.D.}}(Z, W)$ is computed from Eq. (10) using the Thomas-Fermi-Dirac wave functions evaluated on the ENIAC, and $F_{\text{coulomb}}(Z, W)$ is computed from (11). These correction factors are listed in Table II for the radioactive *parent* nuclei; although in computing the $F(Z, W)$, nuclear charges corresponding to the *daughters* must be used.

Table III gives the screening correction factors to allowed positron spectra; these factors were computed in a similar fashion to those of Table II.

It is seen that the screening correction for negatrons acts to decrease their number at low energies, but is very small; for light elements the correction is almost negligible, and for uranium it is only seven percent at 25 kev. For positron spectra, however, the correction can be quite large, and has the effect of increasing the

[23] E. Fermi, Zeit. f. Physik, 88, 161 (1934).

[24] We use here the notation of E. J. Konopinski, Rev. Mod. Phys. 15, 210 (1943).

number of low energy positrons. This increase in the number of positrons was expected since the Thomas-Fermi-Dirac field offers a smaller potential barrier to the positron than the Coulomb field. In fact the correction factors in Table III are in rough quantitative agreement with the ratios of potential barrier factors for the two fields.

Screening correction factors for nuclei with different atomic numbers can be obtained by graphically interpolating the values in Tables II and III. The screening correction can also be estimated from Rose's formula although the formula may be in error by as much as fifteen to twenty percent for positrons from heavy elements.

Rose[1] derives his formula in the following manner. First he splits up the atomic potential into two parts, one for the region about the nucleus in which the screened potential differs from the Coulomb potential by an average value D_0, and the other for the region covering the rest of space in which a W.K.B. solution of the wave equation is effected. (D_0 equals $\alpha^2 Z(128Z/9\pi^2)^{\frac{1}{3}}$ for the case of the Thomas-Fermi screened field.) He then compares two states, one an electron of energy W in the field of the screened nucleus, and the other an electron of energy $W-D_0$ in the Coulomb field, and shows that the quantity $(dn/dW)|\psi|^2$ at any point in the nucleus is the same for both of the states. Expressing $|\psi|^2$ in terms of $F(Z, W)$ and noting that the state density per unit energy range, namely (dn/dW), is equal to

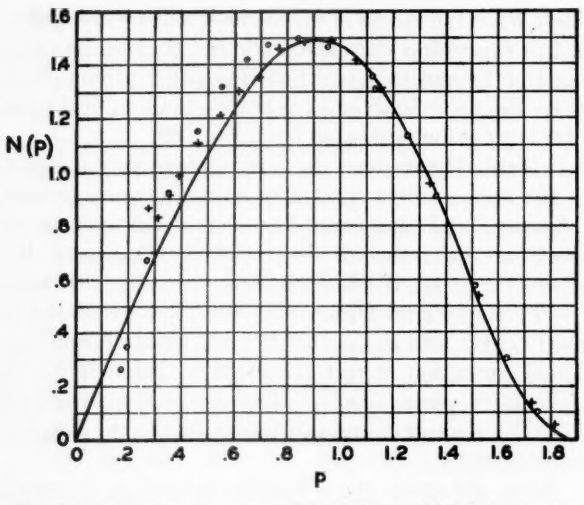

FIG. 1A. Negatron spectrum of Cu^{64}. The solid line is the theoretical curve; the experimental results of Cook and Langer (○), and Wu and Albert (+) are also given.

$(R_\infty W/\pi p)$ we obtain

$$F_{\text{T.F.}}(Z, W)/F_{\text{coulomb}}(Z, W)$$
$$= F_{\text{coulomb}}(Z, W \mp D_0)/F_{\text{coulomb}}(Z, W)$$
$$\times \left(\frac{W-1\mp D_0}{W-1}\right)^{\frac{1}{2}}\left[\left(\frac{W+1\mp D_0}{W+1}\right)^{\frac{1}{2}}\left(\frac{W\mp D_0}{W}\right)\right]. \quad (12)$$

The upper sign is for negatrons, the lower sign for positrons. The factor in the brackets is close to unity, thus Eq. (12) is essentially the same as the correction recently given by Longmire and Brown.[2]

A comparison of Eq. (12) with Tables II and III shows that the formula predicts the screening correction fairly well for negatrons with energies greater than about $4D_0$. For light elements like copper and sulfur, Eq. (12) agrees with the tabulated values within one percent down to 10 kev. For heavier elements deviations start at higher energies; in polonium, for example, the formula agrees down to about 70 kev, but is $2\frac{1}{2}$ percent low at 25 kev. It is known that the formula breaks down for energies in the neighborhood of D_0.

For positrons the agreement is not as good, principally since the magnitude of the correction is so much greater. For positrons from copper the formula predicts a screening correction of 1.025 at 200 kev, is six percent below the values in Table III from 30 down to 10 kev, and becomes equal to the tabulated value at about 6 kev. For polonium the formula gives a value of only 1.05 at 500 kev, is about 15 percent low from 100 down to 40 kev, and equals the value in Table III at 20 kev. In making the above comparisons, Eq. (12) was evaluated completely, including the factor in brackets; however, the non-relativistic approximation for $F_{\text{coulomb}}(Z, W)$ was used, namely:

$$F_{\text{coulomb}}(Z, W) = 2\pi y/(1-\exp(-2\pi y)),$$
$$y = \alpha ZW/p. \quad (13)$$

We may inquire how close the screening correction factors of Tables II and III, which are computed, from the Thomas-Fermi-Dirac potential, will agree with those for the true atomic potential. Since for negatrons $F(Z, W)$ does not change very much in going from an unscreened to a statistically screened field, there will probably be very little change produced in going to the true atomic field. For positrons, however, the value of the wave functions at the nucleus is quite sensitive to the potential barrier, so we can probably expect small deviations from the values in Table III.

IV. EXPERIMENTS ON BETA-RAY SPECTRA

In this section a few of the allowed spectra which have been experimentally determined down to low energies will be compared with the theoretical spectra in which the $F(Z, W)$ are computed for the Thomas-Fermi-Dirac potential.

For S^{35} the screening correction as obtained from Table II is essentially negligible. Albert and Wu have measured[5] the negatron spectrum and have found that for sources thinner than $2\mu g/cm^2$, the results are in agreement with the theory (for energies greater than 20 kev). With thicker samples they obtain a hump in the spectrum at about 25 kev, similar to the one previously obtained by Cook, Langer, and Price.[4]

Cu^{64} emits both positrons and negatrons; and since the corrections are somewhat larger, a more detailed

comparison between theory and experiment will be made. In Table IV are listed the $F_{\text{T.F.D.}}(Z, W)$ for Cu; these functions were computed by applying the screening correction of Tables II and III to the $F_{\text{coulomb}}(Z, W)$ computed from Eq. (11). The F's, as given, are completely relativistic. (It should be noted that many experimenters use the non-relativistic approximation for $F_{\text{coulomb}}(Z, W)$ given in Eq. (13); the relativistic correction has been discussed by Longmire and Brown.[2]

Using Table IV, the positron and negatron spectra of Cu^{64} were computed, namely the $P(p)$. These theoretical curves are given in Fig. 1, along with experimental values obtained by Cook and Langer[3] and Wu and Albert.[4] The experimental points are normalized on the high energy sides of the distributions. It is seen that the results of Wu and Albert are in fairly good agreement with the Fermi theory, and the small deviations which still occur can probably be attributed to the finite thickness of the source.

Cu^{61} and N^{13} are both positron emitters. Their spectra have been investigated by Cook and Langer,[25,26] who found an increase in low energy positrons over that predicted by the theory. The screening correction is in the right direction but not large enough to explain the discrepancy completely. It should be remembered, however, that if many of the higher energy positrons lose energy as they emerge from the source (of finite thickness) and appear in the low energy region, then this region will be greatly accentuated, since the theory predicts almost no low energy positrons.

V. BETA-DECAY LIFETIMES

Theoretically the mean life of an allowed beta-emitter is proportional to the reciprocal of $f(Z, W_0)$, where

$$f(Z, W_0)=\int_0^{p(W_0)} dpp^2(W_0-W)^2F(Z, W). \quad (14)$$

For negatron emitters, the function $f(Z, W_0)$ will be essentially unchanged upon applying the screening correction to $F(Z, W)$. For the screening effect to enter at all into f, the maximum energy, W_0, must be quite low. The H^3 beta-decay, for example, has a very low maximum energy ($W_0=1.0355$), but no effect is expected because the Z-value is so low.[27]

For positron emitters of low maximum energy the effect of screening is considerably larger, and f is increased somewhat as a result. Thus the ft value for positrons from Cu^{64} is increased by about five percent (t is the observed half-life). Two positron emitters which show a larger increase in their ft values are Co^{57} ($W_0=1.51$)[28] and La^{136} ($W_0=2.64$).[29] Both ft's are increased about 10 percent due to screening.

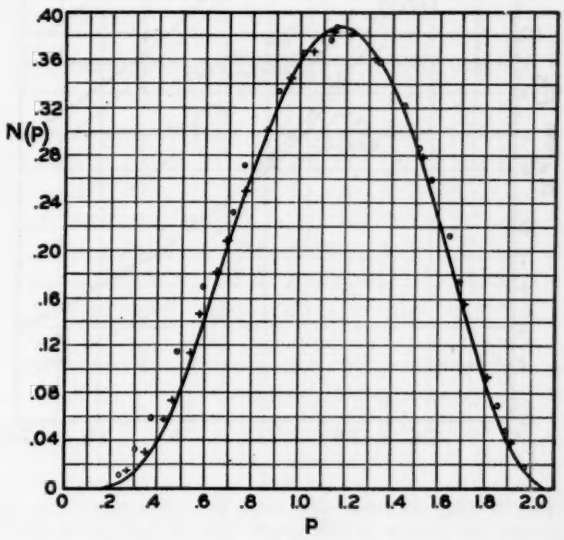

FIG. 1B. Positron spectrum of Cu^{64}. The solid line is the theoretical curve; the experimental results of Cook and Langer (○), and Wu and Albert (+) are also given.

VI. INTERNAL CONVERSION COEFFICIENT FOR THE K-SHELL

Following Dancoff and Morrison[15] we define the internal conversion coefficient to be the ratio of the observed electronic flux, N_e, to the observed flux of the gamma-quanta, N_q, emitted by an atom during a nuclear transition. Theoretically one calculates the internal conversion coefficient for a given multipole character of the radiation, and for conversion by electrons from a given atomic shell. Defining N_e to be the number of K-electrons ejected per unit time, we have as coefficient for the K-shell

$$\alpha_K^{(l)}=N_e/N_q \quad (15a)$$

for electric 2^l-pole radiation, and

$$\beta_K^{(l)}=N_e/N_q \quad (15b)$$

for magnetic radiation.

Let us designate the vector and scalar potentials of the multipole field by

$$\begin{aligned}\mathbf{A}&=\mathbf{A}\exp(-ivt)+\mathbf{A}^*\exp(ivt),\\ \Phi&=\varphi\exp(-ivt)+\varphi^*\exp(ivt),\end{aligned} \quad (16)$$

then for electric dipole radiation

$$\begin{aligned}A_z&=Br^{-1}\exp(ivr), \quad A_x=A_y=0,\\ \varphi&=Br^{-1}[1-(ivr)^{-1}]\exp(ivr).\end{aligned}$$

[25] C. S. Cook and L. M. Langer, Phys. Rev. 74, 227 (1948)
[26] Cook, Langer, Price, and Sampson, Phys. Rev. 74, 502 (1948).
[27] The effect of the coulomb field is usually neglected in computing f for the H^3 decay. By considering the effect of the coulomb field, one finds that f is 1.47 times larger than the value obtained when the field is neglected. Taking $|M|^2=3$, one obtains $|M|^2ft=3000$ sec., which is within a factor of two of the corresponding value for He^6 (see E. J. Konopinski, Phys. Rev. 72, 518 (1947)). In calculating ft the author used $W_0=1.0355$ (Curran, Angus, and Cockroft, Phil. Mag. 40, 53 (1949)) and a half-life of 12 years (A. Novick, Phys. Rev. 72, 972 (1947) and M. Goldblatt, Phys. Rev. 72, 973 (1947)).
[28] J. J. Livingood and G. T. Seaborg, Phys. Rev. 60, 913 (1941).
[29] J. B. Chubbuck and I. Perlman, Phys. Rev. 74, 982 (1948).

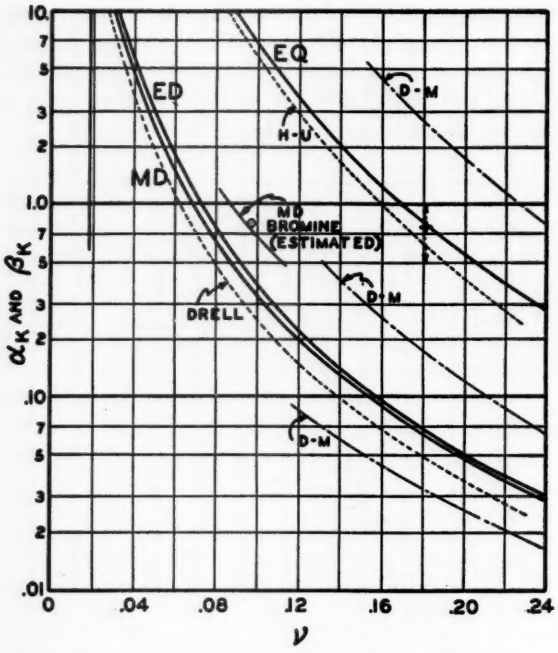

FIG. 2. Internal conversion coefficient for copper. The solid lines are the results of this paper. The dashed curves are the Hebb-Uhlenbeck and Drell formulas for copper, whereas the broken curves are the Dancoff-Morrison results. The Hebb-Uhlenbeck curve for ED radiation was left off the figure in order that the other curves be clearly separated; it is 11 percent below our ED curve at $\nu=0.04$ and at $\nu=0.10$, and is 17 percent low at $\nu=0.20$. Experiment points: + Zn^{67} (Helmholtz), and ⊙ Br^{80} (Siday).

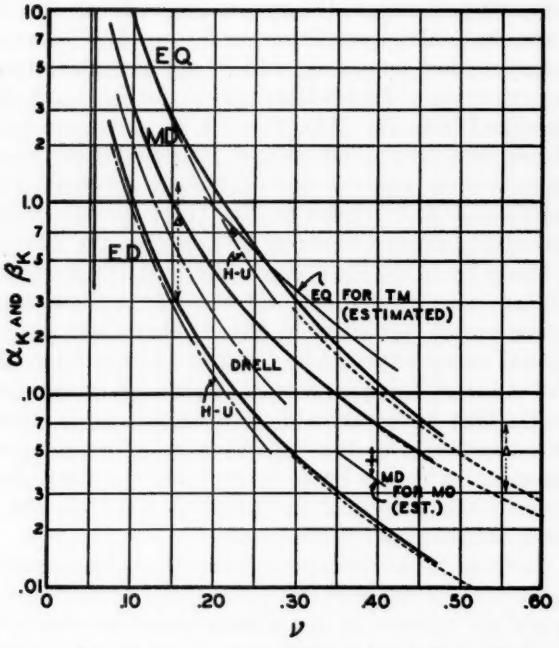

FIG. 3. Internal conversion coefficient for Indium. The solid lines are the results of this paper. The dashed curves are interpolated from Rose *et al.* The broken lines are the Hebb-Uhlenbeck and Drell formulas. Experimental points: + Mo (Huber and Medicus), ⊙ Tm^{171} (McGowan and DeBenedetti), △ Xe^{131} (Metzger and Deutsch).

The corresponding quantities for electric quadripole and magnetic dipole radiations have been given by Taylor and Mott[8] and Fisk and Taylor,[11] respectively. Here ν is the gamma-ray energy (in units of mc^2), t is the time in units of $\hbar/mc^2$, and B is the multipole moment. One then obtains the electronic flux from the K-shell to continuum states f from the well-known formula of perturbation theory:

$$N_e=2(2\pi\alpha^2)\sum_f\left|\int\psi_f^*\{\varphi+\alpha\cdot\mathbf{A}\}\psi_K d\tau\right|^2(R_sW/\pi p). \quad (17)$$

The extra 2 in the formula is because there are two K-electrons; ψ_f is normalized to one particle in a sphere of radius R_s, and the summation is over the allowed final states. The ψ's which were used in evaluating (17) are the Thomas-Fermi-Dirac functions described in Section II; only the radial parts of the wave functions are described there; however, the angular dependence of central field wave functions has been given by Rose[30] for the case of the customary α- and β-matrices. As a result of the angular integrations, electric dipole (ED), electric quadripole (EQ), and magnetic dipole (MD) radiations each allow two final states in the continuum for the case of K-conversion. For ED radiation they are $P_{3/2}(\Delta m_j=0)$ and $P_{\frac{1}{2}}$ $(\Delta m_j=0)$; for EQ, $D_{5/2}(\Delta m_j=0)$ and $D_{3/2}$ $(\Delta m_j=0)$; and for MD, $S_{\frac{1}{2}}$ $(\Delta m_j=0)$ and $D_{3/2}$ $(\Delta m_j=0)$.

In the calculation it is assumed that the nucleus radiates as a classical multiple of the proper order. Taylor and Mott have shown[9] that the number of quanta escaping from a nucleus surrounded by atomic electrons differs from the radiation of the bare nucleus only by a factor of the order of magnitude 1/137, which may be neglected. Thus the energy radiated by either dipole field (ED or MD) is

$$N_q=(4/3)\alpha B^2\nu \quad (18a)$$

quanta per unit time, and by the EQ field

$$N_q=(12/5)\alpha B^2\nu. \quad (18b)$$

The internal conversion coefficient has been evaluated for several nuclei for ED, EQ, and MD radiations using the ratio of Eqs. (17) to (18) as expressed by Eq. (15). The radial integrations in the matrix element of N_e were carried out in a straightforward manner numerically. Wave functions for an electron in a Thomas-Fermi-Dirac atomic potential were used for both initial and final states. The K-shell binding energies which were used to relate the energy of the ejected electron to that of the gamma-ray were obtained from x-ray absorption edges.

The results of the calculations are shown in Table V; they are accurate to about one percent. No correction

[30] M. E. Rose, Phys. Rev. 51, 484 (1937). Rose gives the angular dependence of *Coulomb* eigenfunctions, however, since it does not depend on the form of the potential, it is valid for all central fields. His $f=r^{-1}F$, $g=r^{-1}G$.

was made for the change in the multipole field inside the nucleus, so that the error in the magnetic dipole coefficients may be larger (the principal contribution to the matrix element in this case occurs at small distances from the nucleus).

The internal conversion coefficients are presented in graphical form (heavy solid curves) in Figs. 2–5. For purposes of comparison the low energy calculations of Rose,[13] Hulme,[7] and Griffith and Stanley[12] (calculations in which Coulomb eigenfunctions were used) are also given. In the region in which the calculations overlap, it is seen that screening by atomic electrons consistently has the effect of increasing the coefficient (from one to 13 percent in this region). The effect is smallest for MD radiation and largest for EQ radiation.

TABLE V. Internal conversion coefficients as functions of gamma-ray energy.

ν	$\alpha_K^{(1)}$	$\alpha_K^{(2)}$	$\beta_K^{(1)}$
	Copper		
0.02762	15.5	411.	13.3
0.03762	6.63	184.	5.35
0.06762	1.23	28.0	0.965
0.13762	0.150	2.16	0.142
0.21762	0.0398	0.401	0.0372
	Indium		
0.07472	2.37	17.6	7.50
0.09472	1.18	10.5	3.74
0.13472	0.448	3.83	1.37
0.2547	0.0728	0.542	0.228
0.4547	0.0152	0.0703	0.0487
	Polonium		
0.232	0.244	0.453	7.72
0.282	0.152	0.362	4.40
0.382	0.0732	0.177	2.01
0.682	0.0191	0.0532	0.416
	Uranium		
0.2776	0.178	0.253	10.11
0.3276	0.125	0.221	6.45
0.4776	0.0531	0.127	2.37

In addition the Hebb-Uhlenbeck formulas for ED and EQ radiation, and the Drell formula for MD radiation are plotted for the elements copper and indium. The Hebb-Uhlenbeck formula is given as a function of two parameters,[31] ν and $n=\alpha Z/p$; in evaluating this formula for the graphs, the electron momentum p was obtained from ν by using the x-ray binding energy, and *not* the Coulomb energy. The formula is fairly good (about 10 to 15 percent low) in the low energy region, but shows rather large deviations from our results as the relativistic effects become important. In evaluating Drell's formula, the first form of the equation,[32] in which the variables n and ν are kept separate, was used. The formula is about 25 to 30 percent low for Cu, and is as much as a factor of two low for indium. Nevertheless, one can probably obtain conversion coefficients for other nuclei of low atomic number, by using these approximate formulas, and then estimating the correction to the formulas from the known corrections for copper and indium. The extension of this procedure to higher multipole coefficients is rather risky, however.

The Dancoff-Morrison formula is given for copper. Because the electron binding is neglected in its derivation, the formula is considerably in error in the energy region shown.

VII. EXPERIMENTAL VALUES OF THE INTERNAL CONVERSION COEFFICIENT

Experimental values of the conversion coefficient for the energy region covered by this paper are given on the graph corresponding to the element of nearest atomic number. Experimental errors are given whenever they are quite large. The values of the coefficient have been modified wherever necessary to fit our definition of $\alpha_K^{(1)}$ since some experimenters use the old definition, namely α_K' equals $\alpha_K/(1+\alpha_{\text{total}})$.

Helmholz[33] has concluded that the 92.5-kev gamma-ray from Zn^{67} is EQ radiation; this conclusion is in good agreement with the results of the present paper. The K-conversion coefficient of 0.79 found by Siday[34] for the 49-kev gamma from Br^{80} falls on the estimated MD curve. Siday obtained his value by counting tracks in a cloud chamber, and his experimental error is probably large enough that ED radiation cannot be excluded. The experimentally observed K/L ratio of 12 agrees

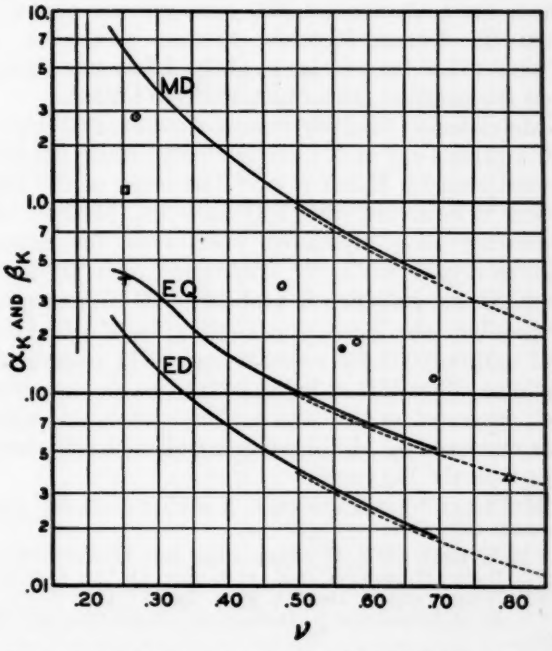

FIG. 4. Internal conversion coefficients for Polonium. The solid curves are the results of this paper. The dashed lines are interpolated from Rose *et al.*, except for ED radiation which comes from Hulme, and Griffith and Stanley. Experimental points: ⊙ Os^{186} (McCreary), + Ir^{193} and △ Hg^{198} (Saxon), □ Ta^{181} (Chu and Wiedenbeck), ● Tl^{203} (Saxon), and ○ RaC (Rutherford, Chadwick, and Ellis).

[31] The notation is that of Dancoff and Morrison, see reference 15.
[32] S. D. Drell, see reference 16, Eq. (4).
[33] A. C. Helmholtz, Phys. Rev. **60**, 415 (1941).
[34] R. E. Siday, Proc. Roy. Soc. **A178**, 189 (1941).

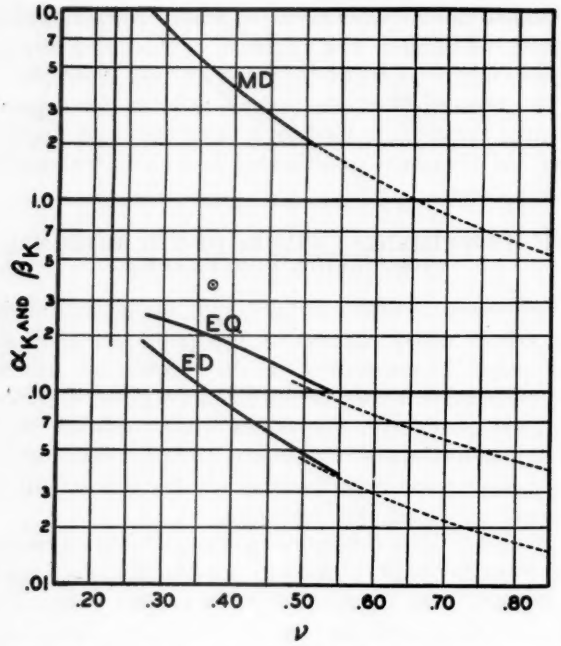

FIG. 5. Internal conversion coefficient for Uranium. The solid curves are the results of this paper. The dashed lines are from Rose *et al.* Experimental point: ⊙ Ra^{226} (Stahel and Johner).

better with the ED value (9.5 according to Hebb and Nelson)[35] than with the MD value of 6.5. On the other hand, the K/L ratio for MD radiation was computed from the Dancoff-Morrison formula which for the K-shell is low by a factor of about 2.5 at this energy; thus the question cannot be considered settled.

Molybdenum resulting from K-capture of 62 day Tc has a gamma-ray at 201 kev ($\nu=0.393$) which has been investigated by Huber *et al.*[36] The value of the coefficient is in accord with MD radiation. Metzger and Deutsch[37] have measured coefficients for several gamma-rays from Xe^{131*} (radiations from I^{131}). For $\nu=0.157$ the radiation is probably MD although ED is possible; the conversion coefficients of 0.05 ± 0.02 and 0.019 ± 0.005 for $\nu=0.554$ and 0.711 respectively could be either MD or EQ since the two curves are not well separated in this region. Tm^{171} ($\nu=0.221$) which was measured by McGowan and DeBenedetti[38] checks best with the EQ curve.

McCreary[39] has obtained a K-shell conversion coefficient of 2.83 for a gamma-ray ($\nu=0.270$) from Os^{186} which results from beta-decay of Re^{186}. The K/L ratio is 0.4. MD radiation gives good agreement with the coefficient and K/L ratio. Os^{193} beta-decays to Ir^{193} which in turn emits a gamma-ray ($\nu=0.250$). According to Saxon[40] it is converted, $\alpha_K=0.41$ and the K/L ratio equals 1.4. EQ radiation is indicated.

Chu and Wiedenbeck[41] have measured the radiations of Hf^{181} which beta-decays to Ta^{181}. If their proposed level scheme is correct, then the gamma-ray ($\nu=0.254$) has a conversion coefficient of 1.15, which is consistent only with electric octopole (EO) radiation.

Several experimenters have observed conversion of the 411-kev gamma of Hg^{198} which results from the beta-decay of Au^{198}. Saxon and Heller[42] give $\alpha_K=0.0356$ which is consistent with EQ radiation. Saxon[43] has also measured the 286-kev gamma-ray of Tl^{203} and finds the K-shell coefficient to be 0.18. The value checks with EO radiation.

Three conversion coefficients for RaC are shown in Fig. 4; they are listed by Rutherford, Chadwick, and Ellis[44] (under radiations from RaB) and are all in accord with EO. Another EO coefficient is indicated for the 190-kev gamma-ray from Ra^{226} measured by Stahel and Johner.[45]

In most cases knowledge of the value of the K-shell conversion coefficient is not sufficient to determine the character of the nuclear transition. However, the K-coefficient will in general give an independent determination of the transition, others being provided by the K/L ratio, the lifetime of the isomeric level and possibly a proposed disintegration scheme between two levels for which the spins are known.

VIII. ACKNOWLEDGMENTS

I should like to express my warm appreciation to Professor E. Teller for suggesting this problem and for his friendly guidance during its progress. It is a pleasure to thank Dr. N. Metropolis for his help and constructive criticisms in setting up the wave function problem for integration on the ENIAC. Thanks are also due to the staff of the Ballistics Research Laboratory at Aberdeen Proving Ground; and to Mr. T. J. Kinyon for evaluating some of the internal conversion matrix elements.

[35] M. H. Hebb and E. C. Nelson, Phys. Rev. **58**, 486 (1940).
[36] O. Huber, H. Medicus, *et al.*, Phys. Rev. **73**, 1211 (1948).
[37] F. Metzger and M. Deutsch, Phys. Rev. **74**, 1640 (1948).
[38] F. K. McGowan and S. DeBenedetti, Phys. Rev. **73**, 1269 (1948).
[39] R. L. McCreary, "A Study of Internal Conversion and Beta Radioactivity of Light Nuclei" (Unpublished Ph.D. dissertation, Department of Physics, University of Rochester, 1942).
[40] D. Saxon, unpublished.
[41] K. Y. Cu and M. L. Wiedenbeck, Phys. Rev. **75**, 226 (1949).
[42] D. Saxon and R. Heller, Phys. Rev. **75**, 330 (A) (1949).
[43] D. Saxon, Phys. Rev. **74**, 849 (1948).
[44] Rutherford, Chadwick, and Ellis, *Radiation from Radioactive Substances* (University Press, Cambridge, 1930), p. 512.
[45] E. Stahel and W. Johner, J. de phys. et rad. **5**, 97 (1934).

Nuclear Disintegrations as Detected with Electron-Sensitive Emulsions Exposed in the Stratosphere*

J. J. Lord and Marcel Schein
Department of Physics, University of Chicago, Chicago, Illinois
(Received September 8, 1949)

The nature of high energy nuclear interactions produced in photographic emulsions was investigated in the stratosphere. Examples are given, which were selected to show the principal modes of interactions, which lead to the emission of groups of particles with ionization energy losses corresponding to the minimum value for singly charged particles. For cases in which more than two particles of minimum ionization were emitted, the incident particle was found to be charged in nearly every case. The angular distribution of emitted minimum ionization tracks was measured as a function of the angle with the direction of the incident track. The zenith angle distribution of incident particles producing groups of minimum ionization tracks is given for two different altitudes in the stratosphere.

INTRODUCTION

THE production of nuclear interactions in very sensitive photographic plates has been investigated in the stratosphere through the use of free balloons. Photographic plates (Eastman[1] NTB-3, Ilford[2] G-5, and Kodak[3] NT-4) 200 microns in thickness were employed, which provided measurable tracks even for particles having an ionization energy loss corre-

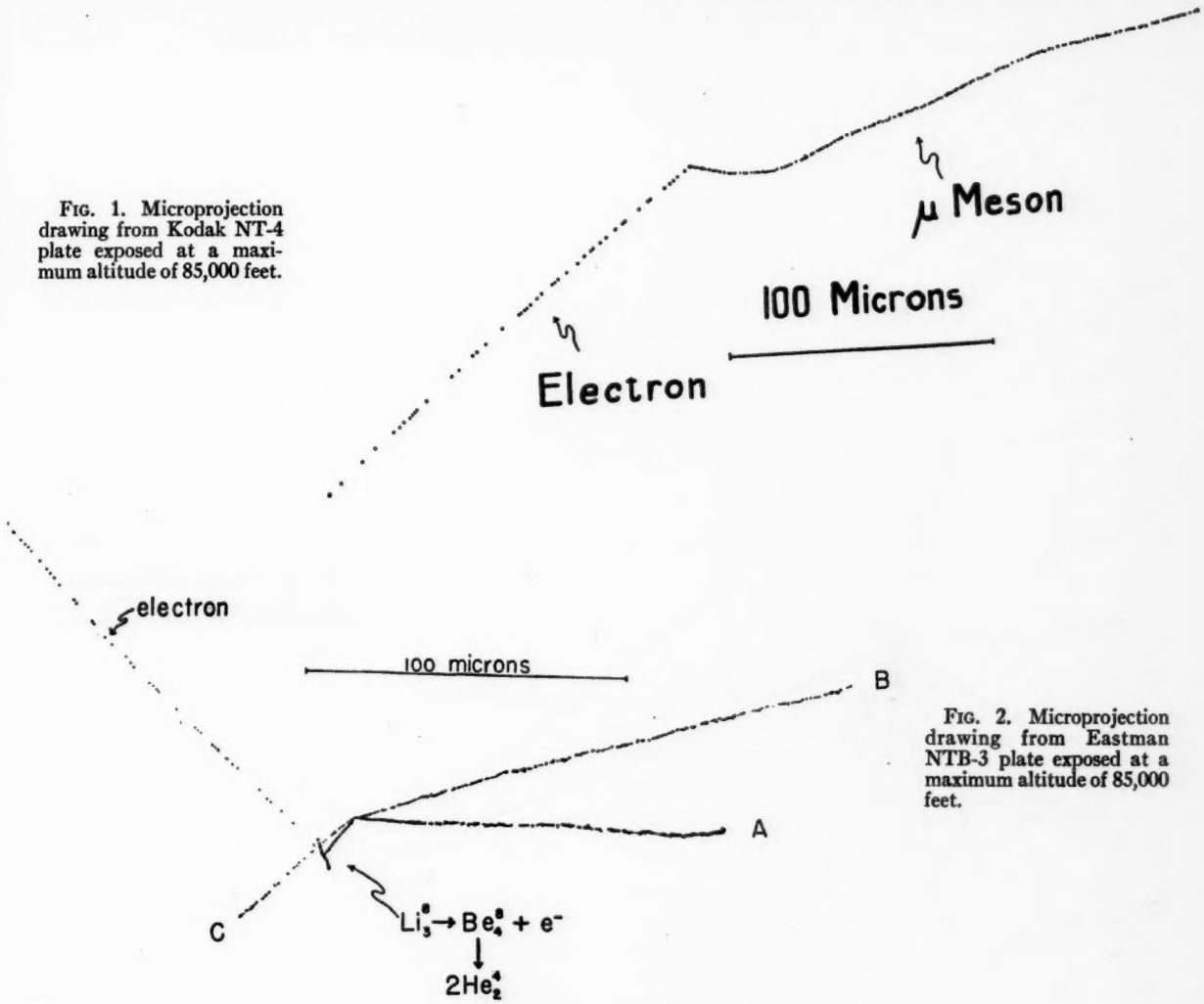

FIG. 1. Microprojection drawing from Kodak NT-4 plate exposed at a maximum altitude of 85,000 feet.

FIG. 2. Microprojection drawing from Eastman NTB-3 plate exposed at a maximum altitude of 85,000 feet.

* Assisted by the Joint Program of the ONR and the AEC.
[1] Plates kindly provided by Dr. J. Spence.
[2] Plates kindly provided by C. Waller.
[3] Plates kindly provided by R. H. Herz.

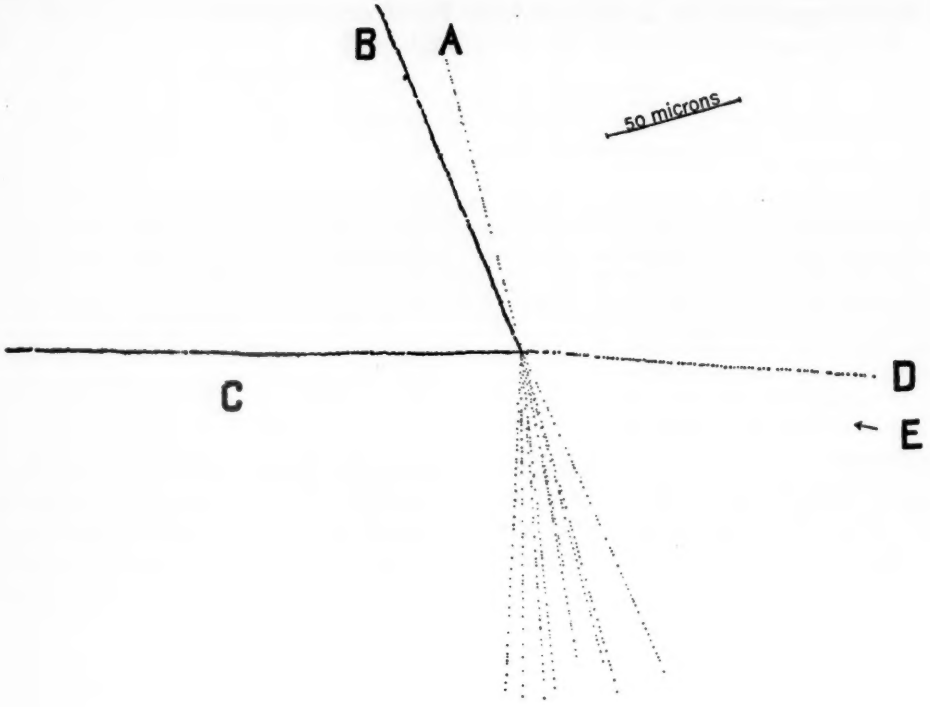

FIG. 3. Microprojection drawing from Ilford G-5 plate exposed at a maximum altitude of 95,000 feet.

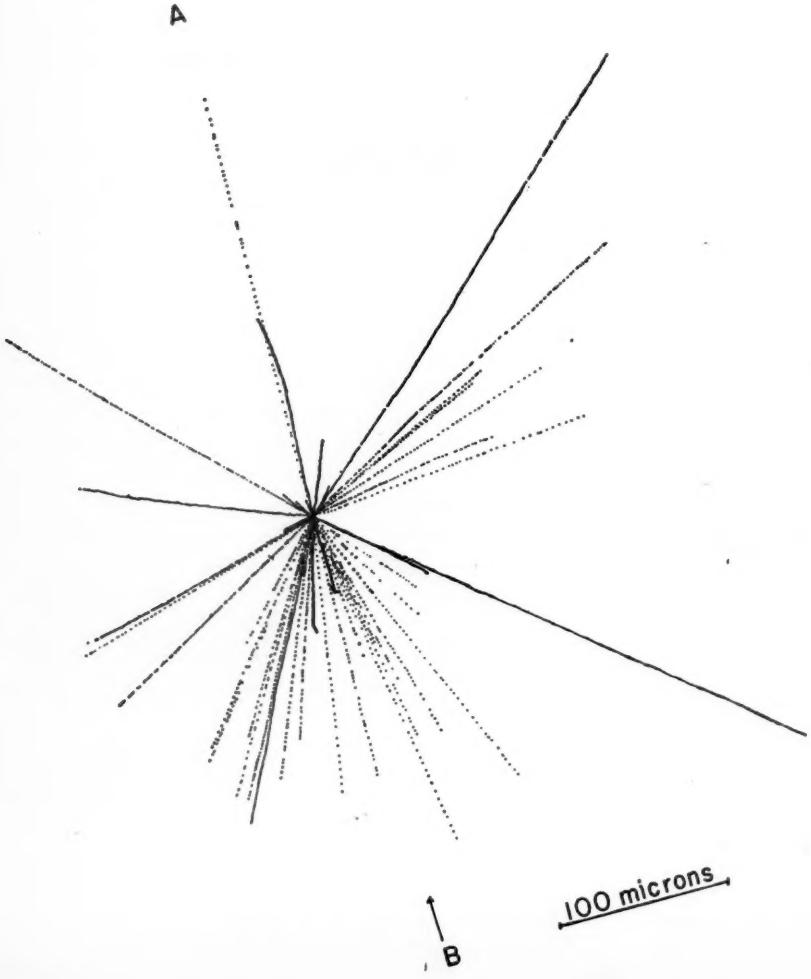

FIG. 4. Microprojection drawing from Ilford G-5 plate exposed at a maximum altitude of 95,000 feet.

sponding to the minimum value for singly charged particles.

The following examples of nuclear interactions were selected principally to show the various modes of nuclear disruptions involving several or many particles with an ionization energy loss close to the minimum value. They were selected from a total of 550 stars largely obtained at an altitude of 95,000 feet. The pictures of these examples were made by projecting the image of silver grains in the photographic emulsion through a microscope and onto a piece of drafting paper. A total magnification between 1200 and 2000 was used, depending upon the size of the event in the emulsion. As each grain of a track was brought into focus, its outline was traced onto the drafting paper.

DESCRIPTION OF SELECTED EVENTS

I

Figures 1 and 2 demonstrate the sensitivity of the emulsions. Figure 1 shows a case in which a μ-meson stops in the emulsion, where it decays with the emission of an electron. The electron track extends 1100 microns through the emulsion, finally passing into the glass backing of the plate. The grain density, 0.27 grain per micron, is constant along the complete range, and this corresponds to approximately the minimum value for the energy loss in this plate. Small angle scattering measurements show that the electron had a momentum of 50 ± 10 Mev/c.

II

In Fig. 2 is shown a hammer track which differs from the familiar examples found in photographic plates[4] in that the decay electron track is visible. The event, according to the usual interpretation,[5] would be the ejection of a Li^8 nucleus in a nuclear disintegration in which three other tracks, *A*, *B*, and *C* were also emitted. After stopping in the emulsion, the Li^8 nucleus decays with the emission of an electron, visible in Fig. 2, to form Be^8. The Be^8 then immediately (10^{-21} sec.) breaks up into two alpha-particles traveling in approximately opposite directions, as is shown in Fig. 2. The electron track is of a grain density corresponding to minimum

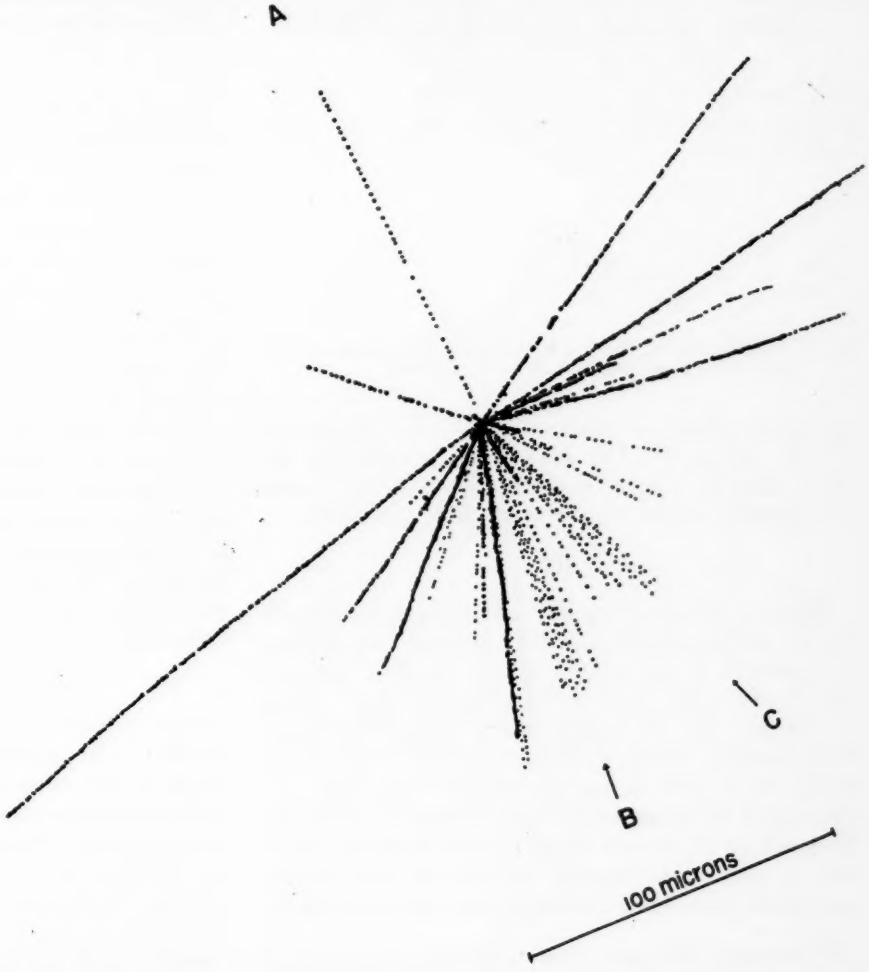

FIG. 5. Microprojection drawing from Kodak NT-4 plate exposed at a maximum altitude of 95,000 feet.

[4] C. P. S. Occhialini and C. F. Powell, Nature **159**, 93 (1947).
[5] Christy, Cohen, Fowler, Lauritsen, and Lauritsen, Phys. Rev. **72**, 698 (1947).

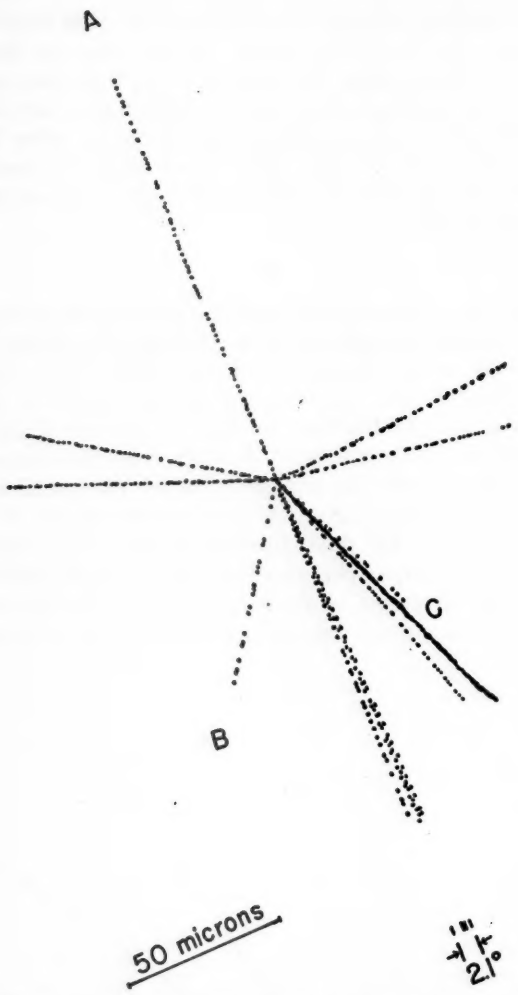

FIG. 6. Microprojection drawing from Kodak NT-4 plate exposed at a maximum altitude of 95,000 feet.

ionization, which is in conformity with the rather high average energy for this beta-decay process. Of the seven hammer tracks observed thus far three cases were found in which the decay electron was visible.

III

Figure 3 shows a nuclear encounter involving 14 visibly ionizing particles. Track *A*, close to minimum ionization,** is interpreted as the incident particle, since in line with it and on the other side of the center of the star are nine other tracks close to minimum ionization in a bundle of angular width 27°. Three heavy tracks, *B*, *C*, and *D* are low energy evaporation nucleons, and the short, heavy track, *E*, almost completely obscured by *D*, is most likely a recoil fragment. Since such a considerable energy was lost by the incident particle in this nuclear encounter, and only four heavily ionizing tracks occurred, it is most likely that this event represents a collision with one of the lighter atoms of the emulsion, such as carbon, oxygen, or nitrogen.

IV

Figure 4 shows a large nuclear encounter involving 45 tracks due to ionizing particles. Track *A* of minimum ionization is interpreted as the incident particle in consideration of the distribution of the 18 minimum ionization tracks involved in the interaction. One of the heavier, short tracks, *B*, near the end of its range, divides into two short tracks and could be either due to collision with a proton in the emulsion, or a hammer track.

V

The microprojection drawing of Fig. 5 shows a star, having a total of 43 prongs, of which 28 are tracks at minimum ionization. From the manner in which the tracks of minimum ionization are distributed, the one marked *A* is interpreted as due to the incident particle causing the nuclear interaction. The arrows *B* and *C* point to two regions in which tracks of minimum ionization are grouped in bundles.

VI

In Fig. 6 an event is shown in which four tracks of minimum ionization are grouped together in a narrow bundle of angular width, 2.1°. Two other minimum ionization tracks, *B* and *C*, are also emitted, but at the much larger angles of 35° and 30°, respectively, as measured from the narrow bundle of tracks. Track *A*, directly opposite the narrow bundle, is of interest, since it has a grain density corresponding to an ionization four times the minimum for singly charged particles. This, then, corresponds to the minimum ionization for a doubly charged particle, so that track *A* is interpreted as a high energy alpha-particle, which causes the resulting nuclear interaction. At minimum ionization the alpha-particle would have an energy in excess of three Bev. This is greater than the minimum energy required for an alpha-particle to penetrate the magnetic field of the earth. (The cut-off energy, due to the earth's magnetic field, for an alpha-particle at 56° magnetic latitude is 1.3 Bev.)

VII

The nuclear interaction in Fig. 7 is represented by 29 tracks of the ionizing particles, and of these, 16 are tracks of minimum ionization. Track *A* of minimum ionization is interpreted as the incident particle causing the interaction. The other tracks of minimum ionization are distributed in a manner quite different from a uniform distribution about an axis defined by track *A*. As shown in Fig. 7, most of them go in the general direction of the arrow, *C*.

A very heavy fragment, *B*, is also emitted, which stops after traversing 62 microns of emulsion. At the

** Throughout this paper "minimum ionization" shall refer to tracks of singly charged particles, which have an ionization energy loss less than 40 percent in excess of the minimum value, registered in the photographic plate.

beginning, the track is 1.2 microns in diameter and thins down continuously to approximately 0.6 micron at the end. From the thinned-down length the nuclear charge, Z, is estimated to be close to 11. If the initial velocity of the fragment is equal to the velocity of an electron in its K orbit, then the transverse momentum of the fragment is approximately one Bev/c.

Since the total momentum of the tracks of minimum ionization appears to have a rather pronounced component in the direction transverse to A, the heavy fragment is the only visible track, responsible for the conservation of momentum in the transverse direction.

VIII

In the nuclear disintegration of Fig. 8 there are involved a total of 35 tracks, produced by charged particles in a plate located vertically, as indicated on the drawing. Nine of these tracks have an ionization energy loss, which, for protons, corresponds to energies somewhat uniformly distributed between 80 and 340 Mev. This event is of interest, since there are no tracks of minimum ionization, although the total number of tracks indicates a large interaction energy. The momentum, due to each particle producing a visible track, can be only roughly estimated in most cases, and for this event, the vector sum of momenta for all of the tracks is quite small in comparison to the arithmetical sum of the momenta.

Of course, minimum ionization tracks could escape detection, if they made very steep angles with the surface of the emulsion, but any grouping of minimum ionization tracks, such as in Fig. 3, would in part be detected, however steep the angle of the incident particle. An examination of the various tracks leads to the conclusion that none of them could satisfy the conditions necessary to be considered the incident particle.

CHARACTERISTICS OF STARS

The characteristics of the stars used for this analysis are given in Fig. 9. Curve A shows the number of stars with more than n prongs as a function of n. In examining the number of minimum ionization tracks involved only those stars were considered, which were at least 40 microns from either surface of the 200-micron thick emulsion. Curve B gives the number of stars having more than n minimum ionization tracks as a function of n. Of the total number of stars, 40 microns from either emulsion surface, 35 percent had at least one and 12 percent had three or more tracks, corresponding to minimum ionization tracks.

ZENITH ANGLE DEPENDENCE OF INCIDENT TRACKS PRODUCING STARS

The zenith angle was measured for those minimum ionization tracks considered to be due to the incident particle, producing a star in which other minimum

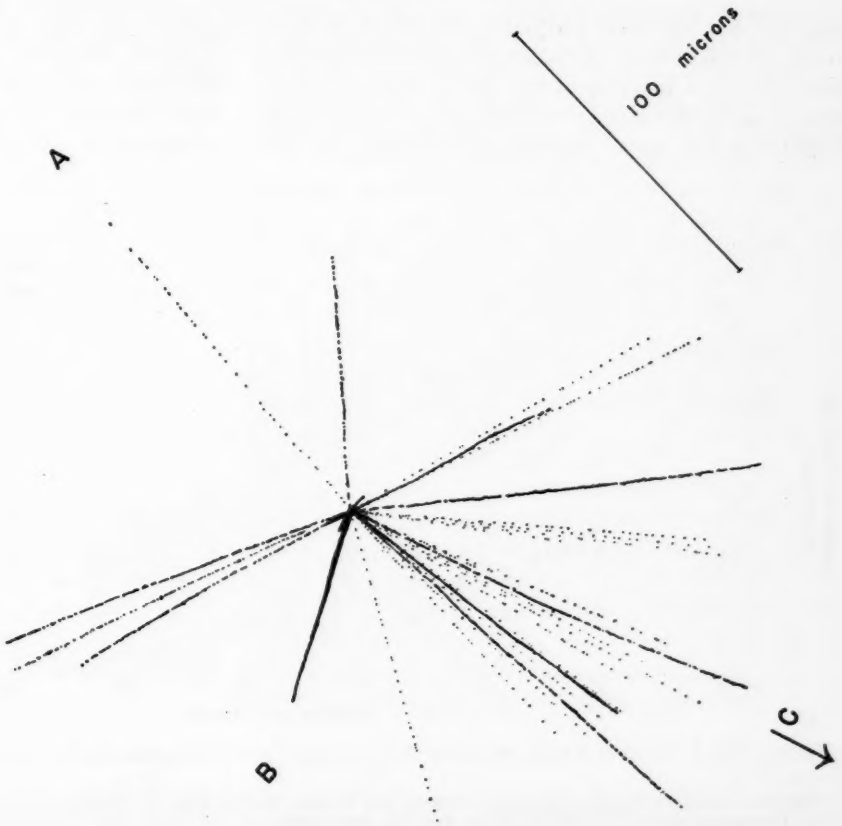

FIG. 7. Microprojection drawing from Ilford G-5 plate exposed at a maximum altitude of 58,000 feet.

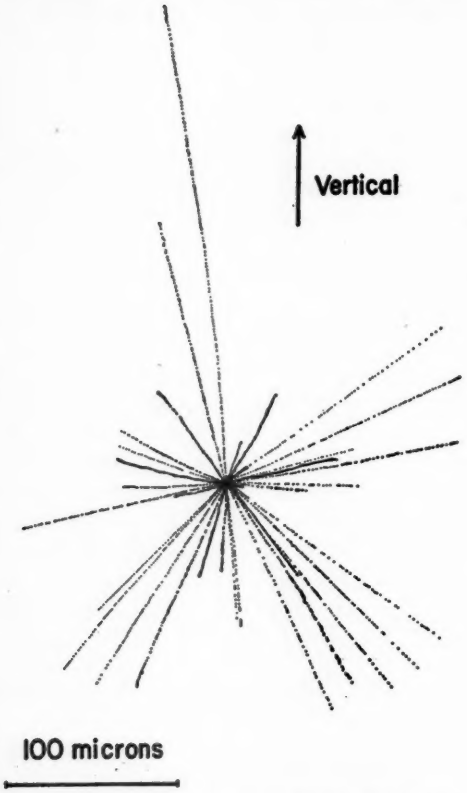

FIG. 8. Microprojection drawing from Kodak NT-4 plate exposed at a maximum altitude of 85,000 feet.

ionization particles were emitted in a forward direction. In Fig. 10 the number of these tracks per steradian has been given as a function of the zenith angle for plates exposed at 95,000 feet and 52,000 feet. The curve for 95,000 feet (15 g/cm² residual atmosphere) was obtained from the measurement of 43 tracks and shows that at 80° from the vertical, the intensity of the incident tracks decreases by $1/e$. This gives for the production of these events an absorption cross section of approximately 3.5×10^{-25} cm² corresponding to a mean free path of 71 g/cm² of air. However, taking into account experimental errors, this can only be considered as an approximate value at the present time. The curve, Fig. 10, at 52,000 feet (109 g/cm² residual atmosphere) based on lower statistics shows a considerably steeper zenith angle dependence. The mean free path was calculated to be roughly the same as that at 95,000 feet.

ANGULAR DISTRIBUTION OF MINIMUM IONIZATION TRACKS IN STARS

In many of the examples shown in Figs. 3–8 it is possible to see a very distinct collimation of the minimum ionization tracks, which was first observed by Powell[6] and later by other groups.[7] Measurements of the angles θ between the emitted minimum ionization tracks and the extension of the incident track showed that for events such as Figs. 3–5, the number of tracks per unit solid angle was largest close to $\theta=0°$, and then fell off exponentially with θ. The intensity dropped to half the minimum for values of θ lying roughly between 7° and 12° for a number of events.

This feature of collimation about the incident track is not present in the case of the star in Fig. 7. Here, there is a spray of minimum ionization tracks in the general direction of C, and in this case, the heavy fragment, B, is most probably an integral part of the elementary act. The spray of minimum ionization tracks describe a cone, the axis of which makes an angle of roughly 20° with the direction of the incident track.

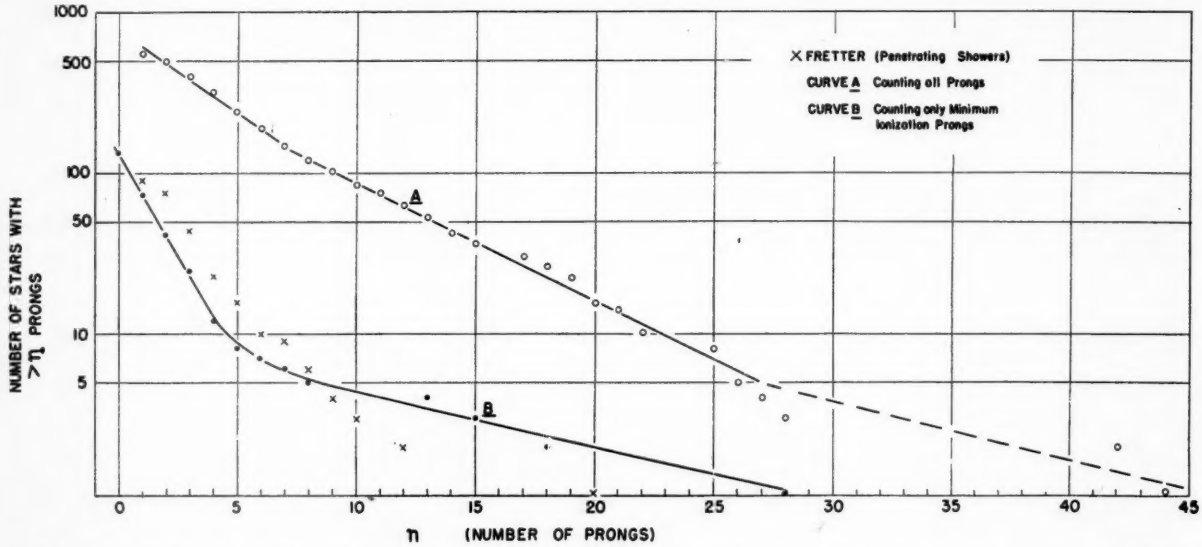

FIG. 9. Curve A: Number of stars with more than n prongs. Curve B: Number of stars with more than n minimum ionization tracks.

[6] Brown, Camerini, Fowler, Muirhead, Powell, and Ritson, Nature **163**, 47 (1949).
[7] J. Hornbostel and E. O. Salant, Phys. Rev. **76**, 468 (1949).

The collimation of the minimum ionization tracks in Fig. 5 about the direction of the incident track shows some bunching in the directions B and C which may correspond to the occurrence of successive collisions inside of the same nucleus.

This pronounced collimation and large multiplicity of minimum ionization tracks in certain stars strongly suggests that these events represent, to a large extent, the production of mesons. The number of minimum ionization tracks per steradian as a function of the angle θ with the extension of the incident track is given in Fig. 11 for two of the stars. Curves A and B were obtained, respectively, from the stars shown in Figs. 5 and 4. A comparison of the angular distribution of these minimum ionization tracks was made with the angular

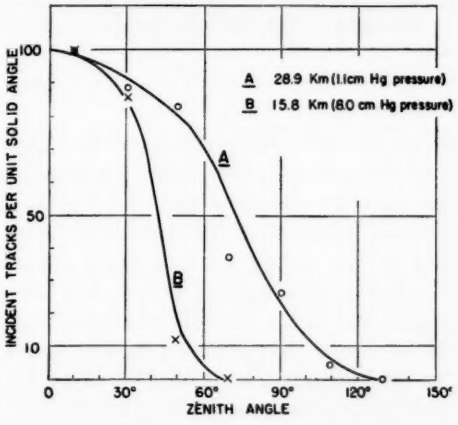

FIG. 10. Incident particles producing large stars in which minimum ionization particles are emitted. Number of incident tracks per steradian at the zenith angle θ. Curve A at 95,000 feet. Curve B at 52,000 feet.

distribution function for the production of mesons, given by Lewis, Oppenheimer, and Wouthuysen.[8] Assuming the multiplicity of meson production to be roughly given by the number of minimum ionization tracks, approximate agreement with the theory was obtained for primary energies of the order of 25 to 50 Bev.

SUMMARY

The examples shown in Figs. 3–8 demonstrate that incident particles of high energy are capable of producing bundles of minimum ionization particles in the general direction of the incident particle. The angular dependence of these tracks seems somewhat similar to that for the penetrating particles obtained in cloud-chamber experiments.[9] The multiplicity with which

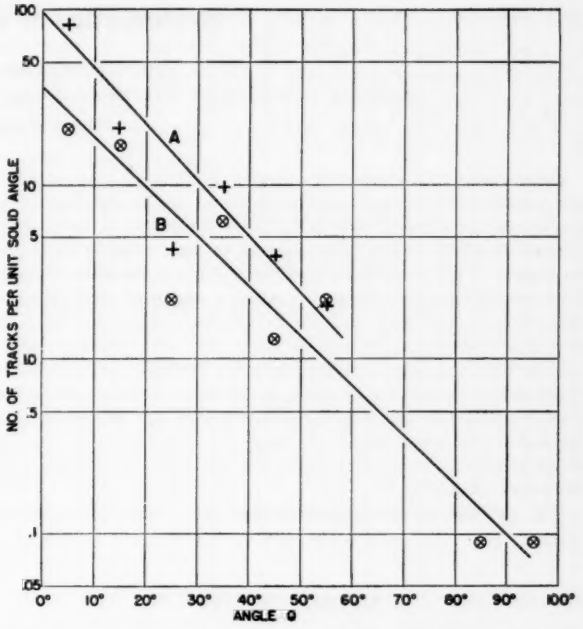

FIG. 11. Number of emitted minimum ionization tracks per steradian at the angle θ with the direction of the incident track. Curve A from star in Fig. 5. Curve B from star in Fig. 4.

penetrating particles are produced in Pb as measured by Fretter[9] is plotted in Fig. 9, and is quite similar to curve B, showing the multiplicity in photographic emulsions.

The nature of the incident particle can be estimated in those cases where the number of minimum ionization tracks is sufficient to define a reasonable cone, and, hence, to give the general direction to the incident track. For this type of event it was found that about 90 percent of the stars was produced by singly charged particles of minimum ionization, which are probably all primary protons. In 10 percent of the cases a track four times the minimum ionization for singly charged particles corresponding to an alpha-particle was found to be the incident track. There were no definite cases found in this analysis, which is primarily concerned with altitudes of 95,000 feet, in which a well defined cone of minimum ionization tracks was not accompanied by a charged incident track. However, Leprince-Ringuet[10] has observed at least one such case.

An interpretation of the above data will be given in a later paper, after more data has been accumulated.

We would like to thank Messrs. A. Elston, M. Vidale, and G. Yodh for assisting in the examination of the photographic plates and in the preparation of the microprojections.

[8] Lewis, Oppenheimer, and Wouthuysen, Phys. Rev. **73**, 127 (1948).

[9] W. B. Fretter, Phys. Rev. **76**, 511 (1949).

[10] L. Leprince-Ringuet (private communication 1949).

Systematics of Alpha-Radioactivity

I. PERLMAN, A. GHIORSO, AND G. T. SEABORG
Radiation Laboratory and Department of Chemistry, University of California, Berkeley, California
(Received September 26, 1949)

Correlations of alpha-decay energies in terms of mass number and atomic number have been made for all of the alpha-emitting species now numbering over 100. For each element isotopes show increase in alpha-energy with decrease in mass number except in the region of 126 neutrons where there is an explainable reversal. This reversal has the effect of creating a region of relatively low alpha-energy and long half-life at low mass numbers for such elements as astatine, emanation, francium, and possibly higher elements as had been noted already for bismuth and polonium. Methods and examples of using alpha-decay data to define the energy surface in the heavy element region are discussed. The regularities in alpha-decay are used for predictions of nuclear properties including predictions of the beta-stable nuclides among the heavy elements.

The half-life *vs.* energy correlations show that the even-even nuclides conform well with existing alpha-decay theory, but all nuclear types with odd nucleons show prohibited decay. The reason for this prohibition is not found in spin changes in the alpha-emission but in the assembly of the components of the alpha-particle, and this theory is discussed further in terms of observations made on nuclides having two or more alpha-groups. Using most of the even-even nuclei to define "normal nuclear radius" calculations are now able to show the shrinkage in the regions of lead and of 126 neutrons to amount to about 10 percent. The much greater change in "effective radius" for bismuth isotopes can be dissociated into the effects of odd nucleons superimposed on the actual decrease in nuclear radius. The simple expression $r=1.48A^{\frac{1}{3}}\cdot 10^{-13}$ cm seems to fit the data for the even-even nuclei outside of the region of 126 neutrons better than more complex functions.

INTRODUCTION

INTEREST in the systematics of alpha-decay properties goes back to the early studies of the natural radioactivities at which time it became apparent that there exists a direct relationship between alpha-energy or velocity and decay constant.[1] Since then there have been numerous efforts to correlate alpha-decay data on an empirical basis and, most important, the successful application of quantum mechanics to give insight into the nature of the process.[2]

Even in general terms the importance of correlations of alpha-decay properties takes several forms. The discovery of artificial radioactivity and the continued development of the means for producing unstable nuclei have made it possible to examine the properties of an increasingly wide variety of nuclear species. In the case of the heavy elements in which alpha-radioactivity is prevalent it is most important to be able to predict, even roughly, the radioactive properties of unknown species because of the extreme range of half-lives that may be encountered. At the present time such predictions can be made with a fair degree of confidence and this facility has aided markedly in the preparation and identification of new nuclear species in the heavy element region. It is perhaps obvious but worth pointing out here that insofar as preparation and observation of new nuclides are concerned, predictions of beta-stability must be considered along with alpha-decay properties.

Another major reason for interest in alpha-decay properties is the insight which these data afford into the nuclear structure of the heavy elements. Alpha-decay energies can be measured precisely and in general are thought to give unambiguous values for decay energies. Since the heaviest elements are joined to the region around lead by continuous decay series it is possible to interrelate on an energy content basis most nuclear species in this region making use of few serious approximations. In brief, it is possible to determine regions of greater nuclear stability from neighboring regions in which the nucleons are less firmly bound. Lastly, so far as this introduction is concerned, it is possible to gain further information on nuclear structure by considering the decay constants in terms of the factors which determine decay constants according to the quantum mechanical explanation for the alpha-decay process and to show to what degree alpha-decay theory is adequate in interpreting all of the new data.

In the last few years the extension of available data has become so considerable as to demand a reexamination of regularities in alpha-decay properties. About 10 years ago only 24 alpha-emitters were known and these were all members of the naturally occurring radioactive families. In the next five years only five more had been reported, one produced by artificial means and the others discovered by more careful examination of the radioactivities occurring in nature. At the present time about 100 alpha-decaying nuclear species have been reported.[3] Most of the large number of new additions may be classified in groups with regard to position among the elements and means of formation. The work on transuranium elements at the University of California and at the wartime Metallurgical Laboratory of the University of Chicago has resulted in the discovery of 16 alpha-emitters in this region.[4] The

[1] H. Geiger and J. M. Nuttall, Phil. Mag. **22**, 613 (1911); **23**, 439 (1912).

[2] G. Gamow, Zeits. f. Physik **51**, 204 (1928); *Structure of Atomic Nuclei and Nuclear Transformations* (Oxford University Press, London, 1937).
E. U. Condon and R. W. Gurney, Phys. Rev. **33**, 127 (1929); Nature **122**, 439 (1928).
H. A. Bethe, Revs. Mod. Phys. **9**, 161 (1937).

[3] G. T. Seaborg and I. Perlman, Revs. Mod. Phys. **20**, 585 (1948).

[4] References for this work as well as other work not specifically cataloged here will be found in the "Table of Isotopes" which is reference 3.

preparation of U^{233} in quantity has added 7 more alpha-emitters as members of the $4n+1$ radioactive family[5,6] while 4 and 18 new species, respectively, were added by the discovery of the U^{230} collateral series[7] and five new short-lived collateral series.[8] Another group of 18 alpha-active species* resulted from preparation of neutron deficient isotopes of bismuth, polonium, astatine, emanation and francium.[9]

The additional alpha-emitters which have been characterized within the past few years are most important because they extend the nuclear types for which alpha-decay is observed and some also fill in gaps between previously known isotopes. The most important new regions for which data are now available are the transuranium elements and isotopes lying on the neutron deficient side of beta-stability. The band of alpha-emitting nuclei has therefore been extended both vertically and laterally.

The regularities in alpha-decay properties are now sufficiently well defined and are broad enough in their coverage to make possible meaningful predictions for all nuclides from bismuth to elements beyond curium. Most of the available alpha-decay energies and some data of half-lives have already been reported in recent brief communications.[10]

ALPHA-DECAY ENERGIES

General Trends

There are clearly a number of ways in which to correlate alpha-decay energies. The most definitive presentation would consist of an energy surface from which could be measured nuclear instability of all types. However, there are great advantages in terms of simplicity and magnification of scale in plotting alpha-decay energies directly. In diagrams of this type one arrives at a family of curves which take different forms depending upon what the alpha-energy is plotted

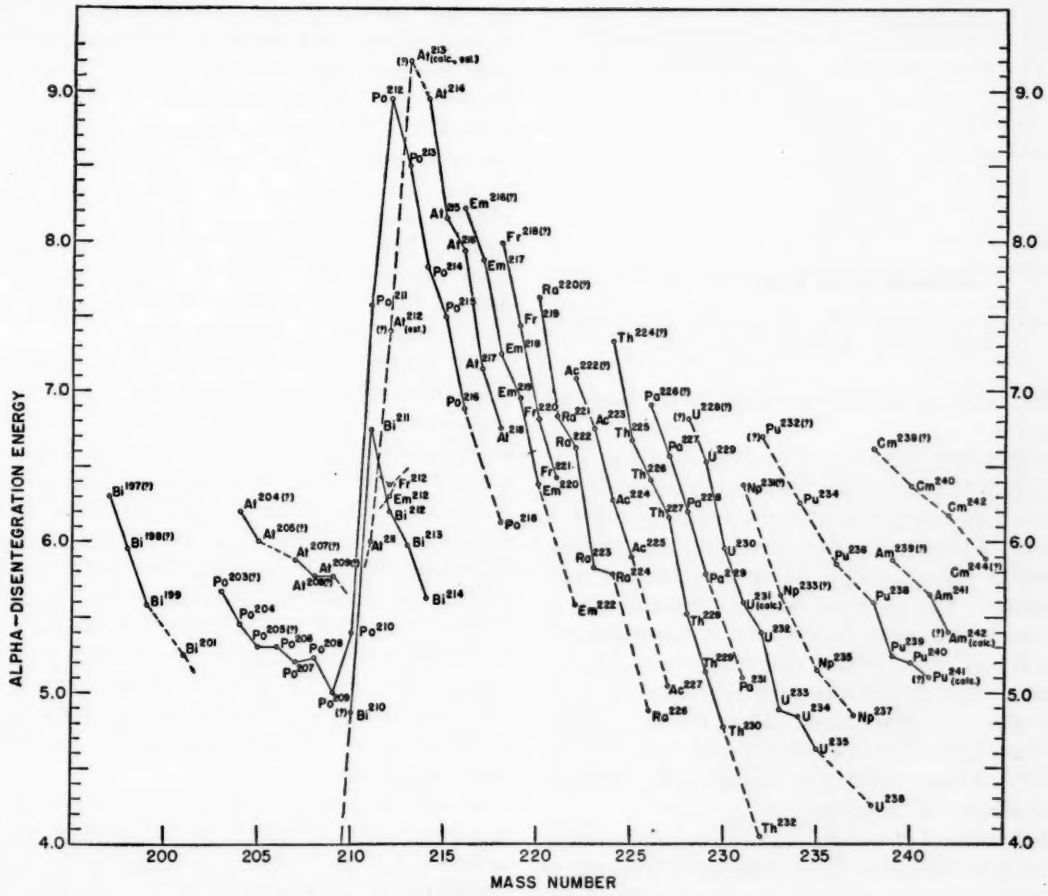

FIG. 1. Alpha-energy *vs.* mass number relationships of the heavy nuclides.

[5] Hagemann, Katzin, Studier, Ghiorso, and Seaborg, Phys. Rev. **72**, 252 (1947).
[6] English, Cranshaw, Demers, Harvey, Hincks, Jelley, and May, Phys. Rev. **72**, 253 (1947).
[7] M. H. Studier and E. K. Hyde, Phys. Rev. **74**, 591 (1948).
[8] Ghiorso, Meinke, and Seaborg, Phys. Rev. **74**, 695 (1948); Meinke, Ghiorso, and Seaborg, Phys. Rev. **75**, 314 (1949).
[9] Templeton, Howland, and Perlman, Phys. Rev. **72**, 527 (1947); D. H. Templeton and I. Perlman, Phys. Rev. **73**, 1211 (1948); for others, see references in the Appendix.
[10] Perlman, Ghiorso, and Seaborg, Phys. Rev. **74**, 1730 (1948); **75**, 1096 (1949).

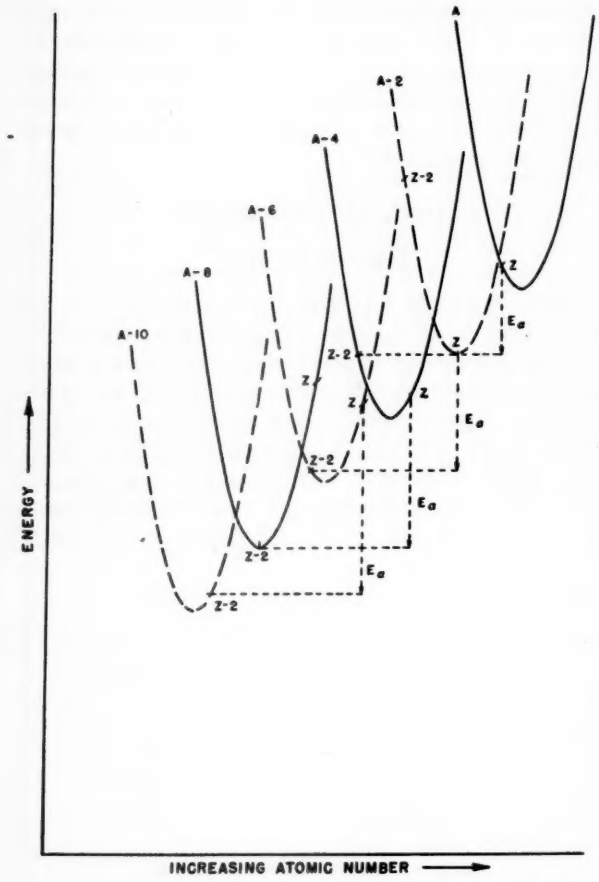

FIG. 2. Parabolic sections of energy surface showing increase in alpha-energy with mass number decrease.

against and which parameter is chosen as the basis for joining points.

One of the early methods of treating data was that of Fournier[11] who plotted the alpha-particle velocity *vs.* mass number and showed that upon joining isotopes of each element a family of parallel straight lines resulted, a few points being notable exceptions to the rule. Schintlmeister[12] has made a similar diagram but in addition has joined points of the same "neutron excess" ($A-2Z$). It will be recognized that members of a decay series linked directly by alpha-particle decay will all have the same "neutron excess." More extensive treatment and interpretation of available data was made by Berthelot[13] and more recently by Karlik[14] using methods somewhat similar to those mentioned.

Another method of correlating data on alpha-decay used recently by Wapstra[15] and Glueckauf[16] consists of a numerical indication of mass defect or alpha-decay energy at the position for the appropriate nuclide on a plot of A *vs.* $A-2Z$ or Z *vs.* $A-Z$. Contour drawn through points of equal instability serve to map trends in this property.

The usefulness of any plot of alpha-decay properties may be measured by the accuracy with which properties of previously unobserved alpha-emitters may be predicted. This in turn depends upon how regularly the data fall into the adopted scheme. There is probably little to recommend one method over another for general purposes since similar uncertainties in extrapolation are inherent in all methods and similar deductions of nuclear properties may be made from all.

At the present time there are sufficient data available over a range of mass numbers for almost every element from bismuth to curium that trends in alpha-decay properties show up well on a plot of alpha-energy *vs.* mass number in which isotopes of the elements are joined. Figure 1 shows such a treatment of the data in which the ordinates give the alpha-disintegration energies* for the ground state transitions which would include gamma-ray energies for those cases in which the most energetic alpha-particle observed is known to be followed by gamma-radiations. If we confine our attention to the heaviest elements, neglecting, for the moment, astatine and lower elements, the most apparent characteristic of the alpha-energies is that the isotopes of each element may be joined by a moderately straight line with increase in energy for decrease in mass number. The trend is roughly linear; that it departs from this condition is not surprising and possible reasons will be discussed below.

The general trend of increase in alpha-energy with decrease in mass number probably can be adequately explained for the present by considering sections of the energy surface at constant mass number. Figure 2 shows a series of such sections in idealized form for A, $A-2$, $A-4$, etc. The parabolic form of these sections at constant A was deduced by Bethe and Bacher[17] from their semi-empirical mass equation and this was transformed into a more convenient form and the parameters evaluated by Bohr and Wheeler.[18] These Bohr-Wheeler parabolas therefore show energy relationships between isobars. The abscissa in Fig. 2 is not continuous. This was done in order to spread the parabolas apart and the notation of Z on each indicates the positions of the same atomic number.

It will be recalled that in the region from lead to uranium there are added on the average almost two neutrons for each proton in attaining a comparable configuration with respect to beta-stability for succeeding elements. Therefore, if as shown in Fig. 2

[11] G. Fournier, Comptes Rendus **184**, 878 (1927); K. Fajans, *Radioelements and Isotopes* (McGraw-Hill Book Company, Inc., New York, 1931), Chapter I.
[12] J. Schintlmeister, Wien. Chem. Zeits. **46**, 106 (1943).
[13] A. Berthelot, J. de phys. et rad. VIII, **3**, 17 (1942).
[14] B. Karlik, Acta Phys. Austriaca **2**, 182 (1948).
[15] A. H. Wapstra, Nature **161**, 529 (1948).
[16] E. Glueckauf, Proc. Phys. Soc. **61**, 25 (1948).

* In this paper the total energy of the transition between ground states will be termed "alpha-disintegration energy" or more simply "alpha-energy" while the kinetic energy of the alpha-particle will be explicitly designated "alpha-particle energy."
[17] H. A. Bethe and R. F. Bacher, Revs. Mod. Phys. **8**, 82 (1936) (pp. 104 and 165).
[18] N. Bohr and J. A. Wheeler, Phys. Rev. **56**, 426 (1939).

element Z lies at the vertex of the parabola for mass number $A-2$, element $Z-2$ will lie approximately at the vertex of $A-8$. It is further assumed that the change in packing fraction is regular in this region so that if the ordinate of Fig. 2 is a function of the mass defect or packing fraction the parabolas will lie as shown. It is a property of identical parabolas arranged in this fashion that the vertical projections of lines representing alpha-decay drawn between points on two parabolas (e.g., A, Z to $A-4, Z-2$) will increase as A decreases. As long as sections of the energy surface at constant A are roughly similar parabolas without sharp irregularities and the slope of the surface is fairly constant, decrease in mass number for each element should be accompanied by increase in alpha-energy. Kohman[19] has developed an expression for alpha-energy in terms of the Bohr-Wheeler mass equation[18] from which the same deductions can be made analytically as those developed graphically here by making equivalent assumptions as to the form of the energy surface. It may be mentioned that the section of the energy surface at constant A will be defined by a single parabola only if A is odd but the same reasoning applies for the condition of "even A" in which odd-odd nuclei lie on a parabola of higher energy than even-even nuclei since alpha-decay is a transition between the same nuclear types.

The above explanation with Fig. 2 considers the parabolic sections of the energy surface to be identical and displaced uniformly on the energy axis. Obviously neither assumption conforms to reality and some further deductions on the shape of the surface may be obtained from more detailed consideration of the alpha-decay data. To do this it is helpful to visualize which parts of the energy surface are under consideration. Accordingly, a schematic sketch is presented as Fig. 3** in which the vertical axis is some function of the mass such as mass defect and the other coordinates are the atomic number and mass number as indicated. The surface has been idealized in that it shows none of the irregularities due to *odd* and *even* relationships but these need not enter into the present considerations of alpha-decay because alpha-transitions occur between the nuclei of the same type. Some contours of constant Z and constant A have been entered as well as a few reference points. Some sharp irregularities are noted in the lower part of Fig. 3 and these will be discussed below. For the present it is worth considering what information may be obtained from alpha-decay data in the region above about mass number 216.

In Fig. 3 is shown a line *ab* which is the contour following the bottom of the valley and is sometimes called the *line of beta-stability*. One may also visualize contours parallel to this stability line which would connect nuclei of the same degree of beta-instability. From alpha-decay energies it is possible to obtain information on the slope of these contours and therefore of the surface. The alpha-decay energies do not indicate the slopes in the direction of the contours but at an angle skew to this direction somewhat as indicated in Fig. 3 by the arrow labeled "α". Bearing in mind this limitation in interpretation it is still possible to observe a definite trend in this region which may be described as a steep slope of the bottom of the valley above mass 216, a tendency toward a plateau between 224 and 236 followed by an increased slope at higher mass numbers. These numbers should not be taken rigidly as there are no sharp breaks in slope and there may be superimposed other effects in a direction not parallel with the valley.

The manner in which these inferences were made may be clarified by reference to Fig. 4. Here are plotted the alpha-decay energies as a function of mass number, and nuclei of constant Z are connected (with light lines) as in Fig. 1. The contours shown in heavy lines on Fig. 4 are intended to map regions of constant degree of beta-instability. For example, the contour XY joins points along the stability line *ab* in Fig. 3, lower contours join points on the Bohr-Wheeler parabolas of Z lower than the most stable value of Z and the contours above XY go through points of higher values of Z than the most stable. The ordinate value, that is the alpha-energy, for each contour is seen to go through a minimum indicating a minimum slope to the energy surface in that region. The reason for the vertical displacement of the contours in Fig. 4 may best be visualized by examining the model in Fig. 3. Since alpha-decay proceeds in a direction skew to that of the valley the alpha-energies of points on the left-hand slope of the valley will become progressively greater the farther one proceeds up the

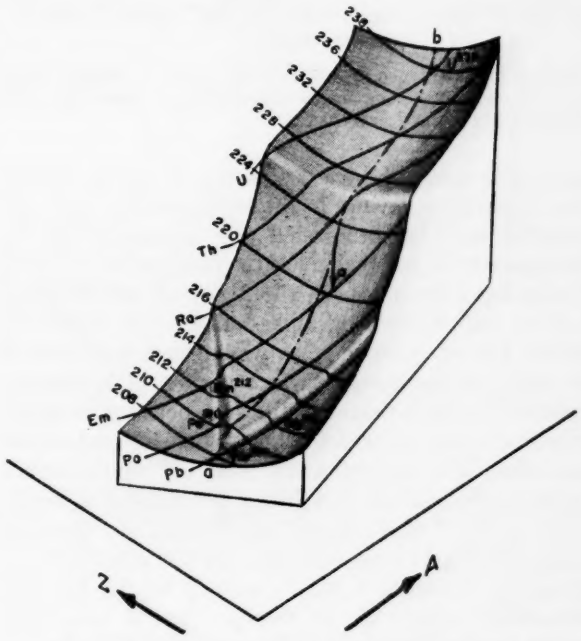

FIG. 3. Energy surface in the heavy element region.

[19] T. P. Kohman, Phys. Rev. **76**, 448 (1949).

** We wish to thank Mr. Robert Olson for the preparation of this sketch.

slope and they will become lower the farther one proceeds up the other slope.

One may also examine contours in the direction of alpha-decay in which points along an alpha-decay sequence are joined. Some of these are shown as dotted lines in Fig. 4 and again show minima. Here, however, the minima arise from at least two effects, the first caused by the plateau in the direction of the valley and the second effect is that of crossing from one slope of the valley to the other.

It is not possible to attach to this plateau any precise

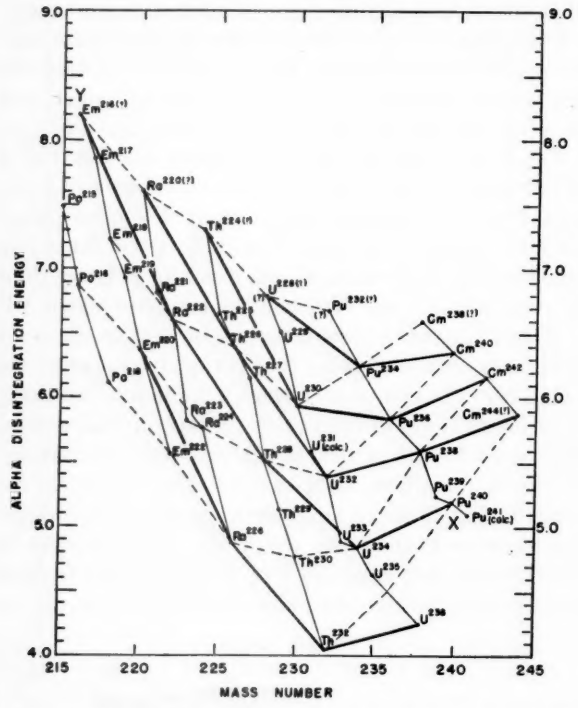

FIG. 4. Alpha-energies trends of heavy nuclides. (Heavy solid lines join nuclides of comparable beta-stability; broken lines join nuclides along alpha-decay chain.)

meaning in terms of nuclear structure in the sense that some sharp irregularities in the region around lead and polonium may be interpreted (see discussion below). The existence of this region has the practical importance of allowing a few nuclei in the region of beta-stability to have sufficiently long alpha-half-lives to persist in nature. Let us examine what would have happened if the slope of the energy surface were a little steeper. Then U^{238} which is assumed still to be beta-stable might have had a ten- or 20-fold shorter half-life and would have essentially decayed away. Now U^{240} would have a longer alpha-half-life but being beta-unstable would decay to Pu^{240} which would again have too short an alpha-half-life. It may be stated that the conditions for persisting in nature is that a nuclide be the heaviest beta-stable isotope of the element, that is that it lie on the proper side of the valley, and that it lie on this plateau. Apparently only two nuclei fulfill these conditions, Th^{232} and U^{238}. The other nucleus with long half-life, U^{235}, is found in nature for another reason having to do with an abnormally long half-life for its decay energy. This will become clearer when half-lives are discussed.

Returning to Fig. 1 it is seen that the smooth trend in energy *vs.* mass number between the heaviest and lightest isotopes of each element from emanation to curium no longer applies to elements below emanation and in fact even emanation and francium now have identified isotopes which do not fall in this sequence. Here the trend of increase in alpha-energy with decrease in mass number is apparent for the heaviest isotopes of each element but a point is reached at which there is a sharp break and alpha-energy decreases with decrease in mass number. At still lower mass numbers there is a minimum in the curve and the initial trend is again resumed.

Bismuth isotopes present an interesting case in that alpha-activity disappears over a wide range of mass numbers and then reappears at very low masses. The condition of increase in alpha-energy with decrease in mass number is fulfilled from Bi^{214} to Bi^{211} while Bi^{210} has a much lower alpha-energy and Bi^{209} (stable bismuth) has an alpha-energy less than 4 Mev as inferred from the inability to detect its alpha-activity. Several bismuth isotopes in the range Bi^{202}—Bi^{207} are known[3,20] but none of these has detectable alpha-activity. However, at still lower mass numbers (Bi^{201} and lower) alpha-activity again appears. The same trend but at higher energies is noted for polonium and astatine and probably for higher elements.

This behavior may be explained by a sharp irregularity in the energy surface of the form indicated in the lower part of the model shown in Fig. 3. It may readily be seen that the Bohr-Wheeler "parabolas" at constant A have a decided depression included as an irregularity and with this it is possible to explain the observed inversion in alpha-energies in a manner similar to that used in Fig. 2. Another method that may be used is to consider contours of the energy surface at constant Z. This has been done in schematic fashion in Fig. 5 for $Z=84$ and $Z=82$. The lengths of the arrows indicate the alpha-energies for the polonium isotopes of the mass numbers indicated and the sequence showing increase in alpha-energy from Po^{220} to Po^{212} followed by a sharp decrease and gradual increase in progressing to lower mass numbers are indicated in this fashion. The exact shapes of these contours must not be taken seriously beyond the point that they will have some such shape if the irregularity in the energy surface sets in at some line of constant neutron number as shown in Fig. 3. The changes in slope of the curves of Fig. 5

[20] Bi^{202} and Bi^{205} decay by electron capture with half-lives of about 2 hr. and 14 days, respectively (D. G. Karraker and D. H. Templeton, unpublished data); Bi^{203} decays by electron capture with 12-hr. half-life (H. M. Neumann and I. Perlman, unpublished).

are made to fit the observed alpha-decay data. It will be noted that the contours were drawn through even-even nuclei only. This was done in order not to complicate the drawing by odd-even alternations. The meaning of the inversion in alpha-energies noted in this region is attributable to abnormally strong nuclear binding associated with 126 neutrons and will be discussed further below.

The preceding paragraphs have dealt with the explanation of the general trends in alpha-decay energies. It is the purpose here to discuss the data presented in Fig. 1 and to point out some of the deductions which can be reached concerning the properties of a number of individual nuclides.

Evaluation of Data

It is inherent in most of the methods used for determining alpha-energies that fairly accurate values are obtained. Almost none of the energies shown should be in error by more than 100 kev, and most of them are known with considerably better accuracy. It will be seen in the final section of this paper that there is hope of making calculations of nuclear radius from alpha-decay data in which uncertainties in alpha-energy of the order of only 10 kev would be meaningful and undesirable. However, for the present considerations such accuracy is not necessary to observe the general trends and the principal uncertainties in interpretation that arise from other sources. There are a number of cases of uncertain assignment of mass number and these are indicated in Fig. 1 by superscript question marks following the mass number. In no cases were the assignments as indicated purely arbitrary; for example, the four neutron deficient bismuth alpha-emitters were arranged in the order shown by excitation function data and the mass numbers of some were assigned by observing the genetic relationship with the lead and thallium daughters arising through successive electron capture decay.[21]

Other entries in Fig. 1 are accompanied by question marks preceding the symbol as in the case of Pu^{232} indicating uncertainty of the energy value, due in this instance to the lack of resolution of this group from others formed in the same irradiation. All energies which are calculated or estimated are similarly denoted.

Beyond the uncertainties already mentioned it should be realized that total decay energy is the property which should be compared and there has been a tacit assumption that the alpha-energies shown represent ground state transitions. Where this condition is known not to apply, corrections have been made by addition of the gamma-ray energy as in the cases of U^{235} and Am^{241} (see Appendix for details). There is good reason to believe that there may be many cases, as yet unproved, in which the observed alpha-particles do not correspond to the ground state transitions. As examples, Pu^{239} and U^{233}, both of which would seem to be out of line in Fig. 1, have associated with them considerable gamma-radiation[3] which may mean that the alpha-groups of the ground state transitions have not been observed. Further reasons lending credence to the existence of this phenomenon will be brought out in the discussion of half-life *vs.* energy relationships.

The alpha-energies for three of the entries, Bi^{210}(RaE), Pu^{241} and Am^{242}, have been calculated from closed decay cycles since the alpha-particles could not be measured directly. In all three cases the alpha-decay process has been evidenced by the appearance of the daughter isotope. Broda and Feather[22] identified the 4-min. thallium as the alpha-decay daughter of RaE and using its beta-decay energy, that of RaE and the alpha-energy of Po^{210}, it was possible to calculate the alpha-energy of RaE. The following diagrams designate the data used in calculating the alpha-energies for Pu^{241} and Am^{242} (see Appendix for further discussion).

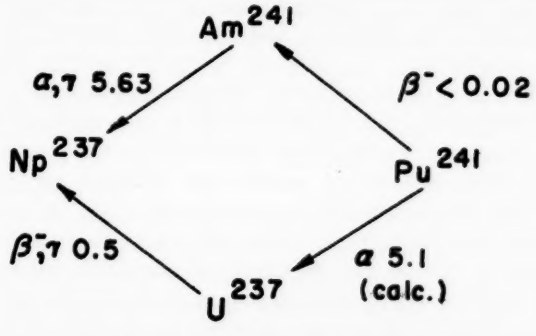

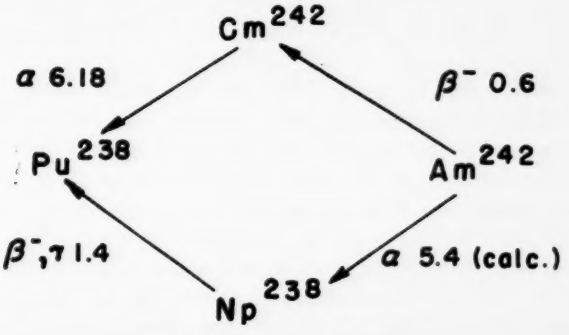

Bismuth and Neighboring Elements, the Effect of 126 Neutrons

The recently discovered alpha-radioactivity of highly neutron deficient bismuth isotopes (Fig. 1) is of interest in marking the "reappearance" of alpha-radioactivity in bismuth at a considerable departure in mass number from the alpha-emitters among the natural radioactivities. A possible explanation has already been advanced in which the trend in alpha-energies for these light bismuth, polonium, and astatine isotopes is

[21] H. M. Neumann and I. Perlman (unpublished).
[22] E. Broda and N. Feather, Proc. Roy. Soc. (London) **A190**, 20 (1947).

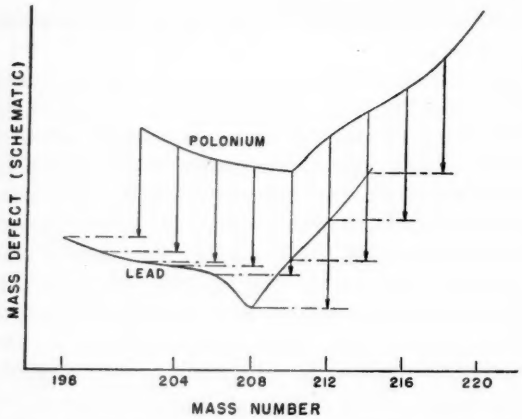

FIG. 5. Schematic sections of energy surface at $Z=84$ and $Z=82$ illustrating trend of alpha-energies of the polonium isotopes (arrows drawn at polonium isotope mass number; length of arrows proportional to alpha-energy).

thought to be a resumption of the trend which all of the heavy isotopes show, namely an increase in alpha-energy with decrease in mass number. This resumption in trend follows an interruption caused by a region of abnormally great nuclear binding.

From the data at hand it is readily seen why no alpha-activity has been noted for previously known isotopes such as Bi^{206} and Bi^{204}. By extrapolations of the curves for bismuth in Fig. 1 it may be estimated that these isotopes have alpha-decay energies around or below 4 Mev. For this energy the alpha-half-life would be perhaps greater than 10^8 years and therefore alpha-particles would be undetectable. As will be discussed below, it would be illuminating to have available the partial decay constants for alpha-emission for these electron capturing bismuth isotopes since the relationship between half-life and energy gives further information on nuclear binding through the effect on nuclear radius. The 5.15-Mev alpha-emitter thought to be Bi^{201} has a measured half-life of one hour and even a crude estimate of its alpha-decay half-life would set it at about 50 years illustrating the extremely low alpha-branching.

The reappearance of high alpha-energies which allow alpha-emission to be detected for the highly neutron deficient isotopes of bismuth, polonium, and astatine gives rise to the thought that elements of still lower atomic number might similarly show alpha-activity. This matter has been considered at greater length by Kohman.[19] Recently in this laboratory[23] there has been observed a number of short-lived alpha-emitters in this region following irradiations of gold with high energy deuterons and two of these have been tentatively assigned to isotopes of gold and mercury. On the other hand, similar experiments[24] were able to show no alpha-activity in lead. This may mean that the region of stability which causes a decrease in alpha-energy and abnormal increase in half-life in a localized region for astatine, polonium, and bismuth is intensified and broadened at the position of lead and possibly thallium so that alpha-activity is no longer exhibited. When this region is passed, alpha-energies and alpha-decay constants are again sufficiently high especially for neutron deficient isotopes.

In considering the reason for the inversion in alpha-energies of bismuth, polonium, and astatine it is necessary to postulate a region of abnormally stable nuclear binding. In proceeding from high toward low mass numbers there is good evidence that this effect sets in at some constant neutron number for each element as indicated in Fig. 3. Thus the highest alpha-energies for bismuth and polonium occur for the isotopes Bi^{211} and Po^{212} and for astatine probably at At^{213} (see next section). All of these decay by alpha-emission into nuclei with 126 neutrons and it is probable that at this neutron number there is abnormally stable nuclear structure as compared with nuclei having greater neutron number.[25,26] It may be worth pointing out that insofar as alpha-decay energies are an index there is no sharp discontinuity in nuclear binding below 126 neutrons as there is above this number.

Neither from Fig. 1 nor from the theory is there any quantitative way of telling how many elements beyond astatine this effect of 126 neutrons will make itself felt. In Fig. 3 the depression in the energy surface due to the 126 neutron configuration is shown to extend to element 88, radium. It may also be seen that for each successive element, the minimum in alpha-energy caused by the depression should lie at progressively higher alpha-energies. Examining the isotopes of Bi, Po, and At, each with 126 neutrons, the alpha-energies are respectively <4 Mev, 5.3 Mev, and 5.9 Mev. Because the differences between successive elements seem to be converging it is difficult to extrapolate to the next nucleus with 126 neutrons, Em^{212}, but a reasonable guess is that its alpha-energy will not be more than 6.4 Mev. As will be pointed out the alpha-decay for nuclei with 126 neutrons or less is highly forbidden and from the curves of Fig. 9 one might expect a half-life for Em^{212} in the range several minutes to an hour, depending, of course upon its energy. Because of the 126 neutron configuration, Em^{212} is possibly sufficiently stabilized to be beta-stable. As a result one would predict that at least this light isotope of emanation should be observable. In summary, as far as predictions are concerned, there is good reason to believe that the curve for emanation (element 86) in Fig. 1 will reach a maximum at Em^{214} and then at lower mass numbers will descend into a region in which the nuclei will have alpha-energies in the range of about 6 Mev.

Very recently in this laboratory,[27,28] attempts have

[23] Thompson, Ghiorso, Rasmussen, and Seaborg, Phys. Rev. 76, 1406 (1949).
[24] D. G. Karraker and D. H. Templeton, unpublished data.
[25] W. Elsasser, J. de phys. et rad. 5, 625 (1934).
[26] M. G. Mayer, Phys. Rev. 74, 235 (1948).
[27] Ghiorso, Meinke, and Seaborg, Phys. Rev. 76, 1414 (1949).
[28] Hyde, Ghiorso, and Seaborg (unpublished).

been made to prepare emanation and francium isotopes of low mass number by spallation of thorium with high energy protons. It was found that there are indeed alpha-emitters in the predicted energy region which must be ascribed to nuclei of lower mass number for these elements than any which had been heretofore examined. In particular, two of these activities have been assigned; a 23-min. period with particles of 6.17 Mev energy to Em^{212}, and a 19-min. period with 6.25 Mev alpha-particle energy to Fr^{212}.

Although this same effect may exist for several higher elements it should become less pronounced and increasingly difficult to observe since not only will the alpha-half-lives be expected to become shorter for higher elements due to larger alpha-energies but at constant neutron number the affected nuclides will be progressively more highly neutron deficient and therefore have short electron capture half-lives.

PREDICTIONS OF NUCLEAR PROPERTIES

Methods and Examples

It is apparent that one may use the correlations of Fig. 1 to predict the alpha-energies of many nuclides just as has been done previously by a number of workers without the benefit of the comprehensive data now available as a guide. In addition, one may use the half-life *vs.* energy correlations which are taken up in a later part of this paper to predict alpha-half-lives. There will be no attempt here to compile a list of predicted nuclear properties of presently unknown species or modes of decay. However, there are a number of generalities of some importance which may be reached through the use of particular data either available or obtainable by prediction, and some of these will be examined. One of these, having to do with relatively long-lived alpha-activities of emanation and francium isotopes of low mass number, has already been discussed. A brief recapitulation of the premises used and methods which are applied may be in order.

The first consideration is that all nuclides in the region under discussion are thermodynamically alpha-unstable and almost all which are either found in nature or artificially prepared would have measurable alpha-activity if alpha-decay were the only type of instability in force. However, alpha-decay may not be discernible in beta-unstable nuclei if the ratio of beta-half-life to alpha-half-life is extremely small. Likewise, a beta-unstable nuclide may not sensibly exhibit its beta-instability if the alpha-half-life is extremely short.

There are a number of reasons for wishing to know whether a nucleus is beta-stable or unstable irrespective of its alpha-decay properties. The beta-stable nuclei in this region are entirely analogous to the stable nuclei lower in the periodic table and their pattern constitutes a source of information on nuclear structure. An example of this will appear in a later section in which is discussed the possibility that astatine (element 85) has no beta-stable isotopes as is apparently the case for two other elements technetium (element 43) and prometheum (element 61). Another, quite different, use of the knowledge of beta-stability has to do with the preparation of nuclear species through the beta-decay process. As an example, the validity of the difficult measurements showing that astatine isotopes arise from rare beta-branching of the "*A* products" (polonium isotopes) of the natural radioactive series must clearly be questioned for these "*A* products" which can be reasonably proved to be beta-stable. All in all, the question of beta-stability is of great importance and an attempt is made (Table I) to list the heavy nuclides accordingly.

Beyond predictions of *type* it is also important to predict *degree* which, for alpha-emission, is the principal part of this paper. The accurate forecast of alpha-half-life along with similar predictions with regard to beta-stability are the requirements in determining how best to prepare and identify unknown species of interest. Such predictions were invaluable in preparing successively the transuranium elements, the transplutonium elements and are the guiding factors in attempting to prepare still higher elements. Therefore, in addition to alpha-decay predictions, it is often important to estimate beta-decay and electron capture decay energies and through modified Sargent diagrams, the half-lives.

The methods of making these predictions vary in kind and reliability. Alpha-energies may be read off a plot such as Fig. 1 by interpolation or extrapolation bearing in mind the sharp changes which occur in the nuclei near closed shell configurations. For example, one may be fairly certain that the alpha-energy of Em^{221} lies between those of Em^{220} and Em^{222} and has an energy of 6.0 ± 0.1 Mev; on the other hand, it would undoubtedly be erroneous to assign At^{213} an alpha-energy between At^{214} and At^{212} since from other correlations we would infer that At^{213} has a higher energy than At^{214} (as shown in Fig. 1) in an analogous fashion to the pairs $Bi^{211}-Bi^{212}$ and $Po^{212}-Po^{213}$.

With information on some decay energies it is often possible to calculate others making use of decay cycles the simplest type of which is shown as follows:

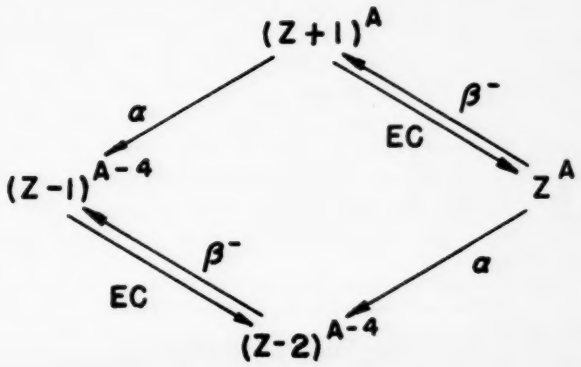

If any three members are known, the fourth is uniquely determined. Sometimes approximations can be made with very little experimental information which in turn can lead to important deductions. As an example, we may use alpha-decay energies to deduce something about nuclear spins near closed neutron and proton shells. The case in point is to obtain information on the spin of Pb^{209} which has one neutron beyond the "closed shell" 126 and Po^{209} which has one neutron less than 126. Known information is shown on the following diagrams with broken line arrows indicating paths of decay not yet observed.

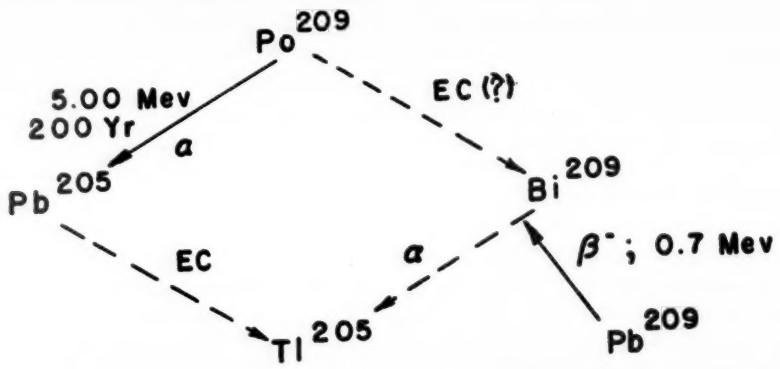

From the failure to observe alpha activity in natural bismuth (minimum half-life $\sim 10^{12}$ yr.) and making use of the half-life energy relationships considered in a following part of this paper, it is almost certain that Bi^{209} has an alpha-decay energy less than 4 Mev and it could be considerably below this, say 3 Mev. Since Pb^{205} must be heavier than Tl^{205} one can immediately decide that Po^{209} is at least 1 Mev heavier than Bi^{209} and perhaps considerably heavier. In preparations of Po^{209} showing considerable alpha-activity the number of x-rays from the electron capture process allows one to set an upper limit of 10 percent for the electron capture branching making the minimum half-life for this mode of decay 2000 years.[24] Realizing that this is a minimum value for the half-life and that the decay energy is at least 1 Mev and might be considerably greater, the decay process is seen to be highly forbidden when compared with a large number of other cases which indicate a half-life of about 100 min. for this decay energy.[29] The spin of Bi^{209} is known to be 9/2 and since one must postulate a large spin change in the $Po^{209}-Bi^{209}$ transition, it is necessary to assign a small spin number such as 1/2 to Po^{209}.

The other isobar decaying to Bi^{209} is Pb^{209} of the U^{233} family which has a 3.3 hr. half-life and 0.7 Mev decay energy. This half-life and energy correspond to an allowed transition which Feather and Richardson[30] associate with a spin change of -1. On this basis one would assign the huge spin number 11/2 to Pb^{209} but in any case it must be close to that of Bi^{209} and therefore large. The point to be made is that Pb^{209} with 127 neutrons has one neutron beyond the configuration 126 and according to Mayer[31] the extra neutron should indeed be in the $7i$ level with spin term $i_{11/2}$. Turning to Po^{209} it is seen that it has 125 neutrons, one below the closed shell of 126. According to the term schemes of Mayer, the last levels to be filled in the shell have the spin term $i_{13/2}$ but as is noted for previous shells these high spin number levels fill only in pairs and there is crossing with a level of lower spin number. In this case the 125th neutron would bear the spin term $4p_{1/2}$ which Mayer lists as the closest level to the first i levels. It is seen that this assignment is in good agreement with the electron capture decay properties of Po^{209} elaborated above. It might be mentioned that Pb^{207} should be an analogous nucleus (125 neutrons) and Nordheim,[32] Mayer,[31] and Feenberg and Hammack[33] assign the odd neutron to a $4p$ state with spin 1/2.

For further illustration of the use of alpha-decay data in predicting nuclear properties the cases of two astatine isotopes will be considered.

One of these has to do with the alpha-energy of At^{213} indicated to be 9.2 Mev in Fig. 1 although this is only a prediction. It will be noted that At^{214} has almost the same alpha-energy as ThC′(Po^{212}) the most energetic alpha-emitter previously known and it would be of interest to know whether At^{213} has still higher decay energy. The point of uncertainty is whether or not Po^{213} is beta-stable and if so what the At^{213} electron capture energy is. Although this cannot be predicted for sure it is probable that it is either β^--stable or is only very slightly unstable with respect to At^{213}. The beta-stability of Po^{213} is discussed in a following section on *beta-stability*. Taking the $Po^{213}-At^{213}$ beta-decay energy as zero, the total decay energy of the Pb^{209} beta-transition as 0.70 Mev and the alpha-energy of Po^{213} as 8.5 Mev, then the alpha-energy of At^{213} is calculated to be 9.2 Mev. This energy would conform with the hypothesis that the highest alpha-energy in this region will reside

[29] S. G. Thompson, Phys. Rev. **76**, 319 (1949).
[30] N. Feather and H. O. W. Richardson, Proc. Phys. Soc. **61**, 452 (1948).
[31] M. G. Mayer, Phys. Rev. **75**, 1969 (1949).
[32] L. W. Nordheim, Phys. Rev. **75**, 1894 (1949).
[33] E. Feenberg and K. C. Hammack, Phys. Rev. **75**, 1877 (1949).

for each element in that isotope which decays to a product with 126 neutrons, in this case $At^{213} \rightarrow Bi^{209}$. To this estimated decay energy of At^{213} must be added the electron capture energy of At^{213} or the β^--energy of Po^{213} must be subtracted, whichever applies.

At^{216} is reported by Karlik and Bernert[34] to arise in the thorium decay series through β^--branching in the decay of ThA(Po^{216}). These authors noted a weak 7.57-Mev alpha-group which decayed with the half-life of separated thoron (Em^{220}) and was attributed to ~0.01 percent branching in ThA decay according to the following scheme:

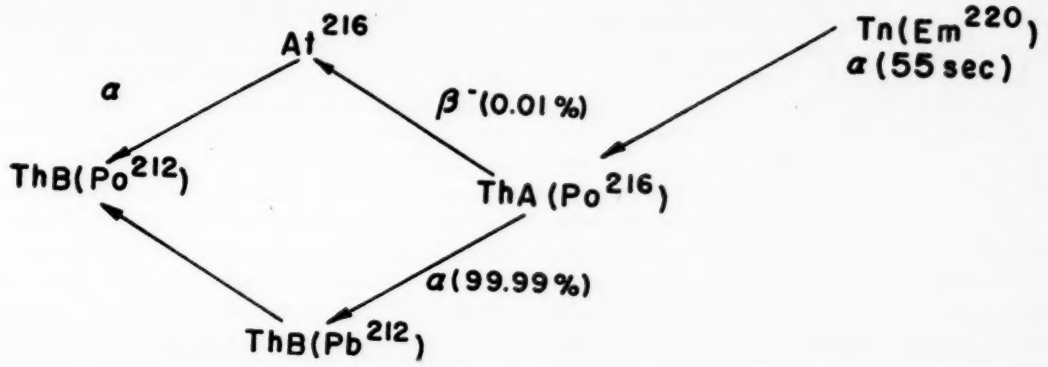

Karlik and Bernert have pointed out a serious difficulty in this interpretation since in summing the decay energies in the closed cycle it turns out that At^{216} (using their value for the alpha-energy of At^{216}) is actually unstable with respect to ThA by 0.15 Mev while the apparently observed β^--branching of ThA would demand an estimated energy of 1 Mev in the opposite direction, thus introducing a discrepancy of 1.15 Mev. They suggest an explanation retaining their assignment of the 7.57-Mev alpha-group to At^{216} by assuming that ThB decays only to a 1.15-Mev excited state of Bi^{212}(ThC) while the alpha-decay of At^{216} proceeds to the ground state. This explanation seems untenable for a number of reasons. If ThC represents the postulated excited state of Bi^{212} then the alpha-energy of the ground state would be 1.15 Mev lower than the measured value (6.1 Mev), that is, about 5.0 Mev. From Fig. 1 it is seen that whereas 6.1 Mev falls directly in line between the energies for Bi^{211} and Bi^{213} a value of 5.0 Mev would be completely out of line. In addition, the explanation is in conflict with the known properties of the collateral decay series[8] starting with 22-hr. Pa^{228} because in this series At^{216} arising from the alpha-decay of Fr^{220} decays to Bi^{212} identical in properties with ThC, that is, the 6.1-Mev energy is noted which would not be possible if At^{216} must decay to the ground state of an isotope for which ThC is an excited state. That the entire Pa^{228} decay series has been wrongly assigned is highly improbable because of the identification of RdTh(Th^{228}) from electron capture branching of Pa^{228}, of ThX(Ra^{224}) from electron capture branching of Ac^{224} and ThC′(Po^{212}) from the β^--decay of ThC(Bi^{212}). All in all, it appears to be highly unlikely that ThA(Po^{216}) is β^--unstable and therefore the 7.57-Mev alpha-group in Tn must arise from some mechanism not involving At^{216}. The At^{216} could not come from Fr^{220} formed by β^--branching of Em^{220} since Em^{220} is surely β^--stable. Perhaps some such explanation as that offered by Feather[35] for the observation of Karlik and Bernert is correct.

These examples of the use of alpha-decay data may serve to indicate some of the methods which have found application while in the following are presented some ideas on beta-stability, the transuranium elements and the rare earth region.

Beta-Stability in the Heavy Elements

As illustrated by the discussion of whether or not At^{216} could arise from the thorium radioactive family it is often important to be able to predict beta-stability. Many of the short-lived alpha-emitters are beta-unstable but this instability is not noted because of overwhelming competition by alpha-decay. Nevertheless, the degree of beta-instability can often be calculated by means of closed decay cycles and conversely the beta-energies can serve as important links in calculating alpha-energies and in predicting branched decay. No attempt will be made in this report to show the calculations of beta-decay energies and Table I tells only whether or not a nuclide is known to be beta-stable or predicted to be so. Predictions are in parentheses. A recent table of Biswas and Mukherjee[36] listing types of instability, differs in some instances from Table I and does not give predictions of unobserved modes of instability or for unknown species.

The greatest uncertainties in predictions of beta-stability involve choosing which isotopes, if any, of astatine and francium are beta-stable. Measurements in this laboratory[8] on the alpha-energy of At^{216} gave 7.79 Mev which when used with the alpha-energy of Po^{216}(ThA) and the decay energy of Pb^{212}(ThB) allows

[34] B. Karlik and T. Bernert, Zeits. f. Physik **123**, 51 (1944).

[35] N. Feather, Nucleonics **5**, 22 (1949).

[36] S. Biswas and A. Mukherjee, Ind. J. Phys. **22**, 80 (1948).

one to calculate that At^{216} is unstable with respect to electron capture to Po^{216} by 0.4 Mev. In a similar fashion, making use of the newly measured[8] alpha-energy of At^{214}, it is possible to show that Po^{214}(RaC′) is beta-stable. Under such circumstances in which both Po^{216} and Po^{214} are beta-stable it is usual that Po^{213} would be expected to be beta-stable, although there are a number of cases known in which there are two beta-unstable even-odd isotopes of lower mass number than the heaviest beta-stable even-even isotope. By closing a decay cycle involving Po^{213}, At^{213}, Pb^{209}, and Bi^{209}, it may be shown that At^{213} must have an alpha-decay energy in excess of 9.20 Mev in order that At^{213} be heavier than Po^{213}. All that can be said from extrapolation in Fig. 1 is that At^{213} could have an alpha-decay energy this high. As a result the question as to whether or not At^{213} is beta-stable cannot be resolved at present.

The other most likely beta-stable isotope of astatine is At^{215}. Here it can be shown that Po^{215} is ~0.8 Mev heavier than At^{215} but it is not at all certain that At^{215} is stable with respect to Em^{215}.

Regarding this question of whether At^{215} is beta-stable with respect to Em^{215} it is possible to show that this is a borderline case insofar as the estimations are valid just as was found for the isobars At^{213}—Po^{213}. The following decay cycle may be drawn with the known values for the decay energies indicated. One may estimate the alpha-decay energy of Em^{215} from Fig. 1 and from this, close the cycle to determine

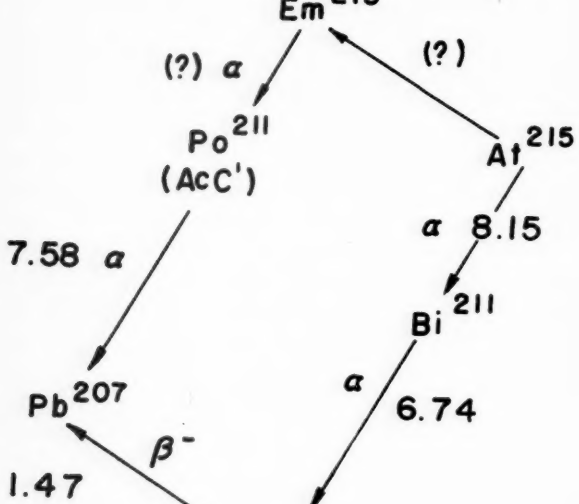

whether Em^{215} or At^{215} is heavier, or alternately, set these isobars equal and determine the alpha-energy which Em^{215} would have to have to satisfy this condition. It is found accordingly that if the alpha-energy of Em^{215} is less than 8.79 Mev then Em^{215} is beta-stable and At^{215} is beta-unstable. In examining Fig. 1 it is seen that the requirement falls in the range of estimation (8.7–8.9) and it may be said that there is probably no more 100 kev difference between Em^{215} and At^{215}. It should be mentioned that the most likely revisions that may be required in the measured values shown in the above decay sequences are in the direction of making At^{215} heavier.

The possible beta-stable isotopes of astatine discussed above are At^{213} and At^{215}. Higher isotopes of astatine such as At^{217} are clearly beta-unstable.

Since there is no measurable isotope of astatine which can be proved to be beta-stable the question arises whether such exists or whether astatine is like two of the other missing elements, technetium (element 43) and prometheum (element 61), which probably have no beta-stable isotopes. In considering this point there are some remarkable analogies between these three elements which upon examination draw attention to a possible reason why no beta-stable isotopes exist. This has to do with the positions which the elements hold with respect to positions of stable configurations or "closed shells" in nuclear structure.¶

In the case of technetium it is necessary to examine the effect of neutron number 50 which apparently promotes added stability in nuclei in which it appears. It should be remembered that in general only one isotope of an odd element has a chance of being stable with respect to its even-element isobars. For technetium one might predict this isotope to be Tc^{97} since it lies midway between $_{39}Cb^{93}$ and $_{45}Rh^{101}$. However, Tc^{97} has two pairs of neutrons beyond the stable configuration of 50 neutrons and since such neutrons may be assumed to have abnormally low binding energies this may be just sufficient to cause it to be heavier than one of its isobars especially if the added assumption is made that for an even element the "closed neutron shell" has a smaller effect on neutron binding energies beyond the shell. From this reasoning all that can be said is that an odd element near the upper limit of elements which have a stable isotope with the neutron number of abnormal stability should be affected but not enough is known about the fine points of nuclear binding to predict whether the affected element should be niobium (41) or technetium (43).

Prometheum (element 61) is in an analogous position with respect to neutron number 82. Here there is a long list of stable nuclei, namely, $_{54}Xe^{136}$, $_{56}Ba^{138}$, $_{57}La^{139}$, $_{58}Ce^{140}$, $_{59}Pr^{141}$, $_{60}Nd^{142}$, $_{62}Sm^{144}$. The remarkable stabilization of 82 neutrons allows both La^{139} and Pr^{141} to be beta-stable even though they differ by just two protons and is presumably responsible for the absence of any stable isotope in the next odd element, prometheum, through reasoning similar to that used for technetium.

¶ *Note added in proof.*—In an article which came to our attention since the preparation of this manuscript, A. Broniewski (Comptes Rendus **228**, 916 (1949)) had already noted the occurrence of the missing elements 43 and 61 near positions of closed neutron shells.

TABLE I. Beta-stability in the heavy elements.*

Element	Beta-stable	*EC* unstable	β^--unstable	*EC* and β^--unstable
bismuth	Bi^{209}	Bi^{197}–Bi^{206}, (Bi^{207})	Bi^{210}–Bi^{214}	(Bi^{208})
polonium	Po^{208}, Po^{210}, Po^{211}, (Po^{212}), $(Po^{213}?)$, (Po^{214}), (Po^{216})	Po^{202}, (Po^{203}), Po^{204}–Po^{207}, (Po^{209})	Po^{215}, (Po^{217}), Po^{218}	
astatine		At^{204}–At^{211}, $(At^{213}?)$	$(At^{215}?)$, (At^{217}, At^{218})	$(At^{212}?)$, (At^{214}), (At^{216})
emanation	$(Em^{212}?)$, (Em^{214}), $(Em^{215}?)$, $(Em^{216}$–$Em^{218})$, Em^{220}, Em^{222}	(Em^{213})	$(Em^{219}?)$, (Em^{221})	
francium	$(Fr^{219}?)$	(Fr^{213})	(Fr^{221}), Fr^{223}	(Fr^{220}, Fr^{222})
radium	$(Ra^{218}, Ra^{220}, Ra^{221})$, Ra^{222}–Ra^{224}, Ra^{226}	$(Ra^{219}?)$	Ra^{225}, Ra^{227}, Ra^{228}	
actinium	Ac^{225}	(Ac^{222}), Ac^{223}	Ac^{226}, Ac^{227}, Ac^{228}	(Ac^{224}, Ac^{226})
thorium	(Th^{224}, Th^{226}), Th^{227}–Th^{230}, Th^{232}	(Th^{223}), Th^{225}	Th^{231}, Th^{233}, Th^{234}	
protactinium	Pa^{231}	(Pa^{226}), Pa^{227}–Pa^{229}	Pa^{232}, Pa^{233}, Pa^{234}	Pa^{230}, (Pa^{232})
uranium	U^{230}, U^{232}–U^{235}, (U^{236}), U^{238}	(U^{227}), U^{228}, U^{229}, U^{231}	U^{237}, U^{239}	
neptunium	Np^{237}	Np^{231}, (Np^{232}), Np^{233}–Np^{235}	Np^{238}, Np^{239}	(Np^{236}, Np^{238})
plutonium	Pu^{236}, Pu^{238}–Pu^{240}, (Pu^{242}, Pu^{244})	(Pu^{232}, Pu^{233}), Pu^{234}, (Pu^{235}), Pu^{237}	Pu^{241}, (Pu^{243})	
americium	Am^{241}, $(Am^{243}?)$	Am^{238}–Am^{240}	Am^{242}, (Am^{244})	(Am^{242})
curium	Cm^{242}, $(Cm^{244}$–$Cm^{246}, Cm^{248})$	Cm^{238}, (Cm^{239}), $(Cm^{240}?)$, Cm^{241}, $(Cm^{243}?)$	(Cm^{247}, Cm^{249})	
element 97	(97^{247})			

* Predictions are enclosed in parentheses.

The next apparent stabilizing neutron number occurs in the region of lead and is presumably the number 126. In the heaviest elements about two neutrons are added for each proton in building from element to element so it is not expected that there should be as many elements each with a stable isotope with the same neutron number as among the lighter elements. For neutron number 126, the known beta-stable nuclei are $_{82}Pb^{208}$, $_{83}Bi^{209}$, and $_{84}Po^{210}$. The interesting possibility has already been considered that $_{86}Em^{212}$ may be beta-stable. As is the case for neutron numbers 50 and 82 it may be expected that an odd element in this region will have no beta-stable isotope, and it is postulated here that astatine (element 85) is that element.

The only possible beta-stable isotopes of francium are Fr^{219} and Fr^{221} since Fr^{223} is known to decay to Ra^{223}(AcX). It is not possible to say for sure whether or not Fr^{219} is beta-stable although tentatively it is decided to be so. The question to be decided is which of the isobars Fr^{219} and Em^{219}(An) is heavier since Ra^{219} is almost surely unstable toward electron capture. A cycle containing these isobars and including At^{215}, AcA^{215}, AcB^{211}, AcC^{211} may be set up using values shown in Fig. 1 (see Table III) for the alpha-energies and 1.40 for the disintegration energy for AcB^{211}. When this is calculated it is found that Fr^{219} is beta-stable with respect to Em^{219}(An) by about 300 kev. In view of the arguments as to the beta-instability of Em^{219} it is almost certain that Em^{221} is a β^--emitter so that the consideration of the beta-stability of Fr^{221} revolve around whether or not Ra^{221} is electron capture unstable. Closing a cycle involving Ra^{221}, Fr^{221}, Em^{217}, Po^{213}, At^{217} and Bi^{213} it is found that Fr^{221} is 100 kev heavier than Ra^{221}, a difference which precludes a decision in view of the uncertainties in some of the data. Tentatively, the only beta-stable isotope of francium will be taken to be Fr^{219}.

Transuranium Elements

For the beta-stable nuclides and those with neutron excess the alpha-decay energies between comparable nuclei progressively increase above uranium. This effect has already been pointed out in the discussion of Fig. 4. This means that comparable nuclei (in their position with regard to the center of beta-stability for each element) will show increased alpha-energy and shorter half-life in going above uranium. If one were to assume that alpha-decay is the only means by which very heavy nuclei could spontaneously degrade to lighter nuclei this effect can be deduced independently of measured alpha-energy values by the fact that transuranium elements have not survived through geological time.

To illustrate this trend the alpha-energies of analogous nuclei are listed in Table II for this region for the even elements. Nuclides in the same horizontal row are considered analogous. A few values obtained by interpolation and extrapolation are included and appear in parentheses.

One of the uses to which these correlations may be put is the prediction of the nuclear properties of transcurium isotopes. The lightest beta-stable isotope of element 98 is 98^{246} or possibly 98^{248}. By following the trends noted 98^{246} and 98^{248} might be predicted to have alpha-energies of 6.8 and 6.6 Mev, respectively. The correlations of half-lives of even-even isotopes as shown in Fig. 6 allow one to extrapolate to element 98 and

TABLE II. Trends of alpha-energies of "comparable nuclei."

U^{232}—5.40	Pu^{238}—5.60	Cm^{244}—5.88
U^{233}—4.89	Pu^{239}—5.24	Cm^{245}—(5.7)
U^{234}—4.84	Pu^{240}—5.2	Cm^{246}—(5.6)
U^{235}—4.63	Pu^{239}—5.24	
	or	
	Pu^{241}—5.1	
U^{236}—(4.6)	Pu^{242}—(4.9)	

predict alpha-half-lives of a few days and about one month, respectively, for the isotopes 98^{246} and 98^{248}.

Alpha-Radioactivity in the Rare Earth Region

It is probably a safe assumption to make that alpha-active isotopes of almost all elements in the upper half of the periodic table may be produced by removal of a sufficient number of neutrons. A possible pattern which such alpha-emitters would follow has been suggested by Kohman.[19] In the region immediately below lead the departure from the region of beta-stability in which alpha-decay rate becomes appreciable is not so great but that the electron capture half-lives allow one to observe the alpha-activity. The gold and mercury alpha-emitters would fall in this category and these are also analogous to the bismuth alpha-emitters around mass number 200. In lower regions of the periodic table where the general slope of the packing fraction curve is less favorable for alpha-emission one might expect to find appreciable alpha-decay rates only at a sufficient degree of instability toward electron capture or positron decay that half-lives would be very short and detection of alpha-decay difficult. However, if there should be localized region of steep slope in packing fraction then a moderate degree of neutron deficiency may enhance the effect sufficiently to produce readily observable alpha-emitters. Just such a region has probably been found recently in this laboratory.

Thompson *et al.*,[23] have produced a number of alpha-active rare earths with half-lives in the range from a few minutes to a few days and alpha-particle energies in the range 4.2–3.1 Mev. Although these activities have not been positively assigned, it is likely that they belong to neutron deficient isotopes of gadolinium, terbium, dysprosium, and holmium, but not samarium and lower rare earths. A most attractive hypothesis is that these nuclei owe their high potential toward alpha-emission to their position relative to the stable configuration of 82 neutrons just as the most energetic alpha-particles in the heavy element region come from nuclei decaying to the vicinity of 126 neutrons. The difference in the case of the rare earths is that these nuclides will in almost all cases lie outside of the limits of beta-stability on the neutron deficient side and the energies of alpha-emitters with 84 neutrons will be relatively lower than those with 128 neutrons because of the generally lower slope of the packing fraction curve. In view of these considerations, it would seem likely that the currently discovered group of alpha-emitters will include and cluster around such nuclides as Gd^{148}, Tb^{149}, Dy^{150}, and Ho^{151}. Perhaps alpha-emission will not be noted for isotopes more than two mass units above Gd^{148} and about four mass units above Ho^{151}. One may turn to some previously available data for confirmatory evidence for this picture. It has long been noted that Sm^{146}, although surely beta-stable, is missing in natural samarium and presumed to be an alpha-emitter. This would indicate that samarium is the only element in this region for which an isotope with high alpha-energy falls within the limits of beta-stability. It would also be tempting to assign the long-lived alpha-emitter in natural samarium to Sm^{147} or Sm^{148} or both on this picture but the best direct evidence to date places the assignment at Sm^{152}.[37]

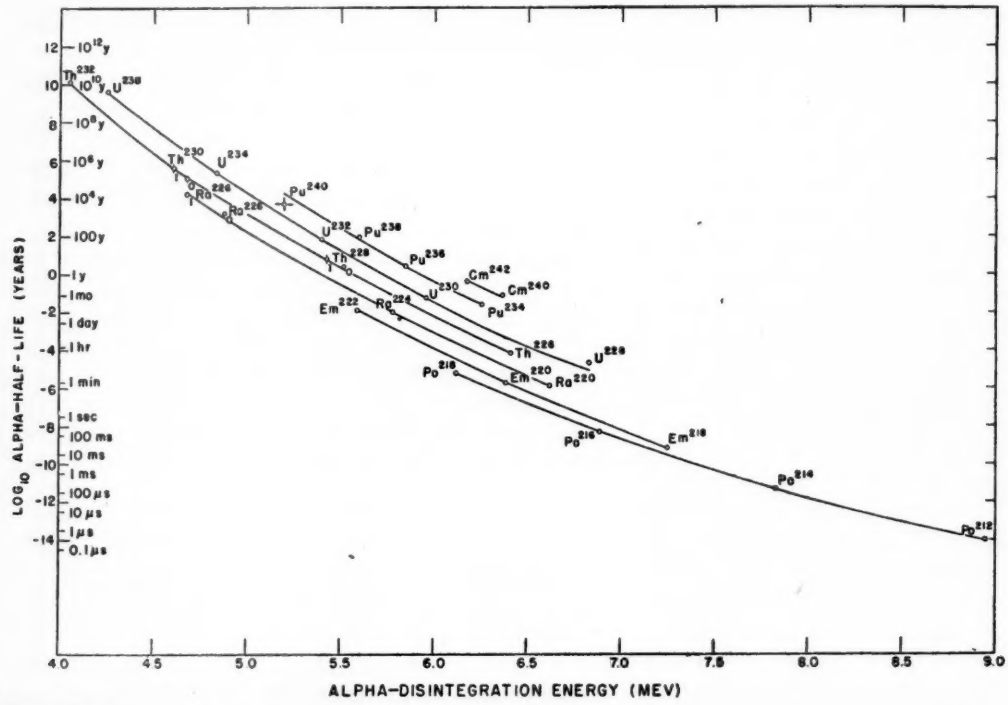

FIG. 6. Half-life *vs.* energy relationship for the even-even nuclides. (Roman numerals indicate short-range groups in fine structure and "0" the ground state transition.)

[37] A. J. Dempster, Phys. Rev. **73**, 1125 (1948).

ALPHA-DECAY RATE

On a simplified model of the alpha-decay process the alpha-particle is considered to exist as an entity within the nucleus of its decay product and its rate of emission is governed by the potential field of that nucleus. The factors which then determine the decay constant are the atomic number, the alpha-energy or velocity and the nuclear radius. For a particular decay energy, an increase in atomic number decreases the decay constant and decrease in nuclear radius decreases the decay constant through its effect in increasing the potential barrier. The quantum mechanical treatment for the decay process resulted in the well-known Gamow formula[2] of which there are a number of modifications and was remarkably successful in explaining the great sensitivity of decay constant to decay energy. The effect of atomic number is predicted to be much less striking and this is borne out by observation. The nuclear radius cannot be independently evaluated with the accuracy required and the formula has been used to calculate the "effective radius" which therefore has become a catch-all for any quantitative shortcomings of the theory. As it turned out, the "effective radius" undergoes rather large changes departing from the $A^{\frac{1}{3}}$ relationship by 25 percent in some cases. One recognized factor in lengthening half-life which appears in the effective radius is change in spin number in the decay process. However, it will be seen that the present availability of much new data has shown up a number of regularities including broad classes of nuclei with abnormally long half-lives and these cannot be explained by spin changes. Rather, it is believed that the simplified one-body model is inadequate in these cases and the process of creating the alpha-particles is slower in certain nuclear types. These nuclear types include those which have an odd number of neutrons, protons or both and in this sense alpha-emission is forbidden in nuclei possessing non-zero spin beyond and independent of any effect due to spin change in the decay process.

References to most of the data which have been used in these correlations will be found in the compilation already cited.[3] Table III shows the alpha-energies and alpha-decay half-lives for all of the alpha-groups used. Those which are not covered in reference 3 or for which additional data are available are discussed in the Appendix. The data in Table III are entered on a series of diagrams (Figs. 6–8, and 9) in which the curves drawn are taken to represent the energy *vs.* half-life relations for non-forbidden alpha-decay processes. These curves, as will be explained, are defined by the even-even nuclei. Other types are, as a rule, comparatively forbidden in their alpha-decay and the last column in Table III indicates the factor of departure between the observed half-life and the predicted half-life if the decay process were not forbidden.

The Even-Even Nuclei

In Fig. 6 are plotted the data for the even-even nuclei relating the half-life and energy in which lines of constant Z are shown. With minor irregularities the points fall on a series of parallel lines. There is still sufficient uncertainty in a few of the points which produce the irregularities (e.g. Pu^{240}, U^{228}) to allow the possibility that the definition of the curves may be even better when the measurements have been refined.

Of the known even-even nuclei only Po^{210}, Po^{208}, Po^{206}, and Po^{204} fall sharply out of line with others and for reasons which will appear below they have been entered on another plot (Fig. 9). It is probable that these species and/or their decay products have abnormally low nuclear radii as compared with the heaviest polonium isotopes and most isotopes of higher elements. These are the polonium isotopes which in Fig. 1 can be seen to lie in the region following the sharp break in the mass number *vs.* energy curve and as would be expected the half-life *vs.* energy relation also shows a discontinuity. However, even taking into account the decreased decay energy these isotopes have abnormally long half-lives, another reflection of the shrinkage in nuclear radius in this region. These will be discussed further below where other isotopes with abnormally long half-life are considered.

Throughout the remainder of this paper these curves for the even-even nuclides form a baseline for comparison of the half-life energy relationships of other nuclear types. This family of curves, in form and without regard to nuclear type, falls directly out of the quantitative treatment of the alpha-decay process in which the parameter Z is held constant for each curve and nuclear radius is assumed to be a smoothly varying function of mass number. This method for treating alpha-decay data has already been applied by Berthelot[38] and Biswas[39] who attempted to fit all nuclear types to the curves. In later discussions in this paper it will be seen that rather good quantitative agreement may be brought about between these data for the even-even nuclides and the Gamow formula by making reasonable assumptions for nuclear radius. In the immediately following sections it will be seen that nuclear types other than even-even do not fall on this family of curves.

The position of the curve for polonium isotopes in Fig. 6 is worthy of note since there is evidence from the calculations that Po^{212} and possibly Po^{214} are showing the effect of decrease in nuclear radius which lengthens the half-life and which becomes pronounced for Po^{210} and lighter polonium isotopes. To this extent we have been inconsistent in placing the baseline curve for polonium through these points (Po^{212} and Po^{214}).

An important part of the discussion in following sections on the nuclides with odd nucleons is the part

[38] A. Berthelot, J. de phys. et rad. VIII 3, 52 (1942).
[39] S. Biswas, Ind. J. Phys. 23, 51 (1949).

which fine structure plays in the degree of prohibition of alpha-decay. There is an important distinction in this respect between the even-even nuclei and all others. There are three well defined cases of fine structure among the even-even nuclides and within the degree of reliability of the experimental data all groups fall on the curves of Fig. 6. That is to say, the partial alpha-half-lives for the two groups of each of the nuclides Ra^{226}, Th^{230}(Io) and Th^{228}(RdTh) are what would be expected for the respective energies of the

TABLE III. Alpha energies and half-lives.

Nucleus	Alpha-energy	Abundance of α-group	Measured half-life	Alpha-branching ratio	Alpha-half-life	Departure* factor
			Even-even species			
Cm^{242}	6.18		150 days		150 days	
Cm^{240}	6.37		26.8 days	>0.8	~30 days	
Pu^{240}	5.2		~6000 yr.		~6000 yr.	
Pu^{238}	5.60		92 yr.		92 yr.	
Pu^{236}	5.85		2.7 yr.		2.7 yr.	
Pu^{234}	6.26		8.5 hr.	~0.03	~10 days	
U^{238}	4.25		4.51×10^{9} yr.		4.51×10^{9} yr.	
U^{234}	4.84		2.35×10^{5} yr.		2.35×10^{5} yr.	
U^{232}	5.40		70 yr.		70 yr.	
U^{230}	5.96		20.8 days		20.8 days	
U^{228}	6.83		9.3 min.	0.8	12 min.	
Th^{232}	4.05		1.39×10^{10} yr.		1.39×10^{10} yr.	
Th^{230}	0 4.76	0.80	8.0×10^{4} yr.		1.0×10^{5} yr.	
	I 4.69	0.20			4.0×10^{5} yr.	
Th^{228}	0 5.52	0.70	1.90 yr.		2.64 yr.	
	I 5.43	0.28			6.79 yr.	
Th^{226}	6.41		30.9 min.		30.9 min.	
Ra^{226}	0 4.88	0.91	1622 yr.		1780 yr.	
	I 4.68	0.09			1.8×10^{4} yr.	
Ra^{224}	5.78		3.64 days		3.64 days	
Ra^{222}	6.62		38 sec.		38 sec.	
Em^{222}	5.59		3.83 days		3.83 days	
Em^{220}	6.39		54.5 sec.		54.5 sec.	
Em^{218}	7.25		0.019 sec.		0.019 sec.	
Po^{218}	6.12		3.05 min.	~1	3.05 min.	
Po^{216}	6.89		0.158 sec.		0.158 sec.	
Po^{214}	7.83		1.5×10^{-4} sec.		1.5×10^{-4} sec.	
Po^{212}	8.95		3.0×10^{-7} sec.		3.0×10^{-7} sec.	
			Even-odd species			
Pu^{241}	5.1 (calc.)		~10 yr.	2×10^{-5}	5×10^{5} yr.	9
Pu^{239}	5.24				2.4×10^{4} yr.	4
U^{235}	0 4.64	0.10	7.07×10^{8} yr.		7.1×10^{9} yr.	1000
	I 4.48	0.90			7.7×10^{8} yr.	13
U^{233}	4.90		1.6×10^{5} yr.		1.6×10^{5} yr.	2
U^{231}	5.6 (est.)		4.2 days	6×10^{-5}	200 yr.	40
U^{229}	6.53		58 min.	0.2	5 hr.	9
Th^{229}	0 5.14	0.1	7000 yr.		7×10^{4} yr.	350
	I 5.04	0.2			3.5×10^{4} yr.	45
	II 4.94	0.7			10^{4} yr.	3
Th^{227}	0 6.16	0.20	18.6 days		93 days	300
	I 6.13	0.038				
	II 6.10	0.25			74.5 days	100
	III 6.08	0.038				
	IV 6.03	0.013				
	V 5.97	0.025				
	VI 5.92	0.013				
	VII 5.87	0.20			93 days	10
	VIII 5.84	0.038				
	IX 5.82	0.15			124 days	8
	X 5.77	0.025			745 days	25
Th^{225}	6.68		7.8 min.	0.9	8.7 min.	5
Ra^{223}	0 5.82	0.55	11.2 days		20.2 days	10
	I 5.71	0.36			31 days	4
	II 5.63	0.90			124 days	5
Ra^{221}	6.83		31 sec.		31 sec.	7
Em^{219}	0 6.94	0.83	3.92 sec.		4.7 sec.	14
	I 6.68	0.085			46 sec.	10
	II 6.56	0.085			46 sec.	3
Em^{217}	7.88		10^{-3} sec.		10^{-3} sec.	4(?)
Po^{215}	7.50		1.83×10^{-3} sec.	~1(?)	1.8×10^{-3} sec.	1
Po^{213}	8.49		4×10^{-6} sec.		4×10^{-6} sec.	1

* Factor by which measured half-life is greater than value for same Z and E_α taken off curves defined by even-even nuclides.

TABLE III. (*Cont.*)

Nucleus	Alpha-energy	Abundance of α-group	Measured half-life	Alpha-branching ratio	Alpha-half-life	Departure* factor
			Odd-even species			
Am^{241}	I 5.58		490 yr.		490 yr.	2
Am^{239}	5.87		12 hr.	10^{-4}	13.7 yr.	3(?)
Np^{237}	4.85		2.2×10^{6} yr.		2.2×10^{6} yr.	4
Np^{235}	5.15		435 days	5×10^{-5}	2.5×10^{4} yr.	4(?)
Np^{233}	5.65		35 min.	10^{-5}	10 yr.	1(?)
Pa^{231}	0 5.10	0.87	3.43×10^{4} yr.		3.95×10^{4} yr.	40
	I 4.82	0.13			2.64×10^{5} yr.	5
Pa^{229}	5.79		1.5 days	0.01	150 days	3(?)
Pa^{227}	6.57		38 min.	0.8	50 min.	6
Ac^{227}	5.04		21.7 yr.	0.012	1810 yr.	7
Ac^{225}	5.90				10.0 days	5
Ac^{223}	6.76		2.2 min.	~1(?)	2.2 min.	7
Fr^{221}	6.45		4.8 min.	~1(?)	4.8 min.	5
Fr^{219}	7.44		0.02 sec.		0.02 sec.	3(?)
At^{217}	7.15		0.021 sec.	~1(?)	0.021 sec.	1
At^{215}	8.15		10^{-4} sec.	~1(?)	10^{-4} sec.	4(?)
			Odd-odd species			
Am^{242}	5.4 (calc.)				$\sim2\times10^{5}$ yr.	20(?)
Pa^{230}	5.5 (est.)		17.7 days	3.5×10^{-5}	1400 yr.	250(?)
Pa^{228}	6.20		22 hr.	~0.02	~50 days	150(?)
Pa^{226}	6.93		1.7 min.	~1(?)	1.7 min.	6
Ac^{224}	6.28		2.9 hr.	0.1	29 hr.	40
Fr^{220}	6.81		27.5 sec.	~1(?)	27.5 sec.	13
At^{216}	7.94		10^{-3} sec.	~1(?)	10^{-3} sec.	10
			Specially forbidden species (Bismuth isotopes and others with 126 neutrons or less)			
Bi^{214}	0 5.61	0.45	19.7 min.	4×10^{-4}	76 days	400
	I 5.55	0.55			63 days	150
Bi^{213}	5.97		47 min.	0.02	39 hr.	350
Bi^{212}	0 6.20	0.27	60.5 min.	0.337	11 hr.	1000
	I 6.16	0.70			4.3 hr.	600
	IV 5.70	0.011			272 hr. (11.3 days)	150
Bi^{211}	0 6.74	0.84	2.16 min.	0.997	2.6 min.	700
	I 6.38	0.16			13.5 min.	150
Bi^{210}	4.86		5.0 days	$\sim3\times10^{-7}$	5×10^{4} yr.	10^{4}(?)
Bi^{199}	5.58		25 min.	$\sim2\times10^{-5}$	2 yr.	3000(?)
Bi^{197}	6.3		2 min.	?	>2 min.	>10(?)
Em^{212}	6.30		23 min.	?	23 min.	10
Fr^{212}	6.37		19 min.	0.5	38 min.	16(?)
At^{211}	6.00		7.5 hr.	0.40	19 hr.	50
Po^{210}	5.40		138 days		138 days	30
Po^{209}	5.02		200 yr.	>0.9	200 yr.	150
Po^{208}	5.24		3 yr.		3 yr.	30
Po^{207}	5.2		5.7 hr.	$\sim10^{-4}$	7 yr.	50(?)
Po^{206}	5.3		9 days	0.1	90 days	6(?)
Po^{204}	5.45		4 hr.	$\sim10^{-4}$	5 yr.	1000
$Au^{<190}$	5.3		4.3 min.	10^{-4}	1 mo.	400(?)

groups. It will be seen that for nuclides with odd nucleons there is a pattern of prohibition of alpha-decay in which the ground state transition is the most highly forbidden.

Even-Odd Nuclei

When the points for nuclei of even Z and odd number of neutrons are entered on a half-life *vs.* energy plot it is found that almost all lie significantly above the curves for the respective elements as determined by the nuclei with even number of neutrons. These are shown in Fig. 7 in which the even-odd nuclei are indicated by their symbols while the reference lines are curves for the even-even nuclei based on those in Fig. 6.

Of especial interest are a number of cases in which the even-odd nuclei emit two or more alpha-groups. For these the partial alpha-half-lives have been calculated (Table III) and plotted with the appropriate energy values. It will be noted that in such cases one or more of the shorter range groups are less forbidden by the criterion adopted than is the alpha-group of the ground state transition. A graphic illustration of this effect is seen in the three alpha-groups of Th^{229} in which comparison with the curve of Fig. 6 for the even-even thorium isotopes shows that the 5.14 Mev group (ground state transition) is 350-fold forbidden while the 5.04 Mev and 4.84 Mev groups are respectively 45-fold and three-fold forbidden. All of the other cases of fine structure are qualitatively similar to that of Th^{229} in the sense that the ground state transition

is most highly forbidden and a low energy group may be relatively non-forbidden.

It is significant that all of the even-odd nuclei (that can be prepared in a state of purity which permits examination) may have important non-ground state transitions as evidenced either by direct observation of the alpha-groups or by the appearance of gamma-radiation in high abundance. The case of Th^{229} in the $4n+1$ family, for which three alpha-groups have been measured, has already been mentioned and in this category of well defined multiple fine structure also lie Th^{227}(RdAc), Ra^{223}(AcX), and Em^{219}(An) of the actino-uranium family.

Because of the abnormally long partial alpha-half-lives of the ground state transitions of the even-odd nuclei cited it is reasonable to suppose that there are other cases in which the ground state transitions have not been observed. There was good reason to suspect that U^{235} was an example of this behavior as a gamma-ray of 160 kev was found in high abundance and hence presumably in cascade with the only observed alpha-group (see Appendix for references and details). We have now found a group in 10 ± 1 percent abundance corresponding to the ground state transition which in unseparated or partially separated U^{235} is obscured by the U^{234} alpha-particle (see Appendix). A consequence of these observations is that while the 4.48 Mev transition is somewhat greater than tenfold forbidden, the ground state transition (4.64 Mev) is 1000-fold forbidden. In view of these findings a re-evaluation of the specific activity and half-life of U^{235} is in order especially since the half-life is involved in calculations of the age of the earth.

With the behavior of U^{235} in mind it would be interesting to examine the relation of the gamma-radiation to the alpha-particles of other even-odd nuclei of which Pu^{239} and U^{233} may serve as examples. It may be that here too the observed alpha-particles do not correspond to the ground state transitions and that the ground state transitions are highly forbidden. Both U^{233} and Pu^{239} have associated gamma-radiation in moderate abundance but it is not yet known whether such transitions are in cascade with the observed alpha-particles. Some indirect evidence to lend further support to the view that the observed alpha-particles do not represent ground state transitions is obtained from Figs. 1 and 7. From Fig. 1 it may be seen that Pu^{239}, U^{233}, and Ra^{223} appear to have abnormally low alpha-decay energies, that is, their decay energies as shown are little greater than their respective higher isotopes Pu^{240}, U^{234}, and Ra^{224}. The inference might follow that to these energies should be added some gamma-ray energies as has been done for U^{235} and Am^{241}. From Fig. 7 it may be seen that with respect to half-life *vs.* energy relationship the observed Pu^{239} alpha-particle is comparable to the short-range (main) group of U^{235} and U^{233} is much like the shortest range group of Th^{229} while the known alpha-groups of Ra^{223} are like the shorter range groups of Th^{227}. From these relationships of Fig. 7, one might infer that the ground state transitions of Pu^{239} and U^{233} are more highly forbidden as are the corresponding groups of their decay products. The significance of the half-life *vs.* energy relationship in the case of fine structure in alpha-decay will be discussed further below.

It will be noted in Fig. 7 that Po^{213} and Po^{215} fall on the polonium curve and hence would appear to be cases of unprohibited alpha-decay. Before accepting these as exceptions one must consider that the baseline in this region of the polonium curve is defined by Po^{212} and Po^{214} and that these nuclei are themselves prohibited due to shrinkage in nuclear radius (see section on Quantitative Treatment of Alpha Decay). There is also the possibility that the observed alpha-particles of Po^{213} and Po^{215} do not represent ground state transitions.

Odd-Even and Odd-Odd Nuclei

The half-lives for these types are plotted in Fig. 8 in which the same reference lines for the even-even nuclei are shown as in Figs. 6 and 7. Interpolated between these curves are broken lines to represent the positions which the isotopes of odd Z elements would have if their alpha-decay rates, like the even-even nuclei, were not forbidden. It is seen that almost invariably these types are forbidden and that the odd-odd species show greater departures from their curves than do the odd-even ones. The quantitative bases for these generalizations may be found in Table III.

For the odd-even species there is reason to doubt that the departures from the reference curves as shown in Table III and Fig. 8 give a true picture of the forbidden character of the ground state transitions since, as has already appeared for the even-odd species, it is not certain that the observed alpha-particles represent these transitions. For example, the measured alpha-particle of 5.48 Mev for Am^{241} almost surely does not correspond to the total decay energy since there is found a gamma-ray of 62 kev in high abundance. If, as seems likely, there should be an unobserved alpha-group of 5.54 Mev, then it must have a very long partial half-life and its emission is highly forbidden. How many others of the odd-even type exhibit the same behavior as Am^{241} is not known.

There are two recognized cases of fine structure in alpha-decay among the odd-even nuclei. These are Pa^{231} and Fr^{221}. In both instances the lower energy group is the less highly forbidden, in fact, the 6.05 Mev group for Fr^{221} does not appear to be prohibited.

In examining the data for the odd-even nuclei in Table III it may be noted that a large fraction of the partial alpha half-lives are calculated from very rare alpha-branching of predominent electron capture decay processes. There is considerable uncertainty in estimating the number of electron capture events and the experience in this laboratory has indicated that it is most likely that they are underestimated. This means

that the true partial alpha half-lives are probably longer than has been tentatively accepted.

The single example of an odd-even nucleus for which both energy and alpha-half-life should be reliable which is not forbidden is At^{217}. There is no apparent explanation for this exception to the general rule unless At^{217} is another case in which the ground state transition is not measured.

It is apparent from the few examples of odd-odd species that alpha-emission in this type is forbidden. With the reservations necessary because of uncertainties in data as already discussed it is probable that odd-odd nuclei are more highly forbidden in their alpha-decay than are the even-odd and odd-even types.

Special Forbidden Species

The special significance of this group plotted in Fig. 9 will be discussed below. Included are all known bismuth alpha-emitters and isotopes of francium, emanation, astatine, and polonium with 126 or fewer neutrons. In the case of polonium this group includes several isotopes of the even-even type and as already discussed should probably include Po^{212} and Po^{214}.

Discussion of Forbidden Alpha-Decay

From the data shown in Figs. 6, 7 and 8 it seems to be a general condition in alpha-radioactivity that nuclei with an odd neutron, proton or both show forbidden decay as compared with the even-even nuclei. This is particularly true of the ground state transitions in those cases in which more than one alpha-group has been measured. Where several alpha-groups are measured, the ground state transition is most highly forbidden and one or more of the shorter range groups is much less forbidden. In contrast, the few cases of fine structure in even-even nuclides indicate no prohibition for either group so that the partial alpha-half-lives correspond to the respective alpha-energies.

According to the Gamow theory a factor which prohibits alpha-decay is spin change in the transition and of course any discontinuity in nuclear radius in the direction of abnormally low nuclear radius will appear as prohibited alpha-decay if the condition is not recognized. There is reason to believe that Em^{212}, Fr^{212}, At^{211}, polonium isotopes of mass 214 and less, and perhaps all of the bismuth isotopes show the effect of shrinkage of nuclear radius. However, it is unreasonable also to attribute an important effect of nuclear radius to all of the heavier nuclides with odd protons and neutrons since, if anything, these species should exhibit somewhat greater radii than neighboring even-even isotopes. It is also not possible to explain the general abnormal half-lives of these types by means of spin changes.

According to the Gamow formulation the spin dependence is such that in order to explain alpha-decay abnormally long by a factor of 10 it would be necessary to invoke a spin change of about 5 units. While such large spin changes have been observed in beta-transitions in which an odd-odd nucleus decays to an even-even type it would be unreasonable to expect such large changes, particularly as a general condition, in the case of alpha-decay in which parent and daughter nuclei are of the same type. In addition, considering a decay series such as the $(4n+1)$ or $(4n+3)$ series in which virtually all members show abnormal decay constants

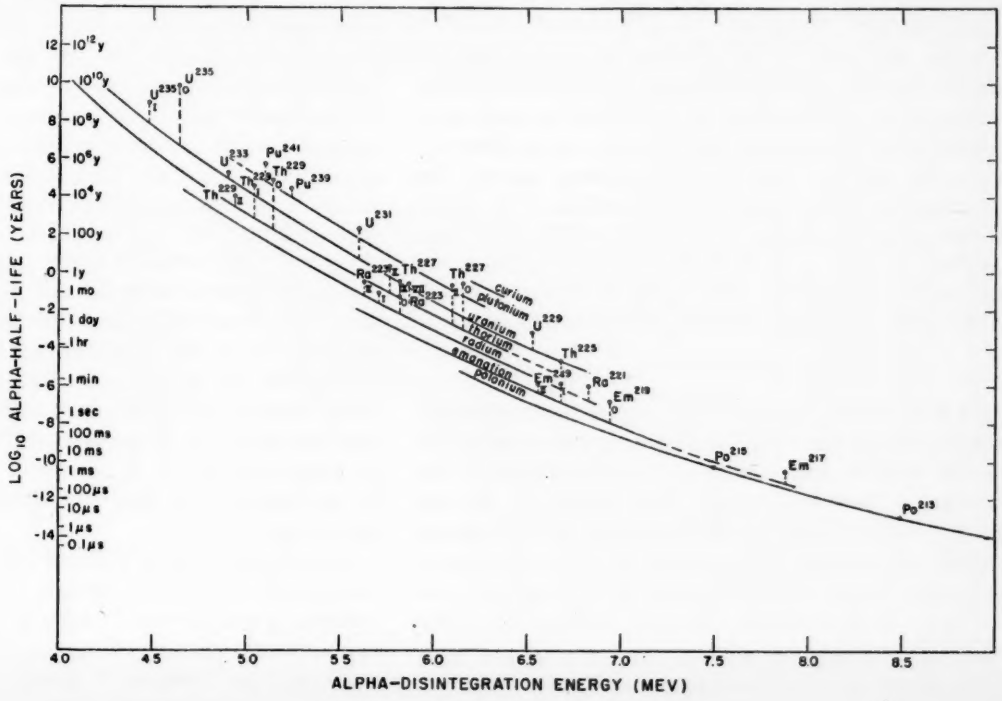

FIG. 7. Half-life *vs.* energy relationship of the even-odd nuclides. (Roman numerals indicate short-range groups in fine structure and "0" the ground state transition.)

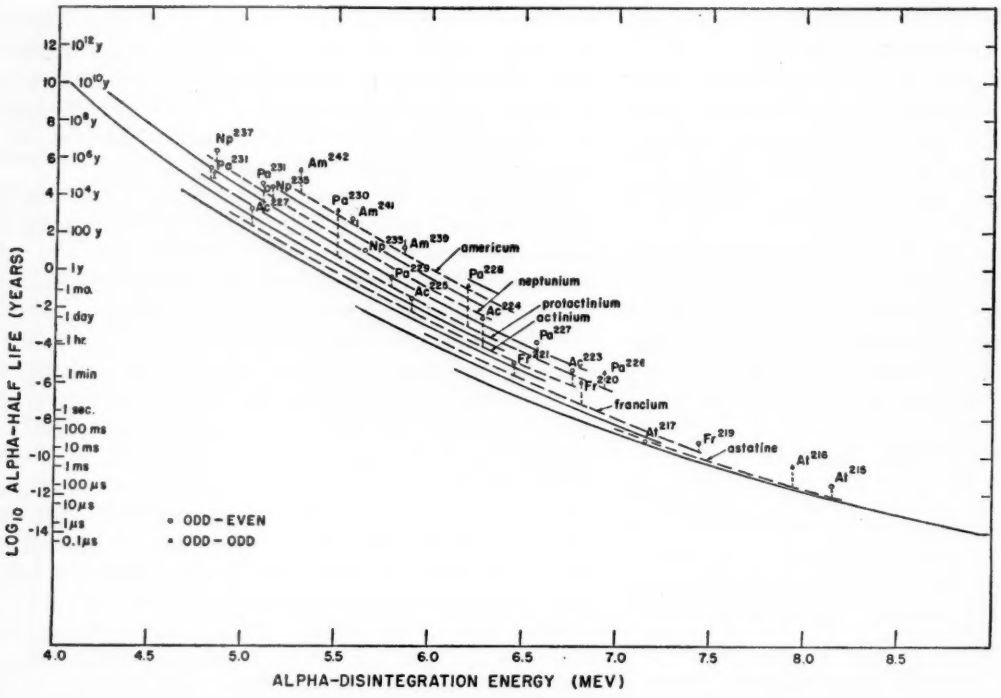

FIG. 8. Half-life *vs.* energy relationship for the odd-even and odd-odd nuclides. (Roman numerals indicate short-range groups in fine structure and "0" the ground state transition.)

it would be necessary to postulate alternation of large and small spin numbers differing by several units each in proceeding down the decay chains. In one case of alpha-decay, namely that of U^{235}, the spin numbers of the ground states have been measured. For U^{235} a value of 5/2 (or 7/2) was obtained[40] while for Pa^{231} a value of 3/2 was measured,[41] thus indicating a spin change of 1 or 2 units in the transition. In order to account for prohibition of the ground state transition of U^{235} by spin change alone it would be necessary that there be a change of about 10 units.

Since present alpha-decay theory does not explicitly account for the forbidden transitions in all of the broad categories in which they are observed a qualitative modification is suggested which is not out of harmony with the Gamow and Condon-Gurney theory. An examination of the Gamow formula shows it to consist of two parts; an exponential term describing the barrier penetration and a coefficient before the exponential term which is a slowly varying function and has been taken to be a constant. This may be written in the form:

$$\lambda = Ce^{-f(v,Z,r)}.$$

Here λ is the decay constant, C is the coefficient mentioned and v, Z and r are the alpha-particle velocity, the atomic number and the effective nuclear radius. The constant C may be thought of as related to the frequency with which an alpha-particle in the parent nucleus encounters the potential barrier and numerically approximates the reciprocal of the length of time it takes the alpha-particle to cross nuclear dimensions.

This model makes the tacit assumption that the alpha-particle which is emitted has been formed in the nucleus and that there is no prohibition toward assembling its components in any one nucleus as compared with any other. It is here that we suggest that the effect of an odd nucleon makes itself felt in slowing the assembly of an alpha-particle. The odd nucleon, presumably the one in the highest quantum state, must be a component of the emitted alpha-particle if the alpha-particle is to leave the nucleus with full kinetic energy; as a result it must pair with a lower lying nucleon of antiparallel spin and perhaps in addition one or more of the remaining nucleons may have to change quantum states. If we assume that these processes require appreciable time we have the basis for forbidden decay in nuclei with odd nucleons. By the same token two odd nucleons should in general prohibit alpha-decay more than single odd nucleons and this would be borne out by comparison of the odd-odd nuclei with the odd-even or even-odd types in Table III and Figs. 7 and 8. It would also follow from these ideas that in all of the forbidden classes lower energy alpha-groups might compete with or supplant the ground state transition since the lower lying nucleons are more likely to be paired and in any case should not be so prohibited in their assembly into an alpha-particle. As is observed, these groups should be less forbidden *for their energies* than the ground state transition.

The abnormality in the half-life *vs.* energy relationships for Po^{210} and all of the naturally occurring bismuth isotopes as compared with other alpha-emitters has been pointed out a number of times and the effect has been attributed to a sudden shrinkage of nuclear radius in

[40] O. E. Andersen and H. E. White, Phys. Rev. **71**, 911 (1947).
[41] H. Schüler and H. Gollnow, Naturwiss. **22**, 511 (1934).

these species. It is worth while to attempt to correlate such abnormalities in nuclear dimensions as evidenced by alpha-decay properties with the newer ideas on stable configurations in nuclear structure. For unambiguous interpretation in a region of rapidly changing nuclear radius bridged by an alpha-decay event it would be necessary to decide whether the increased barrier from a shrunken nucleus may be ascribed to the parent or daughter nucleus. In the one-body model the alpha-particle is considered to be a body moving within the decay product nucleus and the barrier to which it is subjected is that of the decay product. This would mean, as an example, that the alpha-decay of bismuth isotopes is forbidden because the thallium decay products have abnormally low nuclear radii. It is probable that this model is not adequate and that the nucleus responsible for the potential barrier is a hybrid between parent and daughter nuclei.

As already mentioned all of the naturally occurring isotopes of bismuth show very highly forbidden alpha-decay ranging from several hundred-fold to several thousand-fold above the baseline curve. Part of this may now be attributed to odd nucleons in bismuth isotopes, but there is still a considerable degree of prohibition presumably due to nuclear radius effects. If we take a representative departure from the baseline curve as a factor of 500 and attribute 10 or 20 of this to odd nucleons, there is left a factor of 50 or 25 for the effect of decrease in nuclear radius. According to the Gamow formula a shrinkage of about 10 percent could account for a 50-fold increase in half-life. In the following section are discussed more fully some of the quantitative aspects of alpha-decay theory and here it will be seen that there is good agreement with the theory for even-even nuclei except the lighter even-even isotopes of polonium, Po^{212}, Po^{210}, and Po^{208}. In these cases we attribute the entire prohibition of alpha-emission to nuclear radius effects since other even-even nuclides removed from the region of 82 protons and 126 neutrons show rather good agreement. For Po^{210} and Po^{208}, the degree of prohibition is such that a postulated shrinkage of almost 10 percent is necessary to account for it. Since the bismuth isotopes when divested of the effects of odd nucleons show similar prohibition it is only necessary to postulate nuclear shrinkage of the same order, namely, 10 percent or less.

With regard to the new highly neutron deficient bismuth alpha-emitters it is not possible to say whether there is any trend away from that noted for the heavy bismuth alpha-emitters because the branching ratios between alpha-emission and electron capture are not known accurately and the calculated alpha-half-lives shown in Table III must be considered only as rough approximations. The two-minute period assigned to Bi^{197} is only about tenfold forbidden if it decays mainly by alpha-emission. There is no evidence on this point, however. On the other hand the best measured alpha-branching of 25-min. Bi^{199} shows its alpha-decay to be highly forbidden. In attributing and explaining these effects for bismuth in terms of stability of closed shells in nuclear structure perhaps the best that can be done at present is to say that there is abnormally strong binding energies of one or more protons before the closed shell 82 and that for neutrons there are high binding energies for a sizeable number before 126.

With the marked retardation of alpha-decay for bismuth isotopes one might expect that lead isotopes ($Z=82$) would accentuate this trend. As a matter of

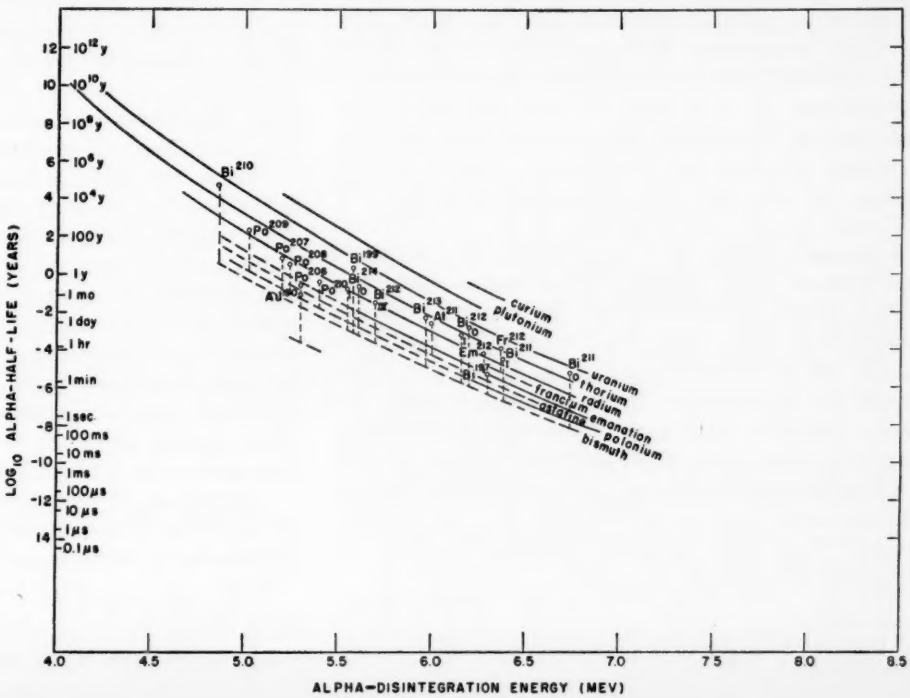

FIG. 9. Half-life *vs.* energy relationship of the specially forbidden nuclear types. (Roman numerals indicate short-range groups in fine structure and "0" the ground state transition.)

fact no lead alpha-activity has been observed even for highly neutron deficient species in corresponding position to the light bismuth isotopes in which alpha-activity does again manifest itself. This might receive adequate explanation by assuming low decay energy for lead isotopes but in addition there could be extremely long half-lives for the decay energies. It is perhaps significant of the position of lead that Thompson *et al.*,[28] have observed alpha-activity again when this region has been crossed, that is, for highly neutron deficient species of gold ($Z=79$) and mercury ($Z=80$).

Besides the bismuth isotopes there is another class that seems to be forbidden in alpha-decay for reasons of abnormal nuclear radius. These are the polonium isotopes of mass 210 and lower, At^{211} and Em^{212}. The significant point here is that all of these have 126 neutrons or less. It will be noted that these are the nuclei in Fig. 1 that show a sharp departure in the mass number *vs.* energy regularities of the heavier isotopes. In this region even the even-even nuclei appear to be forbidden in their alpha-decay.

In Fig. 3 an attempt has been made to demarcate the regions of abnormal nuclear stability. For this purpose use was made of two observations, namely, that all bismuth isotopes show a high degree of prohibition in alpha-decay and that all nuclides with 126 or less neutrons also show this property. The implication of the abnormally long half-lives in both cases is that there are discontinuities in nuclear radius. With regard to nuclei having 126 neutrons or less, it seems fairly clear that there is a region below 126 neutrons in which nuclear binding varies only slightly but that as this neutron number is exceeded there is a sharp decrease in binding energy. This effect shows up as a maximum alpha-energy for a nucleus with 128 neutrons which decays to one with 126 neutrons as is the case for Bi^{211}, Po^{212} and presumably At^{213} and higher nuclei of the type. Likewise nuclei with 126 neutrons and less have low alpha-energy, and what is of equal importance, the half-lives are abnormally long for the alpha-energies. If several neutrons beyond 126 are bound relatively weakly then the alpha-decay energies of nuclei with 127 neutrons should be between those with 126 and 128 neutrons because the alpha-particle here carries off one neutron which is firmly bound and one which is loosely bound. This would account for the observed alpha-energy of Po^{211}(AcC′) and leads to the prediction of that for At^{212} as shown in Fig. 1. Another effect should be observed for these nuclides, namely, the highly forbidden nature of alpha-decay so prominent for nuclei with 126 and less nuclei should begin to show up. For Po^{211} this would lead to the prediction that the half-life might be as long as 50 milliseconds, some tenfold greater than that predicted presumably from the Geiger-Nuttall relations.[42]

This discussion of the effect of 126 neutrons on the energy surface probably applies equally well to the proton number 82 but in this case the almost total absence of measurable alpha-decay potential immediately below bismuth makes any speculation of dubious value. However, the discussion of the effect on alpha-decay of one nucleon beyond a closed shell as applied above with scanty data to the neutron number 127 has more abundant examples in the proton number 83. All of the alpha-energies of bismuth isotopes are sharply lower than those of polonium as compared with the displacement between succeeding elements and the decay rates show a degree of prohibition beyond that expected for nuclides with odd nucleons.

Quantitative Treatment of Alpha Decay

From preceding discussions it seems obvious that if there is to be quantitative agreement between experimental data and existing theory that this agreement can only come for the even-even nuclides. Preliminary calculations*** with these indicate that agreement is indeed good over a wide range of mass number and atomic number. Thus the shape and spacing of the curves shown in Fig. 6 are reproduced rather faithfully by the single body theory of alpha-emission as has already been indicated by Biswas[39] and others who have in addition attempted to fit all nuclear types on the same curves.

Since the nuclear radius is the only parameter in the formula which is not known it is tempting to use curve fitting for the even-even nuclides as a means of determining a function which will describe the nuclear radius in the heavy element region. No comprehensive computations have yet been made, but preliminary attempts would indicate that the simple function $r=1.48A^{\frac{1}{3}}\cdot 10^{-13}$ cm, will fit the data better than a function such as this with an additive term to express the radius of the alpha-particle or the range of its forces as has been suggested.[43,44] One may calculate conversely the explicit value for the nuclear radius for each even-even nuclide which is necessary to give the observed value for the decay constant and to determine the deviation of each such radius from the rule, $r=1.48A^{\frac{1}{3}}\cdot 10^{-13}$ cm. In about a dozen such calculations for nuclides from emanation to curium, the mean deviation encountered was about 1 percent which is considered good agreement when it is considered that often uncertainties in alpha-energy are reflected by greater differences in nuclear radius. Refinement of energy measurements and correlation of more extensive data will show whether there are trends away from this simple formulation for nuclear radius.

Calculations of nuclear radius have also been made for six of the even-even isotopes of polonium for which reliable decay energies and half-lives are available. It

[42] International Radium Standards Commission Report of 1930, Rev. Mod. Phys. 3, 427 (1931).

*** We wish to thank Mr. T. J. Ypsilantis for making most of the computations referred to here.

[43] H. A. Bethe, Rev. Mod. Phys. 9, 163 (1937).

[44] E. Amaldi and B. N. Cacciapuoti, Phys. Rev. 71, 739 (1947).

has long been apparent in the decay of Po^{210} and possibly all bismuth isotopes that a shrinkage in nuclear radius is at play in lengthening the half-lives. In the case of the bismuth isotopes we must attribute part of the prohibition to the general effect of odd nucleons, part possibly to spin changes and part to nuclear radius effects. However, for the even-even polonium isotopes any appreciable prohibition should be ascribed to the abnormality of nuclear radius. In the single body theory of alpha-decay it is assumed that the nuclear radius in effect is that of the alpha-decay product. In the case of polonium alpha-emitters one would then be "measuring" the nuclear radii of the corresponding lead isotopes. Whether or not there is any meaning in ascribing the parameter of distance in alpha-decay explicitly to the radius of the product nucleus, it is almost certain that the binding energy and hence radius of the product nucleus is an important factor in the energy *vs.* half-life relationship. For the decay of polonium isotopes, one may attribute prohibition of alpha-decay to shrunken nuclear radii of the lead daughter isotopes associated with the stable configuration of 82 protons. For Po^{212} and lighter isotopes, the decay products have 126 or less neutrons, and this should increase further the prohibition because of the further decrease in effective nuclear radius. Finally, if we assume that the radius of the parent nucleus is likewise a determinative factor in the effective radius for alpha-emission, polonium isotopes of mass number 210 and lower should have still more highly forbidden alpha-decay since the parent nuclei also have 126 neutrons or less. It is interesting to note that the calculated radii for the even-even polonium isotopes deviate in the manner expected from radii determined by the simple $A^{\frac{1}{3}}$ function. While the Po^{218} radius is found to be low by only 1.4 percent, the isotopes Po^{216}, Po^{214}, Po^{212}, Po^{210} and Po^{208} show deviations respectively of 2.1, 2.8, 5.5, 8.1 and 9.0 percent.

It may be mentioned that further dissociation of factors which affect the nuclear radius may be obtained from observations on nuclides such as Em^{212}. Here both parent and daughter nuclei have 126 or less neutrons but the daughters have 84 protons rather than the 82 for the daughters of polonium isotopes. It will be noted that, perhaps fortuitously, Em^{212} is less forbidden than is Po^{210} and Po^{208}.

This work was performed at the Radiation Laboratory, University of California, Berkeley, California, under the auspices of the AEC.

APPENDIX

Notes and Comments on Individual Activities

Most of the data used in this paper may be found in the compilation "Table of Isotopes."[3] However there are a number of new isotopes not covered there, some of the data have been revised or amplified and some require further explanation in order to indicate the reliability for the purpose used here.

Cm^{238}

As listed[3] this is an alpha-emitter of 6.50 Mev and 2.5-hr. half-life. It is also surely unstable with respect to electron capture (see Table I) and although the branching has not been determined it is probable that the measured half-life is essentially that of the electron capture process. As a result this isotope was not included in Fig. 6 as part of the correlations of the even-even species.

Cm^{240}

This isotope of curium is also predicted to be unstable toward electron capture. However, the branching for this mode of decay has been shown[45] to be less than 20 percent so that little error is introduced in plotting the measured half-life as the alpha-decay half-life.

Cm^{244}

This is a long-lived alpha-emitter of 5.78 Mev alpha-energy discovered by S. G. Thompson[46] from the irradiation of Am^{241} with 38 Mev helium ions. Thompson suggests alternate mass number assignments, Cm^{242} and Cm^{244}, and the assignment to Cm^{244} is favored here from some detailed considerations in the assignment of several curium isotopes.[46] From yield considerations involving considerable uncertainty, Thompson estimates the half-life as 10 years. This point has not been used in Fig. 6 although it fortuitously falls about where expected.

Am^{242}

There is considerable uncertainty in the indicated half-life of the ground state of Am^{242}. The alpha-half-life indicated in Table III is based on the Np^{238} yield from alpha-decay assuming that Am^{242} was formed in the same yield as the 16-hr. excited state, Am^{242m}, from the neutron capture by Am^{241}. There could be a substantial error from this source in either direction. The alpha-energy was determined by closing the cycle consisting of the beta-decay energies of Am^{242} and Np^{238} and the alpha-energy of Cm^{242}. The beta-decay energy of Am^{242} used in closing the cycle is taken to be that of the beta-particle energy (0.6 Mev). If any of the gamma-radiation is in cascade with the beta-particle the decay energy would be greater and this would increase correspondingly the Am^{242} alpha-energy.

Am^{241}

The high abundance of soft gamma-radiation and *L*-x-rays led to the belief that the main alpha-group is in cascade with a gamma-ray. Preliminary alpha-gamma-coincidence measurements[47] tend to confirm this assumption. The gamma-energy is therefore added to the energy of the alpha-particle and recoil nucleus in arriving at the decay energy (5.64 Mev) shown in Fig. 1.

Am^{239}

The listed[3] alpha-branching of ~0.1 percent has been redetermined[48] and a better value 0.01 percent has been used here in determining the alpha-half-life.

Pu^{241}

The alpha-half-life indicated in Table III is based upon the U^{237} yield from alpha-decay estimating the amount of Pu^{241} from yield considerations. The uncertainties are such that the alpha-half-life so calculated is probably correct within a factor of two or three. The alpha-energy is calculated by closing a decay cycle involving beta-disintegration energies of Pu^{241} and U^{237} and alpha-disintegration energy of Am^{241}.

Pu^{239}

It has been mentioned in the text that there is unassigned electromagnetic radiation associated with Pu^{239} and that the pos-

[45] K. Street, Jr. and G. T. Seaborg, unpublished data.
[46] S. G. Thompson, Ph.D. Thesis, University of California (1948) "Nuclear and Chemical Properties of Americium and Curium."
[47] Goeckermann, Robinson, and Stover, unpublished data.
[48] R. A. James and K. Street, Jr., unpublished data.

sibility exists that the measured alpha-particle is not the ground state transition. This phenomenon would be like that which has been established for U^{235}. If this proves to be the case for Pu^{239} the decay energy will be greater than that shown in Fig. 1.

Pu^{234}

The degree of alpha-branching of this 8-hr. period is not accurately known because of difficulties in assessing the counting efficiency of the radiation from the electron capture process. The tentative branching ratio adopted for the present is 0.03, making the alpha-half-life 10 days. The energy has been revised slightly to 6.15 Mev.[49]

Pu^{232}

The alpha-branching of this isotope has been estimated as 20 percent or possibly less from the alpha-activity and x-ray activity.[49] The energy given is also only approximate since the alpha-group falls in the same energy range with its decay product U^{228} which itself is not accurately known.

Np^{235}

The listed[3] alpha-branching of ~0.1 percent has been revised to a value of ~0.005 percent.[50]

Np^{233}

This is a new neptunium isotope prepared by the irradiation of U^{235} and U^{233} with high energy deuterons.[51] It decays predominantly by electron capture with a half-life of 35 min. but also shows a 5.53 Mev alpha-particle in low abundance. As is the case with all of the nuclei decaying by electron capture without daughter activities which can be measured precisely, it is possible at present only to estimate the branching and alpha-half-life. The tentative value for the alpha-branching is $\sim 10^{-3}$ percent.

U^{235}

The main alpha-group (4.396 Mev)apparently does not involve the ground state transition since there is found a 0.162 Mev gamma-ray in high abundance,[3] and the decay energy shown in Fig. 1 includes the gamma-ray.

The abundance of the ground state transition was not known precisely since until recently it had not been observed. On the basis of an apparent 20 percent discrepancy between the number of 4.396 Mev particles relative to those of U^{238},[52] and the number that should be present (if there were one per disintegration) according to mass spectrographic analysis and the yield of the actinium series products it was suggested tentatively[52] that 20 percent of the transitions result in a higher energy alpha-group which is covered up by the U^{234} alpha-particles. Recently this laboratory obtained a sample of highly separated U^{235} † and we were able to resolve a longer range alpha-group occurring in 10 ± 1 percent abundance and at an energy which is 180 kev higher than the main group with an experimental uncertainty of about 20 kev. The ability to resolve this alpha-group makes it possible to determine the specific activity of U^{235} directly on the highly separated material and this may well cause a change in the accepted half-life for U^{235}. However, rather than to attempt to correct existing data we shall retain the old value (7.07×10^8 yr.) until these measurements can be made accurately.

U^{233}

This nuclide like Pu^{239} has associated with it a considerable level of electromagnetic radiation although only a single alpha-group has been identified. It is possible therefore that the observed alpha-group does not represent the ground state transition. Since there is no direct determination of a decay scheme, the measured alpha-energy is used for Fig. 1.

U^{231}

The alpha-energy of this 4.2-day electron capture nuclide cannot yet be measured because it cannot be prepared free of overwhelming levels of alpha-activity of U^{230} and U^{232}. However, the extent of alpha-branching can be measured by isolating the decay products Th^{227}(RdAc) and Pa^{231}. The alpha-half-life was calculated from this as 200 years.[53] The alpha-energy was estimated as 5.6 Mev both from Fig. 1 and also by closing a decay cycle (U^{231}, Pa^{231}, Ac^{227}, Th^{227}) in which the electron capture decay energy for U^{231} was estimated as 0.5 Mev by the relation of Thompson.[29]

Pa^{231}

There is good evidence that the two well established groups of alpha-particles used in this paper themselves possess fine structure and that the high energy group has a component of 5.04 Mev[54] which is about 30 kev greater than what has been taken to be the ground state transition. This makes little difference in the energy plot of Fig. 1 but would have the important effect best visualized from Fig. 8 of making the ground state transition more highly forbidden than as shown. Another minor consequence of this change would be its effect on the U^{231} alpha-energy since it was estimated by closing a decay cycle which includes Pa^{231} alpha-decay. However, other uncertainties in the calculation overshadow the slight increase in alpha-energy for U^{231} that would be entailed.

Pa^{230}

The degree of alpha-branching of this 17-day activity has been estimated[55] by obtaining the ratio of the U^{230} and Ac^{226} which grow from it assuming that the 17-day half-life is substantially that of the electron capture process rather than that of β^--emission. The yields correspond to an alpha-half-life of 1400 years which is plotted in Fig. 8 against the alpha-energy (5.5 Mev) which was interpolated from Fig. 1.

Th^{230}(Io)

Certain aspects of the fine structure of ionium (Th^{230}) have been worked out and warrant incorporation into these correlations. The alpha-particle spectrum has been more carefully examined and seems to consist of at least two groups of energy 4.68 and 4.61 Mev[56] in good agreement with the known gamma-ray of 68 kev.[57, 58] The ratio of the 4.68 Mev to 4.61 Mev groups is estimated by Feather[35] as ~4:1. Rosenblum, Valadares, and Vial[56] also obtained some evidence for a group in low abundance of energy which could correspond to a transition 170 kev above the ground state, which gamma-ray has probably been observed.[57, 58] However, this group is not shown in Fig. 6 and Table III because its abundance is too poorly known.

Th^{228}(RdTh)

Some newer values for the abundances of the two alpha-groups have been given as 0.72 and 0.28 for the respective group energies 5.423 and 5.338.[59]

Th^{224}

The measured alpha-energy (7.20 Mev) is in keeping with a short half-life but it has not yet been measured. This is also true of some other short-lived nuclides such as Ac^{222}, Ra^{220}, Fr^{218}, Em^{216} and Po^{211}.

---

[49] D. A. Orth and G. T. Seaborg, unpublished data.

[50] R. A. James, unpublished data.

[51] Magnussen, Thompson, and Seaborg, unpublished data.

[52] Clark, Spencer-Palmer, and Woodward, British Atomic Energy Project Report, BR-522 (1944).

† We are indebted to Dr. C. E. Larson and other members of Carbon and Carbide Chemicals Corporation, Oak Ridge, Tennessee for making available to us the U^{235} used in this study.

[53] Crane, Ghiorso, and Perlman, unpublished data.

[54] S. Rosenblum and E. Cotton, Comptes Rendus **226**, 171 (1948).

[55] W. W. Meinke, and G. T. Seaborg, unpublished data.

[56] Rosenblum, Valadares, and Vial, Comptes Rendus **227**, 1088 (1948).

[57] A. G. Ward, Proc. Camb. Phil. Soc. **35**, 322 (1939).

[58] I. Curie, Comptes Rendus **227**, 1225 (1948).

[59] Rosenblum, Valadares, and Perey, Comptes Rendus **228**, 385 (1949).

$Ac^{228}(MsTh_2)$

A measurement of the alpha-particle from rare branching has been reported[60] giving 4.54 Mev for the alpha-particle energy, a value which agrees with the predictions according to Fig. 1. However, for this energy and according to Fig. 8, Ac^{228} should have an alpha-half-life of 10^6 years or more making the alpha-branching only 1 in 10^9. It is extremely doubtful that such low alpha-branching could be observed in this particular case.

Ac^{227}

The existence of two alpha-groups one of the ~350 kev below the main group[61] has not been confirmed[62, 63] so for the present it will be assumed that Ac^{227} has a single alpha-group of 4.95 Mev with the reservation that finer measurements may show this group to have closely lying fine structure. The question of whether or not the alpha-particle observed represents the ground state transition remains at present unresolved.

Ra^{226}

There is a well recognized gamma-ray of Ra^{226} of about 0.19 Mev.[64, 65] Stahel[65] found the conversion electrons in abundance of about 5 per 100 alpha-disintegrations and estimated an additional few percent unconverted gammas. Rosenblum and Perrin[66] observed the corresponding short range alpha-group and remarked that the abundance was of the proper magnitude to correspond with the measurements of Stahel. More recently Rosenblum[67] indicated that the abundance of the short-range group is about 9 percent while Chang[68] gives the abundance as 1.8 percent. Because of the agreement between independent measurements of the gamma-ray and the alpha-group by Stahel and Rosenblum, respectively, the higher value is used.

Fr^{212}

This highly neutron deficient francium isotope (predicted β-stable francium is Fr^{219}) was prepared with high energy protons on thorium by Hyde, Ghiorso, and Seaborg.[28] It was isolated chemically and shown to lie in the mass number range well below Fr^{218} since other heavier francium isotopes which could conceivably have the observed alpha-energy and half-life would all give rise to well-known decay products of the natural radioactive series. It was assigned to Fr^{212} through its genetic relationship by alpha-decay with an astatine isotope thought to be At^{208} and by electron capture to a new isotope of emanation assigned to Em^{212} by its genetic relationship with Po^{208}. The measured half-life for Fr^{212} is 19 min. and judging by the rate of growth of Em^{212} alpha-particles the alpha-branching is about 50 percent. The energy of the alpha-particle is 6.25 Mev.

Em^{218}

There is a serious discrepancy in half-life for Em^{218} reported by different investigators. Studier and Hyde[7] reported a half-life of 19 milliseconds for Em^{218} arising as a product in the U^{230} series. Walen,[69] on the other hand, claims to have identified Em^{218} as a 1.3-second activity from the rare β^--branching of At^{218} which itself arose from the rare β^--branching of ThA^{218}. There are several reasons for accepting the value given by Studier and Hyde, the first of which is the greatly simpler experimental situation in their method of production of Em^{218}. Another reason is that the energy and half-life given by Studier and Hyde fit well with the regularities of Fig. 6. With regard to the 1.3-second half-life of Walen, this period is much too long for the energy given by Studier and Hyde, or conversely, if we do not accept this energy but estimate it from the 1.3-second half-life then Em^{218} will have a lower energy than An^{219} which is clearly out of line with the regularities of Fig. 1.

Em^{212}

This new isotope of emanation grows from Fr^{212} as mentioned and has a 6.18 Mev alpha-particle.[28] The measured half-life is 23 min.[27] and since we believe that Em^{212} might be beta-stable this would also be the alpha-half-life.

At^{218}

In the review article[3] the energy of the alpha-particle for At^{218} found by Karlik and Bernert[34] to be 6.63 Mev was erroneously reported as 6.72 Mev.

At^{213}

This nuclide has never been observed and we estimate an alpha-energy (see Fig. 1) following the reasoning that a nucleus in this region with 128 neutrons will have the maximum energy of all of its isotopes. This estimation was made as a prediction to emphasize the belief that this is the expected trend and that the alpha-energy of At^{213} probably should not be obtained by interpolating between At^{212} and At^{214}.

At^{212}

The half-life of this nuclide has been measured as 0.25 second[70] and from Fig. 8 we estimate that the alpha-energy is about 7.4 Mev making allowance for nuclear type both with respect to its odd-odd composition and its decay through 126 neutrons. This energy is probably not reliable to the nearest 200 kev at best. It is to be expected that the alpha-energy will lie between those of At^{211} and At^{213} and to this extent the energy assignments given to both At^{212} and At^{213} are consistent.

At^{210} and lighter astatine isotopes

Kelley and Segrè[71] have for At^{210} a minimum alpha-branching ratio of 10^{-4} which yields accordingly an alpha-half-life >10 years. From Fig. 1 we may estimate the alpha-energy of At^{210} as 5.4 Mev if it is assumed that it bears the same relation to At^{211} as Po^{209} does to Po^{210}. Placing this energy and half-life on Fig. 9 it is seen that the alpha-decay is at least several hundred-fold forbidden. The fact that it is so highly forbidden is attributable partly to its having less than 126 neutrons and partly to its odd-odd configuration. It is interesting to note that (provided the energy has been guessed correctly) the prohibition of alpha-decay is greater than that of At^{211} which fact may be interpreted as the effect noted for an odd-odd nucleus as compared with an odd-even one.

Although alpha-emission is again observed for astatine below mass 210, isotopic assignments for the several activities cannot be made unambiguously. All of these undoubtedly decay principally by electron capture but the degree of branching has not yet even been approximated. Therefore none of these nuclides can be used in the half-life *vs.* energy correlations. However, certain alpha-energies have been measured and isotopic assignments were made as indicated in Fig. 1. It should be emphasized that the half-lives given here are the measured half-lives and not those for alpha-emission.

The assignment of a 5.5-hr. period with alpha-particles of 5.65 Mev energy has been tentatively made to At^{209} based upon the excitation function in the irradiation of bismuth with helium ions and the probable identification of Po^{209} among the decay products of the complex mixture of activities.[72] Another 5.65 Mev alpha-particle decaying with a half-life of 1.7 hr. has been assigned to At^{208}, and was produced through alpha-decay of an activity

[60] G. Guében, Ann. soc. sci. Bruxelles **B52**, 60 (1932); **B53**, 115 (1933).
[61] R. G. Gregoire and M. Perey, Comptes Rendus **225**, 733 (1947).
[62] L. Vigneron, Comptes Rendus **226**, 715 (1948).
[63] Ghiorso, Hollander, and Perlman, U. S. Atomic Energy Commission Document, AECD-2232 (1948).
[64] O. Hahn and L. Meitner, Zeits. f. Physik **26**, 161 (1924).
[65] E. Stahel, Comptes Rendus **194**, 608 (1932).
[66] S. Rosenblum and J. Perrin, Comptes Rendus **195**, 317 (1932).
[67] S. Rosenblum, Nucleonics **4**, 38 (1949).
[68] W. Y. Chang, Phys. Rev. **70**, 632 (1946).
[69] R. Walen, Comptes Rendus **227**, 1090 (1948).
[70] Weissbluth, Putnam, and Segrè, private communication (July 1948).
[71] E. L. Kelley and E. Segrè, Phys. Rev. **75**, 999 (1949).
[72] Barton, Ghiorso, and Perlman, unpublished data.

thought to be Fr^{212}.[28] It was assigned to At^{208} principally on the basis of the appearance of Po^{208} at the rate corresponding to the decay of a 1.8 hr. parent. It may be mentioned that by spallation reactions of bismuth another apparent astatine parent of Po^{208} is produced which decays with a longer half-life than 1.8 hrs. and has no observable alpha-radiation.[72] It is possible that there are isomers of At^{208} which show up in different abundances by the two modes of formation.

Through excitation function measurements a 5.76 Mev alpha-particle decaying with 1.8-hr. half-life has been assigned to At^{207}.[72] Two other probable astatine isotopes are assigned to At^{205} and At^{204} somewhat arbitrarily although the mass number range is defined by excitation experiments. The two activities are respectively a 25-min. period of 5.9 Mev alpha-energy and a 10-min. period with a 6.1 Mev alpha-particle.[72]

Po^{209}

This new isotope of polonium has a 200-year half-life for alpha-decay estimated from yield considerations[71] and the alpha-particle energy has been revised slightly as 4.90 Mev.[72] The electron capture branching is not known accurately but was estimated from the amount of L-x-rays as a maximum of 1 in 10.[24] The electron capture half-life would be accordingly greater than 2000 years.

Po^{205} and lighter polonium isotopes

As in the case of light astatine isotopes there is little accurate information on the alpha-half-lives of these species and the isotopic assignments are not certain. The energies are sufficiently well known and the isotopic assignments are well enough defined for use in Fig. 1 to show the trend expected in this region. The presently accepted decay properties of Po^{205} are a measured half-life of 1.5 hr. with a 5.2 Mev alpha-particle.[24] The 5.35 Mev alpha-particle with 4-hour half-life[3] has been reassigned to Po^{204},[24] while the 40 min., 5.56 Mev alpha-emitter is retained at Po^{203}. In each case the degree of alpha-branching is not known.

[72] A. Ghiorso, unpublished data.

Bi^{208}(?)

In a previous communication[10] a 5.0 Mev alpha-particle found by Howland and Perlman (unpublished) was attributed to Bi^{208}. This alpha-particle appeared as a very weak activity in the bismuth fraction of pile neutron irradiated bismuth and was thought to arise from an $n,2n$ reaction. This assignment was not very attractive since we might expect Bi^{208} to have an alpha-energy not greater and perhaps less than that of Bi^{209}. The interesting possibility is being explored[74] that the 5.0 Mev alpha-group belongs to a metastable state of Bi^{210}(RaE) highly forbidden toward isomeric transition and beta-decay. Partial but inconclusive evidence for this assignment has been obtained.

Bi^{201}

The 60-min. activity with alpha-particles of 5.15 Mev assigned to Bi^{200} [3] has been reassigned to Bi^{201} on the basis of its genetic relationship to 8-hr. Pb and 72-hr. Tl which are tentatively assigned to mass number 201.[21]

Bi^{199}

This is the only one of the neutron deficient bismuth alpha-emitters for which the alpha-branching has now been estimated. Its isotopic assignment has been made[21] by observing the growth through successive electron capture processes of Pb^{199} and the 7.5-hr. Tl^{199}. The alpha-branching calculated from the yields of the Tl^{199} and the observed alpha-emission rate is 1.7×10^{-3} percent which gives an alpha-half-life of 3 years.

Bi^{197}

This 2-min. activity assigned to Bi^{197} is used in these correlations in terms of its minimum alpha-half-life by assuming that the measured half-life is controlled by the alpha-decay process.

Au^{190}

This alpha-emitter[3] has been more positively identified as an isotope of gold and by measuring the other radiation decaying with a 5-min. half-life, the alpha-branching was estimated as 10^{-2} percent.[23]

[74] Neumann, Howland, and Perlman, unpublished data.

PHYSICAL REVIEW VOLUME 77, NUMBER 1 JANUARY 1, 1950

The Beta-Spectra of Cl^{38}*

LAWRENCE M. LANGER**
Los Alamos Scientific Laboratory, Los Alamos, New Mexico
(Received September 23, 1949)

The beta-spectra of the 38-min. activity of Cl^{38} was studied in a magnetic lens spectrometer. The momentum distribution was resolved into three groups with end points of 4.81, 2.77, and 1.11 Mev. The highest energy group was found to have a shape characteristic of a once forbidden transition involving a spin change of 2 units and a change of parity.

INTRODUCTION

THE 38-min. activity of Cl^{38} has been studied by many investigators.[1] Most recent measurements with magnetic spectrometers have been made by Hole and Siegbahn[2] and by Watase and Itoh.[3] In both cases, the beta-transition was found to be complex with at least two and probably three groups of electrons.

By means of a Fermi plot analysis, Hole and Siegbahn arrive at end points of 1.19, 2.70, and 5.2 Mev. However, because of the effect of saturation in the iron of their spectrometer, they express some uncertainty about the accuracy of the high energy group which in turn raises some doubts about the exact determination of the inner end points. They prefer, therefore, to base the value of the beta-end points upon the energy measurement of the two cascade gamma-rays which they measure as 1.60 Mev and 2.15 Mev. They assume that the energy determination of the lowest beta-group is

* This document is based on work performed under government Contract No. W-7405-Eng-36 for the Los Alamos Scientific Laboratory of the University of California.
** Indiana University, Bloomington, Indiana.
[1] Complete references to earlier work may be found in reference 2.
[2] N. Hole and K. Siegbahn, Arkiv. f. Mat., Astr. o. Fys. 33A, No. 9 (1946).
[3] Y. Watase and J. Itoh, Proc. Phys. Math. Soc. Japan 30, 626 (1939).

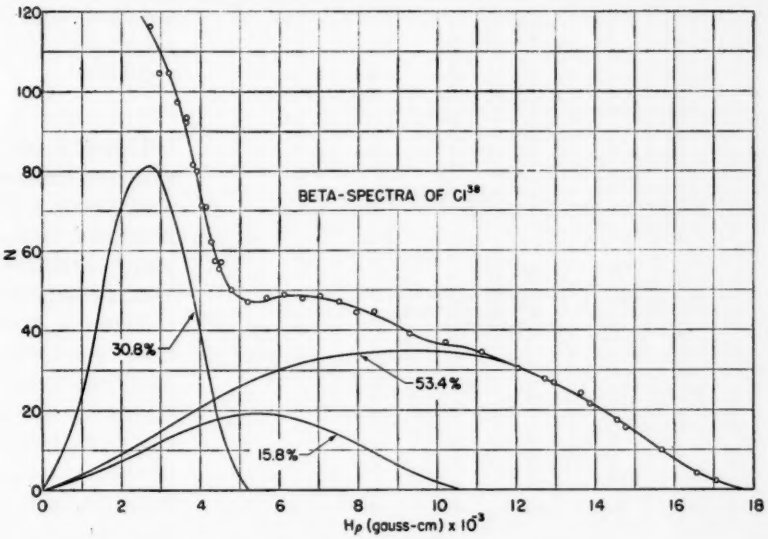

FIG. 1. Momentum distribution of electrons of Cl^{38}. Ordinate is counting rate divided by coil current.

correct. In this way, they obtain 1.19, 2.79, and 4.94 Mev.

By inspection of the momentum distribution, Watase and Itoh find end points at 4.99±0.06 Mev and at about 1.1 Mev. On the basis of a Fermi plot, they report 4.99, 1.08±0.06 and probably a third group at 2.6 Mev. From the distribution of the Compton electrons ejected from a radiator, Itoh[4] has determined the energy of the gamma-rays as 1.64±0.02 Mev and 2.19±0.03 Mev. Coincidence experiments indicate that these gamma-rays are in cascade.

In both investigations, the Fermi plots of the beta-spectra were interpreted as being of the allowed shape and a straight line extrapolation was made on that basis. The results of the present study indicate that the highest energy group has a spectrum of the once forbidden type; the conventional Fermi plot curves toward the energy axis near the end point. The evaluation of this and the lower end points is changed somewhat by this interpretation of the data.

EXPERIMENTAL METHOD

Measurements were made with a large thin lens spectrometer. Preliminary experiments indicated that a rather strong dipole field was being induced in the reenforced concrete of the floor beneath the lens. This trouble was eliminated by banding the spectrometer tube with iron rings in accordance with the suggestion of L. W. McKeehan.[5] One-inch wide transformer iron wound to a thickness of $\frac{1}{8}$ in. and spaced $\frac{1}{2}$ in. apart was employed. This arrangement was found to be quite effective in eliminating interference from all external vertical fields including that of the earth. Under these conditions, it was found that, in spite of the presence of iron, the magnetic focusing field was linearly proportional to the coil current to much better than one percent over the entire range of the instrument, i.e., up to $H\rho=46{,}000$ gauss-cm.

Appropriate baffles and diaphragms were installed, which minimized the possible detection of scattered radiation and of harmonic spectra. A pair of sector baffles which are very effective in discriminating between positrons and electrons, are also of value in suppressing harmonic spectra. These bafflels consist of two identical $\frac{3}{4}$-in. thick aluminum disks each having two diametrically opposed sector openings of just a little less than 90 degrees each. The disks are rotated on their common axis through 45 degrees with respect to each other and spaced experimentally by means of a Wilson-type vacuum seal so as to offer optimum discrimination. Although the transmission of the instrument is reduced somewhat by this arrangement, it is felt that there is less opportunity for scattering than exists with the spiral or "paddlewheel" type baffle.[6]

For the present experiment, the detecting diaphragm opening and the source diameter were 0.75 in. For these conditions, it was found that the resolution, as determined by the full width at half-maximum of the line of internal conversion electrons associated with the 0.663-Mev gamma-ray which follows the decay of Cs^{137}, could be varied from 2.4 to 6.4 percent by setting the position of a disk baffle. This baffle limits the effective annular aperture of the lens. The energy calibration of the instrument is in terms of this 0.663-Mev gamma-ray.

The source was mounted on a skeleton aluminum framework which could be brought accurately and quickly into its proper position through a vacuum gate. The source itself consisted of 10 mg/cm² of NH_4Cl uniformly deposited over a 0.75-in. diameter circle on a 0.0002-in. Al backing. Such a source thickness and backing may be regarded as "thin" for the high energy electrons here under investigation.

Activation was obtained by slow neutron capture in

[4] J. Itoh, Proc. Phys. Math. Soc. Japan 23, 605 (1941).
[5] D. E. Alburger, Rev. Sci. Inst. 19, 474 (1948).
[6] Deutsch, Elliot, and Evans, Rev. Sci. Inst. 15, 178 (1944).

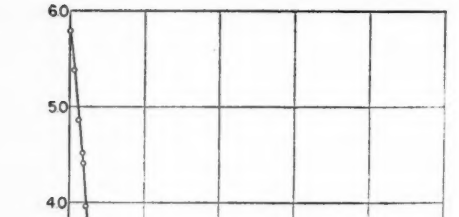

FIG. 2. Conventional Fermi plot of Cl^{38} data. The energy W is in units of m_0c^2.

the thermal column of a nuclear reactor. The same source was used for several bombardments. Measurement of the decay period showed that there was no interference from other activities, e.g., the excitation of 14.8-hr. Na^{24} in the aluminum backing by $Al(n, \alpha)$ was completely negligible.

Detection was by means of a 3.5-mg/cm² mica end window G-M counter. The counter was found to be completely stable and gave reproducible results when operated after the one-hour "warm-up" required to assure drift-free operation of the electronic lens current stabilizer.

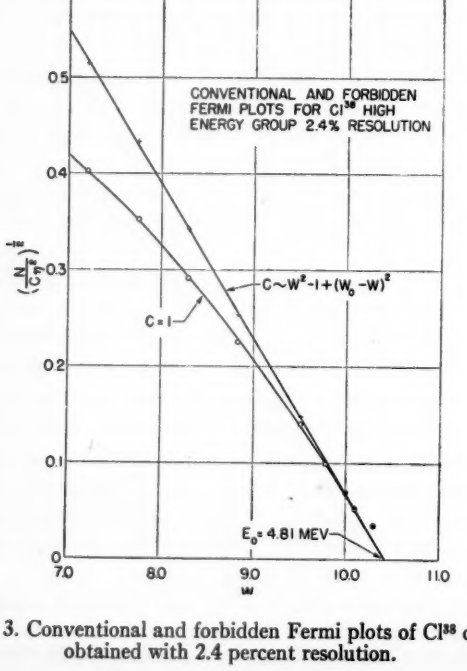

FIG. 3. Conventional and forbidden Fermi plots of Cl^{38} data obtained with 2.4 percent resolution.

RESULTS

Figure 1 shows the momentum distribution of the electrons emitted by Cl^{38}. The ordinate, of course, is the actual counting rate divided by the current, in order to normalize to constant detection sensitivity. From the shape of the curve, it is quite obvious that the distribution is composed of three superposed spectra.

Figure 2 shows the conventional Fermi plot of the data applicable to allowed transitions. The usual Coulomb factor is not shown in the ordinate since for such a low Z element, it is a very good constant over the energy range covered by the data. Careful examination of the points near the maximum energy suggest that the data do not fall on a straight line but rather on a curve which is concave toward the energy axis. If the last two points were corrected for the finite resolution of the instrument, they would be shifted so as to appear with the same ordinate at slightly lower values of the energy. This would make the curvature even more obvious. A curvature of this nature does indeed also occur in the Fermi plot of the data of Hole and Siegbahn.[2] They, however, apparently chose to ignore it, probably because of the previously mentioned saturation effect in the iron of the spectrometer.

Figure 3 shows Fermi plots of the data on the highest energy group obtained with 2.4 percent resolution. The lower curve is the conventional Fermi plot and shows the curvature quite clearly. The upper curve was obtained by dividing the ordinate by the factor $C^{\frac{1}{2}}\sim[W^2-1+(W_0-W)^2]^{\frac{1}{2}}$. This factor uniquely determines the shape of a once-forbidden transition involving a change

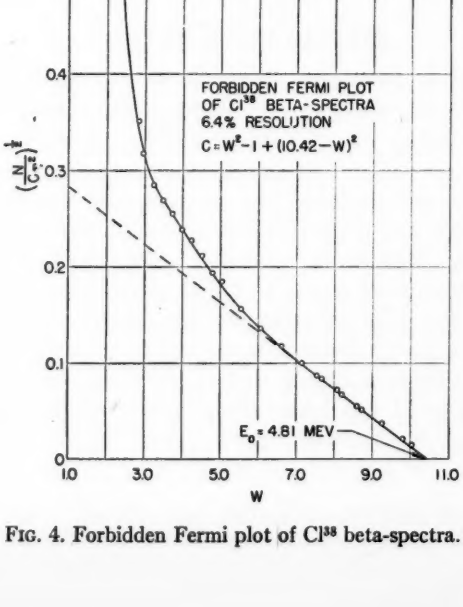

FIG. 4. Forbidden Fermi plot of Cl^{38} beta-spectra.

of two units of angular momentum and a parity change.[7] The end point of the high energy group determined from this plot is 4.81±0.05 Mev. A similar forbidden Fermi plot for all the data obtained at 6.4 percent resolution is shown in Fig. 4. Assuming that only the highest energy group is of the forbidden type, the lower energy groups are separated by proper subtraction as indicated in Fig. 5. The additional end points obtained in this way are 2.77±0.05 Mev and 1.11±0.01 Mev. The partial spectra determined from the Fermi plots are shown in Fig. 1.

DISCUSSION

The fact that the highest energy group has a spectrum which is completely described by applying the once-forbidden factor $W^2-1+(W_0-W)^2$, does not, in this case, uniquely determine that the change of angular momentum is 2 units. In general, according to G-T selection rules, a once-forbidden transition involves a change of parity and may have either 0, 1, or 2 units of angular momentum change. The forbidden factor C, which may modify the shape of the spectrum, may be written[8] as

$$C(W,Z)=\frac{a'}{18}(P_e^2+P_\nu^2)+\tfrac{2}{3}b'P_\nu\left(\frac{\alpha Z}{2R}+\frac{P_e^2}{3W}\right)+c'\left(\frac{\alpha^2Z^2}{4R^2}+\frac{\alpha Z}{3R}\frac{P_e^2}{W}\right),$$

where $P_e^2=W^2-1$ and $P_\nu^2=(W_0-W)^2$. For a spin change of 0 or 1, all three constants a', b', and c' are finite. For elements of medium to high atomic number, Z, the term $\alpha^2Z^2/4R^2$ is much larger than the others and the factor is not very energy dependent. As a result, one may expect such transitions to have spectrum shapes indistinguishably different from those of allowed transitions. However, for once-forbidden transitions involving a spin change of 2 units, only the constant a' remains finite and the characteristic shape described above is obtained. On the other hand, the existence of this shape does not uniquely assure that the spin change in Cl^{38} is 2 units. This arises from the fact that for such a low Z and high energy, is is conceivable that the second and third terms in the forbidden factor might be vanishingly small compared to the first term. Thus, the possibility of a spin change of 0 or 1 is not completely excluded on this basis alone.

According to the theory of nuclear shell structure,[9] one may expect for the $_{17}Cl^{38}$ nucleus that the odd proton will be in a $d_{3/2}$-state and the odd neutron in a $f_{7/2}$-state. These may combine to give a state of odd parity having a resultant spin of either 2, 3, 4, or 5. The product nucleus, $_{18}A^{38}$ has an even number of protons and neutrons and is therefore expected to have zero spin and even parity. A spin change of two units is, therefore, the only value consistent with both experiment and theory. The comparative half-life ($ft\sim2\times10^7$) is also reasonable for a once-forbidden transition from Cl^{38} involving a spin change of 2.

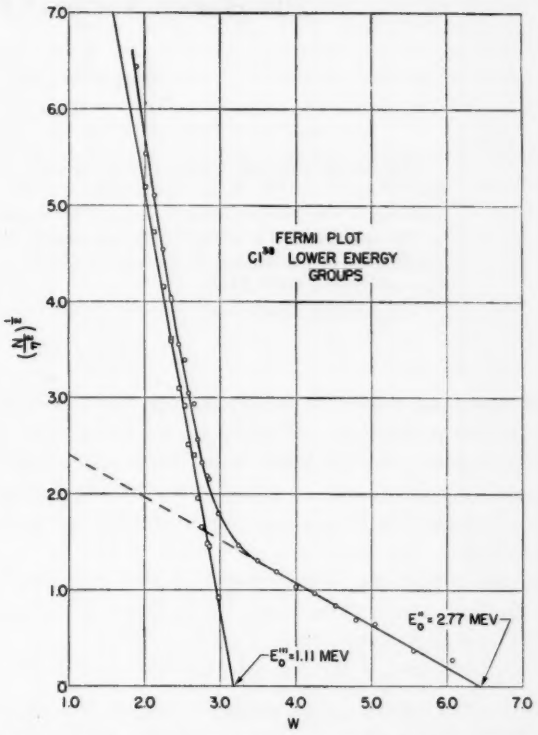

FIG. 5. Fermi plot of lower energy groups of Cl^{38} beta-spectra.

CONCLUSION

The beta-disintegration of Cl^{38} is complex and consists of three groups. The end-point energies and the branching ratios are: 4.81±0.05 Mev, 53.4 percent; 2.77±0.05 Mev, 15.8 percent; 1.11±0.01 Mev, 30.8 percent. The highest energy group was found to have a spectrum shape which is characteristic of a once-forbidden transition involving a spin change of two units and a change of parity. In agreement with the theory of nuclear shell structure this is presumably a transition from the state of $_{17}Cl^{38}$ having spin 2 and odd parity to the ground state of $_{18}A^{38}$ having even parity and zero spin. The intermediate group of electrons with end-point energy of 2.77 Mev has a comparative half-life ($ft\sim10^7$) which is reasonable for a once-forbidden transition having a spin change of 0 or 1. This spectrum is apparently of the allowed shape. The beta-transition having an end point of 1.11 Mev is allowed ($ft\sim10^5$). Therefore, it goes to a level of odd parity. Since the "cross-over" gamma-ray directly to the ground state is not observed, the spin of the second excited level in A^{38} is probably 3. From the beta-ray measurements alone, the excited levels in A^{38} lie at 2.04 Mev and 3.70 Mev above the ground state.

Thanks are due Mr. R. J. S. Brown and Mr. L. M. Baggett for assisting with the measurements.

[7] L. M. Langer and H. C. Price, Jr., Phys. Rev. **75**, 1109 (1949). L. M. Langer and H. C. Price, Jr., Phys. Rev. **76**, 641 (1949).

[8] G. Gamow and C. L. Critchfield, *Theory of Atomic Nucleus and Nuclear Energy-Sources* (Oxford University Press, New York, 1949), p. 139.

[9] M. G. Mayer, Phys. Rev. **75**, 1969 (1949).

The Heavy Nuclei of the Primary Cosmic Radiation

H. L. BRADT AND B. PETERS
University of Rochester, Rochester, New York
(Received September 9, 1949)

The flux of primary cosmic-ray nuclei, heavier than protons, was determined at geomagnetic latitudes $\lambda=55°$ and $\lambda=30°$N. It is shown that at $\lambda=30°$ at least one-half of the incident nucleons and a significant fraction of the incident cosmic-ray energy is due to the heavy component.

The distribution of atomic numbers among the primaries was determined at both latitudes; the relative magnitude of the fluxes of the nuclei H:He:C,N,O:(nuclei of charge $Z>10$) is given approximately by the ratio 4000:1000:35:10.

The possible significance of these results for the theories on the origin of cosmic rays is discussed.

IN previous papers[1–3] evidence has been presented for the occurrence of heavy nuclei in the primary cosmic radiation. Methods have been discussed for determining the charge of these nuclei from the analysis of the tracks they produce when traversing nuclear emulsions.

In this paper we shall present more extensive data on the flux, charge spectrum, and energy distribution of the primary cosmic rays of charge $Z>1$.

The discussion is divided into the following topics:

Section I. Evidence for the primary character of energetic heavy nuclei.
Section II. The identification of particles and the flux of primary helium nuclei.
Section III. The mean free path for nuclear collisions of heavy cosmic-ray primaries.
Section IV. The flux of primary cosmic rays of charge $Z\geq 6$.
Section V. The low energy part of the spectrum at $\lambda=55°$.
Section VI. The contribution of heavy primary nuclei to the total primary and secondary radiation.
Section VII. The latitude effect of the heavy primary radiation and its energy spectrum.
Section VIII. The relative abundance of the different elements in the primary radiation.
Section IX. Remarks on the origin of cosmic radiation.

Our investigations are based on the tracks of particles in emulsions of large stacks of photographic plates[2] exposed at altitudes corresponding to about 16 g/cm, of residual atmosphere.

The results presented in this paper are mainly derived from four high altitude balloon flights, for which the relevant data are listed below in Table I.

I. EVIDENCE FOR THE PRIMARY CHARACTER OF ENERGETIC HEAVY NUCLEI

Our original conclusion that the energetic heavy nuclei observed at high altitudes are cosmic-ray primaries has been greatly strengthened by later observations and it therefore seems desirable to summarize the present evidence.

A

Several hundred particles with at least several g/cm² residual range and atomic number $Z\geq 6$ were recorded in a systematic survey; none has been found to originate in the stack of plates of dimensions 50–100 g/cm² exposed below 16 g/cm² of residual air unless it was the disintegration product of a still heavier incident nucleus. Thus, if the energetic heavy nuclei are secondaries, they could only be produced by a particle which is destroyed at the very top of the atmosphere with a mean free path for destruction of only a few g/cm². The collision cross section of such a particle would therefore have to be extremely large.

Heavy fragments with charges up to $Z\sim 10$ are occasionally emitted in violent nuclear explosions produced by neutral or singly charged particles, but their ranges rarely exceed a few hundred microns.[4]

TABLE I.

Flight No.	Date	Geographical location lat. long.	Geomagn. latitude	Material above plates (mainly air) (in g/cm²)	Time of exposure (hours)	Size of stack
1	10–27–48	44°N 94°W	55°N	16	5	58 plates (3 in.×20 in.)
2	2–4–49	19°N 79°W	30°N	16	6	25 plates (3 in.×10 in.)
3	5–29–49	40°N 76°W	51°N	~10	3	24 plates (3 in.×10 in.)
4	7–30–49	44°N 94°W	55°N	16	6	24 plates (1 in.×3 in.)

[1] Freier, Lofgren, Ney, Oppenheimer, Bradt, and Peters, Phys. Rev. 74, 213 (1948).
[2] H. L. Bradt and B. Peters, Phys. Rev. 74, 1828 (1948).
[3] Freier, Lofgren, Ney, and Oppenheimer, Phys. Rev. 74, 1818 (1948).
[4] A. Bonnetti and C. Dillworth, Phil. Mag. 40, 585 (1949).

B

All observations indicate that the energetic heavy particles enter from the upper hemisphere. The direction of motion of the particle is known:

(1) If the particle slows down as evidenced by a rapid increase in δ-ray density (approximately fifty such cases have been observed, all of which show downward motion).

(2) If one end of the track terminates in a nuclear explosion in the photographic emulsion (Fig. 1). It should be the lower end of the track if the particle produced the star and the upper end if it originated in the star. (In all cases observed, with the exception of tracks of fragments of still heavier nuclei, it is the lower end of the track which terminates in a star.)

(3) If the particle undergoes a nuclear collision in the glass in which it is only partially destroyed.[5] The particle then emerges

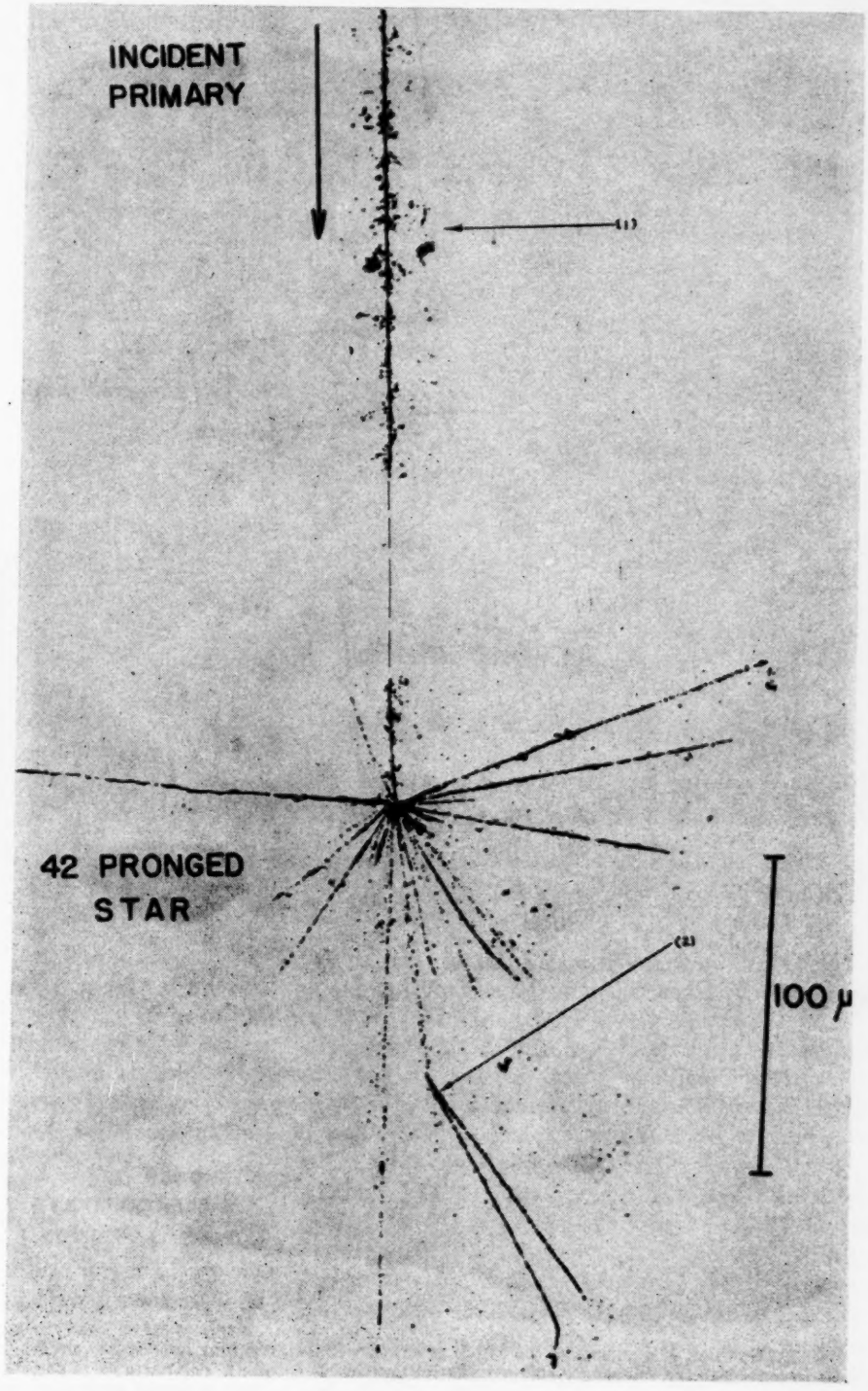

FIG. 1. Collision of a primary Ca nucleus ($Z=20\pm1$) with an energy of the order of at least 100 Bev and an Ag or Br nucleus of a Kodak NTB3 emulsion, flown in Flight No. 2 at $\lambda=30°$N. 42 charged particles are emitted in this violent explosion. 10 prongs are minimum ionization tracks, collimated in the forward direction (they are hardly visible in Fig. 1); most of them probably are tracks of a meson shower. One fast, singly charged particle causes a second nuclear event (2).

[5] H. L. Bradt and B. Peters, Phys. Rev. 75, 1779 (1949).

with reduced charge accompanied by satellites consisting of fast protons and α-particles (see Fig. 3 of reference 5). (About 40 such cases have been observed, all of which show downward motion.)

C

There is an observable concentration of heavy tracks around the zenith direction in plates exposed below

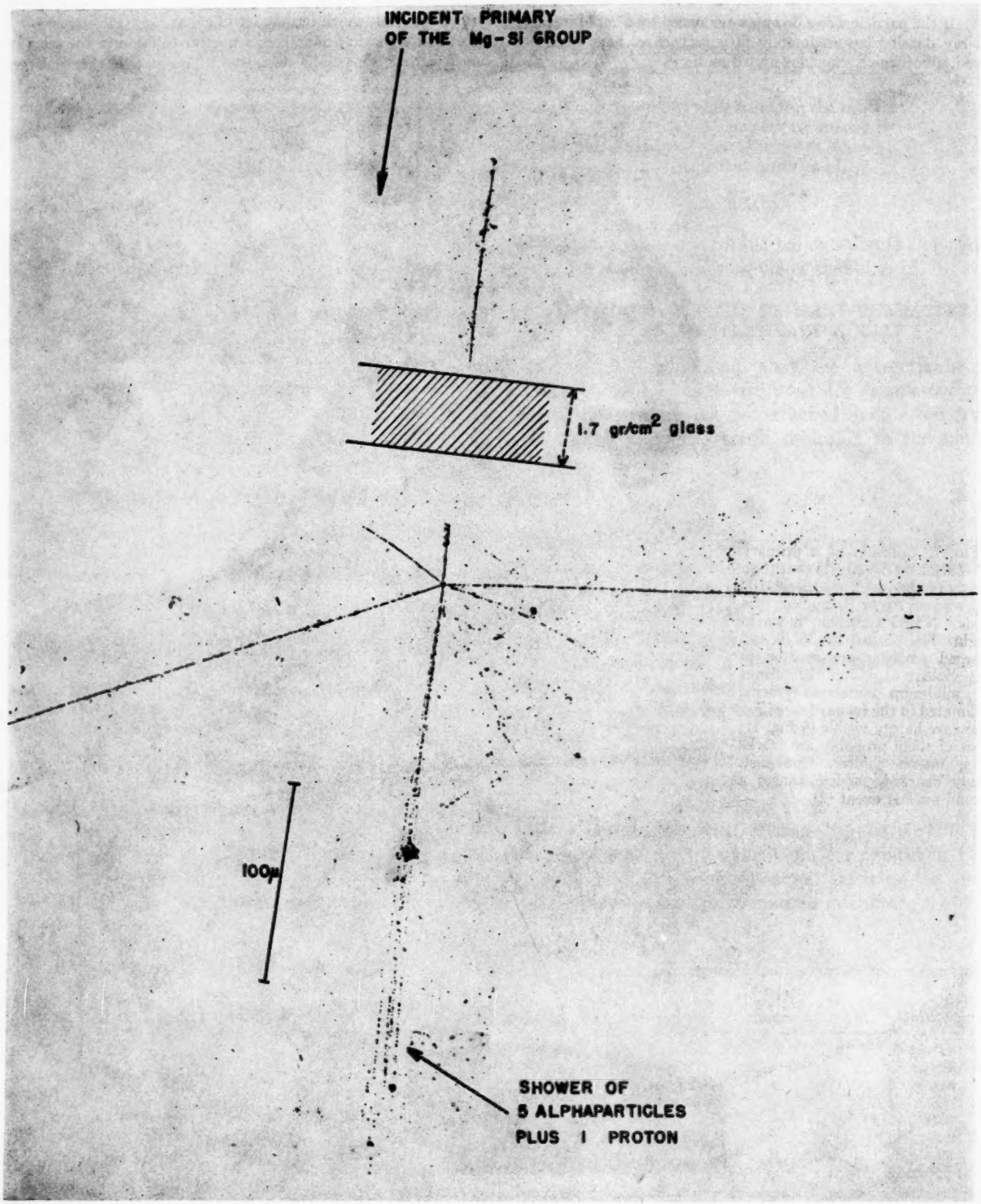

FIG. 2a. Collision of a nucleus of the Mg-Si group ($Z \sim 12$–14), resulting in a narrow shower of five doubly charged relativistic particles (α-particles) and one singly charged relativistic particle (proton). The particles of the shower, carrying 11 units of charge, are considered to be the products of the dissociation of the incident nucleus. A second minimum ionization track emerges with an angle of 30° with respect to the shower axis. Four low energy particles ejected from the star at large angles with respect to the direction of the primary are considered to be fragments of the target nucleus.

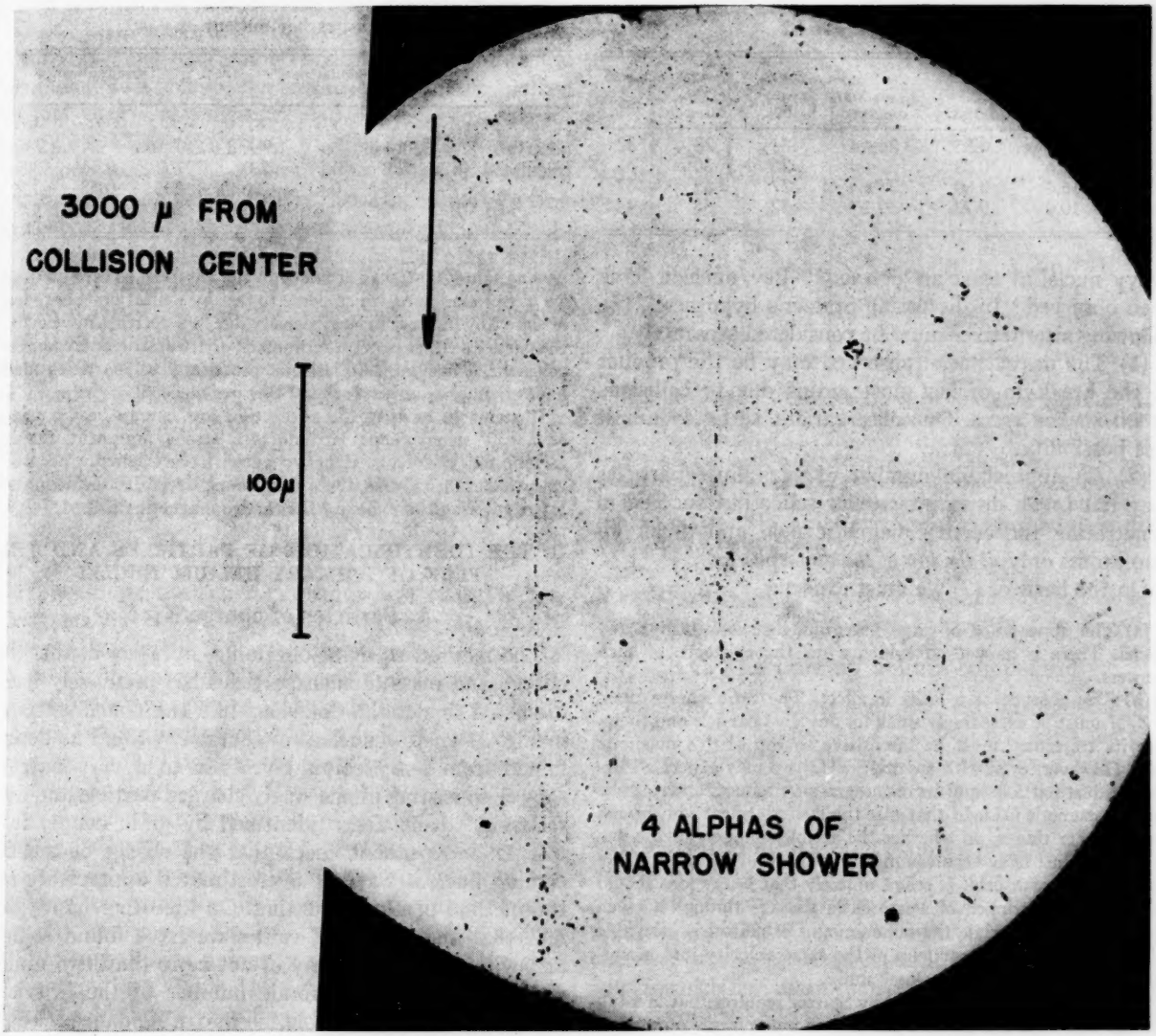

FIG. 2b. Tracks of 4 of the 5 alpha-particles of the shower of Fig. 2a as they appear in the next plate of the stack, after traversal of 3-mm glass. The average angle of the tracks of the five alpha-particles with respect to the axis of the shower is 0.03 radian, corresponding to an energy of the incident nucleus of ~(3–4) Bev per nucleon.

16 g/cm² of air. This indicates a flux of particles entering from the upper hemisphere with an absorption mean free path of the order of, but longer than, 16 g/cm² of air. In a previous communication[5] we have reported values for the mean free path obtained from direct measurements and have shown that these values are consistent with the size of the nuclei as obtained from our charge determination.

D

It has been established with certainty that some of the nuclei observed have atomic numbers much greater than that of air nuclei. This has been demonstrated previously[2] by the self-consistency of charge determinations obtained from δ-ray densities over wide ranges of residual path lengths. It is also conclusively demonstrated by collisions of the type illustrated in Fig. 2, as will be discussed later. Nuclei which are heavier than air nuclei obviously must arrive from the outside.

While the facts listed above show, in our opinion, conclusively that the heavy nuclei observed are not created by a primary proton component, they, of course, do not rule out the possibility that these nuclei may arrive as part of still larger structures.

A plausible mechanism whereby dust grains could be accelerated by the radiation pressure in the neighborhood of supernovae up to energies of the order of 1 Bev per nucleon has recently been suggested by Spitzer.[6] We therefore shall consider the possibility that the heavy primaries observed are remains of larger structures such as dust grains, although energies of the

[6] L. Spitzer, Phys. Rev. **76**, 583 (1949).

TABLE II. δ-ray count for the track of an iron atom (Flight No. 1), $Z=26\pm2$

Plate	Residual range R(gr/cm²)	$\beta=v/c$	δ-rays/100μ observed	$Z=24$ δ-rays/100μ	$Z=26$ calculated	$Z=28$
321	26.0	0.85	26±4	24	28	32
361	21.6	0.83	32±4	26	30	35
401	16.4	0.80	35±4	27	32	37
451	10.0	0.73	39±4	32	38	44

TABLE III. Observed and calculated specific energy loss for a fast carbon nucleus.

		Residual range $R=13.7$ g/cm⁻²			Residual range $R=6.8$ g/cm⁻²		
	Z	K	v/c	n_δ	K	v/c	n_δ
observed		120–140		1.9±.2	140–160		2.9±.2
calculated	6	120	0.59	2.0	160	0.51	2.8
	7	155	0.61	2.6	205	0.53	3.7
	8	190	0.63	3.3	250	0.55	4.8

heavy nuclei at least as high as 10 Bev/nucleon have been observed.[5] In discussing Spitzer's hypothesis, the following alternatives must be considered separately:

(1) The heavy nuclei observed may be the product of the break-up of fast dust grains due to collisions *in interstellar space.* Our observations certainly admit this possibility.

(2) An appreciable number of such dust particles may not break up in interstellar space but succeed in penetrating the earth's magnetic field and break up into atoms only *at the top of the atmosphere.*

On the basis of (2) we must expect:

(a) The appearance of large narrow-angle showers of heavy nuclei. There is as yet no evidence for the existence of such showers.

(b) The absence of a latitude effect. The ratio charge/mass $=Z/M$ must be exceedingly small for any dust particle and therefore its trajectory must be insensitive to the earth's magnetic field. However, even with assumption (2) we may expect a mixture of dust particles and its disintegration products entering the earth's magnetic field. In that case the latitude effect will depend among other things, on whether the atomic products of the disintegrated dust have been completely stripped of electrons before entering the earth field. It seems unlikely that heavy ions should be completely stripped of electrons in passage through a given amount of matter while the same amount of matter is incapable of disintegrating dust particles of the same velocity into atoms, but this point may require closer study.

(c) The mechanism suggested by Spitzer requires that in addition to very high energy dust particles, a much larger number of dust particles with lower energy should be produced. Therefore even if only a small fraction of undisintegrated dust penetrated the earth's magnetic field at latitude $\lambda=30°$ we should nevertheless observe even at this latitude heavy nuclei of low energy.

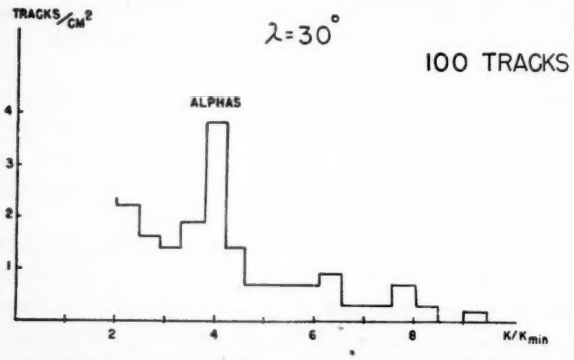

FIG. 3. Frequency of 100 tracks of length $L\geq750\mu$ in an area of 5.8 cm² emulsion of plate No. 190 flown at $\lambda=30°$ plotted against the specific energy loss K (in units of the minimum energy loss of singly charged particles K_{min}) corresponding to their grain density. A definite peak occurs for $K=4K_{min}$; this peak is ascribed to primary α-particles.

Among some 200 tracks of heavy nuclei observed so far at $\lambda=30°$ we have found none which come to rest by ionization energy loss or show any increase in δ-ray density due to a decrease in velocity; the particles either penetrate the stack or are destroyed by nuclear collisions. Thus at that latitude practically all particles must have energies of at least several Bev per nucleon.

It seems to us that the absence of low energy heavy nuclei at $\lambda=30°$ geomagnetic latitude is a strong argument against assumption (2). Thus, if heavy nuclei have originally been accelerated as dust grains, these grains must have been disintegrated *before* entering the region of the earth's magnetic field.

II. THE IDENTIFICATION OF PARTICLES AND THE FLUX OF PRIMARY HELIUM NUCLEI

A. Particles of charge $Z\geq6$

The method used for obtaining, by δ-ray count, the charge and mass of such particles has previously been discussed in detail.[2] Collisions like the one illustrated in Fig. 2, where a nucleus of charge $Z=13\pm1$ as determined from δ-ray count gives rise to a very narrow shower consisting of one singly charged particle and five relativistic α-particles (identified by grain count) furnish an independent check that the charge of the incoming nucleus was not overestimated appreciably by the method of δ-ray counting. On the other hand, the fact that the highest Z-values we have found so far are, within an uncertainty of not more than two units, equal to $Z=26$, the atomic number of the heaviest element with appreciable cosmic abundance (iron), indicates that the charges of the heavy nuclei are also not underestimated.

In emulsions of high sensitivity, which show a comparatively large number of low energy electron tracks, the "background" of unrelated δ-rays, which has to be subtracted from the observed number of δ-rays, is not negligible for the lightest tracks. The background has been determined by comparing δ-ray densities of long ($\sim25000\mu$) tracks of relativistic α-particles with δ-ray densities of minimum ionization tracks. In the plates flown at $\lambda=30°$ in Flight No. 2, for instance, the δ-ray density for minimum ionization tracks was determined to $n_1'=0.26$(δ-rays/100), the δ-ray density of relativistic α-particles to $n_2'=0.44$(δ-rays/100μ). Since the true δ-ray density of relativistic α-particles, corrected for background, n_2, must be four times greater than the corrected δ-ray density of minimum ionization tracks n_1, we obtain for the δ-ray calibration of these plates

$$(n_\delta)_Z=(0.060\cdot Z^2+0.2)(\delta\text{-rays}/100\mu),$$

for particles of charge Z and $\beta=v/c=1$.

For carbon and iron nuclei, this relation yields the values $(n_\delta)_C = 2.4$ and $(n_\delta)_{Fe} = 41$(δ-rays/100μ), respectively. The diagram of Fig. 10, which shows the frequency of tracks observed in these plates plotted against their δ-ray density, shows a definite peak for $n_\delta = (2.3 \pm 0.2)$(δ-rays/100μ), which is therefore ascribed to carbon nuclei. The highest δ-ray densities observed are $n_\delta \sim (39\text{–}45)$($\delta$-rays/100$\mu$), therefore corresponding to charges close to the charge of an iron nucleus.

The same results were obtained in the other flights (see Fig. 11 and Fig. 12). The plates flown at $\lambda = 55°$N in Flight No. 1, for instance, were somewhat less sensitive than the plates of Flight No. 2 and therefore less restrictive criteria were used for the δ-ray counting. As an example, we present in Table II the results of the δ-ray analysis of one of the heaviest tracks found in the plates of Flight No. 1, a-photo-micrograph of which has been reproduced in Fig. 1 of reference 14. The calculated δ-ray densities are based on a calibration corresponding to $n_\delta \cdot \beta^2 = (1.1 \pm 0.1)$($\delta$-rays/100$\mu$) for carbon nuclei.

We estimate the accuracy of our best charge determinations by δ-ray count to be approximately ± 10 percent. However it is possible to improve the accuracy for nuclei of charge $Z \lesssim 10$ by using plates sufficiently underdeveloped to permit grain counting. The accuracy obtainable by this method may be judged from the following example. Consider the track of a heavy particle which entered a stack of Ilford C2 plates making an angle $\vartheta = 17°$ with the zenith direction, traversed 6 plates (13.7 g/cm^{-2} of glass) and came to rest in the emulsion of the seventh plate. The sensitivity of the emulsion was calibrated by measuring the grain density of proton and meson tracks of varying residual ranges and plotting the grain density as a function of the specific energy loss. Table III shows the observed values of the specific energy loss $K = -dE/dR$ in Mev/(g/cm^2) and of the δ-ray density per 100μ track length n_δ. It also shows the calculated values of K and n_δ for three different assumed values of the charge Z.

Comparing the observed and calculated values we conclude that the particle was a nucleus of carbon rather than nitrogen or oxygen and that it entered the stack with an energy of 2.7 Bev ($v/c = 0.59$).

B. Particles of charge $3 \leq Z \leq 5$

These nuclei present a special problem. The δ-ray density is too low to permit accurate charge determination unless the track is exceptionally long. The grain density of relativistic particles of charges $Z = 3$, 4 and 5 is equal to that of protons of residual range 4000μ, 1600μ and 400μ respectively and to that of α-particles of ranges 100,000μ, 28,000μ and 9000μ respectively. Thus tracks of nuclei of charge $3 \leq Z \leq 5$ have to be sorted out from a large background of tracks of slower secondary particles, which have similar appearance. Some tracks of relativistic Li, Be and B nuclei have been identified, but a systematic investigation of such tracks has not yet been carried through.

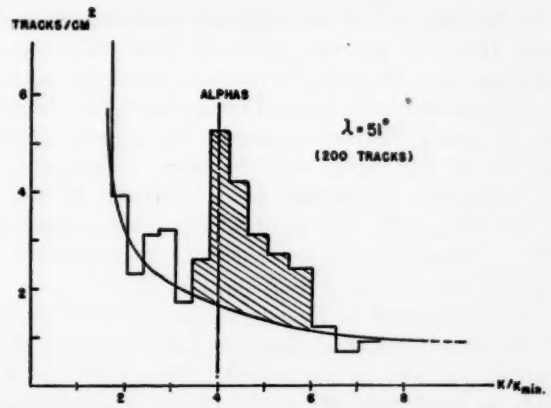

FIG. 4. Frequency distribution of 200 tracks of length $L \geq 750\mu$ in an area $A = 5.1$ cm^2 of emulsions exposed at latitude $\lambda = 51°$, plotted against K/K_{min}. The α-particle peak is broader than the corresponding peak observed at $\lambda = 30°$ (Fig. 3) extending up to about $K/K_{min} = 6$. Indeed, since the geomagnetic cut-off energy at $\lambda = 51°$ is only 0.5 Bev per nucleon primary α-particles with a specific ionization in the interval $K/K_{min} = 4$ to 5.5 can penetrate the earth's magnetic field.

C. The primary helium component

The difficulty connected with establishing the flux of particles of charge $3 \leq Z \leq 5$ does not exist for particles of charge $Z = 2$ because their number is not small compared to the number of slow secondary particle tracks with which they may be confused. The procedure used to identify the primary helium component was as follows:

(1) In an emulsion of a plate flown in Flight No. 2 for a time $t = 22{,}000$ sec. at $\lambda = 30°$, thickness $a = 100\mu$, sensitive to singly charged particles of all energies, all tracks which had more than 200 developed silver grains were recorded and their grain density was determined. 80 percent of all tracks so selected showed grain densities between 9 and 11 grains/75 microns, the remaining 20 percent were distributed between 11 and 80 grains/75 microns. No tracks showed a density of less than 9/75 microns. Thus minimum ionization for singly charged particles corresponds to a grain density of 10 grains/75μ in these plates. This conclusion was verified by grain counting several pairs of thin tracks emerging from a common origin with very small angles between them (which were interpreted as due to electron-positron pairs) and also by counting the tracks in a μ–β-decay.

TABLE IV. Mean free path for nuclear collisions of heavy primaries in glass.

Group	Z	Number of collisions N	L cm	ΔL cm	Path length $L+\Delta L$ cm	Mean free path (gr/cm^2) observed	calculated $\Delta R=0$	calculated $\Delta R=0.85 \cdot 10^{-13}$ cm
I	6–8	40	520	20	540	33±5	20	34
II	10–18	26	255	13	269	25±5	16	25
III	26±2	8	59	3	62	19±6	12	18

(2) An area of 5.8 cm² was surveyed for all tracks longer than 750 microns provided their grain density was larger than 18 grains/75 microns. When the number of tracks so selected is plotted *versus* their grain density, one obtains a distinct maximum at a grain density between 36 and 40/75 microns which corresponds to the minimum ionization of a particle of charge $Z=2(K/K_{\min}=4)$. The width of the peak is consistent with a unique value of grain density, corresponding to a specific energy loss $K=4K_{\min}$ (Fig. 3).

The strong peak at $K/K_{\min}=4$ could, of course, also be due to an abnormal abundance of secondary singly charged particles in the velocity range $0.38<\beta<0.42$. Such an interpretation would require an exceedingly large production in stars of particles of a particular energy (i.e., protons of 80 Mev). Not only is there no such anomaly but it can easily be shown that the peak of the distribution curve of Fig. 3 cannot be due to particles which are locally produced. We conclude that it is due to primary α-particles. Its structure is consistent with a minimum α-particle energy in excess of 3.5 Bev per nucleon, the minimum energy required for the arrival of doubly charged He ions at geomagnetic latitude $\lambda=30°$. The peak accounts for about one-fourth of all the particles of track length $\geq L=750\mu$, equivalent to a particle density of $n=4.5$ alpha-particles/cm².

The flux of alpha-particles is then equal to

$$I_0=\frac{n}{4tp_L}$$

with $$p_L=\int_0^{\pi/2}\exp\left(\frac{-h}{\lambda\cos\vartheta}\right)\sin^2\vartheta d\vartheta$$

$$-\int_\alpha^{\pi/2}\exp\left(\frac{-h}{\lambda\cos\vartheta}\right)\sin\vartheta(\cos^2\alpha-\cos^2\vartheta)^{\frac{1}{2}}d\vartheta$$

and $\sin\alpha=a/L$

$h=16$ g/cm²=amount of material above the plates.

Assuming a mean free path of $\lambda_{\text{air}}\sim 40$ g/cm² we ob-

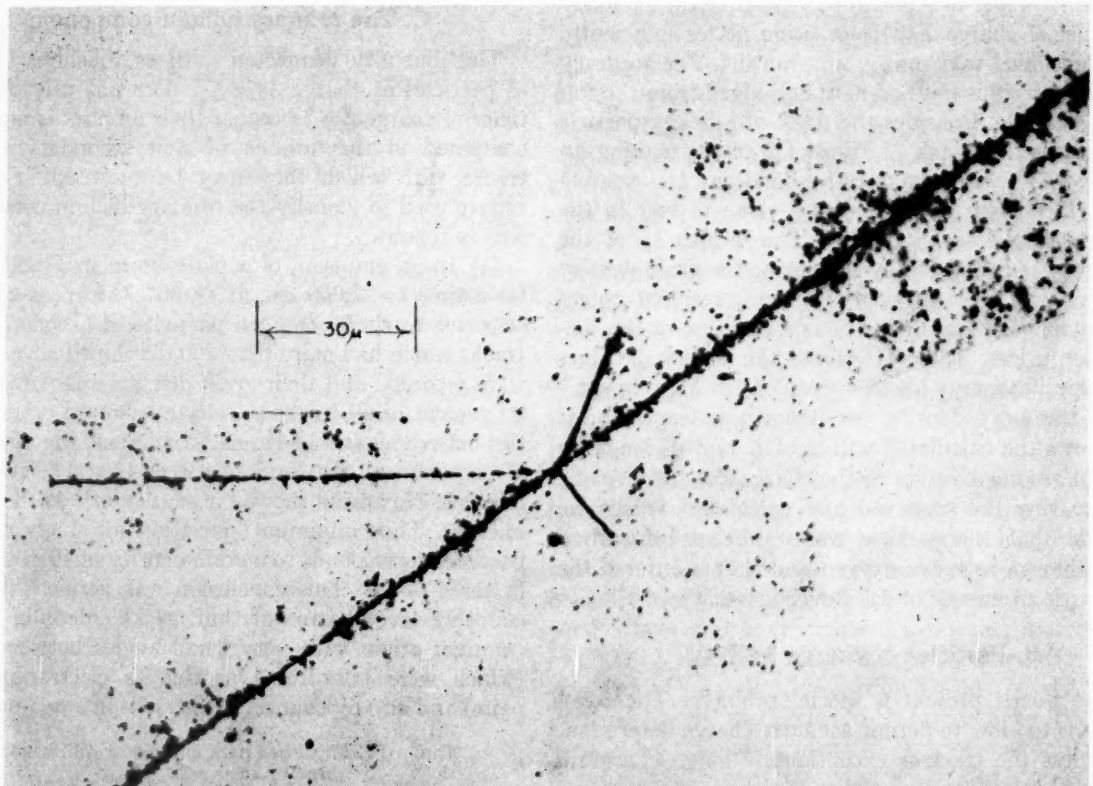

FIG. 5. A nucleus with charge $Z\sim 20$ causes ejection of three charged particles from a target nucleus without suffering any noticeable deflection or loss of charge. This event, which was observed by Dr. E. O. Salant and Dr. J. Hornbostel, may be the result of a rather distant collision. (Courtesy of Dr. E. O. Salant and Dr. J. Hornbostel, Brookhaven National Laboratory.)

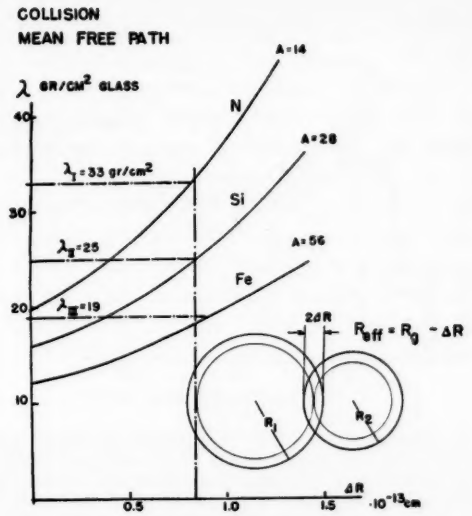

FIG. 6. Mean free path for collisions in g/cm² glass plotted against the decrement of nuclear radius $\Delta R = R_{geom} - R_{eff}$. The curves are calculated for nitrogen, silicon and iron nuclei, respectively, assuming $\lambda = 1/(\Sigma_i n_i \sigma_{ieff})$ and $R_{geom} = 1.45 \cdot 10^{-13} A^{\frac{1}{3}}$ cm for all nuclei involved. The observed values of the collision mean free path: $\lambda_{C,N,O} = 33$ g/cm², $\lambda_{(10 \leq Z \leq 18)} = 25$ g/cm², $\lambda_{Fe} = 19$ g/cm², correspond to a unique value of $\Delta R \sim 0.85 \cdot 10^{-13}$ cm.

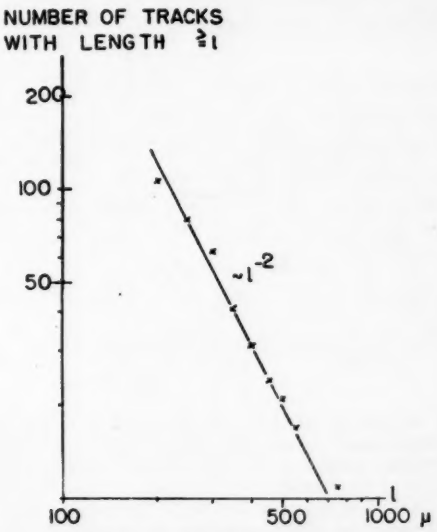

FIG. 7. Integral length distribution of 106 tracks of length $\geq 200\mu$ in a 93μ thick emulsion flown at $\lambda = 30°$. The number of tracks $N(l)$ with length $\geq l$ follows the expected $1/l^2$ distribution.

tain for the flux at the top of the atmosphere:*

$$I_0^{(He)}(30°) = (9 \pm 3) \cdot 10^{-3} \frac{\text{He nuclei}}{\text{cm}^2 \text{ sec. steradian}}.$$

A similar investigation at geomagnetic latitude $\lambda = 51°$ (Flight No. 3) showed also a very distinct α-particle peak of the grain density distribution curve (Fig. 4); at this latitude the peak is broadened toward higher grain densities, as one might expect at a latitude where the magnetic field permits the entrance of primary α-particles with energies of only 0.5 Bev per nucleon.

For the flux of alpha-particles at the top of the atmosphere at geomagnetic latitude $\lambda = 51°$ the value

$$I_0^{He}(51°) = (38 \pm 13) \cdot 10^{-3} \frac{\text{He nuclei}}{\text{cm}^2 \text{ sec. steradian}}$$

is obtained.

(3) As a further check on the interpretation of the peak given above, some individual tracks whose grain density corresponds to four times minimum ionization have been directly identified as tracks of relativistic helium nuclei. One such track, for instance, penetrated 56 g/cm² of glass without showing any change in grain density. A proton producing a track of equal grain density would have an energy of 80 Mev and a range of only 6.5 g/cm². Even if the track is ascribed to a triton nucleus, the heaviest singly charged particle, the range would be only 19.5 g/cm². On the other hand, the grain density of a track produced by a lithium nucleus would have been at least twice the observed grain density. Hence the track must have been produced by a helium nucleus of energy larger than 3 Bev.

Combined with the absolute flux values for all primary cosmic rays as obtained by J. R. Winckler *et al.* (private communication) and by M. A. Pomerantz[7] the α-particle flux values given above indicate, that at both latitudes about 20 percent of the primaries are α-particles. Pomerantz and Hereford[8] have concluded from their observations with low sensitivity coincidence counters that at $\lambda = 50°$ thirty percent of the primaries are α-particles.

(4) Evidence for high energy γ-rays. In the course of this analysis of grain densities we have observed a number of tracks with a grain density corresponding to exactly twice minimum ionization. Some of them, on close inspection, proved to consist of two minimum ionization tracks originating at a point in the emulsion and diverging very slightly. Those tracks can be considered as tracks of an electron-positron pair created by an energetic γ-ray. Long tracks of constant grain density corresponding to twice minimum ionization are most likely unresolved tracks of electron-positron pairs whose angular divergence is smaller than our resolution ($\vartheta \lesssim 5 \cdot 10^{-4}$ radians) produced by γ-rays of energy $h\nu \gtrsim 10$ Bev.

One might have expected that electrons of such high energies should show a substantial relativistic increase of grain density due to the relativistic increase of specific energy loss in solids as calculated by Fermi[9]

* This calculation is based on the assumption that the flux of particles at the top of the atmosphere is isotropic for which evidence will be presented in Section IV.

[7] M. A. Pomerantz, Phys. Rev. **76**, 165 (1949).
[8] M. A. Pomerantz and F. L. Hereford, Phys. Rev. **76**, 997 (1949).
[9] E. Fermi, Phys. Rev. **56**, 1242 (1939); **57**, 485 (1940).

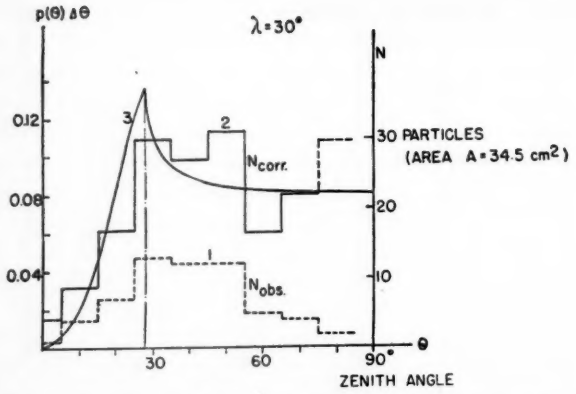

FIG. 8. Angular distribution of 60 tracks of C,N,O nuclei at $\lambda=30°$. Histogram 1 gives the actual number of tracks with length $\geq l=200\mu$ obtained in a systematic survey of an area $A=34.5$ cm² of an emulsion of thickness $a=93\mu$, vertically oriented, flown for $t=6$ hours at $\lambda=30°$N (right scale). Histogram 2 gives the number of tracks, corrected as outlined in the text for absorption in the glass of the plates and the air overhead. Curve (3) is the geometrical factor

$$P_1(\vartheta)\Delta\vartheta=[N_{corr}(\vartheta)]/[A\cdot t\cdot I(\vartheta)].$$

It is seen that, whereas $N_{obs}(\vartheta)$ decreases with ϑ for large zenith angles because of the increasing absorption of the air overhead, the variation of $N_{corr}(\vartheta)$ is within the statistical accuracy given by $P_1(\vartheta)$. This indicates isotropy of the radiation at the top of the atmosphere.

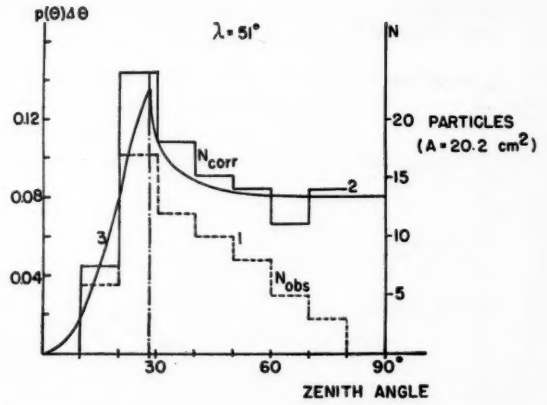

FIG. 9. Angular distribution of 61 tracks of heavy primaries at $\lambda=51°$N.—The 61 tracks of Fig. 9 of length $\geq l=200\mu$, 48 of them due to C,N,O nuclei, were obtained from a complete survey of an area of $A=20.2$ cm² of an emulsion of thickness $a=90\mu$, flown for $t=3$ hours at geomagnetic latitude $\lambda=51°$N. For further explanation see caption to Fig. 8.

and Halpern and Hall.[10] However the sharpness of the peak for tracks with grain density corresponding to minimum grain density observed by us but also by Powell *et al.*[11] seems to indicate that the relativistic increase of grain density in the emulsions used is small.

In addition to what appear to be tracks of very high energy electron positron pairs we have observed the development of a larger mixed shower and cases of direct pair production by electrons (which were themselves members of a pair produced by a γ-ray in the emulsion).[12] While no quantitative work has as yet been done with nuclear emulsions on the soft component of cosmic radiation, it is evident that emulsions will prove to be useful tools for such investigations.

III. MEAN FREE PATH FOR NUCLEAR COLLISIONS OF HEAVY COSMIC-RAY PRIMARIES

Various types of collisions of heavy primaries have been described previously (reference 5). Examples of collisions occurring in the emulsion are shown in Figs. 1, 2, 5 and 14. The mean free path in the glass of the photographic plates for collisions in which the charge of the incident primary is reduced by at least two units, has been determined separately for the nuclei of the C,N,O-group (group I), for nuclei of intermediate charge values $10<Z<18$ (group II) and for nuclei of the iron group (group III).

TABLE V. Flux of heavy primaries at geomagnetic latitudes 55°, 51° and 30°N.

Geom. latitude	Flight No.	$10^3\cdot I_0$(10^3 nuclei)/cm² sec. steradian) $Z=2$	$6\leq Z\leq 10$	$Z>10$
55°	4	—	1.1 ±0.2	0.30±0.1
51°	3	38±13	1.2 ±0.3	0.35±0.07
30°	2	9±3	0.35±0.06	0.10±0.03

The residual length l of all the tracks found in a systematic survey of a number of plates was measured. l is the length of track between the plate surveyed until either the point where the particle leaves the stack or the last plate where the particle is recorded before a collision occurs. Since the exact location of the collision in the glass has in general not been determined, we add in the case of a collision to the observed track length l one-half the path length in the glass before and after collision (Δl). If $L=\sum l$, $\Delta L=\sum\Delta l$, the mean free path is obtained by dividing the total track length $L+\Delta L$ by the number of collision observed. The results are listed in Table IV.

The observed values for the mean free path, listed in column 7 of Table IV, are significantly larger than the values calculated with the assumption that the effective collision cross section σ_{eff} is equal to the geometrical nuclear cross section $\sigma_{geom}(\Delta R=R_{geom}-R_{eff}=0)$. We estimate that with the criteria adopted for the identification of collisions (especially the systematic search for satellite tracks) only a small fraction of actual collisions in the glass would have been missed. Collisions of heavy nuclei in which neither their direction nor their charge is noticeably changed have been observed (Fig. 5),** but seem to be rather infrequent.

It is conceivable that during the passage of an incident nucleus near a target nucleus some small

[10] O. Halpern and H. Hall, Phys. Rev. **73**, 477 (1948).
[11] Brown, Camerini, Fowler, Muirhead, Powell, and Ritson, Nature **163**, 47, 82 (1949).
[12] H. L. Bradt, M. F. Kaplon and B. Peters, Helv. Phys. Acta (in print).

** The event of Fig. 5 has been observed by Dr. E. O. Salant and Dr. J. Hornbostel of the Brookhaven National Laboratory. We are greatly indebted to them for pointing out to us this event and for the loan of the plate.

overlapping of the geometrical nuclear volumes may occur without causing serious damage to either projectile or target nucleus. In order to estimate whether this may possibly explain the rather large observed mean free path values, we make the crude assumption that the effective collision radius R_{eff} is equal to the geometrical radius $R_{geom}=r_0A^{\frac{1}{3}}(r_0=1.45\cdot10^{-13}$ cm) minus a certain decrement ΔR, which may be expected to be of the order of the range of nuclear forces. If R is the geometrical radius of the incident nucleus, R_i the geometrical radius of the nucleus of kind i of the glass, we have for the collision cross section

$$\sigma_i=\pi(R+R_i-2\Delta R)^2,$$

and for the mean free path

$$\lambda=1/\sum n_i\sigma_i,$$

where n_i is the number of nuclei of kind i per unit volume of the glass. Figure 6 shows a plot of the values of λ thus calculated on the basis of the known chemical composition of the glass against the decrement of nuclear radius ΔR. It is seen that the calculated values agree within the experimental error with the observed values $\Delta R=0.85\times10^{-13}$ cm, a decrement of nuclear radius equal to about one-half the range of nuclear forces.

IV. THE FLUX OF HEAVY PRIMARY COSMIC RAYS

In order to obtain the flux of particles at the top of the atmosphere, a number of plates were surveyed for tracks longer than a certain minimum length l and the zenith angle ϑ was measured for each track. Each track within an angular interval $\Delta\vartheta$ was given the statistical weight $\exp[(L'/\lambda_g)+(h/\lambda_a\cos\vartheta)]$ in order to correct for the loss of particles by nuclear collisions taking place above the plate which was surveyed. Here L' is the amount of glass which the particle penetrated before it reached the plate which was surveyed, h is the amount of air above the plates, λ_g and $\lambda_a\approx0.9\lambda_g$ are the mean free paths (in g/cm²) for nuclear collisions in glass and in air, respectively, as obtained in Section III; ϑ is the zenith angle.

After multiplying the number of tracks in a given angular interval, corrected for nuclear collisions, by the appropriate geometric factor, which depends on the orientation of the plates and the criteria used for selection, we obtain for each interval of the zenith angle the number of particles incident at the top of the atmosphere with an energy sufficient to penetrate the air above the plates. The flux at the top of the atmosphere thus calculated has been found to be within the statistical accuracy independent of the zenith angle in all cases.

As an example we shall consider the 60 tracks of length $\geq200\mu$ of nuclei with charge $6\leq Z<10$ found in a systematic survey of $A=34.5$ cm² emulsion of the plates flown in Flight No. 2. The survey was made independently by two observers, which obtained essentially identical results. The plane of the emulsion of thickness $a=93\mu$ was vertical.

Figure 7 shows the integral length distribution of 106 heavy tracks found in a systematic survey of two plates of Flight No. 2. The observed number of tracks with length $\geq l$ follows closely the expected distribution, which is given with sufficient approximation by the relation $N(l)\sim1/l^2$. This provides an additional check that indeed no appreciable number of tracks of length $\geq200\mu$ have been missed in the survey.

TABLE VI. Data for 30 tracks of particles stopping by ionization in the stack of 58 plates flown at Camp Ripley ($\lambda=55°$N).

1	2	3	4	5	6	7	8	9
No.	Number of plates traversed by the particle	Charge Z	Zenith angle ϑ	Range in glass R_g	v/c	Total range R	Energy per nucleon ϵ	Total kinetic energy E
			Degrees	g/cm²		g/cm²	Bev	Bev
1	6	6	17	13.7	0.59	33	0.39	4.7
2	5	6	34	22.7	0.66	56	0.55	6.6
3	4	6	3	41.0	0.74	60	0.57	6.9
4	2	6	49	13.6	0.59	59	0.57	6.8
5	3	6	10	14.5	0.60	30	0.37	4.5
6	6	6	32	14.1	0.60	32	0.38	4.6
7	10	6	29	17.2	0.62	34	0.39	4.7
8	6	6	18	15.8	0.61	32	0.38	4.6
9	8	6	16	24.4	0.66	40	0.44	5.3
10	9	6	26	26.2	0.67	43	0.47	5.7
11	1	6	50	9.6	0.55	32	0.38	4.6
12	6	7	30	26.0	0.71	43	0.52	7.3
13	5	8	39	11.2	0.60	30	0.45	7.2
14	3	8	31	7.8	0.56	25	0.40	6.4
15	7	8	14	24.0	0.70	40	0.53	8.5
16	4	8	12	19.0	0.67	34	0.48	7.7
17	4	10	54	7.4	0.58	33	0.54	11
18	8	11	35	11.8	0.65	26	0.50	11
19	25	12	16	69.0	0.87	85	1.20	29
20	9	12	25	16.4	0.70	35	0.63	15
21	4	12	33	12.0	0.66	30	0.57	14
22	12	12	43	26.6	0.77	42	0.71	17
23	11	14	34	18.0	0.74	36	0.71	20
24	4	14	29	29.4	0.80	89	1.40	39
25	2	14	34	13.0	0.70	31	0.65	18
26	4	20	10	5.6	0.63	21	0.62	25
27	8	22	37	5.9	0.65	25	0.76	34
28	24	26	40	35.0	0.88	55	1.45	81
29	20	26	46	24.6	0.84	48	1.30	73
30	4	26	14	22.8	0.84	38	1.10	62

The number ΔN of tracks of length $L\geq l$ in the interval of zenith angle between ϑ and $\vartheta+\Delta\vartheta$, corrected for the loss of particles by collisions, is related to the true flux $I(\vartheta)$, (the number of particles per cm², per sec. and per unit solid angle) by the relation

$$\Delta N=A\cdot t\cdot I(\vartheta)\cdot P_l(\vartheta)\cdot\Delta\vartheta,$$

where A is the area surveyed and t the time of exposure. The geometrical factor $P_l(\vartheta)$ for vertical plate orientation and selection of tracks of length $\geq l$ in the unprocessed emulsion is given by

$$P_l(\vartheta)=\begin{cases}4\sin^2\vartheta & (\vartheta\leq\alpha)\\ 4\sin^2\vartheta\left[1-\left\{1-\left(\dfrac{a}{l\sin\vartheta}\right)^2\right\}^{\frac{1}{2}}\right] & (\vartheta\geq\alpha),\end{cases}$$

where α is given by $\sin\alpha=a/l$, or $\alpha=28°$.

TABLE VII. Breakdown of flux data for $\lambda=30°$.

	Particles/ m² sec. steradian	%	Nucleons m² sec. steradian	%
Protons	356	79.0	356	45.0
Helium	90	20.0	360	45.3
C, N, O	3.5	.78	49	6.2
$Z>10$	1	.22	28	3.5
Total	450	100%	793	100%

In Fig. 8, histogram 1 represents the observed number of tracks (out of a total of 60 tracks) per 10° interval, plotted against the zenith angle ϑ. Histogram 2 gives the number of tracks, as corrected for absorption in the material overhead. Curve 3 (left scale) gives the function $P_l(\vartheta)\Delta\vartheta$. It is seen that the variation of $N_{corr}(\vartheta)$ with zenith angle ϑ follows within the statistical accuracy the function $P_l(\vartheta)$, as would follow from an isotropic flux distribution $I(\vartheta)=I_0$. The falling off of the observed number of tracks with zenith angle shows the influence of the absorption of the air overhead. The absolute value of I_0 is deduced from Fig. 8 to be

$$I_0=\frac{1}{A\cdot t}\cdot\frac{N_{corr}}{P_l(\vartheta)\Delta\vartheta}$$

$$=\frac{1}{34.5\times2.2\times10^4}(275\pm35),$$

$$I_0(\lambda=30°)=(3.5\pm0.6)10^{-4}\frac{\text{C,N,O-nuclei}}{\text{cm}^2\text{ sec. steradian}}.$$

For the particles with $Z>10$ a value for the flux at the top of the atmosphere of

$$I_0(30°)=(1.0\pm0.3)10^{-4}\frac{\text{nuclei with } Z>10}{\text{cm}^2\text{ sec. steradian}}$$

is obtained.

Figure 9 shows the angular distribution of 61 tracks recorded and followed through the stack in a systematic survey of $A=20.2$ cm² of emulsion of thickness $a=90\mu$, flown for $t=3$ hours at $\lambda=51°$ (Flight No. 3). 47 tracks (77 percent) were tracks of nuclei of the C,N,O group. The criterion used for selection, hence the function $P_l(\vartheta)$ is the same as for Fig. 8, the only difference being that for this survey the particles were required to enter the plate from the side turned away from the stack of plates. Since the same number passed the plate from the other side, the numbers of Fig. 9 have to be multiplied with a factor 2 in order to obtain the flux at the top of the atmosphere. For C,N,O nuclei we obtain

$$I_0=2\cdot0.77\cdot\frac{(167\pm30)}{20.2\cdot1.1\cdot10^4}$$

$$=(1.2\pm.3)\cdot10^{-3}\frac{\text{C,N,O nuclei}}{\text{cm}^2\text{ sec. steradian}}.$$

The flux at the top of the atmosphere of nuclei with $Z>10$ is about $\frac{1}{3}$ of this value.

The flux values of heavy primary ions at the top of atmosphere are summarized in Table V.

The fact that the observed flux is within the statistical error uniform from $\vartheta=0$ to $\vartheta=65°$ indicates that the fraction of particles with ranges between 16 g/cm² and 40 g/cm² of air is a small fraction of the total flux. This conclusion is corroborated by the observation that at $\lambda=55°$ and at $\lambda=51°$ only 10 percent of all particles stop in the stack of plates, while at $\lambda=30°$ none of the 100 particles observed stop in the stack. From this we conclude that at $\lambda=30°$ no particles enter with energies below those observable in this experiment and that the figures quoted therefore represent the true flux values at this latitude.

At $\lambda=55°$, however, a closer analysis of the low energy part of the radiation is required.

V. THE LOW ENERGY PART OF THE SPECTRUM OF HEAVY PRIMARY NUCLEI AT $\lambda=55°$N

At geomagnetic latitude $\lambda=55°$N the magnetic field of the earth will not permit protons of less than $E_0'=1.0$ Bev and completely stripped heavier nuclei ($A=2Z$) of less than $E_0^Z=0.35\times A$ Bev to reach the atmosphere from the zenith direction.[13] The knee of the latitude curve observed at lower altitudes, occurring at $\lambda=40°$ for sea level observation and at $\lambda=48°$N for observation at 25–30,000 feet altitude has in the past fre-

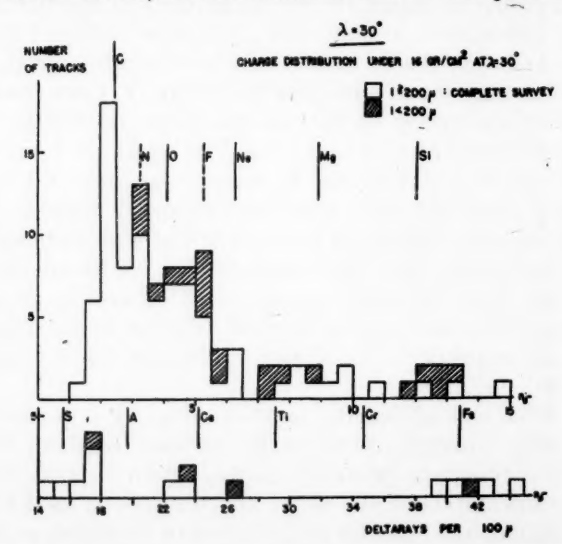

FIG. 10. Charge spectrum under 16 g/cm² air at $\lambda=30°$ (Flight No. 2).—The observed frequency of tracks with length $l\geq200\mu$ is plotted against their δ-ray density (blank squares). Out of a total of 119 tracks of length $\geq200\mu$ found in a systematic survey, 22 are tracks of nuclei with $Z>10$, four of them tracks of iron nuclei. The shaded squares represent additional tracks of length $<200\mu$, found in a survey which is only representative for the higher charge values. Since the heavier nuclei are more rapidly destroyed by collisions in the material above the plates than the lighter nuclei, the charge distribution at the top of the atmosphere will show a somewhat greater proportion of the heavier nuclei than the distribution shown in Fig. 10.

[13] M. S. Vallarta, Phys. Rev. 74, 1837 (1948).

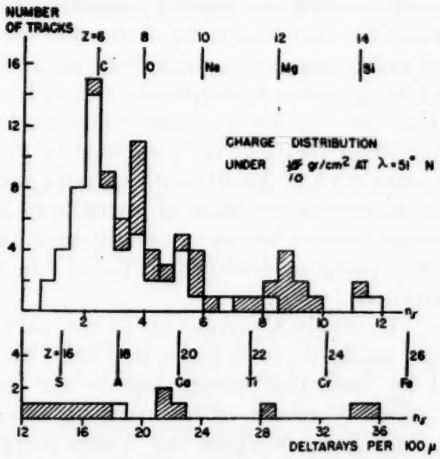

FIG. 11. Charge spectrum under 10 g/cm² of air at $\lambda=51°$ (Flight No. 3).—Of the total of 100 tracks of length $l\geq 200\mu$, 60 tracks result from a systematic survey of an area of 20.2 cm² of emulsion (blank squares), while the remaining 40 tracks (shaded squares) were found in a survey of 26.3 cm² which was complete only for tracks of particles with charge $Z\geq 10$.

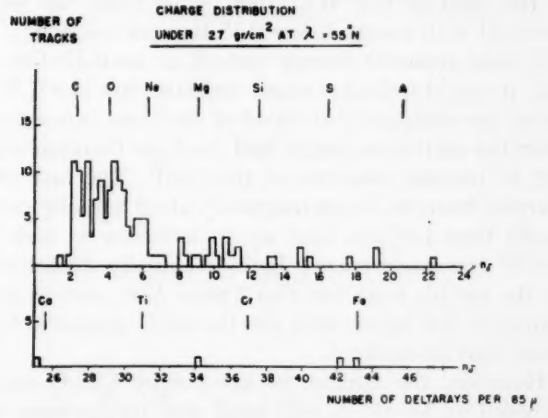

FIG. 12. Charge spectrum under 27 g/cm² of air and glass at $\lambda=55°$ (Flight No. 1).—This histogram is based on 165 tracks found in a complete survey of a given horizontal area for tracks with a projection on the vertical axis $lz=\geq 145\mu$ in 24 vertically stacked plates.

quently been interpreted as an indication that the actual minimum energy of nuclei at $\lambda=55°$N may be considerably higher than the geomagnetic cut-off for this latitude. On the other hand, if the heavy primary ions do not arrive as completely stripped ions, their geomagnetic cut-off energy would be considerably lower than the above value. For instance, the minimum energy per nucleon for penetration of the earth magnetic field at $\lambda=55°$ is $\epsilon_0=0.35$ Bev for completely stripped carbon nuclei, $\epsilon_1=0.15$ Bev for four times ionized carbon, and only $\epsilon_2=0.04$ Bev for doubly ionized carbon.

In order to determine the minimum energy of heavy primaries at $\lambda=55°$N we have selected from some 200 tracks traced through the stack flown at Camp Ripley at 97,000 ft. in Flight No. 1 a total of 30 tracks of particles which were stopped by ionization energy loss in the stack and for which the range thus could be determined. Only two of them stopped in one of the emulsions. In these cases the range can of course be very accurately measured. In general the particles stop between two adjacent glass plates. In these cases the tracks, if followed through successive plates, show increasing δ-ray density in the last few plates before they disappear. (Disappearance of the track without any previous increase in δ-ray density is considered to be due to a nuclear collision in the glass.) If the particle is assumed to stop in the middle between the last emulsion where the track is still seen and the following one, where the track no longer appears, the uncertainty in range ΔR is equal to one-half the path length in one glass plate. Since most of the tracks have been followed through a great number of plates, this uncertainty is relatively small.

Table VI shows the data pertaining to these 30 tracks ending in the stack. Column 1 gives the track number, column 2 the number of plates through which the track has been traced, column 3 the charge Z (determined by δ-ray counting in all the plates penetrated by the particle), column 4 gives the zenith angle, column 5 the range in g/cm² glass, column 6 the velocity $\beta=v/c$ of the particle when entering the stack of plates, column 7 the total range from the top of the atmosphere (air and glass combined), column 8 the energy per nucleon ϵ, and column 9 the total energy at the top of the atmosphere.

The energy per nucleon ϵ can be determined with an accuracy given by

$$\frac{\Delta\epsilon}{\epsilon}=\left[\frac{R'}{E'}\cdot\frac{dE'}{dR'}\right]\left(\frac{\Delta Z}{Z}+\frac{\Delta R}{R}\right),$$

where R' and E' are the range and energy of a proton of equal velocity. (In the range of energies considered the quantity in the square bracket has a numerical value between 0.6 and 0.8.) $(\Delta Z)/Z$ and $(\Delta R)/R$ are the percentage error in the charge determination and the range determination respectively. In most cases ϵ can be obtained with an accuracy better than 10 percent.

In Figs. 2 and 3 of a preliminary communication[14] we have plotted the kinetic energies of these 30 particles stopping in the stack against their charges, and also the frequency of tracks against the energy per nucleon. As is seen also from Table VI energies per nucleon as low as $\epsilon=0.37$ Bev occur for the lighter ions, for which the energy necessary for penetrating the material above the plates is smaller than the geomagnetic cut-off energy for stripped nuclei $\epsilon_0=0.35$ Bev. This minimum energy amounts to 0.25 Bev per nucleon for carbon nuclei incident from the zenith. Actually, about one-half of the 16 nuclei of the C,N,O group stopping in the stack have energies per nucleon

[14] H. L. Bradt and B. Peters, Phys. Rev. 76, 156 (1949).

in the interval 0.37–0.45 Bev, while none has been observed with energy below 0.35 Bev per nucleon.

If this apparent energy cut-off at $\epsilon=0.37$ Bev is real, it would indeed strongly indicate that the C,N,O nuclei are completely stripped of electrons before they enter the earth's magnetic field (and are therefore subject to the full influence of this field). The fact that energies down to the geomagnetic cut-off actually occur would then indicate that up to latitudes as high as $\lambda=55°$ the lower energy limit is actually determined by the earth's field (see also Freier, Ney, and Oppenheimer[15]). An upper limit for the sun's magnetic field could thus be deduced.

However, the number of low energy C,N,O nuclei recorded at $\lambda=55°$ is still small and furthermore the upper few centimeters of the stack of plates of Flight 1 were of uneven sensitivity, a fact which discriminated somewhat against observing particles with energies per nucleon below 0.3 Bev. Though it therefore, may not be entirely safe to draw any definite conclusions about the solar magnetic field from the data presented in Table VI, it is clear that this type of measurement, especially when carried out at higher latitudes and greater altitudes should give useful information on the strength of the sun's magnetic field.

Additional evidence that at least the nuclei with atomic numbers $Z<10$ are completely stripped of electrons when entering the earth's magnetic field is deduced from the fact that none of the 150 completely analyzed nuclei stop in the stack flown at $\lambda=30°$. For, if C,N,O nuclei are not completely stripped, we must expect that the very heavy nuclei retain most of their electrons and are therefore not prevented by the earth's field to enter even at $\lambda=30°$ with energies sufficiently low to be stopped in the stack of plates flown in Flight 2. This is not the case for any of the still small number of very heavy particles observed so far in the stack of plates flown at $\lambda=30°$.

At $\lambda=55°$, about 8 percent of all the particles entering the stack of plates flown in Flight No. 1 were stopped by ionization energy loss in the stack. At $\lambda=51°$ about 7 percent of the particles entering the smaller stack flown in Flight No. 3 were stopped in it by ionization energy loss (17 tracks of particles stopped in the stack in a surveyed area of 80 cm² (0.21 tracks/cm²) as compared to a total of 60 heavy tracks in a surveyed area of 20.2 cm² (3 tracks/cm²)). The energies of most of the stopped particles lie in the interval between E_c and $2E_c$ (E_c=geomagnetic cut-off energy).

VI. THE CONTRIBUTION OF HEAVY PRIMARY NUCLEI TO THE TOTAL PRIMARY AND SECONDARY RADIATION

A discussion of the contribution of heavy primary nuclei to the total primary and secondary radiation

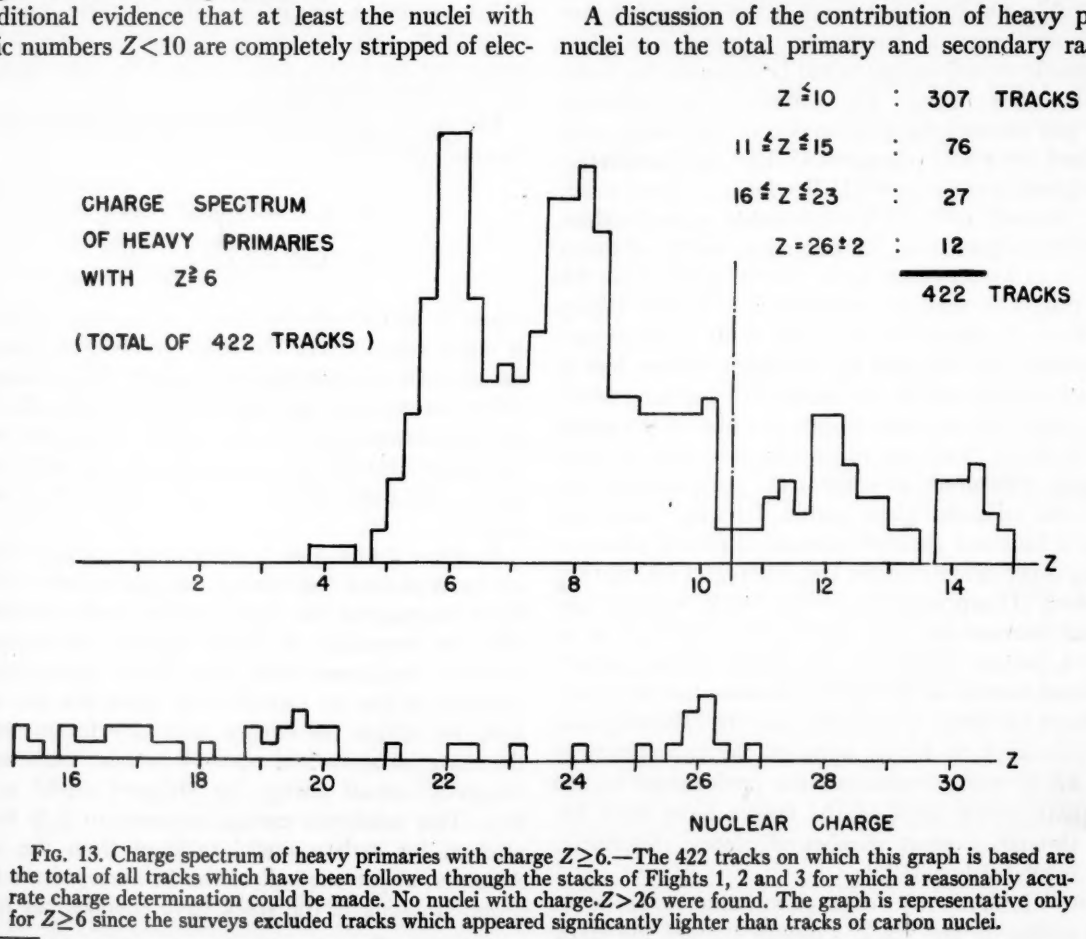

FIG. 13. Charge spectrum of heavy primaries with charge $Z\geq6$.—The 422 tracks on which this graph is based are the total of all tracks which have been followed through the stacks of Flights 1, 2 and 3 for which a reasonably accurate charge determination could be made. No nuclei with charge $Z>26$ were found. The graph is representative only for $Z\geq6$ since the surveys excluded tracks which appeared significantly lighter than tracks of carbon nuclei.

[15] Freier, Ney, and Oppenheimer, Phys. Rev. 75, 991 (1949).

should be based on the data obtained at $\lambda=30°$ for the following reasons:

A. The absence of low energy particles indicates that our flux data, extrapolated to the top of the atmosphere, represent the entire heavy primary radiation.

B. The flux at this latitude has been determined for all masses from helium to iron (except for Li, Be, B).

C. A reasonably close upper limit can be given for the total primary flux using the data obtained by J. R. Winckler.

We shall use for the primary flux at $\lambda=30°$ a value of 450 particles per square meter, sec. and steradian.

Using the flux data for $\lambda=30°$ quoted above the breakdown summarized in Table VII is obtained.

Thus one-half of the incoming nucleons are contained in the incident heavy nuclei and one-quarter of the total number of incoming nucleons are neutrons.

If the nuclei are stripped of electrons, their energies must exceed the geomagnetic cut-off energy at $\lambda=30°$ of $\epsilon_0=3.5$ Bev per nucleon. The energy lost by ionization per mean free path for collision is, on the other hand, equal to: for protons 170 Mev, for nitrogen 180 Mev/nucleon, for silicon 260 Mev/nucleon, for iron 330 Mev/nucleon, and therefore represents for all nuclei only a small fraction of their energy.

Thus most heavy primaries are destroyed in nuclear collisions long before they could be stopped by ionization and hence they ought to be responsible for about one-half of the secondary radiation observed at lower altitudes.

This leads to the conclusion that since the total cosmic-ray intensity at sea level shows only minute diurnal and seasonal variation, the same must be true for that part of the heavy component which is energetic enough to penetrate the earth field at $\lambda=30°$.

VII. THE LATITUDE EFFECT OF THE HEAVY PRIMARY RADIATION AND ITS ENERGY SPECTRUM

The last conclusion makes it legitimate to compare results at different latitudes although the measurements were made at different times.

In comparing the flux data obtained at $\lambda=55°-51°$ and $\lambda=30°$ we observe that the ratio of the number of nuclei of the carbon, nitrogen, oxygen group to the number of nuclei of charge $Z>10$ is within the experimental error the same at both latitudes. Therefore the velocity spectra of these two groups are similar at least up to energies of 5–10 Bev per nucleon. Comparing the absolute numbers at the two latitudes, we find that the latitude effect between latitudes 50° and 30° amounts to about a factor 3.5.*** In addition, we estimate that some 10 percent of the particles observed at $\lambda=55°$ and $\lambda=51°$ geomagnetic latitude have energies between the cut-off energy and twice the cut-off energy (0.35–0.7)(Bev/nucleon) at $\lambda=55°$ and (0.5–1.0)(Bev/nucleon) at $\lambda=51°$.

TABLE VIII. Relative abundance of the nuclei of the light elements in stellar atmospheres (Unsold) and in the primary cosmic radiation at $\lambda=30°$.

		Stellar atmospheres	(Unsold)*	Cosmic radiation at $\lambda=30°$	
Z	Element	Sun	τ-Scorpii		
1	H		$1.6\cdot10^6$	$1.6\cdot10^6$	
2	He		$2.9\cdot10^5$	$4.0\cdot10^5$	
6	C	550	280		
7	N	1150	620		
8	O	1500	1600		
Total $6\leq Z\leq 8$		3200	2500	14000	
10	Ne		1800		
11	Na	5	2		
12	Mg	81	107		
13	Al	6	6		
14	Si	55	100		
Total $11\leq Z\leq 14$		157	215	~2600	~4000
16	S	23			
18	A		?	~1000	
20	Ca	5	5		
26	Fe	150		~400	

* Abundance of Si = 100 in τ-Scorpii. The table contains all the elements with abundance greater than 5 percent of the abundance of Si.

Both these observations are consistent with an energy spectrum for the heavy primaries $\mathfrak{F}(\epsilon)$, which for low energies increases with energy up to a maximum in the neighborhood of $\epsilon_m=2.0$(Bev/nucleon) (same magnetic rigidity as a 5 Bev proton) and falls off beyond this maximum as $1/\epsilon^{2.5}$. Whether or not a maximum actually occurs, $\mathfrak{F}(\epsilon)$ certainly cannot decrease with energy as rapidly as $\epsilon^{-2.5}$ near the geomagnetic cut-off at $\lambda\approx50°$ A change in slope of the energy spectrum around 4 Bev is indicated for the total primary radiation by the observations of Millikan[16] and co-workers and by the change of the slope of the latitude curve of cosmic rays at 30,000 feet as geomagnetic latitude $\lambda=48°$, observed by W. F. G. Swann and co-workers.[17]

Flights at different latitudes are needed in order to obtain more definite information on the shape of the energy spectrum of the heavy primaries.

A detailed comparison of the energy distribution of primary protons with that of heavy primaries may throw some light on the accelerating mechanism of cosmic rays. The low energy part of the spectrum can be investigated by measuring charge and range simultaneously as discussed in reference.[2] This method is not applicable for energies much higher than 1 Bev/nucleon since at these energies almost all particles will

*** As a result of an oversight in the evaluation of the data, the flux value for heavy primaries at $\lambda=55°$ given in a preliminary communication (reference 14) is considerably too low. Since the value for $\lambda=30°$ is correct, the latitude effect has unfortunately been underestimated in this note. The value $I_0(51\text{–}55°):I_0(30°)=3.5:1$ for the ratio of the numbers of heavy primaries at $\lambda=51\text{–}55°$ and at $\lambda=30°$ is in good agreement with the value (3.6 ± 0.4) obtained for the ratio of the numbers of big stars in photographic emulsions by E. O. Salant and J. Hornbostel (private communication).

[16] R. A. Millikan, Rev. Mod. Phys. **21**, 1 (1949).

[17] W. F. G. Swann *et al.*, Fifth Semi Annual Report Bartol Research Foundation (March 1949).

undergo nuclear collisions rather than come to rest by ionization.

In the range from 1–10 Bev/nucleon an integral spectrum could be obtained from the latitude effect and the East-West asymmetry of the radiation.

The frequency of occurrence of even higher energies may be estimated from collisions of the type illustrated in reference 5.

VIII. THE RELATIVE ABUNDANCE OF NUCLEI OF THE DIFFERENT ELEMENTS IN THE PRIMARY RADIATION

Figures 10, 11 and 12 show histograms of the charge spectrum for charges $Z \geq 6$ as observed in the plates flown at latitudes $\lambda = 30°$, $\lambda = 51°$, and $\lambda = 55°$, respectively, below 16, 10, and 27 g/cm² of air. Since the fraction of heavy elements destroyed in the material above the plates is larger than the corresponding fraction of light elements, the actual charge spectrum at the top of the atmosphere will show a somewhat higher percentage of the heavier elements than the histograms.

Figure 13 shows the frequency distribution of 422 tracks of nuclei with charge $Z \geq 6$ (practically all the nuclei for which the charge has been determined with any accuracy) plotted against the nuclear charge. Although this diagram contains a number of tracks which were not found in systematic surveys (mainly tracks of nuclei with charge $Z \geq 10$), it is believed to be fairly representative of the actual charge spectrum of incoming nuclei above $Z = 6$. The number of nuclei with $Z > 10$ in Fig. 13 is about one-third of the C,N,O group. Hence it seems that the emphasis given to the heavier nuclei by inclusion of a number of tracks from non-systematic surveys roughly compensates the deficiency due to the stronger absorption of the very heavy nuclei in the air above the plates.

Although the charge determinations are not accurate enough to permit to distinguish one element from its immediate neighbors for $Z \gtrsim 10$, we can nevertheless draw the following conclusions:

A. The similarity of the spectra obtained at the different latitudes indicates that the velocity spectra of the nuclei from helium to iron are not radically different, if they differ at all. This suggests that the accelerating mechanism does not depend critically on the mass of ions for which the ratio of charge to mass Z/M is approximately equal.

B. Particles of atomic number higher than the one corresponding to elements in the neighborhood of iron have not been observed. This fact seems to be significant in view of the astrophysical data on the relative abundance of elements in stellar atmospheres, which show that iron is the heaviest element with an abundance comparable with the abundance of the lighter elements.

C. About $\frac{3}{4}$ of all the nuclei with charges ≥ 6 belong to the group $6 \leq Z \leq 10$, which we call the C,N,O group, since most of the nuclei of this group are certainly nuclei of carbon, nitrogen, and oxygen. The abundance of carbon and oxygen seems to be approximately equal and greater than that of nitrogen. It is difficult to estimate the actual abundance of nitrogen because the carbon and oxygen peaks overlap (Fig. 13). Though charges below 10 may be identified uniquely in favorable cases (see Table III), the resolution shown in Figs. 10–13 is poor even for this group; but the histograms indicate, nevertheless, that the number of nuclei with charges $Z = 9$ or 10 cannot be insignificant.

A determination of the relative abundance of these nuclei would be especially important, because different assumptions on the origin of cosmic rays may give quite different abundance values for these nuclei. The cosmic abundance of fluorine seems to be very small and F nuclei might occur only as breakup products of heavier nuclei. The same would be true for neon if one assumes a specific accelerating mechanism as for instance that suggested by Spitzer.[6]

D. Of the nuclei with charges $Z > 10$ about 60 percent belong to the Mg-Si group ($11 \leq Z \leq 15$) and some 10 percent to the iron group ($Z = 26 \pm 2$).

The following Table VIII lists the relative flux values of the cosmic-ray primaries together with the relative abundances of nuclei in the atmosphere of the sun and τ-Scorpii according to Russell and Unsold.[18]

There is obviously considerable similarity between these relative abundances, though some differences appear: for instance, the abundance ratio of the metals with respect to He (same Z/M) in the cosmic radiation is *ca.* 10 times greater than in stellar atmospheres. This difference seems to be outside the quite considerable possible error of the figures listed above. (The uncertainty of the astrophysical data is estimated by Unsold to be of the order of a factor two.)

IX. REMARKS ON THE ORIGIN OF COSMIC RADIATION

A. If we assume with Alfven[19] and Richtmeyer and Teller[20] that cosmic rays are accelerated in the neighborhood of the sun and if we further assume that they hit the earth after circling the planetary system during a time short as compared to the time between collisions with interstellar hydrogen atoms, then we would expect that the relative proportion in which particles of different mass are accelerated is the same proportion in which they appear in the cosmic radiation.**** Because of the high ionization potential of He and H, the relative proportion of neutral and ionized helium and hydrogen atoms, which is very large at the solar surface, may possibly even be large in those regions near the sun where acceleration starts, whereas the metal atoms are strongly ionized even in the solar atmosphere. This may be the cause for an excess of heavy nuclei in the initial stages of the acceleration. On the other hand until the heavy atoms have obtained sufficient energy to lose all their orbital electrons their ratio of charge to mass is less than that for helium and it is always less than that for hydrogen. Thus, at some

[18] A. Unsold, Zeits. f. Astrophys. **21**, 1 (1944); **24**, 306 (1946).
[19] H. Alfven, Phys. Rev. **75**, 1732 (1949).
[20] R. D. Richtmeyer and E. Teller, Phys. Rev. **75**, 1729 (1949).

**** Whether the break up of heavy nuclei in interstellar space is important could be tested by studying the relative abundance of the nuclei of certain elements. Nuclei of Li, Be and B, the light elements of extremely low cosmic abundance are expected to occur, if at all, only as products of the break up of heavier nuclei. If Li, Be and B nuclei are produced by the break up of heavier primaries in the earth's atmosphere only, as would be expected in the case of solar origin of cosmic rays, then the intensity *vs.* altitude curve for these nuclei should be a transition curve extrapolating to intensity zero at the top of the atmosphere. On the other hand, if break up of heavier nuclei in interstellar space is important, as it must be if cosmic rays are of galactic origin, then this curve is expected to extrapolate to a finite intensity at the top of the atmosphere.

stage of the accelerating process, hydrogen should be favored and even helium may be accelerated more efficiently than heavier ions. Hence, the observed charge distribution may well be consistent with the hypothesis that cosmic rays originate near the sun.

B. Let us assume that cosmic rays are accelerated in the galaxy and that there exists in the galaxy domains with magnetic fields of the order of $H \sim 10^{-5}$ gauss, as postulated by Alfven and by Fermi.[21] The hypothesis of the existence of such magnetic domains has recently received empirical support by the discovery of the polarization of starlight passing through interstellar clouds, observed by Hall[22] and Hiltner[23] and discussed by Spitzer and Tukey.[24] Thus nuclei accelerated to cosmic-ray energies would be either completely retained in the galaxy or at least execute long and tortuous paths through interstellar space. Collisions with nuclei of interstellar hydrogen will eventually destroy the cosmic-ray primaries or reduce their energy. Because of their much larger cross section, the heavy primaries will be eliminated by these collisions much faster than the protons.

Figure 14 shows an event which is very probably the break up of a heavy primary ($Z=10\pm1$) in a collision with a hydrogen target nucleus. The collision of Fig. 14 is remarkable insofar as it is the only case observed of a collision of a heavy primary where no visible low energy particles are emitted from the target nucleus. It is therefore not improbable that this latter has been a hydrogen nucleus of the emulsion. (The projected hydrogen target nucleus may actually by the particle responsible for track 4.) If this is the case, Fig. 14 is an illustration for the break up of heavy cosmic-ray primaries in collisions with interstellar hydrogen atoms.

It is noteworthy that, even if we make the extreme assumption that originally *only* heavy nuclei such as iron, calcium, silicon, oxygen and carbon are accelerated, we can nevertheless account for the observed abundance of protons and α-particles in cosmic radiation as fragments of collisions suffered by the heavy nuclei in interstellar space.

The cross section for collision between a relativistic nucleus of iron, calcium or silicon and a proton is of the order of $\sigma_M = 0.3\times10^{-24}$ cm^2. With a mean density of interstellar hydrogen in our galaxy of $\rho = 10^{-24}-10^{-25}$ g/cm^3 this corresponds to a mean life of these nuclei in the galaxy of $\tau_M = 3\times10^6-3\times10^7$ years. Therefore the injection mechanism must be capable of reproducing the heavy nuclei in the cosmic radiation at the rate of about once every 10 million years. Heavy nuclei will finally be reduced by collisions to α-particles, protons and neutrons (which in turn decay into protons). According to our observations on the collision of heavy

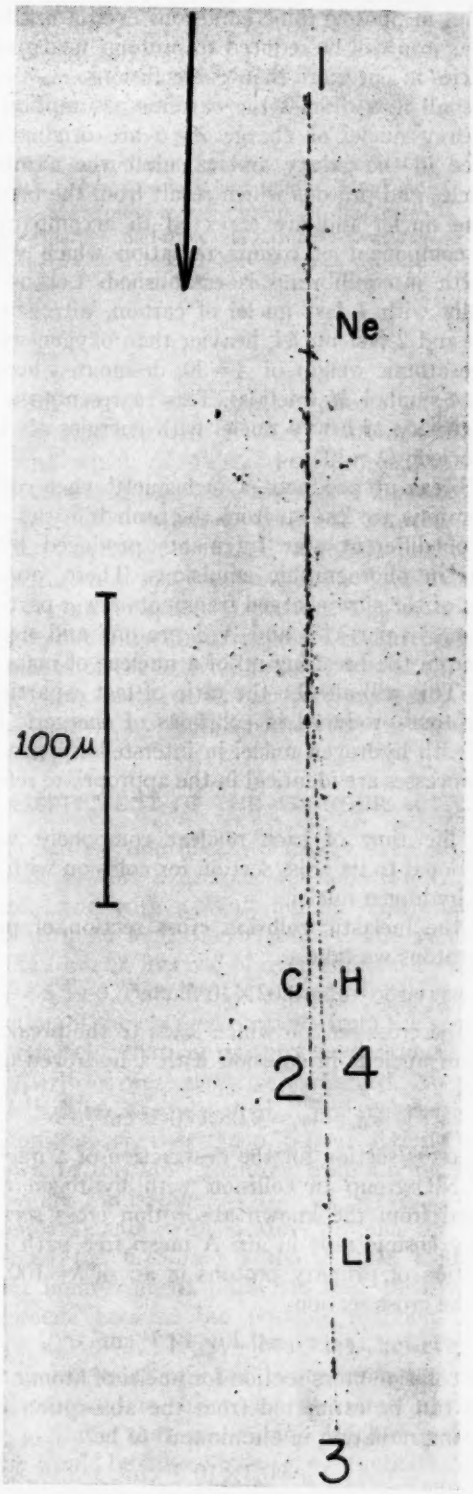

FIG. 14. A heavy primary nucleus of charge $Z=10\pm1$ (track No. 1), after traversal of seven plates (7.5 g/cm^2 of glass) is split up in the emulsion of the eighth plate into at least two fragments, one of charge $Z=6$ or 7 (track No. 2) and one of charge $Z=3$ (track No. 3) diverging with an angle of 1.5°. Track No. 4 is a track with grain density corresponding to a specific energy loss $K/K_{\min}=2.2$ and is probably caused by a proton of 200 Mev. All three tracks 2, 3, and 4 have been traced through the next plate.

[21] E. Fermi, Phys. Rev. **75**, 1169 (1949).
[22] J. S. Hall, Science **109**, 166 (1949).
[23] W. A. Hiltner, Science **109**, 165 (1949).
[24] L. Spitzer and J. W. Tukey, Science **109**, 461 (1949).

primaries in photographic emulsions even a nucleus as heavy as iron will be reduced to protons, neutrons and α-particles in not more than $\sim$3 collisions.

We shall now discuss the extreme assumption that *only* heavy nuclei of charge $Z\geq 6$ are originally accelerated in the galaxy and calculate the number of α-particles and protons which result from the break-up of these nuclei and are expected to accompany the heavy component of cosmic radiation which will hit the earth if equilibrium is established. Let us start originally with 7 fast nuclei of carbon, nitrogen, and oxygen and 2 fast nuclei, heavier than oxygen with an average atomic weight of $A=30$, designated hereafter with the symbol M (metals). This represents the relative intensity of heavy nuclei with energies above 3.5 Bev/nucleon ($\lambda=30°$).

The break-up products of such nuclei when colliding with protons are known from the probability of occurrence of different star fragments produced by fast protons in photographic emulsions. There, about 50 percent of the slow charged fragments are α-particles.[25] Thus $A/6$ α-particles and A/3 protons and neutrons result from the breaking up of a nucleus of mass number A. This will also be the ratio of fast α-particles to fast protons produced in collisions of energetic heavy nuclei with hydrogen nuclei in interstellar space, since both processes are identical in the appropriate reference systems.

The life time of each nuclear component will be proportional to its cross section for collision with interstellar hydrogen nuclei.

For the inelastic collision cross section of protons with protons we take

$$\sigma_p=0.02\times 10^{-24}\ \text{cm}^2.$$

For the cross section which leads to the break up of a helium nucleus in collision with a hydrogen nucleus we take

$$\sigma_{\text{He}}=4\sigma_p=0.08\times 10^{-24}\ \text{cm}^2.$$

The cross section for the destruction of a nucleus of the C,N,O-group in collision with hydrogen can be obtained from the known absorption cross section of primary cosmic rays in air. A mean free path for the absorption of primary protons in air of $\lambda=100$ g/cm^2 gives the cross section

$$\sigma_{\text{C, N, O}}=0.20\times 10^{-24}\ \text{cm}^2.$$

The collision cross section for nuclei of atomic weight $A\sim 30$ can be estimated from the absorption of star producing radiation in aluminum[26] to be

$$\sigma_M=0.3\times 10^{-24}\ \text{cm}^2.$$

We therefore obtain for the number of fast α-particles (N_{He}) in equilibrium with nuclei of charge $Z\geq 6$

$$N_{\text{He}}=\frac{14}{6}\frac{\sigma_{\text{CNO}}}{\sigma_{\text{He}}}N_{\text{CNO}}+\frac{30}{6}\frac{\sigma_M}{\sigma_{\text{He}}}N_M\approx 80$$

and for the number of fast protons (N_p)

$$N_p=\frac{14}{3}\frac{\sigma_{\text{CNO}}}{\sigma_p}N_{\text{CNO}}+\frac{30}{3}\frac{\sigma_M}{\sigma_p}N_M+4\frac{\sigma_{\text{He}}}{\sigma_p}N_{\text{He}}\approx 1900$$

Thus on the assumption that only nuclei of charge $Z\geq 6$ are accelerated we predict that the ratio of elements in cosmic radiation with energies above a certain minimum energy per nucleon should be

$$\text{H:He:C,N,O:}Z\geq 10=1900:80:7:2.$$

Since collision products of relativistic nuclei have roughly the same velocity, hence the same energy per nucleon as the original nucleus the calculated ratios should be compared with the relative fluxes above a given energy per nucleon. Thus if we take for nuclei heavier than H the flux values at geomagnetic latitude $\lambda=30°$ (cut off energy $\epsilon_c=3.5$ Bev per nucleon) we must compare them with the proton flux at latitude $\lambda=42°$ where the cut-off energy ϵ_1 for protons is also 3.5 Bev. Assuming a latitude effect of 1.7 for the proton component between $\lambda=42°$ and $\lambda=30°$, the observed ratio of fluxes is

$$\text{H:He:C,N,O:}Z\geq 10=1200:180:7:2.$$

The comparison shows that the acceleration of heavy nuclei *only* would lead to a flux of protons and α-particles in cosmic radiation which is of the correct order of magnitude.

A direct acceleration of protons and helium nuclei in addition to heavy nuclei is consistent with the observations only if the number of *nucleons* accelerated as protons or α-particles is at most of the same order as the number of nucleons accelerated as heavy nuclei.

The conclusion that, assuming equilibrium in the galaxy to be established, the number of hydrogen and helium nuclei cannot be significantly greater than the number of nuclei in heavier atoms injected in the accelerating process, is difficult to understand if cosmic rays originate as ions accelerated by electromagnetic fields in regions of the galaxy where hydrogen is predominantly ionized. If, on the other hand, a mechanism like that proposed by Spitzer[6] should be considered acceptable by means of which only heavier atoms could be accelerated to cosmic-ray energies in the galaxy, the hydrogen and helium nuclei could be accounted for as fragments from collisions with hydrogen nuclei in interstellar space.

We are greatly indebted to Mr. Robert Brent and Mr. Robert Rickard, who did most of the surveying and δ-counting, to Mr. Lionel Goldfarb who helped carry out the α-particle work and to Mr. Tom Putnam, who prepared the photographs.

We also wish to express our gratitude to Dr. John Spence of Eastman Kodak Company and Drs. E. O. Salant and J. Hornbostel of the Brookhaven National Laboratory for making available to us their facilities in many important phases of this work. This work was assisted by the Joint Program of the ONR and the AEC.

[25] J. B. Harding, Phil. Mag. 11, 530 (1949).
[26] G. Bernardini, Phys. Rev. 75, 1328 (1949).

Assignment and Disintegration Scheme of the 6.75-Hour Molybdenum

D. N. KUNDU, JOHN L. HULT,* AND M. L. POOL
Mendenhall Laboratory of Physics, Ohio State University, Columbus, Ohio
(Received August 29, 1949)

Contrary to previous reports, deuteron bombardment of molybdenum does not produce any measurable amount of the 6.75-hour Mo activity. The assignment of this activity has, therefore, been reinvestigated and correctly found to be still Mo^{93}. Decay does not take place by positron emission or K-capture. A disintegration scheme has been worked out using absorption, beta-ray spectrograph, and coincidence counter measurements. By successive emission of three gamma-rays of energies 0.30, 0.70 and 1.7 Mev of which the first is about 90 percent internally converted, the 6.75-hour Mo^{93} passes into a long-lived isomeric state. Mo K_α x-rays resulting from the conversion have been found.

INTRODUCTION

BY private communication,[1] a 7-hour Mo activity had been reported from a proton bombardment of columbium and tentatively assigned to Mo^{93}. The characteristic radiations were not given. Later workers[2] changed the value of the half-life to 6.7 hours and assigned the activity to Mo^{93} by producing it from columbium by protons and deuterons and from zirconium by alpha-particles. They reported beta-particles of energies 0.3 and 0.7 Mev and one gamma-ray of energy 1.6 Mev. Absence of x-rays was indicated and the method of decay by positron emission was confirmed by others[3] on the basis of Cb+d and Mo+d but no check on the energies of the emitted radiations was available. Recently, however, it has been pointed out[4] that though the value of the half-life was 6.75 hours and the maximum energies of the charged particles were 0.35 and 0.65 in fair agreement with those previously reported, these were not positrons but negative electrons from internally converted gamma-rays. Neither positrons nor x-rays were observed. The presence of a long-lived isomer, Mo^{93}, was also indicated.

The above observations, however, had left the disintegration scheme of the 6.75-hour activity in a very unsatisfactory state. Supposing, even, that the decay took place by internal conversion to the long-lived Mo^{93} isomeric state, the absence of x-rays, resulting from the conversion of the gamma-rays, was not consistent with this mode of disintegration. A study of the decay scheme was, therefore, deemed necessary. This paper reports the results obtained from absorption measurements, beta-ray spectrograph and coincidence methods which were brought together to work out the detailed mode of disintegration.

Another peculiarity connected with the 6.75-hour Mo activity was noticed in connection with our studies of nuclei in the Cb—Mo region. Contrary to the reports of others,[3] that this activity was produced by a deuteron bombardment of Mo, repeated efforts to produce it from metallic Mo with 10-Mev deuterons failed. The ease with which (d, p) reactions proceed, makes this phenomenon difficult to understand. To make certain that other Mo activities were not masking out the 6.75-hour activity, enriched molybdenum** with a concentration of 92.07 percent of Mo^{92} was bombarded by deuterons in order to produce this activity more strongly, but still without success. The correctness of the assignment of the activity to Mo^{93} is thus thrown into considerable doubt. It is, therefore, necessary to check the assignment by using enriched isotopes of neighboring elements.

ASSIGNMENT OF THE 6.75-HOUR ACTIVITY

The Mo fraction obtained from a bombardment of Cb with 10-Mev deuterons was followed with Geiger counters and with a Wulf unifilar electrometer provided with an ionization chamber. The value of the half-life from an interval of over ten half-lives is found to be 6.75±0.05 hours. It was also observed by the deflection of the charged particles from the sample in a magnetic field, that contrary to the previous reports,[2,3] these particles were negatively charged. No positrons of this half-life were detected. These observations open the question whether the 6.75-hour activity is to be assigned to the Mo^{93} resulting from $Cb^{93}(d, 2n)$ or to some other Mo isotope.

Bombardments with 5-Mev protons on Cb also produced the 6.75-hour activity quite readily. The proton bombardment does not lead to any definite assignment because the possible reactions may be $Cb^{93}(p, n)Mo^{93}$ or $Cb^{93}(p, \gamma)Mo^{94}$. It is, however, shown[5] that (p, n) reactions have larger cross sections than (p, γ) reactions in this region of atomic nuclei. It is, thus, plausible that an activity which is produced so readily would be caused by a (p, n) reaction rather than a (p, γ) reaction and, therefore, be assigned to Mo^{93}.

The assignment can be made more definite by the use of separated isotopes of Zr, since as reported

* At present at the Rand Corporation, Santa Monica, California.

[1] G. T. Seaborg and I. Perlman, Rev. Mod. Phys. **20**, 585 (1948).
[2] D. N. Kundu and M. L. Pool, Phys. Rev. **70**, 111 (1946).
[3] M. L. Wiedenbeck, Phys. Rev. **70**, 435 (1946).
[4] D. N. Kundu and M. L. Pool, Phys. Rev. **76**, 183 (1949).

** Supplied by Y-12 Plant, Carbide and Carbon Chemicals Corporation, through the Isotopes Division, A.E.C., Oak Ridge, Tennessee.

[5] D. N. Kundu and M. L. Pool, Phys. Rev. **74**, 1574 (1948).

earlier,[2] the 6.75-hour activity is produced from Zr with 20-Mev alpha-particles. A rotating target arrangement[6] was employed to bombard two samples of Zr enriched respectively in isotopes Zr^{90} and Zr^{91}. It was found that the 6.75-hour activity was produced from Zr^{90} in quantities three times as much as from Zr^{91}. It has been observed that (α, n) reactions proceed more readily, at the alpha-energy used, than $(\alpha, 2n)$ reactions. The ratio $(\alpha, n)/(\alpha, 2n)$ is 45:1 in case[7] of Ru and 72:1 in case[8] of Y. The assignment is, therefore, in favor of Mo^{93} resulting from the reaction $Zr(\alpha, n)$.

The possibility of the assignment to Mo^{94} was further excluded by observing that a fast neutron bombardment on enriched Mo^{95} did not produce the 6.75-hour Mo activity.

The final confirmation was made by a simultaneous bombardment of Mo enriched separately in Mo^{92} and Mo^{94} isotopes, with fast neutrons. In this case, the 6.75-hour activity was produced from Mo^{94} but not from Mo^{92}. The 6.75-hour activity is, therefore, definitely assigned to Mo^{93}.

ABSENCE OF (d, p), (n, γ) AND (γ, n) REACTIONS

It was mentioned previously that the 6.75-hour Mo activity was produced from Mo^{94} by fast neutrons. The yield from the reaction Mo^{94} $(n, 2n)$ was, however, very low.

With regard to the failure of the 10-Mev deuterons to produce any appreciable amount of the 6.75-hour activity from Mo^{92}, it was suggested that the growth of the 5.9-hour Tc^{99} isomer from the 2.79-day Mo^{99} might possibly mask the decay of the 6.75-hour Mo activity. Such a possibility had to be discarded, however, subsequent to deuteron bombardments of Mo of ordinary isotopic composition, enriched Mo^{92}, and enriched Mo^{98}. The percent of Mo^{92} contained in the three samples was 15.84, 92.07, and 0.65 respectively and of Mo^{98} content was 23.78, 1.65, and 95.00 respectively. The percents are so widely different that if in one sample the 6.75-hour decay were compensated exactly by the 5.9-hour growth, then in the other two samples the decay-growth ratio ought to be distinctly seen.

The above results are consistent with the findings recently reported by others[9] that the 6.75-hour Mo

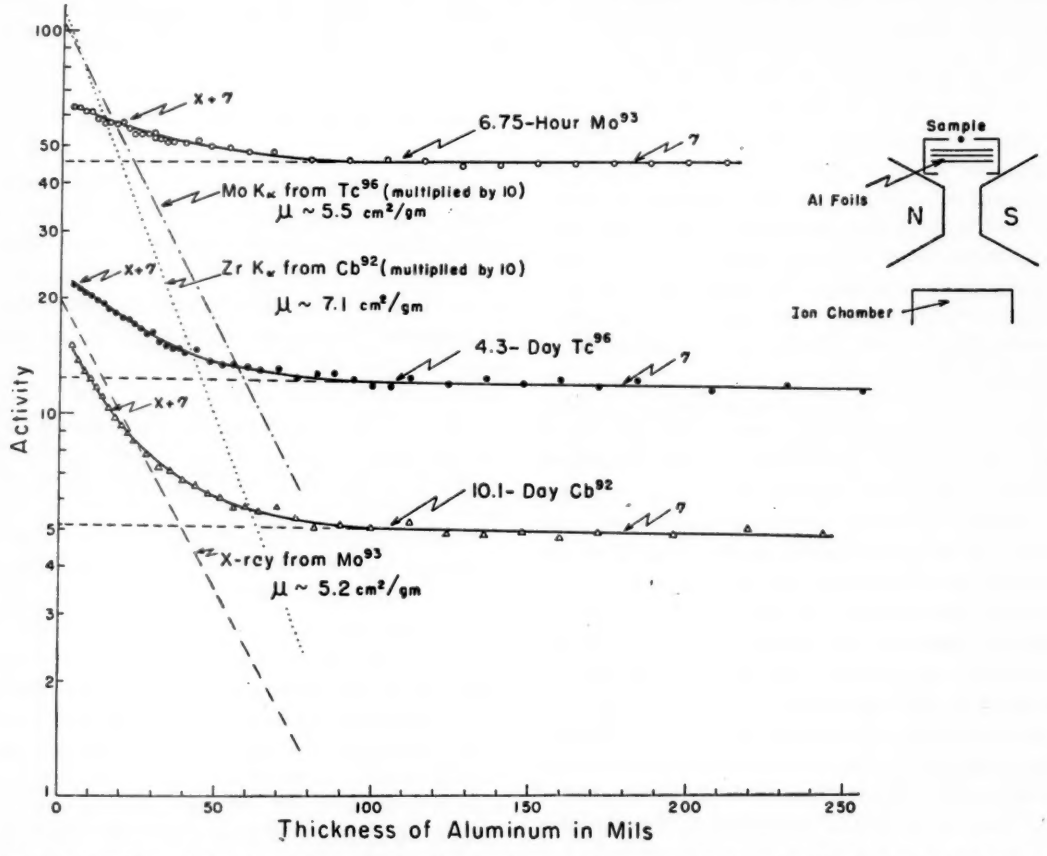

FIG. 1. Comparison of the absorption coefficient in aluminum of the x-rays from the 6.75-hour Mo^{93} with those of the K_α x-rays of Mo and Zr.

[6] D. N. Kundu and M. L. Pool, Phys. Rev. **74**, 1775 (1948).
[7] D. T. Eggen and M. L. Pool, Phys. Rev. **75**, 1464 (1949).
[8] Scott, Robertson, and Pool, Phys. Rev. **76**, 183 (1949).
[9] R. B. Duffield and J. D. Knight, Phys. Rev. **76**, 573 (1949).

activity was not produced by the (n, γ) reaction with slow neutrons. The additional fact that $Mo^{94}(\gamma, n)$ did not produce this activity either, may be understood in the light of the present data that the yield from $Mo^{94}(n, 2n)$ reaction was very low.

The observation that the $Mo^{92}(d, p)$ and $Mo^{92}(n, \gamma)$ reactions were not detected is probably related to the fact that Mo^{92} happens to be a nucleus with the magic number 50 and, therefore, has a very low neutron capture cross section.

COMPONENTS IN THE PRODUCTS OF DISINTEGRATION

Absorption measurements with thin aluminum foils show two end points with values for the maximum energies at 0.30±0.05 and 0.65±0.05 Mev. As mentioned previously these particles were verified to be negatively charged. Since Tc^{93} is not a stable isotope, these electrons are to be suspected as resulting from the internal conversion of γ-rays. In this connection, it may be noted that the ratio of the ionization for the γ-rays and for charged particles indicated that more than one gamma-ray must be involved in each disintegration process.

An absorption measurement with lead showed that apart from the hard γ-ray of 1.7±0.1 Mev, there is a second component of energy 0.70±0.05 Mev. The relative ionization at zero thickness caused by the 0.70-Mev component is 0.9 of that produced by the 1.7 Mev-component. This indicates that there are as many gamma-photons of higher energy as of the lower energy, and also that the small number of 0.65-Mev electrons may possibly result from the internal conversion, to a small extent, of the 0.70-Mev gamma-rays.

The conclusive proof that the 0.30-Mev group was caused by the internal conversion of another gamma-ray was obtained by the use of a beta-ray spectrograph. Two lines were photographed which corresponded approximately to the K and L conversion lines of molybdenum.

To find out if any of the 0.30-Mev group of gamma-rays remained unconverted, the sample was covered with 29 mils of Mo foil which would stop both the groups of charged particles and a thin aluminum absorption made. It was found that charged particles of these energies could still be detected. This shows that the conversion is not complete and also supports the view that these particles are not genuine beta-rays but they are conversion electrons.

The reported absence of x-rays was next examined. Absorption measurements were made in the usual way by placing the sample in a magnetic field and inserting thin aluminum foils immediately in front of the window of the ionization chamber or Geiger counter. In agreement with earlier reports, no definite indication of x-rays could be found. But it was suspected that the diminution of the ionization by x-rays might, perhaps, be just compensated by the increase in the ionization due to the secondary electrons which the gamma-rays

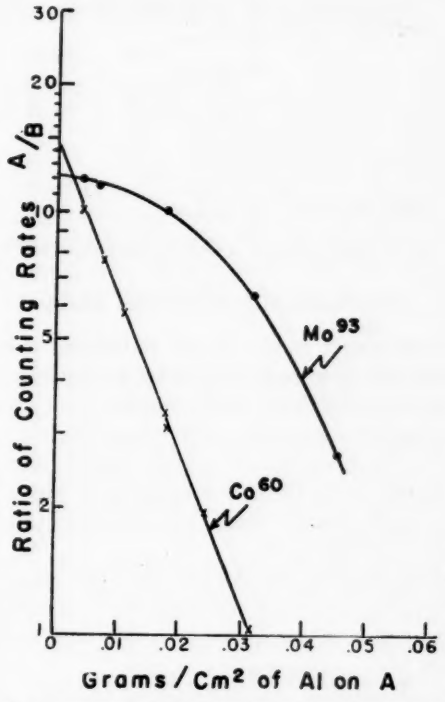

FIG. 2. Comparison of the beta-gamma-counting ratio in the 6.75-hour Mo^{93} with that for Co^{60}.

knocked out of the added aluminum foils. An arrangement was, therefore, devised to place the source and also the absorbing foils both in a strong magnetic field. No secondary electrons resulting from the aluminum foils could then reach the ionization chamber or Geiger counter. The schematic arrangement and the results of measurements are shown in Fig. 1. Distinct evidence of x-rays is indicated. The wave-length of the x-rays is calculated as 0.70A from the half-value thickness equivalent to an absorption coefficient of 5.52 cm^2/g. These x-rays are thus suspected to be Mo K_α. This was proved conclusively by comparing the observed absorption coefficient of x-rays in the 6.75-hour activity with the coefficients of known Mo and Zr x-rays under the same geometry and with intensities of the same order of magnitude. Mo K_α x-rays were obtained from the 4.3-day Tc^{96} and the Zr K_α x-rays from the 10.1-day Cb^{92}. The absorption coefficients were found to be 5.55 and 7.1 cm^2/g respectively. The absorption coefficients thus arrived at are different enough to easily distinguish between Mo x-rays and those from neighboring elements.

During the decay of the 6.75-hour Mo^{93}, the ratio of the ionization from the γ-rays to that from the x-rays is 2.6 for the ionization chamber used. For this chamber, each γ-quantum produces about the same ionization as each 0.70A X-quantum. Each x-ray quantum must, therefore, be associated with at least two γ-quanta. Which of these radiations are in series was determined by coincidence counter measurements, presented in the following section.

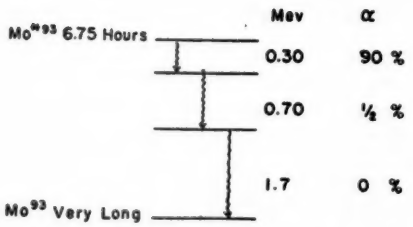

FIG. 3. Disintegration scheme of 6.75-hour Mo^{93}.

COINCIDENCE COUNTER DATA

The coincidence study of the radiations from Mo^{93} was made with thin end-window beta-ray Geiger tubes. When used for the detection of gamma-rays only, thick Lucite absorber-radiators were placed in front of the windows. The gamma-ray energy *versus* gamma-ray detection efficiency for this arrangement was found to be very nearly linear[10] over the calibrated range from 0.4 Mev to 2.8 Mev.

The beta-gamma-coincidence rate per beta-particle *versus* beta-ray absorber thickness was consistent with a simple beta-ray spectrum in series with a total of 2.5±0.05 Mev of gamma-ray energy.

Lead absorption measurements of the gamma-gamma-coincidence rate per gamma-ray indicated that the 2.5 Mev total gamma-ray energy is split principally into two components of approximate energies 1.8 Mev and 0.7 Mev.

The beta-gamma-counting ratio extrapolated to zero beta-ray absorber thickness when compared with that for Co^{60} (0.31 maximum beta-ray energy, 2.50 total gamma-ray energy[11]) indicates that the 0.30-Mev transition in Mo^{93} is 0.9 internally converted. Figure 2 shows the ratio of the counting rate in the beta-ray tube to the counting rate in the calibrated gamma-ray tube with a thick Lucite radiator as a function of the grams/cm^2 of aluminum in front of the beta-tube. It may be shown that

$$\frac{(N_{\beta 1}/N_{\gamma 1})E_1}{(N_{\beta 2}/N_{\gamma 2})E_2}=1+\alpha,$$

when there is a primary beta-spectrum. If, however, there is no primary beta-spectrum, as in the present case, the right-hand side of the above equation reduces simply to α. In the above $N_{\beta 1}/N_{\gamma 1}$=extrapolated e^--gamma-counting ratio in Mo^{93}, $N_{\beta 2}/N_{\gamma 2}$=extrapolated beta-gamma-ratio in Co^{60}, E_1 and E_2 are the total gamma-ray energies in series with the beta-spectra of Mo^{93} and Co^{60}, respectively, and α=the total internal conversion coefficient.

The beta-beta-coincidence rate per beta-particle *versus* aluminum absorber thickness in front of both tubes indicates that no radiation of energy greater than 0.1 Mev, other than the 0.3-Mev transition, is internally converted more than one-half percent.

A delayed coincidence study of beta-gamma-, gamma-beta- and gamma-gamma-coincidence revealed that the half-lives of the intermediate states involving the 0.3-, 0.7-, and 1.7-Mev components are less than 1×10^{-7} seconds.

DISINTEGRATION SCHEME

Summarizing the observations of the two foregoing sections, it is found that in the decay of Mo^{93}, there are three gamma-rays of 0.30, 0.70, and 1.7 Mev. The first of these is almost completely internally converted, giving rise to Mo K_α x-rays. The other two gamma-rays are in cascade with the first gamma. The 0.70-Mev gamma is very slightly converted to the extent of only one-half percent at most. The mode of decay is not by K-capture, unless it be to the extent of a small percent. No positron emission was observed.

The absence of positrons and the presence of Mo K_α x-rays alone coupled with the fact that a high percent of the 0.30-Mev gamma-rays is internally converted indicate that there must be a Mo^{93} isomer, and that this isomer must be long-lived.

Two more facts, already in the literature, also substantiate the above remarks. The first is that the 17-minute Mo activity has been shown[4] to be Mo^{92} and not Mo^{93}, as previously reported by others.[1] The second fact is that the Tc^{93} isomers of half-lives 4.5 minutes and 2.75 hours decay into Mo^{93} primarily by positron emission and K-capture respectively.[6] No growth of the 6.75-hour Mo was observed from Tc^{93}. These observations also indicate that Mo^{93} must have a very long-lived isomer.

On the basis of the above findings, the decay scheme shown in Fig. 3 is, therefore, suggested. After three successive gamma-emissions, the 6.75-hour activity passes into the proposed long-lived isomer Mo^{93}.

ACKNOWLEDGMENT

Acknowledgment is made of the help received from the Development Fund and the Graduate School of the Ohio State University. All chemical separations had kindly been done by Mr. H. L. Finston and Mr. R. M. Dyer. Thanks are also due the Ghosh Board of the Calcutta University for aid in traveling to this country.

[10] Lind, Brown and DuMond, Phys. Rev. **76**, 591 (1949).
[11] C. E. Mandeville and M. V. Scherb, Nucleonics, **3**, 2 (1948).

Assignment and Characteristic Radiations of the 14-day Tin Activity

E. C. MALLARY* AND M. L. POOL
Mendenhall Laboratory, The Ohio State University, Columbus, Ohio
(Received September 13, 1949)

The tin isotope which decays with a 14-day half-life by an isomeric transition is definitely assigned to mass number 117. It was produced by the reactions $Cd^{114}(\alpha, n)$, $Sn^{116}(d, p)$, $Sn^{118}(n', 2n)$, and $Sn^{117}(n', n)$; and by the decay of indium 117 which is produced by the reaction $Cd^{116}(d, n)$. The cross section of the reaction $Sn^{117}(n', n)$ is about 1.8 times larger than the cross section of the reaction $Sn^{118}(n', 2n)$. Characteristic radiations are K and L conversion electrons of 0.146-Mev and 0.171-Mev energy, respectively, tin x-rays, and 0.175-Mev gamma-rays which are about 50 percent internally converted.

I. INTRODUCTION

IT has been reported[1] that a 13-day tin activity was produced by bombarding cadmium with alpha-particles. The characteristic radiation reported was negative particles only. No attempt was made for a mass assignment of this activity. Later it was reported[2] that a 14-day tin activity was produced by bombarding antimony with deuterons. Characteristic radiations reported were 0.13-Mev conversion electrons and 0.17-Mev gamma-rays. The energy of the electrons was measured with a spectrometer and the energy of the gamma-rays was measured by a lead absorption. The mass assignment was tentatively made to tin 119. The purpose of this paper is to report further investigations of this 14-day activity and to give it a definite assignment to tin 117. No previous assignment to tin 117 has been reported.

II. PROCEDURE

Samples of electromagnetically enriched cadmium and tin oxides** and tin metal, obtained by reducing the enriched tin oxide, were bombarded. Fast neutrons, 10-Mev deuterons, and 20-Mev alpha-particles were used as bombarding particles. In Table I are given the isotopic abundances supplied with each sample of enriched cadmium and in Table II are given the isotopic abundance supplied with each sample of enriched tin.

Samples were prepared for deuteron and alpha-particle bombardment by pressing the material into slots in chemically pure aluminum target blocks; while samples were prepared for fast neutron irradiation by placing a capsule containing the material in a small cadmium box placed behind a thick lithium target which was bombarded with 10-Mev deuterons. Measurement of the resulting activities in each case was accomplished with a thin window Geiger tube or with a freon-filled ionization chamber connected to a Wulf unifilar electrometer.

III. ALPHA-PARTICLE BOMBARDMENT OF ENRICHED CADMIUM

Comparison of results obtained by bombarding all eight samples of cadmium oxides, each enriched in a different isotope of cadmium, showed conclusively that the bombardment $Cd^{114}+\alpha$ produced the 14-day tin activity. The activity could then conceivably be attributed to either tin 116 or 117, though the former possibility would be contrary to Mattauch's rule. Figure 1 shows that the end point of the charged particle component of the radiation of the 14-day activity is 31 ± 1 mg/cm^2 of aluminum and that a tin x-ray and a gamma-ray of about 0.17-Mev energy constitute the electromagnetic component of this radiation.

Recently it was reported[3] that the ratio of the number of gamma-rays to the number of x-rays emitted by indium 111 in the 2.84-day activity was 1.72. The x-rays from this activity are indium x-rays and there are an almost equal number of 0.173-Mev and 0.247-

TABLE I. Isotopic abundance of enriched cadmium.

	Percent abundance of isotope of mass number		
	114	116	all others
Sample enriched in Cd^{114}	*94.2*	1.2	4.6
Sample enriched in Cd^{116}	18.4	*71.2*	10.4

TABLE II. Isotopic abundance of enriched tin.

	Percent abundance of isotope of mass number				
	116	117	118	120	all others
Sample enriched in Sn^{116}	*58.4*	8.9	10.3	10.8	11.6
Sample enriched in Sn^{117}	5.4	*75.3*	8.8	5.3	5.2
Sample enriched in Sn^{118}	1.1	2.0	*91.8*	2.2	2.9
Sample enriched in Sn^{120}	0.4	1.1	0.8	*95.4*	2.3

* Lt. Col. USAF, Research under auspices of USAFIT, Wright-Patterson Field, Ohio.

[1] J. J. Livingood and G. T. Seaborg, Phys. Rev. **55**, 667 (1939).

[2] G. T. Seaborg and I. Perlman, Rev. Mod. Phys. **20**, 585 (1948).

** Supplied by the Y-12 plant, Carbide and Carbon Chemicals Corporation through the Isotope Division, AEC., Oak Ridge, Tennessee.

[3] Boehm, Huber, Marimer, Preswerk, and Steffun, Helv. Phys. Acta **22**, 69 (1949).

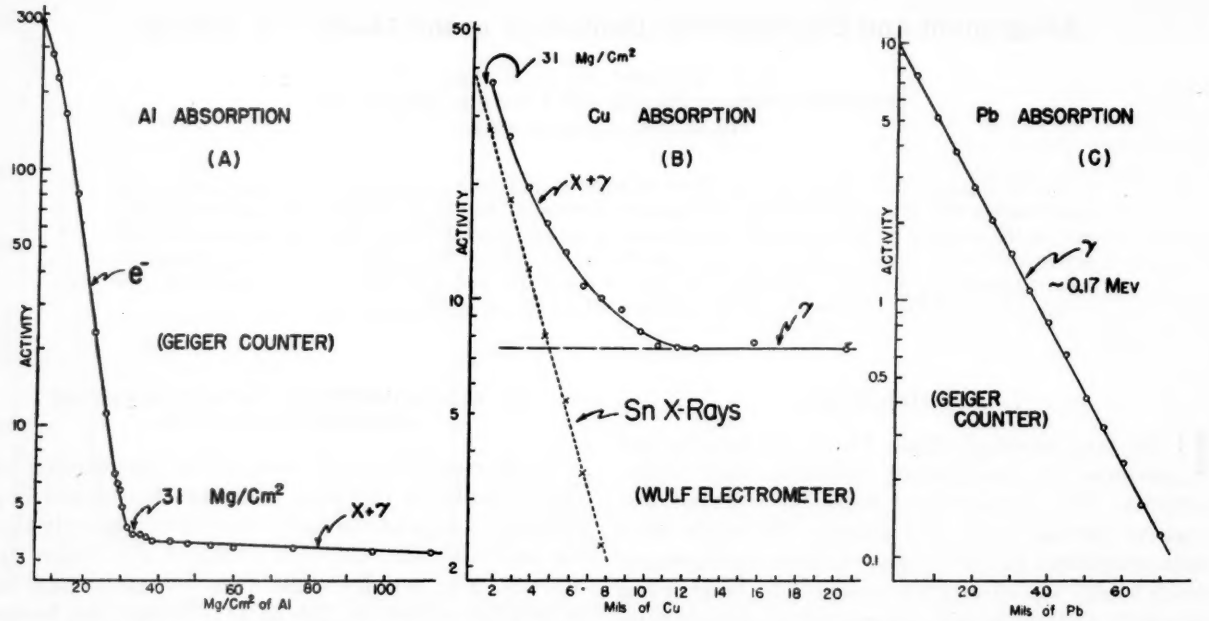

FIG. 1. (*A*) Aluminum absorption of the 14-day activity of tin 117 produced by the reaction $Cd^{114}(\alpha, n)$. The end point of the charged particle radiation is shown to be 31±1 mg/cm² of aluminum. (*B*) Copper absorption of the same activity. The x-ray is shown to be tin x-ray. (*C*) Lead absorption of the same activity.-The gamma-radiation is shown to have an energy of about 0.17 Mev.

Mev gamma-rays. Since the x- and gamma-rays of the 14-day tin activity are comparable in energy to those of indium 111, a direct comparison of these activities can be made. This was done by means of a copper absorption of each activity with the Wulf electrometer. The 2.84-day activity of indium 111 was produced by bombarding cadmium 110 with deuterons. The results of this comparison indicated that the gamma-rays of the 14-day tin activity are about 50 percent internally converted.

IV. DEUTERON BOMBARDMENT OF ENRICHED CADMIUM

Two samples of cadmium oxide enriched respectively in isotopes 116 and 114 were bombarded with deuterons. Only the bombardment of cadmium 116 produced in the tin fraction the 14-day activity with an end point of 31 mg/cm² of aluminum. The parent of the 14-day tin activity could then conceivably be either indium 116 or indium 117, both of which are known to decay to tin. The former possibility would again be contrary to Mattauch's rule.

V. DEUTERON BOMBARDMENT OF ENRICHED TIN

Two samples of tin metal were bombarded with deuterons. One sample was enriched in isotope 116 and the other in isotope 118. Only the bombardment of tin 116 produced in the tin fraction this 14-day activity with an end point of 31 mg/cm² of aluminum. Therefore, the 14-day tin activity is very definitely assigned to tin 117. A copper and a thick aluminum absorption of the 14-day activity both revealed the presence of tin x-rays. A spectrogram, taken during the 14-day tin activity which was produced by this bombardment, showed that *K* and *L* conversion electrons have energies of 0.146±0.006 Mev and 0.171±0.006 Mev respectively, corresponding to a gamma-ray energy of 0.175±0.006 Mev. The beta-ray spectrograph used was calibrated with the annhilation radiation of positrons from copper bombarded with deuterons, using lead foil as the radiator.

VI. FAST NEUTRON BOMBARDMENT OF ENRICHED TIN

A fast neutron bombardment of tin enriched in isotope 120 revealed no 14-day activity nor any activity with an end-point of 31 mg/cm² of aluminum. Samples of tin enriched, respectively, in isotopes 116, 117, and 118 were bombarded with fast neutrons. Each sample contained the 14-day tin 117 activity with an end-point of 31 mg/cm² of aluminum. Comparison of the specific activities of the 14-day tin 117 activity induced in these samples by the same neutron flux, indicated that tin 117 was produced by both the reactions $Sn^{118}(n', 2n)$ and $Sn^{117}(n', n)$ and that the latter has a cross section about 1.8 times as large as the former.

VII. ACKNOWLEDGMENTS

Thanks are due to Mr. H. L. Finston and to Mr. R. M. Dyer for the chemical separations. Grateful acknowledgment is made for the support received from the Ohio State Development Fund and the Graduate School.

Microwave Spectrum and Molecular Constants of Hydrogen Cyanide*

JAMES W. SIMMONS,** WALLACE E. ANDERSON,*** AND WALTER GORDY
Department of Physics, Duke University, Durham, North Carolina

(Received September 20, 1949)

Precision measurements of the frequencies of the $J=0\rightarrow1$ transition of $HC^{12}N^{14}$, $HC^{13}N^{14}$, $DC^{12}N^{14}$, and $DC^{13}N^{14}$ have been made with multiples of a 10-mc/sec. frequency monitored by Station WWV. The B_0 and I_0 values are, respectively: 44300.83 mc and 18.93_{790} g cm$^2\times10^{-40}$ for $HC^{12}N^{14}$; 43154.83 and 19.44_{080} for $HC^{13}N^{14}$; 36207.40 and 23.17_{108} for $DC^{12}N^{14}$; 35587.57 and 23.57_{465} for $DC^{13}N^{14}$. The interatomic distances determined are $d_{CH}=1.061$A and $d_{CN}=1.157$A. The nuclear quadrupole coupling of N^{14} is determined as 4.58 ± 0.05 mc/sec.

THE light-weight linear molecule, HCN, has been carefully investigated with optical spectroscopy.[1] In fact, among the polyatomic molecules its spectrum is one of those most accurately measured by optical techniques. Nevertheless, the newly developed microwave methods are capable of extending significantly the accuracy of certain of its molecular constants.

Using the instruments and techniques previously developed in this laboratory[2] for the wave-length region below four millimeters, we have measured the frequencies of the first rotational lines ($J=0\rightarrow1$ transition) to seven figures for the different isotopic species $HC^{12}N^{14}$, $DC^{12}N^{14}$, $HC^{13}N^{14}$, and $DC^{13}N^{14}$. Only the first two of these species have been investigated with optical spectroscopy. In the preliminary microwave investigations by Smith, Gordy, Simmons, and Smith,[2(a)] the first rotational line of $HC^{12}N^{14}$ was detected, and an approximate measurement was made with a cavity wave meter. The present work extends the range of precision frequency measurements to the region of 88,000 Mc.

The radiation source used was a crystal multiplier which produced harmonics of energy from a Raytheon klystron. The second harmonic was used for measurements on DCN, and the third harmonic for those on HCN. Coin silver *K*-band wave guide was used for the cell, with tapered transition sections to couple it to the *H*-band components. The frequency measurements were made with multiples of a ten-megacycle crystal oscillator continuously monitored by Station WWV, of the Bureau of Standards.[3]

In Table I are listed the measured frequencies of the various lines. The $J=0\rightarrow1$ rotational line of each molecule is split into a triplet hyperfine structure by the nuclear quadrupole coupling of N^{14}. This structure for $DC^{12}N^{14}$ is shown in Fig. 1, where the calculated hyperfine structure is compared with the cathode-ray trace of the observed lines.

The rotational energy of a linear molecule in the ground vibrational state is

$$E_r(\text{cm}^{-1})=B_0J(J+1)-DJ^2(J+1)^2.$$

With the Bohr relation and the selection rule, $\Delta J=1$, this gives the frequency of the first line as

$$\nu(\text{cm}^{-1})=2B_0-4D.$$

The centrifugal stretching constant D cannot be evaluated from the present measurements. Fortunately, since we are dealing with the $J=0\rightarrow1$ line, the centrifugal effects are very small and can be neglected entirely without affecting the accuracy of the molecular structure determination. However, D has been evaluated approximately from the higher rotational lines in the optical region. In determining the B_0 and I_0 values for each of the isotopic forms, the value $D=3.3\times10^{-6}$ cm^{-1} given for HCN by Herzberg[4] was used. The resulting

TABLE I. Observed line frequencies.

Molecule	Transition	ν (mc/sec.)
	$J=0\rightarrow1$	
$HC^{12}N^{14}$	$F\rightarrow F'$	
	$1\rightarrow0$	88603.56 ± 0.30
	$1\rightarrow2$	88601.49
	$1\rightarrow1$	88600.11
$HC^{13}N^{14}$	$1\rightarrow0$	88311.54 ± 0.30
	$1\rightarrow2$	86309.49
	$1\rightarrow1$	86308.12
$DC^{12}N^{14}$	$1\rightarrow0$	72416.68 ± 0.20
	$1\rightarrow2$	72414.62
	$1\rightarrow1$	72413.25
$DC^{13}N^{14}$	$1\rightarrow0$	71177.02 ± 0.20
	$1\rightarrow2$	71174.96
	$1\rightarrow1$	71173.58

* The research reported in this document has been made possible through support and sponsorship extended by the Geophysical Research Directorate of the Air Force Cambridge Research Laboratories under Contract No. W(19-122)ac-35. It is published for technical information only and does not represent recommendations or conclusions of the sponsoring agency.

** Present address: Emory University, Atlanta, Georgia.
*** Present address: The Citadel, Charleston, South Carolina.

[1] (a) G. Herzberg and J. W. T. Spinks, Zeits. f. Physik **91**, 386 (1934); (b) P. F. Bartunek and E. F. Barker, Phys. Rev. **48**, 516 (1935); (c) Herzberg, Patat, and Verleger, Zeits. f. Physik **102**, 1 (1936); (d) E. Lindholm, Zeits. f. Physik **108**, 454 (1938); (e) G. Herzberg, *Infrared and Raman Spectra of Polyatomic Molecules* (D. Van Nostrand Company, Inc., New York, 1945), p. 391.

[2] (a) Smith, Gordy, Simmons, and Smith, Phys. Rev. **75**, 260 (1949); (b) W. Gordy, Rev. Mod. Phys. **20**, 668 (1948).

[3] The method of monitoring is described in reference 2(b).

[4] G. Herzberg, reference 1(e), p. 393.

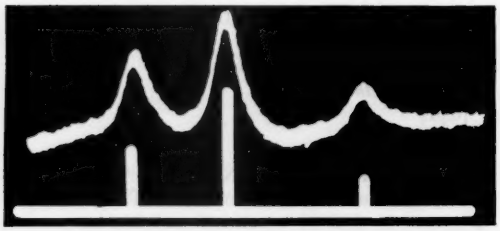

FIG. 1. Calculated and observed hyperfine structure of the $J=0\rightarrow1$ transition of $DC^{12}N^{14}$.

TABLE II. Molecular constants.*

Molecule	ν_0 (mc/sec.)	B_0 (Mc/sec.)	I_0 (g cm$^2\times10^{-40}$)
$HC^{12}N^{14}$	88601.26	44300.83	18.93_{790}
$HC^{13}N^{14}$	86309.26	43154.83	19.44_{080}
$DC^{12}N^{14}$	72414.39	36207.395	23.17_{108}
$DC^{13}N^{14}$	71174.73	35587.565	23.57_{465}

* The ν_0 represents the frequency of the $J=0\rightarrow1$ rotational line corrected for hyperfine splitting. In computing B_0 from ν_0, D was taken as 0.1 mc. The value of h used in computing I_0 is $6.624_2\times10^{-27}$ erg-sec.

TABLE III. Molecular dimensions* of hydrogen cyanide determined from different isotopic combinations.

Molecular pair used	CH or CD distance (10^{-8} cm)	CN distance (10^{-8} cm)
$DC^{12}N^{14}-DC^{13}N^{14}$	1.0817	1.1500
$HC^{12}N^{14}-HC^{13}N^{14}$	1.0665	1.1561
$DC^{12}N^{14}-HC^{13}N^{14}$	1.0610	1.1571
$DC^{12}N^{14}-HC^{12}N^{14}$	1.0605	1.1573
$HC^{13}N^{14}-DC^{13}N^{14}$	1.0593	1.1575
$HC^{12}N^{14}-DC^{12}N^{14}$	1.0586	1.1577
	Av. 1.0647	Av. 1.1560

* The constants used in these calculations are: $M_H=1.00813$, $M_D=2.01473$, $M_{C^{12}}=12.00386$, $M_{C^{13}}=13.00761$, $M_{N^{14}}=14.0075$, all in a.m.u.; $h=6.6242\times10^{-27}$ erg-sec. and the unit atomic mass $M=1.6599\times10^{-24}$ g.

B_0 values are listed in Table II with the frequencies of the hypothetical unsplit rotational lines, ν_0, and the moments of inertia.

The moment of inertia of hydrogen cyanide may be expressed in terms of its structural parameters as

$$I=\frac{1}{M_H+M_C+M_N}\{M_HM_Cd_{CH}^2+M_CM_Nd_{CN}^2+M_HM_N(d_{CH}+d_{CN})^2\},$$

where the subscript H refers to H or D and the subscript C to C^{12} or C^{13}. With the available data, four independent equations can be written which can be combined in six different ways to yield values of d_{CH} and d_{CN}. Because of the differences in zero point energies of the different isotopes, the interatomic distances for the ground vibrational state depend somewhat on the mass of the isotope. This unfortunate circumstance prevents the use of microwave data on different isotopic combinations for highly accurate structural determinations, except in rare instances where it is possible to determine equilibrium values of B. From the degree of consistency of the results obtained with different isotopic combinations one can estimate the probable error arising from this effect.

It is apparent from an examination of Table III that the results are reasonably consistent except for the combination $DC^{12}N^{14}-DC^{13}N^{14}$. This pair gives an anomalously large d_{CD} in comparison with the d_{CH} determined from $HC^{12}N^{14}-HC^{13}N^{14}$. The implication is that the d_{CD} in this case is actually longer than the d_{CH} since the pairs are identical except for the difference in D and H. The probable error is greatest for $DC^{12}N-DC^{13}N$ since here the isotope changed is nearest the center of gravity. However, the difference appears too great to be accounted for entirely by experimental error. In choosing the most probable value for the d_{CH} and d_{CN} we omit those for $DC^{12}N-DC^{13}N$ and average those for the remaining five combinations. The resulting values are: $d_{CH}=1.061_3$A, $d_{CN}=1.157_1$A. The average deviations are 0.002A and 0.0005A, respectively. The average deviations from these values become 0.005A and 0.0015A, respectively, when the values from $DC^{12}N-DC^{13}N$ are included.

The optical spectroscopy measurements included $DC^{12}N^{14}$ and $HC^{12}N^{14}$ only. The most recent values from optical spectroscopy, $d_{CH}=1.058_7$ and $d_{CN}=1.157_4$, are from Herzberg.[5] These are in excellent agreement with the ones determined here from the same pair of isotopes.

The N^{14} nuclear quadrupole coupling constant, $eQ\partial^2V/\partial z^2$ is, within the experimental error, the same for all the different isotopic combinations studied. Table IV lists the values obtained from measurements

TABLE IV. Nuclear quadrupole coupling of N^{14} in HCN.

Molecule	N^{14} nuclear coupling $eQ\partial^2V/\partial z^2$ (mc/sec.)
$HC^{12}N^{14}$	4.58_5
$HC^{13}N^{14}$	4.56_5
$DC^{12}N^{14}$	4.57_5
$DC^{13}N^{14}$	4.59_5
	Av. 4.58_0

TABLE V. Comparison of N^{14} nuclear quadrupole coupling and CN length in HCN with those in the halogen cyanides.

Molecule	CN length (A)	N^{14} nuclear coupling (mc/sec.)
HCN	1.157	4.58[a]
ICN	1.159	3.80[b]
BrCN	1.160	3.83[b]
ClCN	1.163	3.67[b]

[a] Present work.
[b] From Smith, Ring, Smith, and Gordy, Phys. Rev. 74, 370 (1948), and Townes, Holden, and Merritt, Phys. Rev. 74, 1113 (1948).

[5] G. Herzberg, reference 1(e).

on the different molecules. The average value $4.58_0 \pm 0.050$ is slightly lower than the earlier less accurate value.[2] Table V compares the nuclear coupling in HCN with that in the halogen cyanides. The higher value for HCN reveals a small but definite difference in the electronic structure of the CN bond. A slight difference is also revealed by the shorter CN distance for HCN shown in Table V.

We wish to thank Dr. Ralph Trambarulo for preparing the chemicals and Messrs. O. R. Gilliam and C. M. Johnson for assistance in assembling some of the equipment.

PHYSICAL REVIEW VOLUME 77, NUMBER 1 JANUARY 1, 1950

On the Emission Bands of CCl

PUTCHA VENKATESWARLU*
Department of Physics, University of Chicago, Chicago, Illinois
(Received September 7, 1949)

Some new bands of CCl are recorded and these together with those reported by earlier workers are arranged in a vibrational scheme. The electronic transition is $^2\Sigma \rightarrow {}^2\Pi$, the doublet separation for the $^2\Pi$ state being 138 cm^{-1}. By way of comparison it is mentioned that the uncondensed transformer discharge gave CF_2 bands in the case of CF_4, CCl, and Cl_2 bands in the case of CCl_4 and only Br_2 bands in CBr_4. It is pointed out that the supposed CBr bands reported by Durie and Iredale are not due to CBr but due to Br_2.

FLOWING vapor of carbon tetrachloride was excited by an uncondensed transformer discharge and the spectrum obtained was photographed on Medium Hilger quartz and E_1-quartz (Littrow type) spectrographs. Besides the continuous bands of Cl_2 and the CCl bands reported by earlier workers,[1-3] some extra bands of CCl were recorded. The wave-lengths and the wave numbers together with the estimated intensities of the band heads, which are all degraded to shorter wave-lengths, are given in Table I. The intense bands were photographed in the second order of a 21-ft. Wadsworth mounting grating spectrograph, and the rotational structure of the bands could be seen, but the dispersion is not high enough to make any rotational analysis.

All the new bands, marked*, together with those reported by earlier workers can be arranged in the vibrational scheme shown in Table II, which represents an extension of the analysis of Asundi and Karim.[1] The electronic transition, as suggested by Asundi and Karim, appears to be $^2\Sigma \rightarrow {}^2\Pi$, $^2\Pi$ being the ground state. The doublet separation $^2\Pi_{3/2} - {}^2\Pi_{1/2}$ is 138 cm^{-1}. From the analysis the Q heads can be fairly well represented by the following formula.

$$\nu = \left.\begin{matrix}35834\\35972\end{matrix}\right\} + (866v' - 1.5v'^2) - (845v'' - 1.0v''^2).$$

Horie[3] gave a vibrational analysis of the CCl bands** which does not appear to be satisfactory for the following reasons: (1) Some of the extra bands obtained in the present experiments, namely 34098, 34169, and 36012 cm^{-1} do not fit in the scheme proposed by Horie. (2) The $\omega_e'x_e'$ value 18.8 cm^{-1} obtained by Horie's analysis appears to be too high and out of proportion with the value 3.5 cm^{-1} obtained by him for $\omega_e''x_e''$.

TABLE I.

Intensity	λ_{air}	ν_{vac}
1	2931.9	34098
1	2927.4	34150
?	2925.8	34169
1	2919.5	34242
1	2916.3	34280
3	2861.5	34936
5	2857.1	34990
4	2855.5	35010
4	2849.2	35087
5	2846.0	35127
?	2844.2	35149
4	2794.2	35778
6	2789.8	35834
10	2788.3	35854
5	2786.7	35874
8	2782.3	35931
7	2778.9	35975
10	2777.6	35992
?	2776.0	36012
1	2724.0	36700
2	2721.5	36734
?	2717.4	36789
2	2713.9	36836
1	2711.5	36869

* Post Doctoral Research Fellow, Molecular Spectra Research Project.

[1] R. K. Asundi and S. M. Karim, Proc. Ind. Acad. Sci. **6A**, 328 (1937).

[2] Asundi, Singh, and Mishra, Current Science **12**, 204 (1943).

[3] Tadao Horie, Proc. Phys. Math. Soc. Japan **21**, 143 (1939).

** The isotope displacements due to CCl^{35} and CCl^{37}, reported by Horie for three of the bands are, however, not noticed in the present experiments.

TABLE II. Vibrational analysis.

v'\v''	0	1	2	3
0	P 35778 842 Q 35834 844 141 P 35931 844 Q 35975 848 866,858,861	34936 838 34990 840 137 35087 845 35127 847 864,865	34098* 34150 130 34242 34280* 860	
1	... 36700 846 136 36789* 36836 844	... 35854 844 138 ... 35992	... 35010 841 139 35149 864, 863	... 34169*
2			... 35874 138 ... 36012* 860,857	
3			... 36734 135 ... 36869*	

(3) The O−C values for Horie's analysis can be seen to be in general high compared with the O−C values for the present analysis. (4) The transition responsible for the band system, as stated above appears to be $^2\Sigma \rightarrow {}^2\Pi$, with which Horie also agrees. $^2\Sigma \rightarrow {}^2\Pi$ transitions in the iso-electronic molecules SiF (β- and γ-systems),[4] NS[5] and Po[6] (all of which have 23 electrons like CCl) clearly show P_1, Q_1, P_2 and Q_2 band heads. This is true also for similar transitions in NO and SiCl.[7] So it is quite natural to expect the P_1, Q_1, P_2 and Q_2 heads in the CCl band system. Indeed we see four band heads in the different groups of the present band system. Horie's analysis is based on the assumption that all the band heads are just either Q_1 or Q_2 heads and he does not take into consideration the possible existence of P_1 and P_2 heads at all. On the other hand, the present analysis (Table II) shows clearly the expected P_1, Q_1, P_2 and Q_2 heads.

It will be worth while, by way of comparison, to mention briefly some results obtained by the writer in other experiments using a similar uncondensed transformer discharge through CF_4 and CBr_4. In the case of CF_4, a new band system due to the CF_2 molecule is obtained. This will be dealt with in detail in a separate communication. But the excitation of CBr_4 gave only bands due to the bromine molecule and did not give any bands due to either CBr or CBr_2. It may be pointed out that Durie and Iredale[8] reported some supposed CBr continuous bands**,[9] obtained by high frequency discharge through CBr_4 vapor. We also got these bands by the transformer discharge through CBr_4 vapor, but the same bands were also obtained by exciting pure bromine vapor.[10] Hence these bands must be due to the bromine molecule and not due to the CBr molecule.

The author wishes to express his thanks to Professor R. S. Mulliken for his kind interest in the work.

[4] R. K. Asundi and R. Samuel, Proc. Ind. Acad. Sci. **3**, 346 (1936).
[5] A. Fowler and C. J. Bakker, Proc. Roy. Soc. London **136**, 28 (1932).
[6] P. N. Gosh and G. N. Ball, Zeits. f. Physik **71**, 362 (1931).
[7] W. Jevons, Proc. Phys. Soc. **48**, 563 (1936).
[8] R. A. Durie and T. Iredale, Trans. Faraday Soc. **XLIV**, 806 (1948).
** It may be mentioned that these continua agree well with those continuous emission bands obtained by Asundi and Karim (see reference 9) in the excitation of $SiBr_4$, which are also obviously due to Br_2.
[9] See reference 1, p. 282.
[10] P. Venkateswarlu, Proc. Ind. Acad. Sci. **25A**, 138 (1947).

Straggling of Electrons near the Critical Energy. II

L. EYGES*
*The University, Birmingham, England***
(Received August 12, 1949)

The straggling of electrons with energy near the critical energy is discussed, using an approximation to the expression for the radiative cross section which takes into account its variation with energy. From the results the "track length" of electrons (neglecting pair production and Compton effect) is evaluated for some special cases and compared with the numerical calculations of Richards and Nordheim. The agreement appears to be good.

I. INTRODUCTION

THIS paper should be considered as an extension of a previous one with the same title,[1] hereinafter referred to as I. The main advance in the present work is the use of a considerably more accurate expression, suggested by Richards and Nordheim,[2] for the radiative cross section. The paper is essentially in two parts. In Section II we discuss the straggling of electrons using the approximate expression mentioned above; in Section III we discuss the effect of photons and compare our results with some numerical calculations of R.N.

For convenience we will recall here some equations of I; for complete details the reader is referred to that paper. The straggling function $\pi(E, t)$ defined such that $\pi(E, t)dE$ is the probability that an electron has energy in the range E to $E+dE$ at thickness t, satisfies the diffusion equation

$$\frac{\partial\pi(E,t)}{\partial t}=-\int_0^1\left[\pi(E,t)-\frac{1}{1-v}\pi\left(\frac{E}{1-v},t\right)\right]\times\varphi(E,v)dv+\beta\frac{\partial\pi(E,t)}{\partial E}. \quad (1)$$

We shall also use the Mellin transform $M(s, t)$ defined by

$$M(s,t)=\int_0^\infty E^s\pi(E,t)dE \quad (2)$$

with the inverse transform

$$\pi(E,t)=\frac{1}{2\pi i}\int_{\delta-i\infty}^{\delta+i\infty}E^{-(s+1)}M(s,t)ds. \quad (3)$$

II. SOLUTION OF THE STRAGGLING EQUATION

We will first discuss the straggling when collision loss is neglected, but the variation of radiative cross section is taken into account, in order to show as clearly as possible what the latter entails. Following R.N. we take as an approximate expression for the radiative cross section which holds for E of the order of 10^8 electron volts or lower,

$$\varphi(E,v)=\varphi_0(v)+\varphi_1(E,v), \quad (4)$$

where

$$\varphi_0(v)=\frac{4}{3}\frac{dv}{v}(1-v), \quad (4a)$$

$$\varphi_1(E,v)=aEv, \quad (4b)$$

where $a=3/4W_0$ and W_0 is a constant characteristic of the material. $W_0=1.15\beta$ for air and 10β for lead. In Fig. 1 we plot the correct and approximate expressions for various energies in air. If we use the expressions (4) in (1), with β set equal to zero, and apply the Mellin transform (3) we are led after some algebra and the evaluation of a simple integral to an equation for the transform $M(s, t)$

$$\frac{\partial M(s,t)}{\partial t}=-A(s)M(s,t)+B(s)M(s+1,t), \quad (5)$$

where

$$A(s)=\frac{4}{3}(\Psi(s+1)+C)-\frac{4}{3}, \quad (6)$$

$$B(s)=-\frac{as(s+3)}{(s+1)(s+2)}. \quad (7)$$

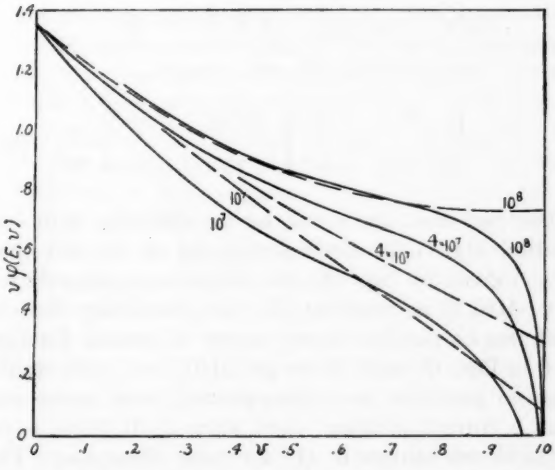

FIG. 1. The approximate expression (4) for the radiative cross section for various energies (electron volts) in air is plotted as dotted lines and the correct expressions as solid lines.

* AEC postdoctoral research fellow.
** President address: Radiation Laboratory, University of California, Berkeley, California.
[1] L. Eyges, Phys. Rev. **76**, 264 (1949).
[2] J. A. Richards and L. W. Nordheim, Phys. Rev. **74**, 1113 (1948). Hereinafter referred to as R.N.

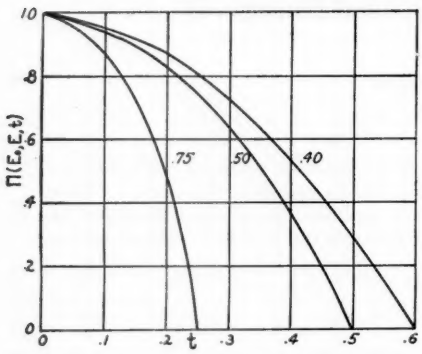

FIG. 2. Integral straggling function $\Pi(E_0, E, t)$, i.e. the probability that an electron of initial energy E_0 has energy greater than E at thickness t, for an electron in air. The numbers attached to the curves are values of E/β and $E_0/\beta=1$.

It is interesting to note that (5) is rather similar in form to the equation one gets taking collision loss into account, but assuming $\varphi(E, v)$ to be a function of v only (see Eq. (5) of I). The main difference is that in the present equation there appears the term $M(s+1, t)$ and in the previous one $M(s-1, t)$. This makes a profound difference in the solution, as we shall see, since the solution we derive for the present equation will hold for $E=0$, whereas the solution of the previous one did not. We attempt to solve Eq. (5) by the following substitution:

$$M(s, t)=e^{-A(s)t}E_0^s(1+\sum_{n=1}^{\infty} c_n(s)t^n). \tag{8}$$

If we put (8) into (5) and equate the same powers of t on both sides of the resulting equation we get for the first three coefficients

$$c_1(s)=E_0B(s), \tag{9a}$$

$$c_2(s)=\frac{E_0^2a^2}{2}\frac{s(s+4)}{(s+2)^2}+\frac{2E_0a}{3}\frac{s(s+3)}{(s+1)(s+2)^2}, \tag{9b}$$

$$c_3(s)=-\frac{E_0^3a^3}{6}\frac{s(s+5)}{(s+2)(s+3)}-\frac{4}{9}\frac{E_0^2a^2s(s+4)}{(s+2)^2}\times\left[\frac{1}{2(s+3)}+\frac{1}{s+2}\right]-\frac{8E_0a}{27}\frac{s(s+3)}{(s+1)(s+2)^2}. \tag{9c}$$

The fact that there will be no difficulty with our solution $\pi(E, t)$ for $E=0$ is reflected in the fact that $M(s, t)$ given by Eqs. (8) and (9) behaves properly for $s=0$. $M(0, t)$ is, recalling (2), the probability that at thickness t a particle of any energy is present. Putting $s=0$ in Eqs. (8) and (9) we get $M(0, t)=1$; this result, that no particles have disappeared, must come out from a correct solution, since when $\beta=0$, there is no physical mechanism in (1) for their absorption. The straggling function $\pi(E, t)$ can be evaluated using Eqs. (3), (8), and (9) in the way discussed in I, i.e. by using the saddle-point method to evaluate the complex integral (3). We shall go into this below in a little more detail.

We now include the effect of collision loss, i.e., we use Eq. (1) as it stands, without setting $\beta=0$. Again applying the Mellin transform (2) and using $\varphi(E, v)$ given by Eq. (4) we are led to the equation

$$\frac{\partial M(s, t)}{\partial t}=-A(s)M(s, t)+B(s)M(s+1, t)-\beta sM(s-1, t). \tag{10}$$

If we now make the substitution

$$M(s, t)=e^{-A(s)t}(E_0-\beta t)^sP(s, t), \tag{11}$$

we are led to an equation for $P(s, t)$:

$$(E_0-\beta t)\frac{\partial P(s, t)}{\partial t}-\beta sP(s, t)=B(s)e^{-[4t/3(s+2)]}(E_0-\beta t)^2P(s+1, t)-\beta se^{[4t/3(s+1)]}P(s-1, t). \tag{12}$$

Finally, we assume

$$P(s, t)=1+\sum_{n=1}^{\infty} d_n(s)t^n, \tag{13}$$

and putting this in Eq. (12) and expanding the exponentials we can determine the coefficients $d_n(s)$ by equating to zero successive powers of t. In this manner we get for the first few after some reduction

$$d_1(s)=-E_0\frac{as(s+3)}{(s+1)(s+2)}, \tag{14a}$$

$$d_2(s)=\frac{E_0^2a^2}{2}\frac{s(s+4)}{(s+2)^2}+E_0a\frac{2}{3}\frac{s(s+3)}{(s+1)(s+2)^2}+\beta a\frac{(s-1)(s+4)}{2(s+1)(s+2)}-\frac{2}{3}\frac{s}{(s+1)}\frac{\beta}{E_0}, \tag{14b}$$

$$d_3(s)=\frac{\beta}{3E_0}(s+2)d_2(s)+\frac{E_0}{3}B(s)\times\left[d_2(s+1)-\frac{4}{3(s+2)}d_1(s+1)+\frac{8}{9(s+2)^2}\right]-\frac{2}{3}B(s)\beta\left[d_1(s+1)-\frac{4}{3(s+2)}\right]+\frac{B(s)\beta^2}{3}-\frac{\beta s}{3E_0}\left[d_2(s-1)+\frac{4}{3}\frac{d_1(s-1)}{(s+1)}+\frac{8}{9(s+1)^2}\right]. \tag{14c}$$

In the last equation we have for simplicity expressed $d_3(s)$ directly in terms of d_2 and d_1 instead of in an

expanded form. Even so, the expression is still very cumbersome, and the higher order terms increase very rapidly in complexity. The linear term $d_1(s)$ is due to the variation of radiation cross section with energy and is, of course, the same as Eq. (9a). As in the previous paper the effect of energy loss comes in first in the second-order term. Using the above expressions one can reassemble $M(s, t)$ and use it in (3) to evaluate the straggling spectrum. This is done in the next section.

III. DISCUSSION

We wish to compare our results with the numerical calculations of R.N., and for that purpose we will calculate the *integral* spectrum $\Pi(E_0, E, t)$ defined in I. It is given by

$$\Pi(E_0, E_1t)=\frac{e^{0.463t}}{2\pi i}\int_{\delta-i\infty}^{\delta+i\infty}\frac{e^{zs-(4/3)\Psi(s+1)t}}{s}\times(1+\sum_{n=1}^{\infty}d_n(s)t^n)ds, \quad (15)$$

where

$$z=\ln\frac{E_0-\beta t}{E}. \quad (16)$$

Noting that the first three coefficients d_1, d_2, d_3 given by Eq. (14) are very slowly varying for large s we can use the saddle-point method and write to a good approximation

$$\Pi(E_0, E_1t)=\frac{e^{0.463t+zs_0-(4/3)\Psi(s_0+1)t}}{s_0\left(-\frac{4}{3}\Psi''(s_0+1)t+\frac{1}{s_0^2}\right)^{\frac{1}{2}}}\cdot(1+\sum_{n=1}^{\infty}d_n(s_0)t^n) \quad (17)$$

whenever s_0, defined by the equation

$$z-(4/3)\Psi'(s_0+1)t-(1/s_0)=0 \quad (18)$$

is large enough. In practice it appears that s_0 greater than 2 or 3 is usually sufficiently large. Using this expression when it holds, and simple variations of the saddle-point method when it does not, we have calculated the spectrum for $E_0/\beta=1$ and $E/\beta=0.75$, 0.50, 0.40. For these values of E/β, t is quite small (it is necessarily less than $1-E/\beta$, and it is sufficient to retain terms only up to order t^3 in Eq. (17). The results of this calculation are given graphically in Fig. 2.

As mentioned in I, the saddle-point method gives an answer about 8 percent high for $t=0$. Thus if we consider the leading term in the spectrum (15), which is the integral

$$\frac{e^{0.463t}}{2\pi i}\int_{\delta-i\infty}^{\delta+i\infty}\frac{e^{zs-(4/3)\Psi(s+1)t}}{s}ds \quad (19)$$

TABLE I. Comparison of the electron track length with the values of Richards and Nordheim.

E/β	$\int_0^\infty \Pi(E_0, E, t)dt$	Richards-Nordheim track length (corrected)
0.75	0.18	0.16
0.50	0.33	0.32
0.40	0.39	0.40

the saddle-point method gives for this integral for $t=0$ the value $e/(2\pi)^{\frac{1}{2}}\approx 1.08$, whereas the correct value is 1. As one would expect, for t not zero but small, the saddle-point method still gives an answer slightly too high. For $E_0/\beta=1$, $E/\beta=0.2$, e.g. it gives for Eq. (19) for $t=0.1$, 0.2, 0.3, 0.4, 0.5 the values 1.08, 1.05, 1.02, 0.98, 0.91. We know that (19) cannot become greater than one. For small t, when the saddle-point method gives values slightly greater than one, we have therefore set these equal to one. This is only a partial correction however and some of our values for small t are probably still too large by a few percent. This will be of no great consequence in most practical computations, but we must consider it now, since we wish to compare our results with those of R.N.

These authors have computed the track length numerically for $E_0/\beta=1$, and various values of E/β, using the expression (4) for the radiative cross section. To compare our results with theirs, we have computed, by numerically integrating the curves of Fig. 1, the "track length" due to the original electron, i.e.

$$\int_0^\infty \Pi(E_0, E, t)dt.$$

These numbers are given in Table I. For an unequivocal comparison with Richards and Nordheim's work we should have to take into account, as they do, the effect of photons in pair production and the Compton effect. It seems clear, however, as discussed in I, that the contribution of photons will be quite small, and we would expect that for energies close to the initial energy, i.e. E/β close to 1, practically all the contribution to the track length will come from the original electron, and our results should agree quite closely with theirs. There is also another difficulty in an accurate comparison. R.N. use an approximate method of simplifying their equations to take into account radiation loss (over and above the use of the expression (4) for the radiative cross section). They state that this introduces an error of about 8 percent for $E=1$, but do not give the sign of the error. We can, however, deduce this with moderate safety by comparing their result at one point with the very accurate calculations of Rossi and Klapman. For $E/\beta=0.1$ and $E_0/\beta=1$ these authors find for the integral track length for air 32 g/cm² or in radiation lengths $32/43=0.740$. We can compare this result in radiation lengths with that of R.N. who find 0.671. Thus Rossi and Klapman's result is about 10 percent

larger. Also if one extrapolates graphically the R.N. results to $E=0$, one gets the value 0.91 instead of the value unity as one should. This can, of course, only be considered as weak corroborative evidence since the extrapolation is rather uncertain. In view of all the facts, however, it seems reasonable to assume that the results of R.N. are about 9 percent too low for $E_0/\beta=1$. To compare their results with ours we have therefore increased their results by this amount. The comparison is given in Table I. We think it reasonable to interpret this table as showing good agreement with R.N. in the following way. For the values of E/β listed in it the contribution of intermediate photons to the track length is practically nil. If this were true our results should be just the same as theirs. Our result is for the first value listed actually several percent greater because the saddle-point method gives an answer about 8 percent high for small t, and for this case the partial correction mentioned above is a very small correction, since Eq. (16) gives values less than one except for very small t. For the following two values of E/β the saddle-point method is rather more accurate, and one gets better agreement with R.N.

A remark here may be interesting if not strictly germane to the present subject. Tamm and Belenky have derived expressions for the track length we have discussed here, taking pair production into account and assuming a constant probability σ_0 for the pair production cross section. One might hope to estimate the effect of photons on the track length by finding what their expression becomes for $\sigma_0=0$, the difference between this and the general expression being the effect of photons. This cannot be done, however, because of the fact, at first sight rather surprising, that their result does not depend on σ_0. It is immediately clear that the track length is really independent of σ_0, however, if one looks at the coupled shower equations written for an incident electron. If one eliminates the photon spectrum from the two equations, leaving an equation involving only the spectrum of electrons, one finds that σ_0 has dropped out, provided it is not zero. The physical reason that the track length is independent of σ_0 is that no matter how small the photon absorption coefficient, photons *eventually* will be absorbed, producing pairs, and since we integrate to infinity in finding the track length we eventually get the contribution from these pairs.

One can get a rough upper limit for the effect of pair production of photons in the following way. Consider a photon of energy W_0 incident on matter, and assume a constant absorption coefficient σ due to pair production. The probability of the photon existing at t is $e^{-\sigma_0 t}$. If we use the rough law that the probability that a photon of energy W_0 produces a pair of electrons one of which has energy in the range E to $E+dE$ in dt is:

$$[2\sigma dEdt]/W_0,$$

then the number of electrons produced at t by one incident photon is

$$\frac{2\sigma dEdt'e^{-\sigma t'}}{W_0}.$$

Assume now an an upper limit for the straggling function

$$\Pi(E_0, E, t)=\begin{matrix}1 \text{ when } E<E_0-\beta t\\ 0 \text{ when } E>E_0-\beta t\end{matrix}$$

then the spectrum of electrons at t, which we call $\Pi_\gamma(W_0, E, t)$, is

$$\frac{2\sigma}{W_0}\int_0^t\int_{E+\beta(t-t')}^{W_0} dE'dt'e^{-\sigma t'},$$

which to first order in t is

$$(2\sigma/W_0)(W_0-E)t.$$

Now consider an electron of energy E_0 incident on matter. If we neglect the straggling, and it will be clear that this again overestimates the effect of photons, there will be one particle of energy $E_0-\beta t'$ at t'. Now use the rough law that the probability that in dt' this particle produces a quantum of energy E' is $(dE'/E')dt'$ where E' can go from 0 to $E_0-\beta t'$. Then the spectrum of particles at t due to the intermediate photon produced is approximately

$$\int_0^t dt'\int_E^{E_0-\beta t'}\frac{dE'}{E'}\Pi_\gamma(E', E, t-t').$$

If we use the above expression for Π_γ we get for the last expression in lowest order

$$\sigma t^2\left[\ln\frac{E_0}{E}+\frac{E}{E_0}-1\right].$$

E.g. for $E_0/\beta=1$, $E/\beta=0.2$, $t=0.5$, $\sigma\sim 0.5$; this gives 0.10 as the increase in probability for an electron being present.

Note that since this expression goes as t^2, the effect of pair production is always negligible for small thickness, compared with the probability that the original electron is present, which probability is of order unity. Also, the above estimate does not take into account electrons produced by the Compton effect, but we would expect its effect to be about the same as that of pair production, since the Compton and pair production cross sections are of the same order in the energy range we have considered.

The expression for the effect of pair production derived above corresponds to the effect of one intermediate photon, in the sense of the Bhabha-Heitler theory.[3] The effect of high numbers of intermediate photons will be much smaller for small thicknesses. One

[3] H. J. Bhabha and W. Heitler, Proc. Roy. Soc. **A159**, 432 (1937).

can get an exact expression, instead of an upper limit for the effect of one intermediate photon by refining the above arguments in an obvious way. The result is then the analogue of Bhabha-Heitler's Eq. (23) for $n=1$, but it involves multiple integrals which cannot be evaluated easily and it is probably not worth writing down, since the effect it describes is so small.

The author would like to thank the U. S. Atomic Energy Commission for a fellowship during the tenure of which this work was done.

PHYSICAL REVIEW VOLUME 77, NUMBER 1 JANUARY 1, 1950

Dimensional Effects Resulting from a High Dielectric Constant Found in a Ferromagnetic Ferrite

FRANK G. BROCKMAN, P. H. DOWLING, AND WALTER G. STENECK
Philips Laboratories, Inc., Irvington-on-Hudson, New York

(Received September 6, 1949)

A variety of a ferromagnetic ferrite is shown to have dielectric properties corresponding to a dielectric constant of the order of 10^5. Coupled with a magnetic permeability of about 10^3, this leads to dimensional resonance effects such that the apparent permeability of a core whose section is 2.5×1.25 cm reduces to very low values in the region of 2 megacycles. An apparent anomaly exists in the dielectric behavior in the vicinity of the magnetic Curie point. A general theory of dimensional effects encountered in measuring magnetic and dielectric constants is developed. This theory is based on the geometry of the infinite slab. When the theory is applied to the ferrite under study, a residual variation of the permeability with frequency remains, which may be explained by magnetic resonance. The theory accounts adequately for the dielectric effects at the Curie point.

I. INTRODUCTION

IN the last few years there was developed in the Philips Laboratories, in Eindhoven, Holland, a series of non-metallic ferromagnetic materials by Snoek, Verwey and their coworkers.[1] Being non-metallic these materials have low electrical conductivity and therefore low eddy current losses when used in an alternating magnetic field. Because of this development, Philips Laboratories, Irvington, New York, were consulted regarding the use of one of these materials in the construction of a special massive ferromagnetic core for use in the lower megacycle region. The chief requirements made of the core material were as high permeability as possible (preferably not less than 1000) together with low losses (hysteresis and residual losses as well as eddy current loss) at frequencies up to 5 megacycles per second. Aside from the problem of the choice of the material based on the magnetic properties, there also existed the purely mechanical problem of the construction of such a core, which would weigh about $\frac{1}{2}$ ton.

One of the commercial varieties of the non-metallic magnetic materials mentioned above is a manganese-zinc ferrite, marketed under the trade mark Ferroxcube III. Consideration of the nominal properties of this material (Table I) indicated that it would probably be acceptable for this application.

Since these materials are not ductile and cannot be cast, it was decided that the large core could be assembled of brick-shaped pieces which would be accurately dimensioned and squared. This latter requirement was imposed to reduce the effects of air gaps in the structure to a minimum.

For preliminary studies a smaller test core was constructed. The sizes chosen for the brick-shaped pieces were $5\times2.5\times1.25$ cm and $10\times2.5\times1.25$ cm. In the core structure these sizes present a minimum dimension, in a direction perpendicular to the magnetic flux, of 1.25 cm. On the basis of the resistivity of the material (Table I) and this dimension, it was estimated that eddy-current losses would not be excessive.

However, when the initial permeability of the bricks was investigated as a function of frequency it was found to decrease rapidly to a very low value at about 2 mc. Because this frequency was considerably lower than had been expected from previous experience, an investigation of the effect was made. This investigation led first to the prediction that the material must possess a dielectric behavior corresponding to an unexpectedly large dielectric constant of the order of 5×10^4 and then to the experimental verification of this fact.

TABLE I. Nominal characteristics of Ferroxcube III.

Initial permeability, μ_0	1000 to 1500
Loss factor, $\tan\delta/\mu_0$, 60 kc	0.1×10^{-4}
Hysteresis resistance coefficient,* 2 kc	1 to 4×10^{-6}
Resistivity	100 ohm cm

* Victor E. Legg, Bell Sys. Tech. J. 15, 39 (1936).

[1] (a) J. L. Snoek, *New Developments in Ferromagnetic Materials* (Elsevier Publishing Co., New York, 1947). (b) J. L. Snoek, Philips Tech. Rev. 8, 353 (1946). (c) E. J. W. Verwey, Philips Tech. Rev. 9, 46 (1947). (d) Verwey, Haayman, and Heilman, Philips Tech. Rev. 9, 185 (1947). (e) E. J. W. Verwey and E. L. Heilman, J. Chem. Phys. 15, 174 (1947). (f) Verwey, Haayman, and Romeyn, Philips Tech. Rev. 15, 181 (1947).

With a permeability of 10^3 and a dielectric constant of 5×10^4, the wave-length of an electromagnetic wave in a core of Ferroxcube III is about 2 cm at 2 megacycles. Dimensional resonance effects may thus be expected at this frequency in a core about 1 cm thick. Furthermore, as the core thickness is decreased, such resonance effects will be pushed to higher frequencies as confirmed by experiment. When dimensional resonance occurs, the real component of the flux decreases to low values or, if the losses be low enough, may pass through zero to negative values. A corresponding variation will be produced in the apparent or effective permeability, thus accounting for the low apparent permeability we found at 2 mc in the bricks of Ferroxcube III.

The origin of the dielectric behavior of Ferroxcube III is not entirely clear. Polder,[2] of the Philips Laboratory, Eindhoven, has advanced an explanation based on a fine-grained texture of this material giving rise to a distribution of barrier layers, and von Hippel has informally suggested a somewhat similar explanation. For large scale measurements such a material will behave as though it had a high dielectric constant, even though it nowhere possesses a significantly large inherent dielectric constant.

When calculations are made according to our theory for the removal of dimensional effects, a considerable dispersion remains in the magnetic permeability so derived. It is possible to account for this, as Snoek[3] has done, by magnetic resonance. His paper contains a misprint for the value of g, the gyromagnetic ratio. When the correct value of 1.76×10^7 is substituted in his formula, the frequency at which the actual permeability of Ferroxcube III reduces to half value comes out to be 1.26×10^7 c.p.s. Our measurements give about 0.5×10^7 for the half value frequency. Snoek has advanced reasons as to why such a discrepancy might be expected.

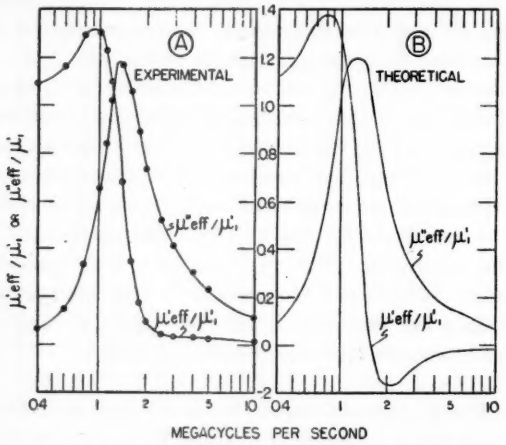

FIG. 1. Core section 2.5×1.25 cm. A. Experimental values of the ratio of the effective permeabilities to the real part of the actual permeability at 1000 c.p.s. B. Theoretical values of the same.

[2] D. Polder, forthcoming publication.
[3] J. L. Snoek, Physica 14, 207 (1948).

II. EXPERIMENTAL

Magnetic Experiments

For the magnetic measurements on the bricks a square core was assembled from two of the 5 cm bricks and two of the 10 cm bricks. The core was thus 10 cm square with a window 5×5 cm. This core was wound with an appropriate number of turns of insulated copper wire and the resulting inductor was measured upon a General Radio Type 916-A Radio Frequency Bridge. The data obtained by these measurements are the equivalent series reactance and resistance between the two terminals of the inductor. This equivalent is the representation usually employed in studies of this kind. The inductance at a low frequency (1000 c.p.s.) was obtained using a General Radio Type 667-A Inductance Bridge. In all cases the current through the measured inductor was kept so small that the measured reactance corresponded to the initial permeability.

At the higher frequencies corrections have been applied for the distributed capacitance. Part of this capacitance, 2.8 mmfd, exists at the Type 916-A bridge terminals and part is due to the winding on the core. This latter value was estimated by preparing a polystyrene duplicate core which was coated, except for a horizontal space to break the eddy current circuit, with a thin layer of Aquadag. A similar winding was applied to this duplicate core and the distributed capacitance evaluated by determining the resonant frequency of this inductor for various values of capacitance using a Boonton Type 160-A Q-meter. By plotting the inverse of the square of the angular resonant frequency against the added capacitance, a straight line relationship is obtained which can be extrapolated to yield a value for the distributed capacitance of the coil.

In Fig. 1A are shown the data on the brick core, plotted as the ratio of the effective permeabilities to the real part of the actual permeability at 1000 c.p.s., i.e., μ_{eff}'/μ_1' and $\mu_{\text{eff}}''/\mu_1'$. The effective permeabilities were

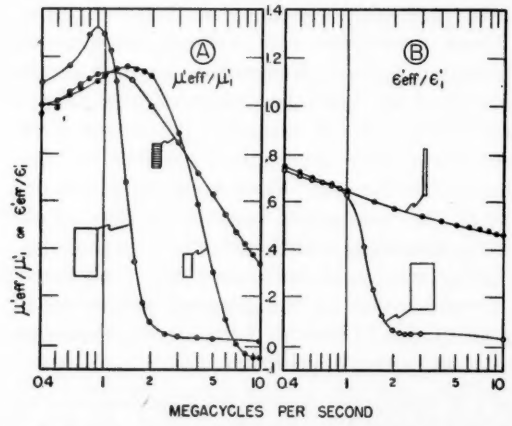

FIG. 2. Dependence of the real part of the effective material constants upon dimensions of the sample, experimental. Sample cross sections shown to scale for each curve. Data given as the ratio of the effective constant to the real part of the corresponding constant at 1000 c.p.s. A. Permeabilities. B. Dielectric constants.

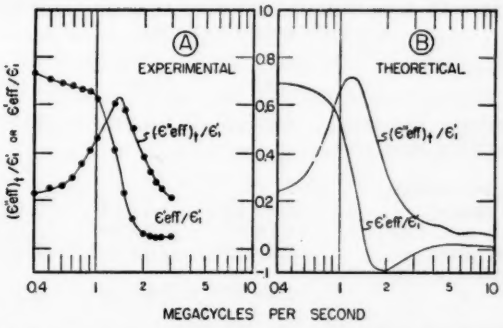

FIG. 3. Sample section 2.5×1.25 cm. A. Experimental values of the ratio of the effective dielectric constants to the real part of the actual dielectric constant at 1000 c.p.s. In the case of the imaginary part the influence of the conductivity has been removed. B. Theoretical values of the same.

computed according to Eqs. (8) in the theoretical section. μ_{eff}' increases to a maximum at about 0.9 mc and then decreases to a very low value at about 2 mc. In some samples, μ_{eff}' was observed to go negative in the neighborhood of this frequency.

When air gaps were introduced into the magnetic circuit,[4] the apparent resonance was shifted to higher frequencies. Because it is an experimental fact that one of the effects of the introduction of an air gap is to decrease the apparent losses of the inductor, another well-known method for reducing core losses was tried, i.e., to reduce the dimensions of the core in a direction perpendicular to the magnetic flux. Again it was found that the apparent resonance effects were pushed to higher frequencies. The shift to higher frequencies also occurred when the over-all core dimensions were not changed, but the core was laminated. The curve obtained with one of these laminations was substantially the same as with the core composed of ten laminations. (See Fig. 2A. In this figure the areas marked off are the core sections drawn to scale. The largest section is 2.5×1.25 cm.)

These phenomena indicated strongly that the deviations of μ_{eff}'/μ_1' from unity were not due alone to an inherent property of the material as would be the case if they were due only to magnetic resonance. Calculations on the effect of ohmic eddy currents indicated clearly that these alone could not account for the results and hence we were led to a consideration of the dielectric properties of the material.

[4] Experiments performed with air gaps at 1000 c.p.s. served to establish the fact that, when no intentional gaps were inserted in the core assembled as described, the faces of the bricks, which were in contact, were sufficiently plane and parallel so that no measurable effect upon the permeability could be observed. These experiments consisted in measuring the low frequency inductance of a given coil upon the core with the bricks pressed firmly together and then with various known gaps. When the reciprocals of the measured inductances were plotted against the gap lengths the line was straight and the intercept on the reciprocal inductance axis coincided with the reciprocal of the inductance measured when the blocks were pressed firmly together.

Dielectric Experiments

The dielectric properties of the material were investigated by applying, by evaporation, gold electrodes to opposite faces of appropriately shaped pieces.

The absence of electrode effects was demonstrated by showing the equality of the direct current resistivity if measured from the dimensions, the current through the electrodes and (a) the voltage drop across the electrodes or (b) the potential difference, measured potentiometrically, between two probe electrodes spaced along the direction of the current flow. Some further proof of the absence of electrode effects is that, with carefully applied electrodes, the low frequency (e.g., 1000 c.p.s. resistance between the electrodes was the same as the d.c. resistance observed.

The equivalent parallel reactance and resistance between the electrodes were measured from 200 to 100,000 c.p.s. on a fully-shielded equal-ratio-arm parallel impedance bridge. Above 100,000 c.p.s. the measurements were made as the equivalent series reactance and resistance between the electrodes, using either a General Radio 917 AL or 917 A Radio Frequency Bridge. These values were converted to equivalent parallel impedances by calculation. On account of the high dielectric constant of the material, no guard rings were necessary. The measured impedances were converted to effective

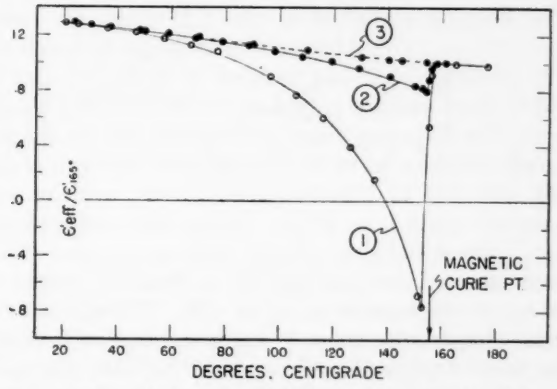

FIG. 4. The variation of the real part of the effective dielectric constant with temperature through the magnetic Curie point. Data plotted as the ratio of the effective constant to the real part of the actual constant at 165°C. (1) Sample section 2.5×1.25 cm. (2) Sample section 2.5×0.358 cm. (3) Actual dielectric constant computed from (2).

dielectric constants, ϵ_{eff}' and $(\epsilon_{eff}'')_t$, by means of Eqs. (8). In the effective dielectric loss factor, $(\epsilon_{eff}'')_t$, the effect of the ohmic current has been eliminated by means of Eq. (3).

Figure 3A shows the results for one of the 10 cm Ferroxcube III bricks, the electrodes being applied to the 2.5×1.25 cm ends. The results are plotted as the ratios of the effective constants to the real part of the actual dielectric constant at 1000 c.p.s.; i.e., $\epsilon_{eff}'/\epsilon_1'$ and $(\epsilon_{eff}'')_t/\epsilon_1'$. Again resonant effects are apparent and again, in the case of some bricks, we have observed

negative values of ϵ_{eff}' in the region of 2 mc. Figure 2B shows the effect on ϵ_{eff}' of reducing the 1.25 cm dimension to 0.127 cm. The areas marked off in the figure are the electrode areas drawn to scale. It is evident that resonant phenomena have been pushed to higher frequencies by making the sample thinner, as in the case of the magnetic permeability.

These experiments show conclusively that the material does have a dielectric behavior corresponding to a very high dielectric constant. The combination of the high dielectric constant and high magnetic permeability in the same material gives rise to the dimensional resonance which accounts for the anomalous results we have observed in our measurements of μ_{eff}' and ϵ_{eff}' in the samples of thicker section. A quantitative explanation will be given in the theoretical section.

When the unusual dielectric properties of the material were established, the question of the behavior of the dielectric properties as a function of temperature was investigated. Special interest was centered in the phenomena which occur at the magnetic Curie point.

The results given in Fig. 4 were obtained by measurements at 10,000 c.p.s. These data are plotted as the ratio of the real part of the effective dielectric constant at a given temperature to the real part of the dielectric constant at a temperature just above the magnetic Curie point. Curve 1 of this figure was obtained from measurements performed on a bar 1.25×2.50×10 cm with electrodes applied to the 1.25×2.50 cm faces. Curve 2 was obtained from a similar sample in which the 1.25 cm dimension was reduced to 0.358 cm and in which electrodes were applied to the 0.358×2.50 cm faces. The apparent dielectric constant for the thicker sample will be seen to become negative between about 138° and 154°C. The magnetic Curie point for the material studied is 155°C. Near this temperature (153°) the initial permeability rises to a rather sharp maximum and then falls rapidly to about 10 percent of its room temperature value at 156°. Throughout the entire temperature range, ϵ'' has no anomalies. It shows the same temperature dependence as does the conductivity. In Ferroxcube III, the conductivity varies with temperature in a manner common to semiconductors.

The apparent anomalies in the variation of the effective dielectric constant with temperature are explained in the theoretical section, and curve 3, obtained by correcting the data of curve 2 as discussed there, shows the course of the real part of the actual dielectric constant.

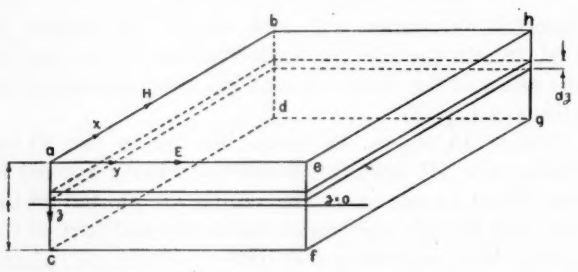

FIG. 5. Fundamental block of material used as the basis for the calculations in the theoretical section.

TABLE II. Actual material constants for samples used for the Curie point experiments.

	20°	150°	158°
Permeability, real part, μ'	1.4×10^3	2.6×10^3	<10
Permeability, imag. part, μ''	0	0	0
Dielectric constant, real part, ϵ'	9.5×10^4	7.5×10^4	7.5×10^4
imag. part, total, ϵ''	13.8×10^5	10.9×10^5	11.7×10^5
imag. part,* ϵ_i''	$\sim2.0\times10^4$	$\sim2.0\times10^4$	$\sim2.0\times10^4$
Conductivity (ohm cm)$^{-1}$, σ	7.5×10^{-3}	5.9×10^{-2}	6.3×10^{-2}

* Associated with true dielectric loss only.

In Table II are given, at three temperatures of interest, the actual material constants of the particular samples used for the investigation of the phenomena at the Curie point.

III. THEORETICAL

Derivation of the Impedance Expressions

Except for the limitations imposed by the assumed geometry, the following considerations are perfectly general and include many possible dimensional effects, of which dimensional resonance is a specific type. Other dimensional effects occur under non-resonant conditions, the ordinary shielding effect of ohmic eddy currents in magnetic cores being a case in point. All such effects lead to apparent material constants which differ in magnitude from the actual constants, are functions of the sample dimensions, and, in general, show a frequency dependence which is superimposed upon any frequency dependence existing in the actual constants.

Figure 5 shows a block of material to which a magnetic field H may be applied by means of a coil whose plane is parallel to the section *aecf* or an electric field E by means of electrodes on the faces *abcd* and *efgh*. Because of the relative simplicity of the resulting expressions, we have assumed H and E to vary only in the z-direction; i.e., perpendicular to the applied fields. This assumption imposes restrictions on the dimensions of the block or toroidal core of which, in the magnetic case, it is a part; i.e., (1) the thickness, t, must be small compared to the width of the section (*ab*, in the case of the dielectric block and *ae* in the case of the magnetic core), (2) the width must be small compared to the diameter of the toroid, (3) all dimensions must be small compared to the wave-length in vacuum of the electromagnetic wave set up by the applied fields. We shall be concerned, then, with dimensional effects connected with the dimension t only. The mathematics is essentially that of the "infinite slab."

Referring to Fig. 5, we take $z=0$ to be the center of the block section for reasons of symmetry. For the

magnetic core, the boundary condition is that at both surfaces, *abhe* and *cdgf*, the magnetizing field reduces to what it would be at zero frequency, H_s. Similarly, for the dielectric block, the electric field at these same surfaces reduces to E_s, the value it would have at zero frequency. Under these conditions, the Maxwell equations lead to the following solutions when the time variations of the various quantities are taken to be sinusoidal.

$$H=H_s\frac{\cos jkz}{\cos jkt/2},\quad E=E_s\frac{\cos jkz}{\cos jkt/2}. \tag{1}$$

Here $k=j\omega\mu^{\frac{1}{2}}\epsilon^{\frac{1}{2}}/c$ and is the propagation constant of the electromagnetic wave in the core.

The impedance of the reactor, of which the magnetic core is a part, is found from the ratio of applied voltage to current, V_m/I_m where $V_m\sim\omega\int Hdz$ and $I_m\sim H_s$. Similarly, the admittance of the condenser formed by the dielectric block is found from the ratio I_d/V_d where $I_d\sim\omega\int Edz$ and $V_d\sim E_s$. When these operations are carried out, we have

Reactor impedance

$$Z_m=-(2c^2/\omega)K(k/\epsilon)\tan jkt/2, \tag{2}$$

Condenser admittance

$$Y_d=2Q\omega(\epsilon/k)\tan jkt/2.$$

Here $K=L/\mu t$ and $Q=C/\epsilon t$ where L is the ordinary low frequency inductance of the reactor and C is the ordinary low frequency capacity of the condenser. K depends only on the number of turns and dimensions of the reactor; Q only on the dimensions of the condenser. With L in henries, C in farads, and all other quantities in the c.g.s. system, Z_m is in ohms and Y_d in mhos.[5] For some calculations, it is convenient to replace ϵ/k in Eqs. (2) by $-c^2k/\omega^2\mu$.

The general expressions for Z_m and Y_d can now readily be derived from (2) by making the substitutions $\mu=\mu'-j\mu''$ and $\epsilon=\epsilon'-j\epsilon''$ where μ'' accounts for losses associated with the magnetization and ϵ'' for losses connected with currents flowing in the material. A detailed consideration of Maxwell's equations shows that ϵ'' may be separated into factors accounting for dielectric losses alone, ϵ_t'', and for ohmic losses alone; i.e.

$$\epsilon''=\epsilon_t''+4\pi\sigma c^2 10^{-9}/\omega, \tag{3}$$

where σ is in (ohm-cm)$^{-1}$. It is convenient to carry ϵ'' alone throughout the calculations. The true dielectric loss factor can then at any time be found by determining σ from d.c. measurements and substitution in (3).

[5] In terms of the dimensions of the reactor core and block, $K=4\pi n^2 w10^{-9}/l$ and $Q=w10^9/4\pi c^2 l$. Here w is the width of core or block section and l the mean flux path of the core or distance between electrodes of the block. When these expressions for K and Q are used, Z_m comes out in ohms and Y_d in mhos.

By inserting the complex values of μ and ϵ, we find $k=\alpha+j\beta$ where

$$\begin{aligned}\alpha&=(\omega/c\sqrt{2})\{(\mu'^2+\mu''^2)^{\frac{1}{2}}(\epsilon'^2+\epsilon''^2)^{\frac{1}{2}}-(\mu'\epsilon'-\mu''\epsilon'')\}^{\frac{1}{2}},\\ \beta&=(\omega/c\sqrt{2})\{(\mu'^2+\mu''^2)^{\frac{1}{2}}(\epsilon'^2+\epsilon''^2)^{\frac{1}{2}}+(\mu'\epsilon'-\mu''\epsilon'')\}^{\frac{1}{2}}.\end{aligned} \tag{4}$$

It should be remembered that in general there is, by virtue of (3), a frequency term under the radical in (4), even though all material constants are independent of frequency. Physically α is the extinction coefficient and ω/β gives the phase velocity of the electromagnetic wave in the material. These quantities appear in the ordinary wave equation thus,

$$E=E_0\{\exp-\alpha x\}\{\exp j\omega(\tau-\beta x/\omega)\}.$$

By taking the real and imaginary parts of (2) after inserting the complex values of μ and ϵ, the following expressions are obtained.

$$\begin{aligned}R_m&=\frac{2K\omega}{\alpha^2+\beta^2}\left\{\frac{B\sinh\alpha t-A\sin\beta t}{\cosh\alpha t+\cos\beta t}\right\},\\ X_m&=\frac{2K\omega}{\alpha^2+\beta^2}\left\{\frac{A\sinh\alpha t+B\sin\beta t}{\cosh\alpha t+\cos\beta t}\right\},\end{aligned} \tag{5}$$

$$r_d=\frac{\omega}{2c^2Q}(\mu'^2+\mu''^2)\left\{\frac{\cosh\alpha t+\cos\beta t}{B\sinh\alpha t+A\sin\beta t}\right\}, \tag{6}$$

$$x_d=\frac{\omega}{2c^2Q}(\mu'^2+\mu''^2)\left\{\frac{\cosh\alpha t+\cos\beta t}{A\sinh\alpha t-B\sin\beta t}\right\},$$

where

$$A=\mu'\alpha-\mu''\beta,\quad B=\mu'\beta+\mu''\alpha,\quad R_m+jX_m=Z_m$$

and

$$1/r_d+1/jx_d=Y_d.$$

These expressions are rigorous and automatically carry the proper sign so that if any reactance term turns out to be positive an inductive reactance is denoted and if negative, a condensive reactance. It should be noted that R_m and X_m are the equivalent series resistance and reactance of the reactor while r_d and x_d are the equivalent parallel resistance and reactance of the condenser. For some calculations it may be convenient to change the coefficients of the transcendental terms in (5) and (6) according to the following identities.

$$\frac{\omega^2}{c^2}\left(\frac{\mu'^2+\mu''^2}{B}\right)\equiv\frac{\alpha^2+\beta^2}{B'},\quad \frac{\omega^2}{c^2}\left(\frac{\mu'^2+\mu''^2}{A}\right)\equiv-\frac{\alpha^2+\beta^2}{A'},$$

where $A'=\epsilon'\alpha-\epsilon''\beta$ and $B'=\epsilon'\beta+\epsilon''\alpha$. Alternate expressions for the impedances may also be derived in terms of $\Re\tan jkt/2$ and $\Im\tan jkt/2$ explicitly. (See reference 8.)

Equations (5) and (6) contain many special cases of importance. For example, when ϵ', ϵ_t'', and μ'' are

neglected, Eqs. (5) reduce to those developed by K. L. Scott[6] for the case of a reactor with ohmic eddy currents alone. In this case α becomes equal to β and is the reciprocal of the ordinary penetration depth. Other special cases will be discussed in the section on effects at the Curie point.

Effective *vs.* Actual Material Constants

From the definitions of the various quantities involved, apparent or effective material constants can be determined. These play the roles of the actual constants for any particular reactor or condenser and any particular frequency under consideration but have no general interest. It is, however, convenient to use the effective values when discussing a particular experiment. In the absence of dimensional effects, the effective constants will be equal to the respective actual constants. The effective values can be obtained from the fundamental impedance and admittance equations,

$$Z_m = jK\omega t\mu_{\text{eff}} \quad \text{and} \quad Y_d = jQ\omega t\epsilon_{\text{eff}}$$

giving

$$\mu_{\text{eff}} = -jZ_m/K\omega t \quad \text{and} \quad \epsilon_{\text{eff}} = -jY_d/Q\omega t. \tag{7}$$

In general, these quantities are complex and their components can be determined directly from measured values of the impedances.

$$\begin{aligned} \mu_{\text{eff}}' &= X_m/K\omega t, \qquad \mu_{\text{eff}}'' = R_m/K\omega t, \\ \epsilon_{\text{eff}}' &= -1/x_dQ\omega t, \qquad \epsilon_{\text{eff}}'' = 1/r_dQ\omega t. \end{aligned} \tag{8}$$

By substituting (5) and (6) in (8), the effective constants can be calculated rigorously from the actual material constants.

Determination of the Actual Values of μ', μ'', ϵ' and ϵ'' from Measured Values of the Impedances

Although Eqs. (8) with X_m, R_m, x_d, r_d substituted from (5) and (6) can, in principle, be solved for rigorous explicit expressions for the actual material constants in terms of the effective constants, these expressions would be cumbersome and it is simpler to return to Eqs. (2) and proceed in a somewhat circuitous way. In the following outline it is assumed that the equivalent series reactance and resistance of the reactor and the equivalent parallel reactance and resistance of the condenser have been measured, i.e. X_m, R_m, x_d, r_d. The relative dimensions of the reactor core and dielectric block are immaterial except that the thickness, t, of the two must be the same and that the before-mentioned limiting conditions are met.

Multiplying Eqs. (2) together leads to the following rigorous expressions from which α and β can be calculated.

$$\begin{aligned} \tan\beta t &= -2\Phi D/\{D^2-(\Psi^2+\Phi^2)\}, \\ \sinh\alpha t &= 2\Psi D/[\{D^2-(\Psi^2+\Phi^2)\}^2+4\Phi^2D^2]^{\frac{1}{2}}, \end{aligned} \tag{9}$$

where

$$\begin{aligned} \Phi &= \mp(1/\sqrt{2})\{(p^2+q^2)^{\frac{1}{2}}-p\}^{\frac{1}{2}}; \\ \Psi &= (1/\sqrt{2})\{(p^2+q^2)^{\frac{1}{2}}+p\}^{\frac{1}{2}}; \end{aligned}$$

$p=R_m/r_d+X_m/x_d$; $q=X_m/r_d-R_m/x_d$; $D=2cK^{\frac{1}{2}}Q^{\frac{1}{2}}$; and Φ takes the sign opposite to q. Care must be taken to insert the values of X_m and x_d, in these expressions, with their proper signs. At a sufficiently low frequency, X_m will be positive and x_d negative. Care must also be taken that βt is chosen in the proper quadrant. In general, a series of measurements at various frequencies will be necessary to establish the proper course of βt. Having the values of αt and βt, the actual dielectric constants can be calculated as follows:

When Eqs. (6) are substituted in (8), the resulting expressions can be solved for ϵ' and ϵ'', giving

$$\begin{aligned} \epsilon' &= \epsilon_{\text{eff}}'U(V+\epsilon_{\text{eff}}''W/\epsilon_{\text{eff}}'), \\ \epsilon'' &= \epsilon_{\text{eff}}''U(V-\epsilon_{\text{eff}}'W/\epsilon_{\text{eff}}''), \end{aligned} \tag{10}$$

where

$$\begin{aligned} U &= (\cosh\alpha t+\cos\beta t)/2(\sinh^2\alpha t+\sin^2\beta t), \\ V &= \alpha t\sinh\alpha t+\beta t\sin\beta t, \\ W &= \beta t\sinh\alpha t-\alpha t\sin\beta t. \end{aligned}$$

In using Eqs. (10), αt and βt are obtained from (9) while ϵ_{eff}' and ϵ_{eff}'' are determined from measured quantities using (8). When the value of ϵ'' has been determined from (10), ϵ_i'' can be computed from (3) in which σ is known from d.c. measurements. The expressions for the actual permeabilities are the same as (10) except that, where they occur explicitly, the ϵ's are replaced by the corresponding μ's. For the calculation of either the ϵ's or the μ's, the factors U, V, W remain the same. (See discussion of Eq. (12) in the section Approximate Expressions. Also in this section, approximations are developed for Eqs. (10).)

Numerical Calculations of the Actual Core Constants

The actual material constants in c.g.s. units are given in Fig. 6, as calculated from the rigorous expressions, using impedance measurements on samples of the following dimensions:

Magnetic toroid: Section, 0.127×0.53 cm; mean flux path, 5.56 cm.
Dielectric block: Section, 0.127×2.5 cm; length, 7 cm.

In this case, the 0.127 cm thickness of the section was taken as determining the dimensional effects. At 10 mc, the maximum effect in any of the constants occurs in ϵ'', where $\epsilon''/\epsilon_{\text{eff}}''=0.69$. Above 10 mc, our measurements become unreliable because of the difficulty of estimating with sufficient accuracy the distributed capacity effects

[6] K. L. Scott, Proc. I.R.E. 18, 1750 (1930).

in the magnetic measurements. Below 10 mc we have been able to correct for such effects. While some corrections may still have to be applied because of geometrical limitations, we believe these will be small. It is evident that a considerable dispersion remains after removal of the dimensional effects, particularly in the magnetic constants. The dependence of the components of the propagation constant on frequency is given in Fig. 6B.

The results of calculating the effective constants for $t=1.25$ cm from the actual constants of Fig. 6, using the rigorous equations, are given in Figs. 1B and 2B. Here they are shown in comparison to experimental values on core and block sections 1.25×2.5 cm. We believe the discrepancies are due, in large part, to the failure of these experimental samples of relatively thick section to satisfy sufficiently well the geometrical limitations. As mentioned in the experimental section, on some samples of Ferroxcube III of these dimensions, we have observed negative values of both μ' and ϵ' in the vicinity of 2 mc. In none of these cases, however, are complete measurements available for the determination of the actual material constants. The values of the effective constants in the resonant region are rather sensitive to both the geometry of the core[7] and the actual material constants.

Calculations have also been made on the effect of an air gap in the magnetic core, using Eqs. (5). In making the calculations, the value of the permeability used was the actual value as reduced by the air gap. Reasonable agreement with experiment was obtained.

It should be emphasized that the major features of such curves as Figs. 1B and 2B are not necessarily determined by a dispersion of the actual core constants. Figures 7A and 7B show similar results, for example, when the actual core constants are taken to be independent of frequency.

Magnetic Flux Distribution

The magnetic flux distribution in the core of the reactor is found from (1) by multiplying by the permeability, $\mu'-j\mu''$. Two standing wave patterns result, differing in phase from each other by 90°. The real pattern, $\Re\mathbf{B}$, is associated with the reactance of the reactor and the imaginary pattern, $\Im\mathbf{B}$, with its effective resistance. The total flux, $\mathbf{B}_{tot}$ is the vector sum of the two patterns. Following are the expressions for the flux distributions.

$$\Re\mathbf{B}=H_s\frac{\mu'S+\mu''T}{\cosh\alpha t+\cos\beta t},\quad \Im\mathbf{B}=H_s\frac{\mu'T-\mu''S}{\cosh\alpha t+\cos\beta t},\quad (11)$$

[7] We have, for example, derived the equations for the effective constants for samples of circular cross section and find the resonance phenomena move to higher frequencies when the diameter of the circular section is the same as the thickness of the "infinite slab."

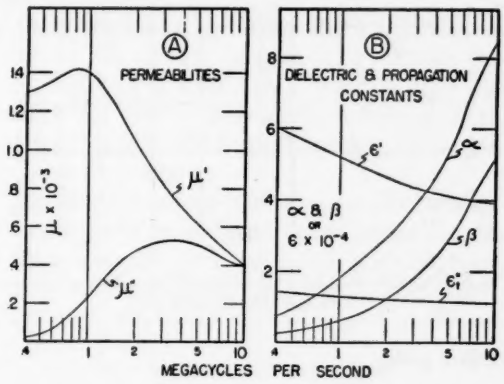

FIG. 6. Actual material constants for Ferroxcube III. A. Permeabilities. B. Dielectric constants. Propagation constants in cm^{-1} for an electromagnetic wave.

where

$$S=\cos\beta(z+t/2)\cosh\alpha(z-t/2)+\cos\beta(z-t/2)\cosh\alpha(z+t/2),$$
$$T=\sin\beta(z-t/2)\sinh\alpha(z+t/2)+\sin\beta(z+t/2)\sinh\alpha(z-t/2).$$

Figure 8 shows these distributions, calculated for the frequency where the reactance first becomes zero in Fig. 7A. Since at the surfaces, $\mathbf{B}=\mu H_s$ and μ'' has been taken to be zero, $\Im\mathbf{B}$ reduces to zero at the surfaces while $\Re\mathbf{B}$ reduces to $\mu' H_s$. The integral of $\Re\mathbf{B}$ across the core section accounts for the reactance of the coil and is zero as it should be for this particular case. It is noteworthy that the total flux density is actually higher within the core than at the surface. To speak of the penetration depth of the flux is obviously meaningless in this case. Similar considerations apply to the distribution of the electric intensity in the dielectric block.

Approximate Expressions

For purposes of approximation, Eqs. (2) can be substituted in (7) and $\tan jkt/2$ developed directly. This

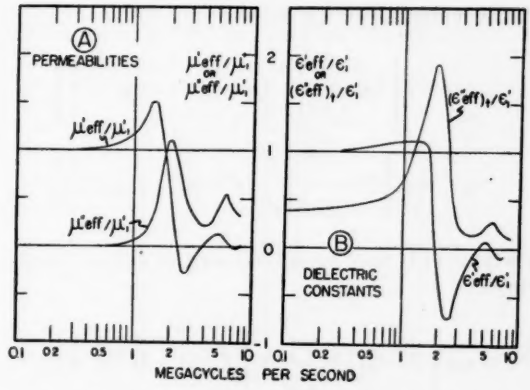

FIG. 7. Effective material constants calculated for sample thickness 1.25 cm assuming actual material constants independent of frequency. $\mu'=10^3$, $\mu''=0$, $\epsilon'=5\times10^4$, $\epsilon_i''=2\times10^4$, $\sigma=5\times10^{-3}$. A. Permeabilities. B. Dielectric constants.

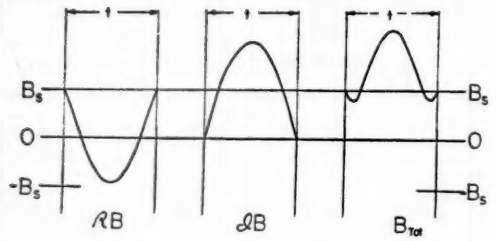

FIG. 8. Flux distribution in the core of Fig. 7A at a frequency where μ_{eff}' has its first zero.

procedure gives

$$\mu_{eff}=\mu\left[1-\left\{\frac{(kt)^2}{12}-\frac{(kt)^4}{120}+\cdots\right\}\right],$$
$$\epsilon_{eff}=\epsilon\left[1-\left\{\frac{(kt)^2}{12}-\frac{(kt)^4}{120}+\cdots\right\}\right]. \tag{12}$$

These equations show clearly the symmetry between expressions for μ_{eff} and ϵ_{eff}. For example, expressions for μ_{eff}' and μ_{eff}'' are obtained from the expressions for ϵ_{eff}' and ϵ_{eff}'' when the ϵ's are replaced, where they occur explicitly, by the corresponding μ's. In the following, then, we shall write only expressions for the ϵ's.

When the complex value for ϵ is inserted in (12) and only the terms of second degree in αt and βt are retained, the effective constants are given by

$$\epsilon_{eff}'=\epsilon'\left[(1-M)-\frac{\epsilon''}{\epsilon'}N\right],$$
$$\epsilon_{eff}''=\epsilon''\left[(1-M)+\frac{\epsilon'}{\epsilon''}N\right], \tag{13}$$

where

$$M=\frac{(\alpha^2-\beta^2)t^2}{12} \quad \text{and} \quad N=\frac{\alpha\beta t^2}{6}.$$

When α and β are substituted in (13) in terms of the actual constants, we have

$$\epsilon_{eff}'=\epsilon'\left[1+\frac{\omega^2t^2}{12c^2}\left\{\frac{\mu'}{\epsilon'}(\epsilon'^2-\epsilon''^2)-2\mu''\epsilon''\right\}\right],$$
$$\epsilon_{eff}''=\epsilon''\left[1+\frac{\omega^2t^2}{12c^2}\left\{\frac{\mu''}{\epsilon''}(\epsilon'^2-\epsilon''^2)+2\mu'\epsilon'\right\}\right]. \tag{14}$$

Equations (13) may be solved for the actual constants, giving

$$\epsilon'=\epsilon_{eff}'\left[(1-M)+\frac{\epsilon_{eff}''}{\epsilon_{eff}'}N\right]\Big/[(1-M)^2+N^2],$$
$$\epsilon''=\epsilon_{eff}''\left[(1-M)-\frac{\epsilon_{eff}'}{\epsilon_{eff}''}N\right]\Big/[(1-M)^2+N^2]. \tag{15}$$

These last equations have the same form as the rigorous Eqs. (10). The approximate expressions for the factors $U\cdot V$ and $U\cdot W$, appearing in (10), can thus be determined from (15) by inspection.

In using these approximations, care must be taken to see that the approximation is warranted. When the actual material constants are complex, the degree of approximation is not a function of $|kt|$ alone as might be inferred from a casual inspection of (12). Actually in arriving at (13), (14), and (15) it is $\tan jkt/2$ which is being approximated. Retaining second degree terms in αt and βt in (12) is equivalent to retaining third degree terms in αt and βt in the development of $\tan jkt/2$. This latter is a very good approximation. For example, so long as αt and βt are each no greater than unity, the error in neither component of $\tan jkt/2$ can be more than about 5 percent. If αt and βt are each no greater than 0.8, the error can be no more than about 1.5 percent. These errors may, however, be greatly magnified in computing the effective material constants. This is because one or the other of the effective constants can always be written rigorously as the difference between two terms; i.e., as $P\cdot\Re\tan jkt/2-Q\cdot\Im\tan jkt/2$, where P and Q are functions of αt, βt and the actual material constants appearing explicitly.[8] When approximate expressions for $\tan jkt/2$ are used, the resulting percentage error in this effective constant is influenced by the ratio of the two terms; i.e., by

$$\chi=(\mu''\beta-\mu'\alpha)\sinh\alpha t/(\mu'\beta+\mu''\alpha)\sin\beta t.$$

As χ approaches unity, the merit of the approximation for the effective constants becomes poorer and the approximation is good only for very small values of αt and βt. Conversely, the merit becomes better when χ approaches zero and the approximation for the effective constants then approaches that for $\tan jkt/2$ itself. Similar considerations apply to the merit of the approximation for the actual constants in Eq. (15). The ratio, χ, is the same as before except that the effective constants replace the actual constants where they occur explicitly.

It should be emphasized further that the presence or absence of dimensional effects does not, as might be inferred from (12), depend on $|kt|$ alone. This is shown by Eqs. (13) where, because of the factor ϵ''/ϵ' or ϵ'/ϵ'', one or the other of the effective constants may differ greatly from the corresponding actual constant, even though αt and βt are each small compared to unity. Under these conditions, the dimensional effects will be important in ϵ_{eff}' if $\epsilon''\gg\epsilon'$ and in ϵ_{eff}'' if $\epsilon''\ll\epsilon'$.

[8] When the effective constants are expressed in this way as functions of $\Re\tan jkt/2$ and $\Im\tan jkt/2$, they may be calculated from tables of these quantities instead of using tables of hyperbolic and circular functions as when working with expressions derivable from (5) and (6). (See Kennelly, *Tables of Complex Hyperbolic and Circular Functions* (Harvard University Press, Cambridge, 1914).) The tables of the tangent of a complex variable can also be used in estimating the errors introduced by approximations of $\tan jkt/2$.

Effects at the Magnetic Curie Point

When the material is carried through the magnetic Curie point, the effective dielectric constant, measured at 10^4 c.p.s. on relatively thick blocks, shows the rather interesting behavior described in the experimental section. Significant dimensional effects are present, even at these relatively low frequencies where there can be no question of dimensional resonance. Some sort of discontinuity is naturally to be expected at the Curie point because of the collapse of the permeability. The rather rapid decline of the effective dielectric constant with increasing temperature below the Curie point, however, has no primary connection with the permeability. It arises, instead, from the fact that the conductivity of Ferroxcube III increases rapidly with temperature.

Calculations from the data of Table II show that the maximum dimensional effects are to be expected just below the Curie point (155°C), where ϵ''/ϵ', αt and βt have relatively large values; i.e. $\alpha t \cong \beta t \cong 0.15$ for a block 1.25 cm thick and $\epsilon''/\epsilon' \cong 150$. Under these conditions the approximations retaining only the second degree terms in αt and βt can be used safely. The second degree terms, however, lead to large dimensional effects, Since $\mu'' \cong 0$ and $\epsilon_t'' \ll \epsilon''$, further approximation in (14). which retains the second degree terms, is warranted and we may write:

$$\epsilon_{eff}' = \epsilon' \left\{ 1 - \frac{4}{3}\pi^2 \frac{\mu'}{\epsilon'} t^2 \sigma^2 c^2 \cdot 10^{-18} \right\}, \tag{16}$$

$$\epsilon_{eff}'' = \epsilon'' = 4\pi\sigma c^2 \cdot 10^{-9}. \tag{17}$$

Equation (17) shows at once that no appreciable discontinuity in ϵ''_{eff} is to be expected at the Curie point. On the other hand, Eq. (16) shows a marked effect of the permeability depending upon the magnitude of $(t\sigma)^2/\epsilon'$.

Just below the Curie point, the difference between ϵ_{eff}' and ϵ' is large and is influenced by the square of the conductivity. Since the latter is a rapid function of the temperature, ϵ_{eff}' becomes very sensitive to temperature changes. In fact it is not difficult to cause ϵ_{eff}' to become negative just below the Curie point, as shown in Fig. 4.

At the Curie point, ϵ_{eff}' will suffer a near discontinuity owing to the sudden collapse of μ'. Above the Curie point, since μ' is now small, there is little difference between ϵ_{eff}' and ϵ' and further changes in the conductivity caused by further increase in temperature will have little effect.[9]

Like all dimensional effects, these phenomena at the Curie point can be made negligible by making measurements on a sample sufficiently thin. ϵ_{eff}' then approaches ϵ' in value throughout the entire temperature range. Otherwise ϵ' can be determined from Eq. (16) as

$$\epsilon' = \epsilon_{eff}' + (4/3)\pi^2 \mu' t^2 \sigma^2 c^2 \cdot 10^{-18}. \tag{18}$$

ϵ' as computed from (18) using the data of curve 2, Fig. 4, is shown as curve 3, Fig. 4. Equation (18) does not give as satisfactory a correction for curve 1 of Fig. 4, not because the approximation is invalid but because the geometrical limitations of our theory are not met as well by the thicker block.

IV. ACKNOWLEDGMENTS

We wish to extend our thanks to Dr. O. S. Duffendack and Dr. F. K. du Pré of this Laboratory, to Dr. H. M. Blewett of the Brookhaven Laboratory, and to Professor G. E. Uhlenbeck for their advice and criticism.

[9] Low frequency dimensional effects in the dielectric block can also be discussed in terms of an equivalent circuit for the block. In the case of our Curie point experiment, this circuit consists of two parallel impedances. One is that of the block considered as a lossless condenser (permeability taken as unity); the other is that of the block considered as a lossless inductor (dielectric constant taken as unity) in series with a resistance (the d.c. resistance of the block). The impedance of the inductive branch can be calculated from $1/Y_d = (2Q\omega)^{-1} k\epsilon^{-1} \cot jkt/2$. When this is developed in the same way as we developed Z_m and Y_d and we put $\epsilon' = 1$, $\epsilon_t'' = \mu'' = 0$, the inductance comes out to be $\mu'/12c^2Q$ henries to the same degree of approximation used in Eqs. (14). Here we have neglected the inductance arising from the field external to the block. Now, when the equivalent circuit is converted to a reactance shunted by a resistance, as it is measured, Eqs. (16) and (17) result. In the conversion, the further approximation is made that in the inductive branch of the equivalent circuit, the resistance is large compared to the reactance. An explanation of the Curie point phenomena in essentially this manner, was given independently by C. G. Koops of the Philips Laboratory, Eindhoven, in a private communication to the authors.

The Influence of Nuclear Structure on the Hyperfine Structure of Heavy Elements

AAGE BOHR
*Department of Physics, Columbia University, New York, New York**

AND

V. F. WEISSKOPF
Department of Physics and Laboratory for Nuclear Science and Engineering, Massachusetts Institute of Technology, Cambridge, Massachusetts

(Received September 27, 1949)

The influence on the h.f.s. of the finite size of the nucleus is considered and the effect is calculated for simple models of the nuclear magnetism. It is pointed out that the distribution of magnetic dipole density over the nuclear volume may vary greatly from nucleus to nucleus depending on the relative contributions of spin and orbital magnetic moments to the total nuclear moment. On this basis an attempt is made to interpret the observed discrepancy between the h.f.s. ratio of the Rb isotopes and the ratio of the magnetic moments as determined by the magnetic resonance method. A study of such anomalies may give some information regarding the structure of nuclear moments, in particular, regarding the nuclear g_L-factor.

I. INTRODUCTION

A RECENT accurate determination[1] of the nuclear moments of the Rb isotopes by the magnetic resonance method has indicated that the ratio of the h.f.s. splittings in Rb^{85} and Rb^{87}, measured previously with great precision,[2] does not agree exactly with the value calculated from the ratio of the moments, if the nuclei are considered as point dipoles. The h.f.s. ratio is found to be larger by 0.33 percent, while the experimental uncertainty involved in the comparison is judged to be about 0.05 percent.

It has been pointed out by Bitter[3] that anomalies of this order may be expected if the nuclear magnetic moments are represented by some distribution of magnetism over the nuclear volume rather than by a point dipole. Since effects of this type might offer information regarding the structure of nuclear moments, we shall attempt a somewhat more detailed analysis of the problem.

II. QUALITATIVE CONSIDERATIONS

In the non-relativistic approximation, the h.f.s. of an s-state is proportional to the average electron density at the location of the nuclear magnetic moment. It is here assumed that the moment distribution is spherically symmetric, but even large angular asymmetries have only a minor effect. At a small distance R from a central charge Ze, the electron density is proportional to $1-2ZR/a_0$ where a_0 is the radius of the hydrogen atom. Inside the nucleus itself, however, the wave function decreases somewhat more slowly with distance. Thus, in a nucleus of uniform charge distribution, the electron density varies approximately as $1-ZR^2/a_0R_0$, where R_0 is the nuclear radius.

In a model in which the nuclear magnetic moment is considered as a smeared-out dipole distribution, the h.f.s. would thus be expected to differ from the value calculated for a point dipole at the nuclear center by a factor $1+\epsilon$, where

$$\epsilon \approx -(ZR_0/a_0)(R^2/R_0^2)_{Av}. \quad (1)$$

For heavy atoms, relativity becomes of importance and its main effect in the present connection is to increase the absolute magnitude of the electron density at the nucleus by a factor of about $(a_0/2ZR_0)^{2(1-\rho)}$, where $\rho=(1-Z^2\alpha^2)^{\frac{1}{2}}$ and α is the fine structure constant. The total h.f.s. is increased in corresponding measure and, thus,

$$\epsilon \approx -(ZR_0/a_0)(a_0/2ZR_0)^{2(1-\rho)}(R^2/R_0^2)_{Av}. \quad (2)$$

The assumption of a uniform distribution of the nuclear charge restricts our considerations to nuclei containing a large number of protons. For the lightest elements the dependence of the electronic wave function on the position of the individual protons must be taken into account.[4]

If the magnetic moment is uniformly distributed over the nucleus, we have $(R^2/R_0^2)_{Av}=\frac{3}{5}$ and, by putting $R_0=1.5\times10^{-13}$ cm $A^{\frac{1}{3}}$, values for ϵ are obtained which for light elements are of the order of 0.01 of a percent and which become quite appreciable, of the order of several percent, for the heaviest elements.

For $p, d\cdots$ states the h.f.s. anomaly is negligible in the non-relativistic approximation, in which the corresponding wave functions vanish at the center. In heavy elements, however, due to relativity effects, the value of ϵ may become appreciable for $p_{\frac{1}{2}}$-states. For these states the small components have the character of s-wave functions and determine the density at the center. The value of ϵ will therefore be of the order of

* On leave from Institute for Theoretical Physics, Copenhagen, Denmark.

[1] F. Bitter, Phys. Rev. 75, 1326 (1949).

[2] S. Millmann and P. Kusch, Phys. Rev. 58, 438 (1940).

[3] F. Bitter, Phys. Rev. 76, 150 (1949); see also H. Kopfermann, *Kernmomente* (Akademische Verlagsgesellschaft, Leipzig, 1940), p. 17.

[4] A. Bohr. Phys. Rev. 73, 1109 (1948).

$Z^2\alpha^2$ of that for an $S_{\frac{1}{2}}$-state. For an electron of higher total angular momentum than $\frac{1}{2}\hbar$, the influence on the h.f.s. of the finite size of the nucleus may be disregarded.

In the particular case of Rb, one obtains from (2) a value for ϵ of about 0.4 percent. Whereas effects of this magnitude are thus to be expected in the h.f.s. of each isotope, it might at first appear surprising that the ratio of the h.f.s. shows an anomaly of the same order. In fact, it becomes necessary to assume an essentially different distribution of magnetism in the two nuclei.

It appears that a natural explanation of such variations is possible if one considers the nuclear magnetic moment as composed of two intrinsically different parts, a spin moment and an orbital moment. In fact, the latter part, originating from currents in the nucleus, will in general be equivalent to a magnetic dipole distribution which increases toward the center, and should therefore produce smaller anomalies in the h.f.s. than the former, the spin part. For example, a rotating charged sphere is equivalent to a magnetization increasing toward the center and would give rise to a value of ϵ only about half that corresponding to a sphere of uniform magnetization. Depending on the proportion of spin magnetic moment and orbital magnetic moment in the nucleus, considerable variations in the h.f.s. anomalies may thus occur. Indeed, a nucleus in which the spin moment is directed oppositely to that of the total nuclear magnetic moment might even have a larger h.f.s. than that corresponding to a point dipole.

In the case of Rb, the values of the angular momenta and the magnetic moments actually indicate a very different alignment of spin and orbital momentum in the two isotopes, and therefore an essentially different distribution of magnetism. Indeed, while the magnetic moment of Rb^{87} ($I=\frac{3}{2}$, $\mu=2.75$) appears primarily due to the spin moment of the odd proton, the moment of Rb^{85} ($I=5/2$, $\mu=1.35$) would seem to be largely of orbital type with only a small, and perhaps even negative, spin contribution. On the basis of such considerations, it thus appears possible to understand the comparatively large decrease in the h.f.s. of Rb^{87} relative to that of Rb^{85}.

It is of interest that no effect of comparable magnitude has been found in the cases of Ga[5] or Tl[6] where the two isotopes have the same spins and comparable moments and, therefore, presumably, similar distributions of magnetism.

III. H.F.S. DUE TO SPIN MAGNETIC MOMENT

In the more quantitative considerations, we shall treat separately the cases of spin and orbital moment. In the former case we represent the nucleus by a distribution of magnetic moment, given by a density function $w(\mathbf{R})$, and having the direction of the spin angular momentum $\mathbf{s}$. Denoting the spin g-factor by g_s, the vector potential produced by the nucleus may be written

$$\mathbf{A}_s(\mathbf{r})=-\int d\tau_R w(\mathbf{R}) g_s \left(\mathbf{s}\times\nabla_r \frac{1}{|\mathbf{r}-\mathbf{R}|}\right), \quad (3)$$

where

$$\int d\tau_R w(\mathbf{R})=1.$$

The magnetic interaction of the nucleus with an atomic electron is given by $e\boldsymbol{\alpha}\mathbf{A}(\mathbf{r})$ and, considering the interval rules, it is necessary only to evaluate the diagonal matrix element of this operator for the state in which the electronic, as well as the nuclear, angular momentum has its maximum component in the z direction. Denoting the electron part of the wave function by ψ, one finds that,

$$W\equiv\int d\tau_r \psi^* e\boldsymbol{\alpha}\mathbf{A}(\mathbf{r})\psi$$
$$=\pm 2e\int d\tau_r F(r)G(r)\frac{1}{r}(\mathbf{A}\times\mathbf{r}_s), \quad (4)$$

where F and G represent the two radial wave functions. The upper and lower sign refer to $s_{\frac{1}{2}}$ and $p_{\frac{1}{2}}$ states, respectively.

Introducing (3) into (4), it is convenient to write

$$W_s=\pm\frac{16\pi}{3}eg_s\int d\tau_R w(\mathbf{R})q_s. \quad (5)$$

If the distribution $w(\mathbf{R})$ is spherically symmetric, q_s takes the simple form

$$q_s=s_z\int_R^\infty FGdr. \quad (6)$$

In the case of angular asymmetries, one must add to (6)

$$\left\{\tfrac{1}{2}s_x\frac{3XZ}{R^2}+\tfrac{1}{2}s_y\frac{3YZ}{R^2}+\tfrac{1}{2}s_z\frac{3Z^2-R^2}{R^2}\right\}\int_0^R\frac{r^3}{R^3}FGdr, \quad (7)$$

but since the effect of such asymmetries for not too extreme models is of only minor influence, we shall in the following use the simple expression (6) for q_s.

Defining

$$\kappa_s\equiv\int_0^R FGdr/\int_0^\infty FGdr, \quad (8)$$

it follows that W_s is decreased by the relative amount $(\kappa_s)_{Av}$, as a consequence of the deviation of the nuclear magnetization from a point dipole.

IV. H.F.S. DUE TO ORBITAL MOMENT

It may first be noted that the magnetic field of a current density distribution $\mathbf{i}$, for which $\operatorname{div}\mathbf{i}=0$, is

[5] R. B. Pound, Phys. Rev. **73**, 1112 (1948).
[6] H. Poss, Phys. Rev. **75**, 600 (1949).

TABLE I. Values of b for $s_{\frac{1}{2}}$- and $p_{\frac{1}{2}}$-states.

Z	$b(s_{\frac{1}{2}})$	$b(p_{\frac{1}{2}})$
10	0.08 percent	
20	0.20	
30	0.38	0.02 percent
40	0.68	0.05
50	1.12	0.13
60	1.71	0.29
70	2.52	0.60
80	3.58	1.16
90	4.80	2.11

equivalent to that produced by a magnetic dipole density $\mathfrak{y}$ given by $\mathbf{i}=-c\,\mathrm{rot}\mathfrak{y}$, and thus the problem of an orbital moment is reducible to that considered in the preceding paragraph.

Still, in many cases, it is more convenient to consider directly the interaction of a moving nuclear particle with the atomic electron. Denoting by Ze and M the charge and mass of the particle, and its wave function by $\varphi(\mathbf{R})$, we may use the expression

$$\mathbf{A}_L(\mathbf{r})=\frac{Ze}{Mc}\int d\tau_R\varphi^*(\mathbf{R})\frac{1}{|\mathbf{r}-\mathbf{R}|}\mathbf{P}\varphi(\mathbf{R}) \tag{9}$$

and, introducing in (4) one finds that W_L can be expressed in the form

$$W_L=\pm\frac{16\pi}{3}eg_L\int d\tau_R w(\mathbf{R})q_L, \tag{10}$$

where $w(\mathbf{R})=|\varphi(\mathbf{R})|^2$ and $g_L=Ze/2Mc$. Furthermore,

$$q_L=L_Z\left\{\int_R^\infty FGdr+\int_0^R\frac{r^3}{R^3}FGdr\right\}, \tag{11}$$

where $\mathbf{L}$ is the orbital angular momentum of the particle. Thus, if

$$\kappa_L\equiv\int_0^R\left(1-\frac{r^3}{R^3}\right)FGdr/\int_0^\infty FGdr, \tag{12}$$

the contribution to the h.f.s. of the orbital angular momentum is decreased by a relative amount $(\kappa_L)_W$.

V. EVALUATION OF ELECTRONIC WAVE FUNCTIONS

In order to calculate κ_s and κ_L, it is necessary to evaluate the electronic wave functions in the interior of the nucleus, in which region they deviate significantly from the wave functions corresponding to a point nucleus. Representing the nucleus by a homogeneously charged sphere of radius R_0, the potential in this region is given by

$$V=(\tfrac{3}{2}-\tfrac{1}{2}x^2)Ze/R_0\quad x\equiv r/R_0<1. \tag{13}$$

Solving the radial wave equations by an expansion in powers of x, one finds, for an $s_{\frac{1}{2}}$-state

$$G=k\left(1-\frac{3}{8}\gamma^2x^2+\frac{1}{10}\gamma^2x^4+\cdots\right)\quad\gamma\equiv Ze^2/\hbar c$$
$$F=\tfrac{1}{2}k\gamma x\left(1-\left(\frac{1}{5}+\frac{9}{40}\gamma^2\right)x^2+\frac{1}{10}\gamma^2x^4+\cdots\right) \tag{14}$$

and, for a $p_{\frac{1}{2}}$-state

$$F=k\left(1-\frac{3}{8}\gamma^2x^2+\frac{1}{10}\gamma^2x^4+\cdots\right)$$
$$G=-\tfrac{1}{2}k\gamma x\left(1+\frac{4}{3}\frac{R_0mc}{\gamma\hbar}-\left(\frac{1}{5}+\frac{9}{40}\gamma^2\right)x^2+\frac{1}{10}\gamma^2x^4+\cdots\right), \tag{15}$$

where k is a constant depending on the normalization of the entire wave function. These approximate expressions have an accuracy of about one percent, even for Z-values corresponding to the heaviest elements.

The integrals in the numerators of (8) and (12) may now be expressed in terms of powers of R. The main term is proportional to R^2 and since the higher terms never amount to more than ten percent of the leading term, one may conveniently replace these terms by appropriate multiples of R^2. If values are chosen intermediate between those corresponding to a uniform distribution $w(\mathbf{R})$ and those corresponding to a surface distribution, the error involved will, for the most plausible models, only amount to a few percent. In this manner, one obtains

$$\int_0^R FGdr=0.23k^2R_0\gamma(1-0.2\gamma^2)\times\frac{R^2}{R_0^2}\left[(-1)\left(1+1.44\frac{R_0mc}{\gamma\hbar}\right)\right] \tag{16}$$
$$\int_0^R FG\left(1-\frac{r^3}{R^3}\right)dr=0.62\int_0^R FGdr,$$

where the factor in square brackets is to be included for $p_{\frac{1}{2}}$-states only.

Outside the nucleus the electron moves in a Coulomb field screened at larger distances by the other atomic electrons. However, we need consider only the unscreened part of the field, since the h.f.s. interaction takes place primarily in this central part of the atom.

The integral in the denominators of (8) and (12) may thus be expressed in terms of the well-known solutions to the wave equation for an unscreened Coulomb field, normalized relatively to the wave functions in the interior of the nucleus by the boundary conditions at

the nuclear surface.[7] One finds approximately

$$\int_0^\infty FG dr = \tfrac{1}{4}k^2 \frac{\hbar}{mc}\left(\frac{2R_0Z}{a_0}\right)^{2(1-\rho)} \frac{3}{\rho(4\rho^2-1)}\{(2\rho-1)!\}^2 \times \begin{cases} (1-\frac{1}{2}\gamma^2)^2 & (s_{\frac{1}{2}}) \\ (-1)\dfrac{4}{3\gamma^2}(1-0.72\gamma^2)^2 & (p_{\frac{1}{2}}) \end{cases} \quad (17)$$

where $\rho=(1-\gamma^2)^{\frac{1}{2}}$. The use of the wave functions for an unscreened field in the evaluation of (17) is always well justified for s-states, and is also valid for $p_{\frac{1}{2}}$-states in heavy atoms.

It follows that the values of κ_s and κ_L are independent of k and, consequently, of the particular $s_{\frac{1}{2}}$- or $p_{\frac{1}{2}}$-state under consideration. One may conveniently write

$$\kappa_s = bR^2/R_0^2 \qquad \kappa_L = 0.62bR^2/R_0^2, \quad (18)$$

where the coefficients b depend only on Z and R_0. For $R_0=1.5\times10^{-13}$ cm$\times A^{\frac{1}{3}}$, the values of b for $s_{\frac{1}{2}}$- and $p_{\frac{1}{2}}$-states are given in Table I.

VI. COMBINED EFFECT OF SPIN AND ORBITAL MOMENT

If the total nuclear magnetic moment is composed of a spin part and an orbital part, the relative change in the total h.f.s. splitting may be written

$$\epsilon = -(\kappa_s)_{Av}\alpha_s - (\kappa_L)_{Av}\alpha_L, \quad (19)$$

where α_s and α_L represent the fractions of the nuclear moment due to spin moment and orbital moment, respectively. These quantities may be expressed in terms of the g-factors:

$$\alpha_s = \frac{g_s}{g_I}\frac{g_I-g_L}{g_s-g_L} \qquad \alpha_L = 1-\alpha_s, \quad (20)$$

where g_I is the total nuclear g-factor.

The experiments determine most easily the difference of the ϵ-values for two isotopes. Of course, the values of $(\kappa_s)_{Av}$ and $(\kappa_L)_{Av}$ may vary somewhat from isotope to isotope, but, it appears that larger effects may be expected due to differences in α_s and α_L. If we neglect the fluctuations in $(\kappa_s)_{Av}$ and $(\kappa_L)_{Av}$ and if, moreover, the values of g_s and g_L are the same for the two isotopes, as seems a plausible assumption for isotopes differing by an even number of neutrons, one obtains the expression:

$$\Delta \equiv \epsilon(1)-\epsilon(2) = ((\kappa_s)_{Av}-(\kappa_L)_{Av})\frac{g_sg_L}{g_s-g_L}\left(\frac{1}{g_I(1)}-\frac{1}{g_I(2)}\right) \quad (21)$$

for the influence of the finite size of the nucleus on the h.f.s. ratio of isotopes 1 and 2.

[7] See G. Racah, Nuovo Cimento 8, 178 (1931); also J. E. Rosenthal and G. Breit, Phys. Rev. 41, 459 (1932).

It is, of course, difficult to estimate the mean values of $(R/R_0)^2$ entering into the expressions for $(\kappa_s)_{Av}$ and $(\kappa_L)_{Av}$. It may be noted that for a uniform distribution over the sphere, the mean value equals $\frac{3}{5}$, but one might well imagine a tendency of the unpaired particles which contribute to the nuclear moment to stay near the surface, in which case the mean value would be somewhat larger. Since, however, it cannot exceed unity, one may tentatively assume a value for $(R^2/R_0^2)_{Av}$ of about $\frac{4}{5}$. On this assumption one obtains, from (18) and (21),

$$\Delta \approx 0.3b\frac{g_sg_L}{g_s-g_L}\left(\frac{1}{g_I(1)}-\frac{1}{g_I(2)}\right), \quad (22)$$

but it need not be emphasized that the approximation may be rather crude.

VII. DISCUSSION AND COMPARISON WITH EXPERIMENTAL DATA

The expression (22) for Δ involves the spin and orbital g-factors, the values of which must be expected to depend on the type of nuclei. The large majority of nuclei having angular momenta contain an odd number of nucleons. In this case it is most often assumed that the spin g-factor equals that of the odd particle, i.e., $g_s=g$ (proton) for Z odd and $g_s=g$ (neutron) for Z even. The choice of g_L, however, is more uncertain and we shall consider two possible assumptions regarding the origin of the orbital momentum.

On the one hand, we may assume with Margenau and Wigner[8] that the nuclear matter as a whole is involved in the orbital momentum. This leads in a plausible manner to $g_L=Z/A$, in units of $e/2Mc$, M being the nucleon mass.

On the other hand, Schmidt[9] has tried to account for nuclear moments by ascribing the orbital momentum to the motion of the odd particle in the nucleus. This leads to $g_L=1$ for Z odd and $g_L=0$ for Z even. It may be added that these g-values do not necessarily imply a single particle model of the nuclear moment. Any model in which, for Z odd, only protons, and for Z even, only neutrons, contribute to the orbital momentum leads to the same g-values and is therefore equivalent for our purpose.

The two assumptions regarding g_L lead to appreciably different values for Δ, and the phenomenon in question might thus offer some evidence regarding the nature of the orbital momentum.

The value of Δ has as yet been measured only for the Rb isotopes ($Z=37$, $A=85$ and 87), for which has been found $\Delta=0.33\pm0.05$ percent for the ground state, which is an $s_{\frac{1}{2}}$ term. Expression (22) gives $\Delta=0.11$ percent for $g_L=Z/A=0.43$ and $\Delta=0.29$ percent for $g_L=1$. The

[8] H. Margenau and E. Wigner, Phys. Rev. 58, 103 (1940).
[9] Th. Schmidt, Zeits. f. Physik 106, 358 (1937).

latter value is in good agreement with the empirical value while the estimate for $g_L=Z/A$ is too small by a factor three. Although the approximations involved in this estimate are somewhat crude, it seems difficult to obtain a sufficiently large value of Δ for $g_L=Z/A$, even under rather extreme assumptions regarding the values of $(\kappa_s)_{Av}$ and $(\kappa_L)_{Av}$ in the two isotopes.

In this connection it may be mentioned that the Schmidt model is also favored by other evidence regarding nuclear magnetic moments. In fact, as is well known, the g_I-values of all odd nuclei fall within the limits given by the Schmidt model, whereas the g_I-values of a number of nuclei with high spin fall outside the limits predicted by the model in which $g_L=Z/A$. Moreover, reference may be made to the recent successes achieved by the individual particle model of nuclear structure in accounting for the angular momenta of nuclei.

Measurements of the h.f.s. anomalies in other elements would be desirable. There exist a number of odd elements (e.g., Sb, Eu, Ir) having isotopes with widely different g_I-values and for which the value of Δ according to (22) should be appreciable. In the case of even elements with isotopes of odd atomic number (22) gives a vanishing Δ for the Schmidt model, whereas for $g_L=Z/A$, values of Δ of more than one percent would be expected in several cases (e.g., Yb and Hg).

A number of elements (e.g., Na and K) have isotopes of odd numbers of protons and neutrons whose spin and h.f.s. have been measured. These nuclei are of special interest for the problem of nuclear structure, and a study of their h.f.s. anomalies might give some indication regarding the composition of their moments.

This work was assisted by the Ernest Kempton Adams Fund for Physical Research of Columbia University and by the Joint Program of the ONR and AEC.

PHYSICAL REVIEW VOLUME 77, NUMBER 1 JANUARY 1, 1950

On the $\alpha-\beta$- and $\alpha-K$-Branching of the Heaviest Natural and Artificial Radioactive Substances*

W. JENTSCHKE

(Received June 24, 1949)

Based on simple empirical regularities in α-decay properties of the heavy elements, the following substances which show β-emission or K-capture should also be α-radioactive with $\alpha-\beta$- or $\alpha-K$-branching ratios of at least 10^{-10}: $MsTh_2$, $MsTh_1$, AcK; $_{88}Ra^{225}$, $_{91}Pa^{233}$, $_{93}Np^{234}$, $_{93}Np^{235}$, $_{93}Np^{236}$, $_{93}Np^{238}$, $_{93}Np^{239}$, $_{94}Pu^{241}$, $_{95}Am^{242}$.

I. INTRODUCTION

IN addition to the long known dual disintegration of the C-bodies of the three natural radioactive disintegration series, the existence of a number of other double disintegrations has been established. M. Perey[1] succeeded in proving that actinium emits a weak α-radiation. This disintegration creates element 87 (francium). B. Karlik's and T. Bernert's[2] proof of the dual disintegration of RaA made it possible to establish the occurrence in the natural disintegration series of element 85 (astasium) through the isotope $_{85}At^{218}$.** Prior to this, element 85 has already been artificially obtained and chemically investigated through reaction $_{83}Bi^{209}(\alpha,2n)_{85}At^{211}$ by D. R. Corson, K. R. McKenzie, and E. Segre.[3] This element shows $\alpha-K$-branching. In the newly established $4n+1$-series $_{83}Bi^{213}$ suffers an $\alpha-\beta$-decay.[4]

II. EMPIRICAL REGULARITIES OF THE α-DISINTEGRATION OF THE HEAVIEST NUCLEI

In the range of α-instability of the heaviest nuclei all elements emitting β-rays or showing K-capture must also be α-radioactive. Based on simple empirical regularities, therefore, branching ratios for some of these radioactive elements which have not as yet been measured are stated below. However, only dual disintegrations with branching-ratios of 10^{-10} or higher will be mentioned.

If the disintegration energies of the natural α-radioactive elements are plotted in a diagram as function of their mass numbers[5] (Fig. 1), a family of curves is formed by lines connecting nuclei of the same atomic

* This paper was written in August, 1947.

[1] M. Perey, J. de phys. et rad. **10**, 435 (1939). M. Perey and Lecoin, J. de phys. et rad. **10**, 439 (1939).

[2] B. Karlik and T. Bernert, Zeits. f. Physik **123**, 51 (1944).

** In the case of ThA and AcA, also, long range α-particles had been observed.[2] The simplest explanation would be a dual decay of ThA and AcA. But applying energy-conservation rules it follows that there exist considerable difficulties in accepting this interpretation.

[3] Corson, McKenzie, and Segrè, Phys. Rev. **57**, 1087 (1940).

[4] Hagemann, Katzin, Studier, Ghiorso, and Seaborg, Phys. Rev. **72**, 252 (1947); English, Cranshaw, Demers, Harvey, Hincks, Jelley, and May, Phys. Rev. **72**, 253 (1947).

[5] J. Schintlmeister, Oesterreichische Chemiker Zeitung Nr. 17, 1938, Nr. 9/12, 1943. Regularities in Geiger Nuttal diagrams referring to the individual values of Z were pointed out by Berthelot in the J. de phys. et rad., serie VIII, **3**, 17 (1942) and by N. Feather, Proc. Roy. Soc. Edinburgh, **62**, 211 (1946).

number. Another family of curves occurs if nuclei with the same neutron-proton differences, $N-Z$, are connected with each other. Of course, other variables can be chosen as abscissae; for instance, the number of the neutrons N, the atomic number, Z, $N-Z$ or N/Z. In each case, similar families of smooth curves are again obtained, for appropriate parameters.

The atom nuclei may be separated into three types in accordance with the number of their constituent protons and neutrons: Even-even (e–e)-types (both particle numbers even), even-odd (e–o)-types (one particle number odd) and odd-odd (o–o)-types (both particle numbers odd). From Fig. 1 can be seen that the (e–e)-nuclei (marked ●●●) lie directly on the curves, while the (e–o)-nuclei (marked ×××) and the (o–o)-nuclei (marked ○○○) are almost invariably situated slightly below or above the curves.

By means of this diagram, the energy of α-rays can be predicted with a fair degree of accuracy for the even–even nuclei and with a little less accuracy for the (e–o)- and (o–o)-nuclei.

One would like to establish with the greatest possible accuracy the corresponding half-life periods, since they must be exactly known in order to ascertain the value of the branching ratio. It is not advisable to determine, with the aid of the Geiger-Nuttal principle, half-lives from the known α-ray energies since this law is of only approximate validity. A calculation with the aid of the Gamow formula does not show very accurate results either, because some of the parameters which enter into the formula vary from nucleus to nucleus in a manner as yet unknown.

For this reason, a second diagram has been inserted into Fig. 2, which again shows as abscissa the mass number. However, the common logarithm of the half-life is used as ordinate, in place of the disintegration energy. The regularities thus obtained resemble those in Fig. 1. All (e–e)-nuclei lie on smooth curves, joining the nuclei with the same atomic number or with the same number of excess neutrons. Generally the (e–o)- and (o–o)-nuclei again lie off these curves. They are almost invariably situated below these curves. But, as Fig. 2 shows, the (e–o)- and (o–o)-nuclei lie with a fair degree of accuracy on separate smooth curves, which are marked by dotted lines. For the radioactive bodies with atomic numbers 83, 84, 85 the differences between (e–e)- and (e–o)- or (o–o)-nuclei seem to be very small.

The artificially produced α-radioactivities such as $_{85}At^{211}$, the members of the $4n+1$-series[4] and the α-radioactive elements[6] with atomic numbers larger than 92 (according to data published to date) are easily classified in Figs. 1 and 2.

III. THE DUAL DISINTEGRATIONS OF THE NATURAL RADIOACTIVE ELEMENTS: $MsTh_2$, $MsTh_1$, $_{87}Fr^{223}$ (AcK) AND RaE

Of the natural elements emitting α-rays, only $MsTh_2$, $MsTh_1$, and AcK show dual disintegration probabilities

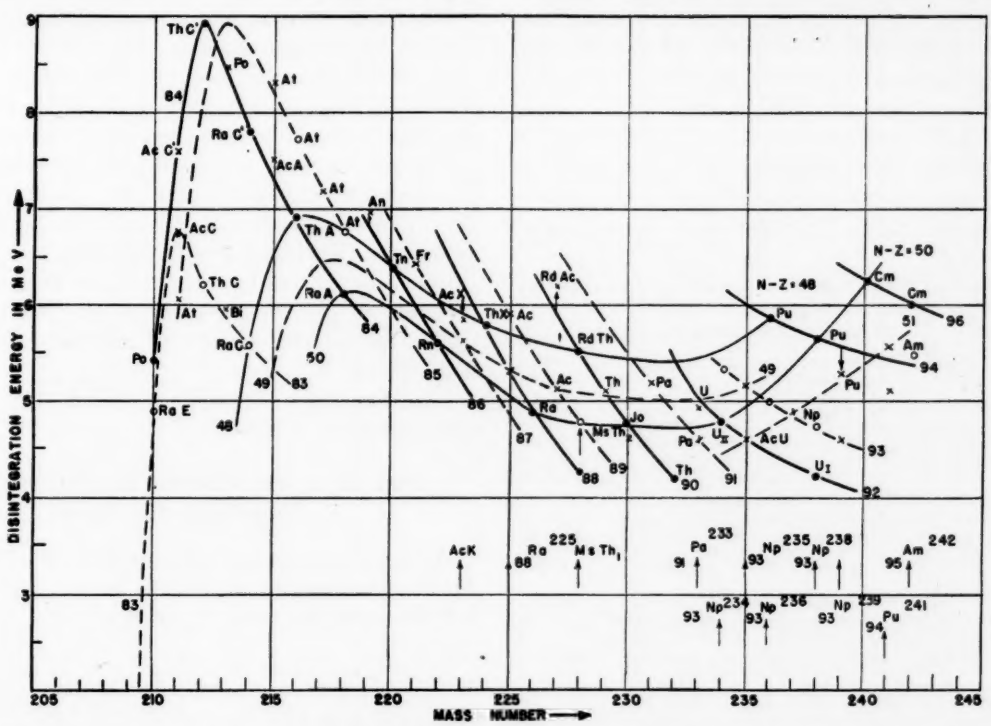

FIG. 1. α-Radioactive elements: disintegration energy and mass number. Even-even nuclei ●●●, even-odd nuclei ×××, odd-odd nuclei ○○○.

[6] Seaborg, James, Florin, Hopkins, Studier, Hyde and Ghiorso, Science, **104**, 379 (1946); Seaborg, James, and Morgan, Chem. Eng. News **25**, 358 (1947); James M. Cork, Radioactivity and Nuclear Physics (New York, 1947).

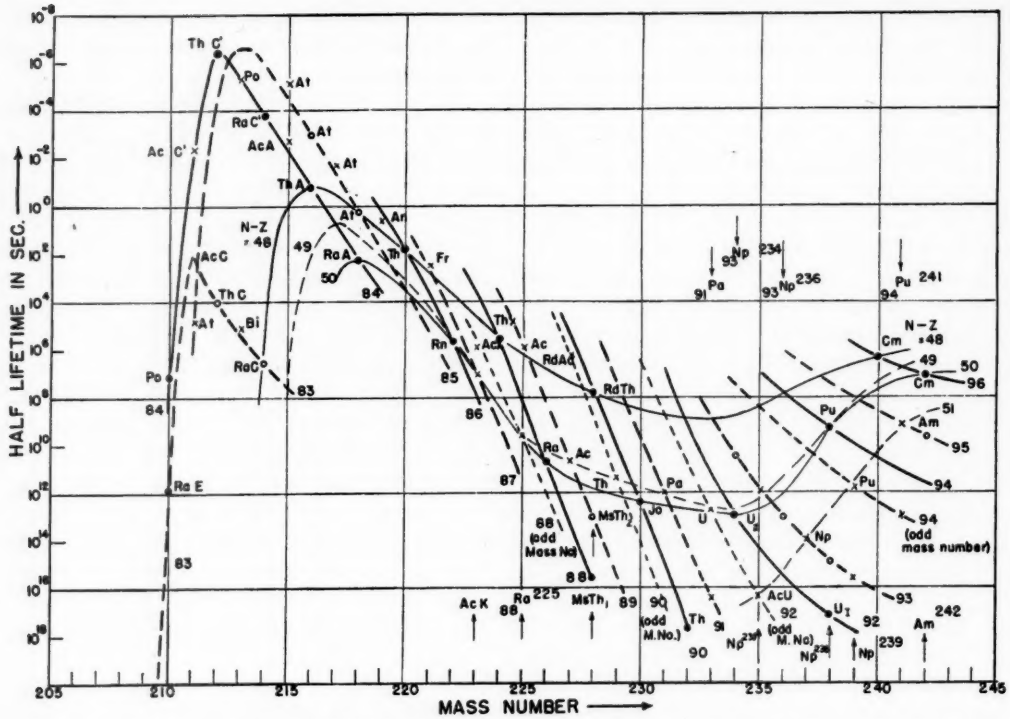

FIG. 2. α-radioactive elements: half-life and mass number. Even-even nuclei ●●●, even-odd nuclei ×××, odd-odd nuclei ooo.

as yet not observed whose branching ratios are higher than 10^{-10}. Recently, the dual disintegration of radium *E* was experimentally demonstrated, as can be seen from a very exhaustive investigation which was published while this paper was being prepared.[7] Data concerning the mentioned radioactive elements have been compiled in Table I. Column 1 indicates the element in question, column 2 the half-life of the β- or *K*-radiation in seconds, column 3 the estimated limits of the half-life of the supposed α-activity, columns 4 the estimated limits of the α–β-branching ratio, column 5 the most probable value of the α-energy.

TABLE I. Branching ratios and α-decay energies of some natural and artificial radioactive substances.

Element	Half-life of β- or *K*-radiation in sec.	Lower and upper limit of the half-life of the supposed α-radiation in sec. values from Fig. 2	Lower and upper limit of the α–β- or α–*K*-branching ratios	α-disintegration energy in Mev. values from Fig. 1
		Natural-radioactive substances		
$MsTh_2$	β^- 2.026×10^{4}	3×10^{12}–3×10^{13}	6×10^{-9}–6×10^{-10}	4.75±0.1
$MsTh_1$	β^- 2.11×10^{8}	2×10^{15}–2×10^{16}	10^{-7}–10^{-8}	4.25±0.1
AcK	β^- 1.26×10^{9}	2×10^{8}–3×10^{7}	6×10^{-4}–4×10^{-5}	5.5 ±0.2
RaE	β^- 4.32×10^{5}	4×10^{9}	5×10^{-7}	4.87
		Artificial-radioactive substances		
$_{88}Ra^{225}$	β^- 1.21×10^{6}	10^{9}–2×10^{10}	10^{-3}–6×10^{-4}	5.2 ±0.2
$_{91}Pa^{233}$	β^- 2.367×10^{6}	3×10^{13}–3×10^{16}	8×10^{-10}–8×10^{-11}	4.50±0.2
$_{93}Np^{234}$	*K* 3.80×10^{5}	$\sim 10^{10}$		5.3
$_{93}Np^{235}$	*K* 2.07×10^{7}	$\sim 5.10^{11}$		5.15
$_{93}Np^{236}$	β 7.2×10^{4}	$\sim 5.10^{12}$		5.0
$_{93}Np^{239}$	β^- 1.73×10^{5}	$\sim 10^{14}$		4.7
$_{93}Np^{239}$	β^- 2.01×10^{5}	$\sim 10^{15}$		4.6
$_{94}Pu^{241}$	β^-	$\sim 10^{13}$		5.1
$_{95}Am^{242}$	β^- 6.48×10^{4}	$\sim 10^{11}$		5.5

The limits of accuracy were estimated according to the following points of view:

As far as even–even nuclei are concerned, the values of the disintegration energy and of the half-life are uncertain only if it is necessary to extrapolate the curves into regions where no measured values are as yet available. This is the case with $MsTh_1$. In spite of this, however, the branching ratio can be stated with an accuracy of, perhaps, a factor of 10.

Generally, as can be seen from the diagram, the uncertainty of the α-decay energy amounts to 0.2 Mev while the uncertainty of the half-life amounts to a factor of ten.

Experimentally determined values are, of course, given for RaE in Table I.

Disintegration Schemes and Experimental Possibilities of Proof

Attempts to demonstrate the dual disintegration of $MsTh_2$ have already repeatedly been made. The disintegration scheme reads as follows:

$$_{89}MsTh_2^{228} \xrightarrow{\alpha} {}_{87}Fr^{224} \xrightarrow{\beta} {}_{88}ThX^{224}.$$
$$\qquad\qquad\qquad\qquad\qquad\qquad\quad \beta \searrow {}_{90}RdTh^{228} \xrightarrow{\alpha}$$

Of all the experiments conducted to date in an at-

[7] E. Broda and N. Feather, Proc. Roy. Soc. **190**, 20 (1947).

tempt to show the dual decay of $MsTh_2$[8] none has even approached the sensitivity of the method used by Hahn and Erbacher.[9,10] By applying chemical separation methods, element 87 was isolated and examined for β-radiation. Negative results obtained places an upper limit on the α–β-branching ratio of $MsTh_2$, dependent upon the assumed value of the half-life of element 87. In Table II are shown the results obtained by Hahn and Erbacher. It appears in comparison with the value of Table I that the sensitivity has been just not large enough for a positive confirmation of the α-radiation of $MsTh_2$ if the β-half-life of the element $_{87}Fr^{224}$ is longer than 10 minutes. Applying energy-conservation rules we obtain for the value of the β-disintegration energy of $_{87}Fr^{224}$ 3.2 Mev. By means of the Sargent diagram it is possible to estimate the half-life of $_{87}Fr^{224}$ to 50 seconds for an allowed transition, for a "first forbidden transition" to 1.4 hours.

The disintegration of $MsTh_1$ occurs as follows:

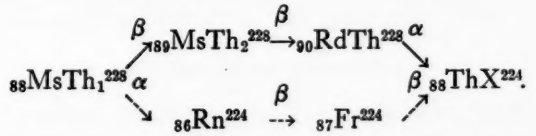

In spite of the higher α–β-branching ratio it seems that here, too, no direct confirmation of the α-radiation of $MsTh_1$ can be obtained because of the fact that it is impossible to prevent the presence of small traces of other α-rays with similar ranges. According to the above mentioned disintegration scheme the same isotope of element 87 is again being formed. In conformity with the estimates made here it can be concluded from these experiments by Hahn,[10] which were conducted with a mesothorium-source, that the α–β-branching ratio of MsTh is lower than 10^{-4}. The β-half-life of $_{86}Rn^{224}$ can be estimated by means of energy considerations to 16 hours if we assume an allowed transition, to 60 days for a first forbidden transition.

A positive confirmation of the dual disintegration of $MsTh_1$ is perhaps possible if the very sensitive method used by Hahn and Erbacher is applied to very strong mesothorium-sources.

The disintegration scheme of $AcK(_{87}Fr^{223})$ can be written as follows:

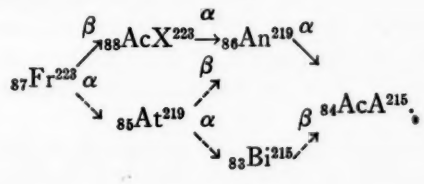

[8] J. Schintlmeister and E. Rona, Akad. Wiss. Wien **147**, 49 (1938); see there also other literature.
[9] O. Hahn and O. Erbacher, Physik Zeits. **27**, 531 (1926).
[10] O. Hahn, Naturwiss. **14**, 159 (1926).

TABLE II. Results of Hahn and Erbacher for the maximal α–β-branching ratio α/β of $MsTh_2$.

Supposed half-life of $_{87}Fr^{224}$	Maximal α–β-branching-ratio
10 minutes	2.9×10^{-8}
9.5 hours	5.5×10^{-9}
1 day	1.6×10^{-8}
10 days	5×10^{-9}
100 days	8×10^{-9}
10 years	1.5×10^{-7}

If it is possible to produce rather strong $_{87}Fr^{223}$ sources, the direct confirmation of the α-radiation of $_{87}Fr^{223}$ should not meet special difficulties. To complete the picture, the disintegration scheme of RaE, already experimentally confirmed, may be mentioned:

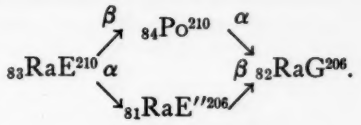

IV. THE BRANCHING RATIOS WITH ARTIFICIAL RADIOACTIVE SUBSTANCES

Concerning the newly established $4n+1$ series, $_{88}Ra^{225}$, in addition to $_{83}Bi^{213}$, should undergo a dual disintegration. Experimentally it has already been established that the α–β-branching ratio for $_{88}Ra^{225}$ is less than 1 percent. The values read off from Figs. 1 and 2 were also recorded in Table I. From this it can be seen that the branching ratio is lower than 10^{-3}.

The disintegration scheme reads:

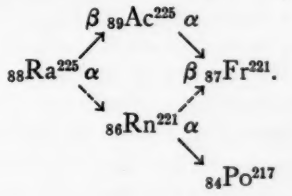

Experimental confirmation should not meet any special difficulties.

In addition the following radioactive substances which show β-radioactivity or K-capture should be also α-radioactive with α–β- or α–K-branching ratios larger than 10^{-10}:

$_{91}Pa^{233}$, $_{93}Np^{234}$, $_{93}Np^{235}$, $_{93}Np^{236}$, $_{93}Np^{238}$, $_{93}Np^{239}$, $_{94}Pu^{241}$, $_{95}Am^{242}$.

The values of the branching ratios for elements with atomic numbers larger than $g2$ are not entered in Table I, because the curves drawn in this range are very inaccurate due to the lack of published data.

Note added at proof:—While this paper was being prepared for publication, the following related articles appeared: Vigneron, Comptes Rendus **225**, 1067 (1947); Feather, Reports Prof. Phys. **11**, 19 (1948); Karlik, Acta Phys. Austriaca **2**, No. 2, 182 (1948); Perlman, Ghiorso, and Seaborg, Phys. Rev. **74**, 1730 (1948).

On the Disintegration Products of the 2.2-μSec. Meson

E. P. HINCKS AND B. PONTECORVO*
National Research Council of Canada, Chalk River Laboratory, Chalk River, Ontario, Canada

(Received September 19, 1949)

An investigation of the penetration through absorbers of various elements by the charged particles that result from the 2.2-μsec. meson decay is reported. Mesons and decay particles are detected by an arrangement of Geiger-Müller counter trays, and delayed coincidence techniques are used to select the desired events. The absorption measurements exhibit two components in the decay radiation, one of which is much more penetrating than the other. In lead, for example, the "soft component" is essentially absorbed by about 20 g/cm², while the "hard component" is easily detected after 38 g/cm².

A different arrangement of counters is used to show that the "hard component" is due to a neutral radiation which accompanies the charged decay particles. This result, and measurements of the intensities of the "hard component" with lead and carbon absorbers, provide strong evidence that the neutral radiation is, in fact, bremsstrahlung from the charged particles which constitute the "soft component."

The bremsstrahlung intensities, together with the form of the absorption curve, are shown to lead to the following conclusions: (1) the charged decay particles are electrons (i.e., they have a mass less than two electron masses); (2) a considerable number of electrons are emitted with energies greater than 25 Mev; (3) the average energy of the electrons is greater than 25 Mev; (4) there is no evidence for electrons of energy much greater than 50 Mev.

The support which these results lend to the currently favored ideas on the meson decay process is discussed.

INTRODUCTION

THE decay process of the ordinary cosmic-ray meson[a] is still not known with certainty, although its instability was first inferred over ten years ago. The earliest direct observations of the decay phenomenon were made in a cloud-chamber photograph by Williams and Roberts[1] in 1940, and by the detection of the delayed emission of charged particles from stopped mesons by Rasetti,[2] and by Auger, Maze, and Chaminade,[3] in 1941.

The photograph by Williams and Roberts (as well as others which have been obtained subsequently[4]), showed that a single lightly ionizing charged particle is emitted in the decay process. This observation provided evidence for the identity of the cosmic-ray meson and the particle postulated earlier by Yukawa to account for nuclear forces,[5] and this identification was made even more convincing by the similarities between the lifetimes and between the masses of the two particles. The hypothetical Yukawa meson has integral spin, and, when free, disappears in the following process:

$$\text{meson} \rightarrow \text{electron} + \text{neutrino}. \qquad (1)$$

Conservation of energy and momentum requires both decay products to receive as kinetic energy about half the rest mass (~100 Mev) of the meson. According to the Yukawa picture, positive mesons when brought to rest should decay with the production of electrons (positive) of about 50 Mev; negative mesons, on the other hand, are expected[6] to be captured by nuclei of the stopping material in a time much shorter than their lifetime for radioactive decay, and so give rise to no decay radiation. The energy—70±35 Mev—of the decay particle in Williams and Roberts' picture was consistent with the assumption of Eq. (1). Moreover, Conversi and Piccioni[7] in 1944 deduced from the numbers of decay particles escaping from iron plates 0.6 cm and 5 cm thick that their mean range is about 2.5 cm of iron. This value corresponds to an electron energy of about 50 Mev, again in agreement with the electron-neutrino hypothesis.

A refutation of the identification of the 2.2-μsec. meson with the Yukawa particle was given by the well-known experiment of Conversi, Pancini and Piccioni,[8] which showed that while in a heavy element (iron) only *positive* stopped mesons decay, in a light element (carbon), on the other hand, both *positive and negative* mesons decay. This result and subsequent confirmative experiments by other workers lead to the conclusion[8,9] that the interaction between the meson

* Present address: Atomic Energy Research Establishment, Harwell, England.

[a] By "cosmic-ray meson" we mean the particle, positive or negative, of mass about 100 Mev, that forms the bulk of the hard component of the cosmic radiation at sea level and decays, when free, with a mean life of 2.2 μsec. It is commonly assumed to be identical with the μ-meson produced in the π-μ-decay process discovered by Lattes, Occhialini, and Powell (Nature **160**, 453 (1947)). In this paper the term meson will refer to the 2.2-μsec. particle unless otherwise specified.

[1] E. J. Williams and G. E. Roberts, Nature **145**, 102 (1940).

[2] F. Rasetti, Phys. Rev. **59**, 613 (1941); **60**, 198 (1941).

[3] Auger, Maze, and Chaminade, Comptes Rendus **213**, 381 (1941).

[4] Fowler, Cool and Street, Phys. Rev. **74**, 101 (1948); R. W. Thompson, Phys. Rev. **74**, 490 (1948); Kan-Chang Wang and S. B. Jones, Phys. Rev. **74**, 1547 (1948). It should be noted that Thompson's cloud chamber was triggered by delayed coincidences, and therefore the correlation was almost certainly established between the events observed and the 2.2-μsec. decay. (See also references 11 and 18).

[5] For a discussion and references see, for example, *Cosmic Radiation*, edited by W. Heisenberg (Dover Publications, New York, 1946).

[6] S. Tomonaga and G. Araki, Phys. Rev. **58**, 90 (1940).

[7] M. Conversi and O. Piccioni, Phys. Rev. **70**, 874 (1946).

[8] Conversi, Pancini, and Piccioni, Phys. Rev. **71**, 209 (1947).

[9] J. A. Wheeler, Phys. Rev. **71**, 320 (1947); E. Fermi, E. Teller and V. Weisskopf, Phys. Rev. **71**, 314 (1947); E. Fermi and E. Teller, Phys. Rev. **72**, 399 (1947); T. Sigurgeirsson and A. Yamakawa, Phys. Rev. **71**, 319 (1947); G. E. Valley, Phys. Rev. **72**, 772 (1947); H. K. Ticho and M. Schein, Phys. Rev. **73**, 81 (1948); G. E. Valley and B. Rossi, Phys. Rev. **73**, 177 (1948);

and the nucleus is much smaller (by a factor $\sim 10^{12}$) than that required for the Yukawa particle, and so precludes the possibility of their identity. In renouncing the "Yukawa character" of the meson, we must also renounce the inferences regarding its decay products and its spin. In particular, we must admit that not only may the neutrino of Eq. (1) be replaced by some other neutral particle, or particles, but also that *the charged decay particle may not be an electron.*

Another decay process which would result in electrons of about 50 Mev, but which would require half-integral spin for the meson, is the following:

$$\text{meson} \rightarrow \text{electron} + \text{photon}. \qquad (2)$$

This process is, however, apparently ruled out by the negative results of several workers[10] who searched for photons from disintegrating mesons.

The observation of a meson disintegration in a cloud chamber, in which the energy of the decay particle is 24 Mev, led Anderson and co-workers[11] to suggest the process:

$$\text{meson} \rightarrow \text{electron} + \text{neutretto}, \qquad (3)$$

the mass of the neutretto, or neutral meson, being 25–30 Mev less than that of the original meson. While the secondary charged particle was assumed to be an electron, by direct measurements of momentum and specific ionization these authors could only place an upper limit to its mass at about 25 electron masses.

The experiments[b] to be described in this paper were undertaken in order to derive some information about the nature and energy of the charged decay particles by observing their penetration through solid matter. The measurements were made at the Chalk River Laboratory, near sea level, in the period May, November, 1948. Since the present work was initiated, new results[4,12,13] relating to the energy spectrum of the charged particles have appeared in the literature. Steinberger,[13] in particular, has made absorption measurements similar in principle to our own, and we shall discuss them further below.

While the form of the energy spectrum of the decay particles still requires further investigation, it seems certain, at least, that it does not consist of a single line. The possible alternatives are several lines (i.e., two or more competing decay processes), or a continuum, (i.e., three or more decay products).

As an example of a process with three decay products, the following has been suggested:[14]

$$\text{meson} \rightarrow \text{electron} + \text{neutretto} + \text{neutrino}. \qquad (4)$$

This process would result in a continuous spectrum of electron energies with a maximum energy equal to less than half the mass of the original meson by an amount dependent upon the mass of the neutretto, and with an average energy somewhat greater than half the maximum. Equation (4) like Eq. (3) requires the existence of a new particle, the neutretto or neutral meson, which might be expected on theoretical grounds to have a very short lifetime for decay into photons. There is some experimental evidence[10,15] against this possibility.

Another process which would result in a continuous distribution of electron energies was mentioned by Nordheim[16] in 1941:

$$\text{meson} \rightarrow \text{electron} + 2 \text{ neutrinos}. \qquad (5)$$

Good evidence for a continuous spectrum of the decay particles was published recently by Brown *et al.*[17] and by Leighton *et al.*,[18] after our work as well as Steinberger's was finished. The California authors measured in a cloud chamber the momenta of a great number of decay charged particles, contributing most of the present knowledge on the energy spectrum. Their results support the process (5).

Part I of the present paper describes measurements pertinent to the problem of the energy of the decay charged particles. Part II concerns the nature (mass) of such particles. We shall discuss our results in relation to the several hypotheses mentioned above, and in particular, at the end of the paper, summarize the evidence supporting process (5).

PART I. ABSORPTION MEASUREMENTS

1. Method

The function of the apparatus used in this experiment is to select charged particles which result from the meson decay process and which have traversed a known thickness of matter. The numbers of such events may then be observed for absorbers of different thicknesses, and of different materials. Some of the more important considerations affecting the choice of a suitable experimental arrangement are worthy of mention.

C. W. Kissinger and D. Cooper, Phys. Rev. **74**, 349 (1948); H. K. Ticho, Phys. Rev. **74**, 492 (1948); **74**, 1337 (1948).

[10] R. D. Sard and E. J. Althaus, Phys. Rev. **73**, 1251 (1948); **74**, 1364 (1948); E. P. Hincks and B. Pontecorvo, Phys. Rev. **73**, 257 (1948); a full report has been submitted for publication in Can. J. Research; O. Piccioni, Phys. Rev. **74**, 1236 (1948); **74**, 1754 (1948).

[11] Anderson, Adams, Lloyd, and Rau, Phys. Rev. **72**, 724 (1947). A second photograph, in which the decay particle energy is 25 Mev, was published by Adams, Anderson, Lloyd, Rau, and Saxena, Rev. Mod. Phys. **20**, 334 (1948).

[b] Partial accounts of the results of these experiments have been presented at the Royal Society of Canada, Vancouver Meeting, June 1948, and at the American Physical Society, Chicago Meeting, November 1948; also in Phys. Rev. **74**, 697 (1948); **75**, 698 (1949).

[12] J. G. Retallack, Phys. Rev. **73**, 921 (1948); Zar, Herschkowitz, and Berezin, Phys. Rev. **74**, 111 (1948); M. H. Shamos and A. Russek, Phys. Rev. **74**, 1545 (1948).

[13] J. Steinberger, Phys. Rev. **74**, 500 (1948); **75**, 1136 (1949). We are indebted to Dr. Steinberger for sending us a complete account of his work in advance of publication.

[14] O. Klein, Nature **161**, 897 (1948); Horowitz, Kofoed-Hansen, and Lindhard, Phys. Rev. **74**, 713 (1948).

[15] E. P. Hincks and B. Pontecorvo, Phys. Rev. **73**, 1122 (1948).

[16] L. W. Nordheim, Phys. Rev. **59**, 554 (1941).

[17] Brown, Camerini, Fowler, Muirhead, Powell, and Ritson, Nature **163**, 47 (1949).

[18] Leighton, Anderson, and Seriff, Phys. Rev. **75**, 1432 (1949).

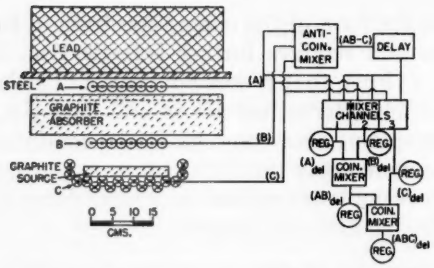

FIG. 1. Experimental arrangement for the absorption measurements, with block diagram indicating the essential functions of the electronic circuits. The geometry perpendicular to the paper may be inferred from the lengths of the source and counters, which are ~40 cm.

To detect both mesons and decay particles, the use of Geiger counters (in trays of many counters each) permits a relatively high rate of useful events to be obtained because large effective areas are possible, and the counters (at the counting rates used) are essentially continuously sensitive. The desired events, i.e., the stopping of mesons, followed by their decay with the emission of charged particles, are selected by the well-known technique of delayed coincidences. We have chosen for its directness and flexibility an arrangement in which the material which absorbs mesons, which we shall refer to as the "source" of decay particles, is separate from the material which absorbs the decay particles, to be called the "absorber."

The choice of source is governed by the requirement that decay particles should not lose too much energy in it before escaping. Therefore its thickness must be small compared with the average range of the decay particles. However, in order that the number of mesons stopped be not too low, a compromise must be made. The use of an element of low atomic number for the source has two advantages: (1) loss of energy by bremsstrahlung, with its resultant severe straggling, will be minimized; and (2) the intensity is enhanced by the decay of negative, as well as positive mesons. The source used was carbon, and its thickness—4.2 g/cm²—is about one-third the average range of 25-Mev electrons.

The requirement of a counting rate high enough to permit absorption measurements to be made in a reasonable time not only limits the thinness of the source, but also restricts the amount of collimation which can be imposed on the decay particles in their passage through the absorber. Thus we expect[19] about 0.03 meson stopped per gram of source per hour, or a total in our source (mass 3300 grams) of about 100 mesons stopped per hour. The condition that the meson should traverse a counter telescope renders only a fraction (~1/3 in our geometry) of these useful as a source of decay particles. Clearly then, "good geometry" for the absorption measurements must be sacrificed for intensity.

[19] Data may be obtained from B. Rossi, Rev. Mod. Phys. **20**, 537 (1948).

Absorbers of carbon, aluminum, and lead were used. Again a low Z material (preferably the same as the source), i.e., carbon, will facilitate interpretation of the results because of smaller bremsstrahlung effects. On the other hand, because of its low density, large thicknesses of such a material cannot be used without expanding the apparatus, and therefore losing intensity. Aluminum is a compromise in this respect, while lead was used to obtain a comparison between absorbers of high and low Z. The areas of all absorbers were such that they extended on all sides well beyond the solid angle defined by the counters.

2. Arrangement of Apparatus

In Fig. 1 we show a vertical section of the arrangement of counters and absorbers together with a simplified block diagram of the counting circuits. The apparatus was situated in a room whose walls and ceiling were concrete. Figure 2 is a photograph of the counter assembly; the components may be easily identified by comparison with the left-hand side of Fig. 1.

Three trays of counters are used, from top to bottom, A, B, and C (Fig. 1). Trays A and B each consist of 8 counters, each 1-in. diameter and 15-in. active length, with 1-mm thick copper walls. They are supported in thin aluminum boxes, but the bottom of box A, and the top and bottom of box B, are cut away to expose the active areas of the counters. The 17 counters of tray C are 1-in. diameter, 16-in. active length, with 0.65-mm thick brass walls, and are supported on a thin (0.5 g/cm²) aluminum shelf about 4 ft. above the floor of the room. All counters used were of the self-quenching type. A graphite block (20 cm×40 cm×4.2 g/cm² thick; density=1.7) resting on the counters of tray C forms the source of decay particles. Mesons traversing trays A and B, and stopping in the source, are detected by the anticoincidence $(AB-C)$. The pulse corresponding to $(AB-C)$, which we shall refer to as the "triggering event," is first delayed ~1 μsec. and then initiates a gating pulse ~5 μsec. wide. The outputs of each of trays A, B, and C are separately mixed with the gating pulse in such a way that if a discharge of either A, B, or C occurs between 1 and 6 μsec. after a triggering event, a "delayed coincidence" is recorded which we designate as $(A)_{del}$, $(B)_{del}$, or $(C)_{del}$ respectively. A decay particle leaving the source between 1 and 6 μsec. after a meson stops will thus be detected in any of the three trays through which it passes. In particular, a decay particle passing upward through *both* B and A gives a delayed coincidence $(AB)_{del}$.

The absorbers are placed in the 10-cm gap between trays A and B. They consist of aluminum sheets, lead sheets, or graphite blocks (density=1.7), and in all cases cover an area about 50 cm square. While the graphite and aluminum absorbers always rested on the top of the B counter box, the lead absorbers (with the exception of the very thick ones), were supported about

midway between trays A and B. When it turned out to be of interest to use graphite absorbers with a thickness greater than 10 cm, a compromise was made by adding a thickness of heavier material—iron or copper—above an initial thickness of graphite.

The lead (15 cm thick = 170 g/cm^2) which is placed above A (together with the concrete ceiling of the room), serves not only to shield the counters from the soft cosmic-ray component, but also, because of the form of the differential range spectrum of mesons,[19] to increase somewhat the "source strength," i.e., the number of mesons stopped in the source. On the other hand we expect that the source strength will not be altered significantly by the addition of the absorbers (up to $\sim$100 g/cm^2) between A and B, an assumption which was verified experimentally by control measurements made during the experiment.

The geometry used, in which decay particles emitted *upward* from the source are detected by the same pair of counter trays that detect the incident mesons, was chosen for its considerable economy in counters for a given intensity. However, although trays A and B are each used for two purposes, two properties of this geometry which reduce the efficiency should be noted: (1) the collimation of the meson beam, similar to that of the decay particles, is unnecessarily high, and (2) at least one counter in both A and B—the one discharged by the meson—is insensitive to a decay particle which may traverse it. The decrease in sensitivity of tray B due to the dead counter would be serious if the source were too close, and a favorable position of the latter (4.1 cm below B) was determined graphically.

The dual use of trays A and B introduces some complication in the electronic circuits, which will be described in the next section. On the other hand the arrangement lends itself to the reduction of the background (casual) counting rate by means of the anticoincidence counters C. The anticoincidence function of tray C for the *triggering event* $(AB-C)$ has already been stated. Moreover, since essentially all the casual *delayed events* are caused by a second meson traversing the apparatus by chance within the delayed resolving time, by recording $(ABC)_{\text{del}}$ together with $(AB)_{\text{del}}$ we can identify a large fraction of these events and disregard them. In effect, therefore, we measure the counting rate

$$(AB-C)_{\text{del}}=(AB)_{\text{del}}-(ABC)_{\text{del}}$$

with various absorbers between trays A and B. While the anticoincidence efficiency of tray C in our arrangement is not very high (of the mesons which traverse A and B, far more "leak" past C than stop in the source), nevertheless it is sufficient to give a very low rate of casual $(AB-C)_{\text{del}}$ events.

3. Electronic Apparatus

Figure 3 is a complete block diagram showing the electronic components used to record the delayed events.

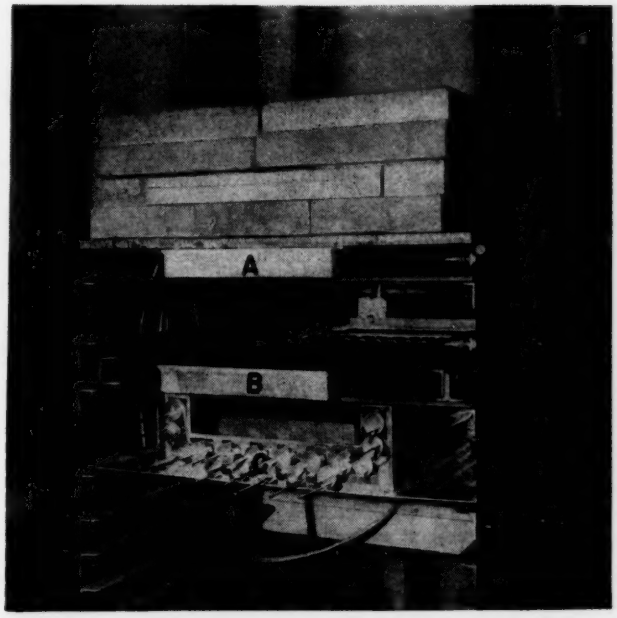

FIG. 2. Photograph of the counter assembly showing the graphite source between trays B and C. Absorbers are placed in the space between trays A and B.

Each counter used has a separate H.T. resistor ($R=10^7$ ohms) by which voltage is applied to the wire, and a separate output condenser ($C=50\ \mu\mu$f). In tray C the counters are simply paralleled by connecting all 17 output condensers to the input of a single cathode-follower. On the other hand the circuits associated with trays A and B must be capable of handling two pulses which may be as close together as 1 μsec. and, moreover, the first pulse of the pair must be accepted by the anticoincidence mixer, while the second must be accepted by the delay mixer. It will be apparent that to satisfy the last requirement it must be ensured that *either* there be no dead-times equal to or greater than one microsecond between the output of the counter tray and the mixing stage of the delay mixer, *or* if there be a long dead-time at some stage, then the first pulse must be prevented from reaching it and rendering it insensitive to the second pulse. The second of these conditions has been satisfied in our apparatus. The delay mixer input circuit has a long dead-time ($\sim$100 μsec.) but when operated from the "threshold amplifier" ("threshold output") it receives only the *second* of two pulses which occur close together. From the "normal output" of the threshold amplifier, on the other hand, the first pulse of the pair is fed to the anticoincidence mixer.

A circuit diagram of the threshold amplifier[9] is shown

[9] The characteristics of the "threshold amplifier" make it of possible use for several purposes. It may have application, for example, as a coincidence (or anticoincidence) mixer in counter arrays in which the functions of the counters are not individually specified. Thus by selecting output pulses of the appropriate magnitude, events in which only one, or only two, or two or

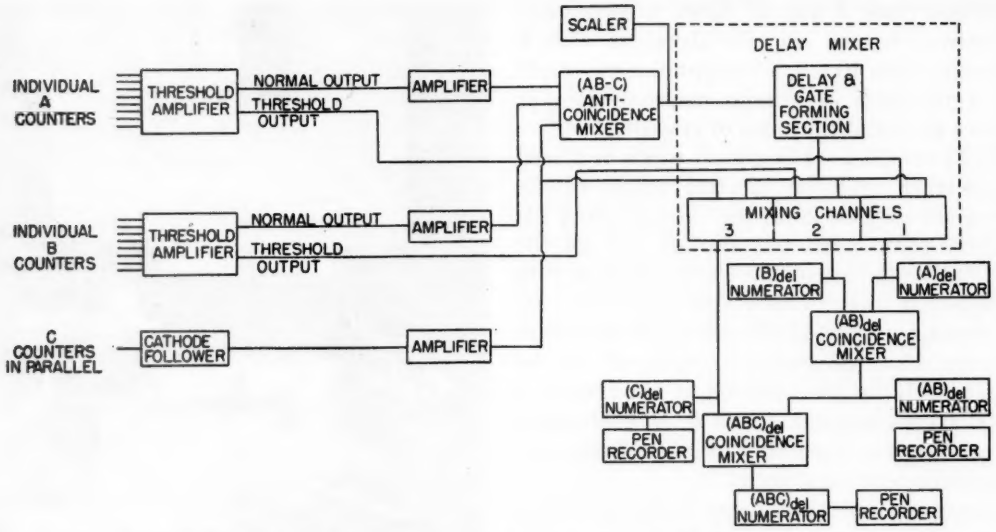

FIG. 3. Detailed block diagram of the circuits used to record the delayed coincidences in the absorption measurements.

in Fig. 4. The output of each counter of the tray is fed to a separate tube (6AU6) whose purpose is to shape and equalize all pulses. Thus, the negative pulse resulting from a counter discharge cuts off the plate current of the associated 6AU6 very quickly (in $\sim$0.1 μsec.) with the result that at the plate an approximately rectangular positive pulse appears whose width (10–15 μsec.) is determined by the differentiating time constant at the grid. The amplitude of this pulse is given by the steady potential drop across the 10K plate resistor of the tube, and standardization of the pulse sizes from different tubes is improved by using both matched tubes and matched plate resistors. The outputs of all tubes are mixed in a resistor network and output stage (6AQ5) whose operation is linear over the region in which it is used. (The use of negative feedback from plate to grid has the advantages of improving the linearity, and of reducing the output impedance.) Thus the discharge of a single counter results in a rectangular negative pulse at the 6AQ5 plate; the simultaneous discharge of two counters produces a rectangular pulse of twice the amplitude, and so on. A diode discriminator (EA50), with its bias adjusted to a voltage just greater than the amplitude of a single pulse, will therefore pass a standard pulse which has been preceded within an interval 0 to $\sim$15 μsec. by another standard pulse. In our application of this circuit, the discharge of one counter by a meson initiates a pulse which reaches the anticoincidence mixer via the "normal output" (no discriminator). On the other hand, only a second pulse, e.g., that due to a decay particle with a delay between 0 and 15 μsec., can pass the "threshold output" to trigger the input circuit of the delay mixer. All components of the circuit (excluding power supply) are mounted directly on the end of the counter box. It is essential that the leads from the counters to the 6AU6 grids be short, and shielded from each other, but the output impedance is sufficiently low to tolerate several feet of low capacity cable.

The "normal outputs" of the threshold amplifiers of trays *A* and *B* feed the two "coincidence inputs" of the anticoincidence mixer through "wave-front amplifiers." The latter are simply fast two-stage saturating amplifiers (gain below saturation $\sim 10^3$) which serve to bring the pulse front above the threshold of the anticoincidence mixer with negligible delay. In the case of tray *C*, where no threshold amplifier is required, the pulses are fed from a cathode-follower through a wave-front amplifier, and thence to the "anticoincidence input" of the mixer.

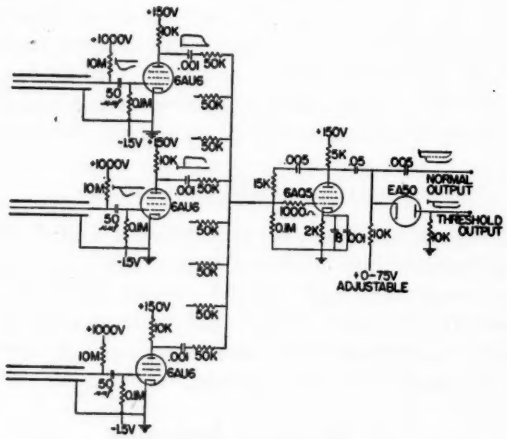

FIG. 4. Schematic diagram of the threshold amplifier circuit, showing three of the eight parallel input stages with G-M counters.

more, etc., counters are discharged may be selected. While the present circuit has been designed for maximum simplicity, some refinements in the pulse shaping stages would give greater uniformity of size, and would be required for coincidences of higher order.

The anticoincidence mixer is of straightforward design, and will not be described in detail. The two coincidence channels and Rossi mixing stage are similar, with minor alterations, to the circuit described by Jelley.[20] Output pulses (positive) from the Rossi plates are shaped slightly and fed to a biased-off control grid of a 6SA7 anticoincidence mixing stage. A coincidence pulse renders the 6SA7 conducting (the second control grid has zero bias), and a large pulse results at the plate. However, should a pulse arrive simultaneously at the anticoincidence input, a large negative pulse is applied by a trigger-pair to the second control grid of the 6SA7, and prevents the passage of plate current until well after the pulse on the first grid is over. The resolving time of either coincidence channel, with respect to a pulse in the other one, is 1.0 μsec. (i.e., ±0.5 μsec). The resolving time of either coincidence channel with respect to a pulse in the anticoincidence channel is {−0.6 to +5 μsec.}. The output pulse from the mixer is delayed by ∼0.6 μsec. with respect to the latest coincidence input pulse.

The delay mixer was designed by Mr. G. B. Parkinson, who also supervised its construction for us in the Electronics Section of this Laboratory. Since a description of this instrument has not hitherto been published, we shall include here a circuit diagram (Fig. 5) and a few points concerning its operation. The instrument consists essentially of one channel in which the initial input pulse (the "triggering" pulse), is delayed and made to generate a gating pulse of fixed width, together with three independent but identical channels in which "naturally" delayed input pulses are mixed with the artificially delayed gating pulse. In every channel an input pulse (negative) after amplification and reversal of sign by the first tube (6AK5), fires a thyratron (6D4). The latter, by virtue of the delay line in its cathode circuit, produces a standard rectangular pulse ∼0.5 μsec. in width, negative at the plate and positive at the cathode. In the "triggering channel," the next stage (½-2C51) accepts the positive pulse from the thyratron cathode and delivers a positive pulse with a selected delay to the gate-forming trigger pair (6J6+½-2C51). If zero delay is desired, the positive pulse is passed directly from the thyratron to the trigger circuit. On the other hand delays of either 1 or 2 μsec. are obtained with a shorted delay line which forms the plate load of the 2C51. The undelayed pulse at the plate of the 2C51 is negative and does not affect the 6J6; the reflected pulse is positive and actuates the trigger pair. The width of the positive rectangular gating pulse which is fed to the mixing stage in each delay channel may also be selected by a switch. Considering again

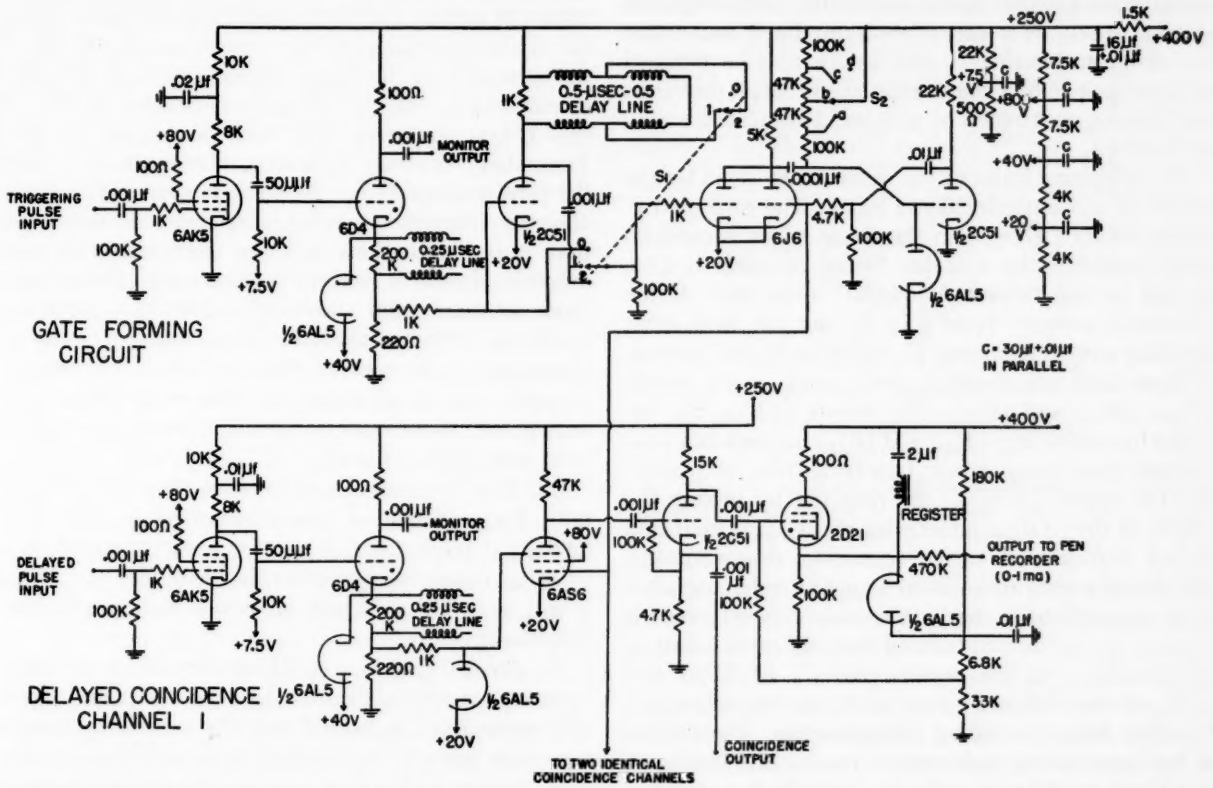

FIG. 5. Schematic diagram of the circuit of the delay mixer. Delayed coincidence channels 2 and 3, not shown, are identical with channel 1. Switch S_1 selects the initial delay, which may be nominally 0 μsec. (position 0), 1 μsec. (position 1), or 2 μsec. (position 2). The finite widths of the pulses produced by each channel have the effect of reducing these values by 0.4 μsec. Switch S_2 provides alternative gate widths of (a) 2 μsec., (b) 3 μsec., (c) 5 μsec., and (d) 7 μsec., approximately.

[20] J. V. Jelley, Can. J. Research A 26, 255 (1948).

TABLE I. Summary of $(AB-C)_{del}$ rates for "no absorber" runs.

Two-week period	Hours of observation	$(AB-C)_{del}=(AB)_{del}-(ABC)_{del}$ Total counts	Counts/hr.*
May 1–15	99	89	0.90±0.10
June 1–15	71	50	0.70±0.10
June 16–30	50	34	0.68±0.12
July 1–15	30	22	0.73±0.16
Aug. 1–15	49	39	0.80±0.13
Aug. 16–31	87	65	0.75±0.09
Sept. 1–15	22	16	0.73±0.18
Total	408	315	0.77±0.05

* All errors ascribed to measured counting rates in this paper are the statistical standard deviations.

one of the delay channels, the mixing tube (6AS6), which is normally cut off, receives positive standard pulses from the thyratron cathode of that channel on its suppressor grid, and positive gating pulses on its control grid. When these are coincident (the total resolving time is slightly less than the sum of the two pulse widths), a negative pulse appears at the mixer plate and drives the output tube ($\frac{1}{2}$-2C51). From the cathode of the latter negative pulses are available for external use; from the plate positive pulses operate a built-in numerator (mechanical register operated by a thyratron). The delayed coincidences in the three channels are thus counted independently by three numerators; a fourth (spare) numerator, with a separate external input, is a useful addition. Each numerator has an output terminal whence a pulse may be obtained to drive the pen of a chart recorder so that, if desirable, the time of occurrence of a delayed coincidence may be observed.

The triggering input of the delay mixer is fed by the output of the anticoincidence mixer. The rate of triggering events $(AB-C)$ in the delay mixer is continuously monitored by a scaler. Delay channels 1, 2, 3, are fed by the "threshold output" from tray A, the "threshold output" from tray B, and the wave-front amplifier output from tray C, respectively; the outputs of these channels therefore correspond to the events $(A)_{del}$, $(B)_{del}$ and $(C)_{del}$. The events $(AB)_{del}$ are detected by mixing the $(A)_{del}$ and $(B)_{del}$ outputs in a two-channel coincidence mixer (resolving time=0.6 μsec.) and the events $(ABC)_{del}$ are detected by mixing the output of the $(AB)_{del}$ mixer with the $(C)_{del}$ output in a second two-channel mixer (resolving time=8 μsec.). All delayed events are counted by individual numerators (it is arranged as a check that each delayed event is counted by two numerators fed from different points of the circuit), and the events $(AB)_{del}$, $(ABC)_{del}$ and $(C)_{del}$ are recorded on the moving charts of synchronized Esterline Angus recording milliammeters. The circuits of the two-channel coincidence mixers are similar to that given by Jelley,[20] while the individual numerators each consist of a mechanical register and driving circuit, as used in the delay mixer.

The a.c. power is supplied to the electronic apparatus, with the exception of a few units whose operation is not critical, through voltage-regulating transformers. The d.c. voltages required for the counters are obtained from compact 1200-v battery boxes with stepped outputs. A separate battery supplies the single operating voltage for each tray of counters.

4. Control Measurements

Many control runs, and tests of the proper operation of the apparatus, were made during the many months taken by the experiment. These checks may be divided into three categories: (a) those obtained continuously during the experimental runs, (b) those made periodically, once or twice a day, and (c) those made only occasionally. They will be described in turn.

(*a*) *Continuous checks.*—(i) The number of triggering events $(AB-C)$ was counted continuously by a scaler. Readings taken usually twice a day showed whether the $(AB-C)$ rate had been normal throughout the preceding interval. The rate varied somewhat (between 30/min. and 37/min.), as expected, when different absorbers were inserted between trays A and B, but for a given condition fluctuations from the mean value were never more than a few percent, and often much less, over long periods.

(ii) The rates $(B)_{del}$ and $(C)_{del}$, and therefore their sum $(B)_{del}+(C)_{del}$, are due chiefly to decay electrons from the source and so constitute an excellent check (a) of the constancy of the "source strength," (b) of the constancy of the delay and gate width of the delay mixer, and (c) of the proper performance of the B- and C-tray counters and their associated circuits. Twice-daily readings furnished interim checks, while the rates averaged over the complete run with a given absorber furnished a suitable reference intensity for that run. Fluctuations in these averaged rates with different absorbers were not appreciably greater than those expected from statistical causes, and, since the statistical errors in the $(AB-C)_{del}$ rates were at all times much greater, corrections for variation in "source strength" could be neglected. The mean $(B)_{del}$ rate during the whole experiment (2155 hours of observation) was 4.1/hr.; the mean $(C)_{del}$ rate was 8.6/hr.

(iii) The Esterline-Angus charts were examined carefully for evidence of non-randomness in the rates $(AB)_{del}$, $(ABC)_{del}$, or $(C)_{del}$, for assurance that each $(ABC)_{del}$ count was properly coincident with an $(AB)_{del}$ count, and for evidence of power failure or other irregularity.

(*b*) *Periodic Checks.*—(i) Measurements of the single counting rates (A), (B), (C) (i.e., the total rate of each tray separately), indicated that the sensitivity of each tray was normal. The single rates varied somewhat with changes in absorber, and, of course, with drifts in the H.T. voltages, but the good reproducibility attained with a given absorber may be attributed in large part to the excellent characteristics of the counters. Typical values of the single rates with a thick absorber (80

g/cm² Pb) are:

$(A) = 720/\text{min.}$
$(B) = 1030/\text{min.}$
$(C) = 2690/\text{min.}$

(ii) The H.T. voltages supplied by the batteries to each tray of counters were checked, and readjusted when a drift $\sim\pm 10$ v occurred.

(iii) Some of the more critical d.c. voltages in the coincidence mixers were checked, and readjusted if they drifted beyond safe limits.

(iv) The shapes of certain standard pulses produced in the delay mixer were observed with a fast oscilloscope.

(*c*) *Occasional Checks.*—(i) Control runs were made at appropriate intervals throughout the experiment with no decay particle absorber. In these "no absorber" runs the rate $(AB-C)_{\text{del}}$ checks the sensitivity and proper performance of the whole apparatus. That this rate did not exhibit significant variation may be seen from Table I, in which the values are grouped according to the two-week period during which they were obtained. The mean rate (0.77 ± 0.05/hr.) has been taken as a measure of the intensity with no absorber.

(ii) On two occasions overnight runs were made with all conditions normal except that the H.T. voltages on the counters were removed. No counts due to faulty apparatus, electrical pick-up, or other spurious causes, were observed.

(iii) A fast triggered oscilloscope was used to verify that the pulses delivered by the counters, together with the pulses appearing at various points of the circuit, were of the proper shape.

(iv) If the counting rate at the "threshold output" of the threshold amplifier is measured for different bias voltages applied to the discriminating diode, a curve is obtained which consists of a series of downward (with increasing bias) steps (Fig. 6). Along the horizontal portion of the first step all discharges (single or multiple) in the tray of counters are detected; the second step corresponds only to discharges of two or more counters, the third step to three or more, and so on. The lack of complete discontinuity between the steps, and the deterioration in rectangular form as the bias is increased, are due, of course, to imperfect standardization of the pulses. The operating bias is chosen to lie just above the transition between the first step and the second, and it is important that neither the shape of the bias curve in this region, nor the position of the operating point, change appreciably. Such an occurrence would result in not only a change in the effective resolving time for genuine delayed pulses but also the possible registration of spurious delayed pulses due to circuit lags. The dotted curves in Fig. 6 which show the number of spurious delayed counts recorded by the delay mixer (position 1) as a function of bias voltage, indicate the importance of the threshold amplifier stability. Bias curves for both A and B threshold amplifiers taken at various times showed that their stability during the experiment was quite adequate.

(v) Two characteristic times are important in determining the sensitivity of the apparatus for the detection of decay particles: the total delay experienced by the triggering pulse ("delay time"), and the resolving time for the delayed coincidence. The former is the time interval between the entrance of a meson and the moment when a decay particle can be first detected; it consists essentially of the sum of two artificially imposed delays, one in the anticoincidence mixer, and one in the triggering channel of the delay mixer. The resolving time is the length of the delayed time interval during which the decay particle can be detected, i.e., the effective gate width of the delay mixer, and is important for the estimation of the casual rate. These times were measured by means of a pulse generator which could supply from separate outputs two pulses whose time separation was adjustable. Thus delayed events could be simulated artificially, and by varying the interval between the pulses the delay time and resolving time were observed. The time separation of a pair of pulses was measured with the fast triggered oscilloscope, whose internal sweep-speed calibrator was checked by independent resolving-time measurements using two random sources with known rates. The delay time is ~ 1.2 μsec.; the value of the resolving time, used below for the computation of chance rates, is

$$\tau = 4.7\pm 0.3 \ \mu\text{sec.}$$

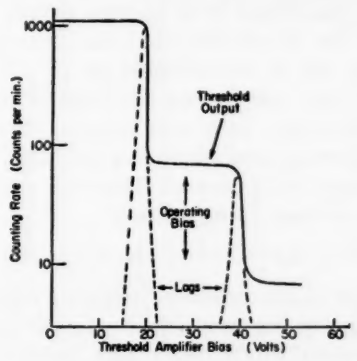

FIG. 6. Bias curve for the threshold amplifier. The dotted curves indicate the number of spurious lags, greater than ~ 1 μsec., which are produced when the bias is varied.

The constancy of these values was confirmed by the appropriate control runs and monitoring rates which have already been described.

(vi) Besides the single rates (A), (B), (C), and the triggering rate $(AB-C)$, to which reference has been made above, knowledge of a number of other (prompt) coincidence and anticoincidence rates is required in order to calculate those rates of chance delayed events which are of significance. Examination of these subsidiary prompt rates also furnished additional evidence that the apparatus was working properly. All rates were measured under circuit conditions approximating

as closely as possible those of the experiment. For example, by means of a three-position switch the anticoincidence mixer could be made to function as a two- or three-channel coincidence mixer, and used to measure either (AB) or (ABC), without other change. For those coincidence events requiring the discharge of at least two counters of trays A or B (*viz.* (AA) or (BB)), the appropriate "threshold output" was used.

Most of these rates depended somewhat on the thickness of absorber present, and so were measured for various conditions; a typical set of values obtained with the 80 g/cm² lead absorber is given below:[d]

$$\begin{aligned}(AB) &= 290\pm6/\text{min.}\\ (ABC) &= 249\pm6/\text{min.}\\ (AAB-C) &= 2.4\pm0.3/\text{min.}\\ (ABB-C) &= 1.6\pm0.3/\text{min.}\\ (AABB-C) &= 0.2\pm0.1/\text{min.}\\ (AB-C) &= 30.5\pm0.3/\text{min.}\end{aligned}$$

The value included for $(AB-C)$ is actually the mean triggering rate for the whole run with the 80 g/cm² lead absorber. These rates will be used in the next section for the computation of the chance rates.

5. Computation of Chance Rates

Because of the importance of a knowledge of the contribution to the $(AB-C)_{del}$ rate by chance events, and the fact that the estimation of their rate for our arrangement is not as straightforward as usual, we shall discuss the chance rates in some detail.

It should be noted first that the chance delayed single events, which we designate by $(A)_{del}^{ch}$, $(B)_{del}^{ch}$ and $(C)_{del}^{ch}$, are due to *any discharge* in the tray in question that occurs, within the delayed resolving time τ, *after a triggering event which does not "kill" the circuit of the associated delay channel.* Thus the chance $(A)_{del}$ rate may be written approximately:

$$(A)_{del}^{ch}=[(AB-C)-(AAB-C)][7/8(A)]\tau.$$

The reduction in the measured triggering rate $(AB-C)$ by subtraction of the term $(AAB-C)$ allows for those triggering events which, since they involve a double discharge in tray A, produce a pulse at the "threshold output" which "kills" the input channel of the delay mixer. They cannot therefore be associated with an $(A)_{del}$ count. On the other hand not all the events represented by the measured (A) rate can give rise to a chance delay, for a fraction (roughly 1/8), are not detected because of the dead counter.

Similarly, we may write:

$$(B)_{del}^{ch}=[(AB-C)-(ABB-C)][7/8(B)]\tau.$$

On the other hand the chance $(C)_{del}$ rate is given simply by:

$$(C)_{del}^{ch}=(AB-C)(C)\tau.$$

Chance events of the type $(AB)_{del}$, $(ABC)_{del}$, or $(AB-C)_{del}$, are due essentially to mesons traversing the apparatus so as to discharge counters in trays A and B between 1 and 6 μsec. after a triggering event that has "killed" neither A nor B delay channel circuits. Following the reasoning already applied to $(A)_{del}^{ch}$ and $(B)_{del}^{ch}$, the following expressions may be written:

$$\begin{aligned}(AB)_{del}^{ch}&=[(AB-C)-(AAB-C)-(ABB-C)\\ &\quad+(AABB-C)][(7/8)^2(AB)]\tau,\\ (ABC)_{del}^{ch}&=[(AB-C)-(AAB-C)-(ABB-C)\\ &\quad+(AABB-C)][(7/8)^2(ABC)]\tau,\\ (AB-C)_{del}^{ch}&=(AB)_{del}^{ch}-(ABC)_{del}^{ch}\\ &=[(AB-C)-(AAB-C)-(ABB-C)\\ &\quad+(AABB-C)][(7/8)^2(AB-C)]\tau.\end{aligned}$$

(The very small term $(AABB-C)$ is properly added in the above expressions because it has otherwise been subtracted twice—as part of $(AAB-C)$ and as part of $(ABB-C)$.)

We give below typical values of the chance rates, calculated for the condition with 80 g/cm² lead absorber.

$$\begin{aligned}(A)_{del}^{ch}&=0.08/\text{hr.}\\ (B)_{del}^{ch}&=0.12/\text{hr.}\\ (C)_{del}^{ch}&=0.39/\text{hr.}\\ (AB)_{del}^{ch}&=0.028/\text{hr.}\\ (ABC)_{del}^{ch}&=0.024/\text{hr.}\\ (AB-C)_{del}^{ch}&=0.0029/\text{hr.}\end{aligned}$$

It is estimated that the error (standard deviation) in the above rates is in each case $\sim\pm10$ percent.

The occurrence of types of casual delays other than chance events has not been mentioned above, and actually is of little importance in this experiment. Such delays may occur as a result of random time lags in the counter discharges, or because exceptionally slowly-rising pulses from the counters may take an appreciable time to cross the threshold point of the threshold amplifier. Counter lags may contribute slightly to the single delayed rate $(C)_{del}$, and to a much smaller extent[e] to $(A)_{del}$ and $(B)_{del}$. On the other hand, a few threshold amplifier lags may be present in the $(A)_{del}$ and $(B)_{del}$ rates. However, the chance that two random lags occur simultaneously to produce multiple delayed events ($(AB)_{del}$, etc.) is quite negligible, and so for these events, which are the significant ones in the experiment, only the chance rates need be considered.

The values of some of the chance rates can be verified experimentally. These checks will be described in the next section.

6. Experimental Results

The measurements made with absorbers of various materials and thicknesses extended over a period of

[d] The meaning of the symbols will be apparent. For example, $(ABB-C)$ refers to those events in which the discharge of at least one counter of tray A is accompanied by the discharge of at least two of tray B, but is unaccompanied by any discharge in tray C.

[e] For example, a casual $(A)_{del}$ event from this cause can only result from a double discharge (AA), one pulse of which is accidentally lagged.

about 5 months, during which the checks described above in Section 4 were applied to ensure that the apparatus was functioning properly. With a given absorber in position, readings were taken customarily twice a day until a sufficient number of hours of observation had been accumulated.

A list of the absorbers used, together with the measured values of all delayed coincidence rates, is presented in Table II. Here, we have termed "nominal absorber thickness" the thickness of the absorber which is placed between trays A and B; the "total absorber thickness" is obtained by adding to the "nominal thickness" half the thickness of the carbon source (2.1 g/cm²) plus the thickness of three (two for tray B, one for tray A) copper counter walls (2.1 g/cm²). Runs with different absorbers were interspersed with short runs with the absorber removed, and all results obtained in these short runs are combined to give the values presented in Table II for the condition "no absorber."

A few points concerning the rates given in Table II are of interest. The rate $(A)_{del}$ of course changes with absorber. The fact that $(A)_{del}$ is consistently higher than the rate $(AB)_{del}$ may be attributed to several causes: (1) decay particles which pass through the dead counter of tray B and traverse the absorber to produce a discharge of tray A; (2) decay particles from mesons stopped in the counter walls of tray C which can "see" tray A without intersecting the sensitive area of tray B; (3) more chance $(A)_{del}$ events than chance $(AB)_{del}$; (4) random lags in A. That random lags contribute little may be seen from the fact that the measured $(A)_{del}$ rate with the "thick lead" absorber is equal, within the error, to the estimated chance rate.

The constancy of the rates $(B)_{del}$, $(C)_{del}$, and thus $(B)_{del}+(C)_{del}$, with different absorbers may be observed. The fluctuations in $(B)_{del}+(C)_{del}$ are neither large enough, nor systematic enough, to warrant corrections to $(AB-C)_{del}$. The mean $(B)_{del}+(C)_{del}$ rate for the whole experiment is 12.7/hr., of which it is estimated that ~9/hr. are due to decay particles from the graphite source, ~1/hr. are due to decay particles from counter walls, 0.5/hr. are chance events, and the rest are random lags.

The rate $(ABC)_{del}$ is also constant, at least to within the large statistical uncertainty, throughout the experiment. Since these events should be only of chance origin, their number furnishes a useful check on the correctness of the calculated value $(ABC)_{del}^{ch}$. In a total of 2155 hours, 65 $(ABC)_{del}$ events were counted, or 0.030±0.004/hr. This rate lies satisfactorily between the estimated extreme values of $(ABC)_{del}^{ch}=0.024$/hr. with 80 g/cm² lead absorber, and 0.037/hr. with no absorber. Since the ratio $(AB-C)_{del}^{ch}/(ABC)_{del}^{ch}$ should be equal to the ratio of prompt coincidences $(AB-C)/(ABC)$(~0.12), this experimental check of $(ABC)_{del}^{ch}$ also is strong evidence that our value (0.003/hr.) of $(AB-C)_{del}^{ch}$ is estimated correctly.[f]

Direct evidence that the chance $(AB-C)_{del}$ rate at least does not greatly exceed our estimate is provided by the results of runs with thick lead absorbers (80 g/cm² and 95 g/cm²). In 369 hours only 2 $(AB-C)_{del}$ events were registered, while in the same time 9 $(AB)_{del}$

TABLE II. Delayed coincidence rates measured with various absorbers in arrangement of Fig. 1.

Absorber	Nominal absorber thickness g/cm²	Total absorber thickness g/cm²	Hours of observation	$(A)_{del}$ counts/hr.	$(B)_{del}$ counts/hr.	$(C)_{del}$ counts/hr.	$(B)_{del}+(C)_{del}$ counts/hr.	$(AB)_{del}$ counts/hr.	$(ABC)_{del}$ counts/hr.	$(AB-C)_{del}=(AB)_{del}-(ABC)_{del}$ counts/hr.
No absorber	0	4.2	408	1.56±0.06	4.0	8.5	12.5±0.2	0.82	0.05	0.77±0.05
Carbon	5.1	9.3	67	1.09±0.13	3.7	8.7	12.4±0.4	0.57	0.03	0.54±0.09
Carbon	13.6	17.8	142	0.53±0.06	4.9	9.2	14.1±0.3	0.21	0.04	0.17±0.04
Carbon	16.1	20.3	250	0.34±0.04	4.0	8.3	12.3±0.2	0.12	0.02	0.10±0.02
Carbon (16.1 g/cm²) +Iron (2.6 g/cm²)*	18.7	22.9	158	0.21±0.04	4.3	8.7	13.0±0.3	0.08	0.02	0.06±0.02
Carbon (13.6 g/cm²) +Copper (14.2 g/cm²)*	27.8	32.0	119	0.18±0.04	4.2	8.3	12.5±0.3	0.08	0.03	0.05±0.02
Aluminum	26.7	30.9	94	0.15±0.04	3.8	7.8	11.6±0.4	0.06	0.02	0.04±0.02
Lead	4.1	8.3	121	0.91±0.09	3.9	7.3	11.2±0.3	0.44	0.02	0.42±0.06
Lead	8.2	12.4	90	0.51±0.08	4.0	10.2	14.2±0.4	0.29	0.01	0.28±0.06
Lead	16.5	20.7	154	0.21±0.04	3.6	10.9	14.5±0.3	0.09	0.04	0.05±0.02
Lead	33.7	37.9	183	0.19±0.03	4.2	8.1	12.3±0.3	0.08	0.04	0.04±0.02
"Thick" lead**		~100	369	0.10±0.02	4.1	8.6	12.7±0.2	0.02	0.02	2 in 369 hours

* The maximum thickness of graphite for which there was sufficient space was 16.1 g/cm² (9.5 cm). When it was observed that an appreciable number of $(AB-C)_{del}$ events were recorded with this thickness, some of the graphite near tray A was removed, and replaced by denser material (iron or copper). In this way the total absorber thickness was increased without changing geometry, but at the sacrifice of homogeneity of absorber. However, it is probable that the results obtained in these cases are not very dissimilar to those which would have been obtained had the absorber consisted of the same thickness of pure carbon, for the first part of the decay particle path, where the rate of energy loss is most sensitive to change of Z, lies in the carbon as before.

** Combined results from two runs, one of 211 hours with 80 g/cm² lead, and one of 158 hours with 95 g/cm² lead; in both cases the lead was supported by 6 g/cm² steel.

[f] Some subsidiary tests, in which the low intensity chance delayed rates were increased by predictable factors to the point where they could be measured without difficulty, also supported the validity of our estimates.

TABLE III. Summary of results obtained with a copper source.

Absorber	Hours of observation	$(AB-C)_{del}$ Total counts	$(AB-C)_{del}$ Counts/hr.
No absorber	45	44	1.0
25 g/cm² lead	197	9	0.05

and 7 $(ABC)_{del}$ events were registered; all are consistent with the estimated chance rates.

Examination of the last column of Table II shows that the $(AB-C)_{del}$ rate is of the order of one per day for all absorbers having thicknesses in the range ~20 to 40 g/cm². Although these low rates have been measured with very poor accuracy, they are, nevertheless, over ten times the chance rate, and so can only be attributed to a very penetrating radiation associated with the meson decay. The immediate consequences of this result are discussed in the succeeding section, while an investigation of the nature of the penetrating radiation forms the subject of Part II of this paper.

In order to check quickly that the penetrating radiation is not associated *only with the decay of negative mesons*, the carbon source was replaced by a copper one of approximately the same area, and 23 g/cm² thick. Now, since all mesons stopped between trays B and C are brought to rest in copper (or brass), only radiation from the decay of *positive* mesons[8] can be responsible for any $(AB-C)_{del}$ effect observed. The essential results of the measurements with copper source, with and without a 25g/cm² lead absorber, are given in Table III. Since the chance rates are approximately the same as with the carbon source, the observed rate with the lead absorber is evidently a genuine decay effect, and establishes that the penetrating radiation is not exclusively a consequence of negative meson decay.

7. Discussion

The rates $(AB-C)_{del}$ presented in Table II are plotted against the total absorber thickness in Fig. 7. Here the reality of the existence of the penetrating radiation is apparent, and the distribution of points for all absorbers strongly suggests the division of the decay radiation into two components according to their relative penetration. Thus, for example, the "soft component" is essentially absorbed by about 25 g/cm² carbon; the "hard component," on the other hand, is easily detected after 38 g/cm² lead.

The interpretation of Fig. 7 must be conditioned by the following considerations: (i) The "geometry" of our experimental arrangement is poor—the ratio of thicknesses of absorber presented to decay particles incident normally, and at extreme inclination, is ~1:2.5; (ii) the statistical accuracy of the points is low because of the low decay particle intensity; (iii) it is inherently difficult to assess the effect of straggling in range of the decay particles due to scattering and to radiative collision (bremsstrahlung) energy losses. While the possibility of deriving the true energy spectrum of the decay particles is therefore immediately precluded, nevertheless certain observations based chiefly on consideration of maximum ranges can be made.

We shall use for reference the values of rate of energy loss and range for *electrons* of 25 and 50 Mev in different elements which are presented in Table IV. These values are calculated from approximate formulas according to Bloch, and to Bethe and Heitler,[21] with rough corrections for the Fermi polarization effect.[22] The quantities

TABLE IV. Approximate values of energy loss, range, and total energy radiated for electrons of 25 and 50 Mev in various elements. (Calculated with rough formulas of Bloch, Bethe, and Heitler.[21])

Element	Carbon		Aluminum		Copper		Lead	
Energy E_0 (Mev)	25	50	25	50	25	50	25	50
$-(dE/dx)_{coll}$ (Mev g⁻¹ cm²)	1.8	1.9	1.7	1.9	1.6	1.7	1.3	1.4
$-(dE/dx)_{rad}$ (Mev g⁻¹ cm²)	0.34	0.74	0.70	1.5	1.4	3.0	3.4	7.0
$-(dE/dx)_{tot}$ (Mev g⁻¹ cm²)	2.1	2.6	2.4	3.4	3.0	4.7	4.7	8.4
R_{max} (g cm⁻²)	14	26	15	27	17	30	19	37
R_{av} (g cm⁻²)	13	22	12	19	12	18	9.5	13
$(E_0)_{rad}$ (Mev)	2.1	7.9	4.2	14	7.3	22	13	33

are defined as follows:

$-(dE_0/dx)_{coll}$ is the average energy loss per unit path length by an electron of energy E_0 due to ionization collisions;

$-(dE_0/dx)_{rad}$ is the corresponding average energy loss due to radiation;

$-(dE_0/dx)_{tot}=-(dE_0/dx)_{coll}-(dE_0/dx)_{rad}$ is the average total energy loss per unit path length by an electron of energy E_0;

$R_{max}=\int_0^{E_0}\frac{dE}{-(dE/dx)_{coll}}$ is the maximum range (integrated path length) of an electron of initial energy E_0 (i.e., radiation loss omitted);

$R_{av}=\int_0^{E_0}\frac{dE}{-(dE/dx)_{tot}}$ is the average range (integrated path length) of an electron of initial energy E_0;

$(E_0)_{rad}$ is the average total energy lost as radiation by an electron of initial energy E_0 before it comes to rest.

We note first the considerable $(AB-C)_{del}$ rate observed with a carbon absorber thickness equivalent to

[21] See H. Bethe and W. Heitler, Proc. Roy. Soc. A **146**, 83 (1934); W. Heitler, *The Quantum Theory of Radiation* (Oxford University Press, London, 1944).

[22] E. Fermi, Phys. Rev. **57**, 485 (1940); G. C. Wick, Ricerca Scient. **12**, 858 (1941); O. Halpern and H. Hall, Phys. Rev. **73**, 477 (1948).

the *maximum* range of a 25 Mev electron (14 g/cm²). The two-particle decay hypothesis (Eq. (3)) for which all electrons have a unique energy ~25 Mev therefore is untenable. That the observed intensity (~0.3 count/hr.) could only be due in small part to bremsstrahlung from 25-Mev electrons may be seen from the following rough argument.[g] The total number of decay particles emitted within the solid angle of acceptance of the counters is ~0.8/hr. ($(AB-C)_{del}$ rate with no absorber). The average total energy radiated by a 25-Mev electron which starts in the carbon source, traverses the counter walls of tray B, and is stopped in the carbon absorber, is estimated to be <5 Mev. For simplicity, we assume that all photons are emitted in the forward direction, and neglect absorption. The maximum efficiency of a counter for detecting an incident photon is taken to be 1 percent/Mev. (See Part II, Section 7.) The counting rate which can be attributed to bremstrahlung assuming all decay particles to be electrons of initial energy 25 Mev is therefore

$$<0.8\times5\times0.01=0.04/\text{hr.}$$

At absorber thicknesses greater than the maximum range of a 50-Mev electron (26 g/cm² carbon), the $(AB-C)_{del}$ rate is ~0.04/hr. This rate we consider to represent the intensity of the "hard component," since it is not reduced very greatly by the introduction of even 38 g/cm² of lead. It might be pointed out here that most of the counting time in the absorption experiments was spent in establishing the reality of the "hard component."

To identify the "hard component" with charged particles is to invoke excessively high energies (e.g., up to 100 Mev or more) which cannot be accounted for by any μ-meson decay process. An alternative explanation is to attribute the effect to a neutral radiation which is associated with the meson decay process or its products, and which can give effects detectable by the counters.

One radiation which does have the required properties to explain qualitatively the "hard component" is the γ-radiation resulting from bremsstrahlung processes suffered by the charged decay particles. It may be noted, in fact, that the points of Fig. 7 suggest a stronger absorption[h] of the "soft component" in lead than in graphite; such a phenomenon would indicate a significant radiation loss. It has been shown above that the counting rate to be expected due to bremsstrahlung from 25-Mev electrons is <0.04/hr. A similar estimate for electrons of 50 Mev gives an *upper limit* of 0.10 counts/hr. The intensity of the "hard component" is not, therefore, inconsistent with the effect to be expected from bremsstrahlung, assuming that the decay particles are electrons, either negative (carbon source), or positive (carbon and copper sources). Furthermore, it may be noted that the relative intensities measured with the three thickest lead absorbers, although measured to a very low accuracy, are not in conflict with the expected[21] absorption coefficient for γ-radiation, which lies in the range 0.45 cm^{-1}–1 cm^{-1} for all energies between 1 and 50 Mev.

In Part II experiments are described which give strong evidence that the "hard component" is, in fact, bremsstrahlung from the particles constituting the "soft component."

Before passing to the description of these experiments, it may be useful to compare our absorption measurements with those of Steinberger.[13] As for the "soft component," our results are in agreement with his. Because his intensity was higher than ours (a much larger number of counters was used), Steinberger was able to analyze his absorption curves in more detail than we felt justified in doing. On the other hand, the fact that the casual rate in Steinberger's experiments was much higher than in our experiment made it impossible for him to investigate the "hard component."

PART II. THE BREMSSTRAHLUNG COMPONENT

1. General Considerations

Because of the limitations described in Part I which are attendant on the interpretation of the absorption measurements, and, in particular, of the effect observed with thick absorbers, attention was turned to an investigation of the nature of the "hard component." This work was directed toward determining two points: (1) whether or not a neutral radiation is responsible for the great penetrating power of the "hard component," and (2) the dependence of the observed intensity of the "hard component" on the atomic number of the absorber. Furthermore it evolved, from the results of these investigations, that it was possible to derive information on the mass of the charged decay particles from considerations of their radiative power.

The method used to investigate question (1) was

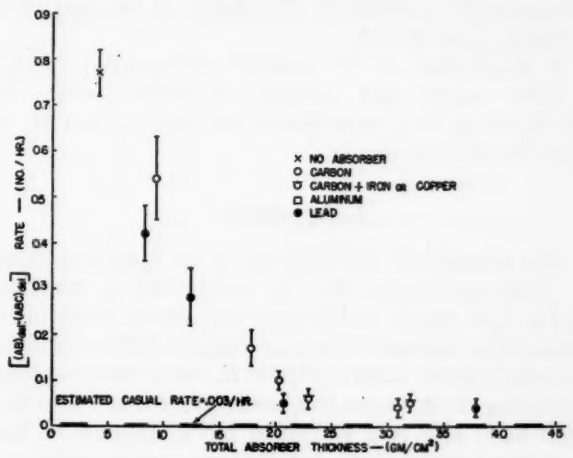

FIG. 7. Results of the absorption measurements. The $(AB-C)_{del}$ rates are plotted against the total absorber thickness for each element used.

[g] A more detailed consideration of this problem is given in Part II.

[h] For more conclusive evidence see Part II.

essentially to divide the (thick) decay particle absorber by an intermediate tray of counters. It is then possible to see whether or not a delayed coincidence due to the hard component (i.e., detected entering and leaving the total thick absorber) is accompanied by a discharge of the intermediate tray. Now, since the efficiency of the intermediate tray for detecting a charged decay particle must be high, the type of geometry (Fig. 1) used for the absorption measurements is unsuitable. Thus the possibility that the decay particle passes through a counter which has been rendered insensitive by the

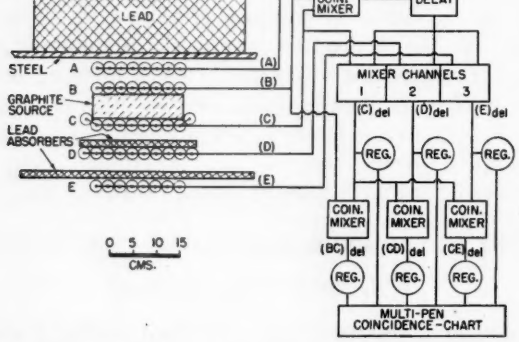

FIG. 8. Experimental arrangement for the detection of bremsstrahlung, with simplified block diagram of the circuits. The lengths of the counters and source are ~40 cm.

incoming meson itself, giving by the absence of a pulse from the intermediate tray an apparent but false anticoincidence, must be avoided. To do this the counters used to detect decay particles must be distinct from those used to detect the stopped mesons; the former have therefore been placed below the source for this experiment, and they detect decay particles travelling in a downward direction.

To observe the Z dependency of the "hard component," a similar arrangement of counters was used in which absorbers of carbon and lead could be interchanged with a minimum disturbance of the apparatus in every other respect.

A description of the counter arrangement, decay particle source, and counting apparatus, which is applicable to both experiments reported in Part II, is given in the next section.

2. Apparatus

The disposition, and function of the apparatus used in these experiments may be understood by referring to Fig. 8, in which the left-hand side shows the arrangement of counters and source (variations in the distances between counter trays C, D, and E, and in the absorbers occupying these spaces will be described later), and the right-hand side is a simplified block diagram of the counting circuits. Cathode-followers, wave-front amplifiers, and a threshold amplifier for tray B, have been omitted for simplicity (compare Figs. 1 and 3).

The counters used—15-inch copper counters in trays A and B, 16-inch brass counters in trays C, D, and E—are described in Part I, Section 2. In trays C and D the aluminum shelves that support the counters have been cut away opposite the sensitive areas of the latter, so that there is no solid material between the source and tray E other than the counter walls and the absorbers which may be inserted. The individual electronic circuits are described in Part I, Section 3.

Mesons stopped in the graphite source (20 cm×40 cm×8.5 g/cm² thick) are detected by the anticoincidence $(AB-C)$ as before. The delayed coincidence events $(C)_{del}$, $(D)_{del}$, or $(E)_{del}$, which may be due to a decay particle traversing trays C, D, or E between 1 and 6 microseconds after a meson stops, are selected by the three channels of the delay mixer. The outputs of these channels are mixed in pairs in two-channel coincidence mixers in order to observe events of the type $(CD)_{del}$ and $(CE)_{del}$. A third two-channel mixer accepts pulses from the first channel of the delay mixer ($(C)_{del}$ pulses) and from the "threshold output" from B, and therefore effectively detects events of the type $(BC)_{del}$. The $(BC)_{del}$, $(CD)_{del}$ and $(CE)_{del}$ pulses are recorded by different pens of an Esterline-Angus ten-pen "Operation Recorder" with a chart speed of 4 inches/hr. Since the rates of these pulses are always small (a few per hour, or less), it is convenient to detect coincidences or anticoincidences between these events by observing their correlation in time on the chart. We shall therefore refer to the ten-pen recorder as the "coincidence chart."

The events $(BC)_{del}$ are recorded in order to reduce the chance rate of delayed coincidences for the three lower trays; thus if an event $(C)_{del}$, $(D)_{del}$ or $(E)_{del}$ is accompanied by a discharge of tray B, we attribute it to the chance passage of a second meson, and disregard it. The significant delayed events defined with reference to the records on the coincidence chart are listed below: $(CD-B)_{del}$ refers to all $(CD)_{del}$ pulses non-coincident with a $(BC)_{del}$ pulse; $(CE-B)_{del}$ refers to all $(CE)_{del}$ pulses non-coincident with a $(BC)_{del}$ pulse; $(CDE-B)_{del}$ refers to those $(CE)_{del}$ pulses which are coincident with a $(CD)_{del}$ pulse, but non-coincident with a $(BC)_{del}$ pulse; $(CE-D-B)_{del}$ refers to those $(CE)_{del}$ pulses which are non-coincident with either a $(CD)_{del}$ pulse or with a $(BC)_{del}$ pulse. The more frequent delayed events $(C)_{del}$, $(D)_{del}$, and $(E)_{del}$ are also recorded separately on the chart, so that their time-distribution can be observed. Finally, another pen is used to indicate mains power failure.

3. Control Measurements

The various control measurements, and checks of the proper functioning of the apparatus, were essentially similar to those described in Part I, Section 4. They are listed briefly below, with comments only in those cases where there are significant differences from the procedures or data of Part I.

(*a*) *Continuous Checks.* (i) The triggering events $(AB-C)$ were counted continuously. The rate was between 75/min. and 80/min. for all runs, and, as expected, was not influenced by the absorbers. That the triggering rate is much higher than in Part I is due mainly to the smaller separation of trays A and B.

(ii) The rate $(C)_{del}$ was used as an over-all check of the "source strength," and sensitivity of the apparatus. No significant variations in this rate (18/hr.) were observed for all runs in which absorbers were present between trays C and D, and D and E; with these absorbers removed there were indications of a slight decrease ($\sim$1/hr. or less). This difference might be explained as being the contribution to $(C)_{del}$ from mesons which "leak" past tray C and decay in the absorber. In the absence of the source (and absorbers) the $(C)_{del}$ rate was $\sim$3/hr. of which we estimate that 0.5/hr. are chance, 0.5–1/hr. are due to decay particles from mesons stopped in counter walls, and the balance may be attributed to random counter lags.

(iii) All coincidence chart records were examined for evidence of spurious events or improper mixing.

(*b*) *Periodic Checks.* (i) The single counting rates for the separate trays were checked daily. Their magnitudes are illustrated by the following mean values obtained during the experiment described in Section 6 below (see Fig. 9, I or II); they are somewhat different for other variations of this geometry, or if the absorbers are removed.

$(A)=1015$/min.
$(B)=1060$/min.
$(C)=1585$/min.
$(D)=1560$/min.
$(E)=1285$/min.

(ii) Checks of voltages and pulse shapes were made as described in Part I.

(*c*) *Occasional Checks.*—(i) Check runs made with no decay particle absorbers will be referred to later. In each arrangement (Section 5, Section 6, below) a short run was made with the source removed as well, to verify that most of the counts which are attributed to decay particles disappeared.

(ii) Several of the occasional check measurements described in Part I were not made during this part of the work. They were felt to be unnecessary since (a) the apparatus was checked carefully at the beginning, (b) the runs described in Section 5 took a relatively short time, and (c) the measurements in Section 6 consisted of the periodic alternation of two conditions which were to be compared.

(iii) The various prompt coincidence rates required for computation of the chance delayed rates were measured for each variation of counter-absorber geometry. The typical set of rates given below applies to Section 6 (I and II); they would be somewhat different for the counter tray separations used in Section 5.

$(ABB-C)$ = 11±1/min.
(BC) =445±11/min.
(CD) =487±10/min.
$(CD-B)$ =202±7/min.
(CE) =267±7/min.
$(CE-B)$ =117±5/min.
$(CE-D)$ = 10.4±1.0/min.
$(CE-D-B)$= 3.6±0.5/min.

$(AB-C)$ = 78±1/min. (mean triggering rate).

Other rates required may be derived from the above; for example,

$$(BCDE)=(CE)-(CE-B)-(CE-D)+(CE-D-B), \text{ etc.}$$

4. Computation of Chance Rates

As in Part I, a knowledge of the chance rates of delayed coincidences of different types is essential in order to interpret the results correctly. Moreover, since in the most significant cases they are too low to measure easily, calculated values must be used. A discussion of the formulas which were used follows.

It should be noted that, for the arrangement shown in Fig. 8, corrections for dead counters and for instrumental dead-times are introduced only when trays B or D cancel chance delayed events. Thus chance rates as $(C)_{del}{}^{ch}$, $(D)_{del}{}^{ch}$, $(E)_{del}{}^{ch}$, $(CD)_{del}{}^{ch}$, $(CE)_{del}{}^{ch}$, etc., are given accurately by such expressions as

$$(C)_{del}{}^{ch}=(AB-C)(C)\tau,$$
$$(CD)_{del}{}^{ch}=(AB-C)(CD)\tau,$$

etc. On the other hand $(C-B)_{del}{}^{ch}$, $(CD-B)_{del}{}^{ch}$, $(CDE-B)_{del}{}^{ch}$ are given only *very approximately* by the simple relations:

$$(C-B)_{del}{}^{ch}\sim(AB-C)(C-B)\tau,$$
$$(CD-B)_{del}{}^{ch}\sim(AB-C)(CD-B)\tau,$$
$$(CDE-B)_{del}{}^{ch}\sim(AB-C)(CDE-B)\tau,$$

TABLE V. Chance rates computed for the experimental arrangements of Part II.

Type of event	Arrangements for the detection of neutral radiation (Section 5) Lead below C counts/hr.	Carbon below C counts/hr.	Arrangements I and II for testing the Z dependence (Section 6) counts/hr.
$(C-B)_{del}{}^{ch}$	0.4 ±0.1	0.5 ±0.1	0.5 ±0.1
$(CD-B)_{del}{}^{ch}$	0.11 ±0.01	0.09 ±0.01	0.10 ±0.01
$(CE-B)_{del}{}^{ch}$	0.08 ±0.01	0.05 ±0.01	0.06 ±0.01
$(CDE-B)_{del}{}^{ch}$	0.07 ±0.01	0.05 ±0.01	0.06 ±0.01
$(CE-D-B)_{del}{}^{ch}$	0.006±0.001	0.004±0.001	0.004±0.001

TABLE VI. Delayed coincidence rates with arrangement of Fig. 8—lead below C.

Condition	Hours of observation	$(CD-B)_{del}$ counts/hr.	$(CE-B)_{del}$ counts/hr.	$(CDE-B)_{del}$ counts/hr.	$(CE-D-B)_{de}$ counts/hr.
Without absorbers measured	21	9.0 ±0.7	4.8 ±0.5	4.6 ±0.5	~0.2 (3 counts)
With absorbers measured	103	0.56±0.08	0.19±0.05	0.09±0.03	0.10 ±0.03
Estimated chance	—	0.11±0.01	0.08±0.01	0.07±0.01	0.006±0.001

TABLE VII. Delayed coincidence rates with arrangement similar to Fig. 8—carbon below C.

Condition	Hours of observation	$(CD-B)_{del}$ counts/hr.	$(CE-B)_{del}$ counts/hr.	$(CDE-B)_{del}$ counts/hr.	$(CE-D-B)_{del}$ counts/hr.
Without absorbers measured	67	5.0 ±0.3	2.6 ±0.2	2.4 ±0.2	0.15 ±0.05
With absorbers measured	90	0.96±0.10	0.19±0.05	0.06±0.03	0.13 ±0.04
Estimated chance	—	0.09±0.01	0.05±0.01	0.05±0.01	0.004±0.001

for after a triggering event $(AB-C)$ we find *either* one dead counter in tray B which is impotent to cancel a delayed event, *or* a dead circuit in the $(BC)_{del}$ mixer (if two or more B counters fired) so that the whole B tray is ineffective for subsequent canceling. It follows then that, for example, $(CDE-B)_{del}^{ch}$ is given very closely by

$$(CDE-B)_{del}^{ch}=\langle[(AB-C)-(ABB-C)]\times[(CDE)-7/8(BCDE)]+(ABB-C)(CDE)\rangle\tau,$$

and similarly for other expressions containing $-B$.

The evaluation of the important rate $(CE-D-B)_{del}^{ch}$ is even more elaborate, and a detailed formulation will not be given here. We shall, however, describe the two chance sequences of events which contribute chiefly to the effect. First, a triggering event $(AB-C)$ may be followed by a chance $(CE-D-B)$ (e.g., by a meson which misses tray B, discharges C, "leaks" through D, and discharges E). Alternatively, a triggering event of the type $(ABD-C-E)$ (e.g., a meson discharges trays A and B, "leaks" through C, discharges D (whose circuit has a long dead-time), and misses E), is followed by a chance $(CE-B)$. The contributions to $(CE-D-B)_{del}^{ch}$ from both of these effects have been estimated, taking into account the corrections for dead counters and dead circuits, and turn out to be of comparable magnitude. Effects due to other combinations of events, in particular those due to the chance

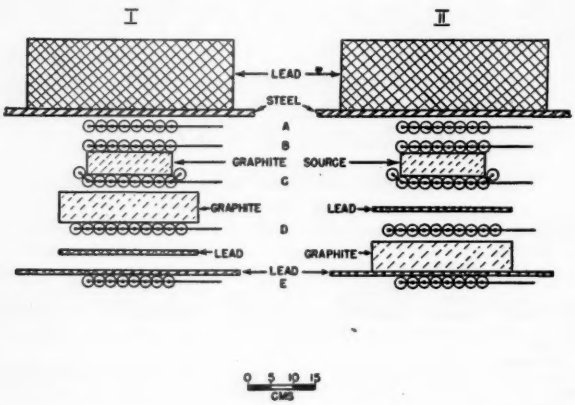

FIG. 9. Two arrangements which were alternated to compare the production of bremsstrahlung in carbon (I) and in lead (II). The circuits are identical to those indicated in Fig. 8.

TABLE VIII. Delayed coincidence rates for the two arrangements of Fig. 9 (corrected for chance events).

Arrangement	Hours of observation	$(CD-B)_{del}^{net}$ counts/hr.	$(CDE-B)_{del}^{net}$ counts/hr.	$(CE-D-B)_{del}^{net}$ counts/hr.
No absorbers	47	5.7 ±0.4	1.8 ±0.2	0.11 ±0.05
I. Carbon below C	392	1.50±0.07	0.02±0.02	0.046±0.013
II. Lead below C	392	1.02±0.06	0.01±0.02	0.13 ±0.02

coincidence of *three* independent events within the resolving time, are much smaller, and are neglected.

The computed values of chance rates for the more important delayed events are listed in Table V; the three columns of values are applicable to the two variations in geometry described in Section 5, and to the variation used in Section 6 (with either absorber arrangement I or II). The resolving time has been taken as 4.7±0.3 μsec.—the value used in Part I.

5. Detection of Neutral Radiation

In the first experiment designed to test whether a neutral radiation is responsible for the "hard component," the particular arrangement of absorbers shown in Fig. 8 was used. The separation between trays C and D (center to center) is 5.4 cm; that between trays D and E is 6.8 cm. The absorbers between trays C and D, and D and E, each consist of 16.5 g/cm² lead. These absorber thicknesses were chosen in order to prevent most of the "soft component" from reaching tray D, and at the same time to allow an appreciable intensity of "hard component" to be detected by tray E (see Fig. 7). Runs were made both with and without these two absorbers, and the measured rates of importance, together with the estimated chance rates for the condition "with absorbers," are given in Table VI.

It will be readily seen that the relative contributions of $(CDE-B)_{del}$ counts and $(CE-D-B)_{del}$ counts to the total $(CE-B)_{del}$ rate are quite different for the two conditions. Without absorbers, nearly all $(CE-B)_{del}$ events are accompanied by a discharge of D: the three $(CE-D-B)_{del}$ events represent about the fraction to be expected as a result of the geometrical transparency of the D tray. On the other hand, taking into account the expected chance rates calculated in Section 4 (Table V), and shown again in Table VI for comparison, it is apparent that with absorbers present few, if any, of the $(CE-B)_{del}$ decay events are accompanied by discharges of tray D. This demonstrates the production in the first part of the absorber (between C and D) of a neutral radiation which can traverse tray D without discharging it, but which may subsequently give rise to an ionizing radiation detected by tray E.

In order to establish the same character of the "hard component" in the case of low Z absorbers, a variation of the above experiment was carried out with the lead between C and D replaced by 13.6 g/cm² carbon. To accommodate the greater absorber thickness, the distance between trays C and D was increased to 13.0 cm.

The absorber between D and E was 16.5 g/cm² lead as before, with a D–E tray separation of 7.1 cm. The results of runs with and without the carbon and lead absorbers, and the estimated chance rate with absorbers, are presented in Table VII.

The data for carbon again demonstrate the presence of a neutral radiation in the "hard component." In view of both these results, the attribution of the "hard component" to bremsstrahlung from the particles of the "soft component" becomes very plausible.

6. Z Dependency of the "Hard Component"

The strong dependency on the atomic number of the stopping material which is characteristic of the bremsstrahlung process should provide a good test of the nature of the "hard component." Thus we see from Table IV that electrons of 25–50 Mev stopped in lead lose on the average more than half their energy by radiation; in carbon, on the other hand, most of their energy loss is by ionization. By comparing the intensities of the "hard component" with lead and carbon absorbers, under conditions in which changes in such factors as the geometry, the absorption of the "hard component," the sensitivity of the counters, etc., are reasonably constant, we can therefore determine whether they are consistent with those to be expected from bremsstrahlung. It should be noted that no attempt was made to keep these factors constant for the two arrangements already used which were described in the preceding section.

The two alternate arrangements of counters and absorbers chosen for comparison are shown in Fig. 9. Here the location of the counter trays is kept fixed, and lead and graphite absorbers are interchanged in position to give alternately the two sequences of counters and absorbers:

I. Tray C—11.0 g/cm² carbon—Tray D—8.2+8.2 g/cm² lead—Tray E;
II. Tray C—8.2 g/cm² lead—Tray D—11.0 g/cm² carbon+8.2 g/cm² lead—Tray E.

The circuits are those already shown in Fig. 8, and the operation of the apparatus has been described in Section 2 (Part II). A few points of particular significance for this experiment will be discussed.

It is convenient to use now the $(CE-D-B)_{del}$ rate as a measure of the "hard component" intensity. We conclude from the results of Section 5 that little or no intensity is sacrificed by doing this; on the other hand the fact that the chance rate for this type of event is so low is an indispensible advantage.

The selection and location of the absorbers is based on the following considerations. An 8.2 g/cm² thickness of lead is kept immediately above tray E for both arrangements I and II. The combination of lead and counters may then be considered together as a photon detector whose sensitivity is fairly independent of the other absorbers immediately above it. The result of the alternation in positions above and below D of the graphite absorber (11.0 g/cm²) and the other lead absorber (8.2 g/cm²) means that the events $(CE-D-B)_{del}$ are due in the one case (I) to neutral radiation produced in carbon, and in the other (II) to neutral radiation produced in lead. At the same time, the total absorbing material between C and E is kept constant. While neither carbon nor lead absorber between C and D is of sufficient thickness to completely remove the "soft component," the fraction left should be sufficiently degraded in energy that it cannot contribute much to the average total radiation (bremsstrahlung), and moreover, because of its penetration, it cannot have suffered appreciable radiation loss in the absorber above D. The significance of this will be seen below. The lead and carbon thicknesses were chosen (see Fig. 7) to stop roughly the same fraction of the "soft component" between C and D in the two arrangements. The lead is placed either above or below tray D at positions which correspond roughly to the center of the graphite in the alternative arrangement.

TABLE IX. Estimated $(CE-D)_{del}^{rad}$ rates due to bremsstrahlung for the two arrangements of Fig. 9.

Particles		$(CE-D)_{del}^{rad}$, counts/hr. Arrangement I	Arrangement II	Ratio: II/I
Electrons	25 Mev	0.015	0.037	2.5
	50 Mev	0.043	0.12	2.8
"Heavy electrons," mass $=2m_e$	25 Mev	0.004	0.015	4
	50 Mev	0.012	0.06	5

The positions of the graphite and lead absorbers were reversed about every three days, for a period of about one month. All check readings indicated that the apparatus behaved consistently throughout. A single run was made with all absorbers between C and E (including the lead immediately above E), removed. A summary of the important rates, from which the appropriate chance rates derived in Section 4 (Table V) have already been subtracted, is given in Table VIII.

The ratio of the $(CE-D-B)_{del}^{net}$ rate for arrangement II to that for arrangement I is 2.8±0.9. It will be shown in Section 7 that the $(CE-D-B)_{del}^{net}$ rates, and in particular their ratio, are consistent with the values to be expected if the neutral radiation is bremsstrahlung from electrons.

The $(CD-B)_{del}^{net}$ rates for arrangements I and II (Table VIII) are due essentially to the "soft component." We observe that the latter is, in fact, more strongly absorbed by 8.2 g/cm² lead than by 11.0 g/cm² carbon, as would be expected if the particles suffer appreciable radiation loss.

7. Discussion

We have estimated the $(CE-D-B)_{del}^{net}$ counting rates to be expected for the two arrangements described in Section 6 as a result of bremsstrahlung assuming that the radiating particles are electrons, responsible for

the observed "soft component" of the absorption curve. Estimates are made for initial electron energies of both 25 Mev and 50 Mev.

A fairly straightforward evaluation of the effect may be based on the fact that the efficiency of a counter for detection of a photon of energy E is approximately proportional to E.[22] This is true except for energies well below 1 Mev, and provided that the thickness of the counter wall is not less than the maximum range of the secondary Compton or pair electrons. In our case the fraction of the energy radiated which is accounted for by photons of <1 Mev is very small because of the form[21] of the radiation spectrum. It should also be noted that in each arrangement there is 8.2 g/cm² lead immediately above tray E. If ϵ (Mev^{-1}) is the efficiency of tray E (with the lead above) for detecting an incident photon per Mev of photon energy, N the number of electrons per hour of initial energy E_0 whose radiation may be assumed to travel in the direction of tray E, and $(E_0)_{\text{rad}}$ the average total energy (Mev) radiated per electron in the material above tray D, then the $(CE-D)_{\text{del}}$ rate[i] due to bremsstrahlung may be written approximately

$$(CE-D)_{\text{del}}^{\text{rad}}=\alpha\epsilon N(E_0)_{\text{rad}} \text{ counts/hr.}$$

The factor $\alpha(<1)$ accounts for the effective reduction in intensity due to absorption of the photons by the material between their point of origin and tray E. It may be approximated by the quantity $e^{-\tau_1 x_1-\tau_2 x_2}$, where τ_1 is a suitable average value of absorption coefficient in carbon over the energy range of the photons, x_1 is a suitable average value of the thickness of the carbon effective for absorption, and τ_2, x_2 are similar quantities for the lead. We have taken[21] for τ_1, 0.03 g^{-1} cm², and for τ_2, 0.06 g^{-1} cm². Since most of the radiative energy loss takes place in the uppermost part of the absorber between C and D, we cannot be greatly in error by taking for x_1 and x_2 the total thicknesses of carbon and lead respectively between C and E. It follows that α is approximately 0.3 for both arrangement I and arrangement II.

For ϵ we assume the value 0.01 Mev^{-1} to be appropriate for a counter with lead wall.[23]

If the angular spreading of the radiation is neglected, then N will be just the rate $(CDE)_{\text{del}}$ measured with no absorber, i.e., the rate of emission of decay electrons from the source, with appropriate delay, which travel in the direction of tray E. We consider this value to be reasonable since the angular divergence of bremsstrahlung at high energies is small,[21] and the loss in intensity due to the deviation of emitted photons from the paths of electrons directed towards tray E is partially compensated by the detection of photons produced by electrons traversing C but not directed towards E. It should be noted that if an electron penetrates the absorber between C and D, and discharges tray D, then any radiation which it may have emitted cannot contribute to the $(CE-D)_{\text{del}}^{\text{rad}}$ effect. The number of such electrons can be estimated and a small correction made for this loss.

Values of $(E_0)_{\text{rad}}$ are estimated in the following manner. Each electron is assumed to start with initial energy E_0 at the center of the source, and to travel always in a direction normal to the counter trays and absorbers. The average energy lost by both radiation and ionization in half the source thickness is computed, giving the average reduced energy E_1 with which the electron enters the C counter walls. Further estimates of radiation and ionization loss in the average thickness of brass in tray C give the average energy E_2 after traversing C. The total energy radiated by an electron of energy E_2 when stopped in carbon (arrangement I) or lead (arrangement II) is finally estimated. The various *radiation* energy losses are totalled to give $(E_0)_{\text{rad}}$. The values used for rate of energy loss by ionization and by radiation, and of total energy radiated, are derived from the formulas of Bloch, and Bethe-Heitler;[21] some of these values are given in Table IV.

The expected values $(CE-D)_{\text{del}}^{\text{rad}}$ for electrons with $E_0=25$ Mev and $E_0=50$ Mev, and for the two arrangements of Section 6 (Fig. 9), are given in Table IX.

It is difficult to evaluate the accuracy to be attached to these estimated rates; we believe they are at least correct to within a factor 2. However the ratio of the two rates for arrangements I and II is known to much better accuracy, for in this case the quantities α, ϵ, and N are not involved, and, because of the similarity in geometry between arrangements I and II, the ratio of counting rates becomes essentially equal to the ratio of the total energies radiated. Moreover this ratio is fairly insensitive to the initial electron energy in the range 25–50 Mev.

A comparison of the experimental values ($(CE-D-B)_{\text{del}}^{\text{net}}$, Table VIII) with the values in Table IX shows that both the counting rates observed in arrangements I and II, and their ratio, are consistent with the rates to be expected due to bremsstrahlung from electrons of 25–50 Mev.[j] The agreement in the values of the ratio is the stronger since, as indicated above, fewer assumptions are involved in deriving the estimated figure. It may be significant that the rates themselves are closer to those computed for 50-Mev electrons than for 25 Mev. This would indicate that the average energy is in fact greater than 25 Mev, but more quantitative estimates would not be justified.

The total energy lost by radiation by fast particles with a given charge and energy (or momentum) depends

[22] See, for example, Fowler, Lauritsen, and Lauritsen, Rev. Mod. Phys. **20**, 236 (1948); Bradt, Gugelot, Huber, Medicus, Preiswerk, and Scherrer, Helv. Phys. Acta **19**, 77 (1946).

[i] It is superfluous here to indicate that tray B is not discharged.

[j] A similar calculation for the absorption experiment (Part I) shows that bremsstrahlung should give a "background" effect of about the magnitude of the "hard component."

very sensitively on their mass. It is possible to conclude from this consideration that the decay particles that radiate in our apparatus are indeed electrons, or, more precisely, that they cannot have a mass much greater than one electron mass. In Table IX we have included values which were calculated for the hypothetical case of particles similar to electrons but with twice the mass ($M=2m_e$). Such "heavy electrons" could hardly produce the amount of bremsstrahlung observed, and of course hypothetical particles with $M>2m_e$ are discriminated against even more strongly. It is reasonable, therefore, to conclude that the charged decay particles are truly electrons, as is generally postulated. The evidence presented here based on their radiative property, is more decisive than evidence from their ionization in a cloud chamber or photographic plate. For example, Leighton, Anderson, and Seriff[18] recently obtained from cloud-chamber evidence a value of $10m_e$ for the upper limit of the mass of the charged decay particles. A similar case analyzed by Fletcher and Forster[24] gave a high probability (0.95) that the mass is less than $7m_e$.

Finally it may be pointed out why bremsstrahlung was not observed in some other experiments[10] designed to detect photons associated with the meson decay. The present authors, for example, looked without success for photons in coincidence with decay electrons in order to test a hypothetical electron-photon decay process (Eq. (2)). The counter arrangement for this experiment could only detect a photon travelling in approximately the opposite direction to the electron; it would thus not detect photons from the bremsstrahlung process, which are strongly concurrent in direction with the electrons. The same directional property would also make the bremsstrahlung difficult to observe in the arrangements of Sard and Althaus, and of Piccioni. In these experiments a photon from the "source" is first required to traverse an anticoincidence row of counters, and the probability that these would be discharged by the accompanying electron would be high for a "radiation" photon. In the present experiment this concurrence in direction of electron and photon is allowed, and in fact constitutes one of the arguments for the interpretation we have placed on our results.

CONCLUSIONS

Our study of the absorption of the charged particles emitted in the meson decay process, and the identification of a very penetrating "background" component with the photons resulting from the bremsstrahlung process, have lead to the following conclusions:

(1) The charged particles themselves are electrons, for if they were heavier (mass $2m_e$ or more) it would be difficult to account quantitatively for the observed intensity of the bremsstrahlung, and for the ratio of the intensities of such radiation produced in lead and carbon;

(2) The absorption curve obtained with carbon absorbers shows conclusively that at least a considerable number of electrons are emitted with energies greater than 25 Mev;

(3) A comparison of measured with calculated intensities of bremsstrahlung indicates that the *average* electron energy is greater than 25 Mev;

(4) The presence of bremsstrahlung obscures the observation of the *maximum* electron energy by absorption measurements. However, it is clear that to interpret our absorption curves, as well as those of Steinberger,[13] there is no need to invoke the presence of electrons of energy greater than $\sim$50 Mev.

The above conclusions referring to the energy of the charged particles are consistent with the extensive data recently obtained by Steinberger[13] (absorption technique), by Thompson[4] (cloud chamber), and by Leighton, Anderson and Seriff[18] (cloud chamber).

Our main conclusion referring to the mass of the charged decay particles excludes the possibility that a new type of meson (charged light meson or λ-meson) is emitted in the 2.2-μsec. decay, and adds to the body of evidence in support of the "electron+2 neutrinos" process (Eq. (5)), requiring a spin $\frac{1}{2}\hbar$ for the μ-meson. This evidence is summarized below with selected references:

(a) There is only one charged particle emitted in the 2.2-μsec. decay (Thompson, reference 4).

(b) The charged particle is an electron (present work).

(c) There are no high energy photons emitted in the 2.2-μsec. decay (reference 10).

(d) The charged particles are emitted with an apparently continuous distribution of energies extending up to about 55 Mev (reference 13 and especially 18).

(e) Assuming an "electron+2 neutrinos" process, the mass of the decaying meson can be calculated from the maximum energy of the decay electrons; the value obtained appears to be in very good agreement with the mass of the μ-meson measured[25] by other methods (reference 18).

(f) The average energy and the form of the energy spectrum of the decay electrons are, within the accuracy of theory and experiments, in agreement with theoretical expectations[26] for the "electron+2 neutrinos" process (reference 18).

(g) The discussions[27] of the experiments[28] on the production and on the nuclear capture of negative μ-mesons strongly suggest that their spin is $\frac{1}{2}\hbar$.

[24] J. C. Fletcher and H. K. Forster, Phys. Rev. **75**, 204 (1949).

[25] A. S. Bishop, Phys. Rev. **75**, 1468 (1949); R. B. Brode, Rev. Mod. Phys. **21**, 37 (1949).

[26] J. Tiomno and J. A. Wheeler, Rev. Mod. Phys. **21**, 144 (1949).

[27] B. Pontecorvo, Phys. Rev. **72**, 246 (1947); R. Serber, Phys. Rev. **75**, 1459 (1949); J. Tiomno and J. A. Wheeler, Rev. Mod. Phys. **21**, 153 (1949); R. E. Marshak, Phys. Rev. **75**, 700 (1949).

[28] Lattes, Occhialini, and Powell, Nature **160**, 453 and 486 (1947), and see also reference 17; E. Gardner and C. M. G. Lattes, Science **107**, 270 (1948); E. Gardner, Phys. Rev. **75**, 1468 (1949); A. S. Bishop, Phys. Rev. **75**, 1468 (1949); C. M. G. Lattes, Phys. Rev. **75**, 1468 (1949); O. Piccioni, reference 10; Sard, Ittner, Conforto, and Crouch, Phys. Rev. **74**, 97 (1948); W. Y. Chang, Rev. Mod. Phys. **21**, 166 (1949).

ACKNOWLEDGMENTS

We are deeply indebted to Mr. G. B. Parkinson for designing and supervising the construction of the delay mixer. Mr. F. MacDonald assisted us greatly in constructing the delay mixer, as well as other electronic apparatus. We wish to thank Miss E. Mooney and Miss C. Walker for their help in taking readings and checking the apparatus during the experiment. Finally, we acknowledge gratefully the interest and encouragement given by Dr. B. W. Sargent and Dr. W. B. Lewis.

PHYSICAL REVIEW VOLUME 77, NUMBER 1 JANUARY 1, 1950

A Study of the Spectra of Columbium and Molybdenum in the Extreme Ultraviolet

GEORGE W. CHARLES*
Mendenhall Laboratory of Physics, Ohio State University, Columbus, Ohio
(Received August 31, 1949)

The spectra of columbium and molybdenum in the range 100–1000A have been investigated. Spectrograms were obtained with a three-meter grazing incidence vacuum spectrograph having a dispersion of 1.0A/mm at 500A. The lines of Cb V and Mo VI previously reported have been remeasured. Attempts to find higher members of the series $4d-np$ and $4d-nf$ have proved fruitless except for the transition $4d-6p$ in Mo VI, for which tentative identification is given. Six low levels of Cb VI and Mo VII have been identified by extrapolation of frequencies in the Kr sequence. Some of the classifications are supported by considerations from theory. By applying a Rydberg formula to the transitions $4p^6-4p^55s$ and $4p^6-4p^56s$, the absolute value of the ground level of Cb VI is estimated to be 829,750 cm^{-1} and that of Mo VII is estimated to be 1,020,460 cm^{-1}.

The Br sequence has been extended to Cb VII and Mo VIII. The separations of the ground doublets were predicted by use of the regular doublet law. Forty-one lines of Cb VII and forty-two lines of Mo VIII have been identified by extrapolation of frequencies and application of the regular doublet law. These lines arise from transitions between the ground doublet arising from $4s^24p^5$ and the configurations $4s4p^6$, $4s^24p^44d$, and $4s^24p^45s$. The absolute values of the $^2P^\circ_{3/2}$ ground levels of Cb VII and Mo VIII are estimated to be 1,005,000 cm^{-1} and 1,235,000 cm^{-1}, respectively.

Results of an approximate calculation of the energy levels of the configuration p^4s in intermediate coupling are given and are compared with the observed levels in Cb VII and Mo VIII. The order of J-values is, with one exception, the same for the calculated levels as for the observed levels. The two sets of levels agree roughly, although the observed levels are more intimately mixed than the calculated levels.

INTRODUCTION

THE spectra of columbium have previously been investigated through Cb V and those of molybdenum through Mo VI (with the exception of Mo III).[1] In the present study, some of the low lying levels of higher stages of ionization of these metals are identified on the basis of extrapolations along isoelectronic sequences.

EXPERIMENTAL

The spectrograms upon which this investigation is based were obtained with the three-meter grazing incidence vacuum spectrograph at the Ohio State University; they cover the range 100–1000A. A condensed spark between electrodes of columbium or molybdenum wires in carbon and in copper was used to excite the spectra. Different stages of ionization were distinguished by varying the capacity from 0.1 to 1.8 μf, and by varying the inductance in the circuit. Exposures of two to four hours were made on Ilford Q-II plates. Standard wave-lengths in carbon, nitrogen, and oxygen were taken from the table of Boyce and Robinson;[2] those in copper were taken from the table of Kruger and Cooper.[3] A supplementary spectrogram of the copper spectrum was taken for the purpose of identifying copper lines not published in the table of Kruger and Cooper. It is estimated that the wave-lengths given below are accurate to 0.01A.

THE SPECTRA OF CB V AND MO VI

Classifications in these spectra isoelectronic with Rb I were given by Trawick;[4] Table I summarizes the measurements made on the classified lines lying in the range of the present instrument. The lines $4d\,^2D_{5/2}-4f\,^2F^\circ$ have now been resolved. The agreement between the present measurements and those of Trawick is quite satisfactory except for the multiplet $4d-4f$ in Mo VI; the present measurements place the $4f$ levels about 400 cm^{-1} lower than their position according to Trawick. Attempts to find higher members of the series $4d-np$ and $4d-nf$ by extrapolation of the quantum defects of the np and nf levels proved fruitless except for the transition $4d-6p$ in Mo VI, for which tentative identification is given in Table I.

Table II gives the relative values of the levels in these spectra, measured from $4d\,^2D_{3/2}$.

* Now at the University of Oklahoma, Norman, Oklahoma.
[1] W. F. Meggers, J. Opt. Soc. Am. 36, 435 (1946).
[2] J. C. Boyce and H. A. Robinson, J. Opt. Soc. Am. 26, 133 (1936).
[3] P. Gerald Kruger and F. S. Cooper, Phys. Rev. 44, 826 (1933).
[4] M. W. Trawick, Phys. Rev. 46, 63 (1934).

CLASSIFICATIONS IN THE SPECTRA OF CB VI AND MO VII

The spectra of the ions isoelectronic with neutral krypton have not been extensively studied. An analysis of the spectrum of Kr I was given by Meggers, de Bruin, and Humphreys[5] and supplemented by Meggers and Humphreys.[6] The spectrum of Rb II was analyzed by Laporte, Miller, and Sawyer.[7] No identifications have been made in the spectra of Sr III, Y IV, or Zr V. Therefore, some of the classifications proposed below for the low levels of Cb VI and Mo VII are regarded as subject to revision.

The starting point for the classification given here was the observation of the resonance lines $4p^6-4p^55s$ in Mo VII. These form a very striking pair near 200A, where there are no other strong lines, so that their identification was readily established. Interpolation of frequencies according to the method of Bowen and Millikan[8] then revealed a corresponding pair in Cb. These identifications are supported by considerations from the theory,[9] according to which we should expect the ratio of the separation of the two levels from $4p^5ns$ with $J=1$ to the separation of the two levels from $4p^5$ to be approximately constant through the sequence. Similar considerations led to the identification of the transition $4p^6-4p^56s$.

Table III shows the classifications made in the spectra of Cb VI and Mo VII by extrapolation of frequencies.

TABLE I. Classified lines of Cb V and Mo VI.

Rel. int.	λ_{vac}(A)	ν(cm^{-1})	Transition
		Cb V	
150	774.017	129196	$4d\ ^2D_{3/2}-5p\ ^2P^\circ_{\frac{1}{2}}$
300	763.752	130933	$4d\ ^2D_{5/2}-5p\ ^2P^\circ_{3/2}$
50	753.011	132800	$4d\ ^2D_{3/2}-5p\ ^2P^\circ_{3/2}$
25	468.627	213389	$4d\ ^2D_{5/2}-4f\ ^2F^\circ_{5/2}$
150	468.325	213525	$4d\ ^2D_{5/2}-4f\ ^2F^\circ_{7/2}$
100	464.555	215260	$4d\ ^2D_{3/2}-4f\ ^2F^\circ_{5/2}$
		Mo VI	
25	790.639	126480	$5p\ ^2P^\circ_{3/2}-6s\ ^2S_{\frac{1}{2}}$
15	760.997	131407	$5p\ ^2P^\circ_{\frac{1}{2}}-6s\ ^2S_{\frac{1}{2}}$
500	548.234	182404	$4d\ ^2D_{3/2}-5p\ ^2P^\circ_{\frac{1}{2}}$
1000	541.282	184747	$4d\ ^2D_{5/2}-5p\ ^2P^\circ_{3/2}$
150	533.820	187329	$4d\ ^2D_{3/2}-5p\ ^2P^\circ_{3/2}$
75	378.118	264469	$4d\ ^2D_{5/2}-4f\ ^2F^\circ_{5/2}$
400	377.540	264873	$4d\ ^2D_{5/2}-4f\ ^2F^\circ_{7/2}$
250	374.472	267043	$4d\ ^2D_{3/2}-4f\ ^2F^\circ_{5/2}$
150	298.358	335168	$4d\ ^2D_{5/2}-6p\ ^2P^\circ_{3/2}$(?)
100	297.326	336331	$4d\ ^2D_{3/2}-6p\ ^2P^\circ_{\frac{1}{2}}$(?)
15	296.087	337739	$4d\ ^2D_{3/2}-6p\ ^2P^\circ_{3/2}$(?)

TABLE II. Relative term values for Cb V and Mo VI.

Level	Rel. value (cm^{-1})	Level	Rel. value (cm^{-1})
Cb V		Mo VI	
$4d\ ^2D_{3/2}$	0	$4d\ ^2D_{3/2}$	0
$4d\ ^2D_{5/2}$	1869	$4d\ ^2D_{5/2}$	2578
$5p\ ^2P^\circ_{\frac{1}{2}}$	129196	$5p\ ^2P^\circ_{\frac{1}{2}}$	182404
$5p\ ^2P^\circ_{3/2}$	132800	$5p\ ^2P^\circ_{3/2}$	187329
$4f\ ^2F^\circ_{5/2}$	215260	$4f\ ^2F^\circ_{5/2}$	267043
$4f\ ^2F^\circ_{7/2}$	215394	$4f\ ^2F^\circ_{7/2}$	267451
		$6s\ ^2S_{\frac{1}{2}}$	313810
		$6p\ ^2P^\circ_{\frac{1}{2}}$(?)	336331
		$6p\ ^2P^\circ_{3/2}$(?)	337739

TABLE III. Classified lines of Cb VI and Mo VII.

Rel int.	λ_{vac}(A)	ν(cm^{-1})	Transition
		Cb VI	
250	325.795	306941	$4p^6\ p_0-4p^54d\ d_2^\circ$
250	248.724	402052	$4p^6\ p_0-4p^55s\ s_4^\circ$
400	238.176	419858	$4p^6\ p_0-4p^55s\ s_2^\circ$
25	180.548	553869	$4p^6\ p_0-4p^55d\ d_0^\circ$(?)
125	177.552	563215	$4p^6\ p_0-4p^55d\ d_2^\circ$(?)
100	170.180	587613	$4p^6\ p_0-4p^56s\ s_4^\circ$
75	164.977	606145	$4p^6\ p_0-4p^56s\ s_2^\circ$
		Mo VII	
200	286.294	349291	$4p^6\ p_0-4p^54d\ d_2^\circ$
500	207.774	481292	$4p^6\ p_0-4p^55s\ s_4^\circ$
800	198.839	502919	$4p^6\ p_0-4p^55s\ s_2^\circ$
75	149.639	668275	$4p^6\ p_0-4p^55d\ d_2^\circ$(?)
150	140.955	709446	$4p^6\ p_0-4p^56s\ s_4^\circ$
50	136.675	731663	$4p^6\ p_0-4p^56s\ s_2^\circ$

The first column gives relative intensities estimated visually; the other columns indicate wave-lengths, frequencies, and transitions, respectively. The notation used for levels is adapted from that used by Meggers, de Bruin, and Humphreys[5] for Kr I. The classifications in the transitions $4p^6-4p^54d$ and $4p^6-4p^55d$ rest upon a correlation of levels of the $4p^54d$ and $4p^55d$ configurations in Rb II[7] with those in Kr I,[6] and may be open to some question. Since the relative energy values are identical with the radiated frequencies, they are not repeated.

An estimate of the absolute values of the ground levels in Cb VI and Mo VII has been made by applying a Rydberg formula to the frequencies $4p^6\ p_0-4p^55s\ s_4^0$ and $4p^6\ p_0-4p^56s\ s_4^0$. The p_0 level of Cb VI is found to be 829,750 cm^{-1} below the $^2P^\circ_{3/2}$ level of Cb VII and the p_0 level of Mo VII to be 1,020,460 cm^{-1} below the $^2P^\circ_{3/2}$ level of Mo VIII. These values correspond to ionization potentials of 103 v and 127 v for Cb VI and Mo VII, respectively.

CLASSIFICATIONS IN THE SPECTRA OF CB VII AND MO VIII

These ions are isoelectronic with bromine. They have an inverted doublet ground state arising from $4s^24p^5$.

[5] Meggers, de Bruin, and Humphreys, Bur. Stand. J. Research 7, 643 (1931).
[6] W. F. Meggers and C. J. Humphreys, Bur. Stand. J. Research 10, 447 (1933).
[7] Laporte, Miller, and Sawyer, Phys. Rev. 38, 843 (1931).
[8] I. S. Bowen and R. A. Millikan, Phys. Rev. 26, 313 (1925).
[9] E. U. Condon and G. H. Shortley, *The Theory of Atomic Spectra* (The Cambridge University Press, New York, 1935), p. 271.

TABLE IV. Classified lines of Cb VII.

Rel. int.	λ_{vac}(A)	ν(cm^{-1})	Transition
150	517.281	193319	$4s^24p^5\ ^2P^\circ_{\frac{1}{2}}-4s4p^6\ ^2S_{\frac{1}{2}}$
300w	470.590	212499	$4s^24p^5\ ^2P^\circ_{3/2}-4s4p^6\ ^2S_{\frac{1}{2}}$
75	386.819	258519	$4s^24p^5\ ^2P^\circ_{\frac{1}{2}}-4s^24p^4(^3P')4d\ ^4D'_{3/2}$
200	378.901	263914	$4s^24p^5\ ^2P^\circ_{\frac{1}{2}}-4s^24p^4(^3P')4d\ ^4D'_{\frac{1}{2}}$
75	369.197	270858	$4s^24p^5\ ^2P^\circ_{3/2}-4s^24p^4(^3P')4d\ ^4D'_{5/2}$
150	360.099	277701	$4s^24p^5\ ^2P^\circ_{3/2}-4s^24p^4(^3P')4d\ ^4D'_{3/2}$
35	353.240	283094	$4s^24p^5\ ^2P^\circ_{3/2}-4s^24p^4(^3P')4d\ ^4D'_{\frac{1}{2}}$
10	325.386	307327	$4s^24p^5\ ^2P^\circ_{\frac{1}{2}}-4s^24p^4(^3P')4d\ ^4P'_{\frac{1}{2}}$
35	320.527	311986	$4s^24p^5\ ^2P^\circ_{\frac{1}{2}}-4s^24p^4(^3P')4d\ ^4P'_{3/2}$
20	316.043	316413	$4s^24p^5\ ^2P^\circ_{\frac{1}{2}}-4s^24p^4(^3P')4d\ ^2D'_{3/2}$
25	312.010	320503	$4s^24p^5\ ^2P^\circ_{\frac{1}{2}}-4s^24p^4(^3P')4d\ ^2P'_{\frac{1}{2}\text{ or }3/2}$
25	306.274	326505	$4s^24p^5\ ^2P^\circ_{3/2}-4s^24p^4(^3P')4d\ ^4P'_{\frac{1}{2}}$
150	301.960	331170	$4s^24p^5\ ^2P^\circ_{3/2}-4s^24p^4(^3P')4d\ ^4P'_{3/2}$
150	297.984	335588	$4s^24p^5\ ^2P^\circ_{3/2}-4s^24p^4(^3P')4d\ ^2D'_{3/2}$
35	297.556	336071	$4s^24p^5\ ^2P^\circ_{3/2}-4s^24p^4(^3P')4d\ ^4P'_{5/2}$
100	294.390	339686	$4s^24p^5\ ^2P^\circ_{3/2}-4s^24p^4(^3P')4d\ ^2P'_{\frac{1}{2}\text{ or }3/2}$
100	286.276	349314	$4s^24p^5\ ^2P^\circ_{3/2}-4s^24p^4(^3P')4d\ ^2D'_{5/2}$
150	274.219	364672	$4s^24p^5\ ^2P^\circ_{3/2}-4s^24p^4(^3P')4d\ ^2F'_{5/2}$
100	265.293	376942	$4s^24p^5\ ^2P^\circ_{\frac{1}{2}}-4s^24p^4(^1D')4d\ ^2D'_{3/2}$
50	263.417	379626	$4s^24p^5\ ^2P^\circ_{\frac{1}{2}}-4s^24p^4(^1D')4d\ ^2P'_{3/2}$
250	262.453	381021	$4s^24p^5\ ^2P^\circ_{3/2}-4s^24p^4(^1D')4d\ ^2D'_{5/2}$
100	261.434	382516	$4s^24p^5\ ^2P^\circ_{\frac{1}{2}}-4s^24p^4(^1D')4d\ ^2P'_{\frac{1}{2}}$
75	257.498	388353	$4s^24p^5\ ^2P^\circ_{\frac{1}{2}}-4s^24p^4(^1S')4d\ ^2D'_{3/2}$
25	252.448	396121	$4s^24p^5\ ^2P^\circ_{3/2}-4s^24p^4(^1D')4d\ ^2D'_{3/2}$
150w	251.973	396868	$4s^24p^5\ ^2P^\circ_{\frac{1}{2}}-4s^24p^4(^3P')5s\ ^4P'_{3/2}$
25	250.737	398824	$4s^24p^5\ ^2P^\circ_{3/2}-4s^24p^4(^1D')4d\ ^2P'_{3/2}$
25h	248.944	401697	$4s^24p^5\ ^2P^\circ_{3/2}-4s^24p^4(^1D')4d\ ^2P'_{\frac{1}{2}}$
250	247.979	403260	$4s^24p^5\ ^2P^\circ_{3/2}-4s^24p^4(^1S')4d\ ^2D'_{5/2}$
35	245.620	407133	$4s^24p^5\ ^2P^\circ_{\frac{1}{2}}-4s^24p^4(^3P')5s\ ^4P'_{\frac{1}{2}}$
25h	245.368	407551	$4s^24p^5\ ^2P^\circ_{3/2}-4s^24p^4(^1S')4d\ ^2D'_{3/2}$
50	240.351	416058	$4s^24p^5\ ^2P^\circ_{3/2}-4s^24p^4(^3P')5s\ ^4P'_{3/2}$
15	234.576	426301	$4s^24p^5\ ^2P^\circ_{3/2}-4s^24p^4(^3P')5s\ ^4P'_{\frac{1}{2}}$
100	234.260	426876	$4s^24p^5\ ^2P^\circ_{\frac{1}{2}}-4s^24p^4(^3P')5s\ ^2P'_{3/2}$
150	227.463	439632	$4s^24p^5\ ^2P^\circ_{\frac{1}{2}}-4s^24p^4(^3P')5s\ ^2P'_{\frac{1}{2}}$
200	224.737	444964	$4s^24p^5\ ^2P^\circ_{\frac{1}{2}}-4s^24p^4(^1D')5s\ ^2D'_{3/2}$
300	224.182	446066	$4s^24p^5\ ^2P^\circ_{3/2}-4s^24p^4(^3P')5s\ ^2P'_{3/2}$
500	219.746	455071	$4s^24p^5\ ^2P^\circ_{3/2}-4s^24p^4(^1D')5s\ ^2D'_{5/2}$
300	217.945	458831	$4s^24p^5\ ^2P^\circ_{3/2}-4s^24p^4(^3P')5s\ ^2P'_{\frac{1}{2}}$
400	215.444	464157	$4s^24p^5\ ^2P^\circ_{3/2}-4s^24p^4(^1D')5s\ ^2D'_{3/2}$
200	205.182	487372	$4s^24p^5\ ^2P^\circ_{\frac{1}{2}}-4s^24p^4(^1S')5s\ ^2S'_{\frac{1}{2}}$
100	197.415	506547	$4s^24p^5\ ^2P^\circ_{3/2}-4s^24p^4(^1S')5s\ ^2S'_{\frac{1}{2}}$

All other levels, except one, are formed by the addition of a valence electron to the configuration $4s^24p^4$ of the ion. The other level comes from $4s4p^6$. Most of the expected even levels from $4s^24p^44d$, $4s4p^6$, and $4s^24p^45s$ of Cb VII and Mo VIII have been identified in this investigation from their combinations with the ground doublet. It has not been possible to identify any combinations between these levels and higher odd levels, although some of them are expected to lie within the range covered.

The spectra of Br I,[10] Kr II,[11] Rb III,[12] Sr IV,[12] Y V,[13] and Zr VI[13] have been previously investigated. The screening constant in the regular doublet law was extrapolated from the results of these investigations. The doublet separation of the ground levels of Cb VII was then predicted to be about 19,100 cm^{-1}, and found experimentally to be 19,185 cm^{-1}. That for Mo VIII was predicted and found to be 23,280 cm^{-1}.

Table IV gives the lines classified in Cb VII, and Table VI gives those classified in Mo VIII, showing estimated relative intensity, wave-length, frequency, and transition. The symbols used in the intensity columns are those used in the M.I.T. wave-length tables.[14] For the sake of consistency, the L–S notation employed in previously reported classifications in this sequence has been retained, although it is no longer significant to use any quantum number except J. This has been indicated by using primed symbols. No levels of $J=5/2$ were identified in Rb III and Sr IV, therefore the levels of $J=5/2$ in the present paper are subject to some question. The assignments of $4s^24p^4(^3P')5s\ ^4P'_{\frac{1}{2}}$ and $4s^24p^4(^3P')5s\ ^4P'_{3/2}$ are not certain. The levels $4s^24p^4(^1S')4d\ ^2D'_{3/2,\,5/2}$ were not found in Br I nor in Rb III or Sr IV; the assignments given here are extrapolations from Y V and Zr VI. They are open to question since these levels might be expected to be separated from the levels $4s^24p^4(^1D')4d\ ^2D'$ by approximately the separation of the levels $4s^24p^4\ ^1S'$ and $4s^24p^4\ ^1D'$ of the ion, as is the case with $4s^24p^4(^1S')5s\ ^2S'$ and $4s^24p^4(^1D')5s\ ^2D'$. This would place the transition $4s^24p^5\ ^2P-4s^24p^4(^1S')4d\ ^2D'$ at shorter wave-length; no acceptable substitute assignment was found. Therefore, the assignments given in Tables IV and VI are retained for the present. The line $4s^24p^5\ ^2P^\circ_{3/2}-4s^24p^4(^1D')4d\ ^2F'_{5/2}$ could not be definitely established in either spectrum. Only one $4s^24p^4(^3P')4d\ ^2P'$ level can be identified, since there is serious doubt of the validity of the assignments in Y V and Zr VI. The J value can only be specified as $\frac{1}{2}$ or 3/2. The data indicate several possibilities for a

Table V. Relative energy level values for Cb VII.

Level	Rel. value (cm^{-1})	Level	Rel. value (cm^{-1})
$4s^24p^5\ ^2P^\circ_{3/2}$	0	$4s^24p^4(^1D')4d\ ^2D'_{5/2}$	381021
$4s^24p^5\ ^2P^\circ_{\frac{1}{2}}$	19185	$4s^24p^4(^1D')4d\ ^2D'_{3/2}$	396124
$4s4p^6\ ^2S_{\frac{1}{2}}$	212501	$4s^24p^4(^1D')4d\ ^2P'_{3/2}$	398817
$4s^24p^4(^3P')4d\ ^4D'_{5/2}$	270858	$4s^24p^4(^1D')4d\ ^2P'_{\frac{1}{2}}$(?)	401699
$4s^24p^4(^3P')4d\ ^4D'_{3/2}$	277702	$4s^24p^4(^1S')4d\ ^2D'_{5/2}$(?)	403260
$4s^24p^4(^3P')4d\ ^4D'_{\frac{1}{2}}$	283097	$4s^24p^4(^1S')4d\ ^2D'_{3/2}$(?)	407544
$4s^24p^4(^3P')4d\ ^4P'_{\frac{1}{2}}$	326509	$4s^24p^4(^3P')5s\ ^4P'_{3/2}$(?)	416055
$4s^24p^4(^3P')4d\ ^4P'_{3/2}$	331170	$4s^24p^4(^3P')5s\ ^4P'_{\frac{1}{2}}$	426310
$4s^24p^4(^3P')4d\ ^4P'_{5/2}$	336071	$4s^24p^4(^3P')5s\ ^2P'_{3/2}$	446064
$4s^24p^4(^3P')4d\ ^2P'_{\frac{1}{2}\text{ or }3/2}$	339687	$4s^24p^4(^3P')5s\ ^2P'_{\frac{1}{2}}$	458824
$4s^24p^4(^3P')4d\ ^2D'_{3/2}$	335593	$4s^24p^4(^1D')5s\ ^2D'_{5/2}$	455071
$4s^24p^4(^3P')4d\ ^2D'_{5/2}$	349314	$4s^24p^4(^1D')5s\ ^2D'_{3/2}$	464153
$4s^24p^4(^3P')4d\ ^2F'_{5/2}$	364672	$4s^24p^4(^1S')5s\ ^2S'_{\frac{1}{2}}$	506552

[10] C. C. Kiess and T. L. de Bruin, Bur. Stand. J. Research 4, 667 (1930).
[11] de Bruin, Humphreys, and Meggers, Bur. Stand. J. Research 11, 409 (1933).
[12] D. H. Tomboulian, Phys. Rev. 54, 350 (1938).
[13] F. W. Paul and W. A. Rense, Phys. Rev. 56, 1110 (1939).

[14] *Massachusetts Institute of Technology Wavelength Tables* (George R. Harrison, Editor) (John Wiley and Sons, Inc., New York, 1939), p. 429.

second $^2P'$ level, but there are no criteria for predicting its position. The $4s^24p^4(^3P')4d\ ^4F'$ levels were not found in Cb VII; their combinations in Mo VIII are quite faint.

The relative values of the energy levels measured from $4s^24p^5\ ^2P^\circ_{3/2}$ are given for Cb VII and Mo VIII in Table V and Table VII, respectively. An estimate of the absolute values of the ground levels may be made by extrapolating Moseley diagrams, keeping them parallel and at the same time making the difference of the squares of their ordinates equal to observed frequencies. This extrapolation has been made with $4s^24p^5\ ^2P^\circ_{3/2}$, $4s^24p^4(^3P')4d\ ^4D'_{3/2}$ and $4s^24p^4(^1D')4d\ ^2D'_{3/2}$. It is estimated that $4s^24p^5\ ^2P^\circ_{3/2}$ of Cb VII is 1,005,000 cm^{-1} below the ionization limit and $4s^24p^5\ ^2P^\circ_{3/2}$ of Mo VIII is 1,235,000 cm^{-1} below the corresponding limit. The ionization potentials are approximately 125 v for Cb VII and 153 v for Mo VIII.

TABLE VI. Classified lines of Mo VIII.

Rel. int.	λ_{vac}(A)	ν(cm^{-1})	Transition
250	474.941	210553	$4s^24p^5\ ^2P^\circ_{\frac{1}{2}}-4s4p^6\ ^2S_{\frac{1}{2}}$
1000w	427.660	233831	$4s^24p^5\ ^2P^\circ_{3/2}-4s4p^6\ ^2S_{\frac{1}{2}}$
150	348.252	287148	$4s^24p^5\ ^2P^\circ_{\frac{1}{2}}-4s^24p^4(^3P')4d\ ^4D'_{3/2}$
50	337.631	296181	$4s^24p^5\ ^2P^\circ_{\frac{1}{2}}-4s^24p^4(^3P')4d\ ^4D'_{\frac{1}{2}}$
200	331.612	301557	$4s^24p^5\ ^2P^\circ_{3/2}-4s^24p^4(^3P')4d\ ^4D'_{5/2}$
150	322.152	310412	$4s^24p^5\ ^2P^\circ_{3/2}-4s^24p^4(^3P')4d\ ^4D'_{3/2}$
25	313.033	319453	$4s^24p^5\ ^2P^\circ_{3/2}-4s^24p^4(^3P')4d\ ^4D'_{\frac{1}{2}}$
150	294.138	339977	$4s^24p^5\ ^2P^\circ_{\frac{1}{2}}-4s^24p^4(^3P')4d\ ^4P'_{\frac{1}{2}}$
50	290.111	344696	$4s^24p^5\ ^2P^\circ_{\frac{1}{2}}-4s^24p^4(^3P')4d\ ^4F'_{3/2}$
25	287.304	348063	$4s^24p^5\ ^2P^\circ_{\frac{1}{2}}-4s^24p^4(^3P')4d\ ^4P'_{3/2}$
250	283.412	352843	$4s^24p^5\ ^2P^\circ_{\frac{1}{2}}-4s^24p^4(^3P')4d\ ^2D'_{3/2}$
200	279.463	357829	$4s^24p^5\ ^2P^\circ_{\frac{1}{2}}-4s^24p^4(^3P')4d\ ^2P'_{\frac{1}{2}\text{ or }3/2}$
50	275.288	363256	$4s^24p^5\ ^2P^\circ_{3/2}-4s^24p^4(^3P')4d\ ^4P'_{\frac{1}{2}}$
20	271.871	367822	$4s^24p^5\ ^2P^\circ_{3/2}-4s^24p^4(^3P')4d\ ^4F'_{5/2}$
25	271.769	367960	$4s^24p^5\ ^2P^\circ_{3/2}-4s^24p^4(^3P')4d\ ^4F'_{3/2}$
100	269.287	371351	$4s^24p^5\ ^2P^\circ_{3/2}-4s^24p^4(^3P')4d\ ^4P'_{3/2}$
150	265.869	376125	$4s^24p^5\ ^2P^\circ_{3/2}-4s^24p^4(^3P')4d\ ^2D'_{3/2}$
150	264.629	377888	$4s^24p^5\ ^2P^\circ_{3/2}-4s^24p^4(^3P')4d\ ^4P'_{5/2}$
500	262.402	381095	$4s^24p^5\ ^2P^\circ_{3/2}-4s^24p^4(^3P')4d\ ^2P'_{\frac{1}{2}\text{ or }3/2}$
200	255.637	391179	$4s^24p^5\ ^2P^\circ_{3/2}-4s^24p^4(^3P')4d\ ^2D'_{5/2}$
150	244.263	409395	$4s^24p^5\ ^2P^\circ_{3/2}-4s^24p^4(^3P')4d\ ^2F'_{5/2}$
100	237.552	420960	$4s^24p^5\ ^2P^\circ_{\frac{1}{2}}-4s^24p^4(^1D')4d\ ^2D'_{3/2}$
25	236.886	422144	$4s^24p^5\ ^2P^\circ_{\frac{1}{2}}-4s^24p^4(^1D')4d\ ^2P'_{3/2}$
75	236.004	423722	$4s^24p^5\ ^2P^\circ_{3/2}-4s^24p^4(^1D')4d\ ^2D'_{5/2}$
250	231.998	431038	$4s^24p^5\ ^2P^\circ_{\frac{1}{2}}-4s^24p^4(^1S')4d\ ^2D'_{3/2}$
150h	225.102	444243	$4s^24p^5\ ^2P^\circ_{3/2}-4s^24p^4(^1D')4d\ ^2D'_{3/2}$
75	224.497	445440	$4s^24p^5\ ^2P^\circ_{3/2}-4s^24p^4(^1D')4d\ ^2P'_{3/2}$
500	223.270	447888	$4s^24p^5\ ^2P^\circ_{3/2}-4s^24p^4(^1S')4d\ ^2D'_{5/2}$
250	220.102	454298	$4s^24p^5\ ^2P^\circ_{3/2}-4s^24p^4(^1S')4d\ ^2D'_{3/2}$
50	213.126	469206	$4s^24p^5\ ^2P^\circ_{\frac{1}{2}}-4s^24p^4(^3P')5s\ ^4P'_{3/2}$
25	208.319	480033	$4s^24p^5\ ^2P^\circ_{\frac{1}{2}}-4s^24p^4(^3P')5s\ ^4P'_{\frac{1}{2}}$
100	203.042	492509	$4s^24p^5\ ^2P^\circ_{3/2}-4s^24p^4(^3P')5s\ ^4P'_{3/2}$
100	198.686	503307	$4s^24p^5\ ^2P^\circ_{3/2}-4s^24p^4(^3P')5s\ ^4P'_{\frac{1}{2}}$
150	198.351	504157	$4s^24p^5\ ^2P^\circ_{\frac{1}{2}}-4s^24p^4(^3P')5s\ ^2P'_{3/2}$
75	192.283	520067	$4s^24p^5\ ^2P^\circ_{\frac{1}{2}}-4s^24p^4(^3P')5s\ ^2P'_{\frac{1}{2}}$
300	190.243	525644	$4s^24p^5\ ^2P^\circ_{\frac{1}{2}}-4s^24p^4(^1D')5s\ ^2D'_{3/2}$
750	189.602	527421	$4s^24p^5\ ^2P^\circ_{3/2}-4s^24p^4(^3P')5s\ ^2P'_{3/2}$
600	186.376	536550	$4s^24p^5\ ^2P^\circ_{3/2}-4s^24p^4(^1D')5s\ ^2D'_{5/2}$
600	184.050	543360	$4s^24p^5\ ^2P^\circ_{3/2}-4s^24p^4(^3P')5s\ ^2P'_{\frac{1}{2}}$
400	182.179	548911	$4s^24p^5\ ^2P^\circ_{3/2}-4s^24p^4(^1D')5s\ ^2D'_{3/2}$
150	174.891	571785	$4s^24p^5\ ^2P^\circ_{\frac{1}{2}}-4s^24p^4(^1S')5s\ ^2S'_{\frac{1}{2}}$
100	168.050	595061	$4s^24p^5\ ^2P^\circ_{3/2}-4s^24p^4(^1S')5s\ ^2S'_{\frac{1}{2}}$

TABLE VII. Relative energy level values for Mo VIII.

Level	Rel. value (cm^{-1})	Level	Rel. value (cm^{-1})
$4s^24p^5\ ^2P^\circ_{3/2}$	0	$4s^24p^4(^3P')4d\ ^2F'_{5/2}$	409395
$4s^24p^5\ ^2P^\circ_{\frac{1}{2}}$	23277	$4s^24p^4(^1D')4d\ ^2D'_{5/2}$	423722
$4s4p^6\ ^2S_{\frac{1}{2}}$	233830	$4s^24p^4(^1D')4d\ ^2D'_{3/2}$	444240
$4s^24p^4(^3P')4d\ ^4D'_{5/2}$	301557	$4s^24p^4(^1D')4d\ ^2P'_{\frac{1}{2}\text{ or }3/2}$	445430
$4s^24p^4(^3P')4d\ ^4D'_{3/2}$	310419	$4s^24p^4(^1S')4d\ ^2D'_{5/2}$(?)	447888
$4s^24p^4(^3P')4d\ ^4D'_{\frac{1}{2}}$(?)	319456	$4s^24p^4(^1S')4d\ ^2D'_{3/2}$(?)	454307
$4s^24p^4(^3P')4d\ ^4P'_{\frac{1}{2}}$	363255	$4s^24p^4(^3P')5s\ ^4P'_{3/2}$(?)	492522
$4s^24p^4(^3P')4d\ ^4F'_{5/2}$	367822	$4s^24p^4(^3P')5s\ ^4P'_{\frac{1}{2}}$	503309
$4s^24p^4(^3P')4d\ ^4F'_{3/2}$	367967	$4s^24p^4(^3P')5s\ ^2P'_{3/2}$	527428
$4s^24p^4(^3P')4d\ ^4P'_{3/2}$	371345	$4s^24p^4(^1D')5s\ ^2D'_{5/2}$	536550
$4s^24p^4(^3P')4d\ ^2D'_{3/2}$	376122	$4s^24p^4(^3P')5s\ ^2P'_{\frac{1}{2}}$	543352
$4s^24p^4(^3P')4d\ ^4P'_{5/2}$	377888	$4s^24p^4(^1D')5s\ ^2D'_{3/2}$	548916
$4s^24p^4(^3P')4d\ ^2P'_{\frac{1}{2}\text{ or }3/2}$	381102	$4s^24p^4(^1S')5s\ ^2S'_{\frac{1}{2}}$	595062
$4s^24p^4(^3P')4d\ ^2D'_{5/2}$	391179		

THEORETICAL CONSIDERATIONS

During the consideration of the configuration $4p^45s$ in Cb VII and Mo VIII, an approximate calculation of the energy levels to be expected in intermediate coupling was made, using the matrices of electrostatic energy and spin-orbit interaction given for p^2s by Condon and Shortley. The electrostatic part of the energy matrix is the same for p^4s as for p^2s.[15] The matrix of spin-orbit interaction for p^4s may be obtained from that for p^2s by reversing the sign of the parameter ζ_p.[16] The secular determinant for $J=5/2$ leads to a quadratic equation, while those for $J=3/2$ and for $J=\frac{1}{2}$ yield cubic equations in the energy. As an example, the secular determinant for $J=3/2$ is

$$\begin{vmatrix} F-G-E' & -(\sqrt{3})^{\frac{1}{2}}/6\,\zeta_p & (15)^{\frac{1}{2}}/6\,\zeta_p \\ -(\sqrt{3})^{\frac{1}{2}}/6\,\zeta_p & 1/3\,\zeta_p-5F & (5)^{\frac{1}{2}}/6\,\zeta_p \\ & -2G-E' & \\ (15)^{\frac{1}{2}}/6\,\zeta_p & (5)^{\frac{1}{2}}/6\,\zeta_p & -1/3\,\zeta_p-5F \\ & & +G-E' \end{vmatrix} = 0.$$

In this determinant, E' is written for $E-F_0$.

When this is expanded and powers of G/F higher than the first are neglected, the equation becomes

$$\begin{aligned}(E'/F)^3&+(9+2G/F)(E'/F)^2\\ &-(75\chi^2/4-15-14G/F-5\chi G/F)(E'/F)\\ &-(225\chi^2/4+25-125\chi^3/4+25\chi^2G/F\\ &\qquad -20G/F+5\chi G/F)=0,\end{aligned}$$

where χ is written for $\zeta_p/5F$. We assume that this

[15] See reference 9, p. 299. The energies are given on p. 199.
[16] See reference 9, p. 301. The matrix for p^3s is given on p. 268.

equation is of the form

$$(E'/F-x/F+lG/F)(E'/F-y/F+mG/F)\times(E'/F-z/F+nG/F)=0,$$

where x and y are the energy values for the levels of p^4 belonging to $J=2$, while z is the value for the level belonging to $J=1$.

$$x/F=-2-5\chi/4+(9+15\chi/2+225\chi^2/16)^{\frac{1}{2}},$$
$$y/F=-2-5\chi/4-(9+15\chi/2+225\chi^2/16)^{\frac{1}{2}},$$
$$z/F=-5+5\chi/2.$$

Equating coefficients of like powers of G/F, we obtain equations for l, m, and n which yield the solutions

$$l=1/4+(3/4+5\chi/16)(1+5\chi/6+25\chi^2/16)^{-\frac{1}{2}},$$
$$m=1/4-(3/4+5\chi/16)(1+5\chi/6+25\chi^2/16)^{-\frac{1}{2}},$$
$$n=3/2.$$

Thus the energy levels are given by

$(^1D_2')_{J=3/2}$:

$$(E-F_0)/F=-2-5\chi/4+3(1+5\chi/6+25\chi^2/16)^{\frac{1}{2}}-G/F[1/4+(3/4+5\chi/16)(1+5\chi/6+25\chi^2/16)^{-\frac{1}{2}}],$$

$(^3P_2')_{J=3/2}$:

$$(E-F_0)/F=-2-5\chi/4-3(1+5\chi/6+25\chi^2/16)^{\frac{1}{2}}-G/F[1/4-(3/4+5\chi/16)(1+5\chi/6+25\chi^2/16)^{-\frac{1}{2}}],$$

$(^3P_1)_{J=3/2}$: $(E-F_0)/F=-5+5\chi/2-3G/2F.$

In the same manner, we obtain for $J=5/2$

$(^1D_2')_{J=5/2}$:

$$(E-F_0)/F=-2-5\chi/4+3(1+5\chi/6+25\chi^2/16)^{\frac{1}{2}}-G/F[3/2-(1/2+5\chi/24)(1+5\chi/6+25\chi^2/16)^{-\frac{1}{2}}],$$

$(^3P_2')_{J=5/2}$:

$$(E-F_0)/F=-2-5\chi/4-3(1+5\chi/6+25\chi^2/16)^{\frac{1}{2}}-G/F[3/2+(1/2+5\chi/24)(1+5\chi/6+25\chi^2/16)^{-\frac{1}{2}}].$$

For $J=\frac{1}{2}$, we find

$(^3P_1)_{J=\frac{1}{2}}$: $(E-F_0)/F=-5+5\chi/2,$

$(^1S_0')_{J=\frac{1}{2}}$: $(E-F_0)/F=5/2+5\chi/2+15/2(1-2\chi/3+\chi^2)^{\frac{1}{2}}-G/F,$

$(^3P_0')_{J=\frac{1}{2}}$: $(E-F_0)/F=5/2+5\chi/2-15/2(1-2\chi/3+\chi^2)^{\frac{1}{2}}-G/F.$

The variation of $\chi^{\frac{1}{2}}$ with Z is approximately linear along an isoelectronic sequence.[17] Using this relation with the data of Table VII of the paper by Robinson and Shortley,[17] we estimate χ to be 0.97 for Cb and 1.13 for Mo. Putting these values in the above equations, we obtain the following expressions for the energy values in the form $(E-F_0)/F$:

Level	Cb	Mo
$(^1D_2')_{J=5/2}$	$2.21-1.11\ G/F$	$2.53-1.13\ G/F$
$(^3P_2')_{J=5/2}$	$-8.65-1.89\ G/F$	$-9.35-1.87\ G/F$
$(^1D_2')_{J=3/2}$	$2.21-0.83\ G/F$	$2.53-0.81\ G/F$
$(^3P_1)_{J=3/2}$	$-2.57-1.50\ G/F$	$-2.18-1.50\ G/F$
$(^3P_2')_{J=3/2}$	$-8.65+0.33\ G/F$	$-9.35+0.31\ G/F$
$(^1S_0')_{J=\frac{1}{2}}$	$13.48-1.00\ G/F$	$14.57-1.00\ G/F$
$(^3P_1)_{J=\frac{1}{2}}$	-2.57	-2.18
$(^3P_0')_{J=\frac{1}{2}}$	$-3.62-1.00\ G/F$	$-3.93-1.00\ G/F$

With the exception of the inversion of $(^1D_2')_{J=5/2}$ and $(^3P_1)_{J=\frac{1}{2}}$, the order of levels predicted by the above considerations is the same as that observed experimentally. Furthermore, the predictions of the theory agree roughly with the observed positions of the levels. Since the energy differences between levels are functions of the parameters F and G, two observed differences may be used to calculate F and G and the other intervals calculated. For this purpose, the intervals chosen were that between $(^1S_0')_{J=\frac{1}{2}}$ and $(^1D_2')_{J=3/2}$ and that between $(^1S_0')_{J=\frac{1}{2}}$ and $(^3P_1)_{J=3/2}$. For Cb, one obtains the equations

$$11.27F-0.17G=42399\ \text{cm}^{-1},$$
$$16.05F+0.50G=60488\ \text{cm}^{-1}$$

from which $F=3764$ cm^{-1}, $G=142$ cm^{-1}. For Mo, the equations are

$$12.04F-0.19G=46146\ \text{cm}^{-1},$$
$$16.75F+0.50G=67634\ \text{cm}^{-1}$$

from which $F=3904$ cm^{-1}, $G=4494$ cm^{-1}. Using these parameters in the remaining expressions for energy intervals, we obtain the values given in the first and third columns of Table VIII for the relative level values. The observed values are given in the second and fourth columns.

TABLE VIII. Comparison of relative level values.

Level	Cb Calculated value (cm^{-1})	Cb Observed value (cm^{-1})	Mo Calculated value (cm^{-1})	Mo Observed value (cm^{-1})
$(^1S_0')_{J=\frac{1}{2}}$	506552	506552	595062	595062
$(^1D_2')_{J=3/2}$	464153	464153	548916	548916
$(^1D_2')_{J=5/2}$	464116	455071	547474	536550
$(^3P_0')_{J=\frac{1}{2}}$	442188	426310	522838	503309
$(^3P_1)_{J=\frac{1}{2}}$	446282	458824	534164	543352
$(^3P_1)_{J=3/2}$	446064	446064	527428	527428
$(^3P_2')_{J=3/2}$	423444	416055	507565	492522
$(^3P_2')_{J=5/2}$	423127		497768	

Although the calculated and observed values are roughly equal, the observed levels are more intimately mixed than the calculated levels.

[17] H. A. Robinson and G. H. Shortley, Phys. Rev. **52**, 720 (1937).

Electronic Specific Heats in Tungsten and Zinc

A. A. SILVIDI AND J. G. DAUNT
Mendenhall Laboratory, Ohio State University, Columbus, Ohio

(Received September 19, 1949)

Calorimetric measurements have been made in the liquid helium temperature region on tungsten and zinc. For tungsten, the specific heat could be resolved into a lattice T^3 function with Debye $\theta=169°K$ and an electronic term γT with $\gamma=51.1\times10^{-4}$ cal./mole/degree^2. The anomalously low θ-value may indicate the existence of a hidden transition at low temperatures. A discussion is given of the high value of γ and it is suggested that a recalculation of the energy spectrum at both high and low temperatures may be required and that correlation forces may be partly responsible for the observed result. For zinc, measurements were also carried out on a powder with average particle size $=1.3\times10^{-4}$ cm in order to assess the significance of size effects. The results showed that the powder had a specific heat identical with that for zinc in bulk, given by a Debye $\theta=291°K$ and an electronic term γT with $\gamma=1.50\times10^{-4}$ cal./mole/degree^2.

1. INTRODUCTION

LOW temperature calorimetric measurements in the liquid helium temperature region have been carried out on tungsten and zinc and are reported herewith. By making the generally accepted assumption that at sufficiently low temperatures the measured specific heat is the sum of two terms, one proportional to T^3 caused by the lattice vibrations and the other proportional to T caused by the electronic contribution, it is possible to assess the specific heats of the lattice and of the electrons separately.

In the case of tungsten a measurement of the specific heat appeared to be of twofold interest. In the first place, no measurements had been previously made below 25°K[1] although detailed computations had been carried out on the electronic energy spectrum by Manning and Chodorow[2] and on the lattice vibrational energy by Fine[3] which could only be checked by very low temperature measurement. In the second place, the electronic energy of the transition elements has been the subject of many investigations in view of the high values of the density of states these elements exhibit[4] and it seemed worth while to extend measurements to include for the first time a metal in group 6 of the periodic table.

The measurements on zinc were carried out partly as a check on other measurements of the electronic specific heat in zinc simultaneously being carried out in the same laboratory by an entirely different method[5] and partly in order to investigate the possible existence of size effects in a powder having small average linear dimensions and at the same time a high purity.

2. EXPERIMENTAL ARRANGEMENTS

(a) The Tungsten Specimen

The tungsten was obtained from the Fansteel Corporation and had a stated purity of 99.9+ percent. The specimen was cylindrical, 7.31 cm long, 1.585-cm diameter and mass of 271.17 g.

The thermometer wire was of leaded phosphor-bronze (diameter 0.002 in.) kindly given to us by Dr. M. C. Desirant and it showed a satisfactory variation of resistance with temperature in the liquid helium range. It was wound on the outside of the specimen together with the electrical heater coil which was of manganin wire (0.0031-in. diameter). The mass of the thermometer and heater coils was 0.030 g, and the coils were insulated from and secured to the specimen by thin layers of varnish. Finally a radiation shield of tin foil of mass 0.153 g covered the entire specimen. The electrical leads to the heater and thermometer coils were of tantalum wire, 0.007-in. diameter, which were maintained at the temperature of the liquid helium bath ($<4.2°K$) at their upper ends. These leads, therefore, were superconducting during the experiments and so electrical and thermal losses were minimized.

(b) The Zinc Specimen

The zinc was obtained from Mallinckradt Chemical Works in the form of powder, of average grain diameter 1.3×10^{-4} cm. A spectrographic analysis revealed a purity of 99.9 percent with a largest single impurity of Pb of about 0.1 percent. For the first measurements on the zinc, 53.347 g of the powder were placed in a small copper vessel, of mass 16.48 g, together with 3×10^{-7} mole of pure helium gas to serve as heat exchanger. This helium gas was admitted through a small tube attached to the copper vessel, after the powder has been thoroughly degassed and subsequently this tube was sealed off.

Thermometer and heater coils, similar to those used for the tungsten, were wound on the copper vessel with suitable varnish insulation and a tin foil radiation shield, of mass 0.153 g. Subsequent measurements on zinc were made on a specimen formed by fusing the powder in vacuum into the form of a solid cylinder of length 8.0 cm, diameter 1.28 cm, and of mass 65.026 g. Thermometer and heater wires, again similar to those used for the tungsten, were wound directly on the zinc cylinder with suitable varnish insulation and again a

[1] Lange, Zeits. f. physik. Chemie **110**, 343 (1924).
[2] M. F. Manning and M. I. Chodorow, Phys. Rev. **56**, 787 (1939). (See also H. Jones and N. F. Mott, Proc. Roy. Soc. **A162**, 49 (1937).
[3] P. C. Fine, Phys. Rev. **56**, 355 (1939).
[4] See N. F. Mott and H. Jones, Properties of Metals and Alloys (Oxford University Press, New York, 1936).
[5] J. G. Daunt and C. V. Heer, Phys. Rev. **76**, 1324 (1949).

TABLE I. Data on specific heat of the tungsten specimen.

Points	Heater Voltage volts $\times 10^{-3}$	Heater Time sec.	Current amp. $\times 10^{-3}$	$\Delta Q \times 10^{-3}$ cal./mole	ΔT°K	T°K	C_v $\times 10^{-3}$ cal./mole-deg.
May 4th, 1949. Thermometer measuring current = 0.2 ma							
1	53.9	65.0	1.222	0.699	0.063	2.063	11.01
2	53.9	119.8	1.222	1.294	0.110	2.140	11.75
3	53.9	119.8	1.222	1.294	0.098	2.229	13.20
4	53.9	119.8	1.222	1.294	0.103	2.273	12.55
5	53.9	119.8	1.222	1.294	0.101	2.320	12.81
6	53.9	179.5	1.222	1.935	0.145	2.377	13.32
7	53.9	181.0	1.222	1.951	0.140	2.430	13.95
8	53.9	150.4	1.222	1.620	0.105	2.675	15.40
9	53.9	149.9	1.222	1.615	0.097	2.738	16.65
10	53.9	179.3	1.222	1.930	0.110	2.895	17.55
11	53.9	119.2	1.222	1.280	0.070	2.955	18.30
May 9th, 1949. Thermometer measuring current = 0.4 ma							
1	84.7	119.9	1.776	2.955	0.339	1.686	8.70
2	84.7	120.0	1.796	2.990	0.307	1.793	9.74
3	84.7	99.9	1.786	2.471	0.252	1.849	9.81
4	84.7	120.0	1.786	2.970	0.281	1.953	10.56
5	84.7	120.0	1.776	2.962	0.265	2.027	11.17
6	84.7	120.5	1.776	2.970	0.257	2.128	11.55
7	84.7	59.5	1.776	1.465	0.120	2.135	12.21
May 16th, 1949. Thermometer measuring current = 0.4 ma							
1	84.7	60.2	1.766	1.481	0.185	1.533	8.00
2	84.7	90.2	1.766	2.210	0.265	1.593	8.34
3	84.7	90.5	1.766	2.210	0.253	1.614	8.73
4	84.7	90.0	1.766	2.189	0.250	1.655	8.77
5	84.7	60.2	1.766	1.472	0.165	1.633	8.87
6	84.7	82.4	1.766	2.020	0.205	1.823	9.84
7	84.7	111.0	1.766	2.721	0.235	2.088	11.55
8	84.7	127.0	1.766	3.112	0.237	2.362	13.10
9	84.7	91.0	1.766	2.311	0.163	2.464	13.70
10	84.7	94.0	1.766	2.305	0.145	2.806	15.89
11	84.7	240.0	1.766	5.880	0.305	3.093	19.25
12	84.7	203.1	1.766	4.972	0.220	3.505	22.60
13	84.7	60.8	1.766	1.489	0.157	1.792	9.49
14	84.7	82.0	1.766	2.011	0.205	1.848	9.81
15	84.7	95.0	1.766	2.330	0.211	1.974	10.61
16	84.7	147.0	1.766	3.612	0.360	1.825	10.01

radiation shield attached. Both heater and thermometer coils were connected by tantalum leads in the same way as for the tungsten.

(c) The Apparatus

Each specimen was hung by three Nylon threads, 0.2-mm diameter, inside a copper vacuum jacket which could either have pure helium exchange gas admitted into it or be highly evacuated. This apparatus was placed in a Dewar vessel filled with liquid helium, the temperature of which could be held at any desired value between 1.3°K and 4.2°K by means of pumping the liquid helium. The temperature of the bath was ascertained by measuring the vapour pressure of the helium over the liquid surface. The liquid helium was provided by a small Simon type liquifier[6] modified to enable the liquid to be withdrawn into exterior Dewar vessels, as reported elsewhere.[7,8]

[6] F. E. Simon, Physik. Zeits. **34**, 232 (1933).
[7] R. B. Scott and J. W. Cook, Rev. Sci. Inst. **19**, 889 (1948).
[8] Daunt, Heer, and Silvidi, Phys. Rev. **75**, 113 (1949).

(d) The Electrical Measuring System

The resistances of the heater coils at 4.2°K were about 40 ohms. To measure the power input, current and potential measurements were made for each heating with an accuracy of ±0.25 percent.

The current in the heater coil was switched on and off by a special switch which simultaneously automatically started and stopped a previously calibrated stop watch, capable of reading to 0.1 sec.

No signs of overheating of the specimens were observed, indicating good thermal contact between the heaters and the specimens.

The resistances of the thermometer coils were about 3.5 ohms. The calibration of the thermometer was made against the vapour pressure of liquid helium, above 1.6°K the measurements of Schmidt and Keesom[9] being taken, whereas below 1.6°K the scale of Bleaney and Simon[10] was used. It was found that below 3°K the variation of the resistance of each thermometer with temperature was essentially linear, having a temperature coefficient of resistance in this region of about 18 percent per degree. Since the resistance of the thermometer wire was current sensitive, care was taken to maintain the measuring current through it constant during any one experiment. Calibrations were made immediately before and after the measurements were taken.

To calculate the resistance of the thermometer coils, current and potential measurements were made, and during experiments the temperature differences ob-

TABLE II. Data on specific heat of the powdered zinc specimen.

Points	Heater Voltage volts $\times 10^{-3}$	Heater time sec.	Current amp. $\times 10^{-3}$	Total ΔQ cal. $\times(10^{-3})$	ΔT°K	T°K	$\Delta Q/\Delta T$ $\times 10^{-3}$ cal./deg.	Heat cap. 0.259 mole Cu $\times 10^{-3}$ cal./deg.	Heat cap. of 0.817 mole of Zn $\times 10^{-3}$ cal./deg.	C_v $\times 10^{-3}$ cal./mole-deg.
July 5th, 1949. Thermometer measuring current—0.1 ma										
1	30.8	5.0	0.944	0.0342	0.0975	1.544	0.351	0.0826	0.2684	0.328
2	30.8	5.6	0.944	0.0383	0.109	1.567	0.351	0.0846	0.2664	0.325
3	30.8	9.6	0.944	0.0657	0.179	1.596	0.367	0.0863	0.2807	0.343
4	30.8	9.2	0.944	0.0630	0.161	1.599	0.391	0.0877	0.3033	0.370
5	30.8	10.0	0.944	0.0684	0.177	1.619	0.387	0.0881	0.2989	0.368
6	30.8	5.0	0.944	0.0342	0.091	1.592	0.376	0.0863	0.2897	0.354
7	30.8	5.0	0.944	0.0342	0.089	1.766	0.385	0.0983	0.2867	0.351
8	30.8	5.4	0.944	0.0370	0.091	1.772	0.408	0.0991	0.3089	0.377
9	30.8	5.8	0.944	0.0397	0.095	1.780	0.417	0.1001	0.3169	0.387
10	30.8	9.0	0.944	0.0616	0.140	1.820	0.440	0.1030	0.3370	0.412
11	30.8	7.2	0.944	0.0493	0.096	2.097	0.513	0.1252	0.3878	0.471
12	30.8	6.4	0.944	0.0438	0.089	2.098	0.493	0.1262	0.3668	0.449
13	30.8	14.0	0.944	0.0959	0.178	2.174	0.538	0.1325	0.4045	0.495
14	30.8	9.8	0.944	0.0671	0.120	2.178	0.559	0.1335	0.4225	0.520
15	30.8	10.1	0.944	0.0692	0.094	2.479	0.736	0.1635	0.5725	0.698
16	30.8	9.1	0.944	0.0623	0.087	2.509	0.717	0.1651	0.5519	0.675
17	30.8	5.9	0.944	0.0404	0.058	2.529	0.696	0.1681	0.5279	0.645
18	30.8	9.2	0.944	0.0630	0.087	2.566	0.724	0.1716	0.5524	0.674
19	30.8	12.0	0.944	0.0823	0.096	2.799	0.886	0.1940	0.6920	0.846
20	30.8	11.0	0.944	0.0754	0.078	2.881	0.966	0.2087	0.7573	0.923
21	30.8	15.0	0.944	0.1029	0.099	2.967	1.036	0.2210	0.8150	0.996
22	30.8	10.0	0.944	0.0684	0.068	2.992	1.005	0.2231	0.7819	0.955
23	30.8	25.5	0.944	0.1745	0.124	3.422	1.345	0.286	1.049	1.280
24	30.8	20.0	0.944	0.1370	0.100	3.483	1.370	0.296	1.074	1.310
25	39.6	15.2	1.128	0.1620	0.109	3.570	1.485	0.312	1.173	1.425
26	49.5	15.0	1.460	0.259	0.165	3.667	1.570	0.328	1.242	1.520
27	30.8	30.0	0.944	0.205	0.111	4.012	1.850	0.392	1.458	1.780

[9] G. Schmidt and W. H. Keesom, Leid. Comm., **250** c.
[10] B. Bleaney and F. E. Simon, Trans. Faraday Soc. **35**, 1205 (1939).

TABLE III. Data on specific heat of the fused zinc specimen.

June 23rd, 1949. Thermometer measuring current = 0.1 ma

Points	Heater Voltage volts $\times 10^{-3}$	Time sec.	Current amp. $\times 10^{-3}$	$\Delta Q \times 10^{-3}$ cal./mole	ΔT°K	T°K	$C_v \times 10^{-3}$ cal./mole-deg.
1	69.3	2.5	1.374	0.0574	0.210	1.515	0.283
2	69.3	3.2	1.374	0.0735	0.226	1.520	0.325
3	69.3	3.5	1.374	0.0805	0.243	1.528	0.331
4	69.3	2.0	1.374	0.046	0.141	1.692	0.328
5	69.3	5.0	1.374	0.115	0.276	1.777	0.417
6	69.3	4.5	1.374	0.1032	0.260	1.793	0.398
7	46.2	4.8	0.916	0.0485	0.140	1.585	0.347
8	46.2	4.0	0.916	0.0408	0.135	1.543	0.303
9	46.2	5.1	0.916	0.0521	0.170	1.590	0.307
10	46.2	5.1	0.916	0.0521	0.129	1.909	0.404
11	46.2	5.7	0.916	0.0581	0.140	1.910	0.416
12	46.2	4.8	0.916	0.0489	0.120	1.901	0.407
13	46.2	6.0	0.916	0.0612	0.1475	1.921	0.416
14	46.2	4.9	0.916	0.0499	0.110	2.005	0.454
15	46.2	5.2	0.916	0.0530	0.124	2.008	0.428
16	46.2	9.8	0.916	0.100	0.201	2.052	0.499
17	46.2	5.8	0.916	0.0591	0.107	2.221	0.552
18	46.2	6.0	0.916	0.0611	0.122	2.230	0.501
19	46.2	3.5	0.916	0.0357	0.060	2.363	0.595
20	46.2	7.1	0.916	0.0724	0.086	2.831	0.841
21	46.2	7.0	0.916	0.0715	0.0865	2.823	0.827
22	46.2	7.1	0.916	0.0724	0.075	3.034	0.965
23	46.2	7.0	0.916	0.0715	0.075	3.022	0.954
24	69.3	6.2	1.374	0.1425	0.1075	3.498	1.325
25	69.3	6.0	1.374	0.138	0.105	3.491	1.310

tained could be estimated with an accuracy of less than 1 percent.

3. EXPERIMENTAL RESULTS

The experimental results are given in Tables I, II, and III and curves of the measured specific heats as functions of temperature are shown in Figs. 1 and 2, the full curves being drawn through the smoothed values.

The total mass of the radiation shield, thermometer coil and heater coil was 0.26 percent of the mass of the zinc powder and only 0.08 percent of the mass of the tungsten. This factor, therefore, made a negligible correction. In the experiments on the zinc powder, corrections were made for the heat capacity of the copper vessel using the specific heat values of copper given by Keesom and Kok.[11] To correct for the heat capacity of the helium gas filling and to check possible effects of adsorption in the experiments on the zinc powder, measurements were made with different fillings of gas. The results given in Table II and Fig. 2 are for the smallest gas filling used, for which it was found that the corrections were negligible.

The accuracy of the results both for W and Zn as represented by the smoothed specific heat curves of Figs. 1 and 2 is estimated to be within ± 0.5 percent.

4. DISCUSSION

(a) Tungsten

Assuming that the full specific heat in this temperature range to be the sum of a Debye term (AT^3) due to the lattice and of a Sommerfeld term (γT) due to the electronic contribution, a plot of the ratio of C_v/T against T^2 should give a straight line. Such plots have been drawn up from our measurements on tungsten and zinc and have been found to be satisfactorily linear, giving support to the assumption made. From such plots the numerical values of A and γ have been obtained. For tungsten:

$$C_v = 464.5(T/169)^3 + 51.1 \times 10^{-4} T \text{ cal./mole/degree.}$$

At the highest temperature of measurement, $T = 3.5$°K, the lattice contribution to the total specific heat was only 19 percent, a result which made the evaluation of θ (Debye) difficult. It is estimated, however, that $\theta = 169$°K± 20, a value which is considerably lower than that estimated by Lange,[1] ($\theta_D = 310$°K), from measurements of the specific heat between 26°K and 90°K. Moreover, the value of θ_D obtained from the high temperature elastic constants is still higher, being given by Honnefelder[12] as 384°K. Calculations of the specific heat of tungsten based on the normal modes of vibration of the lattice have been made by Fine[3] which have indicated the possibility that some of the apparent discrepancies between high and low temperature measurement of the lattice specific heat might be resolved. Fine, however, suggests that at the lowest temperatures his atomic model would give a T^3 specific heat corresponding to a Debye function with $\theta_D = 367$°K. It is considered, therefore, that the low observed value of θ may not be characteristic of the lattice but may be due to an additional term dependent on some hidden transition. The proximity of W to superconducting Ta in the periodic table and in atomic volume and its similarity in crystal structure suggests that such a

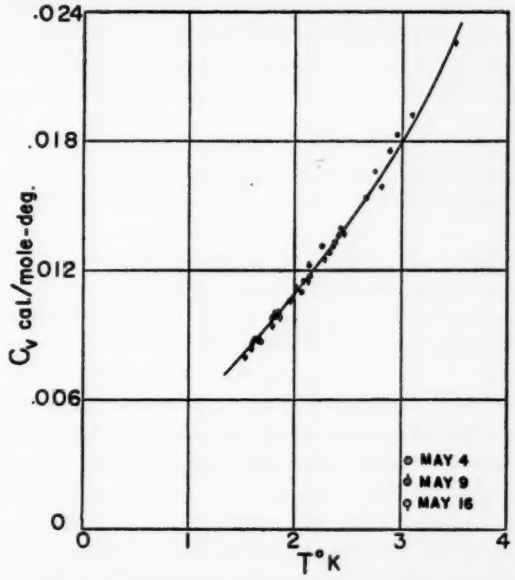

FIG. 1. The specific heat of tungsten as function of temperature.

[11] W. H. Keesom and J. A. Kok, Physica 3, 1035 (1936).

[12] Honnefelder, Zeits. f. physik. Chemie 21, 53 (1933).

transition might be calorimetrically analogous to the phenomenon of superconductivity. Such calorimetric anomalies have been previously observed by Simon and co-workers in beryllium[13] and sodium.[14]

The value of $\gamma=51.1\times10^{-4}$ obtained from our measurements is very high, a feature which has been established generally for the transition elements. For comparison with other transition elements, the values of γ obtained by low temperature measurement are tabulated in Table IV (column 4).

TABLE IV.*

Element	Crystal structure	γ-value (cal./mole/degree²) Calc. ×10⁻⁴	Obs. ×10⁻⁴	Expt. method	Expt. authors
W	b.c.C.	4.8	51.1	C	This paper
Cb	b.c.C.	...	60.0	S-C	Daunt and Mendelssohn[15]
Ta	b.c.C.	6.2	19.4	S-C	Daunt and Mendelssohn[15]
			14.1	C	Keesom and Desirant[16]
Mn	b.c.C.	...	42.1	C	Elson, Grayson Smith and Wilhelm[17]
Fe	b.c.C.	4.6	12.0	C	Duyckaerts[18]
			12.0	C	Keesom and Kurrelmeyer[19]
Co	f.c.C.	...	12.0	C	Duyckaerts[20]
Ni	f.c.C.	11.0	17.4	C	Keesom and Clark[21]
Pd	f.c.C.	...	31.0	C	Pickard[22]
Pt	f.c.C.	...	16.0	C	Keesom and Kok[11]

* In this table the fifth column indicates "C" calorimetric measurements and "S-C" magnetic measurements on superconductors, both methods being carried out at low temperatures. For references to calculated values (column 3), see text.

In Table IV, the third column gives the values of obtained from detailed calculations of the band structure which have been made for W and Ta by Manning and Chodorow,[2] for Fe by Manning,[23] and for Ni by Slater.[24]

The high values of γ for the transition elements cannot be due to s electrons, for which $\gamma\approx1\times10^{-4}$, and the general trend has been explained by Mott[25] as being due to the unoccupied d states for which the density of states per unit energy range is high.

The only transition metals for which a detailed calculation of the density of states has been made are listed in Table IV, column 3. Whereas in the case of Ni, the calculated and observed values are in moderate agreement, for Fe, W, and Ta there are large differences, the observed values being much the higher.

One might suppose these high observed values of γ to be associated with low degeneracy temperatures, and as a result the contribution to the specific heat at high temperatures (circa 1200°K for example) to be approximately $3/2k$ per "positive hole" due to the approximate non-degeneracy of the gas at such temperatures. The observed specific heats at high temperatures for W and Ta measured by Mangus and Holtzmann[26] are 6.44 and 6.77 cal./mole-deg. respectively at 1173°K, values which do not appear sufficiently larger than the lattice specific heat (5.959 cal./mole-deg.) at this temperature to allow for a non-degenerate "positive hole" gas. Such a difficulty in correlating the observed low temperature and high temperature electronic specific heats has already been pointed out by Mott and Jones[4] for the case of Pt and Pd, and again more recently by Mott.[27]

An additional difficulty in the case of W and Ta lies in the fact that the excess specific heat over the Debye term at high temperatures as observed by Mangus and Holtzmann[26] is essentially linearly proportional to temperature, given by $c=\alpha T$, where $\alpha=5.1\times10^{-4}$ per mole of W and $\alpha=7.2\times10^{-4}$ per mole of Ta. If one associates this excess specific heat with the electronic contribution[25] rather than being due to anharmonicity terms,[28] then the correlation between these values and those calculated for γ by Manning and Chodorow might appear too close to be entirely fortuitous. It cannot, however, be excluded that the high apparent γ-value of W at low temperatures may be partly due to a hidden transition, as has been suggested to account also for the anomalous lattice specific heat. Such an argument, on the other hand, cannot be applied to Ta for which one

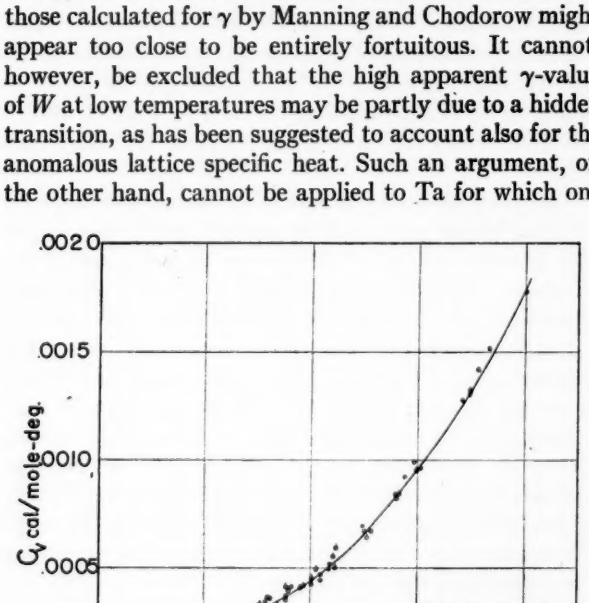

FIG. 2. The specific heat of zinc (powdered and fused) as function of temperature.

[13] Cristescu and F. Simon, Zeits. f. physik. Chemie **25**, 273 (1934).
[14] G. L. Pickard, and F. E. Simon, Proc. Phys. Soc. **61**, 1 (1948).
[15] J. G. Daunt, and K. Mendelssohn, Proc. Roy. Soc. **A160**, 127 (1937).
[16] W. H. Keesom, and M. C. Desirant, Physica **8**, 273 (1941).
[17] Elson, Grayson Smith, and Wilhelm, Can. J. Research **18**, 82 (1940).
[18] G. Duyckaerts, Physica **6**, 401 (1939).
[19] W. H. Keesom, and B. Kurrelmeyer, Physica **6**, 364, 633 (1939).
[20] G. Duyckaerts, Physica **6**, 817 (1939).
[21] W. H. Keesom and C. W. Clark, Physica **2**, 513 (1935).
[22] G. L. Pickard, Nature **138**, 123 (1936). (See also reference 14.)
[23] M. F. Manning, Phys. Rev. **63**, 190 (1943).
[24] J. C. Slater, Phys. Rev. **49**, 537 (1936).
[25] N. F. Mott, Proc. Phys. Soc. **47**, 571 (1935). (See references 2 and 4 also.)
[26] A. Mangus and H. Holtzmann, Ann. d. Physik **3**, 602 (1929).
[27] N. F. Mott, Proc. Phys. Soc. **62**, 416 (1949).
[28] M. Born, and E. Brody, Zeits. f. Physik **6**, 132 (1921); **8**, 205 (1922).

must suppose the γ-value is due to the normal electronic contribution.

It has been suggested by Mott[27] that the apparent discrepancies between the low temperature and high temperature specific heats of the positive holes could be due to a particular form and filling of the *d*-band which at high temperatures might result in a lower specific heat than corresponds to the high density of states at low temperatures. No detailed calculation of these effects has been made. It would appear, however, that the low temperature density of states on such a picture would correspond to the values already calculated (see column 3, Table IV) by Manning[2] for which the discrepancy between theory and observation remains.

On the other hand, it has been pointed out by Wigner[29] that the inclusion of the effects of correlation forces would result in an increase in the density of states and hence the high values of γ at low temperatures might be the result of such correlation effects. The necessity for the inclusion of correlation forces to account for the high paramagnetic susceptibilities of Pd and Pt has already been stressed by Mott and Jones.[4] Other transition metals undoubtedly require the inclusion of similar interaction forces to account for their paramagnetism and hence the high value of γ for tungsten and tantalum may be partly due to the existence of such an extra term, a feature which in the case of W may also be reflected in the observed low θ-value. Further specific heat measurements on W with a more extensive temperature range would be, therefore, of value and are being carried out, and additional experimental investigations of the low temperature paramagnetic susceptibility would appear to be of interest in view of these considerations.

(b) Zinc

By considering the observed specific heat (see Fig. 2) to be the sum of a Debye term (AT^3) and an electronic term (γT), we obtain the following evaluation:

$$C_v = 464.5(T/291)^3 + 1.50\times10^{-4}T \text{ cal./mole/deg.}$$

Since the maximum temperature employed in the measurements on zinc was less than (1/50) θ (Debye), the T^3 approximation for the lattice specific heat should be valid.[30]

The Debye θ-value of 291°K obtained is in fair agreement with that previously obtained by Keesom and Van den Ende,[31] (320°K), and with that calculated by Gruneisen and Goens,[32] (305°K), from elastic data. The value of γ giving the electronic specific heat is slightly higher than that which can be interpreted from Keesom and Van den Ende's measurements.* It is in good agreement with the value recently obtained by magnetic measurements on superconducting zinc by Heer and one of us.[5] The value of γ calculated according to the Sommerfeld formula for a perfect electron gas[33] assuming one free electron per atom is 1.43×10^{-4}, whereas, assuming two free electrons per atom the value is 1.80×10^{-4}. The measured value lies between these two values, as might be expected.[34]

The measurements carried out on the zinc in the form of a finely divided powder (average linear dimensions of the particles = 1.3 microns) were made in order to give some indication, or limit to the order of magnitude, of the size at which size effects in the specific heat might appear. From the work of Frohlich[35] variations from the bulk value of γ are not to be expected in metal pieces of 1 micron linear dimension until temperatures of about 10^{-3}°K are reached. For the lattice contribution to the specific heat, however, effects due to the increase of the ratio of surface to volume in small sizes might be expected in the helium temperature region. It is estimated** that for zinc particles of the size used by us differences in the Debye term of about 5 percent might be expected between the specific heats of the fused and powdered samples at 1.5°K. At this temperature, however, it was found that the Debye term only contributed approximately 20 percent to the total specific heat and consequently any variations due to size effects should have been only about 1 percent, which was within the experimental scatter of individual points. As is shown in Fig. 2, the measured specific heat curve for the zinc in powder form is within experimental error identical with that for the zinc in fused form. It is considered, therefore, that size effects in specific heat measurements should be carried out with insulating materials, having Debye θ-values as high or higher than for zinc.

5. ACKNOWLEDGMENTS

We wish to thank Professor H. H. Nielsen for his support of this low temperature program in the Mendenhall Laboratory and The Ohio State University Development Fund and The Ohio State University Research Foundation for their financial assistance in the purchase of equipment. The later stages of the work were also assisted by a contract between the Office of Naval Research and The Ohio State University Research Foundation.

We also wish to thank Professor J. de Boer and Dr. M. C. Desirant for valuable discussions and Dr. C. V. Heer for his assistance during the experiments.

[29] E. Wigner, Tran. Faraday Soc. **34**, 678 (1938).
[30] M. Blackman, Proc. Roy. Soc. **A149**, 117 (1935).
[31] W. H. Keesom and J. N. Van den Ende, Leid. Comm. 219 b; Proc. Roy. Acad. Amsterdam **35**, 143 (1932).
[32] E. Gruneisen, and E. Goens, Zeits. f. Physik **26**, 250 (1924).
* By plotting C/T against T^2 from Keesom and Van den Ende's measurements, we arrive at a γ-value of 1.25×10^{-4} cal./mole-deg., as against 1.55×10^{-4} cal./mole-deg. as calculated by Burton, Grayson Smith, and Wilhelm, *Phenomena at the Temperature of Liquid Helium* (Reinhold Publishing Corporation, New York, 1940), p. 348, from the same measurements. The discussion given by W. H. Keesom and J. A. Kok, Physica **1**, 770 (1934), of Keesom and Van den Ende's measurements also leads to the lower value of γ.
[33] Sommerfeld, Houston, and Eckart, Zeits. f. Physik **47**, 1 (1928).
[34] A. Sommerfeld, and H. Bethe, *Handbuch der Physik* 24/2, 33 (1933).
[35] H. Frohlich, Physica **4**, 406 (1937).
** We are indebted to Dr. E. W. Montroll for valuable discussions on these size effects.

l-Type Doubling in Polyatomic Molecules and Its Application to the Microwave Spectrum of Methyl Cyanide and Methyl Iso-Cyanide

HARALD H. NIELSEN
Mendenhall Laboratory of Physics, Ohio State University, Columbus, Ohio
(Received August 22, 1949)

The theory of the l-type doubling for polyatomic molecules is developed and applied to explain certain anomalies observed in the microwave spectrum of CH_3CN and CH_3NC. The theory predicts for the transition $J=1\rightarrow J=2$, $\Delta K=0$, where the molecule is in an excited e vibration state, a pattern consisting of two lines separated by about 100 mc/sec. with two lines near the center of this doublet which are about 2 or 3 mc/sec. apart. The predicted patterns can be made to agree quantitatively with the observed patterns by correcting the degenerate Coriolis term for centrifugal distortion.

I. INTRODUCTION

THE spectra of methyl cyanide and methyl iso-cyanide have been investigated by Gordy, Kessler, and Ring[1] in the microwave region from 36,000 to 40,000 mc. These investigators have shown that all but three of the CH_3CN lines and all but four of the CH_3NC lines may be identified readily. It has further been demonstrated that the intensities of the unidentified frequencies are in each case temperature varient and must therefore be ascribed to rotational transitions of the molecule in an excited vibration state. It seems most reasonable to assume, if this is indeed the case, that the excited states in question are the states $\nu_8(e)$ which occur at 380 cm^{-1} and 290 cm^{-1}, respectively.

Gordy, Kessler, and Ring have further shown by studying the Stark pattern that the lines must be ascribed to a transition from $J=1$ to $J=2$. Since the electric moment lies along the axis of symmetry of these molecules, the selection rule $\Delta K=0$ must be obeyed also.

The energy level diagram for the states $J=1$ and $J=2$ for the vibration $\omega_8(e)$, where $\nu_8=|l_8|=1$ are shown in Fig. 1. It will be seen that each state where $K\neq 0$ suffers a degenerate Coriolis-type splitting, $\Delta\nu=4K\zeta_8 C$, where ζ_8 is the Coriolis coupling factor and $C=h/8\pi^2 I_{zz}c$. The transitions $J=1\rightarrow J=2$, $\Delta K=0$ are also indicated in Fig. 1. The patterns observed by Gordy, Kessler, and Ring in the two cases are shown in Fig. 2(a) and (b). The pattern consists, in the case of CH_3CN, of two lines separated by about 72 mc with a line near the center of the two. The pattern, in the case of CH_3NC, consists of two lines separated by about 111 mc with two other lines separated by only 2.5 mc located near the center of the former. The difficulty which is encountered is that on the basis of Fig. 1 only two lines can be accounted for and these differ in frequency only by an amount due to the difference in centrifugal stretching in the rotational states involved. This difference might be expected to be of the order of one or two megacycles per second.[2] Quite evidently certain degeneracies must further be removed.[3] The values B_0 have been given by Gordy[4] for the molecules CH_3CN and CH_3NC and are: 0.3066 cm^{-1} and 0.3351 cm^{-1}, respectively. A quick calculation shows that the splitting is of the order of magnitude (B_e^2/ω_s), where $B_e=h/8\pi^2 I_{zz}^{(e)}c$ and ω_s is cm^{-1} value of the excited vibration frequency. This magnitude is of second order and must be sought for as a part of the second-order Hamiltonian of a molecule which normally does not contribute to the energy in second order. In the following section we shall investigate such a term.

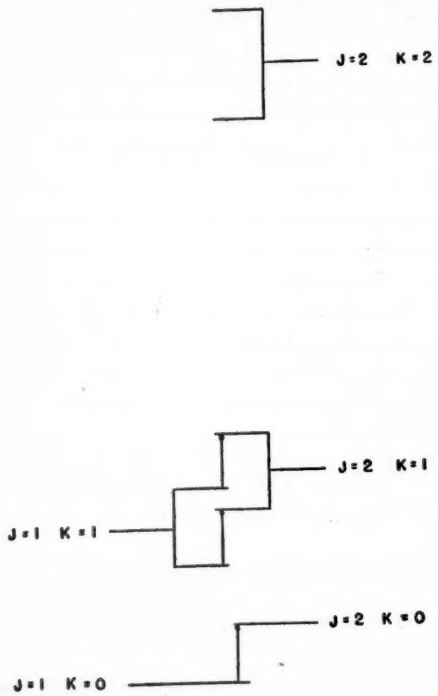

FIG. 1. Rotation levels of a symmetric molecule for $J=1$ and $J=2$ when the molecule is in a vibration state where $l=1$.

II. ANALYSIS OF THE PERTURBING TERMS

The quantum-mechanical Hamiltonian for a polyatomic molecule has been expanded to second order of approximation by Nielsen.[5] The only terms of the

[1] Gordy, Kessler, and Ring (private communication).

[2] See, for example, Z. I. Slawsky and D. M. Dennison, J. Chem. Phys. 7, 520 (1939).
[3] H. H. Nielsen, Phys. Rev. 75, 1961 (1949).
[4] W. Gordy, Rev. Mod. Phys. 20, 711 (1948).
[5] H. H. Nielsen, Phys. Rev. 60, 794 (1941).

Hamiltonian which can be of interest to us will evidently be those which represent corrections to the reciprocals of inertia of the molecule due to the vibration. They will be:

$$H^{(1)}=\cdots-\sum_{\alpha}\sum_{s\sigma}\sum_{s''\sigma''}\zeta_{ss'}{}^{(\alpha)}[(\lambda_{s''}/\lambda_s)^{\frac{1}{2}}q_{s\sigma}p_{s''\sigma''}-(\lambda_s/\lambda_{s''})^{\frac{1}{2}}q_{s''\sigma''}p_{s\sigma}](P_\alpha/I_{\alpha\alpha}{}^{(e)}+\cdots$$

and

$$\begin{aligned}H^{(2)}=\cdots&\tfrac{1}{2}\sum_{s\sigma}\sum_{s'\sigma'}(\hbar^4/\lambda_s\lambda_{s'})^{\frac{1}{2}}\{\sum_{\alpha}[A'^{(\alpha\alpha)}_{s\sigma s'\sigma'}\\&-\sum_{\beta}(a_{s\sigma}{}^{(\alpha\beta)}a_{s'\sigma'}{}^{(\alpha\beta)}/I_{\beta\beta}{}^{(e)})(P_\alpha/I_{\alpha\alpha}{}^{(e)})^2\\&-\sum_{\alpha\beta\gamma}{}''[A'^{(\alpha\beta)}_{s\sigma s'\sigma'}-(a_{s\sigma}{}^{(\alpha\alpha)}a_{s'\sigma'}{}^{(\alpha\beta)}/I_{\alpha\alpha}{}^{(e)})\\&-(a_{s\sigma}{}^{(\beta\beta)}a_{s'\sigma'}{}^{(\alpha\beta)}/I_{\beta\beta}{}^{(e)}+(a_{s\sigma}{}^{(\alpha\gamma)}a_{s'\sigma'}{}^{(\gamma\beta)}/I_{\gamma\gamma}{}^{(e)})]\\&\times P_\alpha P_\beta/I_{\alpha\alpha}{}^{(e)}I_{\beta\beta}{}^{(e)}\}q_{s\sigma}q_{s'\sigma'},\end{aligned}\quad(1)$$

where α, β, γ are summed over x, y, z. In Eq. (1) the notation is slightly different from that used in reference 4. The quantities $A^{(\alpha\beta)}_{s\sigma s'\sigma'}$ are used in place of $A_{s\sigma s'\sigma'}, B_{s\sigma s'\sigma'}, D_{s\sigma s'\sigma'}$, etc., and the $a_{s\sigma}{}^{(\alpha\beta)}$ are used instead of $a_{s\sigma}, b_{s\sigma}, d_{s\sigma}$, etc. Also $A'^{(\alpha\beta)}_{s\sigma s'\sigma'}$ is used as an abbreviation for $A^{(\alpha\beta)}_{s\sigma s'\sigma'}-\sum_{s''\sigma''}\zeta^{(\alpha)}_{s\sigma s''\sigma''}\zeta^{(\beta)}_{s'\sigma' s''\sigma''}$. The $\zeta_{ss'}{}^{(\alpha)}$ are the Coriolis coupling factors so defined that

$$\zeta^{(\alpha)}_{s\sigma s'\sigma'}=\sum_i(l^{(\beta)}_{is\sigma}l^{(\gamma)}_{is'\sigma'}-l^{(\beta)}_{is'\sigma'}l^{(\gamma)}_{is\sigma}).$$

The $l_{is\sigma}{}^{(\alpha)}$ are direction cosines relating the Cartesian coordinates x_i, y_i, and z_i to the normal coordinates, $q_{s\sigma}$, the relationship between these being

$$M_i^{\frac{1}{2}}\delta x_i=\sum_s(\hbar/\lambda_s^{\frac{1}{2}})^{\frac{1}{2}}l_{is\sigma}{}^{(x)}q_{s\sigma},$$

where M_i are the nuclear masses and $\lambda_s=4\pi^2c^2\omega_s{}^2$.

The terms of $H^{(1)}$ cannot contribute to the energy before second order of approximation (except in the degenerate case $s=s''$). The method employed in reference 4 to approximate the energy was to carry out a contact transformation on the Hamiltonian H so that to second order of approximation the transformed first-order Hamiltonian will be absent. When this transformation has been completely carried out, a second-order transformed Hamiltonian will be obtained instead of $H^{(2)}$. This quantity is stated in the relation (21-c) of reference 5. This relation states explicitly, however, only the terms which are diagonal in all the quantum numbers (except K), the terms which are non-diagonal being lumped into $\bar{H}^{(2)}$ which is not given. $\bar{H}^{(2)}$ will, in general, give no contribution to the second-order approximation. When $H^{(2)}$ is restated so as to include these terms explicitly, the part we are interested in will be:

$$\begin{aligned}H^{(2)\prime}=\cdots&-\sum_{\alpha}\sum_{s\sigma}\sum_{s'\sigma'}(\hbar/2\lambda_s{}^{\frac{1}{2}}\lambda_{s'}{}^{\frac{1}{2}}(I_{\alpha\alpha}{}^{(e)})^2)\\&\times\{[A^{(\alpha\alpha)}_{s\sigma s'\sigma'}-\sum_{\beta}(a_{s\sigma}{}^{(\alpha\beta)}a_{s'\sigma'}{}^{(\alpha\beta)}/I_{\beta\beta}{}^{(e)})\\&-2\sum_{s''\sigma''}\zeta^{(\alpha)}_{s\sigma s''\sigma''}\zeta^{(\alpha)}_{s'\sigma' s''\sigma''}\lambda_s/(\lambda_s-\lambda_{s''})]q_{s\sigma}q_{s'\sigma'}\\&-2\sum_{s''\sigma''}[\zeta^{(\alpha)}_{s\sigma s''\sigma''}\zeta^{(\alpha)}_{s'\sigma' s''\sigma''}\lambda_s{}^{\frac{1}{2}}\lambda_{s'}{}^{\frac{1}{2}}/(\lambda_s-\lambda_{s''})]\\&\times(p_{s\sigma}p_{s'\sigma'}/\hbar^2)\}P_\alpha{}^2-\sum_{\alpha\beta\gamma}{}''\sum_{s\sigma}\sum_{s'\sigma'}\\&\times(\hbar/2\lambda_s{}^{\frac{1}{2}}\lambda_{s'}{}^{\frac{1}{2}}I_{\alpha\alpha}{}^{(e)}I_{\beta\beta}{}^{(e)})\{[A^{(\alpha\beta)}_{s\sigma s'\sigma'}\\&-(a_{s\sigma}{}^{(\alpha\alpha)}a_{s'\sigma'}{}^{(\alpha\beta)}/I_{\alpha\alpha}{}^{(e)})-(a_{s\sigma}{}^{(\beta\beta)}a_{s'\sigma'}{}^{(\alpha\beta)}/I_{\beta\beta}{}^{(e)})\\&+(a_{s\sigma}{}^{(\alpha\gamma)}a_{s'\sigma'}{}^{(\gamma\beta)}/I_{\gamma\gamma}{}^{(e)})-2\sum_{s''\sigma''}\zeta^{(\alpha)}_{s\sigma s''\sigma''}\\&\times\zeta^{(\beta)}_{s'\sigma' s''\sigma''}\lambda_s/(\lambda_s-\lambda_{s''})]q_{s\sigma}q_{s'\sigma'}\\&-2\sum_{s''\sigma''}[\zeta^{(\alpha)}_{s\sigma s''\sigma''}\zeta^{(\beta)}_{s'\sigma' s''\sigma''}\lambda_s{}^{\frac{1}{2}}\lambda_{s'}{}^{\frac{1}{2}}/(\lambda_s-\lambda_{s'})]\\&\times p_{s\sigma}p_{s'\sigma'}/\hbar^2\}P_\alpha P_\beta+\cdots.\end{aligned}\quad(2)$$

Equation (2) is the equivalent for the general polyatomic molecule of Eq. (1b) given by Nielsen and Shaffer[6] for the linear molecule, in particular, the linear X_2Y_2 model.

The above terms cannot, in general, contribute to the energy in second order unless $s=s'$ and $\sigma=\sigma'$. An exception to this may present itself in axially symmetric molecules where there occur twofold degenerate frequencies. In such cases two coordinates, q_{s1} and q_{s2}, are associated with the frequency ω_s. It may further be shown that for such molecules, simple relations exist between the $A^{(\alpha\beta)}_{s\sigma s'\sigma'}$, the $a_{s\sigma}{}^{(\alpha\beta)}$ and the $\zeta_{ss'}{}^{(\alpha)}$, so that Eq. (2) will reduce to

$$\begin{aligned}H^{(2)\prime}=\cdots&\bar{\sum_{+}}\sum_{s}(B_e/4\omega_s)\{[(A^{(xx)}_{s1s1}-A^{(xx)}_{s2s2})-((a_{s1}{}^{(xx)})^2\\&-(a_{s2}{}^{(xx)})^2+(a_{s1}{}^{(xy)})^2-(a_{s2}{}^{(xy)})^2)/I_{xx}{}^{(e)}\\&-((a_{s1}{}^{(xx)})^2-(a_{s2}{}^{(xx)})^2)/I_{zz}{}^{(e)}](e^{\pm i\chi_s}r_s)^2\\&+2\sum_{s'}(\zeta_{ss'}{}^{(x)})^2[\lambda_s/(\lambda_s-\lambda_{s'})]\\&\times e^{2i\chi_s}[r_s{}^2+((p_{r_s}\pm p_{\chi_s}/r_s)/\hbar)^2]\}\\&\{P_x\mp iP_y\}^2/I_{xx}{}^{(e)},\end{aligned}\quad(3)$$

where q_{s1} and q_{s2} have, respectively, been replaced by $r_s\cos\chi_s$ and $r_s\sin\chi_s$ and the conjugate momenta p_{s1} and p_{s2} by their equivalents in r_s and χ_s.

FIG. 2. Microwave absorption pattern observed by Gordy, Kessler, and Ring for (a) methyl cyanide, (b) methyl isocyanide.

[6] H. H. Nielsen and W. H. Shaffer, J. Chem. Phys. 11, 140 (1943).

The matrix components of $e^{\pm ix_s}r_s$ (i.e., $q_{s1}\pm iq_{s2}$) have been evaluated by Shaffer.[7] The quantities

$$e^{\pm ix_s}[p_{r_s}\pm ip_{x_s}/r_s]$$

are readily recognized as $p_{s1}\pm ip_{s2}$ and, with the aid of Shaffer's relations and the commutation relation

$$(p_{s1}\pm ip_{s2})(q_{s1}\mp iq_{s2})-(q_{s1}\mp iq_{s2})(p_{s1}\pm ip_{s2})=-2ih,$$

it is readily shown that:

$$\begin{aligned}
&(V_s, l_s|e^{-ix_s}r_s|V_s-1, l_s+1)\\
&\quad=(V_s-1, l_s+1|e^{ix_s}r_s|V_s, l_s)=[(V_s-l_s)/2]^{\frac{1}{2}},\\
&(V_s, l_s|e^{ix_s}r_s|V_s-1, l_s-1)\\
&\quad=(V_s-1, l_s-1|e^{-ix_s}r_s|V_s, l_s)=-[(V_s+l_s)/2]^{\frac{1}{2}},\\
&(V_s, l_s|e^{-ix_s}(p_{r_s}-ip_{x_s}/r_s)|V_s-1, l_s+1)\\
&\quad=-(V_s-1, l_s+1|e^{ix_s}(p_{r_s}+ip_{x_s}/r_s)|V_s, l_s)\\
&\quad=ih[(V_s-l_s)/2]^{\frac{1}{2}},\\
&(V_s, l_s|e^{ix_s}(p_{r_s}+ip_{x_s}/r_s)|V_s-1, l_s-1)\\
&\quad=-(V_s-1, l_s-1|e^{-ix_s}(p_{r_s}-ip_{x_s}/r_s)|V_s, l_s)\\
&\quad=-ih[(V_s+l_s)/2]^{\frac{1}{2}}.
\end{aligned}\tag{4}$$

The only non-vanishing matrix components of (3) which are diagonal in V_s are then seen to be:

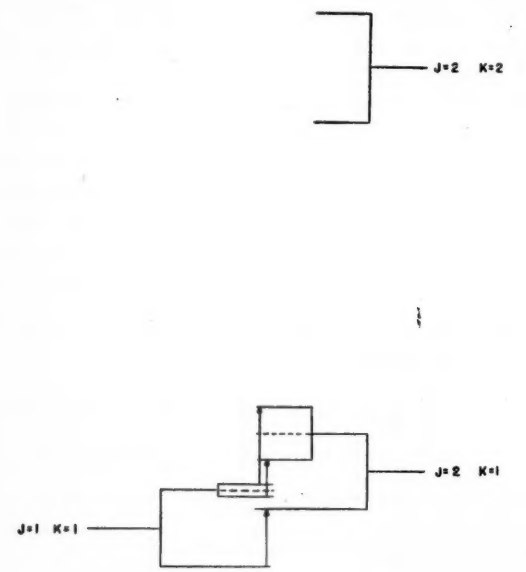

FIG. 3. Rotation levels of a symmetric molecule for $J=1$ and $J=2$, showing l-type doubling, when the molecule is in a vibration state where $l=1$.

$$\begin{aligned}
&(V_s, l_sK|H^{(2)\prime}|V_s, l_s\pm2, K\pm2)\\
&=-hcB_e(B_e/2\omega_s)\{(A^{(xx)}_{s1s1}-A^{(xx)}_{s2s2})-[(a_{s1}{}^{(xx)})^2\\
&\quad-(a_{s2}{}^{(xx)})^2+(a_{s1}{}^{(xy)})^2-(a_{s2}{}^{(xy)})^2]/I_{xx}{}^{(e)}\\
&\quad-[(a_{s1}{}^{(xz)})^2-(a_{s2}{}^{(xz)})^2]/I_{zz}{}^{(e)}\\
&\quad+4\sum_{s'}(\zeta_{ss'}{}^{(x)})^2\lambda_s/(\lambda_s-\lambda_{s'})\}\{[J(J+1)\\
&\quad-K(K\pm1)][J(J+1)-(K\pm1)(K\pm2)]\\
&\quad\times[(V_s\mp l_s)(V_s\pm l_s+2)]\}^{\frac{1}{2}}.
\end{aligned}\tag{5}$$

The relation (5) enables one to compute the l-type splitting for a polyatomic molecule. It is possible to show in the case of linear molecules, where $\sum_i(l^{(\alpha)}_{is\sigma})^2=\sum_{s\sigma}(l^{(\alpha)}_{is\sigma})^2=1$ and where $\sum_i l^{(\alpha)}_{is\sigma}l^{(\alpha)}_{is'\sigma'}=\sum_{s\sigma}l_{is\sigma}l_{i's\sigma}=0$, that $A^{(xx)}_{s1s1}-A^{(xx)}_{s2s2}=-1$, $a_{ss\sigma}{}^{(\alpha\beta)}=0$ and that

$$\sum_{s'}(\zeta_{ss'}{}^{(x)})^2=1.$$

The coefficient of (5) for the linear molecule will, therefore, be $hcB_e(B_e/2\omega_s)[1+4\sum_{s'}(\zeta_{ss'}{}^{(x)})^2\lambda_s/(\lambda_{s'}-\lambda_s)]$. This differs from the coefficient given by Nielsen and Shaffer[6] by the second term which contains the resonance denominator. An error was incurred in their work involving the sign of the matrix components of the operators $e^{\pm ix_s}(p_{r_s}\pm ip_{x_s}/r_s)$ which caused the resonance denominator to be absent.

It was pointed out by Herzberg[8] that in linear molecules where $|K|=|l|=1$, the two degenerate components are split because the perturbing elements (5) will in that case link the two states $l=1$ and $l=-1$. The splitting for the linear molecule will be found to be for the state $V=l=1$

$$\Delta\nu=2B_e(B_e/\omega_s)[1+4\sum_{s'}(\zeta_{ss'}{}^{(x)})^2\lambda_s/(\lambda_{s'}-\lambda_s)]J(J+1).\tag{6}$$

This is the value suggested by Herzberg[7] as the correct value.

III. APPLICATION TO THE SPECTRUM OF CH_3CN AND CH_3NC

We shall consider now the effect of such a perturbation on the lines in the microwave spectrum of methyl cyanide and methyl iso-cyanide which originate from rotational transitions of the molecules in an excited vibration state. It has been pointed out earlier that the transitions involved are $J=1\rightarrow J=2$, $\Delta K=0$, and that the vibration state excited is in all likelihood the perpendicular state ω_8 where $V_8=l_8=1$. The energy of the molecule in a vibration state $V_8=l_8=1$ and in the rotation state J, K may be written:

$$\begin{aligned}
(E/hc)=&T_v+J(J+1)B_v-K^2(B_v-C_v)-2Kl_8\zeta_8{}^{(z)}C_v\\
&-D_JJ^2(J+1)^2-D_{JK}J(J+1)K^2-D_KK^4,
\end{aligned}\tag{7}$$

where T_v is the vibration term value, B_v and C_v are

[7] W. H. Shaffer, Rev. Mod. Phys. 16, 245 (1944).

[8] G. Herzberg, Rev. Mod. Phys. 14, 219 (1942).

the reciprocals of inertia $h/8\pi^2 I_{zz}^{(v)}c$ and $h/8\pi^2 I_{zz}^{(v)}c$, D_{JK}, etc., the centrifugal stretching coefficients and ζ_8 is the Coriolis coupling coefficient associated with the degenerate frequency ω_8. Relation (7) quite evidently also represents the elements of the energy matrix which are diagonal in the quantum number l and K.

The secular determinant of the submatrix for the state $J=1$ is shown in Eq. (8).

	$l=1$ $K=1$	$l=-1$ $K=-1$	$l=1$ $K=-1$	$l=-1$ $K=1$	$l=1$ $K=0$	$l=-1$ $K=0$
$l=1$ $K=1$	$T_v+2B+(C-B)$ $-2\zeta C-4D_J$ $-2D_{JK}-D_K-\epsilon$	$-2(B_e^2/\omega_s)a$				
$l=-1$ $K=-1$	$-2(B_e^2/\omega_s)a$	$T_v+2B+(C-B)$ $-2\zeta C-4D_J$ $-2D_{JK}-D_K-\epsilon$				
$l=1$ $K=-1$			$T_v+2B+(C-B)$ $+2\zeta C-4D_J$ $-2D_{JK}-D_K-\epsilon$			
$l=-1$ $K=1$				$T_v+2B+(C-B)$ $+2\zeta C-4D_J$ $-2D_{JK}-D_K-\epsilon$		
$l=1$ $K=0$					T_v+2B $-4D_J-\epsilon$	
$l=-1$ $K=0$						T_v+2B $-4D_J-\epsilon$

. (8)

It will be seen to factor into the roots $T_v+2B_v+(C_v-B_v)+2\zeta C_v-4D_J-2D_{JK}-D_K$, $T_V+2B_v-4D_J$, and $[T_v+2B_v+(C_v-B_v)-2\zeta C_v-4D_J-2D_{JK}-D_K]\pm 2(B^2/\omega_s)a$, where a is the coefficient in (5) which depends upon the $A_{ssss}^{(\alpha\alpha)}$, $a_{ss}^{(\alpha\beta)}$, and $\zeta_{ss'}^{(z)}$. For the states $J=2$ the submatrix may similarly be set up and factorization of the secular determinant leads to the term values: $T_v+6B_v+(C_v-B_v)+2\zeta C_v-36D_J-6D_{JK}-D_K$, $T_v+6B_v+(C_v-B_v)-2\zeta C_v-36D_J-6D_{JK}-D_K\pm 6(B^2/\omega_s)a$, $T_v+6B_v+4(C_v-B_v)+4\zeta C_v-36D_J-24D_{JK}-16D_K$ and

$$\epsilon=\tfrac{1}{2}\{2T_v+12B_v+4[(1-\zeta)C_v-B_v]-72D_J-24D_{JK}-16D_K\}$$
$$\pm\left\{\left(\frac{4[(1-\zeta)C_v-B_v]-24D_{JK}-16D_K}{2}\right)^2+24(B^4/\omega_s^2)a^2\right\}^{\frac{1}{2}}.$$

It may be pointed out with reference to the last two roots that the quantity

$$\left\{\frac{4[(1+\zeta)C_v-B_v]-24D_{JK}-16D_K}{2}\right\}^2 \gg 24(B^4/\omega^2)a^2$$

so that the last term may be expanded. This leads to the values $T_v+6B_v+4[(1-\zeta)C_v-B_v]-36D_J-24_{JK}-16D_K+[6(Be^4/\omega_s^2)a^2]/[(1-\zeta)C_v-B-6D_{JK}-4D_K]$ and $T_v+6B_v-36D_J-[6(Be^4/\omega_s^2)a^2]/[(1-\zeta)C_v-B_v-6D_{JK}-4D_K]$.

An energy level diagram for the states $J=1$ and $J=2$ is shown in Fig. 3 for molecules like CH_3CN and CH_3NC where $I_{zz}\gg I_{zz}$ assuming $\zeta^{(z)}$ to be negative. It will be seen that only one component of the state $K=1$ is split in both states. The component which splits corresponds to the condition where the framework of the molecule is at rest and is not spinning about the axis of symmetry. This may be seen in the following manner. The quantity $-2Kl\zeta C_v$ is positive for $K=l=\pm 1$, but is negative when $K=\pm 1$, $l=\mp 1$ if one assumes, as we have done, that ζ is negative. Now the total angular momentum of the molecule about the axis z is characterized by K and the internal angular momentum associated with the oscillation ω_8 by l. The angular momentum associated with the spinning framework of the molecule about its axis of symmetry therefore might be characterized by $K-l$. The upper component of $K=1$ which is the one where also $l=1$ will have $K-l=0$ and therefore will be the state where the framework is at rest. This is, of course, consistent with the state of affairs in the linear molecule where K is always equal to l.

One may, in fact, prove an interesting theorem concerning the manner in which the states will split in higher approximations.[9] For the state ω_8, $v_8=1$, and $l_8=\pm 1$. This vibration state is characterized by a vibrational wave function of species E. The molecules we here are considering belong to the point group C_{3v}. The rota-

[9] I am indebted to Professor D. M. Dennison for suggesting this to me.

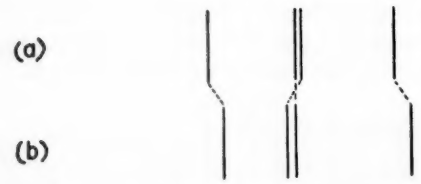

FIG. 4. Microwave absorption patterns predicted on the basis of l-type doubling, (a) assuming the centrifugal stretching of both Coriolis components to be alike; (b) when the difference in centrifugal stretching of the two Coriolis components is taken into account.

tional part of the wave function will therefore be of the species A for the rotation states where $K=3q$ (q being an integer). The complete rotation-vibration wave functions for these states will therefore be of the species $A\times E=E$. The rotational wave functions of the states where $K=3q\pm1$ will, on the other hand, be of the species E so that the complete rotation-vibration wave functions for such states will have the species $E\times E=A+A+E$.

A perturbation which has the same symmetry as the molecule may remove the degeneracy of two levels of the A species, the level of species E will, however, remain degenerate. The C_{3v} symmetry is, however, resident in the framework of the molecule so that the levels associated with a given value of K which are of species A must be ascribed to the values of $|K-l|$ which are multiples of 3.

Consider now the case where $K=\pm1$. The values of l are, of course, also equal to ±1. The quantity $|K-l|$ may, therefore, be equal to 0 or 2. The former is, of course, the upper component and as a multiple of 3 must be of the species A which may further be split. The lower component is of the species E and must remain degenerate. When $K=\pm2$ and $l=\pm1$ the quantity $|K-l|$ may be equal to 1 or 3. The former of these is evidently the upper component which is of the species E and will, therefore, not split. The other being a multiple of 3 is of species A and may, therefore, split in higher approximations. The quantity $|K-l|$ will, however, take the values 2 and 4 when $K=\pm3$ with $l=\pm1$, neither of which are multiples of three. Neither of these levels will, therefore, be split by the perturbation in any approximation.

We shall finally apply the foregoing to interpret the microwave spectrum of CH_3CN and CH_3NC. It is easily shown that the selection rules are such as to permit the transitions indicated in Fig. 2. This will give rise to lines at the following positions $4B_v-32D_J-6[(B_e^4/\omega_s^2)a^2]/[(1-\zeta)C_v-B_v-6D_{JK}-4D_K]$, $4B_v-32D_J-4D_{JK}$ and $4B_v-32D_J-4D_{JK}\pm4(B_e^2/\omega_s)a$. The first two lines are the same except for terms of the order of the centrifugal stretching. This difference cannot be accurately computed without a knowledge of the nature of the normal coordinate problem. An estimate of this difference may, nevertheless, be had from the work of Slawsky and Dennison[2] since this is essentially the centrifugal stretching of a CH_3 group. The value given by them for D_{JK} is -0.976×10^{-5}. The frequency difference between the first two lines should, therefore, be of the order of 4×10^{-5} cm^{-1} or about 1.2 mc/sec. The last two lines are separated by an interval $\Delta\nu=8(B_e^2/\omega_s)a$. The B values for the two molecules CH_3CN and CH_3NC have been given by Gordy[4] as 0.3066 cm^{-1} and 0.3351 cm^{-1}, respectively. The frequencies ω_8 for these molecules are known to have the values 380 cm^{-1} [10] and 290 cm^{-1}, respectively. This leads to the values for (B_e^2/ω_s), 0.000247 cm^{-1} (i.e., 67.3 mc/sec.) and 0.000387 cm^{-1} (i.e., 92.9 mc/sec.), respectively, for the two molecules CH_3CN and CH_3NC. A knowledge of the normal coordinate problem and the normal frequencies is needed to calculate the coefficient a. This problem has not been solved and to make progress we proceed by observing that $C_e\gg B_e$ so that the molecule resembles a linear molecule. In such cases, as we have seen, the part of a depending upon the $A_{ss\sigma\sigma}^{(\alpha\alpha)}$ is equal to unity. The portion which depends upon the $(\zeta_{ss'}^{(\alpha)})^2$ we can not estimate with great accuracy. There will, on the other hand, be four terms in the sum $4\sum_{s'}(\zeta_{ss'}^{(x)})^2\times\lambda_s/(\lambda_s-\lambda_{s'})$ which, if replaced by $4\langle(\zeta_{ss'}^{(x)})^2\rangle_{Av}\times\sum_{s'}\lambda_s/(\lambda_s-\lambda_{s'})$ where $\langle(\zeta_{ss'}^{(x)})^2\rangle_{Av}$ is an average value of $(\zeta_{ss'}^{(x)})^2$ and the linear molecule approximation that $\sum_{s'}(\zeta_{ss'}^{(x)})^2=1$ is also here adhered to, reduces to $\sum_{s'}\lambda_s/(\lambda_s-\lambda_{s'})$. Taking the values of ω_1, ω_2, ω_3, and ω_4 to be those given by Herzberg,[10] we obtain values for the sum of 0.33[11] and 0.17. We may, therefore, except the coefficient a will be slightly greater than unity, say about 1.2. This yields a separation between the outermost lines of 80 mc/sec. and 110 mc/sec. for CH_3CN and CH_3NC, respectively, compared to the measured values 72 mc/sec. and 111 mc/sec.

The pattern predicted by this theory for the transitions $J=1\rightarrow J=2$, $\Delta K=0$ for these molecules is illustrated in Fig. 4(a) and is in qualitative agreement with experiment. It consists of two lines separated by intervals close to 100 mc/sec. with two lines near the center of these separated by an interval of about one or two mc/sec. Our theory predicts, however, that one of the central lines should lie at the exact center of the outer two components while in reality they are both observed to be displaced a few mc/sec. from the center. This displacement is again of the order of the centrifugal stretching. It may, in fact, be shown that if a set of terms included in $\bar{H}$ of Eq. (21-c) of reference 5, namely,

$$\sum_{s\sigma}(\hbar^2/\lambda_s)^{\frac{1}{2}}\sum_{\alpha}\{[(a_{s\sigma}^{(\alpha\alpha)}/(I_{\alpha\alpha}^{(e)})^2)p_\alpha-\sum_{\beta}{}'(a_{s\sigma}^{(\alpha\beta)}/I_{\alpha\alpha}^{(e)}I_{\beta\beta}^{(e)})p_\beta]P_\alpha\}q_{s\sigma} \quad (9)$$

[10] G. Herzberg, *Infrared and Raman Spectra of Polyatomic Molecules* (D. Van Nostrand Company, Inc., New York, 1945), suggests that an alternate assignment $\omega_8=1124$ cm^{-1} may also be made.

[11] If the alternate value 1124 cm^{-1} is chosen for ω_8 instead of 918 cm^{-1} in the case of CH_3CN the sum $\Sigma_{s'}\lambda_s/(\lambda_s-\lambda_{s'})$ becomes about 0.22.

be included in the calculation of the centrifugal stretching a contribution of significance may be had here. This comes about when twofold degenerate oscillations occur in which case p_s will contain a set of operators $-ih\sum_{s''}\zeta_{s''}^{(z)}\partial/\partial\chi_{s''}$ which has non-vanishing matrix components only which are diagonal in $V_{s''}$ and $l_{s''}$. The proof will not be given here but a method like that used in reference 5 will show that the contribution to be added to the term value (7) will be

$$2\sum\zeta_{s''}^{(z)}l_{s''}K\{(2D_J+D_{JK})J(J+1)+(2D_K+D_{JK})K^2\}.$$

Only the second term will be of interest to us since the first cancels out when $\Delta K=0$. With $\sum_{s''}l_{s''}=l_8=1$ a term $4(2D_J+D_{JK})\zeta_8^{(z)}$ must be added, where $J=K=1$, to the upper Coriolis component which is split by l-type doubling and a similar amount must be subtracted from the lower component which is not split. When $J=2$ the amounts to be added to the upper Coriolis component and subtracted from the lower component will be $12(2D_J+D_{JK})\zeta_8^{(z)}$. Slawsky and Dennison have shown that for molecules like those we are considering D_J is negligible compared to D_{JK}. The two extreme lines will, therefore, both be shifted to higher frequencies by an amount $8D_{JK}\zeta_8^{(z)}$ mc/sec. if $\zeta_8^{(z)}$ is indeed negative and if D_{JK} is negative as predicted by Slawsky and Dennison. Likewise the central line will be shifted toward lower frequencies by an equivalent amount $8D_{JK}\zeta_8^{(z)}$ mc/sec.

The new pattern is seen in Fig. 4(b) where the two outside components are still separated by about 100 mc/sec. Near the center of these, but displaced toward lower frequencies, there will still be two lines separated by an amount $-4D_{JK}-8D_{JK}\zeta_8^{(z)}$ mc/sec. The center most line will then be displaced from the center of the outer components by an amount $16D_{JK}\zeta_8^{(z)}$ mc/sec. The predicted patterns are now substantially in complete agreement with the observed patterns, particularly if one assumes in the case of CH_3CN the difference is so small that the two central lines are not resolved.

It is of interest to insert the data of Gordy, Kessler, and Ring in the above expressions involving D_{JK} and $\zeta_8^{(z)}$. Consider first the case of CH_3CN for which they give the following positions 36870.94, 36903.40, and 36942.15 mc/sec. The two central lines are assumed to be unresolved so that the value $-4D_{JK}-8D_{JK}\zeta_8^{(z)}=0$. The value $16D_{JK}\zeta_8^{(z)}$ will, moreover, be equal to 3.14 mc/sec. so that for $\zeta_8^{(z)}$ one obtains a value -0.5 and for D_{JK} a result -0.4 mc/sec.

There are four lines reported in the spectrum of CH_3NC at the positions 40313.37, 40364.07, 40366.55, and 40424.49 mc/sec. The only assignment of lines which gives reasonable results gives $-4D_{JK}-8D_{JK}\zeta_8^{(z)}=2.48$ mc/sec. and $16D_{JK}\zeta_8^{(z)}=2.38$ mc/sec. This leads to the values $D_{JK}=-0.9$ mc/sec. and $\zeta_8^{(z)}=-0.16$. In each case the values of D_{JK} are of the same order of magnitude as that predicted by Slawsky and Dennison,[2] namely, from -0.3 mc/sec. to -0.5 mc/sec. although the value of D_{JK} obtained for CH_3NC appears a little large.

The author wishes to express his gratefulness to the John Simon Guggenheim Memorial Foundation for a fellowship which has made it possible for him to work at this problem without interruption.

Letters to the Editor

PUBLICATION of brief reports of important discoveries in physics may be secured by addressing them to this department. The closing data for this department is five weeks prior to the date of issue. No proof will be sent to the authors. The Board of Editors does not hold itself responsible for the opinions expressed by the correspondents. Communications should not exceed 600 words in length.

The Angular Correlation of Scattered Annihilation Radiation*

C. S. WU AND I. SHAKNOV
Pupin Physics Laboratories, Columbia University, New York, New York
November 21, 1949

AS early as 1946, J. A. Wheeler[1] proposed an experiment to verify a prediction of pair theory, that the two quanta emitted in the annihilation of a positron-electron pair, with zero relative angular momentum, are polarized at right angles to each other. This suggestion involves coincidence measurements of the scattering of both the annihilation photons at various azimuths. The detailed theoretical investigations were reported by Pryce and Ward[2] and by Snyder, Pasternack, and Hornbostel.[3] The predicted maximum asymmetry ratio of coincidence counts when the two counters are at right angles to each other to coincidence counts when the counters are co-planar is as large as 2.85 and occurs at a scattering angle of $\vartheta=82°$. Bleuler and Bradt[4] used two end-window G-M counters as detectors and observed an asymmetry ratio not inconsistent with the theory. Nevertheless, the margin of error associated with their results is so large that a detailed comparison between the theory and experiments is made rather difficult. In the meantime, Hanna[5] performed similar experiments with more efficient counter arrangements and found the asymmetry ratio observed to be consistently smaller than those predicted. Therefore, it appeared to be highly desirable to reinvestigate this problem by using more efficient detectors and more favorable conditions.

The recently developed scintillation counter has been proved to be a reliable and highly efficient gamma-ray detector. With this improved efficiency, which is around ten times that of G-M counters, there will be an increase in the coincidence counting rate of one hundred times. In our experiments, two RCA 5819 photo-multiplier tubes and two anthracene crystals $1\times1\times\frac{1}{2}$ in. were used. The efficiency for the annihilation radiation obtained with these anthracene crystals is seven to eight percent which compares favorably with the calculated value. The geometrical arrangement is schematically shown in Fig. 1.

The positron source Cu^{64} was activated by deuteron bombardment on a copper target in the Columbia cyclotron. The electroplating method was employed to separate Cu activity from other contaminations. The active Cu^{64} was packed in a small Al capsule of 8-mm diameter and 8-mm length. The annihilation radiation was collimated by a lead block $6\times6\times6$ in. with a $\frac{3}{4}$-in. channel drilled through the center of the block, such that the spread of the beam was found to be less than 3°. The aluminum scatterers were $\frac{1}{2}$ in. in diameter and 1-in. long. They were designed to absorb about 40 percent of the annihilation radiation lengthwise and to limit the multiple scattering of the radiation scattered at 90° to less than 15 percent. The crystal of the counter subtends an angle of 43° at the point in the scatterer where 20 percent of the incident radiation has been absorbed—that is, at the absorption midpoint of the scatterer. The mean scattering angle is very close to 82°, the predicted maximum of anisotropy. Under these conditions, the scattered radiation taken as the counting difference detected by the scintillation counter with and without the scatterer in place is three times the over-all background.

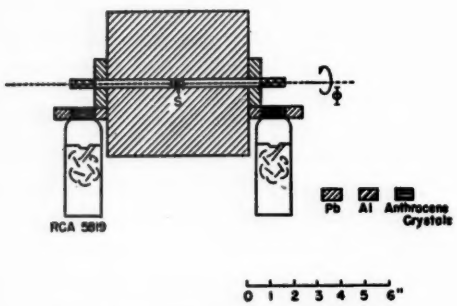

FIG. 1. Schematic diagram of experiment.

In taking the coincidence measurements, one detector was kept fixed in position, and the second detector was oriented to four different positions with azimuth differences (φ) of 0°, 90°, 180°, and 270° between the detector axis. After that, the second detector was kept fixed and the first one rotated. The total period of measurement lasted about 30 continuous hours. On account of the high coincidence rate observed (the true coincidence rates for the perpendicular position at the beginning was of the order of four per minute), the statistical deviations are much improved as compared to the results from G-M counters. The asymmetry ratio from our best run is

$$\frac{\text{Coincidence counting rate } (\perp)}{\text{Coincidence counting rate } (\parallel)}=2.04\pm0.08,$$

where ±0.08 is the probable mean error. The calculated asymmetry ratio for our geometrical arrangement is 2.00. Therefore, the agreement is very satisfactory. Further work is being planned to extend the investigations to more ideal geometrical conditions.

We wish to express our appreciation to Professors J. R. Dunning, W. W. Havens, Jr., and L. J. Rainwater for their constant interest and encouragement. We also wish to thank the cyclotron group for preparing the Cu^{64} source and the U. S. AEC which aided materially in the performance of this research.

* Partially supported by the AEC.
[1] J. A. Wheeler, Ann. New York Acad. Sci. 48, 219 (1946).
[2] M. H. L. Pryce and J. C. Ward, Nature 160, 435 (1947).
[3] Snyder, Pasternack, and Hornbostel, Phys. Rev. 63, 440 (1948).
[4] E. Bleuler and H. L. Bradt, Phys. Rev. 73, 1398 (1948).
[5] R. C. Hanna, Nature 162, 332 (1948).

The Optical Detection of Radiofrequency Resonance

M. H. L. PRYCE
Clarendon Laboratory, Oxford, England
October 31, 1949

IN a recent paper under this title, Bitter[1] discusses the effect of a radiofrequency field on the optical Zeemann effect. He illustrates the question by treating an atomic system whose ground state is ^2S, making optical transitions to a ^2P state. The atoms are in a steady magnetic field H_z on which is superposed a rotating radiofrequency field H_0, in the xy plane, of angular frequency ω. According to Bitter, when there is a resonance between ω and $\omega_0=g\mu_0H_z/\hbar$, the precession frequency of the spin moment in the ^2S ground state, certain observable changes happen to the Zeeman effect.

Such an effect certainly occurs, but Bitter's discussion is incorrect, and it is very doubtful if the effect could be observed in practice. Bitter calculates the frequencies of the Zeemann lines by means of a *mean energy* of the ground level in the presence of the radiofrequency field. This is a fallacious argument. The fre-

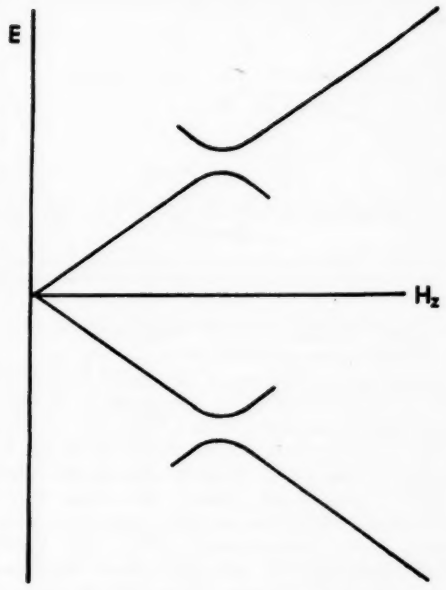

FIG. 1. Effective energy of ground level $J=\frac{1}{2}$ in the presence of a radiofrequency field.

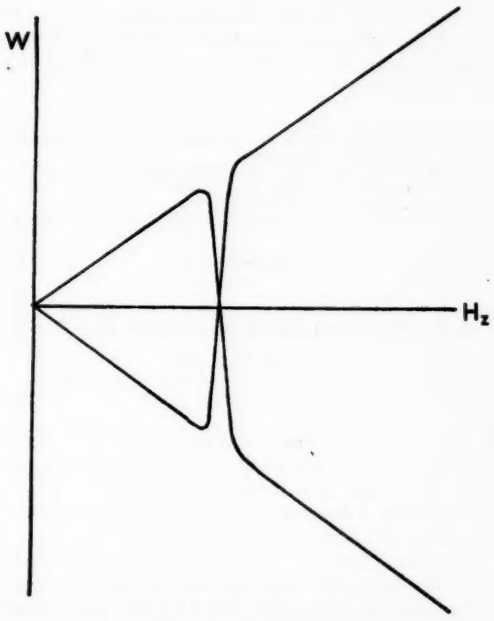

FIG. 2. Mean energy according to Bitter.

quencies are those which are associated with the non-vanishing matrix elements of electric dipole moment coupling ground and excited states, which are simply calculated from the time-dependent wave functions quoted by Bitter. These frequencies are such as would occur if the ground level had energies

$$E=\pm\tfrac{1}{2}\hbar\omega\pm\tfrac{1}{2}[\hbar^2(\omega_0-\omega)^2+(g\mu_0H_0)^2]^{\frac{1}{2}}. \quad (1)$$

In this expression all four combinations of the $\pm$ signs are to be taken. The appearance of four effective energy values, instead of two, can be understood in terms of the possibility of the emission or absorption of one quantum or no quantum by the radiofrequency field. The intensities of the lines are obtained from the intensities in the absence of radiofrequency field, by multiplying by a factor

$$\frac{1}{2}\left[1\pm\frac{\hbar(\omega_0-\omega)}{[\hbar^2(\omega_0-\omega)^2+(g\mu_0H_0)^2]^{\frac{1}{2}}}\right], \quad (2)$$

the sign being + if the two signs are equal in Eq. (1) and − if unequal.

Equation (1) for the effective energy should be contrasted with Bitter's result for the mean energy,

$$W=\pm\tfrac{1}{2}g\mu_0H_z\left[\frac{\delta+H_0/H_z}{(1+\delta^2)^{\frac{1}{2}}}\right]$$

$$=\pm\tfrac{1}{2}\hbar\omega_0\left[\frac{\hbar(\omega-\omega_0)+g\mu_0H_0^2/H_z}{[\hbar^2(\omega_0-\omega)^2+(g\mu_0H_0)^2]^{\frac{1}{2}}}\right]. \quad (3)$$

The two expressions are plotted in Figs. 1 and 2.

The intensity factors (2) are such that the intensity becomes very small when the energy deviates appreciably from the straight lines of Fig. 1. The changes of frequency associated with an appreciable intensity are therefore smaller than predicted by Bitter, namely, of order $\frac{1}{2}g\mu_0H_0/\hbar$ instead of $\frac{1}{2}g\mu_0H_z/\hbar$. Their detection will probably be rather difficult, as the mean position of the two components into which each Zeemann line is split weighted with their intensities, coincides with the position without radiofrequency field. The splitting would therefore have to be nearly resolved to detect significant changes in the polarization distribution on the Zeemann pattern.

[1] F. Bitter, Phys. Rev. **76**, 833 (1949).

The Beta-Spectrum of Ca^{45}*

P. MACKLIN, L. FELDMAN, L. LIDOFSKY, AND C. S. WU
Pupin Physics Laboratories, Columbia University, New York, New York
November 21, 1949

CALCIUM[45] was first produced in the cyclotron by bombarding calcium with deuterons or neutrons. The radioactivity consists of a soft beta-radiation of long half-life (152 days).

The upper energy of the Ca^{45} beta-spectrum is listed in Seaborg and Perlman[1] as 0.260 or 0.21 Mev by the aluminum absorption method and 0.25 Mev by spectrometer measurement. The details of the spectrometer measurement are unfortunately not available since they appear in the Plutonium Project Reports. The most recent value reported, 0.22 Mev,[2] was obtained by absorption methods.

Recently, we received a shipment of Ca^{45} from the Isotopes Division of the AEC at Oak Ridge of specific activity around 2 μc/mg which is sufficiently high for investigation of the upper energy region of its beta-spectrum in our spectrometer. Several sources with approximate average thicknesses varying from 200–450 μg/cm^2 were prepared on collodion backings of 12–14 μg/cm^2. The spectrum was investigated in the Columbia magnetic solenoidal spectrometer, using a counter with a collodion window of about 40 μg/cm^2 thickness and with three percent resolution (full

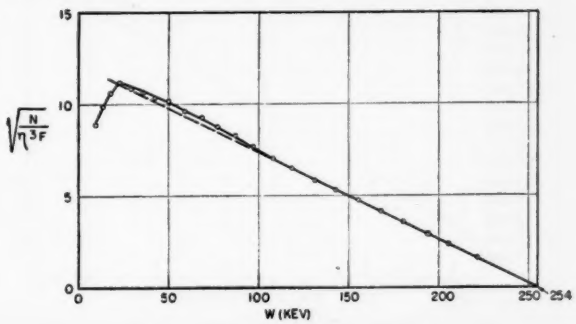

FIG. 1. Fermi plot of Ca^{45} beta-spectrum.

width at half-maximum). The end point of the spectrum as extrapolated from the Fermi plot is 254±3 kev. In constructing the Fermi plot, the non-relativistic Coulomb factor was used. A typical plot for a source of about 200 $\mu g/cm^2$ average thickness is shown in Fig. 1. The graph is linear from the end point to about 90 kev and deviates above the straight line below this energy. Previous experience in the investigation of low energy beta-spectra has shown that a 200-$\mu g/cm^2$ source has quite a distorting effect on the Fermi plot below 90 kev, yielding a greater relative abundance of slow electrons. We therefore attribute the non-linearity of the Fermi plot in the low energy region to the unfavorably thick source used and conclude that thinner and more uniform sources would probably yield a linear Fermi plot to energies below 90 kev.

The above end point combined with the half-life of 152 days gives an approximate *ft* value of 0.7×10^6, which empirically classifies Ca^{45} in the first-forbidden group. The linear Fermi plot is not contra-indicated by theory since, for certain types of interaction, a forbidden transition may yield a linear Fermi plot.

We should like to thank the U. S. AEC which aided materially in the performance of this research.

* Partially supported by the AEC.

[1] G. T. Seaborg and I. Perlman, Rev. Mod. Phys. **20**, 592 (1948).
[2] J. L. Meem, Jr. and F. Maienscheim, Phys. Rev. **76**, 328 (1949).

Temperature Dependence of Scintillation Pulses in Anthracene*

G. G. KELLEY AND M. GOODRICH
Oak Ridge National Laboratory, Oak Ridge, Tennessee
November 16, 1949

MEASUREMENT has been made of the decay constant and light output of anthracene scintillation pulses as a function of temperature. Values of the decay constant were obtained by photographing a series of individual pulses at each temperature using an oscilloscope with a vertical rise time of 6×10^{-9} sec. Because of statistical fluctuation in the individual pulses, many pulses had to be averaged in some manner. Two methods of averaging were used. First, exponentials were drawn by eye through twenty pulses selected at random at each temperature and averaged. Then on the suspicion of systematic errors, these twenty pulses were added graphically. This second method was employed at only two points because it was much more tedious and agreed with the first within two percent. It gave evidence, however, that the decay is exponential within the accuracy of the experiment over nearly a decade. Figure 1 shows the dependence on temperature. It appears to be linear with positive slope and to have an intercept with the temperature axis at −273°C. The

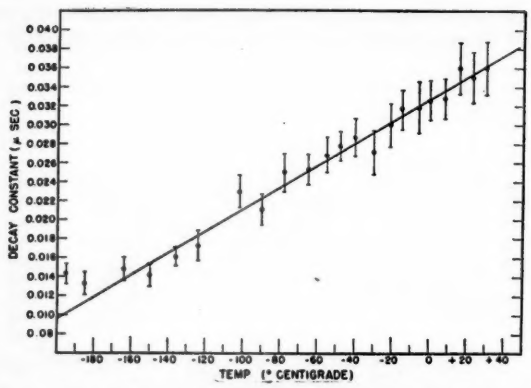

FIG. 1. Decay of scintillation pulses in anthracene. Brackets indicate 95 percent confidence interval based on spread of data.

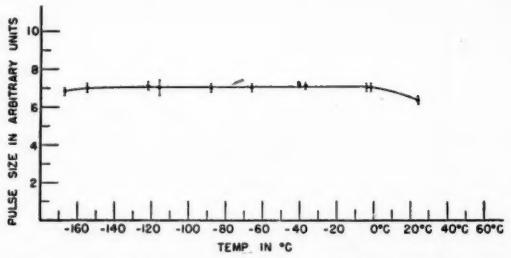

FIG. 2. Variation with temperature of the light pulse size in anthracene. (Conversion electrons from Cs^{137} measured with 1P28 photo-multiplier.)

decay constant at liquid nitrogen temperature is in agreement with the measurements of Collins.[1]

The temperature dependence of the size of the pulses has been investigated with a scintillation spectrometer of the type described by Jordan and Bell.[2] With a 1P28 photo-multiplier, the results, Fig. 2 show an essentially constant pulse size from room temperature to near liquid nitrogen temperature. With a 1P21 tube, however (results not shown), the pulses were some 30 percent larger at −60°C than at room temperature. This confirms qualitatively earlier measurements made at this laboratory by P. R. Bell. Since the 1P28 tube has a lower short wave-length cut-off than the 1P21, it seems likely that the pulse size using the 1P21 may then be attributed either to a lowering of the short wave-length limit of its envelope or to a shift to higher wave-lengths of the scintillation spectrum. We have obtained spectrographic evidence for the former. Either explanation requires that the scintillation spectrum extend below 3400A which is the short wave-length cut-off of the 1P21. This is considerably lower than has been reported.[3]

* This document is based on work performed under Contract No. W-7405, eng. 26, for the Atomic Energy Project at the Oak Ridge National Laboratory, Oak Ridge, Tennessee.
[1] George B. Collins, Phys. Rev. **74**, 1543 (1948).
[2] W. H. Jordan and P. R. Bell, Nucleonics **5**, 30 (1949).
[3] Louise Roth, Phys. Rev. **75**, 983 (1949).

A 7×10^{-9} sec. Isomeric State in $_{79}Au^{197}$ *

F. K. MCGOWAN
Oak Ridge National Laboratory, Oak Ridge, Tennessee
November 10, 1949

USING sources of Hg^{197} and an experimental arrangement similar to that described in a previous letter,[1] an excited state of Au^{197} with a half-life $(7.0\pm1.0)\times10^{-9}$ sec. has been observed. In Fig. 1 the number of delayed coincidences is plotted as a function of delay time. The portion of the solid curve for delays less than 3.5×10^{-8} sec. and points indicated by circles represent the gross data. After subtraction of random coincidences the solid curve for delay time $T\geqslant3.5\times10^{-8}$ sec. represents the decay of the short-lived isomeric state which has been produced by the *K*-capture decay of Hg^{197}.

Figure 2 shows the number of coincidences as a function of delay time obtained with a source of Te^{125*} (∼58 day). This resolution curve is typical of a negative result. The majority of the radioactive species investigated give similar curves exhibiting a sharp break at a delay of 3.0 to 3.5×10^{-8} sec. For larger delays the coincidence rate is constant and equal to the computed random coincidence rate.

The stilbene crystals, which are cemented to the tube envelope with Canada balsam, and Type 5819 multiplier tubes were operated at room temperature. The background (single counts) with phosphor in place is ∼200 c/m of which only 60 c/m is due to thermionic electrons leaving the photo-cathode. This corresponds to a pulse discrimination level such that incident radiation as low as 50 kev energy is detected.

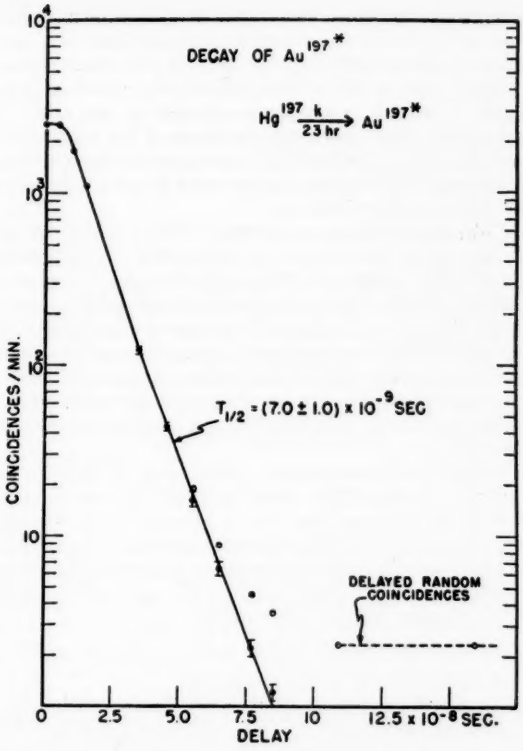
DECAY OF Au197*
Hg197 k 23 hr Au197*
T1/2 = (7.0 ± 1.0) x 10-9 SEC
DELAYED RANDOM COINCIDENCES
COINCIDENCES / MIN.
DELAY
0 2.5 5.0 7.5 10 12.5 x 10-8 SEC.

FIG. 1. Delayed coincidences as a function of delay time.

Using a high speed synchroscope developed by G. G. Kelley[2] photographs of the individual signals from the Type 5819 multiplier showed the presence of delayed signals due to the decay of the isomeric state.

Hg^{197} as listed in the Table of Isotopes[3] is known to decay by K-capture with periods 23 hr. and 64 hr. All points on the decay curve of Au^{197*} appeared to decay according to the 23-hr. period. Huber *et al.*[4] have observed that 4 percent of the disintegrations of Hg^{197} (23 hr.) lead to a 7.5 sec. isomeric state in Au^{197*} and that 96 percent of the disintegrations are followed by γ-ray transitions corresponding to 165 and 135 kev which are strongly converted.

A delayed coincidence scintillation spectrometer[1] is being used to investigate both the radiation spectrum announcing the formation of the isomeric state and the spectrum resulting from its decay. These results and a discussion of the disintegration scheme will be reported later.

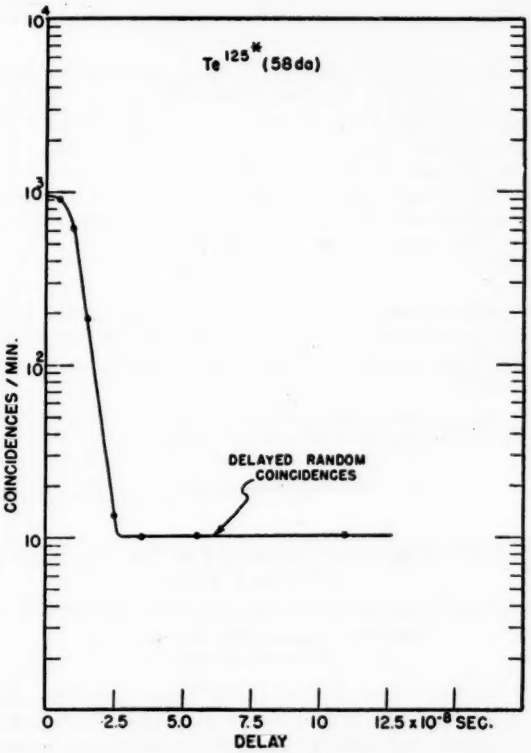

FIG. 2. Coincidences as a function of delay time obtained with a source of Te^{125}.

* This document is based on work performed under Contract No. W-7405, eng. 26 for the Atomic Energy Project at Oak Ridge National Laboratory.

[1] F. K. McGowan, Phys. Rev. **76**, 1730 (1949).
[2] G. G. Kelley (to be published).
[3] G. T. Seaborg and I. Perlman, Rev. Mod. Phys. **20**, 630 (1948).
[4] Huber, Steffen and Humbel, Helv. Phys. Acta **21**, 192 (1948).

Lifetimes of Excited States of Au^{197}, Fe^{57}, Cd^{111}, Hg^{198}, and Tl^{203} *

MARTIN DEUTSCH AND W. E. WRIGHT
Laboratory for Nuclear Science and Engineering and Department of Physics, Massachusetts Institute of Technology, Cambridge, Massachusetts

November 10, 1949

WE have applied the method of delayed coincidences to the measurement of nuclear lifetimes between 5×10^{-9} sec. and 1×10^{-6} sec. in several radioactive decays. Scintillation counters using stilbene or anthracene with RCA 5819 photomultiplier tubes were used with wide band amplifiers of a design due to Elmore and a fast electronic coincidence circuit. Beta-beta-, beta-gamma-, and gamma-gamma-coincidences were studied. In most cases the lifetimes of the excited states were too short to be measured by our instrument and only upper limits can be set. Table I summarizes some of our results. The 8×10^{-8} sec. state in Cd^{111} had been previously reported by Deutsch and Stevenson[1] in the decay of In^{111}. We have now also found it in the decay of the 43′ isomeric state of Cd^{111}. The new 8×10^{-9} sec. states in

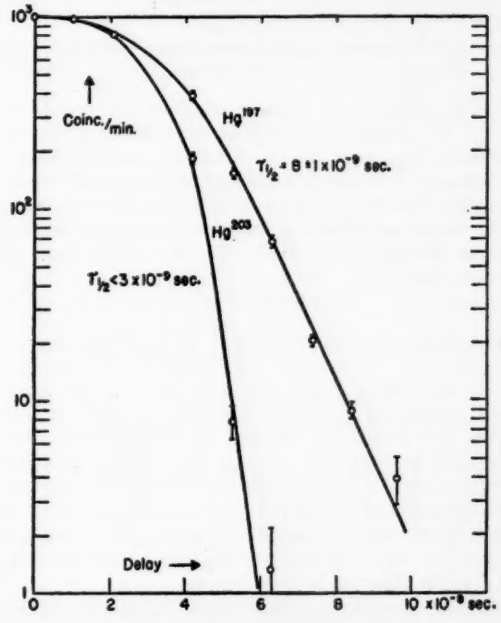

FIG. 1. Typical decay curves.

TABLE I. Life-times of excited states.

	Parent	$\tau_{\frac{1}{2}} \times 10^6$ sec.	$E\gamma$ Mev
Au^{197}	Hg^{197}	0.8 ± 0.1	0.13
Fe^{57}	Co^{57}	11 ± 1	0.014
Cd^{111}	In^{111} Cd^{111*}	8 ± 1	0.247
Hg^{198}	Au^{198}	<0.4	0.411
Tl^{203}	Hg^{203}	<0.3	0.28

An^{197} appears in the 23 hr. Hg^{197} decay but not in the 18 hr. Pt^{197}. The probable energy of 135 kev is assigned on the basis of the decay scheme of Frauenfelder *et al.*,[2] and the fact that the delayed conversion electrons are more readily absorbed than those preceding the delay. The 1.1×10^{-7} sec. state in Fe^{57} appears in the decay of 270 d Co^{57}. The 14-kev gamma-ray has been established by magnetic spectrometer and proportional counter measurements of Hedgran and Deutsch (to be published). Assignment of the observed life time to this transition is based on absorption of the delayed and preceding radiations. Most of the counts in both components are due to iron K x-rays which are quite well detected with anthracene crystals. The upper limit of 4×10^{-9} sec. on the lifetime of the 411-kev state in Hg^{198} is established beyond doubt. It contradicts the result of MacIntyre[3] on the same transition. Besides the activities listed in Table I we studied and failed to find measurable periods in the decay of Ir^{192}, $Te^{121, 123, 125}$ (Sb and d), Au^{199}, Cs^{134}, Co^{60}, Rh^{106}. Bittencourt and Goldhaber[4] had reported a 3×10^{-8} sec. state in the decay of Te^{121} which we are not able to confirm. Figure 1 shows typical decay curves obtained.

Some of the radionuclides were obtained from the AEC, the others were prepared in the MIT cyclotron.

* This work was supported in part by the Joint Program of the AEC and the ONR.

[1] Deutsch and Stevenson, Phys. Rev. **76**, 184 (1949).
[2] Frauenfelder *et al.*, Helv. Phys. Acta **20**, 238 (1947).
[3] W. J. MacIntyre, Phys. Rev. **76**, 312 (1949).
[4] Bittencourt and Goldhaber, Phys. Rev. **70**, 780 (1946).

Applications of Total Reflection of Neutrons*

M. HAMERMESH
Argonne National Laboratory, Chicago, Illinois
November 17, 1949

TOTAL reflection of neutrons provides a powerful technique for the measurement of coherent scattering cross sections and phases. Some examples of its possible application are:

1. Low cross section.—A typical application would be to vanadium. Shull and Wollan[1] using crystal diffraction have been able only to set an upper limit of 0.1 barn for σ_{coh} and are unable to determine the sign of the amplitude. The critical angle for total reflection is given by

$$\theta_c = \lambda(NC/\pi)^{\frac{1}{2}},$$

where λ is the neutron wave-length, N is the number of nuclei per cc, and C is the coherent amplitude (or the average of the coherent amplitudes of the constituent nuclei in the case of compounds). Assuming $\sigma_{coh} = 0.01$ barn, for $\lambda = 4.4$A we find $\theta_c \sim 7$ minutes. The presence or absence of total reflection determines the sign of the amplitude without any precise measurements. Even for $\sigma_{coh} = 0.01$ barn, θ_c will be ~ 4 minutes. Any impurities in the vanadium of the mirror could cause large errors. Another possible mirror would be vanadium carbide; for a vanadium cross section of 0.1 barn, the two possible signs of the amplitude give critical angles differing by ~ 20 percent.

2. Highly absorbing materials.—It is difficult to apply crystal diffraction methods to measurement of σ_{coh} for strong absorbers. But the real part of the index of refraction, and the critical angle depend very little on the absorption cross section.[2] With $\sigma_{coh} = 1$ barn and $\sigma_{abs}/\lambda = 2 \times 10^3$ barns/A, the effect of the absorption on the critical angle is only $\sim$three percent. By mirror experiments it should be possible to measure σ_{coh} for Cd, B, and other strong absorbers. We should note that the shape of the reflection curve depends on the absorption.[3] In the presence of absorption we no longer obtain "total" reflection; the curve of reflectivity smoothes out as the absorption increases.

3. Coherent amplitude of hydrogen.—Measurement of critical angle for a given wave-length can be applied to a determination of the coherent amplitude of hydrogen by using hydrogen compounds as mirrors. This method has one great advantage over those previously used (ortho-parahydrogen scattering and crystal diffraction) in that no complicated calculations and no uncertain corrections are necessary. In total reflection we are dealing with the forward-scattered beam (zero-order Bragg reflection) so that form factors due to molecular structure or thermal agitation are *always* unity.

4. Neutron-electron interaction.—Here again the form factor for the electron scattering is unity so that the neutron-electron interaction contributes fully. For a tungsten mirror a neutron-electron interaction of 5000 volts will contribute 1.4 percent to θ_c. The nuclear amplitude would have to be determined by a separate experiment in which the electron form factor is made to approach zero (e.g., by use of short wave-lengths).

* Condensed from Argonne National Laboratory Report-4298 (May 12, 1949).

[1] C. G. Shull and E. O. Wollan (unpublished).
[2] M. L. Goldberger and F. Seitz, Phys. Rev. **71**, 294 (1947).
[3] A. H. Compton and S. K. Allison, *X-Rays in Theory and Experiment* (D. Van Nostrand Company, Inc., New York, 1935), p. 305 ff.

Note on Rotational Universe

C. Y. FAN
Institute for Nuclear Studies, University of Chicago, Chicago, Illinois
November 10, 1949

THE model of rotational universe was proposed by Gamow,[1] and studied in detail by Gödel.[2] The angular velocity calculated by Gödel is $2(\pi\kappa\rho)^{\frac{1}{2}}$ where κ is Newton's gravitational constant and ρ is the density of the universe. This result is rather strange because the angular momentum is not conserved during expanding. Assume that the universe is an ellipsoid of major axes "a" and minor axis "b", the rotation is along the minor axis, then the angular momentum in classical sense is

$$m = \tfrac{2}{5} M a^2 2(\pi\kappa\rho)^{\frac{1}{2}},$$

where M is the mass of the universe. During expanding, ρ is only decreasing inversely as a^2 or a^3 and so m will be increasing as a or $a^{\frac{1}{2}}$. This is impossible except introducing new concept or new mechanism.

[1] G. Gamow, Nature **158**, 549 (1946).
[2] Kurt Gödel, Rev. Mod. Phys. **21**, 447 (1949).

On the Hyperfine Structure of the $^2P_{\frac{1}{2}}$ State of Tl^{205} and Tl^{203}

A. BERMAN, P. KUSCH AND A. K. MANN*
Columbia University, New York, New York
November 21, 1949

IT has been found that an atomic beam of thallium may be evaporated from an iron oven of the type conventionally used in molecular beam research and that the beam may be detected by the formation of positive ions on a hot oxidized tungsten filament. It has therefore been possible to observe the hyperfine

structure of the $^2P_{\frac{1}{2}}$ ground state of Tl^{205} and Tl^{203} by the atomic beam magnetic resonance method.

Since the zero field h.f.s. separation of the two F levels is very large, observation of the lines $\Delta F=\pm 1$ presents large technical difficulties. The $\Delta\nu$ has, therefore, been determined from an observation of the lines $\Delta F=0$, $\Delta m_F=\pm 1$. The largest contribution to the frequencies of the lines occurs from the terms $g_F\mu_0 H/h$, but a small term, quadratic in H, permits $\Delta\nu$ to be determined.

The spin of both Tl^{205} and Tl^{203} is known to be $\frac{1}{2}$. Thus, only two lines $(1,1)\leftrightarrow(1,0)$ and $(1,0)\leftrightarrow(1,-1)$ of the specified type exist for each isotope. If it is assumed that $g_J(^2P_{\frac{1}{2}}, \mathrm{Tl})=g_J(^2P_{\frac{1}{2}}, \mathrm{In})$, then it is possible from the known values[1,2] of $g_I(\mathrm{Tl})/g_I(\mathrm{H})$ and $g_I(\mathrm{H})/g_J(^2P_{\frac{1}{2}}, \mathrm{In})$ [3] to find $g_I(\mathrm{Tl})/g_J(^2P_{\frac{1}{2}}, \mathrm{Tl})$. By application of the well-known relationships which describe the energies of the magnetic levels of an atom for which $J=\frac{1}{2}$, the two observed line frequencies then determine both $\Delta\nu$ and the parameter

$$x=(g_J-g_I)\mu_0 H/h\Delta\nu.$$

It is found that

$$\Delta\nu^{(205)}=(21312\leftrightarrow 3)\times 10^6 \text{ sec.}^{-1}$$

and

$$\Delta\nu^{(203)}=(21113\pm 3)\times 10^6 \text{ sec.}^{-1}.$$

Since the data of the experiment are reduced to the frequencies of four lines at a fixed magnetic field, the quantity $x\Delta\nu/(g_J-g_I)$ should be the same when calculated for each of the two isotopes of thallium. The agreement is excellent and justifies the precision for the $\Delta\nu$'s if both g_I values are assumed to be negative. The negative g_I's are in agreement with the positive magnetic moments deduced from observations of the nuclear magnetic resonance of thallium by the nuclear induction method. From these results, the ratio

$$\frac{\Delta\nu(205)}{\Delta\nu(203)}=1.00947\pm 0.00020$$

is in excellent agreement with the ratio

$$\frac{\Delta\nu'(205)}{\Delta\nu'(203)}=1.00966\pm 0.00046$$

of the h.f.s. splittings of the $\lambda 4946$ line in the spectrum of Tl II, measured by Schuler and Korshing.[4]

Poss has found that

$$\frac{g_I^{205}}{g_I^{203}}=1.00986\pm 0.00005.$$

The discrepancy between this value and the ratio of the $\Delta\nu$'s is well beyond experimental error.

This appears to be another example of an effect observed previously for other pairs of isotopic nuclei[5-7] which has been explained,[8] in the case of H and D in terms of effects arising from the finite structure of the nucleus.

* Now at the University of Pennsylvania, Philadelphia, Pennsylvania.
[1] H. L. Poss, Phys. Rev. **75**, 600 (1949).
[2] W. G. Proctor, Phys. Rev. **75**, 522 (1949).
[3] H. Taub and P. Kusch, Phys. Rev. **75**, 1481 (1949).
[4] H. Schuler and H. Korshing, Zeits. f. Physik **105**, 168 (1937).
[5] J. E. Nafe and E. B. Nelson, Phys. Rev. **73**, 718 (1948).
[6] F. Bitter, Phys. Rev. **76**, 150 (1949).
[7] P. Kusch and A. K. Mann, Phys. Rev. **76**, 707 (1949).
[8] A. Bohr, Phys. Rev. **72**, 1109 (1948).

The Electric Quadrupole Moment of the Deuteron*

G. F. Newell
University of Illinois, Urbana, Illinois
November 14, 1949

As has been pointed out previously,[1-3] the determination of the quadrupole moment of the deuteron requires finding the ratio of the quadrupole interaction energy to the value of the electric field gradient at the D nucleus.

The interaction energy in HD and D_2 molecules has been determined experimentally,[1] but the field gradient must be calculated from a suitable electronic wave function for the molecule. This calculation was originally done by A. Nordsieck[2] and later by E. Ishiguro[3] with resulting values $Q=2.73\times 10^{-27}$ cm² and 2.79×10^{-27} cm², respectively. Both calculations were estimated to be within ± 2 percent, overshadowing the experimental error of 0.6 percent.

By means of the variation principle, a new six-parameter electronic wave function has been determined for the ground state of the molecule. The field gradient as calculated from this wave function leads to the value $Q=2.766\times 10^{-27}$ cm². In spite of considerable effort to reduce the over-all calculational error in the electric field gradient to a minimum, it was unfortunately not found possible to reduce the error below 0.6 percent. It is felt that any substantial improvement in the accuracy of the calculation would require high speed automatic computing means.

The total probable error in Q, due to both experiment and calculation is thus taken to be $\sqrt{2}$ (0.6) percent = 0.9 percent:

$$Q=(2.766\pm 0.025)\times 10^{-27} \text{ cm}^2.$$

The author wishes to thank Professor A. Norsieck for suggesting the problem and for his helpful discussions. Details of the calculation will be published later.

* Assisted by ONR and AEC.
[1] Kellogg, Rabi, Ramsey, and Zacharias, Phys. Rev. **57**, 677 (1940).
[2] A. Nordsieck, Phys. Rev. **58**, 310 (1940).
[3] E. Ishiguro, J. Phys. Soc. Japan **3**, 133 (1948).

Functions Used in Flügge's Method of Predicting Approximate Spatial Neutron Distributions*

L. Secrest
Laboratory for Nuclear Science and Engineering, Masschusetts Institute of Technology, Cambridge, Massachusetts
November 16, 1949

A method due to Flügge,[1] which permits prediction of the approximate spatial distributions of neutrons in an infinite hydrogenous medium due to a point source of monoenergetic neutrons of energy E_0, applies age theory to the distributed source of those neutrons that have made one slowing-down collision. The assumption is made that these neutrons have an average energy E_0/e. The resulting distribution equation can be put into the form

$$qr^2=\frac{Q}{4\pi\lambda_0}[xe^{-x^2}][F(a+x)-F(a-x)], \quad x=r/2L_s, \quad a=L_s/\lambda_0,$$

where the slowing-down distance, L_s, is measured from the energy E_0/e, λ_0 is an "effective" mean-free-path for a first collision with hydrogen, r is the space coordinate, and Q is the source strength. The functions $F(Z)$ and $[-F(-Z)]$ are tabulated by Flügge for values of Z from zero up to and including $Z=3.0$.

This method was applied to the analysis of various experimental distributions in collaboration with Professor C. W. Tittle of North Texas State College, the results of which will be the subject

Table I. Tabulation of $F(Z)$ and $-F(-Z)$.

Z	$F(Z)$	$-F(-Z)$	$\log[-F(-Z)]$
3.0	1.20	2.93×10^3	3.46687
3.5	1.28	6.49×10^4	4.81224
4.0	1.35	2.43×10^6	6.38561
4.5	1.41	1.54×10^8	8.18752
5.0	1.47	1.64×10^{10}	10.21484
5.5	1.52	2.94×10^{12}	12.46835
6.0	1.57	8.76×10^{14}	14.94250
6.5	1.61	3.80×10^{17}	17.57978
7.0	1.65	3.60×10^{20}	20.55630

of a later report. It was necessary to extend Flügge's tables to include values of $F(Z)$ and $[-F(-Z)]$ for Z up to $Z=7.0$. The new values are given in Table I.

* This research has been supported by the Joint Program of ONR and the Bureau of Ships.

[1] S. Flügge, Physik. Zeits. **44**, 445–455 (1943).

Radioactive Xenon 125, and Xenon 127

D. L. ANDERSON*
Harvard University, Cambridge, Massachusetts
AND
M. L. POOL
The Ohio State University, Columbus, Ohio
November 17, 1949

XENON 125: Cyclotron bombardments by alpha-particles on two samples of tellurium† have been made. In one sample the Te^{122} isotope had been enriched to 79.4 percent, and in the other sample the Te^{124} isotope had been enriched to 83.9 percent. A previously unreported 20±1-hour activity appeared in the Te^{122} sample.

By means of a chemical separation this 20-hour activity was shown to be due to a gas, presumably xenon. The bombarded sample of Te^{122} was dissolved in a melted flux of sodium carbonate and sodium nitrate, to which had been added some potassium bromide to serve as a carrier for any iodine produced by an α,p reaction during bombardment. The mixture was heated in an evacuated chamber until any gaseous products of the bombardment had been driven off. The fluxing chamber was then cooled, to allow the mixture to solidify and to condense any possible, although unlikely, halogen vapors. The remaining gas was swept, with air, into a thin-window glass sample holder. This technique was first checked by use with a sample of Hilger tellurium bombarded with alpha-particles, from which the 5.3-day $xenon^{133}$ was found to be separated satisfactorily.

The reaction leading to the 20-hour activity is then $Te^{122}(\alpha,n)Xe^{127}$. Few positrons, if any, are emitted by this xenon activity.

The presence of x-rays that would accompany K-capture or internal conversion was investigated. Aluminum foil absorption measurements were made with a Wulf electrometer fitted with a magnet arranged to deflect any primary or secondary charged particle radiation away from the ionization chamber. The absorption data showed the presence of x-rays of wave-length 0.44A, corresponding to the K x-rays of iodine. From absorption measurements repeated at intervals it was possible to show that the intensity of the x-radiation decayed with a half-life of the order of 20 hours. This would seem to establish that the 20-hour Xe^{125} activity decays, in large measure, by K-capture.

Absorption measurements with copper indicated that a weak 0.6 Mev gamma-ray was also associated with this activity.

Xenon 127: An activity of 34-days half-life has been obtained by a proton bombardment of iodine.[1] The assignment was tentatively made to Xe^{127}.[2] This assignment may now be considered reasonably certain since the activity is readily obtained by bombarding enriched Te^{124} with alpha-particles. The activity obtained by the reaction $Te^{124}(\alpha,n)Xe^{127}$ has a half-life of 32±2 days.

The support received from The Ohio State University Development Fund and the Graduate School is gratefully acknowledged. The chemical separations in the course of this work were ably performed by Mr. H. L. Finston and Mr. R. M. Dyer.

* Now at Oberlin College, Oberlin, Ohio.
† Supplied by the Y-12 Plant, Carbide and Carbon Chemicals Corporation, through the Isotopes Division, U. S. Atomic Energy Commission, Oak Ridge, Tennessee.

[1] Creutz, Delsasso, Sutton, White, and Barkas, Phys. Rev. **58**, 481 (1940).
[2] G. T. Seaborg and I. Perlman, Rev. Mod. Phys. **20**, 585 (1948); Josef Mattauch and Arnold Flammersfeld, "Isotopenbericht," Zeits. f. Naturforschung, Tübingen (1949).

Units of Radioactivity

L. F. CURTISS,* R. D. EVANS, WARREN JOHNSON, AND GLENN T. SEABORG

IN November, 1947, a joint committee of the Divisions of Chemistry and Chemical Technology and of Mathematical and Physical Sciences of the National Research Council was appointed to make recommendations regarding standards and units of radioactivity. This committee unanimously adopted the recommendations quoted below. The committee would like to point out that these recommendations effectively divorce the curie from the disintegration rate of radium by assigning to the former an arbitrary magnitude (3.7×10^{10} disintegration/sec.) approximately equal to the disintegration rate of radium. This arbitrary figure is therefore not influenced by any future revisions of the generally accepted disintegration rate of radium. This recommendation has been submitted to the Joint Commission on Standards, Units, and Constants of Radioactivity of the International Unions of Chemistry and Physics for the purpose of obtaining international agreement.

This changes, slightly, the meaning of the curie when applied to radium. For example 1 curie of radon is no longer, on the basis of these recommendations, the amount in equilibrium with 1 gram of radium, but is the amount undergoing 3.7×10^{10} disintegrations per second. Similarly, 1 mg and 1 mc of radium are no longer rigorously synonymous. This distinction has a number of precedents in physics; for example the international ampere, now abolished, was not quite equal to the absolute ampere and the angstrom unit is nearly, but not quite, equal to 1000 x units.

> "*curie.*—The curie should be defined as that quantity of any radioactive species (radioisotope) undergoing exactly 3.700×10^{10} disintegrations per second.
> "*rutherford.*—The rutherford should be defined as that quantity of any radioactive species (radioisotope) undergoing 10^6 disintegrations per second.
> "*rhm.*—For the quantitative comparison of radioactive sources emitting gamma-rays, for which disintegration rates cannot be determined, the *roentgen per hour at one meter* (rhm) is recommended. This is not essentially a new unit since all units involved are well established, explicitly defined, and are in common usage."

The recommendation of this latter unit is a practical step to insure that, by its use, gamma-ray measurements are so made with instruments and under such conditions that measurements on a given isotope (nuclear species) made in any laboratory will be directly comparable with similar measurements made in other laboratories. This will result, if the procedures used comply with the definition of the unit; that is, a source is 1 rhm if it produces 1 roentgen per hour at a distance of 1 meter.

* Chairman.

Effect of He^3 on the λ-Point of He^4

O. K. RICE
Department of Chemistry, University of North Carolina, Chapel Hill, North Carolina
November 14, 1949

IN a recent letter de Boer[1] has discussed the effect of He^3 on the λ-transition of He^4, and has come to the conclusion that admixture of He^3 will cause the transition to become first-order, instead of second-order. The possibility of the transition becoming first-order was pointed out by London and Rice;[2] however, later considerations have led me to believe that the transition will remain second-order.[3]

Both of our treatments[1,3] are based on the assumption of Taconis, Beenakker, Nier, and Aldrich[4] that He^3 is soluble only in the normal part of He^4, and not in the superfluid part, below the λ-point. The difference in our conclusions appears to arise from the fact that de Boer has made the assumption that the ratio of superfluid to normal fluid depends only on the temperature, and is independent of the concentration of He^3, below the λ-point;

I, on the other hand, have assumed that the normal fluid and superfluid are in equilibrium with each other. Since the solution of He^3 in the normal part of the He^4 reduces the escaping tendency of the latter, it is natural to suppose that superfluid will be caused by the osmotic forces to go over into normal fluid, thus shifting the equilibrium between the two. Indeed, Stout,[5] in a recent calculation, has also indicated that a second-order transition will occur only if the distribution of superfluid and normal fluid depends upon the concentration of He^3, but he has used an expression for the distribution which must be considered arbitrary except for very small concentrations of He^3, and he has not indicated why the dependence on He^3 concentration occurs.

According to my view,[3] which also is consistent with Stout's[5] statement, the λ-point is the temperature at which the first small trace of superfluid can appear in a sort of fibrous form. The superfluid is stabilized above 0°K only by the fact that it has a partial molal entropy of mixing. This partial molal entropy, remarkably enough, seems to be finite (instead of infinite) even when the concentration of superfluid approaches zero. Thus the stabilization of superfluid begins at a definite temperature; but since the entropy of mixing does depend on the concentration, more superfluid will appear only if the temperature is lowered. This qualitative picture is the same, regardless of whether or not He^3 is present. However, since He^3 tends to stabilize the normal fluid, it will lower the temperature at which the superfluid first appears.

According to this picture, the liquid differs only infinitesimally just below the λ-point, where only a negligible amount of superfluid has appeared, from the liquid just above the λ-point, and this will be true at any concentration of He^3. Therefore, the entropy, enthalpy, volume, and solubility of He^3 in He^4 can show no abrupt change at the λ-transition, which thus continues to satisfy all the criteria of a second-order phase change.[6]

The fact that the presence of He^3 shifts the equilibrium between superfluid and normal fluid in He^4 means that, as the concentration of He^3 becomes appreciable, the calculations of Taconis, Beenakker, Nier, and Aldrich on the vapor pressure of He^3 from He^4 solutions will need to be modified. This shift of equilibrium will also need to be taken into account in calculating the complete curve for the effect of He^3 on the λ-point. With the information available in my recently published article,[3] this should become, formally at least, a standard thermodynamic calculation. It is hoped to carry out this calculation in the near future.

[1] J. de Boer, Phys. Rev. **76**, 852 (1949).
[2] F. London and O. K. Rice, Phys. Rev. **73**, 1188 (1948).
[3] O. K. Rice, Phys. Rev. **76**, 1701 (1949).
[4] Taconis, Beenakker, Nier, and Aldrich, Phys. Rev. **75**, 1966 (1949).
[5] J. W. Stout, Phys. Rev. **76**, 864 (1949).
[6] J. W. Stout, Phys. Rev. **74**, 605 (1948).

Processes Involving Vector Mesons

JAMES N. SNYDER
Department of Physics, University of Illinois, Urbana, Illinois
November 16, 1949

A PARTICLE subject to spontaneous decay could conceivably have its decay constant altered by interaction with other particles. This *stimulated decay* for the case of a scalar particle, subject to a two-particle decay and interacting with a nucleon, has been treated[1] by means of a more refined perturbation method.[2] For this model the effect was found to be very small and the ratio of the stimulated to unstimulated decay constant depended on the initial energy of the particle as $\log E/E$ for large E (in units of the rest energy).

If the particle under consideration is a vector meson, the effects of stimulation would be expected to be much more important. Very rough computations on the basis of a similar model yield an expression for the ratio of stimulated to unstimulated decay constant similar to that given in the first reference, but with an energy dependence which is approximately E^3 for large E. This stronger energy dependence is due to the presence in the interaction energy of spin terms which become important at high energies.

If the π-meson is a vector particle, its lifetime in the presence of matter should be shortened by this effect. A crude estimate gives $E=10^5\ mc^2$ (m is the meson mass) as the energy at which the lifetime of a vector meson traversing solid matter will be reduced by one-half. The shortening is expected to be more important during the production of mesons by the collisions of primary protons with atmospheric nucleons. The reason for this is that the effect is proportional to $\lambda\!\!\!^{-}_0{}^3 n$, where $\lambda\!\!\!^{-}_0$ is the Compton wave-length of the meson and n is the density of nucleons. This number is of the order of one in the interior of a nucleus where a primary event occurs but is $\sim 10^{-14}$ in solid matter. For high enough energy, a π-meson may be expected to decay to a μ-meson before it has moved a distance of the order of nuclear dimensions from the scene of the collision in which it was produced. If μ-mesons would be identified coming from primary cosmic-ray events, there would be a strong reason to believe that π-mesons are vector particles, since current meson theory denies any appreciable coupling between μ-mesons and nucleons.

In connection with the above-mentioned difference in the energy dependence of the process for scalar and vector particles, it is interesting to note that Schiff[3] has investigated the radiation produced in connection with the creation of mesons by nucleon collisions. He finds that the dependence of the process on nucleon energy is stronger for the vector case as compared to the scalar case by a factor $\sim E^4/\log E$. Here again the stronger energy dependence is due to the presence of the spin terms in the interaction energy.

It must be again emphasized that the treatment of the stimulated decay in the vector case is very crude. A careful treatment would certainly require the use of the ideas of radiation damping and multiplicity of meson production. Without these modifications the model must be regarded as suspect since it predicts a cross section for simple elastic scattering of vector mesons by nucleons which depends quadratically on the energy. It seems probable that the theory of radiation damping which serves to decrease and correct the energy dependence of the elastic cross section would weaken the energy dependence of the stimulated decay probability in a somewhat similar fashion.

[1] W. H. Furry and J. N. Snyder, Phys. Rev. **75**, 1265 (1949).
[2] J. N. Snyder and W. H. Furry, Phys. Rev. **76**, 359 (1949).
[3] L. I. Schiff, Phys. Rev. **76**, 89 (1949).

Ultrasonic Interferometry for Low Acoustic Impedance*

JAMES L. STEWART AND ELLEN S. STEWART
Rutgers University, New Brunswick, New Jersey
October 18, 1949

HUBBARD'S[1] original theory of the ultrasonic interferometer has been modified by Alleman[2] to include the effect of dissipative reflection coefficients. The amplitude absorption coefficient per cm, α, and the exponential form of the amplitude reflection coefficient, β, are determined as follows. From the current, i, in the parallel resonance circuit a function, ϕ, is calculated which is proportional to the relative acoustic pressure P at the source. Thus $\phi=SP$ where

$$\phi=(\sigma/1-\sigma)\cdot(1-\sigma_{00}/\sigma_{00})-1, \quad \sigma=i/I_0,$$

and S and σ_{00} are constants which are discussed below. P has maxima $P_{mn}=1/\tanh(\alpha r+\beta)$ at reflector displacements r which are even multiples of quarter wave-lengths, and minima $P_{0n}=\tanh(\alpha r+\beta)$ at odd multiples of quarter wave-lengths. Assuming $\tanh(\alpha r+\beta)\doteq(\alpha r+\beta)$ for small values of α and β, the plot of $1/\phi_{mn}$ against r is a straight line with a slope α/S and an

intercept β/S. S is finally determined from the peak structure and α and β are calculated.

The first simplification of this procedure and the exact solution has come independently from Hubbard and Stewart,[3] and Fox and Hunter.[4] It must be used in regions of large α and β for which the approximation $\tanh(\alpha r+\beta)\doteq(\alpha r+\beta)$ is invalid. They introduced the measurement of the currents i_{00} when $P=P_{00}=0$ (for a vacuum) and i_∞ when $P=P_\infty=1$ (for the fluid without reflection). These give simple determinations of $\sigma_{00}=i_{00}/I_0$ and of $S=\phi_\infty$ without precise knowledge of peak structure. The $P=\phi/\phi_\infty$ are then calculated, and α and β are determined from the slope and intercept respectively of $\tanh^{-1}P_{0n}$ and $1/\tanh^{-1}P_{mn}$ plotted as functions of r.

It should be emphasized that σ_{00} and S are constants of the interferometer only if the acoustic impedance surrounding the source is constant. Thus σ_{00} is a function of the acoustic impedance of the media contacting the unused surfaces of the source, while S is a function of the acoustic impedance of the fluid contacting the used surface of the source.

A second simplification of the procedure is suggested when it is observed that the ϕ may be expressed as $\phi=E\delta$ where $\delta=i-i_{00}$ is the excess of the current i over the background current i_{00} and

$$1/E=(i_{00}/I_0)(I_0-i_{00})[1-(i-i_{00})/(I_0-i_{00})].$$

In the region of low acoustic impedance $(i-i_{00})/(I_0-i_{00})$ is negligible, and E is a constant for a given run. Consequently ϕ and therefore P are proportional to δ, and $P=\delta/\delta_\infty$. It is possible to record only the δ on a linear meter, divide each δ by $\delta_\infty=i_\infty-i_{00}$, and obtain the corresponding P. α and β are then determined from the P as above. No measurement of I_0 or of the absolute magnitude of i is necessary.

In practice i_∞ can be measured with the reflector at such a distance that the reflected waves are completely absorbed. i_{00} need not be measured if the current excesses δ' over the current of the first minimum i_{01} are known. Thus $\delta'=i-i_{01}$, and $\delta=i-i_{00}=\delta'+\delta_{01}$. Since $P_{m1}P_{01}=P_{m2}P_{02}=\cdots=P_\infty^2=1$, we have $\delta_{m1}\delta_{01}=\delta_{m2}\delta_{02}=\cdots=\delta_\infty^2$. This yields $\delta_{01}=(\delta_\infty')^2/(\delta_{m1}'-2\delta_\infty')$ which can be added to each δ' to give the corresponding δ.

The above simplification is particularly applicable to the number of investigations in gases at low pressures now in progress.

* This work was supported by the Rutgers University Research Council.

[1] J. C. Hubbard, Phys. Rev. **38**, 1011 (1931); **41**, 523 (1932).
[2] R. S. Alleman, Phys. Rev. **55**, 87 (1939).
[3] E. S. Stewart, Phys. Rev. **69**, 632 (1946).
[4] F. E. Fox and J. L. Hunter, Proc. I. R. E. **36**, 1500 (1949).

Cosmic Radiation and the Maintainance of a Potential Gradient in the Atmosphere

S. A. KORFF
New York University, New York, New York
November 14, 1949

IT has been well known for over a century that the earth's atmosphere exhibits a potential gradient. The total difference of potential between the ionosphere and the surface of the earth is thought[1] to be around 400,000 volts. The atmosphere is rendered partially conducting by ionization, produced mainly by cosmic radiation and by radioactive contamination in the lower portions. Taking the resistance of a square cm column of the atmosphere as about 10^{21} ohms, the average current in this column will be about 4×10^{-16} amperes or 1800 amperes total, and the total power developed is 7.2×10^8 watts, over the entire earth. The current would of course rapidly neutralize the potential difference if there were no mechanism which maintains it. It has been postulated that thunderstorms provide the mechanism for maintaining this gradient, but to date no satisfactory theory has been proposed as to just how this operates.

Cosmic radiation is thought today to consist in the main of positively charged primaries, probably protons. A total of 5.7×10^{17} rays arrive over the entire earth per second, corresponding to a total current of 0.09 ampere. The influx of energy is estimated[2] at 9.8×10^{18} Bev per sec., or about 1.4×10^9 watts. The primary cosmic radiation would, if it consists of only positively charged particles, cause the earth to charge up at the rate of $dV/dt=dQ/Cdt=i/C$ or about 10^7 volts per day. It is evident that this effect would soon shut off the influx of additional primary radiation. It is therefore necessary to suppose that an equal number of electrons accompany the primary protons, although these need not have high energies and in this case will not penetrate far into the earth's atmosphere. Indeed if the electrons share the average velocity of the protons they will have average energies lower by three orders of magnitude.

It is evident that if the positive incoming radiation penetrates on the average to a lower depth than does the negative, charged layers will be set up. In the steady state, the current, consisting of electrons or ions drifting through the air to neutralize the potential difference produced by the penetrating primary radiation, will equal the current initially incident, minus the amount lost by the absorption of the incident beam at any depth. Therefore the amount of current flowing through the atmosphere will be a function of depth in the atmosphere. If, because of absorption processes, the net unbalanced number of charged particles surviving at any depth decreases exponentially, then the current may be expected to vary with depth in a similar manner.

The primary radiation produces many secondaries, both charged and uncharged, in the atmosphere. Since some of these secondaries, the mesons, are more penetrating than the primary particles, it is actually these which propagate the intensity to lower depths in the atmosphere. It is known that there is a small positive excess in the number of charged cosmic-ray particles (mostly mesons) arriving at sea level. This situation is consistent with the view that charge is conserved in secondary-production processes, and that if one primary positive particle produces n negative secondaries it will produce $n+1$ positives. Thus, in any event, the positive charges are projected down directly, and negatives must drift downward or other positives drift upward at the same total rate to enable a steady state to be maintained.

However, it should be pointed out that whereas the incoming radiation undoubtedly does establish and maintain a potential difference in the atmosphere, it is not possible to ascribe all the observed current through the air to cosmic radiation. Also, whereas the cosmic radiation does bring to the earth more than enough power to maintain the observed potential difference, most of the energy is used up in producing nuclear and atomic transformations. The actual number of charges per sq. cm per second arriving in the form of cosmic radiation does not equal the number required to account for observed currents through the atmosphere. Therefore some other mechanism is also at work.

[1] J. A. Fleming (Editor), *Terrestrial Magnetism and Electricity* (McGraw-Hill Book Company, Inc., New York, 1939).
[2] T. H. Johnson, Rev. Mod. Phys. **10**, 193 (1938).

Dispersion in NH_3 in the Microwave Region[1]

GEORGE BIRNBAUM
National Bureau of Standards, Washington, D. C.
November 14, 1949

IT is well known that NH_3 strongly absorbs centimeter-wave radiation due to the inversion of the molecule in its ground vibrational state. The contribution of this inversion to the electric susceptibility has been demonstrated by recent measurements which have shown a small but significant difference in susceptibility between two frequencies, 2802 Mc (0.0934 cm^{-1}) and 9270 Mc (0.309 cm^{-1}), in the pressure range 10 to 76-cm Hg. In the

TABLE I. Values of parameters in (1) which fit (1) to NH_3 absorption data. Values in ( ) are for another fit.

	Pressure, cm Hg					
	10		30		76	
$\pi\gamma p \times 10^4$	10.4	(9.5)	31.2	(28.4)	79	(72)
ν_0 (cm^{-1})	0.77	(0.77)	0.72	(0.72)	0.40	(0.46)
$\Delta\nu$ (cm^{-1})	0.13	(0.125)	0.31	(0.28)	0.50	(0.47)

TABLE II. Experimental and calculated difference in susceptibility of NH_3 between 0.0934 and 0.309 cm^{-1}. Values in ( ) were calculated from the values in ( ) in Table I.

$[\epsilon'(0.0934)-\epsilon'(0.309)]\times 10^4$	Pressure, cm Hg 10	30	76
Experimental	-0.34 ± 0.17	-0.93 ± 0.50	$+2.9\pm1.3$
Calculated	$-0.53(-0.48)$	$-0.94(-0.98)$	$+2.1(+1.1)$

present work, this difference in susceptibility is shown to be consistent with the absorption.

When certain analytic conditions are satisfied by the complex dielectric constant, $\epsilon(\nu)=\epsilon'(\nu)-i\epsilon''(\nu)$, the real or imaginary part is uniquely determined if the other is known over the entire frequency range. This statement is usually expressed in the form of two integral transformations, first given by Kramers and Kronig.[2]

In the calculation of $\epsilon'(\nu)$ from the data on absorption ($\alpha(\nu)=2\pi\nu\epsilon''(\nu)$ cm^{-1}), the absorption is first represented analytically. Above 10-cm Hg, the fine structure of the NH_3 inversion spectrum is completely obliterated by the merging of the various collision-broadened lines. At these pressures, several observers investigating collision-broadening effects have found it possible to represent the resultant absorption curve by

$$\frac{\alpha(\nu)}{\nu^2}=\pi\gamma p\left(\frac{\Delta\nu}{\Delta\nu^2+(\nu+\nu_0)^2}+\frac{\Delta\nu}{\Delta\nu^2+(\nu-\nu_0)^2}\right), \qquad (1)$$

provided that empirical values of ν_0 (cm^{-1}), and $\Delta\nu$ (cm^{-1}) are used to give the best fit at each pressure p (cm Hg). In the present work, values were obtained for these parameters and for $\pi\gamma$ treated as a constant, by visually fitting (1) to absorption data obtained by Weingarten[3] in the frequency range 0.31 to 1.2 cm^{-1}. These values are given in Table I which also shows an anomalous result reported previously: ν_0 decreases with increasing pressure.[3,4] The values in parentheses are for another fit, and are included to give an idea of the accuracy with which (1) represents the absorption data.

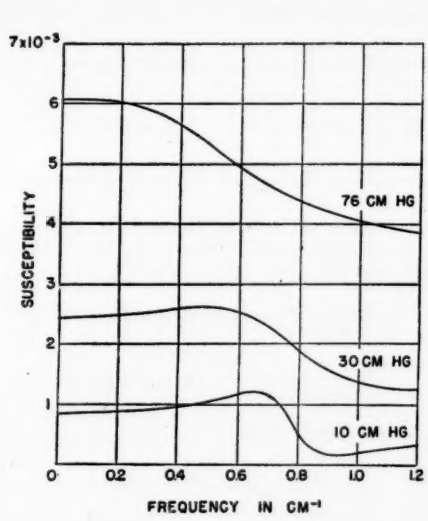

FIG. 1. Calculated dispersion in NH_3 ($T=25$°C). Values of parameters, not in parentheses in Table I, were used.

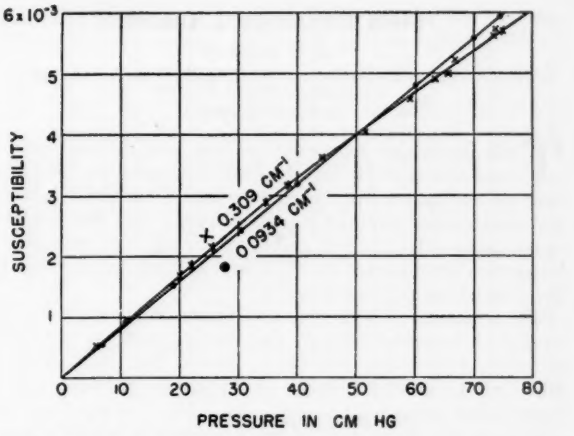

FIG. 2. Susceptibility of NH_3 as a function of pressure. The data were taken at room temperature and were corrected to 25°C.

Equation (1) and

$$\epsilon'(\nu)-1=\frac{\gamma p}{2}\left(\frac{\Delta\nu^2+\nu_0(\nu+\nu_0)}{\Delta\nu^2+(\nu+\nu_0)^2}+\frac{\Delta\nu^2-\nu_0(\nu-\nu_0)}{\Delta\nu^2+(\nu-\nu_0)^2}\right) \qquad (2)$$

have been derived to describe the absorption and susceptibility for spectral lines broadened by collisions.[5] Semi-empirical significance has been attached to (1) in the present type of application by treating the absorption as if due to a single line of resonance frequency ν_0, with a line width $\Delta\nu$ and an intensity $\pi\gamma p$ which is equal to the sum of the intensities of the individual lines. However, since (1) and (2) are consistent with the Kramers-Kronig relations, $\epsilon'(\nu)$ as calculated from (2) by using the values of the parameters given in Table I is actually independent of any special theory of line shape.

To obtain the behavior of the total susceptibility shown in Fig. 1, the contributions of all polarizations other than that due to the microwave inversion must be added to (2). These contributions which are taken as independent of frequency from 0 to 1.2 cm^{-1} are given by $(\gamma'-\gamma)p$, where $\gamma p=\epsilon'(0)-1$ is given by (2) for $\nu=0$, and where $\gamma'=8.02\times10^{-5}$ per cm Hg is averaged from susceptibility measurements at 1 Mc.[6] A noteworthy feature of the curves of Fig. 1 is the disappearance of the maximum and minimum points in the curve at 76 cm Hg. Analytically, this occurs at a pressure such that $\Delta\nu=\nu_0$.

Dispersion in NH_3 was checked by susceptibility measurements at 0.0934 and 0.309 cm^{-1}, where apparatus was readily available. The experimental results shown in Fig. 2 were determined with approximately 1.5 percent error from the change in resonance frequency of a cavity resonator due to the admission of the gas. The variation of susceptibility with pressure, shown in Fig. 2, is evidently in qualitative agreement with this variation obtained from the curves of Fig. 1. Adequate agreement between experimental and calculated values of the difference in susceptibility between 0.0934 and 0.309 cm^{-1} is shown in Table II.

It is planned to make susceptibility measurements in the 0.8 cm^{-1} region,[7] where dispersion should be pronounced.

[1] Some of this work is from a thesis presented for the M.S. degree at George Washington University; G. Birnbaum, Phys. Rev. 76, 178(A) (1949).

[2] H. A. Kramers, Atti del Congresso Internazionale dei Fisici, Como, 2, 545 (1927); R. de L. Kronig, J. Opt. Soc. Am. 12, 547 (1926). See also Radiation Laboratory Report 735 by J. H. Van Vleck.

[3] I. R. Weingarten, Columbia Radiation Laboratory Report (May, 1949).

[4] B. Bleaney and R. P. Penrose, Proc. Phys. Soc. London 59, 418 (1947); B. Bleaney and J. H. N. Loubser, Nature 161, 522 (1948).

[5] J. H. Van Vleck and V. Weisskopf, Rev. Mod. Phys. 17, 227 (1945); H. Fröhlich, Nature 157, 478 (1946).

[6] F. G. Keyes and J. G. Kirkwood, Phys. Rev. 36, 1570 (1930); and C. T. Zahn, Phys. Rev. 27, 455 (1926).

[7] J. E. Walter and W. D. Hershberger (J. App. Phys. 17, 814 (1946)) have reported the following data at 76 cm Hg: $(5.3\pm0.3)10^{-3}$ at 0.314 cm^{-1} and $(5.5\pm0.3)10^{-3}$ at 0.807 cm^{-1}. There is a discrepancy between these results and the calculated dispersion.

Field Dynamics. I. Classical

K. V. ROBERTS
King's College, Cambridge, and H. H. Wills Physical Laboratory, University of Bristol, England
October 10, 1949

THE interaction representation has been derived[1] from the non-covariant Heisenberg-Pauli treatment via the Heisenberg representation, but it is evident from the lengthy deduction[2] and justification[3] required in meson theory that this method is unsatisfactory. In this note and the following one,[4] we derive the interaction Hamiltonian by a classical method and indicate how the S-matrix is to be constructed.

The treatment of both Bose and Fermi fields depends on classical field dynamics because the starting point is a Lagrange principle. Heisenberg and Pauli reduced the problem to one involving an infinite number of degrees of freedom, and one independent variable t, but used a particular Lorentz frame. In a relativistic treatment it still seems reasonable to adopt a classical approach and the mode of attack has been shown by Weiss.[5] We extend it and show the connection with the interaction representation.[6] It might be thought that this approach is unnecessarily highbrow for practical purposes. This is not so: it leads to shorter calculations, as shown by Matthews.[7]

The generalization from particle to field dynamics is based upon two analogies: (i) between equations in l and n independent variables, (ii) between hyperbolic equations in $m+1$ variables, all m. Essentially, the Lagrangian part of the theory uses the first analogy; the Hamiltonian part the second. Quantities transform according to two groups, the Lorentz group and the group of transformations of an arbitrary space-like surface σ.

σ is a *parametrized* space-like surface, u^r the three parameters. N_μ are the three-rowed minors of $(\partial u^r/\partial x^\mu)$. w is a locally normal coordinate satisfying $(\partial x^\mu/\partial w)N_\mu=1$. Field quantities are denoted collectively by $\varphi^\alpha(x)$, α standing for an unspecified tensor or spinor index. $\varphi_\mu{}^\alpha=\partial\varphi^\alpha/\partial x^\mu$. $\mathfrak{L}$ is the Lagrangian.

In this theory, canonical coordinates and momenta are variables $\mathbf{q}$, $\mathbf{p}$ whose values are *functions* on any arbitrary σ with domain the u^r or any transform of them. The fundamental coordinate and momentum functions are $\varphi^\alpha(u)$ and $\pi_\alpha(u)=(\partial\mathfrak{L}/\partial\varphi_\nu{}^\alpha)N_\nu$. $U_\nu{}^\mu=\mathfrak{L}-\varphi_\nu{}^\alpha\pi_\alpha{}^\mu$. The Hamiltonian functions are

$$\mathfrak{H}(u)=U_\nu{}^\mu N_\mu(\partial x^\nu/\partial w) \quad \text{and} \quad \mathfrak{h}_r(u)=U_\nu{}^\mu N_\mu(\partial x^\nu/\partial u^r)$$

expressed in terms of φ^α, $(\partial\varphi^\alpha/\partial u^r)$, and π_α. $H=\int_\sigma\mathfrak{H}(u)du$ and $h_r=\int_\sigma\mathfrak{h}_r(u)du$ are the Hamiltonians; the canonical equations, determining the variation with w and u^r for fixed σ, are

$$\begin{aligned}&\frac{\partial}{\partial w}\varphi^\alpha(u)=-\frac{\delta H}{\delta\pi_\alpha(u)}, \quad \frac{\partial}{\partial w}\pi_\alpha(u)=\frac{\delta H}{\delta\varphi^\alpha(u)},\\ &\frac{\partial}{\partial u^r}\varphi^\alpha(u)=-\frac{\delta h_r}{\delta\pi_\alpha(u)}, \quad \frac{\partial}{\partial u^r}\pi_\alpha(u)=\frac{\delta h_r}{\delta\varphi^\alpha(u)}.\end{aligned} \tag{1}$$

They are equivalent to the field equations. δ denotes functional differentiation. The energy-momentum vector is

$$P_\mu=\int_\sigma U_\nu{}^\mu(u)N_\mu(u)du.$$

Poisson brackets (P.B.) may be defined[8] and shown to be constants of the motion; (Eq. (1) may be restated in terms of them. A canonical transformation (c.t.) is any transformation from $\mathbf{p}_\beta$, $\mathbf{q}^\beta$ to $\mathbf{p}_\gamma{}^*$, $\mathbf{q}^{*\gamma}$ such that

$$\int_\sigma p_\gamma{}^*(w)\delta q^{*\gamma}(w)dw-\int_\sigma p^\beta(v)\delta q^\beta(v)dv$$

is the perfect differential of a functional W of $\mathbf{p}$, $\mathbf{q}$, and possibly σ. *Any functional of σ must satisfy the integrability conditions*, given by Dirac[8]

$$[W_r(u),W_s(u')]-\frac{\delta W_r(u)}{\delta u^s(u')}+\frac{\delta W_s(u')}{\delta u^r(u)}=-W_r(u')\frac{\partial}{\partial u^s}\delta(u-u')-W_s(u)\frac{\partial}{\partial u^r}\delta(u-u'),$$

$$[W_r(u),W_n(u')]-\frac{\delta W_r(u)}{\delta w(u')}+\frac{\delta W_n(u')}{\delta u^r(u)}=W_n(u)\frac{\partial}{\partial u^r}\delta(u-u'), \tag{2}$$

$$[W_n(u),W_n(u')]-\frac{\delta W_n(u)}{\delta w(u')}+\frac{\delta W_n(u')}{\delta w(u)}=-\frac{\partial}{\partial u^s}\delta(u-u')\times\{\gamma_{rs}(u)W_r(u)+\gamma_{rs}(u')W_r(u')\},$$

where $W_n(u)=\delta W/\delta w(u)$, $W_r(u)=\delta W/\delta u^r(u)$, and γ_{rs} is the metric tensor of the surface.

Any c.t. preserves the P.B. relations. Infinitesimal c.t.'s are generated by a functional $K[\mathbf{p},\mathbf{q},\sigma]$ which can depend on σ;

$$dq/d\theta=-\delta K/\delta p, \quad dp/d\theta=\delta K/\delta q. \tag{3}$$

$\int_\sigma\{\mathfrak{H}(u)\delta w(u)+\mathfrak{h}_r(u)\delta u^r(u)\}du$ generates the c.t. induced by an arbitrary infinitesimal deformation of σ. H and h_r correspond to displacements along w, u^r, respectively, P_μ to displacements along the x^μ axis.

Any c.t. may be specified by $W[\mathbf{q},\mathbf{q}^*,\sigma]$; $p=-\delta W/\delta q$, $p^*=\delta W/\delta q^*$, $\mathfrak{H}^*=\mathfrak{H}+\delta W/\delta w$, $\mathfrak{h}_r{}^*=\mathfrak{h}_r+\delta W/\delta u^r$, and preserves the canonical form of the equations. The Hamilton-Jacobi equations define a W which transforms the original $\mathbf{p}$, $\mathbf{q}$ to constants;

$$\mathfrak{H}+(\delta W/\delta w)=0, \quad \mathfrak{h}_r+(\delta W/\delta u^r)=0. \tag{4}$$

This appearance of the Hamiltonian functions as derivatives shows that they must satisfy the conditions (2). Their derivation from a Lagrange principle automatically ensures this.

[1] J. Schwinger, Phys. Rev. **74**, 1439 (1948). S. Tomonaga, Prog. Theor. Phys. **1**, 27 (1946).
[2] See, e.g., S. Kanesawa and S. Tomonaga, Prog. Theor. Phys. **3**, 1 (1948).
[3] F. J. Belinfante, Phys. Rev. **76**, 66 (1949).
[4] K. V. Roberts, Phys. Rev. **77**, 146 (1950).
[5] P. R. Weiss, Proc. Roy. Soc. **169**, 102 (1938).
[6] Also discussed by T. S. Chang, Phys. Rev. **75**, 967 (1949).
[7] P. T. Matthews, Phys. Rev. **75**, 1270 (1949).
[8] P. A. M. Dirac, Phys. Rev. **73**, 1092 (1948).

Field Dynamics. II. Quantum

K. V. ROBERTS
King's College, Cambridge, and H. H. Wills Physical Laboratory, University of Bristol, England
October 10, 1949

THE state of a system is defined[1] on a *parametrized* σ by a state functional or vector Ψ; dynamical variables by operators defined with respect to σ. Here we employ canonical variables $\varphi^\alpha(u)$, $\pi_\alpha(u)$, corresponding to those of I^2, and functions or functionals of them.

The Heisenberg equations (equivalent to the field equations) are

$$\frac{\partial}{\partial w}\xi(u,\sigma)=[\xi,H], \quad \frac{\partial}{\partial u^r}\xi(u,\sigma)=[\xi,h_r]. \tag{1}$$

A transformation of the surface defines a unitary transformation (u.t.);

$$\xi(u,\sigma)=U^{-1}[\sigma,\sigma_0]\xi(u,\sigma_0)U[\sigma,\sigma_0] \tag{2}$$

from the variables on σ_0 to those on ∂, with

$$\begin{aligned}&i\hbar\frac{\delta}{\delta w(u)}U[\sigma,\sigma_0]=\mathfrak{H}(u,\sigma)U[\sigma,\sigma_0],\\ &i\hbar\frac{\delta}{\delta u^r(u)}U[\sigma,\sigma_0]=\mathfrak{h}_r(u,\sigma)U[\sigma,\sigma_0].\end{aligned} \tag{3}$$

The Schrödinger equations are

$$\begin{aligned}&i\hbar\frac{\delta}{\delta w(u)}\Psi[\sigma]=\mathfrak{H}(u)\Psi[\sigma],\\ &i\hbar\frac{\delta}{\delta u^r(u)}\Psi[\sigma]=\mathfrak{h}_r(u)\Psi[\sigma].\end{aligned} \tag{4}$$

Either representation may be employed. Notice that for the validity of this formalism σ must be parametrized. The generating functional for any u.t. must satisfy the integrability conditions.

The Heisenberg representation for any field theory may formally be set up by taking everything over unchanged from classical dynamics. It is readily verified in simple cases that no inconsistency arises. The interaction representation may be constructed with the help of the general theorem, that any c.t. generated by an infinitesimal c.t. may always be performed before transition from classical to quantum mechanics.

Divide the classical $\mathcal{H}$ and $\mathfrak{h}_\tau$ into two parts, $\mathcal{H}=\mathcal{H}^f+\mathcal{H}^i$, $\mathfrak{h}_\tau=\mathfrak{h}_\tau{}^f+\mathfrak{h}_\tau{}^i$, $\mathcal{H}^f$ and $\mathfrak{h}^f$ being derived from the "free" Lagrangian $\mathcal{L}^f$. Then each part will satisfy Eq. (2) of I. New variables $\varphi^{*\alpha}(\sigma,\tau)$, $\pi_\alpha{}^*(\sigma,\tau)$ depending on two surfaces are introduced by the c.t. $(\delta W/\delta w)+\mathcal{H}^f=0$, $(\delta W/\delta u^\tau)+\mathfrak{h}_\tau{}^f=0$ for variations of τ. They satisfy canonical equations with H^i, $h_\tau{}^i$ for variations of σ, and are equal to the original variables when $\sigma=\tau$. This is identical with classical perturbation theory.

With the aid of a one-parameter family of surfaces τ: $x^\mu=f^\mu(\rho,u^1,u^2,u^3)$ with σ as one member, one may introduce field variables $\varphi^{*\alpha}(\sigma,x)$ related to $\varphi^{*\alpha}(\sigma,\tau)$ and $\pi_\alpha{}^*(\sigma,\tau)$ by a transformation depending on τ. These depend on both a point and a surface σ and satisfy "free" field equations and P. B. relations.

Now use the Heisenberg representation for variations of τ and the Schrödinger representation for variations of σ. Then the operators vary only with τ and the wave functional only with σ, according to Eq. (2) with $\mathcal{H}^f$, $\mathfrak{h}_\tau{}^f$ and Eq. (4) with $\mathcal{H}^i$, $\mathfrak{h}_\tau{}^i$. *It is most important to notice that these equations refer to parametrized surfaces.* In particular the variation of Ψ is determined relative to a basis formed by the eigenvectors of a complete commuting set of variables constant under all transformations of τ.

But it is more usual to employ a representation whose basis is defined by a complete set of commuting functions of the field variables which commute with $P_0{}^f$. The two are not the same: The field quantities are related to the canonical variables by a transformation which depends on the particular set of surfaces τ. In the new representation the surfaces are no longer parametrized, and a solution of the Schrödinger equation is

$$\Psi[\sigma_1]=\Phi[\sigma_0]+\left(\frac{1}{i\hbar}\right)\int_{\sigma_0}^{\sigma_1}\mathcal{L}^i(x)\Psi[\sigma]dx, \tag{5}$$

where $\mathcal{L}^i$ is the interaction Lagrangian. The S matrix is

$$\sum_{n=0}^{\infty}\left(\frac{1}{i\hbar}\right)^n\frac{1}{n!}\int_{-\infty}^{\infty}dx^{(1)}\cdots\int_{-\infty}^{\infty}dx^{(n)}P[\mathcal{L}^i(x^{(1)})\cdots\mathcal{L}^i(x^{(n)})]. \tag{6}$$

Expressions equivalent to (6) have been found in particular cases by Belinfante[3] and Matthews.[4] The results of I and this paper will be discussed in detail elsewhere.

[1] P. A. M. Dirac, Phys. Rev. **73**, 1092 (1948).
[2] K. V. Roberts, Phys. Rev. **77**, 146 (1950), designated as I.
[3] F. J. Belinfante, Phys. Rev. **76**, 66 (1949).
[4] P. T. Matthews, Phys. Rev. **76**, 684 (1949).

Determination of g-Values in Paramagnetic Organic Compounds by Microwave Resonance

A. N. Holden, C. Kittel, F. R. Merritt, and W. A. Yager
Bell Telephone Laboratories, Murray Hill, New Jersey
November 23, 1949

MICROWAVE magnetic resonance absorption was observed near 24,000 mc/sec. at room temperature in three organic free radical compounds, and accurate determinations of the g-values in the resonance equation $\hbar\omega=g\mu_B H$ were made by comparison with the proton resonance frequency in the same magnetic field. Preliminary results on one of the compounds were reported in an earlier communication.[1] Measurements at 50 and 450 mc/sec. on another free radical, pentaphenyl cyclopentadienyl, have been reported by Kosirev and Salekov.[2] The results of our measurements on polycrystalline specimens are summarized below.

(a) Diphenyl-trinitro phenyl hydrazyl: $(C_6H_5)_2N-NC_6H_2(NO_2)_3$.

The g-value is 2.0036 ± 0.0002, and the half-width of the resonance line at half-power is 1.35 oersteds, which appears to be the sharpest line yet reported for electronic spin resonance. It is possible that the substance may be useful for magnetic field calibration and stabilization. The g-value determination was repeated a large number of times under various experimental conditions; the standard error of the observations is actually less than 1 part in 20,000. Approximate agreement with our g-value is reported independently by Townes and Turkevich.[3] The g-value was calculated by comparing the observed ratio of (proton frequency/electron frequency) with the value

$$\omega_p/\omega_e=(1.51927\pm0.00008)\times10^{-3}$$

for the frequency ratio given by Taub and Kusch,[4] which we take to correspond to the theoretical g-value for electron spin, $g_e=2(1+\alpha/2\pi)=2.0023$, where vacuum polarization and radiation interaction effects are included.

(b) Di-para-anisyl-nitric oxide: $(p-CH_3OC_6H_4)_2NO$.

The g-value is 2.0063 ± 0.0005, and the half-width at half-power is 15.7 oersteds. Crystalline material in which approximately one part of this compound was diluted with ten parts of the isomorphous non-magnetic compound p,p'-dimethoxy benzophenone gave a half-width of 29.6 oersteds. The increase in line width on dilution suggests that the original line was sharpened by exchange narrowing. In both cases the line was quite flat on top which suggested a hyperfine splitting of about 45 mc/sec. over-all; however, measurements in liquid solution gave a sharper (7 oersteds) and well-rounded single line. The flat top in the solid may have been caused by anisotropy of packing of the individual crystallites.

(c) β-(phenyl nitrogen oxide)-β-methyl pentane-δ-one oxime N-phenyl ether: $ON(C_6H_5)C(CH_3)_2CH_2C(CH_3)N(C_6H_5)O$.

The g-value is 2.0057 ± 0.0002, and the half-width at half-power is 9.2 oersteds. The larger width we reported previously[1] was caused in part by magnet overheating. Single crystals of this substance have been grown and some measurements made. As expected, the g-value is quite anisotropic, ranging between 2.0035 and 2.0073 in different orientations. This compound was also measured in benzene solution: the resonance was rather weak and broad, with no observable hyperfine splitting.

The half-widths calculated for the above compounds on the basis of dipole-dipole interactions alone are of the order of 100 oersteds. The observed widths are between 6 and 70 times sharper, even in polycrystalline specimens, and the effect may be ascribed to the Gorter-Van Vleck process of exchange narrowing. The existence of significant exchange forces is supported in the case of compound (a) above by magnetic susceptibility measurements,[5,6] which give an antiferromagnetic θ in the Curie law of 10°K to 20°K; and in compound (b) the antiferromagnetic θ is 13°K.

The deviations of the g-values from the spin-only value of 2.0023 are 0.0013, 0.0040, 0.0034, in compounds (a), (b), (c), respectively. The excess is presumably to be ascribed to spin-orbit coupling[7] of the "odd" electron, and the sign of the deviation suggests that the odd electron may be partly localized in a more than half-filled shell, perhaps the $2p$ shell of an oxygen, nitrogen, or carbon atom.

We have employed a super-regenerative circuit for detecting proton resonance, and have found that it is possible in some cases for significant errors to arise with this method, as revealed by a dependence of the apparent g-value on the quench frequency of the oscillator. In the worst case, using paraffin wax at 80 kc/sec. quench frequency, the errors in g were of the order of 0.1 percent. In other materials, such as mineral oil, glycerine, and triethanolamine, the objectionable effect did not occur.

We wish to thank J. K. Galt for assistance in setting up the proton resonance equipment, and S. Millman for several valuable discussions.

[1] Holden, Kittel, Merritt, and Yager, Phys. Rev. 75, 1614 (1949).
[2] B. M. Kosirev and S. G. Salekov, Akad. Nauk, Doklady 58, 1023–1025 (1947).
[3] C. H. Townes and J. Turkevich, Phys. Rev. 77, 148 (1950).
[4] H. Taub and P. Kusch, Phys. Rev. 75, 1481 (1949).
[5] Muller, Muller-Rodloff, and Bunge, Ann d. Chem. 520, 235 (1935).
[6] H. Katz, Zeits. f. Physik 87, 238 (1933).
[7] C. Kittel, Phys. Rev. 76, 743 (1949).

Hyperfine Structure and Exchange Narrowing of Paramagnetic Resonance†

C. H. TOWNES* AND J. TURKEVICH**
Brookhaven National Laboratory, Upton, Long Island, New York
November 21, 1949

THE free radical α, α-diphenyl β-picryl hydrazyl, $(C_6H_5)_2N-NC_6H_2(NO_2)_3$, shows the strongest and narrowest electronic paramagnetic resonance absorption so far reported. This resonance was observed by its effect on the transmission of microwaves (frequency approximately 24,000 mc) through a TE_{01} cavity with a small amount of the free radical placed approximately on the axis of the cavity. The microwave frequency was tuned to give maximum transmission through the cavity while the cavity was in place between the pole pieces of an electromagnet. With an amount of the free radical as small as 2 mg the transmitted power was reduced by a factor of three when the magnetic field was of the proper value (approximately 8600 oersteds) to give resonance. The half-width of the resonance at half-maximum absorption was 1.45 oersteds. Because of its sharpness and intensity, this resonance may be of value for stabilizing or measuring magnetic fields in cases where the signal produced by the proton resonance is not sufficiently strong.

The electronic g-value was obtained by measuring the electron's resonant frequency and the proton frequency in the same magnetic field. The ratio of proton to electron frequencies obtained was 15.178×10^{-4} which, combined with results of Taub and Kusch,[1] gives a g-value of 2.0042 ± 0.0004. The g-value and line width obtained are in fair agreement with the results of Holden, Kittel, Merritt, and Yager,[2] who have made measurements parallel to those presented here and with whom we have enjoyed very helpful discussions.

The unusually narrow line-width observed is evidently due to exchange narrowing[3] since spin-spin interactions alone would lead one to expect a half-width of approximately 50 oersteds. The free radical was dissolved in concentrations of 3.0 and 1.5 weight percent in benzene and the resonance width examined. With these dilutions exchange effects should be negligible, and indeed the resonance half-widths (half-widths at half-maximum) were greater than in the solid, being 7.5 and 5 oersteds respectively for the two solutions. These latter widths are, as closely as can be calculated, just those to be expected from spin-spin interactions. Motion of the molecules in solution gives no appreciable narrowing of the line at the frequencies used since the relaxation time is 10^{-10} sec. or larger.

Gaseous NO has been examined by Beringer and Castle[4] with a somewhat similar technique. They find associated with the electronic resonance a hyperfine structure due to coupling between the N^{14} and electronic magnetic moments. If the odd electron in NO is considered to be on the nitrogen atom in an essentially atomic $2p$ state, the expected interaction is approximately 75 $I\cdot J$ megacycles/sec. Here the average inverse cube of the electron's distance from the nucleus has been taken from a previous estimate for nuclear quadrupole effects.[5] The experimental results give an interaction of 31 $I\cdot J$ mc, indicating that the probability of finding the odd electron on the nitrogen atom is approximately $\frac{1}{3}$. This is what may be expected if the electron participates in a 3-electron bond.[6]

The free radical examined here is in a $^2\Sigma$ electronic state and the odd electron might be assumed to be in a $2p$ orbit on the nitrogen atom which has only two bonds. In this case hyperfine structure consisting of three equally spaced, equal intensity lines separated by 125 mc or 45 gauss may be expected. If exchange interactions between the electrons in adjacent molecules are as large as the electron-nuclear coupling, this hyperfine structure may be considerably modified or eliminated. Since the exchange effects are evidently important in the solid material, failure to find hyperfine structure is perhaps not surprising. However, in the diluted solutions of the free radical hyperfine structure of the type described was expected, but not found. What hyperfine splitting is present must be less than the line width, hence the probability of finding the odd electron on the nitrogen which formerly has only two valence bonds must be less than 0.15. In order to produce such a small hyperfine structure, this electron must either have considerable probability of being found on nuclei of zero spin such as oxygen, or perhaps circulate over a considerable region of the molecule and hence average out a large number of small interactions with nuclei.

Study of hyperfine structure in other molecules with magnetic moments of electronic origin should give considerable information about the electron distributions.

The interest and encouragement of Dr. W. V. Cohen during this investigation is appreciated. In addition we are indebted to Mr. Walter Merkle for making available the Brookhaven cyclotron magnet in which this work was carried out, and to Mr. George Brush and others of the cyclotron group for considerable assistance.

† Work performed at Brookhaven National Laboratory under contract with the AEC.
* Permanent address: Columbia University, New York, New York.
** Permanent address: Princeton University, Princeton, New Jersey.
[1] A. H. Taub and P. Kusch, Phys. Rev. 75, 1481 (1949).
[2] Holden, Kittel, Merritt, and Yager, Phys. Rev. 77, 147 (1950).
[3] J. H. Van Vleck, Phys. Rev. 74, 1168 (1948).
[4] R. Beringer and J. G. Castle, Jr., Phys. Rev. 76, 868 (1949).
[5] C. H. Townes and B. P. Dailey, J. Chem. Phys. 17, 782 (1949).
[6] L. Pauling, *Nature of the Chemical Bond* (Cornell University Press, Ithaca, New York, 1945).

Microwave Spectrum of CH_2CFCl

J. K. BRAGG, T. C. MADISON, AND A. H. SHARBAUGH
Research Laboratory, General Electric Company, Schenectady, New York
November 14, 1949

THE microwave spectrum of the asymmetric top molecule CH_2CFCl has been observed and analyzed. The molecular parameters for both isotopic species are given in Table I. The frequencies computed with these parameters for the transitions which have been identified appear in Table II, together with the observed frequencies corrected for quadrupole effect.

The assignments of these lines were further confirmed, in every case, by the agreement (0.5 percent) of the observed quadrupole multiplet structure with that computed by first-order theory.[1] The quadrupole parameters used were $\chi_{aa}=-73.3\pm0.3$ megacycle/second and $\chi_{bb}=39.8\pm0.2$ megacycle/second. The quan-

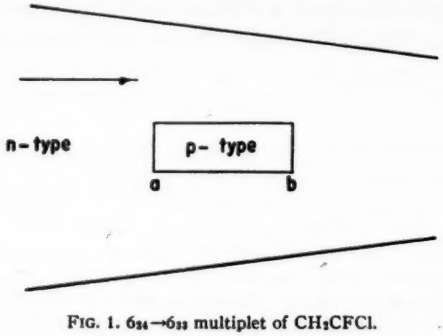

FIG. 1. $6_{34}\rightarrow6_{33}$ multiplet of CH_2CFCl.

TABLE I. Molecular parameters for the isotopic species of CH_2CFCl.*

	$(a+c)/2$	$(a-c)/2$	κ
CH_2CFCl^{35}	7065.00	3616.62	−0.542724
CH_2CFCl^{37}	7030.91	3650.42	−0.568678

* The number of significant figures quoted appears to be justified by the very close agreement of the five transitions of $J<6$ for the Cl^{35} species. This would indicate that the deviations of about a megacycle in the $J\leq 6$ transitions, which are consistent in sign, may be accounted for in terms of centrifugal distortion.

TABLE II. CH_2CFCl^{35} transitions.

Transition	Frequency calculated (Mc)	Frequency observed
$1_{01}\rightarrow 2_{12}$	21,026.7	21,026.70
$2_{12}\rightarrow 3_{03}$	20,214.2	20,214.29
$6_{42}\rightarrow 7_{34}$	22,420.4	22,419.13
$2_{12}\rightarrow 2_{21}$	21,699.7	21,699.70
$3_{12}\rightarrow 3_{22}$	24,362.3	24,362.48
$5_{05}\rightarrow 5_{14}$	24,601.4	24,601.24
$6_{15}\rightarrow 6_{24}$	20,392.4	20,391.51
$6_{24}\rightarrow 6_{33}$	24,896.3	24,895.46
$7_{16}\rightarrow 7_{25}$	25,657.3	25,656.30
$7_{25}\rightarrow 7_{34}$	23,897.8	23,896.29
	CH_2CFCl^{37} transitions	
$1_{01}\rightarrow 2_{12}$	20,822.8	20,822.8
$8_{44}\rightarrow 9_{45}$	22,848.8	22,852.40
$2_{12}\rightarrow 2_{21}$	21,902.5	21,902.50
$3_{12}\rightarrow 3_{22}$	24,427.4	24,427.38

tities χ are products of eQ and $(\partial^2V/\partial a^2)$ and $(\partial^2V/\partial b^2)$, the appropriate components of the molecular field gradient at the Cl nucleus. a and b are the principal axes of least and intermediate moments of inertia, respectively.

The assignments were initially made solely on the basis of the observed multiplet structure. Particularly helpful in this regard were certain of the Q-branch transitions of $J>2$, which appear as quadruplets of lines with a ratio of certain component separations which is determined only by the J value involved. Figure 1 shows the $6_{24}\rightarrow 6_{33}$ multiplet; the ratio of the differences A and B agreeing with that calculated from the first-order formulas for a $6\rightarrow 6$ transition. Although a P or R branch transition gives rise to a similar quadruplet, the ratio of spacings depends on the quadrupole coupling factors of the two levels involved and will not usually be confused with that expected for any Q-branch transition. The amount of the separation depends, however, on the magnitude of the individual coupling factors, so that, due to limitations of resolution, some of the transitions may appear as singlet or doublet lines.

Because the a axis is very nearly parallel to the C−Cl bond, one may calculate with reasonable assurance -74.4 ± 2 mc/sec. as the value of the quadrupole coupling along the bond.

The corresponding deuterated compound is now being prepared, with whose results we hope to determine the structure of the molecule.

We wish to express our gratitude to Dr. M. Prober of this laboratory for the preparation of the compounds used in this investigation. We also wish to thank Miss V. G. Thomas for her assistance with the numerical computations involved in this work.

[1] J. K. Bragg, Phys. Rev. **74**, 533 (1948); J. K. Bragg and S. Golden, Phys. Rev. **75**, 735 (1949).

Erratum: A Theory of Pressure Absorption

[Phys. Rev. **76**, 1268 (1949)]

MASATAKA MIZUSHIMA
Physics Department, Faculty of Science, Tokyo University, Tokyo, Japan

SOME numerical values must be corrected as follows: The experimental intensity of the Q-branch of O_2 band near 1556 cm^{-1} is 4.4×10^6 cm^{-1} instead of 4.0×10^8 cm^{-1}, at 1 atm. Thus $\beta^2+(11/30)\gamma^2$ in (6) must be assumed to be 1.9×10^{-52} in order to explain the above experimental results.

The estimation of the intensity ratio of the quadrupole absorption to the pressure absorption must be revised as follows,

$$1:\left(\frac{c}{\nu}\right)^2\frac{n}{R_0^6}\left(\beta^2+\frac{11}{30}\gamma^2\right)\doteq 1:10^4.$$

Coherent Scattering of X-Rays by Atoms with More Than One Electron According to the One-Electron Theory and the Positron Theory

E. ARNOUS
*Swiss Federal Institute of Technology, Zürich, Switzerland**

October 21, 1949

THERE is no doubt that the "one-electron theory" and the "positron theory" cannot give identical expressions for the *coherent scattering* of x-rays by atoms. Recently Halpern and Hall[1] announced the results of this calculation, which exhibited this fact, but from the very beginning it is clear that the one-electron theory cannot give rise, for example, to the terms due to vacuum polarization. The real problem consists therefore in determining the order of magnitude of the differences in the results of the two theories.

On the other hand, it is evident that these differences may be separated into two classes from the beginning: Those which are encountered for the atom with many electrons as well as for the hydrogen atom and those which are specific to the atom with many electrons, and which are due, if they exist, to the interactions between electrons. The terms of the first class are to be looked for in the "one-particle parts" (in the sense defined by Schwinger[2]), the other in the two- and many-particle parts. It is these latter terms we tried to find.

Let N be the number of electrons, $\varphi_1\varphi_2\cdots$ the wave functions of a single electron in the field of the nucleus. Let

$$\psi(x)=\Sigma\, a_n\varphi_n\exp(itE)_n$$

be the matter field, H the coupling between the matter field and the transverse electromagnetic field, and H^c the Coulomb interaction of the electrons. We introduce S and T by

$$\partial S/\partial t=H,\quad \partial T/\partial t=\tfrac{1}{2}i[S,H]-H_{self}^{tr}\text{ and }\epsilon(t)=\pm 1\text{ if }t\gtrless 0.$$

H^c shall be treated as a perturbation. To the one-particle parts of $\frac{1}{2}i[S,H]$ which give to the well-known terms (Waller):

$$\sum_z\sum_{i=1}^{N}\varphi_i^*(\boldsymbol{\alpha}\cdot\mathbf{A}_0)\varphi_z\varphi_z^*(\boldsymbol{\alpha}\cdot\mathbf{A}_1)\varphi_i/(E_z-E_i\pm|k|),\qquad(1)$$

we must add the two-particle terms of

$$\tfrac{1}{2}i^2[S,(S,H^c-H^c{}_{self})]+i(T,H^c-H_{self}^c)$$
$$=-\tfrac{1}{4}\int\{[H^c(t)-H_{self}^c(t),H(t')],H(t'')\}\epsilon(t-t')\epsilon(t'-t'')dt'dt''.$$

As the calculation shows, this is equivalent to replacing in (1) the function φ by $\varphi+\varphi'$, where φ_i', for instance, is given by

$$\varphi_i'=\sum_{\lambda\neq i}\sum_{j\neq i}^{N}\varphi_\lambda\frac{\langle\lambda j|H^c-H_{self}^c|ij\rangle}{E_i-E_\lambda}.$$

In other words, the scattering due to the ith electron is to be calculated for an electron moving in the field of the nucleus and the mean field of the other electrons. But this is exactly the result of the one-electron theory, if the interaction between electrons is treated as a perturbation.

Thus, we are led to the following conclusion: If there is a non-negligible difference between the results of the one-electron theroy and the positron theory, this difference cannot be attributed to the interaction of the electrons within the atom.

* Chargé de Recherches au C.N.R.S. Paris.

[1] O. Halpern and H. Hall, Phys. Rev. **73**, 1322 (1949).
[2] J. Schwinger, Phys. Rev. **75**, 651 (1949).

On the Treatment of Quantum Electrodynamics without Eliminating the Longitudinal Field

NING HU
University of Wisconsin, Madison, Wisconsin
November 16, 1949

THE aim of the present note is to clarify certain points in a recent paper under the same title.[1] It should first be pointed out that the original derivation of equivalence of (34) and (36) in I is incomplete.* The correct derivation which applies only to the case $\sigma=\infty$ will be given as follows. $H_2(x)$ given by (25) may be written in the following form by using (8a) and (9a)

$$H_2(x)=H_2^{(+)}(x)+H_2^{(-)}(x),$$

$$H_2^{(\pm)}(x)\Omega_0=-(-i)^2 j_\mu(x)A_\mu^{(1)(\pm)}(x)\int_{\sigma(x)} j_\alpha(x')B^{(\mp)}(x')d\sigma_\alpha'\Omega_0$$

$$=-\frac{1}{2\sqrt{2}(2\pi)^3}\int\int j_\mu(x)j_\alpha(x')n_\mu^{(1)}(k)\times e^{\pm i(k,x-x')}\frac{d^3k}{k^2}d\sigma_\alpha'\Omega_0, \quad (1)$$

where $A_\mu^{(\pm)}(x)$ and $B^{(\pm)}(x)$ denote the $(\pm)$-frequency part of $A_\mu(x)$ and $B(x)$. $I_n(i)$ given by (30) (with $\sigma=\infty$) can accordingly be written $I_n(i)=I_n^{(+)}(i)+I_n^{(-)}(i)$ where $I_n^{(\pm)}(i)$ contains the integral $\int H_2^{(\pm)}(x')dx'$. (32) will still hold if $A_\mu^{(s)}(x)$ and $B(x)$ are replaced by $A_\mu^{(s)(\pm)}(x)$ and $B^{(\pm)}(x)$. We shall call the relation thus obtained (32±) and use (32+) to push the surface integral in $I_n^{(+)}(1)$ to the right side of the last factor $\int H_1(x_n)dx_n$ as in I and then replace it by a volume integral from $-\infty$ to σ_n, the surface integral at $-\infty$ being equal to zero if we assume as in all collision problems that the interaction between the particles vanishes at $-\infty$. We have similar to (33)

$$I_n^{(+)}(i)\Omega_0=\Sigma\Big[\cdots\int j_\mu(x')dx'\cdots\int j_\alpha(x'')dx''\cdots\Big]\times A_\mu^{(1)(+)}(x')A_\alpha^{(s)(-)}(x'')\Omega_0$$

$$=-\frac{1}{2(2\pi)^3}\Sigma\Big[\cdots\int j_\mu(x')dx'\cdots\int j_\alpha(x'')dx''\cdots\Big]\times\int n_\mu^{(1)}(k)n_\alpha^{(s)}(k)e^{i(k,x'-x'')}\frac{d^3k}{k}\Omega_0, \quad (2)$$

where $\cdots$ are the other factors in (33) except that the upper limit of integration of the first integral factor is ∞ instead of σ. For $I_n^{(-)}(i)$ we shall push the surface integral to the *left* side instead of the right side using the relation (32−) in the reverse direction. The last surface integral at the extreme left side is then replaced by a volume integral from $-\infty$ to $+\infty$, the surface integral at $+\infty$ being equal to zero by the same argument as at $-\infty$. Here we see the reason for considering the case $\sigma=\infty$ since otherwise we would still have a surface integral over σ. We obtain after letting $x'\rightleftarrows x''$ and $\mu\rightleftarrows\alpha$,

$$I_n^{(-)}(i)\Omega_0=-\Sigma\Big[\cdots\int j_\mu(x')dx'\cdots\int j_\alpha(x'')dx''\cdots\Big]\times A_\alpha^{(1)(-)}(x'')A_\mu^{(s)(+)}(x')\Omega_0$$

$$=-\frac{1}{2(2\pi)^3}\Sigma\Big[\cdots\int j_\mu(x')dx'\cdots\int j_\alpha(x'')dx''\cdots\Big]\times\int n_\mu^{(s)}(k)n_\alpha^{(1)}(k)e^{i(k,x'-x'')}\frac{d^3k}{k}\Omega_0, \quad (3)$$

Equations (2) and (3) should further be summed over $i=0, 1, 2, \cdots, n$. We shall now pick out from each sum on the right-hand side of $\Sigma_i I_n(i)=\Sigma_i I_n^{(+)}(i)+\Sigma_i I_n^{(-)}(i)$ the terms which have $j_\mu(x')$ and $j_\alpha(x'')$ in the same position. We have then

$$\Sigma_i I_n(i)\Omega_0=-\frac{1}{2(2\pi)^3}\Sigma_i\Sigma\Big[\cdots\int j_\mu(x')dx'\cdots\int j_\alpha(x'')dx''\cdots\Big]\times\int[n_\mu^{(0)}n_\alpha^{(0)}-n_\mu^{(3)}(k)n_\alpha^{(3)}(k)]e^{i(kx'-x'')}\frac{d^3k}{k}, \quad (4)$$

where we have used the relation

$$n_\mu^{(1)}(k)n_\alpha^{(s)}(k)+n_\mu^{(k)}(k)n_\alpha^{(1)}(k)=n_\mu^{(0)}n_\alpha^{(0)}-n_\mu^{(3)}(k)n_\alpha^{(3)}(k).$$

If we define a new state vector by the condition

$$A^{(0)}(k)\Omega_0'=0, \quad A^{(3)}(k)\Omega_0'=0, \quad (5)$$

it can easily be seen that $\Sigma_i I_n(i)\Omega_0$ is equal to

$$-\frac{1}{2(2\pi)^3}\Sigma_i\Sigma\Big[\cdots\int j_\mu(x')dx'\cdots\int j_\alpha(x'')dx''\cdots\Big]\times\langle\sum_{s=0,3}A_\mu^{(s)}(x')\sum_{t=0,3}A_\alpha^{(t)}(x'')\rangle_0'\Omega_0, \quad (6)$$

where $\langle\ \rangle_0'$ represents the "vacuum expectation value" with "vacuum" defined by (5). Ω_0' might formally be considered as the state with no longitudinal and scalar photons if $A^{(0)}(k)$ instead of $A^{(0)*}(k)$ would be considered as the absorption operator as whatsoever the application of "hole theory" to Einstein-Bose particles may mean. This shows that (34) and (36) are equivalent if (36) is understood as containing only the virtual emission and absorption processes with vacuum defined by (5). This Ω_0' is the state "with no longitudinal photons" referred to in the footnote on p. 395, and is just the vacuum state vector used by Feynman and Schwinger. It should be noted that in the present derivation we need not concern ourselves with the true vacuum expectation value of (36). Equation (36) can now be extended to include the virtual transverse photons and the same argument leading from (37) to (38) and (40) can be used when more $\int H_2(x)dx$ factors are added. We obtain finally the same result (40) *except that σ should be put equal to infinity.*

The situation will be complicated if σ is finite. Then $S[\sigma]$ will be given by (40) *plus* terms containing the surface integrals that have been pushed over to the left side of $I_n^{(-)}(i)$, $I_n^{(-)}(i, j)$, etc., by the relation (32−). These additional terms vanish when $\sigma=\infty$; this means that they contain no matrix elements over the states of the same energy. The appearance of these terms means at least that the application of Feynman's method must be cautious when we are considering the problems of bound states in which the knowledge of $S[\sigma]$ for finite σ is necessary. It should be noted that the matrix elements between states of different energies are usually ambiguous depending on the methods of perturbation. For instance, each term of $S[\sigma]$ obtained by the method of canonical transformation is hermitian, while that obtained by the straightforward perturbation is not. Therefore the present result cannot decide whether (40) is right or wrong. Further investigation will be necessary to decide this point. Finally we wish to point out some important misprints and mis-statements: (1) The last equation of (8a) should have a plus sign on the right-hand side, (2) the left-hand side of (14) should read $[\partial A_\mu/\partial x_\mu, x]$, (3) the first sentence below (30) should be omitted.

The author is indebted to Drs. F. J. Belinfante and S. T. Ma for the helpful discussions. He also wishes to thank Wisconsin Alumni Research Foundation for the financial support.

[1] Ning Hu, Phys. Rev. **76**, 391 (1949). This will be referred to later as I.

* The validity of the condition $\bar{\Omega}_0 A_\mu^{(k)}(x')A_\alpha^{(k)}(x'')\Omega_0=0$ used in the derivation is questionable. Furthermore the correctness of the statement on p. 395 has to be shown.

On the Infra-Red Absorption of the Hydrogen Molecule

MASATAKA MIZUSHIMA
Physics Department, Faculty of Science, Tokyo University, Tokyo, Japan
November 10, 1949

THE hydrogen molecule, being a homonuclear diatomic molecule, has no dipole infra-red absorption; but recently, 0–2, 0–3 vibrational absorption lines were observed by Herzberg,[1] and 0–1 lines by Welsh, Crawford, and Locke.[2]

There are two reasons to expect these absorptions: The quadrupole absorption and the pressure absorption[3] (absorption induced by the intermolecular forces). The 0–1 lines observed by Welsh,

Crawford, and Locke are apparently due to pressure, while there are many reasons to believe that the absorption lines observed by Herzberg are due to the change of the quadrupole moment.[4]

The present author proposed a theory of the pressure absorption[3] by which the intensity of this absorption is given by

$$I_P=\frac{192\pi^4\nu P^2}{25hcR_0^5}n^2(a|\alpha|b)^2, \quad (1)$$

where ν is the frequency of the absorption line (which corresponds to the transition $a\rightarrow b$), P is the quadrupole moment of the molecule, n is the number of molecules in unit volume, $(a|\alpha|b)$ is the ab-matrix element of the polarizability α, and R_0 is the shortest distance to which the molecules can approach to each other.

For the Q-branch of 0–1 lines, the experimental results of Welsh and others[2] gives $I=3.41\times10^7$ cm^{-1} at 1 atmos. In this case $\nu=1.246\times10^{14}$ sec.$^{-1}$, $n=2.98\times10^{19}$ cm^{-3}, and $P=5.85\times10^{-27}$ c.g.s. e.s.u.[5] From the transport phenomena of hydrogen gas we obtain $R_0=2.72$A. Thus $(0|\alpha|1)$ must be 1.83×10^{-25} in order to explain the experimental results by Eq. (1). Although the theoretical estimation[6] by the Heitler-London wave function yields $(0|\alpha|1)=0.53\times10^{-25}$, it is not an absurd value when compared to the value of polarizability (an average of the diagonal elements of α) 8.02×10^{-25}.

The intensity of the pressure absorption in the harmonic lines 0–2, 0–3 due to the anharmonisity were estimated as follows.

The frequencies of the lines observed by Herzberg[1] fit well with the theoretical one, if we put $D=8.2496\times10^{-12}$ erg, $a=1.8553\times10^8$ cm^{-1} and $r_e=7.501\times10^{-8}$ cm in the Morse potential

$$U=D(1-\exp[-a(r-r_e)])^2.$$

If we put $\alpha(r)=\alpha_e+\alpha_e'(r-r_e)+\cdots$ and neglecting the terms higher than α_e'', it can be shown that the matrix elements of α calculated by the Morse wave function[7] are

$$(0|\alpha|1)=\alpha_e'\frac{(k-3)^{\frac{1}{2}}}{a}\{\psi(k-1)-\psi(k-2)\},$$

$$(0|\alpha|2)=\alpha_e'\frac{1}{\sqrt{2}a}\left(\frac{k-5}{k-2}\right)^{\frac{1}{2}}\{-(k-2)\psi(k-1)+2(k-3)\psi(k-2)-(k-4)\psi(k-3)\}, \quad (2)$$

$$(0|\alpha|3)=\alpha_e'\frac{1}{\sqrt{6}a}\left\{\frac{k-7}{(k-2)(k-3)}\right\}^{\frac{1}{2}}\{-(k-2)(k-3)\psi(k-1)+3(k-3)(k-4)\psi(k-2)-3(k-4)(k-5)\psi(k-3)+(k-5)(k-6)\psi(k-4)\},$$

where $\psi(x)$ is the digamma function, and

$$k=4\pi[(2\mu D)^{\frac{1}{2}}/ah].$$

By the above obtained numerical values we obtain

$$(0|\alpha|1)=9.281\cdot10^{-10}\alpha_e',$$
$$(0|\alpha|2)=-1.039\cdot10^{-10}\alpha_e',$$
$$(0|\alpha|3)=-2.034\cdot10^{-11}\alpha_e'.$$

Thus the intensity ratio of the absorption lines calculated by Eq. (1) is

$$I_{01}:I_{02}:I_{03}=1:0.0225:0.00094. \quad (3)$$

The intensities of the pressure absorption for the Q-branch of each band calculated by it, is shown in Table I, together with the values of intensity of the quadrupole absorption calculated by the James-Coolidge value.[5]

TABLE I. Intensity of each absorption. (Q-branch, at 1 atmos., 300°K, in cm^{-1}).

Absorption lines	0–1	0–2	0–3
$I_Q\times10^{-7}$	1.8	1.65	0.34
$I_P\times10^{-7}$	3.4	0.086	0.0022
$(I_Q/I_P)\times10^5$	5	190	1500

The ratio I_Q/I_P is always less than 10^{-1}, the pressure absorption being larger. We must, however, take note of the fact that what is measured is not the integrated intensity I itself, but rather the absorption coefficient. The maximum absorption coefficient of each line is proportional to I, and inversely proportional to the width of the line. The width of the pressure absorption is about 10^2 cm^{-1}, while that of the quadrupole absorption may be assumed to be about 10^{-3} cm^{-1}. Thus the ratio of the maximum absorption coefficient of two absorptions for each line may be given by the figures in the last row of Table I, from which we can see that even at 10 atmos. the quadrupole absorption may be observed in the harmonic lines, while in the 0–1 lines the pressure absorption is predominant as we see in the experiments.

I wish to thank Professors G. Herzberg and M. Kotani for advice and encouragement.

[1] G. Herzberg, Nature **163**, 170 (1949).
[2] Welsh, Crawford, and Locke, Phys. Rev. **76**, 580 (1949).
[3] M. Mizushima, Phys. Rev. **76**, 1268 (1949).
[4] G. Herzberg (private communication).
[5] H. M. James and A. S. Coolidge, Astrophys. J. **87**, 447 (1938).
[6] B. Mrowka, Zeits. f. Physik **84**, 448 (1933).
[7] P. M. Morse, Phys. Rev. **34**, 57 (1929).

Search for Photons Emitted by Long-Life Species of Nickel

D. G. THOMAS AND J. D. KURBATOV
Ohio State University, Columbus, Ohio
November 23, 1949

AVAILABLE information concerning disintegrations of two species of nickel, Ni^{59} and Ni^{63}, is confined to their half-lives. The $T_{\frac{1}{2}}$ for Ni^{59} disintegrating by orbital electron capture was estimated to be about $(2\text{–}3)\times10^5$ yr. and that for Ni^{63}, disintegrating by negatron emission, several hundred years.[1,2] The beta-disintegration u.e. of Ni^{63} was given as ~50 kev.

The present study of long-life isotopes of nickel was made with 9.7 g of nickel activated at Oak Ridge National Laboratory of AEC. The nickel salt was chemically purified by repeated precipitation of nickel in the presence of carriers for radioactive impurities.

Due to the low specific activity of the nickel species and to their very long lives, the study was made with a G-M counter and with a cloud chamber, both mainly for the emission of photons. A specially constructed large aluminum window gamma-tube was employed. To secure low background and small fluctuations of the tube, a sample of active nickel was shielded and the emitted radiation was collimated.

The results obtained showed the presence of photons of the following energies: 7.5±1 kev, 15±2 kev, and 38±3 kev, by absorption in aluminum. Absorption of radiation in copper verified the presence of photon of 38±3 kev and indicated the existence of photon of 80±5 kev energy. The order of relative intensities of photons of 7.5±1 kev, 15±2 kev, 38±3 kev, and 80±5 kev was estimated as 6:1:1:1, respectively.

The very low intensity of radiation did not allow the establishment of the presence of higher energy photons. Absorption in lead showed the existence of at least one photon of energy higher than 500 kev.

If it is assumed that the 7.5±1-kev photon is due to x-rays of orbital electron capture and to internal conversions, the emitted gamma-rays can be ascribed to Ni^{59}.

Electron tracks in the cloud chamber with and without a magnetic field revealed the presence of monochromatic electron groups.

An attempt to obtain a continuous spectrum of beta-disintegration of Ni^{63} in the cloud chamber was not successful.

Since Ni^{59} disintegrates into Co^{59} and Ni^{63} into Cu^{63} efforts were made to obtain information on the already known excited

states of Co^{59} and Cu^{63}. No experimental evidence was secured for the existence of such states in the disintegration of Ni^{59} and Ni^{63}.

We greatly appreciate the financial help given by the Graduate School for this research and the grant-in-aid for the construction of equipment extended by The Ohio State University Development Fund.

[1] G. Friedlander, Progress Report, Brookhaven National Laboratories (January 1–June 30, 1949).
[2] Q. T. Seaborg and I. Perlman, Rev. Mod. Phys. 20, 596 (1948).

Non-Linear I-V Characteristic of Ge at Very Low Temperatures

F. K. Du Pré
Philips Laboratories, Inc., Irvington-on-Hudson, New York
November 14, 1949

BOTH Estermann[1] and Gerritsen[2] have found in pure Ge samples, in the temperature region of liquid He, that the current-voltage relation is non-linear and usually shows a small asymmetry. At sufficiently high temperatures, however, the non-linearity and asymmetry disappear and at room temperature, a linear $I-V$ characteristic is found.

These facts may be qualitatively understood if we assume, as was done by Estermann, that in the "pure" samples, the concentrations of donors and acceptors are (almost) equal. In that case, we must expect local fluctuations in the concentrations causing the existence of n type domains and p type domains with $n-p$ barriers between them. As has been pointed out by James,[3] who considered an analogous situation for PbS, we may expect that the domains will combine to form a small number of continuous n type paths or p type paths. In each path there will be islands and pensinsulas of the other type. The current will mainly flow in the n paths and p paths, avoiding the islands and peninsulas and therefore it uses only a fraction of the total cross section. This is so because the $n-p$ barriers are quite high at low temperatures namely about 0.7 ev for Ge.

A qualitative explanation of the observed non-linear $I-V$ characteristic follows now directly from the above picture. For let us consider a p type island in an n type path with the electron current flowing in the direction of the arrow (see Fig. 1). The flow

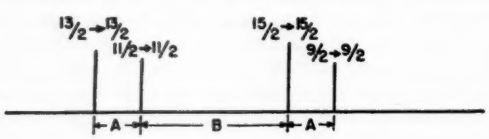

FIG. 1.

through the island will be prevented by barrier a as the flow is in the backward direction for this barrier. As soon, however, as the voltage over the specimen has been increased to such a value that the voltage difference between a and b becomes 0.7 V, the barrier at a will be wiped out and the current will flow through the island too. An analogous reasoning holds for the peninsulas. Also if a favorable voltage difference develops between a certain point of an n path and the adjacent point of a p path, the barrier between them may break down, thus causing a more favorable flow pattern. The described effects will cause a non-linear $I-V$ characteristic of the observed type in which the current increases "too much" with increasing voltage. At higher temperatures the effect will be much less marked because the conductivity increases so quickly that it will be hard to build up sufficient voltage between a and b without causing disturbing heat effects at the same time.

The slope of the characteristic at $V=0$ gives the resistance of the continuous n paths and p paths and its temperature dependence should be characteristic of the material without barriers.

In order to account for the asymmetry we must realize that the electron current can pass from the p path to the adjacent n path but not in the other direction. Therefore, the flow pattern will usually not be the same for both directions of applied voltage. As, however, there are a large number of obstructions for the current in both directions we must expect only a small resultant asymmetry. As this asymmetry is caused by the recifying property of $n-p$ barriers, it will not show up for voltage drops across the barrier corresponding with kT. Therefore we will find less asymmetry at higher temperatures where the applied voltage will be low in order to limit the current density. Furthermore, the barrier height is less at higher temperatures.

The shape of the $I-V$ characteristic is determined by the distribution of the $n-p$ barriers and the conductivities of the n and p paths. The fact that the shape of the $I-V$ characteristic is almost invariant with temperature in the liquid He range is in accordance with the experimental result that the conductivity of the n and p paths is independent of temperature in that range. However, an explanation for this behavior of the conductivity appears to be missing.

If the above considerations are correct we expect the high frequency resistance of pure Ge in the liquid He range to be considerably lower than the d.c. resistance and the $I-V$ characteristic shluld be linear at very high frequencies.

The author is indebted to Professor G. E. Uhlenbeck and Dr. I. Estermann for their encouragement and advice.

[1] I. Estermann, International Conference on the Physics of Very Low Temperatures, Cambridge, Massachusetts, 1949.
[2] A. N. Gerritsen, Physica 15, 427 (1949).
[3] H. M. James, Science 110, 254 (1949).

A Preliminary Report on the Fine Structure of the Microwave Absorption Spectrum of Oxygen*

James H. Burkhalter, Roy S. Anderson, William V. Smith, and Walter Gordy
Department of Physics, Duke University, Durham, North Carolina
November 23, 1949

USING a Zeeman modulation spectrograph, we have observed the microwave absorption spectrum of oxygen at low pressures ($\sim 10^{-1}$ millimeters of Hg), where the fine structure is completely resolved. Though several previous studies of the microwave absorption of oxygen have been made at pressures of the order of an atmosphere, no one has before detected this absorption at sufficiently low pressures to resolve completely the fine structure,** which has been theoretically predicted by Van Vleck.[1] Some experimental evidence for the fine structure was obtained by Beringer[2] in his wartime measurement of the resonance absorption of oxygen in the region of 5 millimeters wave-length. Recently, this work has been repeated by Strandberg, Meng, and Ingersoll[3] at pressures of 80 cm of Hg with the result that somewhat better evidence was obtained for the fine structure. The overlapping absorption of many lines at such high pressure prevented the accurate measurement of several properties of oxygen such as the line breadth parameter and the spacing of the fine structure levels.

In our work an absorption line is detected by a narrow-band, phase sensitive detector and is displayed on an Esterline Angus Automatic Recorder. The receiver operates at 4000 c.p.s. The absorption lines are modulated at the same frequency with an alternating magnetic field, which is applied by means of a solenoid which is placed around the wave guide cell. The field strength used in modulation is usually the order of a gauss. To reduce eddy currents, the wave guide cell is slotted down the center.

So far, sixteen of the fine structure lines have been detected and measured with a cavity wave meter. These tentative frequencies are listed in Table I. They are now being measured more precisely

TABLE I.

K	Transition*	Theoretical freq.** mc/sec.	Actual freq.† mc/sec.
11	−	57,620	57,610
9	−	58,330	58,330
3	+	58,460	58,420
7	−	59,170	59,160
5	+	59,600	59,610
7	+	60,430	60,440
9	+	61,140	61,120
11	+	61,780	61,800
13	+	62,380	62,420
3	−	62,470	62,480
15	+	62,960	62,970
17	+	63,520	63,530
19	+	64,060	64,100
21	+	64,630	64,640
23	+	65,140	65,220
25	+	65,680	65,770

* (+) indicates $J=K+1\rightarrow K$, (−) indicates $J=K-1\rightarrow K$.
** From Schlapp formulas, R. Schlapp, Phys. Rev. 51, 342 (1937).
† Actual frequency tentatively measured as $f/2$ wave meter accuracy. Estimated error ~15 mc/sec., now being remeasured with a frequency standard.

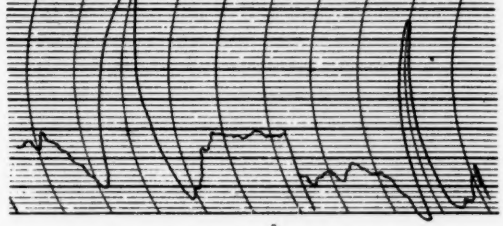

FIG. 1. Recorder tracing of the $J=12\rightarrow 11$, $K=11$ transition of oxygen at pressures of 14 and 7 mm of Hg.

with an electronic frequency standard monitored by station WWV. Figure 1 shows the recorder tracings of one of these lines at different pressures. Over the range of pressures so far studied, the line breadth appears to be proportional to the first power of the pressure. The observed frequencies agree with the theoretical ones within experimental error (about ± 15 = mc) for low K values, but a consistent deviation is observed for high K numbers. Reassignment of theoretical parameters will be made when the precision frequency measurements are completed.

* The research reported in this document has been made possible through support and sponsorship extended by the Geophysical Research Directorate of the Air Force Cambridge Research Laboratories under Contract No. W19-122-ac-35. It is published for technical information only and does not represent recommendations or conclusions of the sponsoring agency.

** The interesting recent work of Beringer in the 3-cm wave region, which included measurements at pressures down to 1.5 cm of Hg was concerned with paramagnetic relaxation in a strong magnetic field (R. Beringer, Phys. Rev. 70, 53 (1946)).

[1] J. H. Van Vleck, Phys. Rev. 71, 413 (1947).
[2] R. Beringer, Phys. Rev. 70, 53 (1946).
[3] Strandberg, Meng, and Ingersoll, Phys. Rev. 75, 1524 (1949).

Lifetimes of Mercury and Potassium Atoms in Excited States

B. MISHRA
Cuttack, India
October 31, 1949

FOR any $S-P$ transition, the lifetime T is given by the equation

$$T^{-1}=\frac{1}{2JH}\frac{64\pi^4\nu^3}{3hc^3}\Sigma|\psi_i r\psi_f d\tau|^2=3.54\times 10^5 \text{ (energy emitted in ev)}^3 \times\left[\int_0^\infty S_i r^3 S_f dr\right]^2 \text{sec.}^{-1}, \quad (1)$$

TABLE I. Calculated and observed lifetimes for $S-P$ transitions in mercury and potassium.

Atom	Calculated lifetime	Observed lifetime	Observer	Year
Mercury	0.6×10^{-9} sec.	0.3×10^{-9} sec.	Garrett[1]	1932
		1.6×10^{-9} sec.	Ladenburg and Wolfsohn[2]	1930
		1.3×10^{-9} sec.	Wolfsohn[3]	1930
Potassium	2.28×10^{-8} sec.	2.7×10^{-8} sec.	Weiler[4]	1939

where

$$S=Pr^{-1}.$$

Using the above formula the lifetimes of the excited mercury and potassium atoms were calculated. The ground state of mercury is $(6S)^2$ and that of potassium $4S$. The radial wave functions of the above ground states have been calculated by Hartree. Using the same self-consistent field method $6P$ and $4P$ wave functions of mercury and potassium atoms were calculated and the lifetime was evaluated by Eq. (1). Observation of Table I will indicate that the agreement between theoretical and experimental values is satisfactory. The high accuracy of potassium is due to polarization of the core being taken into consideration in the calculation of the wave function.

[1] P. H. Garrett, Phys. Rev. 40, 779 (1932).
[2] R. Ladenburg and G. Wolfsohn, Phys. Rev. 65, 207 (1930).
[3] G. Wolfsohen, Zeits. f. Physik 63, 634 (1930).
[4] J. Weiler, Ann. d. Physik 1, 361 (1929).

On the Nature of the π-Meson

B. FERRETTI
Instituto di Fisica della Università, Centro di Fisica Nucleare, Rome, Italy
AND
S. GALLONE
Istituto di Fisica Superiore della Università, Milan, Italy
November 14, 1949

WE want to discuss briefly some aspects of the question of the nature of the π-meson. Following a well-known argument of Oppenheimer and Serber[1] it seems quite proved that the spin of the π-meson is integral, and so we have only two reasonable possibilities for its spin: either it is one or zero. Professor Wentzel[2] has already suggested a method of distinguishing between these two possibilities; furthermore, there are several theoretical reasons which make unlikely the existence of elementary particles having spin one.[3]

We want, therefore, to discuss now the spin zero possibility only. If we were sure that the nuclear forces are due to the π-mesons only, we could conclude that they cannot be scalar. However, we are not sure that this is really the case, and the question, therefore, whether the π-mesons are scalar or pseudoscalar remains open. It has been pointed out, for instance, that the cross section of production of a π-meson by a gamma-ray should increase with the energy just above the threshold more quickly in the case of the scalar meson than in the case of a pseudoscalar meson.[4] There are already some data about the production of mesons by gamma-rays;[5] however, it is not clear whether the energy dependence of the relevant cross section is modified by the fact that in the actual case the production process takes place in a complex nucleus and not in a single nucleon, as it is supposed in the calculations. In order to decide experimentally the question whether the π-meson is scalar or pseudoscalar, it seems therefore surer to devise an experiment in which only a simple process and a very simple nucleus are involved. Such a very simple nucleus could be a nucleus of hydrogen or deuterium only. One of us[6] has already considered the absorption process of a meson in deuterium, pointing out that scalar and pseudoscalar mesons of a very low energy should behave very differently with respect to such a process. In fact, owing to the Pauli exclusion principle, scalar meson waves of even azimuthal quantum number cannot be

TABLE I.

$E-\mu c^2$ (Mev)	$\frac{1}{2}\lvert H_D/H_N\rvert^2$ pseudoscalar elastic scattering	$\frac{1}{2}\lvert H_D/H_N\rvert^2$ scalar elastic scattering
0	0.083	0
20	0.068	
40	0.057	0.005

absorbed in deuterium, at least in non-relativistic approximation. However, it seems very difficult to perform an experiment in order to decide whether π-mesons are scalar or pseudoscalar by studying the nuclear absorption of these mesons in deuterium, since in order to have an observable effect due to the selection rules, the lifetime for nuclear absorption in deuterium should be greater than 10^{-10} sec. and the probability of absorption ought to be decreased by a factor 10^5 at least by the selection rules. This seems very unlikely in view of a number of possible relativistic corrections. However, the same selection rules are very effective in diminishing the scattering cross section in deuterium for scalar mesons of a rather low energy (of the order of 20–40 Mev). One has to expect, therefore, that for mesons of such an energy the ratio of the scattering cross section in deuterium and in hydrogen should be considerably lower in the case of the scalar meson than in the case of the pseudoscalar meson. This ratio may be calculated quite exactly. In fact if H_N is the matrix element for the scattering of a meson against a single nucleon, and H_D the corresponding matrix element for deuterium, the relevant ratio in the case of the *elastic scattering* is $|H_D/H_N|^2$. Using natural mesonic units ($\hbar=1$, $c=1$, $\mu=$ mass of the π-meson $=1$) one has that the matrix element for elastic scattering in deuterium is given by

$$H_D=\frac{G^2}{8\pi^2}\frac{2\beta M}{E}\int\int\int d\mathbf{P}\left[\frac{1}{(\mathbf{P}+\mathbf{k})^2+\beta^2}-\frac{1}{(\mathbf{P}-\mathbf{k})^2+\beta^2}\right]\times\left[\frac{1}{(\mathbf{P}+\mathbf{k}')^2+\beta^2}-\frac{1}{(\mathbf{P}-\mathbf{k}')^2+\beta^2}\right]\cdot\left(\frac{1}{P_0^2-P^2}-\frac{1}{P_0^2+P^2}\right), \quad (1)$$

in the case of the scalar meson, and by

$$H_D=\frac{F^2}{8\pi^2}\cdot(2k)^2\frac{2\beta M}{E}\times\int\int\int d\mathbf{P}\left[\frac{2}{P^2+k^2+\beta^2}\right]^2\cdot\left(\frac{1}{P_0^2-P^2}-\frac{1}{P_0^2+P^2}\right) \quad (2)$$

in the case of pseudoscalar meson (and initial magnetic quantum number of the deuteron equal to zero). Here G and F are the mesonic charge of the nucleons, $2k$ is the initial momentum, and $2k'$ the final momentum of the meson, P the momentum of the nucleus in the intermediate state, E the energy of the meson ($E=(1+4k^2)^{\frac{1}{2}}$), M the mass of the nucleon, $P_0^2=EM$ and β is a constant which is involved in the ground state of the deuteron.[7] The Eqs. (1) and (2) are derived neglecting the recoil energy of the deuteron and the interaction of the nucleons in the intermediate state. The integrals in the right side of (1) and (2) may be very easily evaluated. The result for the ratio $H_D/H_N{}^2$ is given in Table I.

One may see that the relevant effect is very large. There is an interference effect due to the scattering by the two different nucleons in the deuteron which reduces rather strongly the cross section in both cases (scalar and pseudoscalar). However, in the scalar case effect of the selection rules remains very important. The absolute value of the elastic cross section in deuterium for energy of about 40 Mev and in the pseudoscalar case may be of the order of 10^{-27} cm^2 which is rather low but not completely out of the experimental possibilities in a not very far future.

[1] J. R. Oppenheimer and R. Serber, Solvay Conference, 1948.
[2] G. Wentzel, Phys. Rev. **75**, 1810 (1949).
[3] See, for instance, L. Van Hove, Phys. Rev. **75**, 1519 (1949). Also, the vacuum polarization difficulties seem worse with particles of spin one, than usual.
[4] G. Hamilton and H. W. Peng, Proc. Roy. Irish Acad. **49A**, 197 (1944); Leslie L. Foldy, Phys. Rev. **76**, 372 (1949).
[5] E. M. McMillan and J. M. Peterson, Science **109**, 438 (1949).
[6] B. Ferretti, Phys. Soc. Camb. Rep. (1947). B. Ferretti, Rendiconti del Seminario Fis. Mat. della Università di Milano, **19** (1948).
[7] H. A. Bethe and R. F. Bacher, Rev. Mod. Phys. **8**, 82 (1936).